

CONNECTING THE DOTS:
**DUST PARTICLE TRACKING
AT COMET
67P/CHURYUMOV-GERASIMENKO**

DISSERTATION

zur Erlangung des mathematisch-naturwissenschaftlichen Doktorgrades

“Doctor rerum naturalium”

der Georg-August-Universität Göttingen

im Promotionsstudiengang Physik

der Georg-August University School of Science (GAUSS)

vorgelegt von

MARIUS PFEIFER

aus Hildesheim

Göttingen, 2024

Betreuungsausschuss

Prof. Dr. Ulrich Christensen
Max-Planck-Institut für Sonnensystemforschung, Göttingen

Prof. Dr. Jessica Agarwal
Institut für Geophysik und Extraterrestrische Physik, Technische Universität Braunschweig

Prof. Dr. Eberhard Bodenschatz
Max-Planck-Institut für Dynamik und Selbstorganisation, Göttingen

Mitglieder der Prüfungskommission

Referent: Prof. Dr. Stefan Dreizler
Institut für Astrophysik und Geophysik, Georg-August-Universität Göttingen

Korreferentin: Prof. Dr. Jessica Agarwal
Institut für Geophysik und Extraterrestrische Physik, Technische Universität Braunschweig

Weitere Mitglieder der Prüfungskommission:

Prof. Dr. Eberhard Bodenschatz
Max-Planck-Institut für Dynamik und Selbstorganisation, Göttingen

Prof. Dr. Ansgar Reiners
Institut für Astrophysik und Geophysik, Georg-August-Universität Göttingen

PD Dr. Matthias Schröter
Max-Planck-Institut für Dynamik und Selbstorganisation, Göttingen

Dr. Bart Geurten
Department of Zoology, University of Otago, Dunedin, Neuseeland

Tag der mündlichen Prüfung: 03.07.2024

License

Connecting the Dots: Dust Particle Tracking at Comet 67P/Churyumov-Gerasimenko © 2024 by Marius Pfeifer is licensed under Creative Commons Attribution-NonCommercial-ShareAlike 4.0 International (CC BY-NC-SA 4.0). To view a copy of this license, visit <https://creativecommons.org/licenses/by-nc-sa/4.0/>.



All third-party images are all rights reserved, and you must request permission from the copyright owner to use this material.

Imprint

This document was typeset in \LaTeX with the help of the KOMA-Script. It is the result of merging **Federico Marotta's** kaobook class with **André Miede's** Classic Thesis template, and customizing it with additional augmentations.

The illustration on the cover page is an artistic interpretation of real particle tracking data. While the general configuration of the scene is pictured as we observed it, some of the particle trajectories are extended beyond where the particles were seen last.

ABSTRACT

Comets and their characteristic plasma and dust tails have been intriguing people for millennia. Early theories about their nature were for example already developed by the ancient Chinese and Greek, but it was not until the late 1500s that we started to understand that comets were small bodies in our Solar System. It then took another few hundred years to reliably predict their complex orbital motion, and only in the 1950s did we begin to develop plausible theories about their origin and makeup. In 1986, a spacecraft visited a comet for the first time and confirmed that comets indeed have solid nuclei and are not just a cloud of ice and dust. Finally in 2014, the Rosetta mission arrived at comet 67P/Churyumov-Gerasimenko and continued to accompany it for over two years—an unprecedented feat. The mission yielded an equally unprecedented wealth of information, which revolutionized our understanding of comets. And yet the exact mechanism by which comets eject their solid surface material is still not fully understood. Solving this “activity paradox” is currently one of the main challenges in cometary science. One way to learn more about the ejection process is by studying the dynamics of the ejected material. Consequently, the scientific camera system on board the Rosetta spacecraft recorded several image sequences of 67P’s near-nucleus coma. Tracking these dust particles is however highly non-trivial due to sparse data, complex particle motions, fluctuating camera pointing, a high particle density, and other factors. In the scope of this work, I therefore developed a novel tracking algorithm specifically optimized for Rosetta data and used it to track thousands of individual dust particles through several image sequences. Focusing on the four most suitable image sequences, I then continued to trace hundreds of decimeter-sized “particles” back to the nucleus surface and determined their potential source regions, size distributions, and dynamics. The results, which were additionally corroborated by extensive dust coma modeling, reveal that the observed activity cannot be explained by heightened solar radiation alone. Instead, the local surface structure and composition likely play important roles. Most notably, we found that the particles likely gained most of their speed already during their ejection events, which hints at a more “explosive” mechanism. Due to this discovery, we may therefore be one step closer to solving the activity paradox.

ZUSAMMENFASSUNG

Kometen und ihre charakteristischen Plasma- und Staubschweife faszinieren die Menschen schon seit Jahrtausenden. Frühe Theorien über ihre Natur wurden beispielsweise bereits von den alten Chinesen und Griechen entwickelt, aber erst gegen Ende des 16. Jahrhunderts begannen wir zu verstehen, dass Kometen kleine Körper in unserem Sonnensystem sind. Es dauerte dann noch einige hundert Jahre, bis wir ihre komplexe Bahnbewegung zuverlässig vorhersagen konnten, und erst in den 1950er Jahren begannen wir, plausible Theorien über ihren Ursprung und ihre Zusammensetzung zu entwickeln. Im Jahr 1986 besuchte erstmals eine Raumsonde einen Kometen und bestätigte, dass Kometen tatsächlich feste Kerne besitzen und nicht nur aus einer Eis- und Staubwolke bestehen. Schließlich erreichte 2014 die Rosetta-Mission den Kometen 67P/Churyumov-Gerasimenko und begleitete ihn über zwei Jahre lang – eine beispiellose Leistung. Die Mission lieferte eine ebenso beispiellose Fülle an Informationen, die unser Verständnis von Kometen revolutionierten. Doch der genaue Mechanismus, durch den Kometen ihr festes Oberflächenmaterial ausstoßen, ist noch immer nicht vollständig verstanden. Die Lösung dieses „Aktivitätsparadoxons“ ist derzeit eine der Hauptherausforderungen in der Kometenforschung. Eine Möglichkeit, mehr über den Ausstoßprozess zu erfahren, besteht darin, die Dynamik des ausgestoßenen Materials zu untersuchen. Folglich zeichnete das wissenschaftliche Kamerasystem an Bord der Rosetta-Raumsonde mehrere Bildsequenzen der Koma nahe des Kerns von 67P auf. Die Verfolgung dieser Staubpartikel ist jedoch aufgrund spärlicher Daten, komplexer Teilchenbewegungen, schwankender Kamerapositionierung, hoher Teilchendichte und anderer Faktoren äußerst schwierig. Im Rahmen dieser Arbeit habe ich daher einen neuartigen Tracking-Algorithmus entwickelt, der speziell für Rosetta-Daten optimiert ist, und ihn verwendet, um Tausende einzelner Staubpartikel durch mehrere Bildsequenzen zu verfolgen. Mit Fokus auf die vier bestgeeignetsten Bildsequenzen habe ich dann Hunderte von dezimetergroßen „Partikeln“ zurück zur Nukleusoberfläche verfolgt und ihre potenziellen Ursprungsregionen, Größenverteilungen und Dynamiken bestimmt. Die Ergebnisse, die zusätzlich durch umfangreiche Staubkoma-Modellierungen bestätigt wurden, zeigen, dass die beobachtete Aktivität nicht allein durch erhöhte Sonneneinstrahlung erklärt werden kann. Stattdessen spielen die lokale Oberflächenstruktur und Zusammensetzung wahrscheinlich wichtige Rollen. Am bemerkenswertesten fanden wir, dass die Partikel den größten Teil ihrer Geschwindigkeit wahrscheinlich bereits während ihrer Ausstoßereignisse erhielten, was auf einen eher „explosiven“ Mechanismus hinweist. Durch diese Entdeckung sind wir somit möglicherweise einen Schritt näher daran, das Aktivitätsparadoxon zu lösen.

PUBLICATIONS

- Pfeifer, M., Agarwal, J., and Schröter, M. (2022). "On the Trail of a Comet's Tail: A Particle Tracking Algorithm for Comet 67P/Churyumov-Gerasimenko". In: *A&A* 659, A171. doi: 10.1051/0004-6361/202141953.
- Pfeifer, M., Agarwal, J., Marschall, R., Grieger, B., and Lemos, P. (2024). "Dynamics and Potential Origins of Decimeter-Sized Particles around Comet 67P/Churyumov-Gerasimenko". In: *A&A* 685, A136. doi: 10.1051/0004-6361/202346380.
- Lemos, P., Agarwal, J., Marschall, R., and Pfeifer, M. (2024). "Ejection and Dynamics of Aggregates in the Coma of Comet 67P/Churyumov-Gerasimenko". In: *A&A* 687, A289. doi: 10.1051/0004-6361/202348692.

To my *family, my friends, my loved ones.*
To everyone who *supported and believed* in me.

Comets are like vitamin tablets. Both have an air of mystery that surrounds them, and in many cultures, they are seen as the heralds of hope in a time of despair. Ok, maybe that last part was not “exactly” right. But they do end up happily fizzing away if you were to put them in a glass of water. In fact, comets are so excited about showing you their neat little trick that they already start fizzing when they are still millions of kilometers away from your glass. And just like when a kid tugs your sleeve and asks you to watch them perform, you should pay attention, because it’s beautiful.

One of the most memorable experiences that inspired me to become an astrophysicist I had in 2015, when I was part of an excursion to a telescope site in the South-African Karoo Desert. One night we were trying to use the university telescope, and a lot of things went wrong. I actually can’t remember if it eventually worked, but I do know that most of us ended up stranded in the middle of the freezing African night, with only time on our hands (and some gloves if you were lucky). This was very frustrating, and it would have likely remained that way were it not for the absolutely amazing sight of the southern night sky. And so for the longest time we would just stand there, gazing at the stars, with our eyes and mouths wide open, resembling baby chicks waiting to be fed. We simply couldn’t get enough.

Now I study comets, and my fascination hasn’t subsided. Comets are the last survivors from the time when our Solar System formed. By asking them the right questions, we can learn a lot about our history. They may even be the reason we are alive today. When the Earth was still young, comets crashed onto it and likely brought with them the essence for all its life—water. Maybe the exact same water you now use to dissolve your vitamin tablets in.

—Pfeifer (2021). “Origin Story” (slightly modified; written during a free writing session as part of the “Write Like a Thought Leader” workshop).

*There is a phenomenon that attends each Comet, and is peculiar to them,
called its tail.*

— Unknown (1757). *An Account of the Remarkable Comet.*

ACKNOWLEDGMENTS

First of all, thank you **Jessica Agarwal**, for being a great supervisor. I was your first PhD student, which made this endeavor new to both of us, but you clearly cared about me and my work, and so I never really felt left alone or without guidance. Thank you for our regular (virtual) meetings, especially during the height of the corona pandemic, and despite moving your work place to Braunschweig. Thank you for trying your best to keep me focused on the important bits whenever I got distracted. I very much enjoyed our personal and working relationship.

Thank you to the other two members of my thesis advisory committee (TAC), **Ulrich Christensen** and **Eberhard Bodenschatz**. You provided valuable feedback during our TAC meetings, supported the three extensions of my project, and encouraged me to go on parental leave during the first three months after my son was born, which was great advice.

Thank you **Stefan Dreizler**, **Jessica Agarwal**, **Ansgar Reiners**, **Eberhard Bodenschatz**, **Matthias Schröter**, and **Bart Geurten**, for agreeing to referee and examine this work.

A big thank you to my colleagues **Pablo Lemos**, **Raphael Marschall**, **Xian Shi**, and **Nick Attree**, for extensively discussing issues, ideas, and results (either in person or online), being my co-authors (Pablo and Raphael) or (proof)reading my manuscripts (Xian and Nick), providing tools or information, and just generally being very helpful and showing great interest in my work.

Thank you to my other two co-authors, **Matthias Schröter** and **Björn Grieger**. Without hesitation, both of you became deeply involved in my work even though I was a stranger to you. Thank you Matthias, for essentially becoming a second supervisor during the time when I was developing my tracking algorithm. Drawing from your experience in the particle tracking business was integral to the success of my project. Thank you Björn, for so happily helping me out and engaging with my work. You already went beyond what I was asking and provided additional material to examine my results when we hadn't even discussed your co-authorship.

Thank you to the other members of my working group, **Johannes Markkanen**, **Yoonyoung Kim**, **Yuna Kwon**, **Manuela Lippi**, and **Maria Mastropietro**. Thank you for providing feedback, articles, and information, and for tolerating when it took a bit longer to discuss my work during our group meetings. It's a shame that we mostly met online, but it made me cherish the moments even more whenever we did meet in person. You were always easy and fun to be around.

Thank you **Vera Maria Passegger**, for being a great friend and proofreading all my manuscripts with such immediacy and despite your already

insane workload. You were my set of fresh eyes and without you, this dissertation would still be riddled with bloopers.

Thank you to the many other people (from my institute, my community, or elsewhere) that I reached out to, interacted with, met at conferences, workshops, or online, who answered so, so, many questions (yes, this will be a theme here), or who helped me in various other ways (and hopefully won't mind that I bunch them together like that in a roughly chronological order): thank you **Michael Mommert**, for introducing me to the Source Extractor and getting me started with my project; thank you **Carsten Güttler** and **Jakob Deller**, for allowing me to use your Python routine to read PDS images; thank you **Gábor Kovács**, **Cecilia Tubiana**, and **Holger Sierks** (and also Carsten) for happily answering questions about the OSIRIS cameras; thank you **Kyle Barbary**, **Benne Holwerda**, and **Peter Stetson**, for patiently answering so many questions about SEP, the Source Extractor, and DAOPHOT; thank you **Roberto Vio**, for extensively answering questions about matched filters, and **Wilhelm Burger**, for providing resources on them; thank you **Maurizio Berti**, for gladly answering questions about PyQt5; thank you **Andrew Liounis**, for readily answering so many questions about your particle tracking algorithm; thank you **Jean-Yves Tinevez**, **Thomas Caswell**, **Jerry Westerweel**, and **Peter Lu**, for answering questions about particle tracking in your fields and your tracking software; thank you **Matt Taylor** and **Pascal Regnier**, for answering questions about Rosetta's star tracker, and **Fabio Curti**, for answering questions about your star tracking software (and even meeting me on Zoom to do so!); thank you **Amy Mainzer**, **Brian Skiff**, **John Tonry**, and **Larry Denneau**, for answering questions about your sky surveys and small body trackers; thank you **Monique Kelley**, for thoughtfully answering questions about particle tracking during the Deep Impact/EPOXI mission; thank you **Theresa Ott** and **Esther Drolshagen**, for answering questions about your particle tracking results; thank you **Asmus Freytag**, for proofreading the manuscripts of my papers; thank you **Steve Chesley**, for reviewing my first paper; thank you **Koji Wada**, **Noah Molinski**, and **Bastian Gundlach**, for answering questions about and discussing the formation of particle ejection cones; thank you **Miryam Merk**, for providing statistical consulting; thank you **Matthias Läuter**, **Tobias Kramer**, and **Michael Combi**, for answering questions about your respective surface gas production models and Matthias and Tobias for providing your data; thank you **Elias Odelstad** answering questions about the effect that plasma might have on particles; thank you **Frank Preusker**, for providing the (texturized) shape model of 67P; thank you **Mohamed Ramy El-Maarry**, for answering questions about the definition of surface regions and **Nicolas Thomas**, for providing the surface regions tool, which took you a lot of hassle; thank you **Mauro Ciarniello**, for helping with the surface illumination maps; thank you **Jean-Baptiste Vincent**, for helping with your shapeviewer software, answering questions about surface changes within our regions of interest, and even searching your database for potential correlations; thank you **Sonia Fornasier**, **Pedro Hasselmann**, and **Stefano Mottola**, for discussing and providing your data of bright spots and boulders counted on the surface of 67P; thank you **Maurizio Pajola** and **Giovanna Rinaldi**, for answering questions about and discussing particle/boulder size-frequency distributions and power-law indices; thank you Aaron Clauset for discussing the difficulties of power-law fitting; thank you **Marco Fulle**,

for answering questions about your activity model, discussing particle size-frequency distributions, and (proof)reading the manuscript of my second paper; thank you **Yuri Skorov**, for answering questions about your particle ejection models and also (proof)reading the manuscript of my second paper; thank you **Doro Bischoff** and **Moritz Goldmann**, for answering questions about your particle ejection experiments; thank you **Jean-luc Doumont**, for discussing and providing valuable feedback about the layout and presentation of my dissertation; thank you **Rhea Wessel**, for supporting my layout idea; thank you **Michael Fire**, for helping to find resources of publication rates; thank you **David Nicholas**, **Carol Tenopir**, **Naomi Baron**, and **Angus Phillips**, for discussing the decline in long-form reading; thank you **Gloria Mark**, for answering questions about your attention span plot; thank you **Lynn Nygaard**, **Susan Smith**, **Patricia Thomson**, **Dwight Atkinson**, **Brian Paltridge**, **Nell Duke**, **Kristin Solli**, and **John Swales**, for discussing the popularity of cumulative dissertations; thank you **Aileen Fyfe**, **Otto Kruse**, **Adriaan van der Weel**, **Geoffrey Crossick**, **Paul Thompson**, **Charles Bazerman**, and **Agata Mrva-Montoya**, for discussing the history of monographic dissertations and science communication; thank you **Michael Dougherty** and **Brian Copenhaver**, for discussing the last person to “have read everything”; thank you **Steve Heard**, for discussing alchemists and books on writing; thank you **Hans Rickman**, for discussing the intricacies of the comet designation system; thank you **Alessandro Morbidelli**, **David Nesvorný** and **Luke Dones**, for (extensively) discussing comet populations and helping with my plots; thank you **Jessica Sunshine**, for discussing hyperactivity and distributed sources; **Calvin Knoop**, for providing your lab recordings of particle ejections; thank you **Stephanie McLaughlin**, for helping to figure out the imaged scale comet Halley; thank you **Lucie Maquet**, **Giovanni Valsecchi**, and **Massimiliano Guzzo**, for providing information about 67P’s dynamic history; thank you **Luca Penasa**, for providing your figure data; thank you **Thies Staack**, for helping with Chinese crediting practices; thank you **Urs Mall** and **Helga Washausen**, for helping with my literature search; thank you **Sonja Schuh** and **Johanna Wagner-Farssi**, for your IMPRS support; thank you **Julia Marín-Yaseli de la Parra**, **Oksana Shalygina**, **Stavro Ivanovski**, and **Vladimir Zakharov**, for being interested in my work and actually asking *me* questions; and thank you **Martina Kováčová**, **John Junkins**, **Martin Hilchenbach**, **Thurid Mannel**, **Lioudmila Kolokolova**, **Guus Bertens**, **Jan Molacek**, and so many of you that I have already named for providing articles and information.

I would also very much like to thank all the kind **internet strangers** that I encountered (directly or indirectly) on public platforms dedicated to archiving and sharing knowledge, such as Wikipedia, StackOverflow (and derivatives), GitHub, YouTube, ResearchGate, and other online forums or tutorial websites. Thank you for asking questions, giving answers (to my questions), providing tools, reporting bugs, just generally discussing relevant topics, and most importantly letting me borrow countless code snippets that made my program run and my \LaTeX documents compile. Without you and your passion to teach and learn I would have not been able to conclude this project successfully.

Lastly, but very importantly, I would like to thank my dear family and friends for your amazing support. Thank you so much for being there

Some of you provided articles and information in the context of my small literature research side project where I asked you to tell me which work(s) from our community you highly recommend, and which of your own works you were really proud of. Thanks again to everyone who participated! Your answers were very interesting and helpful. I got this idea from Helen Sword’s book *Stylish Academic Writing* (which I highly recommend). To learn more about what makes good scientific writing, the author not only asked scientists from several different fields to name their favorite articulate authors and well-written works, but also interviewed over 100 established academic writers about their work.

Thanks also to **Hardi Peter**, who discussed with me whether it is appropriate to thank all these people already in the acknowledgments of my first paper. Ultimately I decided against it because it might have been too irritating, but here in my thesis I am very happy to do so!

And of course sorry and thank you to everyone who I may forgot to mention!

when I needed it, and taking care of all the things that I could not care for, especially during the most stressful times. Thank you for your help, thank you for your constant encouragement, and thank you for believing in me. We did this together.

FORMAL ACKNOWLEDGMENTS

Because this work is built on the analysis of images recorded by the Optical, Spectroscopic, and Infrared Remote Imaging System (OSIRIS) of the Rosetta spacecraft, I would like to acknowledge the operation and calibration team at MPS and the Principal Investigator Holger Sierks on behalf of the OSIRIS Team for providing the OSIRIS images and related data sets. OSIRIS was built by a consortium of the Max-Planck-Institut für Sonnensystemforschung, Göttingen, Germany; the CISAS University of Padova, Italy; the Laboratoire d'Astrophysique de Marseille, France; the Instituto de Astrofísica de Andalucía, CSIC, Granada, Spain; the Research and Scientific Support Department of the European Space Agency, Noordwijk, The Netherlands; the Instituto Nacional de Técnica Aeroespacial, Madrid, Spain; the Universidad Politécnica de Madrid, Spain; the Department of Physics and Astronomy of Uppsala University, Sweden; and the Institut für Datentechnik und Kommunikationsnetze der Technischen Universität Braunschweig, Germany. The support of the national funding agencies of Germany (DLR), France (CNES), Italy (ASI), Spain (MEC), Sweden (SNSB), and the ESA Technical Directorate is gratefully acknowledged. We thank the Rosetta Science Ground Segment at ESAC, the Rosetta Missions Operations Centre at ESOC and the Rosetta Project at ESTEC for their outstanding work enabling the science return of the Rosetta Mission.

This work was supported by the International Max-Planck Research School (IMPRS) for Solar System Science at the University of Göttingen and funded by the ERC Starting Grant No. 757390 Comet and Asteroid Re-Shaping through Activity (CAstRA).

PREFACE

*The vitality of thought is in adventure. Ideas won't keep.
Something must be done about them.*

— Alfred North Whitehead in Lucien Price (1954).
Dialogues Of Alfred North Whitehead.

This dissertation is written in a special cumulative style. Its overarching structure still follows that of a classical monograph—or by extension that of a typical cumulative thesis—and is divided into a general introduction, a main body, and a final discussion. But its layout significantly changes within its main body, where I incorporated the two first-author papers that I wrote within the context of my PhD project (Pfeifer et al. 2022, 2024). The papers, which I respectively refer to in this dissertation as the “methods” and the “science” paper for convenience, are included unaltered and in full, but with a twist: each page from the papers is dedicated an entire double-page. On its right side, I show an original page from the papers, while on its left side, I directly expand on some of the content of the respective paper page (more specific details are discussed at the end of this preface).

Knowing that this is a rather unusual dissertation format, I motivate my choice in the following paragraphs. There are, however, far too many arguments for or against either the monograph or the cumulative dissertation for me to address (see e. g., Duke et al. 1999; Paltridge 2002; Sharmini et al. 2015; Smith 2015; Freeman 2018; Mason 2018; Rigby et al. 2020; Paltridge et al. 2020, 2023; Chong et al. 2022). The value of the monograph has been extensively discussed among scholars since at least the serials crisis, which started in the 1980s and later turned into the monograph crisis (e. g., Smith 1990; Thompson 2005; Savage 2010; Adema 2015; Buranyi 2017; Bosch et al. 2022; although signs of it may be found as early as 1927, Armato 2012). Especially in the Humanities, Arts, and Social Sciences, where, unlike in the Natural Sciences, the monograph still plays a central role in scholarly communication beyond the dissertation, scholars continue to debate its demise in the context of the digital age (e. g., Steele 2008; van der Weel 2015, 2016; Thomas et al. 2016; Crossick 2016; Mrva-Montoya 2016; Gould 2016; Paré 2019; Clark et al. 2020; Shaw et al. 2022). Because my approach will certainly not end this debate, I merely focus briefly on the arguments that I regard to be most important.

Today’s scientific monographs are rooted in medieval manuscripts, which in turn are rooted in codices, and ultimately ancient scrolls (Leeuwen 2016). Over the course of this transformation, many practices changed and new standards emerged (e. g., Meadows 1980; Paltridge et al. 2020). To name just a few major (but simplified) examples: The predominant language in writing changed from Greek to Latin to several European languages and eventually to English (e. g., Hamel 2007; Englander 2014, albeit that Chinese might replace English in the future); the approach at conveying knowledge changed from Plato’s conversational dialogues intended for a general public (e. g., Plato 2006; Adler et al. 2014), to the

The main purpose of the methods paper is to introduce and explain my tracking algorithm, whereas the science paper focuses on its application and the implications of my findings to cometary science.

I used to think that the cumulative dissertation was a rather new format that emerged from the digital age, but that is not so; the format goes back to at least the 1960s (e. g., Reid 1978; Monaghan 1989; Wilson 2002).

The serials crisis describes the massive hike in journal prices by commercial publishers in the fields of Science, Technology, Engineering, and Mathematics (STEM). To finance journal subscriptions, research libraries thus had to significantly reduce their purchase of monographs, which they struggled to sell. As a consequence, it became difficult for scholars to find an outlet for their monographs (especially when dealing with niche subjects), as “publishers increasingly determined what gets published based on market-value instead of on scholarly merit” (Adema 2015).

In medieval times, “scientists”, such as alchemists, often wrote in code or used cryptic symbols to protect their research from rivals (e. g., Long 2003; Smith 2004; Heard 2016; Nummedal 2016). This changed with the founding of scientific communities like the Royal Society of London in 1660, which were based on principles of open communication and collaboration, ideas most notably advocated by Francis Bacon (e. g., Peltonen 1996; Heard 2016). At the same time however, scientific writing also became increasingly obfuscated, contrived, and verbose, potentially in an attempt to “gate-keep” or feign superiority (e. g., Williams et al. 1995). Complaints about such writing and calls for clear and direct language thus date back at least as far (e. g., Sprat 1667; see also Pinker 2014). In modern times, this sentiment was prominently expressed by Strunk and White in *The Elements of Style* (e. g., 1959, first published in 1920). Yet even though by now, clarity and concision have long been established as important pillars of scientific communication, researchers continue to have legitimate concerns about the current state of writing (e. g., Schimmel 2012; Sword 2012; Greene 2013; Heard 2016; Ball 2017).

Notable recent exceptions from the standard dissertation format are for example: Nick Sousanis’s award-winning dissertation *Unflattening* (2015), which deals with the relationship between text and images and explores new ways of thinking, conveyed entirely in the form of comics; or A.D. Carson’s dissertation “Owning My Masters” (2017), which combines videos, audio recordings, and interviews, but only cites 13 references and is just 37 pages long, of which many contain song lyrics or a single image.

I came across a quote in this regard that is simply too cynical not to share: “The monograph was supposed to be exhaustive, exhausting the ‘sources’ as well as the reader” (Smith 1990). In all fairness however, it is curious that right around the same time when monographic dissertations started to emerge in a “modern” format, in the Natural Sciences, journal papers began to replace monographs as the primary medium of scientific communication. This sparks the question if monographic dissertations ever had a readership or impact comparable to that of journal papers.

early scientific books—by authors such as Galilei, Kepler, or later Darwin—that were often still vernacular and comprehensible by a lay audience (e. g., Meadows 1980; Adler et al. 2014), to the modern, much more neutral, but often jargon-heavy language of today, intended for an expert audience (e. g., Sword 2012; Ball 2017); the publication practices changed substantially with the invention of the printing press from the distribution of hand-written manuscripts to the marketing of mechanically printed books at industrial scales (e. g., Meadows 1980; Hunter 2016; Wilding 2016; Fyfe et al. 2022); modern citation practices, now universally regarded as a hallmark of serious scientific work, only emerged during the 19th century (first as a recognition of debt, e. g., Bazerman 1988); and the nowadays typical IMRaD structure (Introduction, Methods, Results, and Discussion; the so-called “simple traditional” dissertation format, e. g., Paltridge 2002) only established itself as the standard during the 20th century (Bazerman 1988; Day 1989; Atkinson 1998; Sollaci et al. 2004). Throughout the middle ages and the early modern period, doctoral candidates at German universities (where the PhD in its current form originated) were judged solely on the basis of their disputation (Allweiss 1979). Dissertations only emerged in the 17th and 18th centuries as optional writings to the disputation, were often composed by the referee instead of the doctoral candidate (Kruse 2006), and were so different from today’s dissertations in their form and function prior to the early to mid 1800s, that they are regarded as separate kinds of works (Allweiss 1979). In short, the (monographic) dissertation has never been a static genre. Although its current form is regarded as the gold standard in many disciplines, it has a long history of evolution, and—as the emergence of the cumulative dissertation and the more recent move to open-access online publications shows (e. g., Grimme et al. 2019; Clark et al. 2020; Shaw et al. 2022)—it is evolving still.

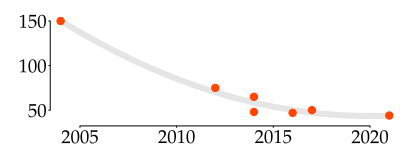
I developed my own dissertation layout because I believe that monographic dissertations have fallen out of time: virtually nobody reads them anymore. One of the core ideas of the monograph lies in that ideally, each part is written with the whole in mind. In that sense, it has a low hierarchy with just one synthesis layer, whereas cumulative dissertations have two: each constituting paper was synthesized with only its specific scope in mind and is ideally self-contained; a good paper should not rely on external material to be properly understood by the target audience. The cumulative framework of the dissertation then forms the second synthesis layer. And even though monographs, too, typically consist of parts, chapters, sections, and so on, a cumulative work might never achieve the same level of coherence. To the reader then, the strength of the monograph unfolds when it is read *as a whole*.

But in my experience as a natural scientist, people just don’t read monographic dissertations as a whole anymore (unless they are asked to). They usually lack the time for such a commitment. Well-written dissertations are still recommended to people who seek a good entry point into a particular field of research, and they are often used to look up specific details that are not mentioned in related articles. But in both instances, cumulative dissertations can serve the same purpose, and do so potentially even better than the monograph. For one, introductions of cumulative dissertations can be equal in quality to those of monographs, but cumulative dissertations may hold an advantage over monographs in that following

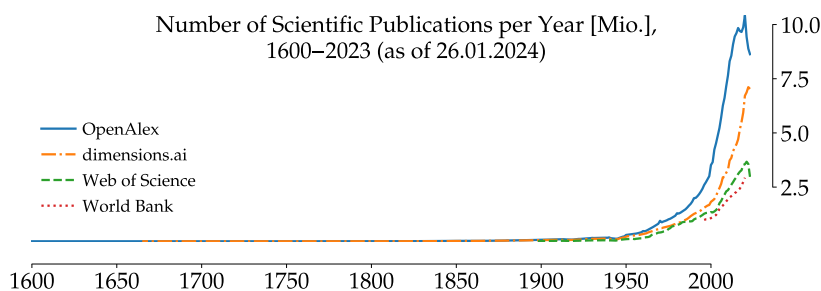
the introduction, they transition into the works that are more typically sought after and debated by the scientific community: the papers. But especially when dissertations are used to look up specific details, the strength of monographs is lost, and cumulative dissertations may actually prove more useful as well, as their layered structure of self-contained units can make it easier to locate supplementary material.

To take up the cudgels for the monograph however, there is another important advantage to it, but it's to its author. In 2019, for example, the Cambridge and Oxford University Presses published a joint report on "Researchers' Perspectives on the Purpose and Value of the Monograph" in the Humanities and Social Sciences (Clark et al. 2020). While the authors conclude that the monograph "must evolve to remain relevant to the way academics work in an increasingly digital world", they also found that many respondents of their survey regard the monograph as an important "organizing principle of research ... that helps them to clarify their thinking ... and supports the development of their ideas." This is a compelling argument for the monograph, and I assume that it is also one of the primary reasons why many universities still prefer the monograph over the cumulative dissertation. And yet in the Natural Sciences, the monograph has long been replaced by the journal article as the primary medium of scientific communication (e. g., Mabe 2009, 2010; Mabe et al. 2011; Ware et al. 2015; Johnson et al. 2018; Tenopir et al. 2019; Dietz 2022), and cumulative dissertations have become a common format (e. g., Dong 1998; Wilson 1998; Sharmini et al. 2015; Autry et al. 2016; Frick 2016; Anderson et al. 2020, 2021; Donner 2021; Kubota et al. 2021; Paltridge et al. 2023; Solli et al. 2023). Nowadays, writing a monographic dissertation is probably the one and only time that most researchers may engage in such long-form scientific writing. And while the mode of thinking enabled by monograph writing is important, I think that it is not lost when writing a cumulative dissertation. This form, too, requires synthesis, and emerges from the framework of a PhD project, which seeks to answer a central question and guides the research.

Thus given the publication and research culture in the digital age, I believe a cumulative dissertation to be the more viable choice. For one, due to the internet, smartphones, social media, and content recommendation algorithms, people are constantly flooded with (irrelevant) information competing for their attention. As a result, the human attention span (or at least the time that we allocate to any specific activity) may have significantly declined over the past two decades (e. g., Duffy et al. 2022; Ducharme 2023; Mark 2023; niplav 2023). But declining attention span or not, there is no denying that the number of scientific publications per year has massively increased over the past few decades (see, e. g., also

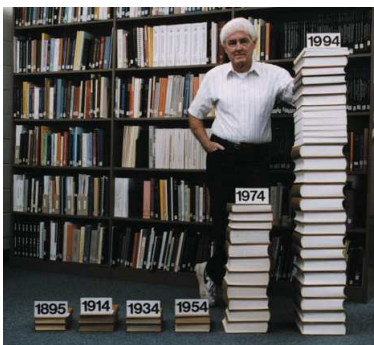


Average attention duration on a computer screen in seconds, 2004–2021 (adapted from Mark 2023). The orange circles indicate measurements from different studies; the gray curve merely illustrates the trend.



The four resources in the previous diagram record various forms of data, including (journal) articles, books, reports, editorials, letters, datasets, or (in the case of the Web of Science) even music, film, or dance performance reviews. Which of those should be considered as relevant sources for scientific work is of course debatable and depends on the subject. What actually constitutes a (scientific) book is for example also not easy to define (e. g., Frasca-Spada et al. 2000; Hunter 2016; Phillips et al. 2022). Naturally, none of the resources claim to be comprehensive, but the curves nevertheless give a good idea about the general trend of the publication rate. Judging from the OpenAlex data for example, since I was born in 1989, the total number of publications has more than quintupled.

There is this notion that the last person to have read or known everything available to them was Giovanni Pico della Mirandola (1463–1494, e. g., Herman 2013). But considering that the ancient Library of Alexandria may have already held hundreds of thousands of documents (El-Abbadi 2023), the point at which it was still possible to read every available work of note likely lies many centuries further in the past.



Then-Editor-in-Chief of the *Astrophysical Journal*, Helmut A. Abt, standing next to book stacks of the journal’s publications to illustrate the dramatic increase of astronomical literature over the past decades (Heck 2003, reprinted with permission from NOIRLab).

Fire et al. 2019). Consequently, it has become impossible to be familiar with every published work even in the smallest of subfields—a trend already predicted by Thomas Henry Huxley during his retiring address as president of the Royal Society in 1885:

It has become impossible for any man to keep pace with the progress of the whole of any important branch of science. If he were to attempt to do so his mental faculties would be crushed by the multitude of journals and voluminous monographs which a too fertile press casts upon him. This was not the case in my young days. A diligent reader might then keep fairly informed of all that was going on without demoralizing his faculties by the accumulation of unassimilated information. It looks as if the scientific, like other revolutions, meant to devour its own children; as if the growth of science tended to overwhelm its votaries; as if the man of science of the future were condemned to diminish into a narrower and narrower specialist as time goes on.

Even Johannes Kepler already noted in 1606 that (Jardine 1988):

After the birth of printing, books became widespread. Hence everyone throughout Europe devoted himself to the study of literature ... Every year, especially since 1563, the number of writings published in every field is greater than all those produced in the past thousand years.

And so while today, researchers may be spending more time reading than ever before (Van Noorden 2014; Tenopir et al. 2015), deciding what to read and how much of it has never been more crucial (e. g., Nicholas et al. 2004, 2007; Baron et al. 2021). As Baron (2015) aptly puts it: “One of the major effects of digital screens is to shift the balance from continuous reading to reading on the prowl ... The result? The meaning of ‘reading’ increasingly becomes ‘finding information’—and often setting for the first thing that comes to hand—rather than ‘contemplating and understanding’.” Thanks to the recent boom in AI-based (writing) tools such as OpenAI’s ChatGPT, Google’s Gemini, or Anthropic’s Claude however, companies and journals now also start to offer AI-tools that can summarize and “study” scientific articles (e. g., R Discovery, Kudos’ AI Summaries, or Myreader; although automated abstraction tools were already developed much earlier, e. g., Luhn 1958; Mathis et al. 1973). If reliable, such tools should make literature research considerably more effective, but I suspect it will likely also result in scientists straying even further from long-form reading.

Ultimately, when it comes to writing, one should always ask themselves who they are writing for. In case of dissertations, it’s typically a balance between writing for yourself, the examiners, and a scientific audience of a certain expertise. When it comes to my dissertation, I would like to write for the contemporary, interested reader, who likely doesn’t have the time to read an entire work potentially comprising hundreds of pages, but who appreciates if the information they are looking for is easy to find and ideally self-contained. The cumulative style of this dissertation is my attempt at meeting this reader’s needs while honoring the standards of dissertation writing that have been established over the past centuries. With this dissertation, I try not only to make a new contribution to my field, but—in the spirit of science—also to innovate how such results may be presented.

My dissertation layout is inspired by the book *Trees, Maps, and Theorems* (2009) by Jean-luc Doumont. The book deals with the first (design) principles of clear and effective communication, and in doing so, sets an example of how they may be applied by relying on a double-page layout as a core structural concept. I find this layout to be well-suited for cumulative dissertations: If a reader is only interested in the primary information encapsulated in the papers, my layout allows them to study the papers without interruption. At the same time however, they also have the option to read up on additional information right where it's relevant thanks to the in-situ discussions. This was one of the main drivers for developing my layout, as it benefits the people that are most likely interested in my dissertation—namely those that are already familiar with my work, but that would like to look up details that are not mentioned in my papers. With my layout, they don't have to skim (or even read) through large parts of the dissertation (and don't have to be uncertain if they missed something), but can immediately see if the aspects they are interested in are further discussed in my dissertation just by going to the relevant paper section.

The illustration below shows how this double-page layout is structured. Orange lines visually connect key words or phrases from the original paper pages on the right side with the in-situ discussions on the left. While the two papers incorporated in this dissertation represent the essence of my work, there are several things—dead ends, side projects, minor results, background information, thoughts and ideas—that didn't make the cut. Most of this extra content is provided in the in-situ discussions. Sometimes longer, sometimes shorter, they address specific aspects mentioned in the papers, in the hopes that they add valuable information and make certain things clearer. As this preface already demonstrated, the wide margins to the side of the discussions are also a feature in other parts of this dissertation. They naturally arise from typographic guidelines developed to alleviate information intake while reading, which state that the text width should be around 30 times longer

Another inspiration were the Wikipedia-style page previews that pop up when hovering over hyperlinks to different Wikipedia articles. It would be really interesting to apply such an interactive feature in the context of dissertations, but the current doctorate regulations do not allow it (in particular because it's impossible to implement in the static format of a PDF and because the printed and digital versions would likely not be identical).



Admittedly, the strength of my layout primarily unfolds when reading the printed version of my dissertation, because it's easier to read double-pages on paper than on screen. Opting for this layout may therefore seem somewhat counter-intuitive given the universal demand for easily accessible and thus virtual information. Yet many if not most scientists still prefer reading on paper (as do I; e. g., Tenopir et al. 2015, 2019; Baron et al. 2017; Mizrachi et al. 2018), and may retain more information when doing so (e. g., Delgado et al. 2018; Kong et al. 2018; Clinton 2019; Stiegler-Balfour et al. 2023). I therefore designed my dissertation having analog reading in mind, but its digital version is still perfectly readable on screen (although it may involve more scrolling than usual).

than the font size (e. g., Bringhurst 2004). In this case, the main text has a (standard) font size of 10 pt and a text width of 304 pt \equiv 10.7 cm; and since the page format is DIN A4 with a page width of 21 cm, these specifications result in a wide side margin. This empty space does not have to go unused however, so here, they sometimes contain a local table of contents or figure captions, but are primarily reserved for small figures and side notes: by way of the proximity principle (which roughly states that in design, related elements should be close, e. g., Doumont 2009; Cairo 2012) they allow content that would traditionally be found in footnotes to be as close to their relevant text passages as possible—presenting ancillary information quite literally as asides. And because they are kept relatively self-contained, it also eliminates the need for footnote markers, resulting in an overall cleaner and direct design. Additionally, this division into papers, discussions, and side notes, as well as the decreasing space that each part is allocated, immediately conveys their relative importance.

In a similar spirit (as reflected by my rather long acknowledgments), I also like to give credit where credit is due. Research is a community effort, and so in the hopes that they may be useful to a reader, I tried to provide references for every unoriginal claim that I made, even, or especially so, if they are about a well-known fact (for which conversely, the original sources are sometimes curiously hard to find as they are often omitted).

Finally, just as with the overall layout and the science itself, I also cared a lot about my writing and figure design. Even though I am neither a professional writer nor a trained layout or graphic designer, as a scientist, I still see myself in both these roles. Rigorous research and novel insights are fundamental parts of science, but I believe that it should also be communicated well: quality science deserves quality communication. Science already deals with complicated issues, and so their comprehension should be as effortless as possible, now more than ever. Effortless communication not only allows to potentially reach a larger audience and keep its interest, but it also respects the underlying work and the audience's time and energy—the mental burden of unraveling a message should not be with its audience but with its author. So rather than feeling frustrated or exhausted, I would like my readers to feel refreshed or engaged. It's a Herculean task for sure, and I may not have achieved it, but I tried my best with every word that I wrote, and every figure that I crafted. I hope you will appreciate.

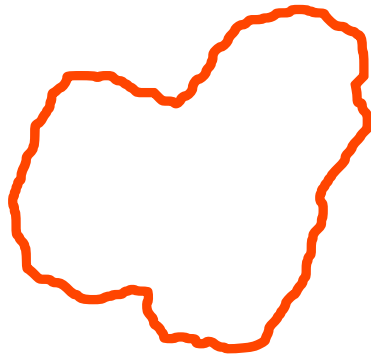
MARIUS PFEIFER

Contents

Abstract	i
Publications	iii
Acknowledgments	ix
Preface	xiii
INTRODUCTION	1
1 Comets and Rosetta	3
1.1 Comet History	4
1.2 Comet Populations	7
1.2.1 Kuiper Belt	7
1.2.2 Oort Cloud	10
1.2.3 Classifications	11
1.3 Comet Activity	14
1.3.1 Tail and Trail	14
1.3.2 Activity Paradox	17
1.3.3 Comet Formation	19
1.3.4 Particle & Gas Dynamics	21
1.4 Rosetta Mission	22
1.5 Comet 67P	26
1.5.1 Basic Properties	26
1.5.2 Seasonal Changes	29
1.5.3 Surface Material	30
1.5.4 Distributed Sources	32
1.6 This Work	34
2 Particle Tracking	37
2.1 Methodological Context	37
2.1.1 Comet Particle Tracking	38
2.1.2 Asteroid Particle Tracking	39
2.1.3 Star and Debris Tracking	40
2.1.4 SSSB Tracking	41
2.1.5 Optical Particle Tracking	41
2.1.6 Optical Tracking	42
2.1.7 Other Particle Tracking	43
2.1.8 Conclusion	43
2.2 A Brief Philosophical Aside	43

THE METHODS PAPER	47
3 Preamble	49
4 The Methods Paper	50
4.1 Introduction	51
4.2 Data	53
4.3 Tracking algorithm	57
4.4 Parameter optimization	67
4.5 Results and discussion	71
4.6 Summary and outlook	77
4.7 Appendix	81
5 Additional Thoughts	83
5.1 The Detection Threshold	83
5.2 More on Quality Control	85
5.3 Last Words on Simulations	87
THE SCIENCE PAPER	89
6 Preamble	91
7 The Science Paper	92
7.1 Introduction	93
7.2 Data selection	95
7.3 Particle tracking	95
7.4 Results and discussion	103
7.5 Summary and conclusions	123
7.6 Appendix	129
FINAL REFLECTIONS	151
8 Final Reflections	153
8.1 Methodology	153
8.2 Comet Physics	154
Bibliography	161

INTRODUCTION



COMETS AND ROSETTA

Comets are like cats: they have tails, and they do precisely what they want.

— Levy (1998). *Comets: Creators and Destroyers*.

COMETS are small Solar System bodies (SSSBs) that formed in the outer regions of our Solar System (or even beyond) and consist of a mixture of dust and various ices (mostly water and CO₂, e. g., Cochran et al. 2015; Bockelée-Morvan et al. 2017; Altwegg et al. 2019; Rubin et al. 2020; Filacchione et al. 2022). Unlike the rocky asteroids, which formed in the inner Solar System and constantly experience physical or chemical alterations (e. g. due to meteorite impacts, solar radiation, or heating; e. g., Asphaug 2009; Asphaug et al. 2015; Murdoch et al. 2015; Pieters et al. 2016), comets have remained mostly unchanged ever since they formed around 4.6 billion years ago along with the rest of our Solar System (e. g., Blum et al. 2022). They are thus regarded as the most primitive Solar System objects, which makes them highly interesting targets for scientific space missions, as they are key to understanding the origin of the Solar System itself (e. g., Bonnet 1985).

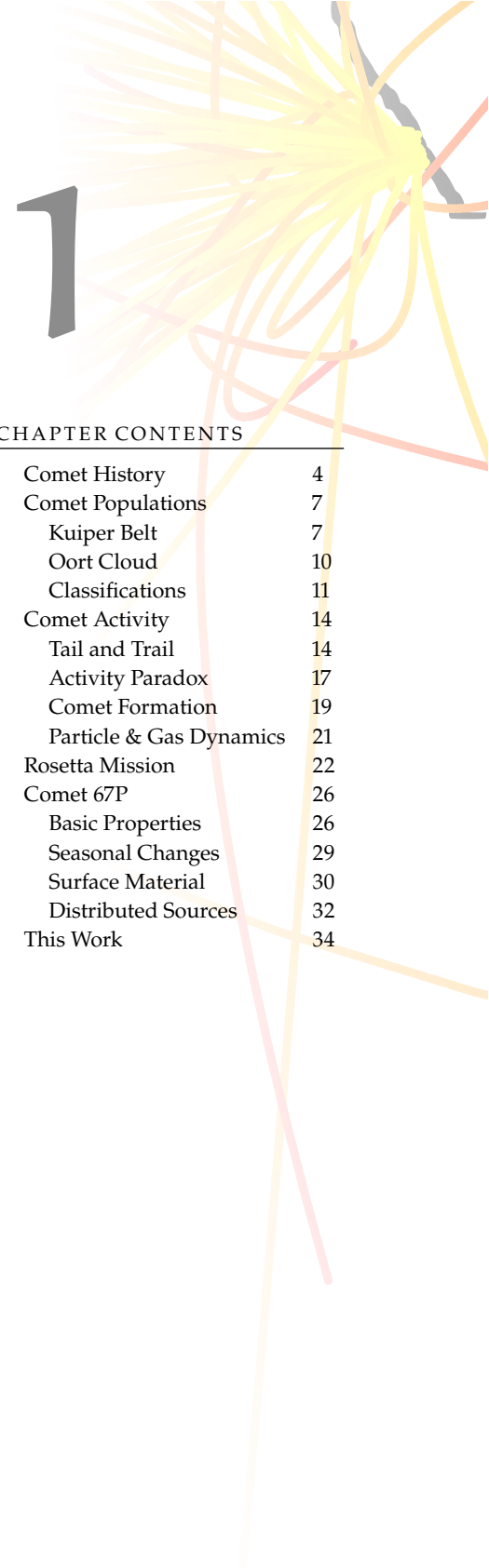
Only when the orbits of comets are changed enough that they enter the inner Solar System (e. g., due to gravitational perturbations from planets, galactic tides, or neighboring stars, Levison et al. 1997; Fouchard et al. 2017a,b) do comets become *active*: heated by solar radiation, their ices start to sublimate, creating gases that expand and remove dust from the cometary surface. This gas and dust then manifest as the characteristic cometary coma, tail, and trail (e. g., Agarwal et al. 2023).

How exactly the dust is ejected however, is not yet fully understood (e. g., Gundlach et al. 2015b; Skorov et al. 2017; Markkanen et al. 2020; Agarwal et al. 2023; Bischoff et al. 2023). Learning more about the responsible processes therefore was, and still is, a declared goal of the European Space Agency’s (ESA’s) Rosetta mission to comet 67P/Churyumov-Gerasimenko (Bonnet 1985; Glassmeier et al. 2007; Taylor et al. 2017). Thus, during Rosetta’s rendezvous-phase with comet 67P, the narrow- and wide-angle cameras (WAC and NAC) of its Optical, Spectroscopic, and Infrared Remote Imaging System (OSIRIS, Keller et al. 2007) recorded many image sequences of 67P’s near-nucleus coma to capture the dynamics of recently ejected dust particles. Studying their dynamics allows not only to indirectly probe the near-nucleus gas environment, but also to draw conclusions about their potential ejection events. I therefore developed a particle tracking algorithm specifically tailored to OSIRIS data, and used it to analyze several image sequences.

But before the methodology and results of this approach are presented and discussed in detail, I first provide a brief introduction into the history, populations, and physics of comets, the Rosetta mission, and comet 67P, followed by a motivation for developing my own tracking algorithm in the context of related algorithms.

CHAPTER CONTENTS

Comet History	4
Comet Populations	7
Kuiper Belt	7
Oort Cloud	10
Classifications	11
Comet Activity	14
Tail and Trail	14
Activity Paradox	17
Comet Formation	19
Particle & Gas Dynamics	21
Rosetta Mission	22
Comet 67P	26
Basic Properties	26
Seasonal Changes	29
Surface Material	30
Distributed Sources	32
This Work	34



1.1 COMET HISTORY

The birth of modern science is commonly attributed to the work of Galileo Galilei from the early 17th century (e.g., Barboianu 2022). And of course—because how else could it be—, one of his most important texts, *Il sagggiatore* (“The Assayer”), sprang from a controversy on comet sightings (Galilei 1623; Galilei et al. 1960).

One culture with a positive view of comets were the !Kung of the Upper Omuramba (in today’s Namibia) who “saw the comet as a guarantee of good times ahead [in] an unusually cheerful interpretation” (Sagan et al. 2011).

The original version of Aristotle’s *Meteorologica* has long been lost, but it was likely written around 340 BCE (Boyer 1959).

Parallax describes the apparent positional shift of foreground objects relative to a fixed background when they are viewed from different locations (e.g., Hirshfeld 2013).

Long before comets were of scientific interest (and in fact, long before modern science was even born), they were of significant cultural importance all around the world (e.g., Green 2004; Sagan et al. 2011). That significance was overwhelmingly negative however, as most cultures saw their appearances as bad omens. The oldest known records of comets were kept in ancient China and inscribed on animal bones and turtle shells (the so-called oracle bones), possibly as early as 1500 BCE (Zhen-Tao et al. 1995). About 1300 years later (although the time periods likely overlap, Sagan et al. 2011), the Chinese had already categorized comets according to their appearance into 29 different “classes”, which are attributed with different events and preserved in the Mawangdui Silk Texts (Gu 1978; Xi 1984, see Fig. 1.1).

Roughly around the same time, Aristotle was also pondering about the nature of comets. In his *Meteorologica*, he disputed previous theories, in particular those of Pythagoras and Hippocrates, who believed that comets were similar to planets (Aristotle 1952). Aristotle instead proposed that comets were meteorological phenomena akin to the aurora borealis or shooting stars, an idea that would be prominent in Western culture well into the early modern period (Green 2004).

But when the Great Comet of 1577 appeared, Danish astronomer Tycho Brahe showed that comets are in fact part of our Solar System (although he still believed in a geocentric system, Brahe 1588). Because the comet was visible for a long time, he and his contemporaries were able to make many precise measurements of the comet’s celestial position. Brahe then used these measurements to determine its parallax relative to background stars and found that the comet must be much further away than the moon, thus placing it with the planets.

The next important step for cometary science was taken by Johannes Kepler, who assisted Brahe shortly before his sudden death, and became his successor as the Imperial Mathematician in Prague (Caspar et al. 1993). Being a strong advocate of Copernicus’ heliocentric system (Copernicus et al. 1543), Kepler made good use of Brahe’s extensive records and discovered that all planets must move on elliptical orbits with the Sun located at one of the foci (the first of Kepler’s three laws, Kepler et al. 1609).

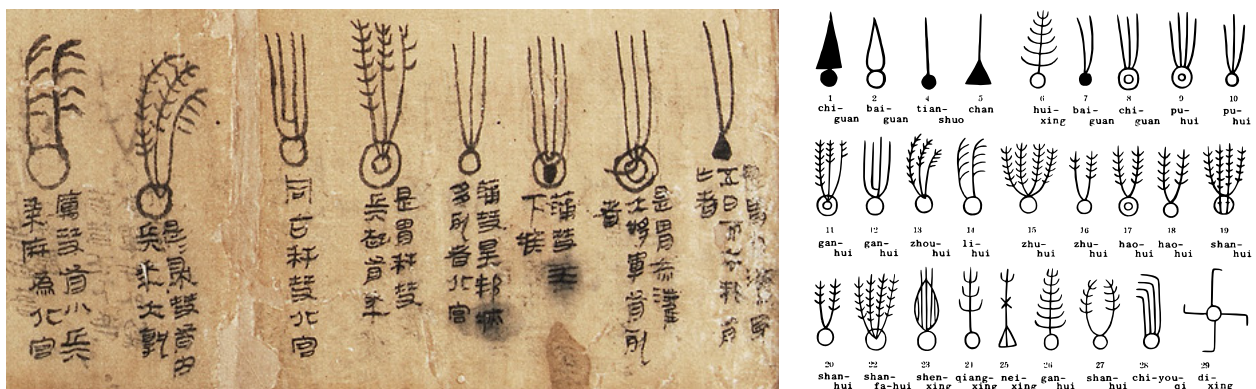


Figure 1.1: Comet classes recorded on the Mawangdui Silk Texts. Left: Image of the original silk drawings showing a sub-set of the 29 different classes (credit: Hunan Museum). Right: 27 recreated depictions of the 29 classes (Xi 1984, reprinted with permission from Elsevier).

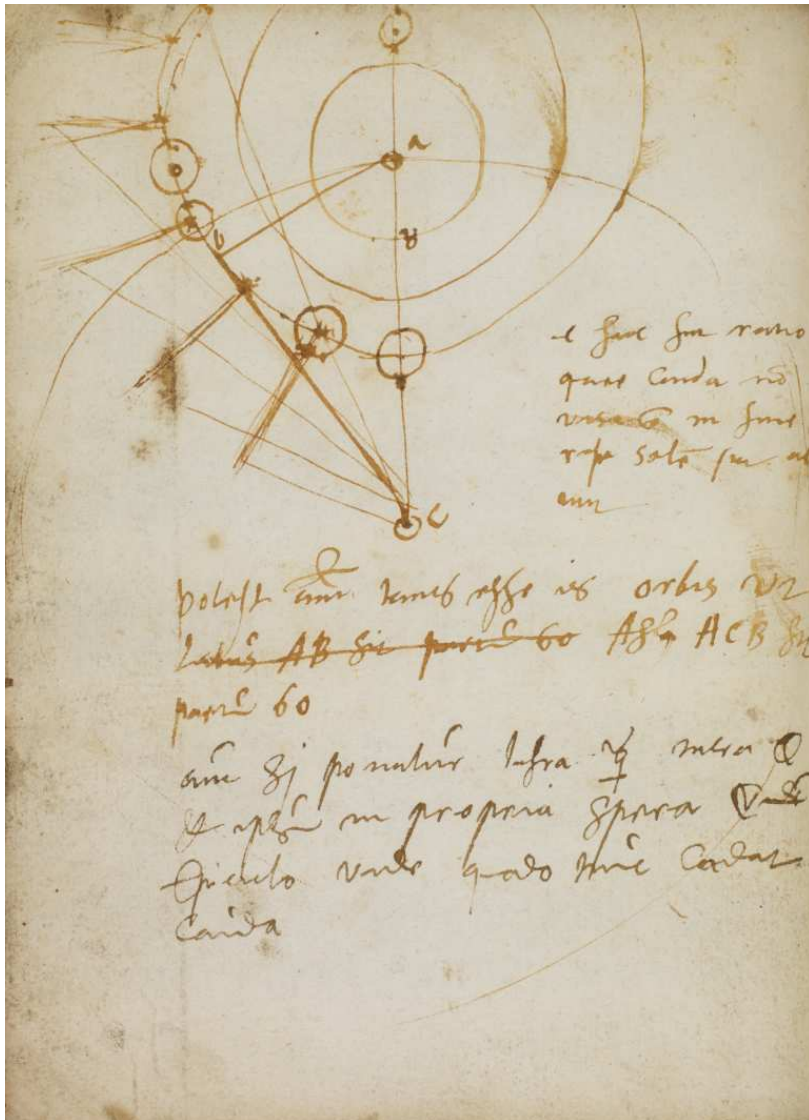


Figure 1.2: Page of Tycho Brahe's notebook showing his observations of the Great Comet of 1577 (credit: Royal Danish Library).

Yet curiously, he did not arrive at the same conclusion regarding comets, but instead believed that they were moving on straight lines (Kepler 1619a; Hellman 1975).

That comets, too, moved on elliptical orbits was finally proven by Isaac Newton in the third book of his magnum opus *Philosophiæ Naturalis Principia Mathematica* (Newton 1687). In December 1680, there was another great comet (luckily, there seemed to have been plenty of them at the time; e. g., Seargent 2008), which drew the attention of many contemporary astronomers, including John Flamsteed (the first Astronomer Royal of the British Crown) and Giovanni Domenico Cassini (the director of the Paris Observatory). They believed that it was the same comet that Brahe observed in 1577 and which later reappeared in January 1681 (Cassini 1681). Newton first dismissed this idea, as it was essentially unprecedented at the time (Sagan et al. 2011), but was later persuaded to put his novel theory of gravity to the test (Hughes 1988). Based on Flamsteed's measurements of the 1680 and 1681 apparitions, he was able to show that the apparitions were indeed of the same comet, observed before and after its perihelion passage. This made Newton the first person to determine a cometary trajectory.

Newton apparently commented that “the discussion of comets was the most difficult part of the book” (Hughes 1988), which probably says something about the feat.

“Some hint of [the idea of a returning comet] can be found in the writings of Aristotle (who firmly rejected it) and Seneca (who ... embraced the suggestion of Apollonius of Myndos that comets move as the planets do)” (Seneca 1972; Sagan et al. 2011). Other than that, it was “explicit only in the folk tradition of the Bantu-Kavirondo people of Africa” (Sagan et al. 2011).

In Paris, the return of Halley's comet was first noticed by the young Charles Messier (Wilson 1993).

Yet he did not achieve this entirely on his own, as Newton received strong support from another astronomer famous for his contributions to cometary science: Edmond Halley. Halley not only inspired and supervised Newton's work, he also paid for the printing and publication of the first *Principia* edition (Ackroyd 2006). Eighteen years later in 1705, Halley published his own seminal work, *Astronomiae cometicae synopsis* (Halley 1705). In it, he made use of Newton's method, and claimed that the comet sightings of 1456, 1531, 1607, and 1682 were all of the same comet, and predicted its return for the year 1758. The French astronomer Alexis-Claude Clairaut later refined the prediction by taking the gravitational perturbations of Jupiter and Saturn into account, and estimated its return to occur in mid-April 1759 (Clairaut 1760). The comet eventually returned 17 years after Halley's death on the 13th of March, 1759, and was named after Halley to honor his accomplishment.

Besides being the first confirmed periodic comet, 1P/Halley (which is the proper scientific designation of Halley's comet, see side note on page 11) also turned out to have been continuously observed for millennia due to its bright appearance, stable orbit, and relatively short orbital period of 74 to 79 years (Yeomans et al. 1986). Its first verified sighting was recorded by the Chinese in 240 BCE (Yeomans et al. 1986), but it most famously appeared during the Norman invasion of England in 1066 and was consequently stitched onto the Bayeux Tapestry, where it is depicted as part of the events of the Battle of Hastings (Rud 1992, see Fig. 1.3). This depiction was likely not only the first depiction of 1P/Halley, but also the first depiction of any comet in the Western world (Green 2004). (Yet Section 1.3.1 shows that the cultural and scientific importance of Halley's comet didn't stop there.)



Figure 1.3: Halley's comet depicted on the Bayeux Tapestry, which shows the events of the Battle of Hastings in 1066 (credit: Detail of the Bayeux Tapestry - 11th Century. City of Bayeux).

1.2 COMET POPULATIONS

Once the orbital mechanics of comets were mostly figured out, scientific interest shifted toward their origin, nature, and formation. Based on their typically highly eccentric orbits, comets were found to mainly originate from two reservoirs in the outer Solar System (e. g., Weissman et al. 2020): the Kuiper Belt region and the Oort Cloud (Kuiper 1951; Oort 1950, see Fig. 1.4).

1.2.1 KUIPER BELT

The Kuiper Belt region has an average temperature of around 40 K and is primarily divided into five dynamical groups: the hot and cold classical Kuiper Belt objects (KBOs), resonant KBOs, scattered disc objects (SDOs), and detached objects (see Fig. 1.5; although how they are separated depends on the classification system, e. g., Elliot et al. 2005; Gladman et al. 2008, 2021; Petit et al. 2011). While the former three groups reside in a region that roughly stretches from 30 AU (the orbit of Neptune) to 50 AU or even 100 AU (depending on the definition, e. g., Fernández 1980; Duncan et al. 1988; Weissman et al. 2020), the latter two reside in a region that roughly stretches from 30 to 10^3 AU (Duncan et al. 1997; Levison et al. 1997). Generally, objects from these regions are collectively referred to as trans-Neptunian objects (TNOs), which include not just small bodies, but also dwarf planets such as Pluto.

Classical Kuiper Belt objects (CKBOs) move on stable, non-resonant, almost circular orbits that are mostly confined to the ecliptic (e. g., Morbidelli et al. 2007; Gladman et al. 2008; Thomas 2020). The division into

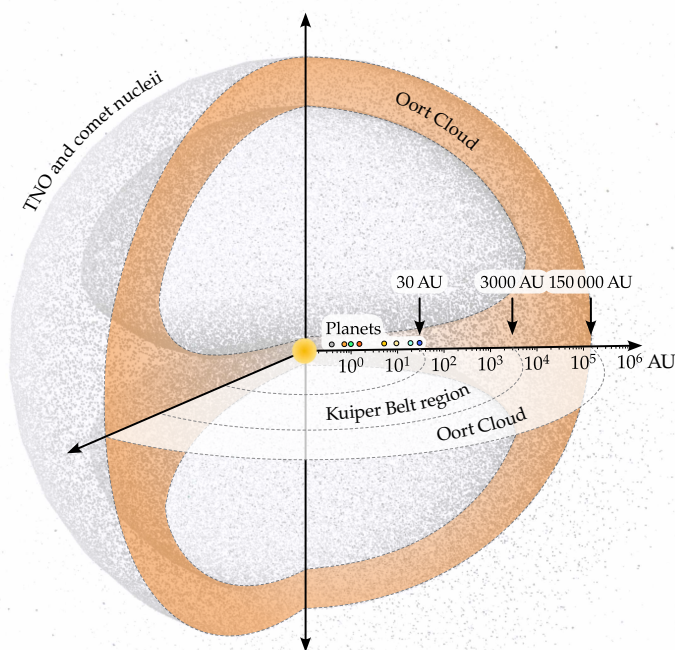


Figure 1.4: Artistic representation of the Solar System indicating the approximate size and shape of the Kuiper Belt region and Oort Cloud.

It's astounding how many notable scientists had worked on the orbital mechanics of comets, for example (Szebehely 1967; Marsden 1974; Wilson 1993; Kronk 1999; Musielak et al. 2014; Valtonen et al. 2016): Euler (1743) was the first to develop a method to determine the orbit of a comet from three observations; Lagrange (1785) developed his price-winning “variation-of-parameters” method (which is used to solve differential equations) to determine (not only, but also) the orbit of comets; Laplace (1805) dealt with the perturbations of comets based on Lagrange’s method; Legendre (1805) developed his least-squares method to determine the orbits of comets (also partially attributed to Gauss); Gauss (1809) developed his theory of motion for celestial bodies, including comets; Jacobi (1836) discovered the only conserved quantity for the circular restricted three-body problem; Bessel (1836a) was the first to suggest that non-gravitational forces may affect cometary orbits; Cauchy (1846) developed yet another method to determine cometary orbits; and Poincaré (1890) discovered chaos theory trying to solve the circular restricted three-body problem. Overall, comets seemed to have been tremendously important for the advancement of science and mathematics as a whole.

Although the term Kuiper belt is commonly used, its naming is actually fairly controversial (Green 1999). In Kuiper’s relevant work (Kuiper 1951), he in fact disputes the belt’s existence, while others before him had already suggested it (Leonard 1930; Edgeworth 1943, 1949). Responsible for this misattribution is likely the much-cited paper by Fernández (1980), who overlooked the work by Edgeworth, and later Duncan et al. (1987). Many other authors who wrote on this topic at the time simply followed suit (Green 1999). Additional scientists with a claim for the naming may for example also be Cameron or Whipple (Cameron 1962; Whipple 1964a,b; Whipple 1972b).

At least in case of the Oort cloud, there is no controversy regarding its naming, but it is worth mentioning that an outer reservoir of comets was already suggested by Leuschner (1907) and Öpik (1932).

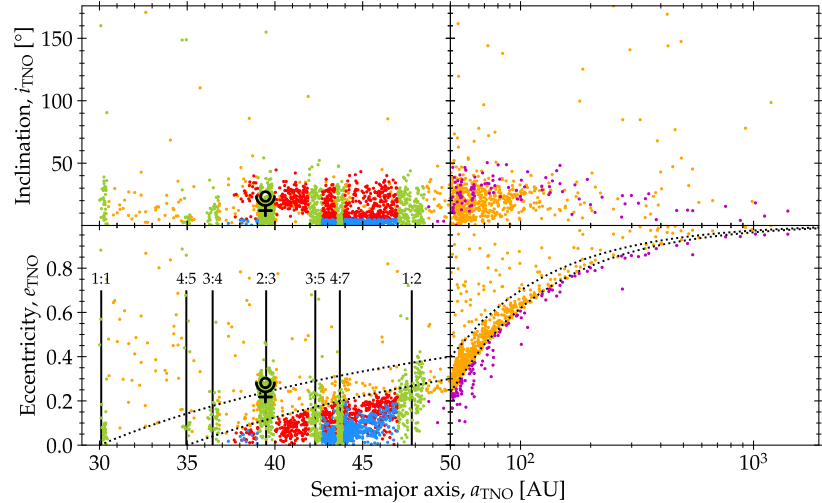


Figure 1.5: Inclinations, i_{TNO} , (top) and eccentricities, e_{TNO} , (bottom) of the different TNO populations as a function of their semi-major axes, a_{TNO} (inspired by Fig. 2 of Morbidelli et al. 2007). The data was retrieved from the MPC’s list of TNOs, SDOs, and Centaurs and was filtered for objects with $a_{\text{TNO}} > 30$ AU, that have been observed for at least three years (2966 objects in total as of April 8, 2024). Hot CKBOs are shown in red, cold CKBOs in blue, SDOs in orange, resonant populations in green, and detached objects in violet. The location of Pluto is marked by its symbol ($\♇$). The vertical lines and integer ratios mark the locations of Neptune’s mean-motion resonances up to 50 AU. For simplicity, objects within certain approximate a_{TNO} ranges around these locations were assumed to be in resonance (data from Robutel et al. 2001), although in reality, their orbital evolutions must be determined numerically to confirm their resonance (e. g., Morbidelli et al. 1995; Gladman et al. 2008). To better highlight the different features of the Kuiper Belt region, the plots are split at 50 AU, with a linear x -axis scale on the left, and a logarithmic x -axis scale on the right. Notably, in the area between the 4:7 and 1:2 resonances, the eccentricities of hot and cold CKBOs are significantly overlapping, which cannot be properly shown in this plot due to the large number of objects. The two dotted curves in the bottom plots roughly indicate the parameter space that most SDOs reside in, defined by a top perihelion distance limit of $q_{\text{TNO}} = 30$ AU, and bottom limits of $q_{\text{TNO}} = 35$ AU (left) and $q_{\text{TNO}} = 38$ AU (right).

hot and cold CKBOs however has nothing to do with their temperatures, but is instead a reference to gas kinetic theory and relates to the objects’ encounter velocities within each group, which strongly depend on their (relative) ecliptic inclinations (Morbidelli et al. 2007). Accordingly, hot and cold CKBOs are primarily separated based on their inclination, since objects with highly inclined orbits (hot CKBOs) can have much higher encounter velocities than those that move in essentially the same orbital plane (cold CKBOs). The dividing line between hot and cold CKBOs typically sits (somewhat arbitrarily) at an inclination of 4 to 5° (e. g., Brown 2001; Levison et al. 2003; Delsanti et al. 2006; Gladman et al. 2008).

In the context of SSSBs, the term “color” generally refers to their spectral appearance in the visible wavelength range, i. e., the relative spectral slope between received and reflected sunlight, where objects that reflect more in the longer than the shorter wavelengths are said to be “red”, and “blue” in the opposite case, (e. g., Morbidelli et al. 2007).

But apart from their dynamics, hot and cold CKBOs also differ in physical properties like their size and “color”, with hot CKBOs tending to be larger and “bluer” and cold CKBOs smaller and “redder” (e. g., Levison et al. 2001b; Trujillo et al. 2002; Morbidelli et al. 2007; Petit et al. 2023). Because of the color difference, Peixinho et al. (2008) also suggested to use an inclination of 12° as the boundary between hot and cold CKBOs, as it is where they found the spectral appearance to change. The different physical properties additionally indicate different formation processes of CKBOs: despite some discrepancies (e. g., Dawson et al. 2012; Morbidelli et al. 2014; Gomes 2021), cold CKBOs likely formed in the region where they are still located today (e. g., Tegler et al. 2003; Batygin et al. 2011; Wolff et al. 2012; Schwamb et al. 2019; Kavelaars et al. 2021; Petit et al. 2023), while hot CKBOs likely formed closer to the Sun and were later

dispersed into the Kuiper Belt region during the late planetary migration (e. g., Nesvorný 2018; Schwamb et al. 2019). Many cold CKBOs are also made up of loosely bound binary pairs (Noll et al. 2008), which should have been destroyed if collisions among KBOs were common (Petit et al. 2004b). In combination with the crater density well below saturation observed on the TNOs Pluto, Charon, and Arrokoth (Singer et al. 2019; Spencer et al. 2020), this strongly supports the primitiveness of CKBOs.

Unlike CKBOs, SDOs move on unstable and typically more eccentric and inclined orbits. Due to interactions with Neptune, they experience significant changes in their semi-major axes on astronomically short timescales (Gladman et al. 2021; e. g. 10 Myr according to the classification scheme of Gladman et al. 2008). Consequently, even though their name may suggest otherwise, scattered disk objects are still very much in the process of scattering away from their current orbits (e. g., Gladman et al. 2008, 2021). Today's SDOs may in fact be the diminishing remnants ($\sim 1\%$) of a once vast primordial scattering population that formed when the giant planets dispersed the residual planetesimal disk (e. g., Duncan et al. 1987, 1997; Gladman 2005; Gladman et al. 2021). But since their perihelion distances do not change much after an encounter with Neptune, SDOs perform somewhat of a random walk within the parameter space displayed in Figure 1.5 (Morbidelli et al. 2007). Eventually however, they leave the scattered disk and for example enter the inner Solar System where they replenish and interchange with a group of objects called Centaurs, which orbit between the orbits of Neptune and Jupiter (e. g., Thomas 2020). Due to gravitational perturbations of the giant planets, centaurs also have typically short dynamical lifetimes (on the order of Myr) and are seen as a sort of “gateway” population of objects that transit between the outer and inner Solar System (e. g., Levison et al. 1997; Morbidelli 2008; Thomas 2020; Wood et al. 2022).

Resonant populations on the other hand move on orbits that are stable over timescales of the age of the Solar System (e. g., Morbidelli et al. 1995; Duncan et al. 1997; Robutel et al. 2001; Gladman et al. 2008, 2021; although these populations are slowly decaying due to chaotic diffusion, Morbidelli 1997; Tiscareno et al. 2009). These orbits derive their stability from having orbital periods that are (small) whole-number multiples of Neptune's orbital period. Objects in such a configuration are said to be in mean-motion resonance with Neptune (there are also so-called secular resonances that relate to the objects' precession rates and that influence the shape of the Kuiper Belt region as well, e. g., Morbidelli 2008). In case of the 2:3 mean-motion resonance for example (see Fig. 1.5, following the notation of, e. g., Morbidelli 2008), this means that during the time Neptune orbits around the Sun thrice, a resonant object would move around the Sun twice. Given the right geometrical configuration (e. g., in the form of a sufficient temporal shift between the respective perihelion passages), a resonant object can thus avoid any close encounters with Neptune that would otherwise disrupt its orbit even if it were to periodically cross Neptune's trajectory (e. g., Murray et al. 1999; Morbidelli et al. 2007). To determine if any particular TNO moves in resonance with Neptune however, their orbits need to be numerically calculated (e. g., Robutel et al. 2001; Gladman et al. 2008). Similar to the scattered disk, the prominent resonant populations likely also formed as a result of

the giant planet migration (e. g., Luu et al. 2002; Morbidelli et al. 2007; Malhotra 2019; Kaib et al. 2024).

Finally, the detached objects (also called extreme TNOs) have orbital parameters similar to those of SDOs, which is why they are also seen as an extension of the scattered disk. Yet because they have larger perihelion distances than SDOs, they are essentially dynamically detached from Neptune’s influence and thus move on orbits that are much more stable (e. g., Emel’yanenko et al. 2003; Delsanti et al. 2006; Morbidelli et al. 2007; Gladman et al. 2008, 2021). So far, only relatively few such objects have been discovered, but not just because they are difficult to detect due to their extreme distances; they also reside in the transition region between the Kuiper Belt and the inner Oort Cloud, which seems to be sparsely populated (also known as the “Kuiper Cliff”, e. g., Chiang et al. 1999; Trujillo et al. 2014; Sheppard et al. 2019; Gladman et al. 2021; de la Fuente Marcos et al. 2024).

1.2.2 OORT CLOUD

Accordingly, the Oort Cloud is located even more remotely than the Kuiper Belt region. It has an average temperature of around 10 K, and stretches from a more disk-like, inner structure beginning around $3 \cdot 10^3$ AU to an almost spherical, outer structure ending around $150 \cdot 10^3$ AU (e. g., Levison et al. 2001a; Weissman et al. 2020). Its outer limit is defined by the tidal truncation radius of the Solar System, at which point the gravity of other stars and massive objects can strip away comets from the cloud (e. g., Levison et al. 2007). The cloud was postulated by Oort (1950) to solve a conundrum (see, e. g., also Levison et al. 1997, 2007; Jewitt 2002): For one, observed comets (i. e., those that entered the inner Solar System and became active) move on orbits that are unstable over the age of the Solar System: due to gravitational perturbations from the planets, they should have long been ejected from the Solar System, become “sun-grazers” (i. e., comets with perihelion distances $q_c < 0.01$ AU, Bailey et al. 1992; Levison et al. 1994) and evaporated, or collided with the Sun, the planets, or other massive Solar System bodies. Second, observable comets should also have long since lost all their volatiles due to sublimation, rendering them inactive or even causing them to disintegrate. Levison et al. (1997) estimated the average dynamical and physical lifetimes of such objects to be 4.5×10^7 and 1.2×10^4 years, respectively. Comets are therefore inherently short-lived and cannot have formed on the orbits on which they are observed, but must instead originate from somewhere else: the Oort Cloud.

In fact, even though Oort (1950) only had reliable data from 19 comets, he already noticed that the orbital binding energy of most observed comets is much smaller (around $10 \times$) than the average planetary “kick” (i. e., kinetic energy transfer) that comets should receive when they pass through the planetary system (see Fig. 1.6). These comets (also known as “Oort Spike comets”, e. g., Królikowska et al. 2020) therefore must be dynamically “new”, that is, when they were observed, they must have entered the planetary system for the first time. To do so, Oort Cloud comets must have perihelion distances $q_c > 15$ AU prior to their entry, as they may otherwise be kicked out of the spike by the giant planets. Consequently, they only enter the planetary system if galactic tides or

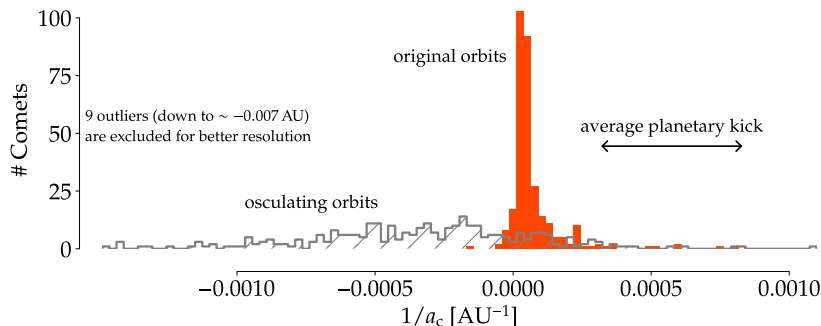


Figure 1.6: Distribution of the inverse semi-major axis, a_c , of the original and osculating orbits of 312 LPCs (data as of April 27, 2024, from the “Catalogue of Cometary Orbits and their Dynamical Evolution”, Królikowska et al. 2020). Also indicated is the average planetary kick ($\sim 0.0005/\text{AU}$) according to van Woerkom (1948) and Oort (1950). The inverse semi-major axis is proportional to the orbital binding energy of comets, $-GM_\odot/2/a_c$, where G is the gravitational constant and M_\odot the solar mass (e. g., Rimrott 1989). Although negative values imply hyperbolic orbits (due to eccentricities $e_c > 1$, as $a_c = q_c/(1 - e_c)$, where q_c is the comet’s perihelion distance, e. g., Thomas 2020), in case of the original orbits, the values instead resulted from inaccurate measurements and computations (e. g., Levison et al. 2007). The difference between the two distributions clearly shows how strongly the planets can affect cometary orbits once the comets enter the planetary system.

neighboring stars disturb their orbits enough to change their perihelion distances by at least ~ 10 AU within one orbit (e. g., Levison et al. 2007; Fouchard et al. 2017a,b).

1.2.3 CLASSIFICATIONS

Once discovered (to be active), comets are traditionally classified based on their orbital period and separated into two groups: short-period comets (SPCs), which have orbital periods, T_c , less than 200 years, and long-period comets (LPCs), which have orbital periods larger than 200 years (e. g., Weissman et al. 2020). SPCs are then further divided into Jupiter-family comets (JFCs), which have $T_c < 20$ yr and are considered to mostly stem from the scattered disc (e. g., Duncan et al. 2004), and Halley-type comets (HTCs), which have $T_c > 20$ yr and are considered to mostly stem from the Oort Cloud (e. g., Thomas 2020). This additional distinction is based on the observation that comets with aphelion distances $\lesssim 10$ AU are mostly concentrated close to the orbit of Jupiter and the ecliptic (see Fig. 1.7), while comets with aphelion distances $\gtrsim 10$ AU have much more dispersed inclinations, or even move on retrograde orbits (including 1P/Halley, Thomas 2020).

Yet the original distinction into these classes is not rooted in physics but was instead driven by practical reasons, as orbital measurements have only been reliable for about 200 years (Levison 1996). The classes are additionally based on the assumption that comets move on Keplerian orbits, that is, that their semi-major axis, a_c , is related to their orbital period via Kepler’s third law (Kepler 1619b):

$$\frac{a_c^3}{T_c^2} = G \frac{M_\odot + m_c}{4\pi^2}, \quad (1.1)$$

where G is the gravitational constant, M_\odot the solar mass, and m_c the mass of the comet. Yet Keplerian orbits are only an approximation; in reality, cometary orbits are much more complex. As already mentioned

“Original” orbits refer to the state of current apparition orbits when the comets were still far outside (the influence of) the planetary system (e. g., at $r_{h,c} = 250$ AU, Królikowska et al. 2020) and effectively orbited the Solar System’s barycenter (e. g., Bailey et al. 1990; Wiegert et al. 1999). Thraen (1894) was the first to accurately calculate such an orbit (see also Fabry 1893; Fayet 1906; Strömgren 1914). Osculating orbits on the other hand reflect the current state of cometary orbits, which is typically around the comets’ perihelion passages (e. g., Królikowska et al. 2020; Thomas 2020). Because the cometary orbits are constantly perturbed by the planets during this phase, osculating orbits only represent “snapshots” of specific orbital states.

The current (and recently updated) designation system of comets is also based on the distinction between SPCs and LPCs (Marsden et al. 1994; Williams 2017). It is overseen by the Working Group on Small Body Nomenclature of the International Astronomical Union and enacted by the Minor Planet Center, which documents positional data and approves new discoveries of SSSBs. According to their system, SPCs receive a “P/” as a prefix, LPCs a “C/”, comets that disappeared a “D/”, interstellar comets an “I/”, comets that turned out to be asteroids or minor planets an “A/”, and comets whose orbit could not be reasonably established an “X/”. Following the prefix, the designation consists of the year of discovery, an upper-case letter that indicates the half-month of discovery (e. g., “A” for the first half of January and “B” for its second half, continuing in alphabetical order excluding “I” and “Z”), and a sequential number representing the order of discovery within the respective half-month. Once sufficient observations were made to reliably determine the trajectory of a periodic comet, the letters are additionally preceded by a sequential number, and the comet receives a proper name after its discoverer(s) that follows the prefix (there are however many ideosyncrasies and complications regarding the designation and naming of comets, Rickman 2017).

The circular restricted three-body problem describes a case where two of the three bodies move on circular orbits around their barycenter while the third body has a negligible mass (e. g., Kresák 1972; Murray et al. 1999).

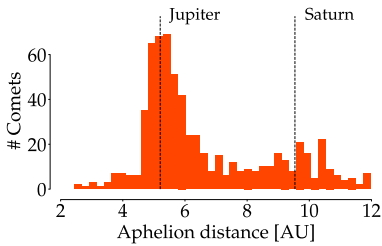


Figure 1.7: Distribution of aphelion distances, Q_c , of 1334 periodic comets with $Q_c < 12$ AU and reasonably well-determined orbits (error in $Q_c < 10\%$; data as of April 27, 2024, from the Jet Propulsion Laboratory). The orbits of Jupiter and Saturn are also indicated for reference.

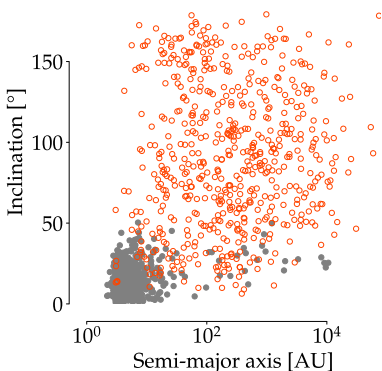


Figure 1.8: Inclination versus semi-major axis for 743 ecliptic (filled, gray circles) and 591 nearly-isotropic (open, orange circles) comets with reasonably well-determined orbits (error in $a_c < 10\%$; data as of April 27, 2024, from the Jet Propulsion Laboratory).

several times, cometary orbits can be significantly perturbed, in particular by the gravitational interaction with planets in the Solar System. But in a gravitational system with more than two bodies, their orbits cannot be described analytically and instead must be determined numerically, which requires good approximations and is a difficult problem to solve (which is also why so many different methods have been developed to calculate cometary orbits, e. g., Musielak et al. 2014). Active comets are additionally affected by non-gravitational forces due to their constant mass loss and the associated rocket forces (e. g., Whipple 1950; Marsden et al. 1973; Micheli et al. 2018; Kramer et al. 2019a; Attree et al. 2019, 2023, 2024b).

Thus, because the distinction into SPCs and LPCs was essentially arbitrary, and to address the perturbations caused especially by the large planets of the Solar System, Levison (1996) proposed to use the so-called Tisserand parameter to distinguish between the different comet populations (building on Kresák 1972; Carusi et al. 1987a). The Tisserand parameter is derived from Tisserand’s relation (Tisserand 1896) and approximates the Jacobi integral (Jacobi 1836), which is a property that is conserved in the circular restricted three-body problem (see, e. g., also Murray et al. 1999). During a real encounter between a small body and a planet, the Tisserand parameter remains roughly constant (with an error of a few percent, Kresák 1972; Murray et al. 1999). Since Jupiter is the most massive planet in the Solar System and is likely mainly responsible for “injecting” new comets into the inner Solar System, the Tisserand parameter is usually determined with respect to Jupiter via

$$T_J = \frac{a_J}{a_c} + 2\sqrt{\frac{a_c}{a_J}(1 - e_c^2)} \cos i_c, \quad (1.2)$$

where a_J is Jupiter’s semi-major axis, and e_c and i_c are the comet’s eccentricity and inclination, respectively. The relative velocity, $v_{J, \text{rel}}$, between Jupiter and a comet in a close encounter can then be expressed in terms of T_J via (Kresák 1954)

$$v_{J, \text{rel}} = \sqrt{3 - T_J}. \quad (1.3)$$

This means that (in the circular restricted case) comets with $T_J > 3$ cannot cross Jupiter’s orbit, and must therefore stay either entirely within or outside its orbit. Levison (1996) therefore divided comets with $T_J > 3$ into Encke-type ($a_c < a_J$, named after its first member comet 2P/Encke, e. g., Encke 1819) and centaurs ($a_c > a_J$, also known as Chiron-type comets, named after its first member 95P/Chiron, Kowal et al. 1979). Together with the JFCs, which Levison (1996) defined as having $2 < T_J < 3$ (meaning they are allowed to cross Jupiter’s orbit), these groups make up the class of ecliptic comets. Ecliptic comets have $T_J > 2$, and move, as the name suggests generally close to the ecliptic. Conversely, comets with $T_J < 2$ can move on arbitrarily inclined (or even retrograde) orbits and are thus called nearly-isotropic comets (see Fig. 1.8). This group is then further divided into dynamically new comets that have $a_c > 10^4$ AU, and returning comets that have $a_c < 10^4$ AU (see also Oort et al. 1951). Finally, because it was found that many returning comets with $a_c < 40$ AU were temporarily trapped in mean-motion resonances with one of the giant planets (e. g., Carusi et al. 1987a,b; Levison et al. 2014), returning comets are split once

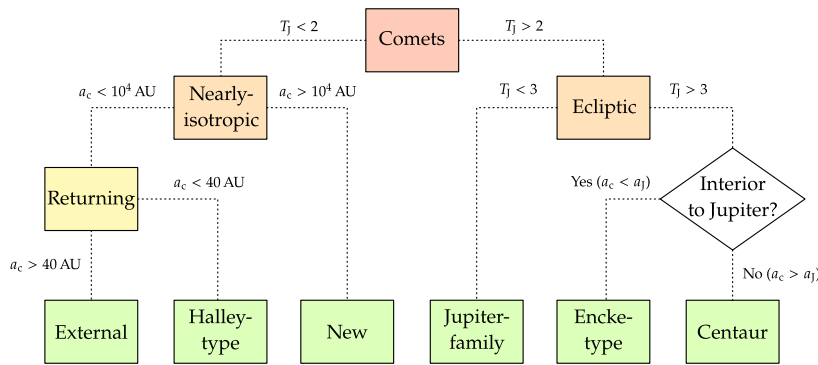


Figure 1.9: The current comet classification scheme according to Levison (1996, diagram also partly based on Fig. 1.4 of Thomas 2020).

more into Halley-type ($a_c < 40$ AU) and external ($a_c > 40$ AU) comets, although it's still unclear where exactly the boundary between these objects should lie (e. g., Levison 1996; Thomas 2020, 40 AU e. g. marks the outer edge of Neptune's 2:3 resonance, see Fig. 1.5). Figure 1.9 shows Levison's classification scheme in its entirety.

This classification scheme is still generally used today, although some minor changes have been proposed since its introduction. Most notably, Gladman et al. (2008) suggested to use $T_j = 3.05$ as the dividing line between JFCs and centaurs, since Jupiter moves on an orbit that is sufficiently elliptic to allow comets with T_j slightly larger than or oscillating around 3 to cross its orbit (see also Duncan et al. 2004). But because this would still classify some highly inclined TNOs as JFCs despite the TNO's large heliocentric distances, Gladman et al. (2008) argued that JFCs should additionally have perihelion distances $q_c < 7.35$ AU (halfway between Jupiter and Saturn) to better separate them from centaurs. Objects with T_j slightly larger than or oscillating around 3 are also interesting because they may pass through Jupiter's Roche limit where they would be torn apart by its tidal forces and may even impact Jupiter or one of its moons (Melosh et al. 1993; Zahnle et al. 1994). Such an event was famously observed in case of comet D/Shoemaker-Levy 9 (see Fig. 1.10).

Next, there is the group of the so-called active asteroids. Active asteroids are highly intriguing objects, since they blur the line between (traditionally active) comets and (traditionally inert) asteroids (e. g., Hsieh 2015, 2017; Jewitt et al. 2022). They occupy the inner Solar System on asteroid-like orbits, but show comet-like activity despite their continuous proximity to the Sun (e. g., Jewitt 2012; Jewitt et al. 2015). The first of their kind, comet 133P/Elst-Pizarro, was discovered by Elst et al. (1996) and subsequently observed to display recurring activity during its following perihelion passages (e. g., Hsieh et al. 2004, 2010; Jewitt et al. 2014). It therefore belongs to an important sub-group of active asteroids, whose periodic activity is best explained by water-ice sublimation: the so-called Main-Belt comets (MBCs, Hsieh et al. 2006; see e. g. also Kim et al. 2022; Mastropietro et al. 2024, for recent analyses). Although water-ice can generally not survive for long when exposed on asteroid surfaces, thermal models show that it can remain frozen for billions of years when located within the asteroid interiors, where the ice is protected from the continuous solar irradiation and the associated heating by an insulating crust. This "buried snow-line" may even only lie a few meters below the surface (Fanale et al. 1989; Schorghofer 2008; Prialnik et al. 2009; Schorghofer 2016; Snodgrass et al. 2017; see also Lebofsky et al. 1981), which would

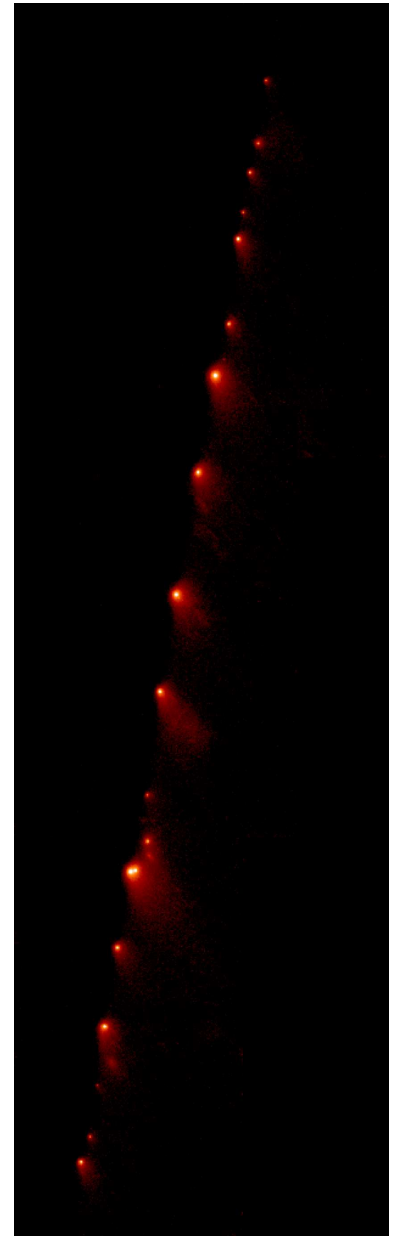


Figure 1.10: 21 fragments of comet D/Shoemaker-Levy 9 as observed by Hubble on May 17, 1994, after it was disrupted by Jupiter's tidal forces in 1992. The fragments span a distance roughly three times that between Earth and Moon and later collided with Jupiter (credit: NASA/ESA/H. Weaver and E. Smith, STScI).

allow for meteorite impacts to effectively excavate the ice and trigger sublimation-driven activity (e. g., Hsieh et al. 2004; Haghhighipour et al. 2016).

In cases of active asteroids where sublimation-driven activity is unlikely, Jewitt et al. (2015) propose a number of alternative causes, including rotational mass loss, meteorite impacts (by themselves), thermal disintegration, radiation pressure sweeping, and electrostatic “gardening”. The recent space mission OSIRIS-REx to near-Earth asteroid (101995) Bennu (e. g., Hergenrother et al. 2020, and references therein), for example, also found Bennu to be surprisingly active (albeit only very little). In this case, either micro-meteorite impacts (Bottke et al. 2020) or thermal fatigue (Molaro et al. 2020) may be responsible. Similarly, the equally recent space mission Hayabusa2 to near-Earth asteroid (162173) Ryugu may have also found evidence of slight activity on its surface (Watanabe et al. 2019).

Conversely, there are also inactive SSSBs that have been found to move on comet-like orbits: Damocloids (named after its first member 5335 Damocles, Asher et al. 1994) move on HTC-like orbits, while another group of inactive SSSBs move on JFC-like orbits. These objects are believed to be the nuclei of inactive, dormant comets (e. g., Hartmann et al. 1987; Jewitt 2005; Gundlach et al. 2016). At the other end of the activity spectrum, some comets have recently been observed to be active at heliocentric distances beyond 20 AU (e. g., Jewitt et al. 2017; Meech et al. 2017a; Hui et al. 2019; Farnham et al. 2021). Jewitt et al. (2021) therefore argue that cometary activity already starts at Kuiper Belt distances (see also Gkotsinas et al. 2022).

Finally, 1I/‘Oumuamua and 2I/Borisov make up the latest group SSSBs: they are the first confirmed interstellar objects that visited our Solar System (e. g., Meech et al. 2017b; Drahus et al. 2018; Jewitt et al. 2019b; Siraj et al. 2020; Borisov et al. 2021). This makes them incredibly interesting targets for science missions as they may, for example, be key in understanding planet formation (e. g., Hibberd et al. 2021; Hsieh et al. 2021; Opatom et al. 2021; Hein et al. 2022; Moro-Martín et al. 2022).



Figure 1.11: Simple schematic illustrating the orientation of a comet’s ion (blue) and dust (gray) tail. Since the tails always point away from the Sun, they precede the nucleus post-perihelion (schematic based on figures from Faure et al. 2007; Freedman et al. 2007).

1.3 COMET ACTIVITY

1.3.1 TAIL AND TRAIL

Observed from a distance, the most striking features of an active comet are certainly its ion and dust tails, a fact that also explains where comets got their name: the ancient Greeks called them *astēr komētēs* meaning “long-haired star” (e. g., Whipple 1974). The dust tails can reach lengths of up to $\sim 10^7$ km, and once the dust particles are decoupled from the gas, they move on independent orbits that are primarily affected by the solar gravity,

$$F_{G, \odot} = m_p \frac{GM_{\odot}}{r_h^2}, \quad (1.4)$$



Figure 1.12: Different dust tail features. The left and center images (reprinted from Jones et al. 2017) show Comet C/1975 V1 (West) observed on different dates, demonstrating both synchrones (credit: Observatoire de Haute-Provence) and striae (credit: P. Stättmayer/ESO). The right image shows comet C/1956 R1 (Arend-Roland) and its sunward spike (credit: Lick Observatory, UC Regents).

and solar radiation pressure (a concept first suggested by Kepler 1619a),

$$F_R = \sigma_p \frac{L_\odot Q_R}{4\pi c r_h^2}, \quad (1.5)$$

which is a force generated by the momentum transfer from incident photons to the dust particles, where m_p is the particle mass, σ_p the particle cross-section, r_h the heliocentric distance, L_\odot the solar luminosity, c the speed of light, and Q_{rad} the radiation pressure coefficient averaged over the solar spectrum (e. g., Burns et al. 1979; Brandt 2014; Beth et al. 2022; Agarwal et al. 2023). Both forces are proportional to $1/r_h^2$, but while the solar gravity is pulling the particles inwards, the solar radiation pressure is pushing them outwards, which effectively results in a reduced solar gravity

$$F_{\text{net}} = F_R - F_{G,\odot} = (1 - \beta)F_{G,\odot}, \quad \text{with} \quad (1.6)$$

$$\beta := \frac{F_R}{F_{G,\odot}} = \frac{3L_\odot}{16\pi GM_\odot c} \frac{Q_R}{\rho_p r} = C_\beta \frac{Q_R}{\rho_p r}, \quad (1.7)$$

where r is the particle radius and $C_\beta = 5.77 \times 10^{-4} \text{ kg/m}^2$. Accordingly, small particles experience only little solar gravity and are effectively pushed away from the nucleus in the anti-solar direction where they form the dust tail (see Fig. 1.11), whose curvature increases with increasing β (Brandt 2014). Occasionally, the dust tail can also show so-called synchrones and striae (see Fig. 1.12). Synchrones are linear features that point toward the nucleus and are likely generated by the simultaneous release of differently sized dust particles, whereas striae are parallel features that only seem to form post-perihelion and may be caused by solar wind interaction and particle fragmentation, but are so far unexplained (e. g., Jones et al. 2017; Price et al. 2019).

Larger particles on the other hand are only weakly affected by the solar radiation pressure and remain relatively close to the nucleus and its orbital plane. If viewed from inside the comet's orbital plane, due to projection effects, these particles can appear as so-called sunward spikes (generated from particles trailing in the orbital plane, e. g., Boehnhardt 2003, see Fig. 1.12) or necklines (generated from particles emitted half an orbit before observation with non-zero velocities perpendicular to the



Figure 1.13: Comet 67P's dust trail (vertical feature) and neckline (feature angled to the lower left), as observed on March 8, 2016 (credit: Subaru Telescope, National Astronomical Observatory of Japan, NAOJ).

comet's orbital plane, e. g., Kimura et al. 1977, see Fig. 1.12). Eventually however, they spread out over the cometary orbits to form the cometary trails, that are also responsible for meteor showers whenever Earth passes through one of them (e. g., Sykes et al. 1992a; Brandt 2014; Ye et al. 2022; Agarwal et al. 2023).

Like the dust tail, the ion tail is also strongly influenced by the solar radiation. But rather than accelerating the ions away from the Sun, the solar radiation instead ionizes the gas molecules in the first place and breaks them apart (e. g., Beth et al. 2022). These ions may in turn be excited by the solar radiation, and although cometary gas is initially mainly composed of water molecules (H_2O), it is the fluorescence of CO^+ ions from other gas species such as carbon dioxide (CO_2), carbon monoxide (CO), or formaldehyde (CH_2O), that creates the characteristic blue shimmer of the plasma tail (e. g., Deslandres et al. 1907; Evershed 1907; Larsson et al. 2012; Beth et al. 2022).

Additionally, the gas molecules can also be ionized by the solar wind, which itself consists of highly energetic electrons and ions. Which of the different ionization processes dominates however, depends on the cometary activity and the nucleocentric distance of the gas (e. g., Heritier et al. 2018; Wedlund et al. 2019, 2020). In any case, once ionized, the gas molecules also start to interact in complex ways with the magnetic field generated by the solar wind, causing large-scale structures in the plasma environment—most notably the ion tail (e. g., Hoffmeister 1943; Biermann 1951, 1952; Parker 1958; Beth et al. 2022; Götz et al. 2022a,b): cometary ions are picked up by the magnetic field and carried away almost radially from the Sun.

Yet while it is comparatively straightforward to explain the presence of the ion tail in so far as it results from sublimating ices that make up part of the surface layers of cometary nuclei heated up by the Sun, the mechanism responsible for the dust particle ejection is still not well understood (e. g., Kührt et al. 1994; Skorov et al. 2012; Blum et al. 2014; Fulle et al. 2019b; Gundlach et al. 2020; Bischoff et al. 2023). In his seminal works, Whipple (1950; 1951) was the first to propose an elaborate theory stating that at the center of a comet sits a cohesive nucleus made of ice and dust, a model which soon became to be known as the “dirty snowball” model. Although the idea of a cohesive nucleus was not exactly new at that point, dating back to at least Laplace (1813) and Bessel (1836b), prior to Whipple's proposal, a commonly accepted theory was that comets consist of a “gravel bank” (e. g., Whipple 1974; Mendis 1988). The dirty snowball model nevertheless quickly became consensus as it could explain how comets survive close encounters with the Sun, how they remain active after many passages through the inner Solar System, and how their activity affects their orbits due to non-gravitational forces (see also Marsden et al. 1973; Micheli et al. 2018; Kramer et al. 2019a; Attree et al. 2019, 2023, 2024b). But it was not until 1986, when the Giotto spacecraft visited comet 1P/Halley during its return to the inner Solar System, that the existence of a solid nucleus at the center of a comet was finally confirmed (Keller et al. 1986, see Fig. 1.14; and also Sagdeev et al. 1986b).

In rare cases, comets were also observed to display a yellow tail made of neutral sodium atoms (e. g., Cremonese et al. 1997; Ip et al. 1998; Cremonese et al. 2002; Afghan et al. 2024). The atoms are driven away by solar radiation pressure and most likely originate from fragmenting dust in the coma (see also Birkett 2017). In an even rarer case, Fulle et al. (2007) report the first (and so far only) discovery of a neutral iron tail.

If SSSBs are constantly exposed to significant solar radiation over long periods of time, their orbits can even be notably affected by solar radiation pressure or the Yarkovsky and YORP (Yarkovsky-O'Keefe-Radzievskii-Paddack) effects, which are driven by thermal radiation (although these effects primarily apply to spacecraft, asteroids, and meteoroids, e. g., Öpik 1951; Rubincam 2000; Bottke et al. 2006). Briefly, the Yarkovsky effect has a diurnal and seasonal component, but generally describes how the orbit of SSSBs can change due to asymmetric thermal radiation caused by the body's thermal inertia and depending on its heliocentric distance, rotational state, axis tilt, and physical characteristics. Similarly, the YORP effect describes how the reflection and re-emission of sunlight can alter the rotational frequency of small bodies, which in turn is relevant for the Yarkovsky effect (e. g., Bottke et al. 2006).

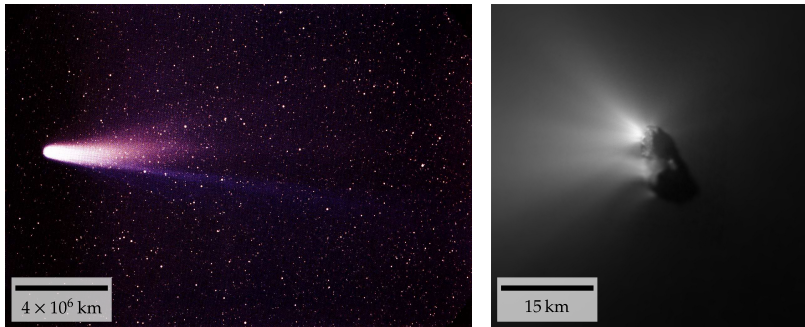


Figure 1.14: Halley’s comet in 1986 as observed from the ground (left; credit: NASA/W. Liller) and from the Giotto spacecraft (right; credit: MPS).

1.3.2 ACTIVITY PARADOX

It turned out however that “icy dirtball” may actually be the more fitting description of cometary nuclei (Keller 1989), as Giotto showed that they primarily consist of dust instead of ice (e. g., Sykes et al. 1992b; Fulle et al. 2000). This was a major insight that was later reconfirmed by the Rosetta mission to comet 67P, but it also led to one of the major challenges in contemporary comet science (e. g., Kührt et al. 1994; Skorov et al. 2012, 2017; Blum et al. 2014; Gundlach et al. 2015b; Fulle et al. 2019b; Vincent et al. 2019): “[First,] how is it possible that water-ice sublimation from the nucleus surface does not lead to an insulating crust, stopping every gas and dust ejection within a few days? [And second,] how is it possible that the gas flow crossing the refractory surface crust ejects dust particles bonded by tensile strengths larger than tens of [Pascal] when the perihelion gas pressure at the nucleus-coma interface is less than one [Pascal]?” (Fulle et al. 2019b). These questions are commonly known as the “activity paradox”, and although significant progress has been made in recent years towards solving it (e. g., Fulle et al. 2020a; Gundlach et al. 2020; Ciarniello et al. 2022; Davidsson et al. 2022a), it currently remains unsolved (e. g., Bischoff et al. 2023; Attree et al. 2024a).

The tensile strength of cometary surface material is badly constrained and can vary several orders of magnitude depending on the relevant length scale (e. g., Biele et al. 2022; Blum et al. 2022). For meter-sized surface material of comet 67P, Attree et al. (2018a) report tensile strengths on the order of ~ 1 Pa, while the (internal) tensile strength of centimeter-sized “pebbles” and smaller particles is possibly much higher (e. g., up to \sim kPa, Blum et al. 2006, 2014, 2015; Gundlach et al. 2018b; Güttler et al. 2019; Bischoff et al. 2020; Fritscher et al. 2022). Yet in the coma of 67P, even micrometer-sized particles were detected (e. g., Mannel et al. 2016; Merouane et al. 2016; Longobardo et al. 2019) even though the gas pressure beneath the nucleus surface was likely less than 1 Pa (e. g., Pajola et al. 2017b). Likewise, Jewitt et al. (2019a) found a special case of the activity paradox which they dubbed the “cohesion bottleneck”. They showed that the activity displayed by comets beyond ~ 7 AU cannot be explained with current understanding either. At those distances, activity is driven by super-volatiles like CO, but the gas pressure they generate is two to three orders of magnitude too small to lift millimeter-sized particles against interparticle cohesion.

To solve the activity paradox, Fulle et al. (2019b, 2020a) proposed a macrophysical activity model assuming that the nucleus is made from centimeter-sized pebbles. They argue that the (water-driven) erosion

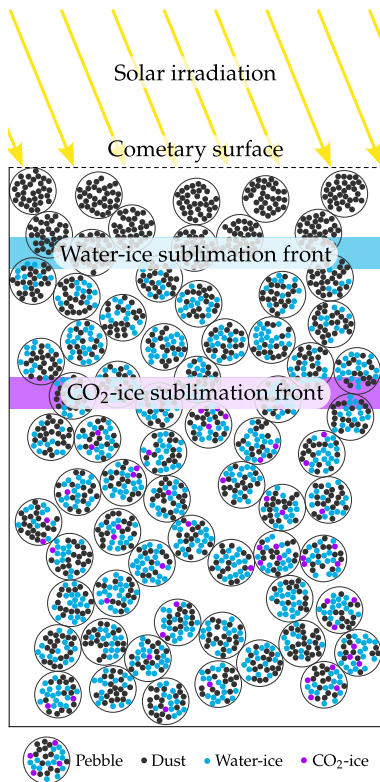


Figure 1.15: Pebble model of Gundlach et al. (2020).

There are several other studies that used thermophysical models to recreate observed characteristics of 67P (e.g., Hu et al. 2017b; Macher et al. 2019; Skorov et al. 2020; Herny et al. 2021), but none were able to explain every observation.

Sintering describes the temperature-driven process of materials to minimize their surface area, which for example means that two touching ice particles start to grow a “neck” that connects them (e.g., Blackford 2007; Gundlach et al. 2018a).

and dehydration of surface material are independent from one another: while the erosion rate only depends on the average dust bulk density, the size of the largest ejected dust, and the pebble heat conductivity and capacity, the dehydration rate only depends on the nucleus bulk density, the water vapor flux, and the refractory-to-water-ice (mass) ratio. Notably, their model implies no insulating nucleus crust, and allows for the gas pressure inside pebbles to reach over 1 kPa.

In tandem with Fulle et al. (2019b, 2020a), Gundlach et al. (2020) simulated the activity of a pebble-based nucleus containing both water- and CO₂-ice (see Fig. 1.15) on a microphysical level, and compared the results to Rosetta observations. They found that the ejection of decimeter-sized particles is driven by the sublimation of CO₂-ice because it already starts to sublimate at much lower temperatures and thus deeper surface layers than water-ice, whereas water-ice sublimation is responsible for ejecting centimeter-sized chunks and pebbles due to its much shallower sublimation front (confirming previous theories about comet activity, e.g., A’Hearn et al. 2011; Skorov et al. 2012). The simulations were however unable to eject sub-centimeter-sized dust and the resulting size-frequency distributions of the coma particles did not match those observed at comet 67P. Similarly, the simulated gas and dust production rates did not (simultaneously) reproduce observations either, and importantly, the model also required an (artificially) low gas diffusivity to allow for the gas pressure to overcome the tensile strength of the surface material and eject the dust particles.

In follow-up studies (Fulle et al. 2020b; Fulle 2021; Ciarniello et al. 2022, 2023), the macrophysical model of Fulle et al. (2019b, 2020a) was further developed and most notably reconciled with the existence of water-ice-enriched blocks (WEBs) discovered on 67P’s nucleus surface (e.g., Fornasier et al. 2023). This refined model assumes that ~ 94% of the surface material is made from water-ice-poor pebbles, while ~ 6% is made from water-ice-rich pebbles concentrated in meter-sized WEBs (both mixed with some CO₂-ice), and is able to reproduce the observed water and CO₂ production rates of 67P as well as its seasonality (see also Sect. 1.5.2). Similarly, Davidsson et al. (2022a) were also able to reproduce the observed water and CO₂ production rates in a different macrophysical model, but needed to shift the fit parameters around perihelion to do so. They also used the observed dust production rate as an input parameter and thus did not explicitly model the ejection process of dust particles.

Finally, the most recent microphysical simulations by Bischoff et al. (2023) showed that a simple pebble-based model cannot (simultaneously) reproduce the observed (trends of) water, CO₂, and dust emissions. The model for example either required artificially low tensile strength or reduced gas diffusivity to eject dust, but the changes also resulted in outgassing rates inconsistent with observations. The authors therefore conclude that “a quantitative description of 67P’s dust and gas production remains enigmatic” and that “to really understand the dust-ejection mechanism in comets ... sintering, thermal cracking, and other phenomena might have to be taken into account.”

1.3.3 COMET FORMATION

The activity paradox also goes hand in hand with another major contemporary challenge: the formation of comets. Currently, there are mainly two competing theories (e. g., Weissman et al. 2020; Simon et al. 2022): the hierarchical agglomeration scenario (e. g., Weidenschilling 1977, 1997; Windmark et al. 2012a,b; Davidsson et al. 2016) and the gravitational collapse scenario (e. g., Youdin et al. 2005; Johansen et al. 2007; Blum et al. 2017, 2022; Fulle et al. 2017a). Both theories generally agree that at the beginning, sub-micrometer- to micrometer-sized grains were condensing out of the protoplanetary disk once it was cool enough (e. g., Blum et al. 2022; Simon et al. 2022, see also Fig. 1.16). These grains then formed larger particles via low-velocity collisions (e. g., $\lesssim 1$ m/s for silicate, Blum et al. 2008; or $\lesssim 10$ m/s for water-ice, Gundlach et al. 2015a), which allows them to stick together via inter-molecular forces like the van der Waals attraction (e. g., Dominik et al. 1997). Initially, these particles are very “fluffy” (i. e., highly porous), but as they grow, they may be increasingly deformed and compacted (e. g., Zsom et al. 2008; Weidling et al. 2009; Güttler et al. 2010), or even abrade and fragment (e. g., Kothe 2017). Once the particles reach a certain size however, they encounter the so-called bouncing barrier, which prevents similar-sized particles from growing any larger as they bounce off of each other under moderate velocity collisions (e. g., Blum et al. 1993; Weidling et al. 2012; Brisset et al. 2016). This size limit is likely around a few millimeters to centimeters, but depends on many factors such as where in the protoplanetary disk the particles were forming, their material properties, and the properties of the protoplanetary disk (e. g., Zsom et al. 2008; Lorek et al. 2018). Particles at this stage are commonly referred to as the previously-mentioned “pebbles”, and it is where the two models diverge.

Advocates of the gravitational collapse scenario argue that this bouncing barrier cannot be overcome, and even if some particles manage to grow past it, they would quickly encounter new challenges (e. g., Blum et al. 2022; Simon et al. 2022; Drażkowska et al. 2023). For one, unlike very small particles ($\ll 1$ m), which essentially follow the gas flow, or very large bodies ($\gg 1$ m), which are essentially decoupled from the gas and move on Keplerian orbits, particles on meter-scales experience significant radial drift towards the protosun, which may accrete them much faster than they can grow out of the critical size range (e. g., Whipple 1972a; Adachi et al. 1976; Weidenschilling 1977; Blum et al. 2022). Second, as particles grow to a few centimeters in size and beyond, it becomes increasingly likely for them to fragment already at low collisional speeds of $\gtrsim 1$ m/s (Blum et al. 2008). But even if they do not fragment, erosion due to high-velocity impacts by small dust particles or grains should stop them from growing past several tens of centimeters (Schräpler et al. 2018). Thus rather than finding ways to overcome these barriers, advocates of the gravitational collapse scenario instead propose that comets are formed via gravitationally collapsing pebble clouds (Blum et al. 2017; Fulle et al. 2017a). To achieve this, pebbles must first be pre-concentrated, for example via eddies, vortices, and pressure bumps, which can occur in turbulent protoplanetary disks (e. g., Johansen et al. 2014). Next, the pebble clouds are further concentrated via so-called streaming instabilities (Youdin et al. 2005): essentially, pebbles that travel in groups experience less friction from the surrounding gas (much like

There also was the theory that comets may be “collisional rubble piles” having formed from fragments of larger parent bodies (e. g., Stern 1988a,b; Farinella et al. 1996; Stern et al. 2001), but it seems to have lost all support (e. g., Davidsson et al. 2016).

Curiously, it was Immanuel Kant who first suggested that planets form from collapsing clouds (Kant 1755).

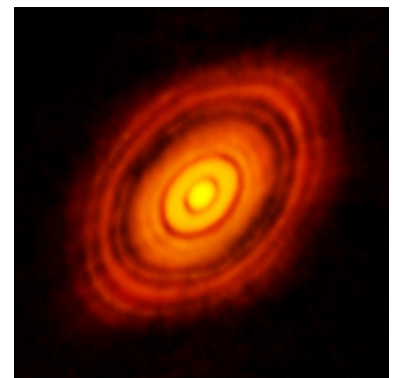


Figure 1.16: Example of a protoplanetary disk, in this case of star HL Tauri (credit: ALMA/NRAO/ESO/NAOJ).

migratory birds), which allows them to overtake more isolated pebbles and potentially incorporate them into their group. This is a crucial step because it allows pebble clouds to reach high enough mass concentrations and become gravitationally bound. Subsequently, they gently ($\lesssim 1$ m/s) collapse into cometesimals, the precursors of comets (Johansen et al. 2007).

Although advocates of the hierarchical agglomeration scenario do not dismiss the gravitational collapse of pebble clouds, they argue that it mostly leads to planetesimals $\gtrsim 50$ km, while smaller bodies likely disintegrated due to steam pressure (Merk et al. 2006; Davidsson et al. 2016). Comets then form from the pebbles that survived this initial phase of gravitational collapse, but they do so via hierarchical agglomeration. The pebbles therefore need to overcome the bouncing barrier, which may be achieved either through sufficient size differences, where the larger particles can “sweep up” much smaller particles (Windmark et al. 2012b; Drążkowska et al. 2013), or through “lucky” series of low velocity collisions (Windmark et al. 2012a). The key to this is that (at the same heliocentric distance) particles of different sizes move at different speeds because they interact differently with the surrounding gas flow. Accordingly, particles grow by accreting (mostly three to six times) smaller particles where the relative velocity is high. Fragmentation or erosion are effectively inhibited at this stage by taking water-ice into account, which is significantly stickier than dust and thus allows for much higher relative velocities (Wada et al. 2009). The particles that made it past the bouncing barrier then continue to grow to a few meters in size, where streaming instabilities may prevent them from drifting into the protosun (Davidsson et al. 2016). From there on, the particles continue to grow via hierarchical agglomeration at low relative velocities (~ 1 m/s), until they eventually form cometesimals of a few kilometers in size.

Both scenarios have their own strengths and weaknesses, but neither can currently explain all of the observed characteristics of cometary nuclei (e. g., Weissman et al. 2020; Blum et al. 2022). The gravitational collapse scenario can for example explain how fluffy particles that were discovered in the coma of 67P may have survived for so long (see also Sect. 1.5.3), whereas in the hierarchical agglomeration scenario, they should have been destroyed due to the high velocity collisions (e. g., Blum et al. 2017). The hierarchical agglomeration scenario on the other hand might be able to explain the layered nucleus structure observed on comet 9P/Tempel 1 (Belton et al. 2007; Thomas et al. 2007; Belton et al. 2018) and comet 67P (Massironi et al. 2015, see also Sect. 1.5.1), because it allows for relatively high collisional velocities between two cometesimals. In such a case, one of them might break apart into its meter-sized constituents, which then settle as a global layer on the other cometesimal (Davidsson et al. 2016; Weissman et al. 2020). Meanwhile, advocates of the gentle gravitational collapse scenario admit that their model cannot currently explain the formation of layers (Blum et al. 2022). In addition to several other differences, neither comet formation model can currently explain the existence of WEBS. And so in conclusion, although the gravitational collapse scenario is currently favored over the hierarchical agglomeration scenario, the debate about comet formation and the activity paradox is not yet settled.

1.3.4 PARTICLE & GAS DYNAMICS

So even though it is not clear yet *how* exactly particles are ejected, it is clear that they *are* ejected. Once they have left the surface, they are exposed to a number of different forces that govern their dynamics. The solar gravity (Eq. 1.4) and radiation pressure (Eq. 1.5) were already mentioned previously (see Sect. 1.3.1), but especially close to the nucleus, the most critical force for most particles is likely the gas drag F_D .

Yet close to the nucleus, the gas environment can also be highly complex due to the nucleus shape, topography, and composition (e. g., Marschall et al. 2020c). Generally, such rarefied gas flows cannot be described analytically by the Euler or Navier-Stokes equations (Euler 1757; Bistafa 2017). These equations are only valid in the continuous flow regime, where the fluid is in thermal equilibrium, or rather, where the velocity distribution is Maxwellian (see, e. g., Fig. 1.17). But in case of (active) comets, the velocity distribution is non-Maxwellian close to the surface (commonly assumed to be “half-Maxwellian”), since there is a net “gain” in gas molecules due to the sublimating ice (e. g., Davidsson 2008). As a consequence, a so-called Knudsen layer forms with a scale height of roughly 10 to 100 molecule mean free paths (mfp ; e. g., Ytrehus 1975). Above this layer, the gas may transition into an equilibrium flow, but because the gas becomes increasingly rarefied with nucleocentric distance, it will eventually take on a non-equilibrium flow again due to insufficient inter-molecular collisions (e. g., Marschall et al. 2020c). These different flow regimes are characterized by the Knudsen number (Knudsen 1909)

$$Kn = \frac{mfp}{L}, \quad (1.8)$$

where L is the characteristic size of the system (e. g., the radius of the nucleus). For $Kn < 0.01$, the flow field is considered continuous, for $0.01 < Kn < 100$ transitional, and for $Kn > 100$ free molecular. If the gas production rate is high, three different flow regimes can therefore be discerned around the nucleus (e. g., Marschall et al. 2020c):

- ▶ a subsonic non-equilibrium flow near the surface,
- ▶ followed by a supersonic continuous flow layer,
- ▶ and a supersonic non-equilibrium flow above.

If the gas production rate is low however, the near-surface Knudsen layer and the outer non-equilibrium flow merge together and cannot be distinguished. The gas environment around an active comet can therefore generally be rather complex.

Nevertheless, it can usually be assumed that the dust particle size is much smaller than the mean free path of the gas molecules, which means that the flow can be treated as free molecular regarding the dust dynamics (e. g., Finson et al. 1968a; Gombosi et al. 1985, 1986; Gombosi 1987; Sengers et al. 2014; Marschall et al. 2016; Agarwal et al. 2023). And while in case of strong outbursts for example, the particles’ influence on the gas as well as particle-particle interactions need to be considered (Shou et al. 2017), it is generally fair to assume that the particle number density is low enough so that they do not significantly affect the gas flow and for

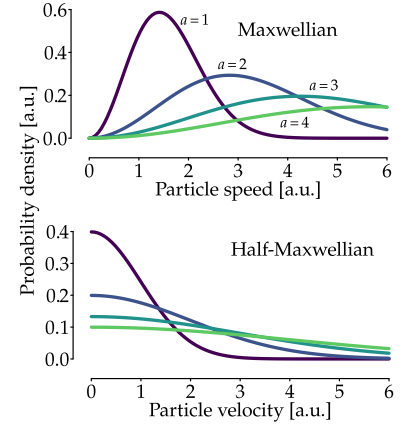


Figure 1.17: Arbitrary (half-)Maxwellian distributions with different scaling parameter a . Maxwell–Boltzmann distributions describe the distribution of particle *speeds* in ideal gases (Maxwell 1860a,b; Boltzmann 1872). A specific instance of such a distribution is often called a “Maxwellian”. Half-Maxwellians on the other hand describe the distribution of particle *velocities* in one direction and correspond to Gaussian distributions centered at zero and multiplied by two (and defined only for positive numbers, e. g., Zudin 2021).

example decelerate it or heat it up (Tenishev et al. 2011). Assuming a spherical particle, the gas drag can then be written as

$$F_D = \frac{1}{2} C_D m_g n_g \sigma_p |v_g - v_p| (v_g - v_p), \quad (1.9)$$

where m_g is the mass of a gas molecule, n_g the gas number density, v_g the gas velocity, σ_p the particle cross section, v_p the particle velocity, and C_D the (dimensionless) drag coefficient, defined as (Baines et al. 1965; Bird 1994)

$$C_D = \frac{2\zeta^2 + 1}{\sqrt{\pi}\zeta^3} e^{-\zeta^2} + \frac{4\zeta^4 + 4\zeta^2 - 1}{2\zeta^4} \operatorname{erf}(\zeta) + \frac{2(1 - \epsilon)\sqrt{\pi}}{3\zeta} \sqrt{\frac{T_d}{T_g}}, \quad (1.10)$$

where T_p is the particle temperature, T_g the gas temperature, ϵ the fraction of specular reflection, and

$$\zeta = \frac{|v_g - v_p|}{\sqrt{\frac{2k_B T_g}{m_g}}}, \quad (1.11)$$

where $k_B \simeq 1.38 \times 10^{-23}$ J/K is the Boltzmann constant. Which forces dominate accordingly depends on many different factors such as the heliocentric distance, the particle size, their nucleocentric distance, the gas production rate of the nucleus, and how well the particles couple with the gas. Smaller particles ($\lesssim 1$ cm) are for example predominantly affected by the gas drag and may only decouple from it beyond ~ 10 nucleus radii, where solar gravity and radiation pressure become increasingly relevant (e. g., Agarwal et al. 2023). Larger particles ($\gtrsim 1$ dm) on the other hand likely only weakly couple with the gas and are thus predominantly affected by the nucleus gravity.

How much certain particles are affected by the gas drag is however still not entirely understood. Highly porous particles may for example experience significantly higher accelerations (Skorov et al. 2016, 2018; Reshetnyk et al. 2018), while oblate, prolate, or irregularly-shaped particles may start to rotate, which can also affect their dynamics (Ivanovski et al. 2017a,b; Moreno et al. 2022; see also Ivanovski et al. 2024). Finally, there are also several other forces that may affect the particle dynamics (e. g., Chesley et al. 2020; Jiang et al. 2020; Agarwal et al. 2023), most importantly “rocket forces” induced via asymmetric outgassing, which is discussed separately in Section 1.5.4.

1.4 ROSETTA MISSION

The Rosetta mission to comet 67P/Churyumov-Gerasimenko was, and still is, the first space mission that performed a rendezvous maneuver with an (active) comet (Bonnet 1985; Schwehm 1989; Schwehm et al. 1994; Kolbe et al. 1997; Glassmeier et al. 2007; Taylor et al. 2017). It subsequently accompanied 67P for over two years as it passed through the inner Solar System and even managed to deploy a lander on 67P’s surface (although due to some unfortunate circumstances, the lander was only able to perform a fraction of its intended measurements).

The mission was approved in 1993 as one of the cornerstones of ESA's new Horizon 2000 long-term science program, but early planning for the mission however already began in 1985 (Bond 2020), the year when the first space mission to visit a comet, the International Cometary Explorer (ICE), was crossing through the tail of comet 21P/Giacobini-Zinner (von Rosening et al. 1986). Shortly afterwards, in 1986, ICE also performed a far flyby of comet 1P/Halley, which was visited via flybys by five additional spacecraft that same year: the two Soviet spacecraft Vega 1 and Vega 2 (Sagdeev et al. 1986a), the two Japanese spacecraft Sakigake and Suisei (Hirao et al. 1988), and of course the ESA spacecraft Giotto (Reinhard 1986). In 1992, the Giotto spacecraft additionally flew by comet 26P/Grigg-Skjellerup (although without a working camera, McBride et al. 1997). This was followed by NASA's Deep Space 1 mission to comet 19P/Borrelly in 2001 (Boice et al. 2002), NASA's CONTOUR mission intended to visit comets 2P/Encke and 73P/Schwassmann–Wachmann 3, which unfortunately exploded on the way to its first target (Cochran et al. 2003; Kerr 2003), NASA's Stardust mission to 81P/Wild 2 (Brownlee et al. 2003), where it collected coma dust samples in 2004 and brought them back to Earth in 2006 (e. g., Brownlee et al. 2004, 2006; Brownlee 2014), and NASA's Deep Impact mission to comet 9P/Tempel 1, where it released a copper probe to collide with the comet in 2005 (A'Hearn et al. 2005; Schultz et al. 2007). In 2010, the Deep Impact spacecraft additionally passed by comet 103P/Hartley 2 (by then renamed EPOXI, A'Hearn et al. 2011), and finally in 2011, the repurposed Stardust spacecraft visited comet 9P/Tempel 1 to reexamine the aftermath of the artificially induced impact (by then renamed Stardust-NEXT, Veverka et al. 2013). While there are currently several new cometary space missions under development (most notably Comet Interceptor, Snodgrass et al. 2022; Jones et al. 2024), for the moment, the Rosetta mission marks the most recent space mission to a comet.

During its long development, the mission underwent several major changes, most notably a downgrade from a sample-return mission to a "simpler" rendezvous mission with a lander (which was still incredibly ambitious), and a reassignment of the main target from comet 46P/Wirtanen to comet 67P due to some delays (Lamy et al. 2007). The mission was eventually launched on March 2, 2004, and arrived at comet 67P on August 22, 2014, after several gravitational assists by Mars and Earth, two flybys of asteroids (2867) Steins and (21) Lutetia (Schulz 2010; Schulz et al. 2012), and a 31-month-long hibernation phase while it was waiting for the comet to make its way back to the inner Solar System.

The prime scientific objectives of the Rosetta mission were (slightly modified from Schwehm et al. 1999; Glassmeier et al. 2007; Taylor et al. 2017):

- ▶ to globally characterize the nucleus, and to determine its dynamic properties, surface morphology, and composition,
- ▶ to determine the chemical, mineralogical, and isotropic compositions of volatiles and refractories,
- ▶ to determine the physical properties and the interrelation of volatiles and refractories in a cometary nucleus,
- ▶ to study the development of cometary activity and the processes in the surface layer of the nucleus and the inner coma (dust–gas interaction),

The Rosetta mission was fittingly named after the world-famous Rosetta stone (Budge 1913), which was discovered in 1799 and finally allowed the deciphering of the ancient Egyptian hieroglyphs. The fact that Rosetta became a *cornerstone* mission makes this even better.

- ▶ to learn about the origin of comets, the relationship between cometary and interstellar material, and the implications for the origin of the Solar System,
- ▶ and to globally characterize the asteroids, and to determine their dynamic properties, surface morphologies and compositions.

To address all these challenging tasks, the Rosetta spacecraft was equipped with a diverse suite of eleven scientific instruments (taken verbatim from the ESA/ATG medialab with added references, see also Fig. 1.20):

- ▶ ALICE: Ultraviolet Imaging Spectrometer (characterizing the composition of the comet nucleus and coma, Stern et al. 2007)
- ▶ CONSERT: Comet Nucleus Sounding Experiment by Radio wave Transmission (studying the internal structure of the comet with lander Philae, Kofman et al. 2007)
- ▶ COSIMA: Cometary Secondary Ion Mass Analyser (studying the composition of the dust in the comet's coma, Kissel et al. 2007)
- ▶ GIADA: Grain Impact Analyser and Dust Accumulator (measuring the number, mass, momentum and velocity distribution of dust grains in the near-comet environment, Colangeli et al. 2007)
- ▶ MIDAS: Micro-Imaging Dust Analysis System (studying the dust environment of the comet, Riedler et al. 2007)
- ▶ MIRO: Microwave Instrument for the Rosetta Orbiter (investigating the nature of the cometary nucleus, outgassing from the nucleus and development of the coma, Gulkis et al. 2007)
- ▶ OSIRIS: Optical, Spectroscopic, and Infrared Remote Imaging System Camera (a dual camera imaging system consisting of a narrow-angle (NAC) and wide-angle camera (WAC) and operating in the visible, near infrared and near ultraviolet wavelength range, Keller et al. 2007)
- ▶ ROSINA: Rosetta Orbiter Spectrometer for Ion and Neutral Analysis (determining the composition of the comet's atmosphere and ionosphere, and measuring the temperature, velocity and density of the gas flow, comprising: DFMS (Double-focusing mass spectrometer), RTOF (Reflectron Time-Of-Flight mass spectrometer) and COPS (Comet Pressure Sensor), Balsiger et al. 2007)

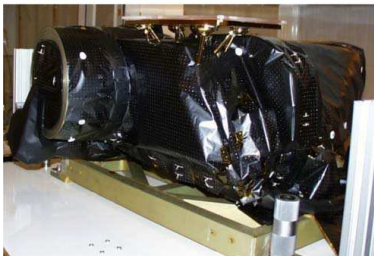
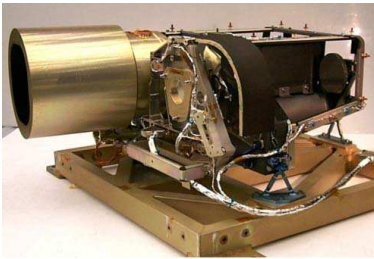


Figure 1.18: “NAC Flight Model during integration and in flight configuration” (Keller et al. 2007, reprinted with permission from Space Science Reviews).



Figure 1.19: Rosetta spacecraft in preparation for thermal testing. OSIRIS/NAC (black cover) and OSIRIS/WAC (golden cover) are indicated by the orange circle (credit: ESA/A. Van Der Geest).

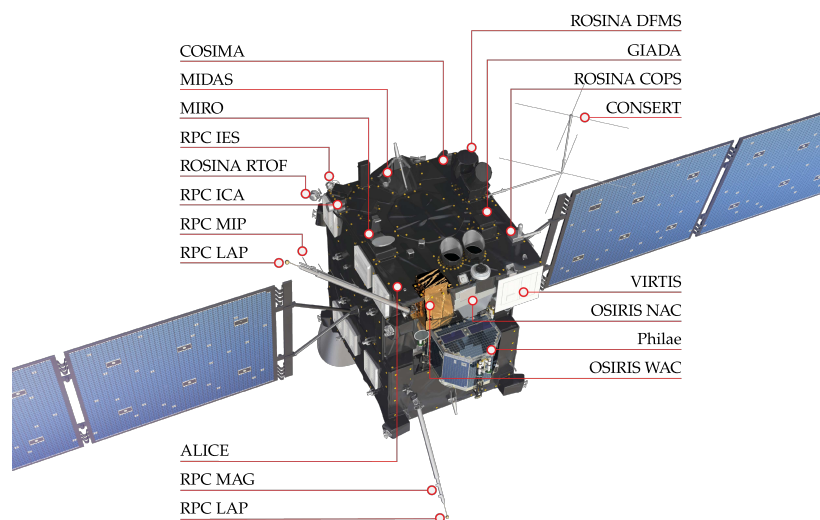


Figure 1.20: The Rosetta spacecraft and its instruments (credit: ESA/ATG medialab; label size increased for better readability).

- ▶ RPC: Rosetta Plasma Consortium (studying the plasma environment of the comet, comprising: ICA (Ion Composition Analyser), IES (Ion and Electron Sensor), LAP (Langmuir Probe), MAG (Flux-gate Magnetometer), MIP (Mutual Impedance Probe), PIU (Plasma Interface Unit), Carr et al. 2007)
- ▶ RSI: Radio Science Investigation (tracking the motion of the spacecraft to infer details of the comet environment and nucleus, Pätzold et al. 2007)
- ▶ VIRTIS: Visible and Infrared Thermal Imaging Spectrometer (studying the nature of the comet nucleus and the gases in the coma, Coradini et al. 2007)

Rosetta's lander, called *Philae*, came with an additional ten instruments (see, e. g., also the ESA/ATG medialab), but because they are only of minor importance for my PhD project, they are not listed here. Of central importance on the other hand are the wide-angle and especially the narrow-angle camera of Rosetta's scientific camera system OSIRIS (see also Figs. 1.19 & 1.18). While OSIRIS/NAC was designed to obtain high-resolution images of 67P's surface with an angular resolution of $18.6 \mu\text{rad}/\text{px}$ and a FOV of $\sim 2.20 \times 2.22^\circ$, OSIRIS/WAC was intended to capture images of 67P's near-nucleus environment with an angular resolution of $101 \mu\text{rad}/\text{px}$ and a FOV of $\sim 11.35 \times 12.11^\circ$ (Keller et al. 2007, see also Fig. 1.21). They also both had various filters specifically selected for their respective tasks as well as doors in front of their lenses to not only protect them from dust impacts while they were not in use, but also to use the door backsides as screens for calibration.

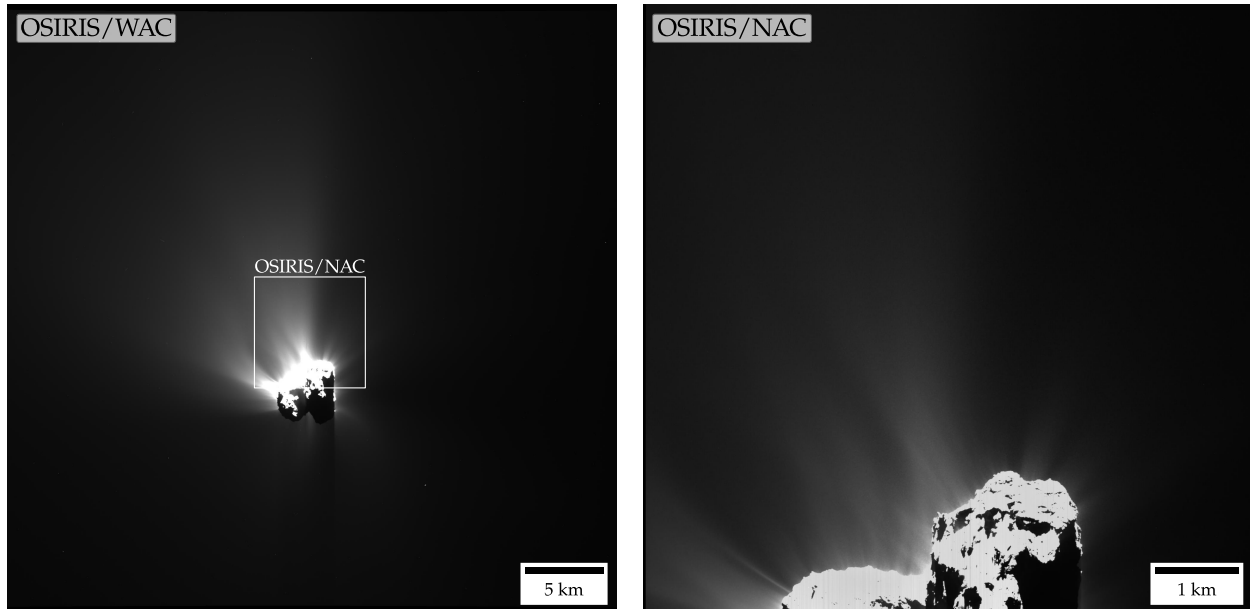


Figure 1.21: Comet 67P as recorded by WAC and NAC on June 23, 2015, illustrating the significant difference in the camera's FOVs.

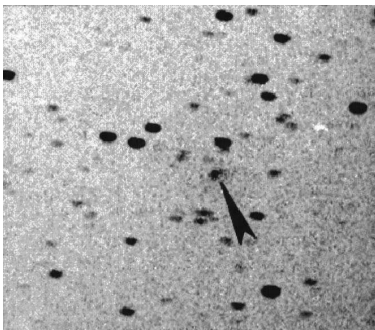


Figure 1.22: The (brightness-inverted) discovery image of comet 67P/Churyumov–Gerasimenko (Lamy et al. 2007, reprinted with permission from Space Science Reviews).

1.5 COMET 67P

Rosetta’s target, comet 67P, was discovered by the soviet scientist Svetlana Gerasimenko during an excursion led by Klim Churyumov to the Alma-Ata Institute of Astrophysics in Kazakhstan in September 1969 (Lamy et al. 2007). While using a 50-cm Maksutov telescope to look for comet 32P/Comas-Solá, she spotted an object on the faded background of a defective photographic plate (see Fig. 1.22) and decided to keep the plate for later inspection. This was indubitably the right decision, since once they were back at their home institute in Kiev and after some close inspection, Gerasimenko and Churyumov realized that the mysterious object on the defective plate was in fact a new comet.

1.5.1 BASIC PROPERTIES

Comet 67P currently has an orbital period of ~ 6.4 years, a perihelion distance of ~ 1.2 AU, an aphelion distance of ~ 5.7 AU, an eccentricity of about 0.65, and an inclination of around 3.8° (according to the MPC). This classifies 67P as a typical JFC with $T_j = 2.75$, which also means that its orbit is highly unstable. In 1959, it experienced a close encounter with Jupiter, dramatically changing its orbital elements: its perihelion distance was reduced from roughly 2.7 to 1.3 AU, its semi-major axis decreased from 4.3 to 3.5 AU, its eccentricity increased from 0.38 to 0.63, and its inclination decreased from 23.2° to 7.2° (Carusi et al. 1985; Belyaev et al. 1986; Krolkowska 2003; Maquet 2015; see also Groussin et al. 2007; Guzzo et al. 2015, 2017). These changes put 67P on an orbit favorable for a rendezvous mission, which was already recognized by Yeomans (1985). Yet when 67P was selected as the new target for the Rosetta mission almost two decades later, nothing much was known about the physical properties of its nucleus, sparking “highly targeted observational campaigns with the most appropriate telescopes, as well as thorough theoretical investigations” (Lamy et al. 2007). As a result, 67P’s nucleus likely became the best studied nucleus not visited by spacecraft prior to Rosetta’s arrival.

Yet even these measurement campaigns did not manage to accurately predict 67’s most striking feature (e. g., Lamy et al. 2006; Lowry et al. 2012): its bi-lobed, “duck-like” nucleus (Sierks et al. 2015, see e. g., Fig. 1.23). The larger lobe (body) is about $4.1 \times 3.3 \times 1.8$ km in size, whereas the smaller one (head) is only about $2.6 \times 2.3 \times 1.8$ km in size. Although this bi-lobed shape seems to be fairly common among comets (see e. g., Fig. 1.24 and Noll et al. 2008; Nesvorný et al. 2018), the cause for this particular shape is still a matter of debate. Because both lobes also show concentric stratifications roughly perpendicular to their respective gravity vectors (i. e., they are layered like an onion, e. g., Massironi et al. 2015; Ruzicka et al. 2019; Penasa et al. 2017, see Fig. 1.25), the two lobes likely formed independently from one another, and may have later merged during a gentle collision (Jutzi et al. 2015; Massironi et al. 2015; de Niem et al. 2018; Nesvorný et al. 2018). Such a contact binary would have mostly preserved the pristine state of the two lobes, but it was also suggested that 67P may have formed via a sub-catastrophic collision, or even a coagulation of fragments from catastrophic collisions (Morbidelli et al.

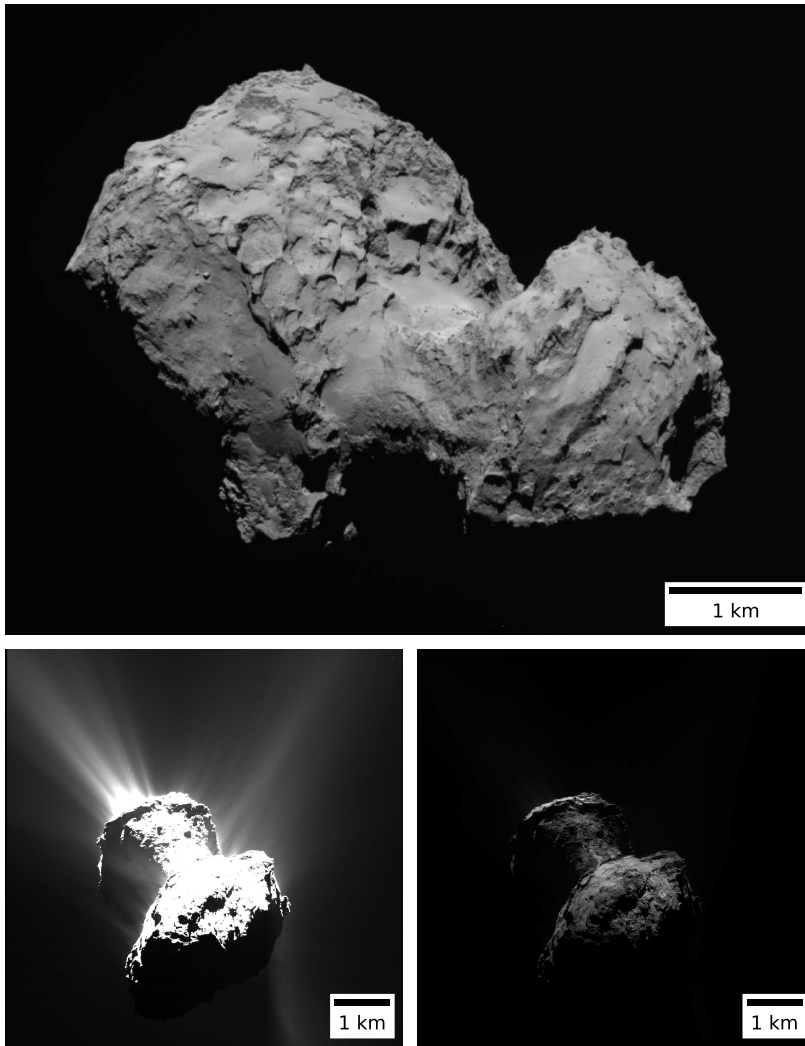


Figure 1.23: Three images of 67P’s nucleus recorded by OSIRIS/NAC on August 3, 2014, in the near-infrared filter (top), and on June 27, 2015, in the orange filter (bottom). The top image was cropped to better show the nucleus and highlighting its bi-lobed shape, while the two bottom images show the same source image, but with different contrast settings to highlight 67P’s strong activity and the enormous dynamic range of the camera.

2015; Rickman et al. 2015; Jutzi et al. 2017a,b). Yet because the deuterium to hydrogen ratios of both lobes were found to be identical within their margins of error (Schroeder et al. 2019), it seems at least likely that both lobes formed within the same region of the protoplanetary disk.

The nucleus is extremely porous with a bulk porosity between 65 and 79% (Pätzold et al. 2019) or even up to 85% (at least in case of the small lobe, Kofman et al. 2015; Herique et al. 2016; Ciarletti et al. 2017), depending on its refractory-to-ice (mass) ratio, δ_{RI} , which may for example lie between 3 and 7 (Pätzold et al. 2019), but is difficult to determine (e. g., Fulle et al. 2017b, 2019a; Choukroun et al. 2020). Overall however, the nucleus structure is likely very homogeneous without any larger voids (Pätzold et al. 2016), although the porosity may also increase with depth (Kofman et al. 2020). The nucleus bulk density and mass on the other hand have been reliably determined and measure 537 kg/m^3 (Preusker et al. 2017) and almost 10^{13} kg (Pätzold et al. 2019), respectively. Accordingly, the nucleus generates a gravitational surface acceleration on the order of

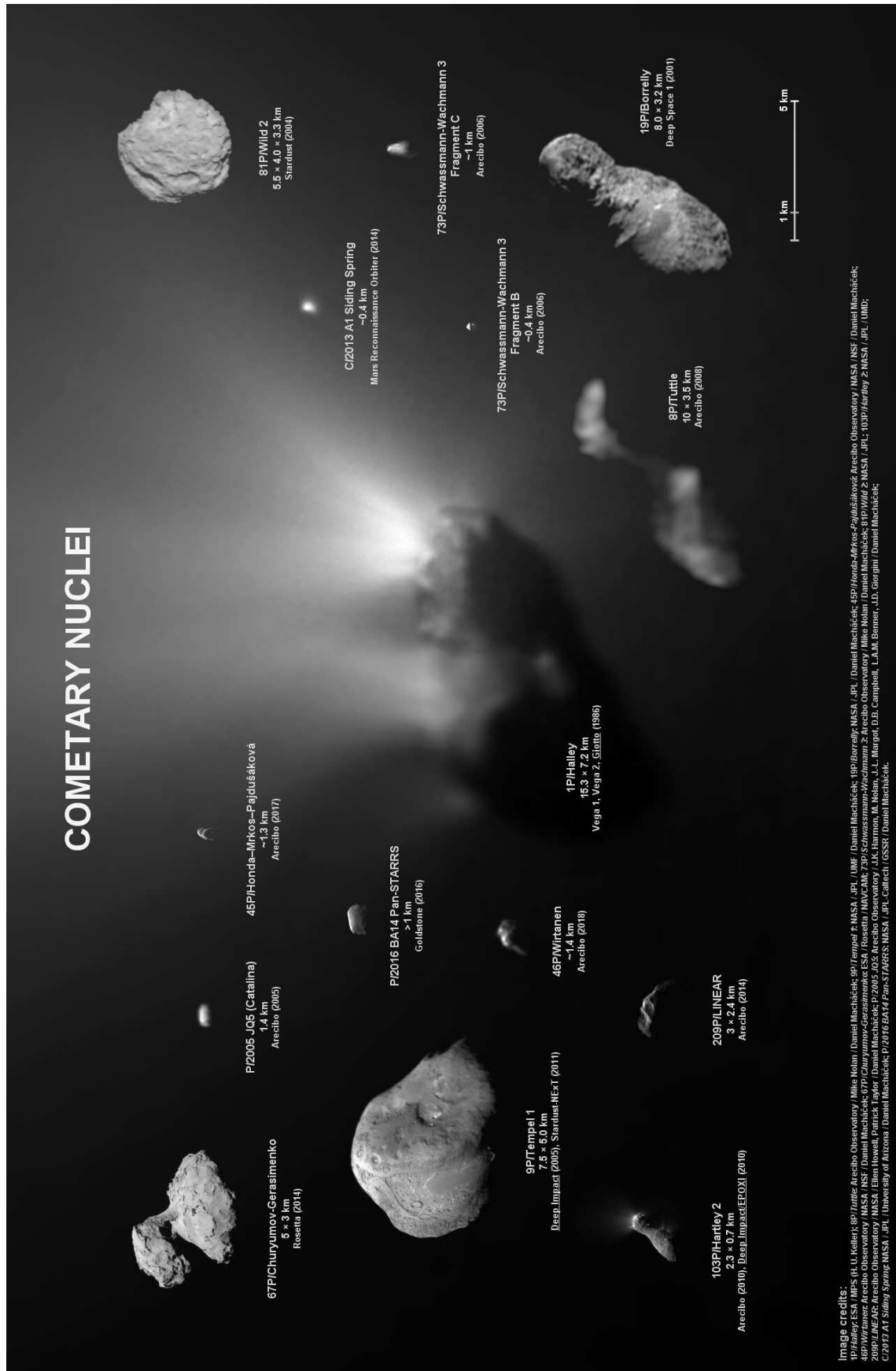


Figure 1.24: “[To-scale] collage of all cometary nuclei imaged by spacecraft and planetary radars” (credit: Daniel Macháček).

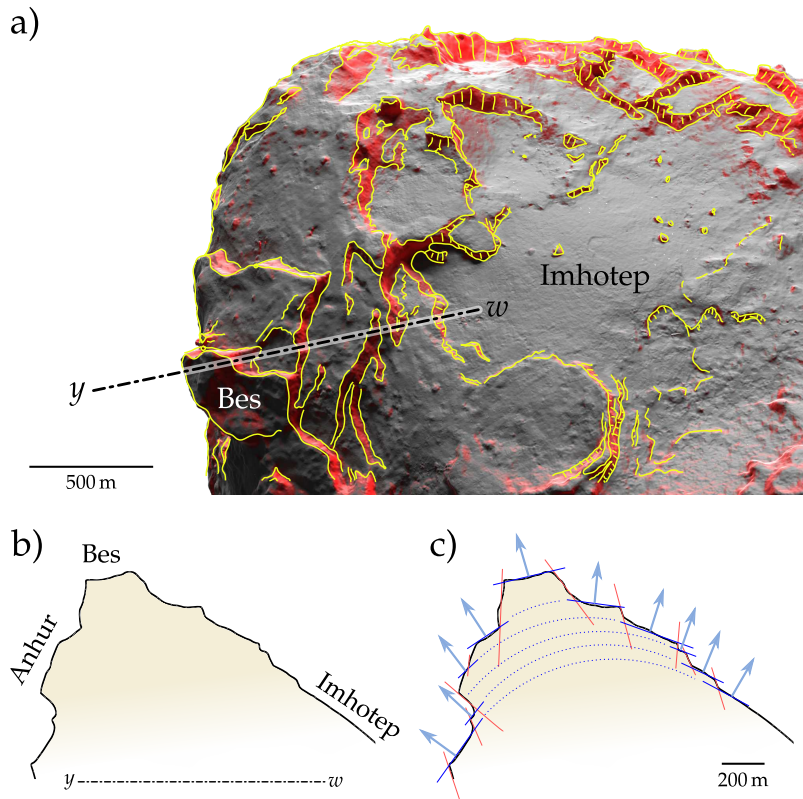


Figure 1.25: Stratifications observed on the big lobe of 67P suggesting a layered nucleus structure: “(a) A render of the three-dimensional shape model by Preusker et al. (2017), centered on the Imhotep region on the [big lobe]. High-slope regions (> 35°) have been shaded in red and highlighted in yellow to demonstrate their elongated and laterally persistent geometry. It is evident that cliffs and terraces create a staircase pattern. (b) Topographic profile obtained cutting the model along the y - w direction from Bes towards Imhotep region further illustrates the alternation of flats and cliffs. In cross-section (c) cliffs and terraces are highlighted by red and blue lines, respectively. Arrows illustrate how the terraces change orientation along the topographic profile. To maintain [these orientations coherent,] the surfaces forming the terraces must indeed be curved within the nucleus interior” (Penasa et al. 2017, figure shows recreation of their Fig. 1, figure elements kindly provided by Luca Penasa).

10^{-4} m/s^2 (e. g., Marschall 2017), while it also shed about 0.28% of its mass during Rosetta’s rendezvous phase due to activity (Laurent-Varin et al. 2024).

1.5.2 SEASONAL CHANGES

Because of this mass-loss and the outgassing, 67P’s rotational period changed by about 21 minutes from about ~ 12.4 hours in March 2014 to ~ 12.1 hours in September 2016 (Godard et al. 2017; Kramer et al. 2019b; see also Jorda et al. 2016; Kramer et al. 2019a). An almost identical decrease in its rotational period was also already observed after its perihelion passage in 2009 (Mottola et al. 2014). Notably, these changes may only be explained when taking another characteristic feature of 67P into account: its strong seasonal and diurnal change in activity (e. g., Keller et al. 2015b; Attree et al. 2019, 2023, 2024b).

67P’s nucleus has an obliquity (i. e., axis tilt relative to its orbital plane) of about 52° (e. g., Sierks et al. 2015) in a configuration such that its southern solstice coincides with 67P’s perihelion passage, which causes strong

seasonal and diurnal effects in several regards. For one, because of the complex shape of the nucleus and its high obliquity, there are areas that lie in constant shadow after the outbound equinox. As a result, the surface temperatures of these areas are lower than the core temperature for a certain time due to the low thermal inertia of the nucleus. And because CO₂-ice is much more volatile than water-ice, this temperature inversion then allows for CO₂-ice to sublimate in deeper layers and subsequently re-condense on the surface, resulting in a seasonal CO₂-cycle (Filacchione et al. 2016). For similar reasons, there is also a diurnal water-cycle where water-ice sublimates during the day and re-deposits on the surface during the night (e. g., De Sanctis et al. 2015; Ciarniello et al. 2016; Fornasier et al. 2016; Tosi et al. 2019; Hu et al. 2021).

Additionally, while the overall appearance of the nucleus is very dark, with a geometric albedo of around 6% (which is roughly that of asphalt, e. g., Lin et al. 2010), there is also a seasonal color-cycle of the nucleus surface: during the southern summer, CO₂-ice sublimation in deeper surface layers continuously removes larger ($\gtrsim 1$ cm) chunks of surface material from the southern hemisphere and exposes fresh water-ice to the sunlight (notably also in the form of water-ice-enriched blocks, so-called WEBS, Ciarniello et al. 2022; which have been observed on the nucleus as bright spots, e. g., Fornasier et al. 2016, 2017, 2023; Oklay et al. 2016, 2017; Deshapriya et al. 2018). Most of the ejected material that is too slow to escape from the nucleus gravity settles again on the much less active northern hemisphere, where it builds up smooth blankets of fall-back material (e. g., Keller et al. 2015a, 2017; Thomas et al. 2015a; Lai et al. 2016; Hu et al. 2017a; Cambianica et al. 2020, 2021; Davidsson et al. 2021). But because of the exposed water-ice on the illuminated southern hemisphere, the nucleus surface appears significantly bluer during the southern summer than during other orbital phases further away from the Sun, when the northern hemisphere becomes increasingly exposed and the surface temperatures are getting too low for sustained water-driven erosion. This causes the surface to appear significantly redder due to the blankets of (at least partially) dehydrated fall-back material (e. g., Ciarniello et al. 2016, 2022, 2023; Fornasier et al. 2016; Filacchione et al. 2020; conversely, the opposite color-cycle was found for the dust coma, Filacchione et al. 2020). Water activity in these northern regions only sets in again during the inbound phase when they are sufficiently illuminated, and dominates the global activity up to about the pre-perihelion equinox, when the activity in the southern hemisphere takes over (e. g., Bockelée-Morvan et al. 2015; Lara et al. 2015; Lin et al. 2015; Sierks et al. 2015; Fougere et al. 2016; Marschall et al. 2016).

1.5.3 SURFACE MATERIAL

This dichotomy in the hemispherical activity and the consequential mass transfer also significantly affect 67P's surface morphology (see also El-Maarry et al. 2019). While the northern hemisphere is characterized by large areas covered in smooth dust blankets created by the fall-back material (e. g., El-Maarry et al. 2015; Thomas et al. 2015b), such areas are entirely absent from the southern hemisphere, which instead features mostly rough, consolidated terrains and outcroppings (e. g., El-Maarry et al. 2016, 2017a). Notably however, this does not mean that the latter

features are absent from the northern hemisphere, and especially on smaller scales, almost any kind of geological feature can be seen anywhere on the nucleus including “ridges, terraces, scarps, niches, (coarse or fine grained) dust-blankets, boulders (El-Maaray et al. 2015, 2016; Thomas et al. 2015b, 2018; Ferrari et al. 2018; Leon-Dasi et al. 2021), (steep) cliffs (Attree et al. 2018a), fractures and other linear features (Giacomini et al. 2016; Lee et al. 2016), [and] even clods or ‘goosebumps’ (Sierks et al. 2015; Davidsson et al. 2016)” (to cite my science paper, see, e. g., Fig. 1.26). Based on this surface morphology and topography, El-Maaray et al. (2015, 2016, 2017a) defined 26 different surface regions (named after Egyptian deities, see Fig. 1.27), which Thomas et al. (2018) later subdivided even further to address intra-regional changes.

Largely independent of its macro-structure or location however, the surface material likely has an average compressive strength of no more than ~ 800 Pa (Heinisch et al. 2019), whereas the primordial ice embedded in boulders was discovered to have a much lower compressive strength of < 12 Pa, making it softer than freshly fallen snow (O’Rourke et al. 2020). Additionally, the average tensile strength of the nucleus material is even lower, at no more than a few Pascal (Groussin et al. 2015; Attree et al. 2018a). Based on the analysis of sub-millimeter dust particles collected in the coma of 67P, it was found that the refractory material consists of nearly equal amounts of anhydrous mineral phases and organic matter made from large macro-molecular compounds (Fray et al. 2016; Bardyn et al. 2017; Rubin et al. 2020). In terms of size, the collected coma particles ranged from tens of nanometers to a few tens of micrometers (in case of

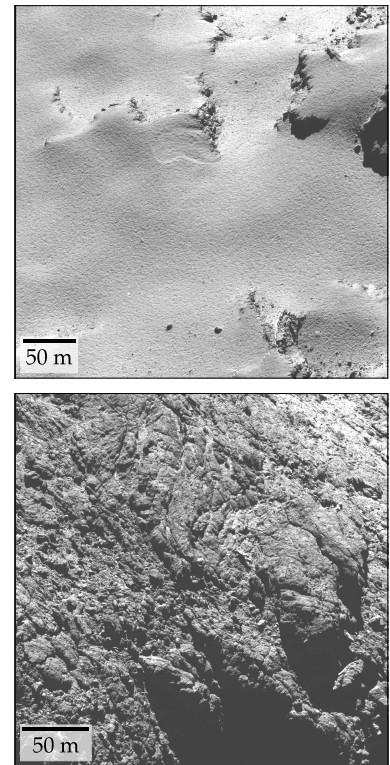


Figure 1.26: The diversity of 67P’s surface material: smooth terrain in the Ash region, recorded on October 20, 2014 (top), and consolidated terrain in the Bastet region (bottom), recorded on August 15, 2014.

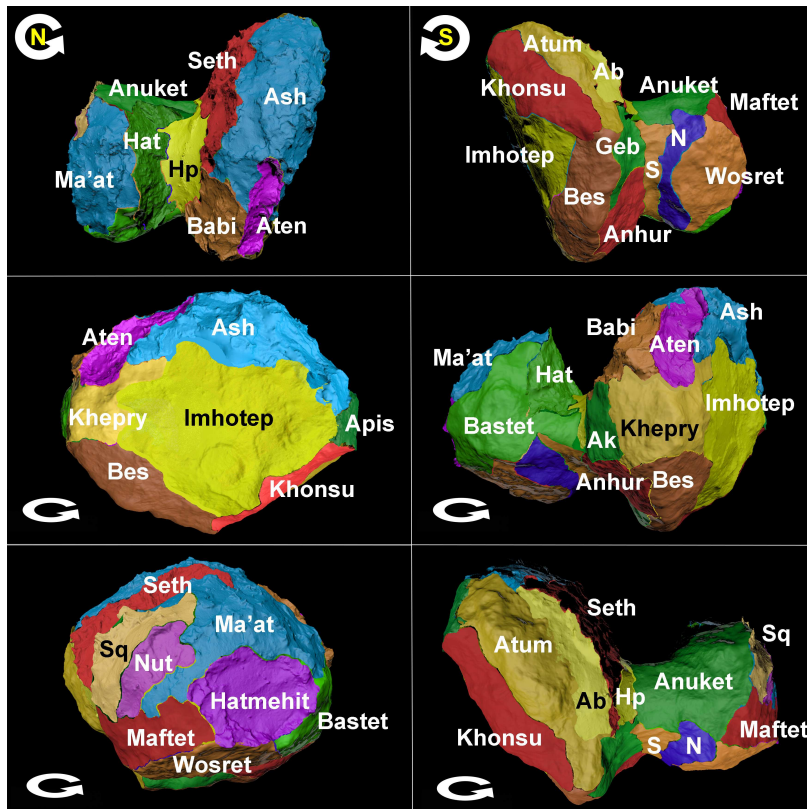


Figure 1.27: The 26 surface regions of comet 67P according to El-Maaray et al. (2015, 2016, 2017a, reprinted with permission from Astronomy and Astrophysics).

MIDAS, e. g., Bentley et al. 2016; Mannel et al. 2016, 2019; Kim et al. 2023), from about 10 micrometers to sub-millimeters (in case of COSIMA, e. g., Hilchenbach et al. 2016; Langevin et al. 2016, 2017; Merouane et al. 2016, 2017), and from sub-millimeters to a few millimeters (in case of GIADA, e. g., Fulle et al. 2015a, 2017a; Rotundi et al. 2015; Longobardo et al. 2019, 2020, 2022).

Because these particles were observed to have vastly different structures and material properties, they can be roughly divided into three distinct groups (e. g., Güttler et al. 2019):

- ▶ solid particles with low porosity ($< 10\%$) and high strength, notably including grains, which are the smallest observed particles starting at tens of nanometers and are thought to be the building blocks of the larger particles;
- ▶ porous particles with “intermediate” porosity (10–95%) and low strength, comprising (hierarchical) agglomerates in the micro- to millimeter size range;
- ▶ and fluffy particles with high porosity ($> 95\%$) and very low strength, notably including fractal particles in the micro- to millimeter size range.

By tracing GIADA particles back to the nucleus surface, Longobardo et al. (2019, 2020) conclude that porous and solid particles likely originated from the processed smooth terrains, whereas fluffy particles likely originated from the pristine rough terrains. This fits well with the cometary formation model of gentle gravitational collapse, because unlike more energetic collisions, which should have compacted or dispersed the fluffy particles, a gentle collapse allows for the fluffy particles to be preserved in the voids between the centimeter-sized pebbles, which the model postulates as the single-size building blocks that cometary nuclei are made of (e. g., Blum et al. 2017, 2022, see also Sect. 1.3.3). Additionally, Pestoni et al. (2023) found via a multi-instrument analysis that fluffy particles likely still contained ices by the time they arrived at the spacecraft, which supports their pristine nature.

1.5.4 DISTRIBUTED SOURCES

Nevertheless, whether or not especially larger ($\gtrsim 1$ cm) particles still contain significant amounts of water-ice after being ejected and thus continue emitting gas and dust while traversing the coma is still a matter of debate. On the one hand (e. g., Cambianica et al. 2020; Fulle et al. 2020a; Fulle 2021; Ciarniello et al. 2022, 2023), it is argued that most of the water-ice is contained in pebble-based water-ice-enriched blocks (WEBs), which have refractory-to-ice (mass) ratios $\delta_{RI} < 5$ and are responsible for the sub-centimeter erosion of the nucleus surface. Such WEBs then only constitute around 6% of the southern surface material, which would be enough to explain the observed fine-dust emission solely via WEB erosion. The rest of the surface material is much dryer in this scenario with $\delta_{RI} > 5$, which prevents the material from water-driven erosion and causes it to dehydrate instead. This dryer material is then ejected in larger chunks via CO_2 -ice sublimation and quickly forms an insulating crust during its coma passage before falling back and settling on the (northern) surface. Accordingly, the larger particles do not contain large amounts of

water-ice, because if they did, their erosion during their coma passage would produce much more fine dust than what was measured by Rosetta (especially because most of the coma dust mass is contained in the larger particles).

On the other hand, much evidence has been found in support of outgassing particles due to their contribution to the gas coma of 67P (e. g., Altwegg et al. 2016; De Keyser et al. 2017; Biver et al. 2019; Hadraoui et al. 2019; Schuhmann et al. 2019; Hänni et al. 2020; Hadraoui et al. 2021). These so-called distributed (or earlier “extended”) sources help to explain overabundances of certain (gas) molecules in the coma that typically cannot be accounted for via sole nucleus activity (e. g., Ip et al. 1974; Cottin et al. 2008). Importantly, the previously described model also implies the existence of distributed sources, since it only allows for particles to be ejected whenever erosion dominates over dehydration, which means that the ejected material must necessarily still contain water-ice. So although an abundance of distributed sources in the coma of 67P was previously disputed by advocates of this model (Fulle et al. 2016a), their latest work actually predicts that the water production of distributed sources contributed significant and even dominating amounts to the total water production observed over the course of Rosetta’s rendezvous phase (Fulle 2021; Ciarniello et al. 2023). According to the authors, the existence of distributed sources is also not conflicting with the dust production based solely on surface erosion, since the sublimating water-ice inside the ejected particles should not be able to build up enough pressure to overcome the particles’ internal tensile strengths, because otherwise, they should have already eroded on the surface.

Yet there are also other studies that predict the ice-content of dust particles in the coma: Gundlach et al. (2020) for example used a thermophysical model of the nucleus surface material to study the particle ejection process, and assumed that the material was made from millimeter-sized pebbles consisting of dust, water-ice, and CO₂-ice particles. Depending on the input-parameters, they found that decimeter-sized particles can still contain up to 90% of their original water-ice content when they are ejected. Once they are part of the coma, decimeter-sized particles may however continue to retain most of their water-ice content: using a different thermophysical model that also accounts for gas advection in the energy-balance of a particle, Davidsson et al. (2021) investigated the ice-retention of dust particles while they were migrating through the coma from the southern to the northern hemisphere. They found that decimeter-sized particles with $\delta_{RI} = 4$ lose less than 10% of their water-ice content during their coma passage. Davidsson et al. (2021) therefore favor the scenario of Keller et al. (2017), who suggested “wet” fall-back material to explain the water-dominated activity in the northern regions prior to the inbound equinox. This was further corroborated by Davidsson et al. (2022a), who used the same code to model the water and CO₂ production rates of 67P and found that distributed sources only contributed $\sim 8\%$ to the total water production rate at perihelion (in conflict with Fulle 2021; Ciarniello et al. 2023). But while decimeter-sized coma particles may only lose small amounts of their water-ice content, this is likely quite different for centimeter-sized particles and below: using yet another thermophysical model, Markkanen et al. (2020) not only found that centimeter-sized icy dust particles should lose their

In the context of (significant) overabundances of water, this phenomenon is also known as hyperactivity (e. g., Rickman et al. 1998; Lis et al. 2019; Sunshine et al. 2021), and was for example first confirmed in case of comet 103P/Hartley 2 (A’Hearn et al. 2011).

The model of Davidsson et al. (2021) theoretically even includes crystallization of amorphous water-ice and heating via radioactive decay, but in this case, the former was not considered and the latter completely negligible.

entire ice content within hours after being ejected, but they also suggest that internal gas pressure within these particles may even become high enough for them to disintegrate.

Finally, the outgassing of such particles may noticeably affect their dynamics, especially if it occurs asymmetrically (i. e., predominantly in one direction) and thus manifests as a “rocket force” (e. g., Reach et al. 2009; Kelley et al. 2013; Agarwal et al. 2023, equivalent to the non-gravitational forces experienced by the nucleus itself):

$$a_{\text{rocket}} = \frac{3}{4} \frac{m_{\text{H}_2\text{O}} Z v_{\text{th}} f_{\text{ice}}}{\rho_{\text{p}} r} \kappa, \quad (1.12)$$

where a_{rocket} is the acceleration a particle experiences due to the rocket force, $m_{\text{H}_2\text{O}} = 3 \times 10^{-26}$ kg is the mass of a water molecule, Z the sublimation rate, v_{th} the mean thermal expansion speed of the gas, $f_{\text{ice}} = 1/(1 + \delta_{\text{RI}})$ the particle ice fraction, $\rho_{\text{p}} = 537$ kg/m³ the particle density (approximated via the nucleus bulk density, Pätzold et al. 2019), r the particle radius (assuming the particle is spherical), and $0 \leq \kappa \leq 1$ the degree of asymmetric outgassing, where $\kappa = 0$ and $\kappa = 1$ correspond to isotropic and one-directional outgassing, respectively. Not all of these parameters are easy to determine however, in particular the sublimation rate (strictly speaking, it is also the sublimation rate *per surface area*, but f_{ice} is likewise the ice fraction of the surface area, so the dependency cancels out). To nevertheless estimate an upper limit of Z , it is helpful to assume that all of the solar energy is used for water-ice sublimation (i. e., no loss via scattering, thermal emission or other effects), which allows to calculate the maximum sublimation rate Z_{max} via (e. g., Kelley et al. 2013; Güttler et al. 2017)

$$Z_{\text{max}} = \frac{(1 - A_{\text{B}}) S_{\odot} N_{\text{A}}}{r_{\text{h}}^2 L}, \quad (1.13)$$

where $A_{\text{B}} = 0.0157$ is the Bond albedo (derived for 67P at 649 nm, Fornasier et al. 2015), $S_{\odot} = 1361$ W/m² the solar constant, $N_{\text{A}} = 6.022 \times 10^{23}$ mol⁻¹ the Avogadro constant, r_{h} the heliocentric distance, and $L = 51\,000$ J/mol the latent heat of sublimating water-ice at a temperature of 300 K (Murphy et al. 2005). Assuming $\delta_{\text{RI}} = 5$, $r_{\text{h}} = 2$ AU, and $v_{\text{th}} = 500$ m/s, which are representative values for our observations, the corresponding rocket acceleration of a decimeter-sized particle is around 1.3×10^{-4} m/s². Although this is an upper-limit estimate, it still shows that the rocket force is likely on the same order of magnitude as the nucleus gravity, and thus may be noticeable in the particle dynamics. Agarwal et al. (2016) and Güttler et al. (2017), for example, who previously studied the dynamics of particles in the coma of 67P have likely already found evidence for asymmetric outgassing as they observed particles being accelerated in the anti-solar direction.

1.6 THIS WORK

This work systematically examines the dynamics of dust particles in the near-nucleus coma of comet 67P. Understanding these dynamics provides key insights into various aspects of cometary science, a fact already

recognized during Rosetta's mission planning and in-situ operations. Consequently, throughout Rosetta's rendezvous phase, OSIRIS/NAC routinely recorded image sequences of 67P's near-nucleus coma to capture the motion of recently ejected dust particles (see also the OSIRIS Science User Guide). Our analysis focuses on these sequences, which primarily consist of image pairs—two images taken in quick succession, followed by a longer pause before the next pair. This structure allows for the assignment of instantaneous velocities to particles detected in both images of a pair, and thus significantly improves their tracking. Due to large particle-observer distances however, the particles could not be spatially resolved by the camera and instead appear as point-sources in the images. Each of the sequences shows thousands of such point-source-like dust particles moving through the coma, necessitating a reliable algorithm that can track them automatically. The successful development of this algorithm is the main technical achievement of this work and represents a major improvement over any previous studies on dust particle dynamics, as they only relied on tracking small numbers of particles by hand.

Within the scope of this work, we then apply our tracking algorithm to dozens of the previously mentioned image sequences, although only a fraction of them are shown here. Specifically, we concentrate our scientific analysis on four image sequences that proved to be most suitable. Of the thousands of particles that we tracked through these four sequences, we trace hundreds of them back to the nucleus surface and determine their potential source regions, size distributions, and dynamics. Using a state-of-the-art coma model, we then further corroborate our results with simulations of 67P's gas and dust coma as it was observed during the respective time periods.

Overall, we most notably find that: (a) the suspected source regions correlate with rough terrain types or steep slopes like scarps, cliffs, or fractures, that facilitate activity; (b) the observed ejection of large, roughly decimeter-sized dust particles is locally confined and does not necessarily correlate in neither place nor time with the much more homogeneous ejection of small, roughly sub-centimeter-sized dust particles; (c) neither solar irradiation nor the local gravity and centrifugal forces can explain the local confinement of the observed ejection of large dust particles, indicating a local overabundance of CO₂-ice; (d) a significant amount of dust particles seem to show notable accelerations in the anti-solar direction, which may be evidence for asymmetric outgassing; and (e) the large dust particles couple only weakly with the escaping gas and instead likely received most of their speed, around 0.5 m s^{-1} , during their ejection events. Collectively, these findings help to constrain the conditions that are necessary for the ejection of such large particles, bringing us a step closer to solving the activity paradox. The strong evidence for significant initial velocities in particular implies that the corresponding ejection events must be considerably more energetic than gradual lift-offs.

In the following chapter, I motivate our choice to develop our own tracking algorithm, while the algorithm itself is described in detail in Part two. Part three discusses our scientific results including the comparison to our dust coma modeling, followed by a general closing discussion in Part four.

PARTICLE TRACKING

The competent tracker is both scientist and storyteller. You must critically observe, collect good data, and avoid rash conclusions, as well as use your imagination to interpret and celebrate the signs you've discovered.

— Elbroch (2003). *Mammal Tracks & Sign*.

BEFORE my tracking algorithm and its intricacies are explored in detail in the next chapter, it is important to put it in the proper disciplinary context. “Optical cometary dust particle tracking” is currently a very niche application that branches off of a highly nested tree of partly well-established tracking disciplines. It may therefore seem natural to use one of these already existing techniques for our purposes, which is why we also briefly investigated this option at the beginning of my PhD project (November 2018). Yet after a few tests, we quickly realized that our image sequences came with a number of challenges unique in their combination: low time-resolution (i. e., down to around two images every six minutes), changing time intervals (i. e., pair-wise image recording, with short time periods between two images of a pair and a long pause in between pairs), alternating exposure times (requiring different sensitivity settings for the detection algorithm), strongly fluctuating particle signals (potentially preventing their continuous detection), thousands of particles with complex dynamics and densely populated areas (requiring dynamic criteria to separate particles), and fluctuations in the camera pointing (adding spatial displacement that needs to be corrected), just to name the most severe. Third-party software would therefore likely not be able to track our particles “straight out of the box”, and there was no guarantee that they would be able to do so eventually. Consequently, we decided that I should develop my own tracking algorithm that would address these challenges and properly utilize all the features of our image sequences.

2.1 METHODOLOGICAL CONTEXT

In the following, I give a (by no means comprehensive) overview of other tracking applications to provide reasons for our decision and to put our application into context. In doing so however, it is unavoidable to explain or reference technicalities that may only become clearer once our approach is understood. It might therefore be advantageous to read the methods paper first. In any case, here is the list of other tracking techniques, starting with those that are most closely related to mine (and that I am most familiar with):

2

CHAPTER CONTENTS

Methodological Context	37
Comet Particle Tracking	38
Asteroid Particle Tracking	39
Star and Debris Tracking	40
SSSB Tracking	41
Optical Particle Tracking	41
Optical Tracking	42
Other Particle Tracking	43
Conclusion	43
A Brief Philosophical Aside	43

My technique is *optical*, because it relies on image sequences instead of other media or sensor data; the particles are *cometary*, because they were recorded in space around a comet instead of in a laboratory experiment, for example, and dust, because they are agglomerates of refractory material (and possibly ice) instead of elemental particles, for example; and the target of my tracking algorithm are *particles* instead of mice, cars, people, or aircraft, for example. Technically, *automated* should also be added to chain of descriptors, since things can also be tracked manually, but that is probably too fine a distinction.

Although there are review articles of tracking techniques in many of the fields that are listed here, as far as I know, nobody has yet attempted to create an overview of the entire field of (object) tracking as I attempt here. The groupings are therefore entirely my own, and likely miss some relevant entries. But if nothing else, the list at least demonstrates the diverse meaning of the word “particle”.

2.1.1 OPTICAL COMETARY DUST PARTICLE TRACKING

In the introduction of the methods paper, we mention many studies that use various techniques to *detected* dust particles around comet 67P (see p. 53), but of those, only Marín-Yaseli de la Parra et al. (2020) automatically *tracked* a single particle throughout an image series. They did so with the help of the TrackMate software, which was originally developed for tracking single particles in live cell microscopy images (Tinevez et al. 2017). TrackMate is also one of the tools that we briefly considered for our application, but which turned out to be inadequate for several of the reasons listed above (e. g., sparse data, changing time intervals, simultaneous tracking of thousands of particles). Yet to be fair, TrackMate is much more versatile by now (Ershov et al. 2022) and thus may actually be configured to also work with our image sequences if they are appropriately pre-processed.

But apart from Marín-Yaseli de la Parra et al. (2020), so far, the only other instance where cometary dust particles were optically tracked was in case of the Deep Impact/EPOXI flyby past comet 103P/Hartley 2 (Hermalyn et al. 2013, which has more to do with the scarcity of space missions to comets than anything else; see also Kelley et al. 2013, 2015). Similar to our case, Hermalyn et al. (2013) were also faced with sparse data and a larger number of particles to track. Yet because their data is from a flyby mission with a high relative encounter speed between the spacecraft and the nucleus, they only had a short observation window of around three minutes, which meant that the main motion of the observed particles was due to parallax. This allowed them to rely on “epipolar” geometry to locate and track the dust particles in 3D. In our case however, this is not possible because the relative speed between spacecraft and nucleus is much slower, and the observational periods much longer (almost two hours), which means that the main motion of our particles is due to their ejection. This is additionally complicated by the camera pointing fluctuation, which can be on the order of the apparent motion of sidereal background objects.

Finally, Moretto et al. (2023) announced a novel approach of tracking dust particles around comet 67P using track-oriented multiple hypothesis tracking (MHT, e. g., Blackman 2004) based on Kalman filtering (Kalman 1960), but they have yet to publish their results. Kalman filtering is a widely-used technique to recursively predict the state of parameters (such as particle locations and velocities) in a noisy dynamical system (e. g., Humpherys et al. 2012). It does so in a two-step iteration, where it first estimates the new parameter state from the previous estimate and the dynamical model that describes the system, and then updates the estimate by averaging it with the current measurement of the parameter state. In a linear dynamic system, the Kalman filter is the best unbiased estimator, and because it only needs the information of the previous step to make a prediction, it can do so effectively in real-time. It is thus employed in many tracking applications and was also famously used for guidance of the Apollo spacecraft (Grewal et al. 2010).

MHT is a technique that is particularly useful for tracking many closely-spaced targets at once (Blackman 2004). It provides decision logic based on Bayesian statistics for handling situations where a single detection may for example be associated with several tracks or vice versa. It does

Epipolar geometry is for example important in stereo vision and describes the relation between different views of the same scene (e. g., Hartley et al. 2003). In such a geometry, the vectors that connect the observers with their respective images of an object in the scene can be extended outwards from their FOVs, where they eventually intersect, marking the exact location of the object.

During the early stages of my project, I also tried to use Kalman filtering with our data via a third-party software. But unfortunately, that software came with a built-in detection algorithm that was unsuitable for our images. It relied on relatively stable image backgrounds that contrast with the motion of objects in the foreground. But because of the low time resolution of our image sequences and their alternating exposure times, their image backgrounds can change drastically from one image to the next due to the rotation of the nucleus and the diffuse dust coma. This approach therefore seemed unfeasible and I stopped investigating the Kalman filter any further due to time constraints.

so by maintaining the corresponding potential track states and their likelihoods (hypotheses) and propagating them into the future, where the conflicts may be resolved with the help of subsequent data. Track-oriented MHT is a particular derivative of this technique where instead of maintaining and updating the hypotheses, they are discarded and new ones formed with each iteration. At its core, MHT seems quite similar to our approach in terms of how to resolve association conflicts, although we do not maintain multiple hypotheses and also do not encounter cases where single detections may be associated with several tracks out of principle. Both Kalman filters and MHT (Levesque et al. 2008, as well as their employed iterative background removal method by) may therefore be a viable alternative to our approach, but it remains to be seen how Moretto et al. (2023) for example resolve the issues generated by the spatial shifts due to the pointing fluctuation.

2.1.2 OPTICAL ASTEROIDAL DUST PARTICLE TRACKING

Next, there are the works of Liounis et al. (2020, and references therein), who tracked dust particles around active asteroid (101955) Bennu. Their application is therefore still closely related to ours in that it deals with simultaneously tracking multiple dust particles in space recorded in sparse data. Yet setting-wise, it also already differs in at least two significant ways: For one, unlike active comets, active asteroids do neither have a complex gaseous environment that needs to be considered nor a diffuse coma that has to be subtracted. And second (at least in this case), their image sequences contain far fewer particles than ours (factor of up to at least ~ 100).

Implementation-wise, their approach relies on a multiple-object-tracking extended Kalman filter (EKF, Al-Shakarji et al. 2017) and is thus quite similar to the approach of Moretto et al. (2023). The EKF is a derivative of the Kalman filter used for non-linear dynamical systems as it produces the best unbiased estimates for linearized systems (e. g., Humpherys et al. 2012). The overall structure of their tracking algorithm is nevertheless notably similar to ours (cf. their Fig. 5 with Fig. 7 in the methods paper), although like Moretto et al. (2023), they create new track variants whenever there is more than one option for a track to continue, and propagate all variants till the end. Only then do they decide on which tracks to keep and which to discard based on residuals after backward smoothing the fitted trajectories.

In our case however, we realized early on that pursuing every possible track variant was computationally not feasible because our images typically contain several thousands of detections, which would produce an unmanageable amount of track variants after only a few steps. We therefore decided for a more economic solution by only pursuing the track variants that produce the best fit at each step. A core strength of our algorithm is also that it takes advantage of the pair-nature of our data sets, which is something that Kalman filters can generally not do.

Yet despite all the differences, their approach may still be a viable option for our data and it would be interesting to see how well it fares. But because it was developed in parallel to our approach, we only learned

Very recently, Deshapriya et al. (2023), Moreno et al. (2023), and Dotto et al. (2024) also published the first analyses of the ejecta plume that was generated by the impact of the DART spacecraft with the asteroid Dimorphos (a satellite of asteroid 65803 Didymos) in September 2022. While they did measure and track some morphological features, it seems that no individual particles could be detected (somewhat reminiscent of the Deep Impact event, e. g., Richardson et al. 2007).

Based on the data from asteroid Bennu, Azzalini et al. (2023) just suggested a curious way of dealing with the low time-resolution of such image sequences: Instead of using a standard frame-based camera, they suggest to use an event-based camera, whose pixels trigger independently whenever their brightness values notably change. Accordingly, the particles would basically be tracked in real-time. This is certainly an interesting technique, but I am not sure if it could also be adapted for observations around an active comet due to its diffuse coma.

about it when our algorithm was essentially finished, so we could not take advantage of their insights.

2.1.3 OPTICAL STAR AND DEBRIS TRACKING

Because our particles are typically unresolved and therefore appear as point sources in the images, they look very similar to stars. The next closest thing to our application may thus be star trackers. Much like sailors at sea, star trackers (i. e., camera-software-combos) on spacecraft scan the celestial surroundings for familiar constellations and use them for navigation and guidance (e. g., Cole et al. 2004, 2006; Mortari et al. 2004; Curti et al. 2015; Zhang 2017; Christian et al. 2021; Zapevalin et al. 2023). These systems have played a crucial role in space exploration for a long time (e. g., Junkins et al. 1977; Strikwerda et al. 1981), and rudimentary versions relying on sextants were already famously used during the Apollo missions (Hoag 1983).

Just like with our application, star trackers also have to potentially distinguish between thousands of objects at once when they are in an active cometary environment. Yet they have the advantage that they are tracking fixed patterns that they cross-correlate with star catalogs, and which do not change unless the spacecraft is reorienting (which usually happens under controlled conditions). Notably, Rosetta’s star tracker (Buemi et al. 2000; Airey et al. 2003) was nevertheless irritated by dust particles several times during the rendezvous-phase with 67P, as it was unable to distinguish them from stars (Accomazzo et al. 2016; Regnier et al. 2016). This even caused the spacecraft to go into “survival mode” after one such occasion at the end of May 2015 (Accomazzo et al. 2017). Grün et al. (2016) on the other hand made practical use of the fact that Rosetta’s star trackers are also sensitive to 67P’s dust coma. They identified brightness changes in the background signal recorded in the star trackers’ housekeeping data and used that information to corroborate measurements made by Rosetta’s scientific instruments of a strong outburst.

The significant overlap between particle and star trackers may have also been exploited during the development of the previously described algorithm that was used to track particles around asteroid (101955) Bennu. According to Liounis et al. (2020), they built their algorithm using the same software that was used to create the star trackers for the mission (Jackman et al. 2013, 2017; Wright et al. 2018; Liounis et al. 2019).

Lastly, due to the massive use of commercial, scientific, and military satellites around Earth, star tracking (or more generally optical navigation) is also explored as a space-based means for hazard prevention by detecting and tracking debris and other resident space objects (RSOs) in (low) Earth orbit and even near-Earth objects (NEOs, i. e., typically asteroids; e. g., Feiteirinha et al. 2019; Spiller et al. 2020; Mastrofini et al. 2023). But star trackers or not, such space-based systems proposed for Space Situational Awareness (SSA) seem to have really gained traction only recently (just last year, e. g., ESA organized the 2nd NEO and Debris Detection Conference) and were consequently developed essentially in parallel to our application as well. One reason for the increasing interest in such systems may also be that they should ideally run completely autonomously on the spacecraft

they are deployed on, which means that they are severely limited by the (computational) power of the spacecraft and thus need to be optimized for their specific application (e. g., Spiller et al. 2020).

So while such systems are still reasonably closely related to our application in that they are space-based and have to simultaneously track multiple objects that appear as point sources (or streaks), they also seem to be generally intended for data with a better time-resolution, and more importantly, they do not have to deal with an active cometary environment, and thus likely have to track far fewer moving objects on simpler trajectories through much less crowded fields.

2.1.4 OPTICAL TRACKING OF SMALL SOLAR SYSTEM BODIES

Still reasonably closely related to our application are also the algorithms that are used to track and discover asteroids and other small Solar System bodies (SSSBs) in the massive sky surveys such as Pan-STARRS or LSST (e. g., Kubica et al. 2007; Denneau et al. 2013; Jones et al. 2018). Such algorithms emerged from a long tradition of manually inspecting pairs of images through a process called blinking, where a device is used to quickly switch back and forth between two images of the same area of the night sky, making small changes in their composition more apparent (e. g., due to moving objects, e. g., Knox-Shaw 1934; Groeneveld et al. 1954; Gehrels 1981). With the advent of the CCD, this technique was subsequently replaced by digital processes that were already able to automatically detect and track moving objects through multiple images (e. g., McMillan et al. 1986; Gehrels 1991; Helin et al. 1997; Larsen et al. 2007). But, to say it in the words of Liounis et al. (2020): “These techniques have largely been developed for terrestrial-based observations of planets, asteroids, and comets, where the distance between the observer and the target is very large, and thus, the apparent motion in subsequent images is small and fairly linear ... While [they] are effective when the observer is largely stationary and there is a low density of moving objects that are captured in the field of view in each frame with near-linear motion in the detector, they begin to break down when the observer is moving and there is the potential for a high density of objects in each frame with substantial nonlinear motion observed in the detector, as may be the case when a spacecraft encounters an active asteroid or comet.”

Other sky surveys for which tracking engines have been developed include: Spacewatch (Rabinowitz 1991); CFHT, SKADS, OSSOS (Petit et al. 2004a; Gladman et al. 2009; Bannister et al. 2016); (NEO)WISE (Mainzer et al. 2011); PTF (Waszczak et al. 2013); and ZTF (Masci et al. 2019). “Recently, also more general-purpose SSSB discovery engines have been developed, such as HelioLinC (Holman et al. 2018), THOR (Moeyens et al. 2021), or tracee (Ohsawa 2021)” (to cite the methods paper).

2.1.5 OPTICAL PARTICLE TRACKING

While the previous four categories are basically all twigs at the very top of the discipline tree, this category is the next big branch further down. It sprouts a huge family of different tracking techniques or applications from all kinds of fields, and so only some of them are mentioned here:

- ▶ Lagrangian particle tracking (LPT) and particle tracking velocimetry (PTV; e. g., Ouellette et al. 2006; Westerweel et al. 2013; Schröder et al. 2023), which are popular and well-established techniques in the field of fluid dynamics, where tracer particles like oil droplets are dispersed into fluid media and subsequently tracked to study their dynamics.

- ▶ Tracking of nanoparticles or colloids in the field of microrheology (and other soft matter physics, e. g., Crocker et al. 1996; Rose et al. 2020), which is a technique similar to PTV, where the properties of fluids is studied by analyzing the behavior of suspended tracer particles (a particle tracker developed for such colloidal studies is for example trackpy, Allan et al. 2021, although like TrackMate, it is also more versatile).
- ▶ Particle tracking in granular media like sands or gravel (e. g., Ermilov et al. 2022; Schroeter et al. 2022), which is used to study geological processes.
- ▶ Particle tracking in microbiology (e. g., Chenouard et al. 2014; Ulman et al. 2017; Fukai et al. 2023), which generally encompasses the tracking of anything from single molecules up to cells (this is e. g. also where TrackMate fits in).

What probably sets most of these applications fundamentally apart from those mentioned in the previous four groups is that they are developed for much more controlled environments like laboratory experiments. So while we only have sparse data that cannot be reproduced and thus have to make every pixel count, workers in these fields can often repeat experiments and optimize their set-ups. Naturally, these applications of course come with their very own sets of challenges such as big data, extremely crowded fields, chaotic particle motion, or particle-particle interaction, but going into detail is out of the scope of this overview. Because of these unique challenges however, the respective tracking techniques are usually highly specialized and tailored to the specific needs of their applications (much like in our case) and thus cannot be directly applied to our data.

2.1.6 OPTICAL TRACKING

Due to the recent advancements in (AI-driven) computer vision, there is an enormous demand from both science and industry for highly versatile tracking engines that can essentially track any kind of object (e. g., Fiaz et al. 2019). Many of the above-listed applications by now also heavily rely on AI technology (e. g., like the very popular, versatile, and powerful YOLO engine, e. g., Redmon et al. 2018; Bochkovskiy et al. 2020; Wang et al. 2022), which has become a lot easier to access and implement. In the early development phase of my algorithm, we therefore also briefly considered to integrate AI routines. But due to our small number of data sets and the lack of training data, this was not feasible.

The next even broader branch of applications sprouts straight from the stem of the discipline tree, and is accordingly even farther away from my area of expertise. It encompasses the tracking of anything that moves in videos or image sequences. In the following, I therefore again only give a few examples of this category in an attempt to highlight its scope:

- ▶ the tracking of coronal bright spots on the Sun (e. g., Shahamatnia et al. 2016; Pires et al. 2019);
- ▶ the tracking of air bubbles in flowing water (e. g., ur Rahman et al. 2019);
- ▶ the markerless tracking of animals as a non-invasive means to study their behavior (e. g. using deep learning, Mathis et al. 2020);
- ▶ the tracking of vehicles (e. g., Liu et al. 2021; Li et al. 2022) or pedestrians (e. g., Sighencea et al. 2021), which is paramount for the development of fully autonomous vehicles;
- ▶ the satellite-based tracking of objects on Earth, for example to monitor sea ice, wildfires, traffic, or shipping commerce, and for other civilian or military applications (e. g., Aguilar et al. 2022; Zhang et al. 2022);
- ▶ or even the tracking of Unidentified Aerial Phenomena (UAPs, Szenher et al. 2022).

2.1.7 OTHER PARTICLE TRACKING

Finally, as a sort of sister-branch to optical particle tracking, there is also a group of particle tracking techniques that do not rely on image analysis. Among them are for example techniques to track elemental particles, which cannot be detected—or tracked—with classical imaging techniques, during experiments conducted at facilities like the CERN Large Hadron Collider (e. g., DeZoort et al. 2021; Akiba et al. 2023). But more importantly, the particle “tracking” that was performed with the help of Rosetta’s Grain Impact Analyser and Dust Accumulator (GIADA, Colangeli et al. 2007; Della Corte et al. 2014, see also Sect. 1.4) should also be mentioned in this context. GIADA had an impact sensor and a laser curtain to measure the momentum and speed of infalling (\lesssim mm-sized) particles. Although the tracking technique was rather rudimentary, the data that GIADA collected was also used to trace particles back to the nucleus of 67P (Longobardo et al. 2019, 2020, 2022).

2.1.8 CONCLUSION

In conclusion, my (particle) tracking application is clearly only one of a myriad of different tracking techniques. Yet as stated at the beginning of this chapter and as explained in the subsequent discussions, due to our unique set of challenges as well as for historic reasons (i. e., the parallel development of closely related and potentially viable techniques), we saw the need to come up with our own tracking algorithm.

2.2 A BRIEF PHILOSOPHICAL ASIDE

[The standard account of identity] requires that we either deny that Oscar minus a hair is a dog—and a Dalmatian—or else that we must affirm that there is a multiplicity of Dalmatians, all but one of which is incapable of independent action and all of which bark in unison no more loudly than Oscar barks alone.

— Deutsch et al. (2022). “Relative Identity”.

In its most abstract form, the particle tracking that I am concerned with can be understood as an undertaking that constantly needs to solve the conundrum of identity: are two point sources recorded in separate images impressions of the same particle?

To answer this question I first had to define what it means for two point sources to be impressions of the same particle, and so I introduced a set of tracking parameters that provide clear criteria against which the properties of point sources can be tested (see Sect. 3.2 in the methods paper). Coming up with such criteria is mostly a technical problem that is governed by the available information, but there is also a more fundamental aspect to consider: when are two *particles* identical?

This may seem like a deeply philosophical question—which it is (and it is currently also unsolved, Deutsch et al. 2022)—that is nonsensical in the context of my work. In the strictest sense, two particles might only ever be identical if they had the same physical configuration down to their elemental particles (spatial location and rotational state aside). But this

Our particles may for example change due to sublimation or thermal radiation, which raises the question if an object at different temperatures is still considered the same object. What if its chemical composition or structure changes? A block of clay molded into the shape of a mug is still the same block of clay—until you heat it up. What if you melt down iron ore and let it solidify as a bar? Is it still the same iron? I would say so. A lake that freezes in the winter and thaws in spring is still considered the same lake. But what if water-ice sublimates and redeposits again? Is it still the same ice? I'm not sure. A cake pre- and post-baking? Likely not. There seems to be no universal answer. Things apparently can change and yet remain the same.

Notably, the simulation software doesn't simulate images. It's purpose is not to test the detection of particles, but their tracking, so it only simulates the locations of where signal may have been detected.

is obviously not a helpful interpretation, especially considering that our particles are likely constantly changing. I did however encounter at least one situation where the identity of a particle is crucial—but to explain it, I need to jump a little ahead:

Once my tracking algorithm was fully functional and delivered satisfying results, I wrote simulation software to test it. The software is actually significantly more complex and versatile than what the brief section in the methods paper gives away (see also discussion on p. 72 as well as Sect. 5.3). Other than simple noise, it can for example also simulate particle tracks in all kinds of “flavors” by changing, among other things, how often they were “detected” throughout an “image sequence” (their so-called miss-rate), or how much their detections scatter from their true locations (their offset).

So I simulated many different scenarios, and subsequent tracking runs showed solid results (see e. g. Fig. 2.1). This was easy enough to confirm by eye. But how can this actually *quantified*? Because naturally, it would be good to know if the algorithm managed to find 70, 80, or even 90% of the simulated tracks, and how many it generated out of noise. But how to decide if a track was found or not? Or in the opposite case: opposite: When should a track be considered spurious and generated from noise? Of course the limiting cases are simple. If none of the detections that constitute a simulated track are part of the tracks that the algorithm found, then the track was not recovered. And if all of them (and them alone) were identified as being part of the same track, then the track was found. But there are many intermediate cases where it is difficult to decide one way or the other—and yet to quantify the tracking results,

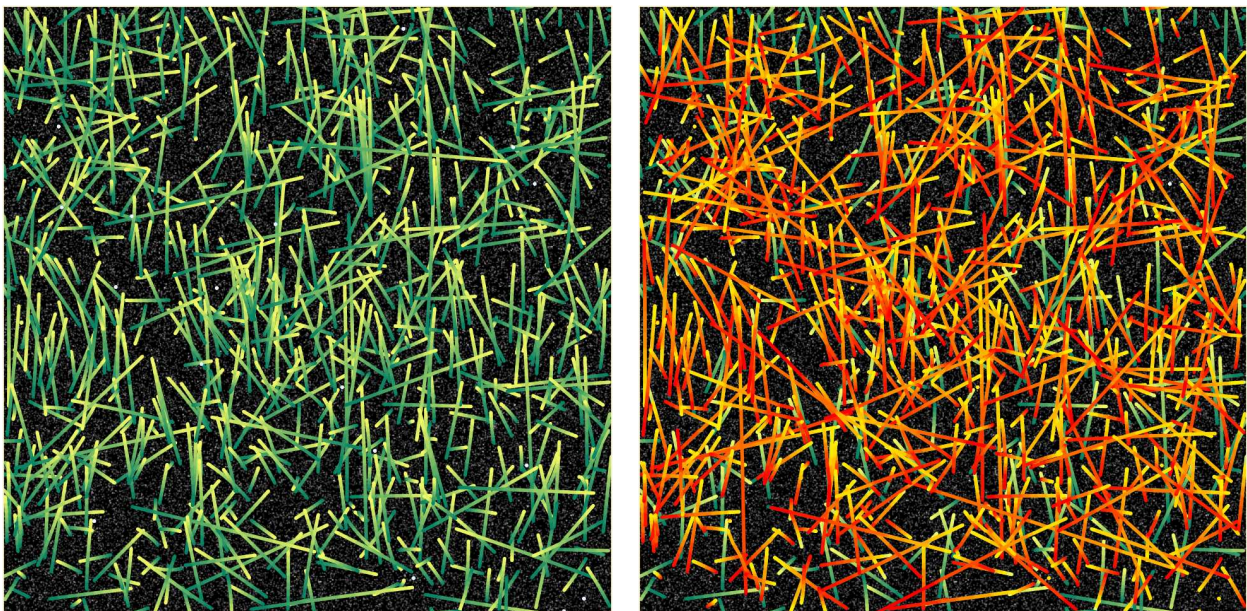


Figure 2.1: Comparison between an exemplary set of simulated (yellow to green gradient) and recovered (yellow to red gradient) tracks. Even though it seems as if many simulated tracks were not recovered, this is actually not the case. Most (if not all) of these simulated tracks consist of too few detections to be accepted as a track, either because they have high miss-rates, or because they have partially left the field of view. There are also a few simulated stars in the image, but because in this instance no camera motion was added, they are stationary and appear as small white dots in the image on the left (not to be confused with the noise in the background image, which is only generated to vaguely imitate proper master images and to give an idea about the detection density; it is not used for detection or tracking). But despite their static nature, the algorithm still managed to find them.

they nevertheless need to be categorized. Here are some of them (see also Fig. 2.2):

- (a) *One or more detections of the simulated track are missing from the recovered track.* This is still fairly easy to solve by for example calculating the percentage of missing detections and reporting it as a recovery rate.
- (b) *The recovered track includes unrelated detections from other tracks or noise.* This is already more complicated depending on the degree of contamination. If only a few detections are unrelated, it may be handled like case (a), but otherwise it is difficult (cases (d) and (e)).
- (c) *Same as case (b), but this time, the replaced detections were not simulated.* Was the simulated track completely recovered? Basically yes, because all of its detections are part of the same recovered track; and yet the recovered track is not correct. Does that make it better or worse than case (b)?
- (d) *The simulated track is shared (in equal parts) by two (or multiple) recovered tracks.* This can for example happen when the algorithm stops to pursue a track at some point because it cannot find any subsequent detections, but later-on starts a new track with the missing detections. Is it fair to say that the simulated track was recovered? Or maybe only part of it?
- (e) *The recovered track consists of (two equal parts of) different simulated tracks.* This may be easier to solve than case (d) by claiming that at least one of the simulated tracks was recovered (although incorrectly).

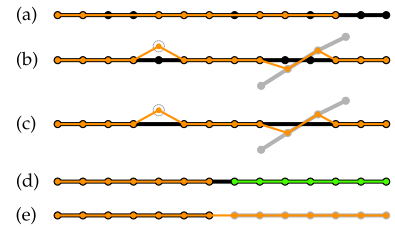


Figure 2.2: Different classes of track recovery from simulations. The black and gray lines and dots represent two simulated tracks and their detections, the dashed circles represent the simulated noise, and the orange and green lines and dots represent two recovered tracks and their detections.

Another aspect to consider about incorporated, unrelated detections might also be how strongly they affect the properties of a track. Some might only slightly change its general course, while others, particularly in case (e), might notably redirect it or alter its speed and acceleration.

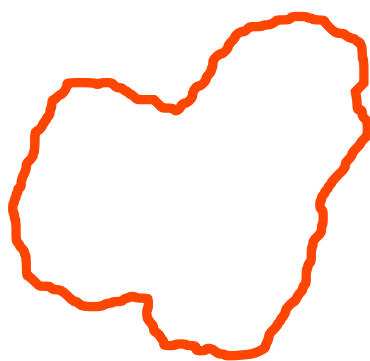
Technically however, all these cases are solvable in so far as they only require clear definitions. But because it would have taken significant time and effort to come up with meaningful definitions, implement the corresponding decision tree, and create the routine that matches simulated and recovered tracks, we ultimately decided to focus on the tracking of simulated noise only.

Still, being able to compare and match tracks like this would also be very useful when comparing results from different tracking runs on real data. It would for example allow us to determine which tracks were only found with a certain tracking parameter set, and help us to identify strengths and weaknesses of said parameters. And although when assessing the results from a particular tracking run on real data, there is no objective truth to compare them against, being aware of these different cases can still be beneficial for manual evaluation.

Finally, with the real data, there is also another possibility to consider: the particles might lose matter, be it via outgassing or because of solid material that is breaking off. While outgassing may be less of an issue, material breaking off can be reason for an identity crisis. Shedding small bits and pieces is likely fine, but if the particle breaks in two (or more) roughly equal parts, which one should the tracking algorithm continue to follow? Even multiple hypothesis tracking would not help in this regard, since in the end, there can only be one valid track: allowing for detections to be shared among tracks would open the floodgates and drown any

genuine particle tracks in a sea of imposters. So far however, I also haven't seen any evidence in my data of particles breaking apart (or of particles colliding for that matter). Such events are likely incredibly rare, but they would also be exciting to find and might even help to better understand the particle's composition and structure. Coming up with a solution to this problem may therefore be worthwhile.

THE METHODS PAPER



PREAMBLE

IN my first paper, “Dynamics and potential origins of decimeter-sized particles around comet 67P/Churyumov-Gerasimenko” (which in this dissertation is called the “methods paper” for convenience), I introduce and explain the functionality of our particle tracking algorithm. The methods paper is now presented unaltered and in full (as it was published in the journal *Astronomy & Astrophysics*) following the layout described in the Preface. Each page of the original paper is reprinted on the right side of a double-page and augmented by in-situ discussions on the left side to provide additional information. Because it is currently not possible to include pdf pages with working hyperlinks in a \LaTeX -document, I manually added all hyperlinks back into the methods paper (except for those found in its bibliography). Citations within the digital version of this document therefore redirect to the bibliography at the end of the dissertation.

* * *

Contribution disclosure

I wrote the entire methods paper except for parts its introduction, which were formulated by Jessica Agarwal, and created all its figures. The tracking algorithm was entirely written by myself and developed and analyzed under the advice of Jessica Agarwal and Matthias Schröter.

PART CONTENTS

Preamble	49
The Methods Paper	50
Introduction	51
Data	53
Tracking algorithm	57
Parameter optimization	67
Results and discussion	71
Summary and outlook	77
Appendix	81
Additional Thoughts	83
The Detection Threshold	83
More on Quality Control	85
Last Words on Simulations	87

4

Factors that influence the appearance of a PSF are for example (Gábor Kovács, priv. com.): the filter (the blob becomes larger with longer wavelengths), the location on the CCD (the blob becomes larger toward the sides), or the spacecraft movements (the blob becomes slightly larger or elongated).

In theory, point sources are infinitely small sources of light, but in reality, they do not exist. So in practice, point sources are radiating (or reflecting) objects that are too small or too far away from the observer to be resolved. A typical example are stars. In optical systems however (like our eyes, telescopes, cameras, etc.), such point sources do not appear as tiny dots, but as small, spread-out blobs. On CCDs for example, the images of point sources often occupy several pixels in radius. Their exact appearance is determined by the so-called point spread function (PSF).

The PSF not only depends on the optical system and its imperfections, but is also a consequence of the wavelike behavior of light: while a flawed optical system can blur or distort the image of a point source, due to the diffraction of the light with the aperture, even a perfect optical system can also only focus the point source down to a certain size—the so-called Airy disk (Airy 1835). Because modeling the PSF for a specific optical system can be very difficult and depends on a lot of factors, the central peak of the diffraction pattern is often approximated by a 2D Gaussian. In case of OSIRIS/NAC, the fitted 2D Gaussian has a standard deviation of roughly one pixel (see Fig. 4.1).

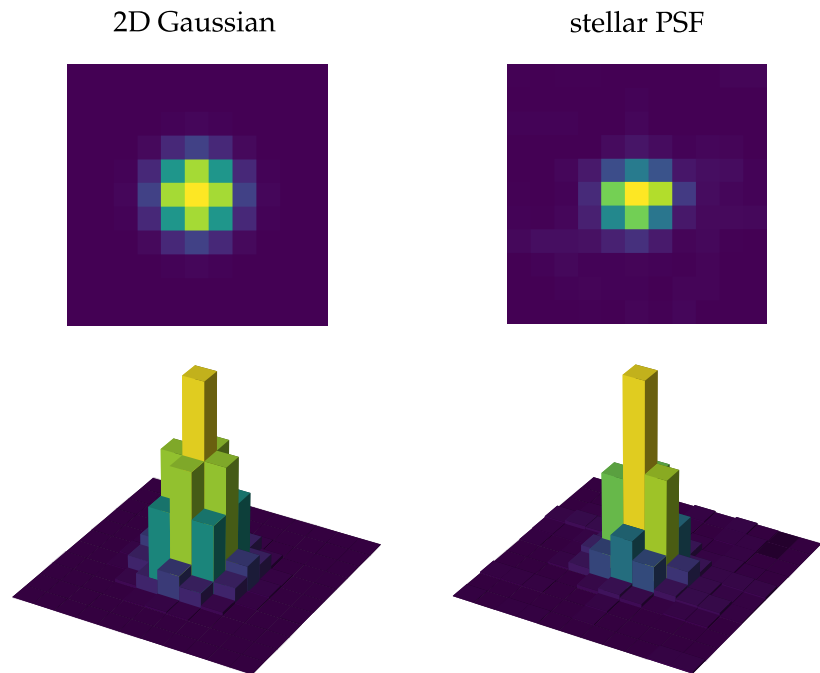


Figure 4.1: Comparison between a 2D Gaussian ($\sigma = 1$ px) and the PSF of a star detected in one of the images OSIRIS images that we used. The top row shows the “top” view (i. e., the image plane), the bottom row the same data represented as a 3D histogram.

As I explain in Section 1.3.3, the formation process of comets has not yet been solved. There is however no doubt that once the comet has reached a certain size, the formation process is dominated by gravity. Since the smooth areas consist mostly of ejected material that fell back onto the nucleus, but that can clearly be distinguished from consolidated terrain, the consolidated material likely underwent additional processing after it was gravitationally bound to the nucleus during its formation.

On the trail of a comet's tail: A particle tracking algorithm for comet 67P/Churyumov-Gerasimenko

Marius Pfeifer¹, Jessica Agarwal^{1,2}, and Matthias Schröter³

¹ Max Planck Institute for Solar System Research, Justus-von-Liebig-Weg 3, 37077 Göttingen, Germany
e-mail: pfeifer@mps.mpg.de

² Institute for Geophysics and Extraterrestrial Physics, TU Braunschweig, Mendelssohnstraße 3, 38106 Braunschweig, Germany

³ Max Planck Institute for Dynamics and Self-Organization, Am Faßberg 17, 37077 Göttingen, Germany

Received 2 August 2021 / Accepted 9 December 2021

ABSTRACT

Context. During the post-perihelion phase of the European Space Agency's Rosetta mission to comet 67P, the Optical, Spectroscopic, and Infrared Remote Imaging System on board the spacecraft took numerous image sequences of the near-nucleus coma, with many showing the motion of individual pieces of debris ejected from active surface areas into space.

Aims. We aim to track the motion of individual particles in these image sequences and derive their projected velocities and accelerations. This should help us to constrain their point of origin on the surface, understand the forces that influence their dynamics in the inner coma, and predict whether they will fall back to the surface or escape to interplanetary space.

Methods. We have developed an algorithm that tracks the motion of particles appearing as **point sources** in image sequences. Our algorithm employs a point source detection software to locate the particles and then exploits the image sequences' pair-nature to reconstruct the particle tracks and derive the projected velocities and accelerations. We also constrained the particle size from their brightness.

Results. Our algorithm identified 2268 tracks in a sample image sequence. Manual inspection not only found that 1187 (~52%) of them are likely genuine, but in combination with runs on simulated data it also revealed a simple criterion related to the completeness of a track to single out a large subset of the genuine tracks without the need for manual intervention. A tentative analysis of a small ($n = 89$) group of particles exemplifies how our data can be used, and provides first results on the particles' velocity, acceleration, and radius distributions, which agree with previous work.

Key words. comets: general – comets: individual: 67P/Churyumov-Gerasimenko – zodiacal dust

1. Introduction

Comets are relatively well-preserved remnant building blocks of our planets. Their interiors may provide us with clues about planetesimal formation and the composition of the outer solar nebula. One of the key quantities relevant in this context is the relative abundance of refractories and volatiles inside the cometary nucleus, often referred to as the refractory-to-ice (mass) ratio.

This ratio cannot be measured directly with current spacecraft or remote observation techniques. An alternative is to determine it indirectly by measuring the dust-to-gas (mass) ratio of the material that was released from the nucleus into interplanetary space. This technique however comes with caveats. For one, estimating the lost dust mass relies on models that require knowledge of or assumptions about the dust size distribution and either optical properties (for remote sensing data) or spatial distribution (for in situ data).

Then, translating the dust-to-gas to the refractory-to-ice ratio is not straightforward. Part of the refractory material is contained in blocks that are too heavy to be accelerated past the comet's escape speed, and so they never leave the nucleus or fall back onto its surface (Choukroun et al. 2020). The blocks' volatiles on the other hand may have escaped entirely. Based on the coma dust-to-gas ratio, the refractory-to-ice ratio would thus be underestimated. Meanwhile, investigation of the surface would tend to overestimate it because of the refractory deposits.

Such deposits may also quench the nucleus' outgassing (e.g., Gundlach & Blum 2016), while ejected material may be outgassing too (Reach et al. 2009), making the translation to the refractory-to-ice ratio more complicated. Both issues would be better understood with a firmer grasp of the material's dynamics.

The European Space Agency's Rosetta mission to comet 67P/Churyumov-Gerasimenko has revealed that fall-back of refractory material is a common phenomenon, as wide parts of 67P's surface are uniformly covered in loose material (Thomas et al. 2015). Images obtained during the final descents of both the lander Philae (Mottola et al. 2015; Pajola et al. 2016) and the Rosetta orbiter (Pajola et al. 2017) show the ground coated in a loose assembly of irregularly shaped blocks with typical sizes down to the centimeter-scale resolution limit of the images. Compared to the consolidated terrains thought to be more representative of the comet's "bedrock", from further out, **these areas look relatively smooth.**

Smooth terrains are predominantly found in the northern hemisphere (Thomas et al. 2015). This regional distribution of fall-back material is likely related to the asymmetric seasons on 67P, with short (~1 yr), hot perihelion summers in the southern hemisphere and long (~5.5 yr), yet colder aphelion summers in the north (Keller et al. 2015). Pajola et al. (2017) have plausibly modeled the inter-region transport of fall-back material driven by the differences in local gas pressure due to varying solar irradiation. They showed that debris should be carried from regions

In this context, it would have been better to for example cite Schröder et al. (2023) instead of Westerweel et al. (2013), because the latter give an overview that is more focused on the developments in particle image velocimetry (PIV), which is a statistical approach where no individual particles are tracked, while the former focuses more Lagrangian particle tracking (LPT) and particle tracking velocimetry (PTV), which are much closer related to our application. For a more detailed discussion of other tracking applications see Chapter 2.

Likely the only other study that is missing from this list is that of Cremonese et al. (2016), who also developed a semi-automatic algorithm to detect elongated particle trails in image pairs. Their approach is based on Laplace filtering (i. e., edge detection; e. g., Burger et al. 2009), and they identified 70 particle tracks in 6 image pairs. Additionally, since the methods paper was published, there is now also the work by Lemos et al. (2023) and Lemos et al. (2024), who used the technique of Frattin et al. (2021) to identify over 30 000 particle trails in 189 OSIRIS images, the work of Shi et al. (2024), who (manually) studied the dynamics of boulder clusters, and Moretto et al. (2023), who announced another method for tracking dust particles around comet 67P similar to our approach (see also Chap. 2).

of high gas pressure to regions where gas pressure is too low to keep the material afloat. [Lai et al. \(2016\)](#) have followed a more global approach studying the trajectories of dust particles embedded in a 3D Direct Simulation Monte Carlo model, and found that regional change in dust mantle thickness can be on the meter-scale.

For such models, it is mandatory to have good knowledge of the debris' source distribution, (i.e., its production rate as a function of time and surface region), and the constituents' initial velocities and accelerations. But accelerations can also provide information about the ice content of larger chunks, because sublimating ice may manifest as an acceleration component toward the antisolar direction ([Kelley et al. 2013, 2015](#); [Agarwal et al. 2016](#)).

To learn more about these factors, [Agarwal et al. \(2016\)](#) manually tracked 238 decimeter-sized particles in an image sequence obtained by the Optical, Spectroscopic, and Infrared Remote Imaging System (OSIRIS) on January 6, 2016. Of the particles whose projected velocities were measured, at least 10% were faster than the local escape speed of the nucleus; hence they likely reached interplanetary space, contributing to the comet's debris trail (e.g., [Sykes & Walker 1992](#)). [Keller et al. \(2017\)](#) estimated that of the remaining 90%, at least 20% fell back to the surface within several hours, possibly accumulating in a regional layer of debris that still contains some water ice.

Other studies that looked for ejected debris in OSIRIS images also did so manually, or mostly by making use of the elongated particle trails in long-exposure images: [Bertini et al. \(2015\)](#) searched for satellites near 67P using the SExtractor software ([Bertin & Arnouts 1996](#)), but found no unambiguous candidates. A moon (dubbed “churymoon”) was later discovered visually by [Roger \(2019\)](#), and in the following tracked by [Marín-Yaseli de la Parra et al. \(2020\)](#) using TrackMate ([Tinevez et al. 2017](#)). [Rotundi et al. \(2015\)](#) and [Fulle et al. \(2016\)](#) manually identified ~400 and 204 particles respectively using image differencing. [Davidsson et al. \(2015\)](#) detected, manually tracked, and determined the orbital elements of four particles. [Ott et al. \(2016\)](#) developed an algorithm to detect elongated particle trails based on Canny edge detection ([Canny 1986](#)) and Hough transformation ([Hough 1959](#)), and used it to measure 262 particles ([Drolshagen et al. 2017](#); [Ott et al. 2017](#)). [Güttler et al. \(2017\)](#) used the blurriness of defocussed particles—instead of the parallax effect used in most of the previous studies—to derive the properties of 109 particles semi-automatically. Finally, [Fratin et al. \(2017\)](#) developed an automated detection method based on line-shaped matching functions to detect elongated particle trails, and identified 1925 tracks (and again 1916 tracks in [Fratin et al. 2021](#)). No algorithm however has been developed for OSIRIS images to automatically track point-source-like particles.

During the post-perihelion phase of the mission, OSIRIS has regularly obtained image sequences like the one analyzed by [Agarwal et al. \(2016\)](#). Many of them show fountains of debris that seem to stem from locally confined sources. Exploiting the sequences' very specific properties, we have created a tool that can automatically detect and track the motion of the point-source-like debris.

Instead of tracing particle tracks manually on a stacked image sequence as performed by [Agarwal et al. \(2016\)](#), our algorithm first examines each image individually before recovering tracks from the gathered data. Because the particles scatter sunlight but are not spatially resolved, they appear as point sources in the images, which already distinguishes them from most other features. Nevertheless we further clean the images to improve

their signal-to-noise ratio and then use the SExtractor software ([Bertin & Arnouts 1996](#)) to detect them. Once located, their positions are passed on to the core of our project, the tracking algorithm. Here, we exploit the dataset's pair-nature to reconstruct the particle motions.

Our work presents a **new approach** in the large field of particle tracking (for other disciplines see e.g., [Westerweel et al. 2013](#); [Chenouard et al. 2014](#); [Ulman et al. 2017](#); [Rose et al. 2020](#)). In astronomy, tracking algorithms were developed to discover small Solar System bodies (SSSBs) in large-scale sky surveys, such as: Spacewatch (MODP, [Rabinowitz 1991](#)); CFHT, SKADS, OSSOS (MOP, [Petit et al. 2004](#); [Gladman et al. 2009](#); [Bannister et al. 2016](#)); Pan-STARRS, LSST (MOPS, [Kubica et al. 2007](#); [Denneau et al. 2013](#); [Jones et al. 2018](#)); (NEO)WISE (WMOPS [Mainzer et al. 2011](#)); PTF (PTF MOPS, [Waszczak et al. 2013](#)); and ZTF (ZMODE, [Masci et al. 2018](#)). Recently, also more general-purpose SSSB discovery engines have been developed, such as HelioLinC ([Holman et al. 2018](#)), THOR ([Moeyens et al. 2021](#)), or tracee ([Ohsawa 2021](#)). All these algorithms were however mostly designed for Earth-based observations of SSSBs, where the object density is low, the apparent speed small, and the motion near linear (as pointed out by [Liounis et al. 2020](#)). They are therefore not very well suited for the dense and more dynamic dust environment in the coma of 67P.

Much closer related to our project are the methods for particle tracking around asteroid (101955) Bennu, which were developed in parallel to our own algorithm and recently published by the OSIRIS-REx team (see [Hergenrother et al. 2020](#) for an overview of the special issue). Following the discovery of Bennu's activity ([Hergenrother et al. 2019](#); [Lauretta et al. 2019](#)), [Liounis et al. \(2020\)](#) developed a dedicated algorithm to detect and track the ejected material. [Pelgrift et al. \(2020\)](#), [Leonard et al. \(2020\)](#), and [Chesley et al. \(2020\)](#) then estimated the trajectories and orbits of the identified particles and traced them back onto the surface of Bennu to reconstruct the ejection events.

In this paper we describe our methodology in detail and apply it to the same image sequence analyzed by [Agarwal et al. \(2016\)](#). Because our algorithm can detect much fainter tracks, we find more than three times as many tracks than the manual procedure and hence significantly improve the statistics.

The data and image processing are described in Sect. 2. The tracking algorithm is described in Sect. 3, and the parameter optimization in Sect. 4. In Sect. 5, we evaluate the performance of the algorithm and present initial scientific results. Our findings are summarized in Sect. 6. The entire project is written in the Python programming language version 3.7.7 ([Van Rossum & Drake 1995](#)) and we are happy to provide access to the code on request.

2. Data

The source material for our tracking algorithm are the previously discussed image sequences recorded by OSIRIS' Narrow Angle Camera (NAC) on board the Rosetta spacecraft (for NAC specifications see Table 1 and [Keller et al. 2007](#)). The sequences typically show (parts of) 67P's nucleus and coma from ~20–400 km distance, and share a characteristic that is essential for our tracking algorithm: their images were recorded in pairs with the time interval between pairs being much longer than the intra-pair cadence (see Sect. 3.1).

We refer to the image sequence that we exemplarily analyze in the following as STP090. It was obtained with NAC on

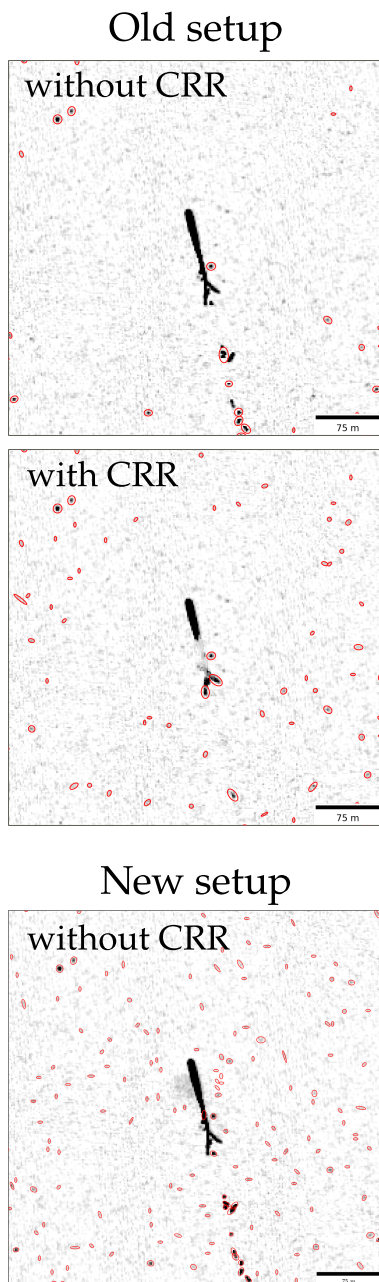


Figure 4.3: Close-ups of the area around the large cosmic ray hit discussed in Fig. 4.2 (top and bottom) showing the effect of different detection set-ups (detections indicated by red ellipses).

Technically, because the first nine pixel columns on the left and the last three on the right side of the NAC CCD were dead, the width of the images is twelve pixels shorter (in our orientation anyways), reducing the resolution to only $2036 \text{ px} \times 2048 \text{ px}$.

Even though the sharp intensity spikes caused by cosmic ray hits do not resemble the brightness profiles of point sources and therefore should not get picked up by the detector, we found that they can still affect the detection process. Since we estimate the background signal locally, particularly numerous, bright, or extensive cosmic ray hits can lead us to overestimate the background signal of the section they reside in—so much so that when we remove the background signal, we also discard enough of the point source signal that our detection algorithm failed to pick them up (see Fig. 4.2). I thus implemented the option to remove cosmic ray hits prior to the background removal, making use of the Astro-SCRAPPY Python package (McCully et al. 2018) that is based on the Laplacian cosmic ray identification by Van Dokkum (2001).

But during test runs, it turned out that we were not able to calibrate the tool in a way that would produce satisfying results. Not only were particularly protruding features not fully removed (see Fig. 4.3), but more importantly, a significant number of point sources were mistakenly removed instead. Eventually, we decided to make the local background mesh several times finer, and set up our detection algorithm to be more sensitive to point sources. This significantly reduced the impact of cosmic ray hits. The few additional spurious detections due to cosmic ray hits are also dwarfed by the number of detections caused by residual background noise and other artifacts, and have virtually no effect on the tracking results. This was later also confirmed by tracking tests using simulations. We hence decided against removing any cosmic ray hits.

There may however still be a way of dealing with them, assuming that the detection algorithm generally doesn't pick up many cosmic ray hits (particularly the disturbing bright ones): the detection algorithm also produces a segmentation map where all the extracted pixels are marked. So after running it once, this map could then be fed into the cosmic ray detection algorithm to stop it from removing point sources. Afterwards, the detection algorithm can be run properly. But for this to have a noticeable effect, the cosmic ray detection of course also has to work well.

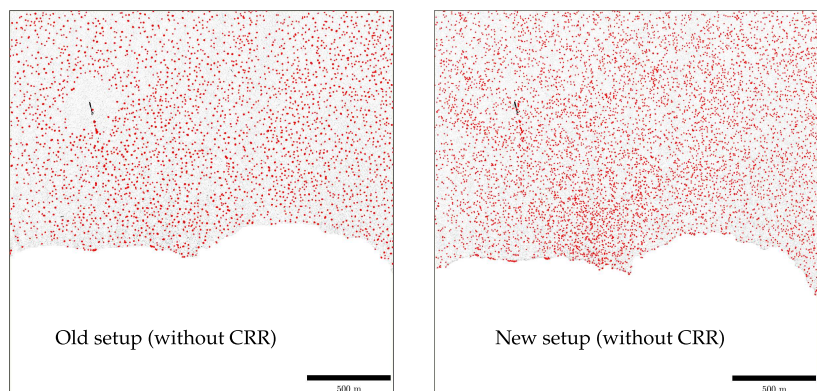
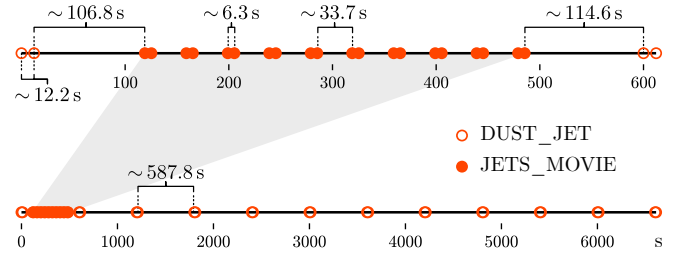
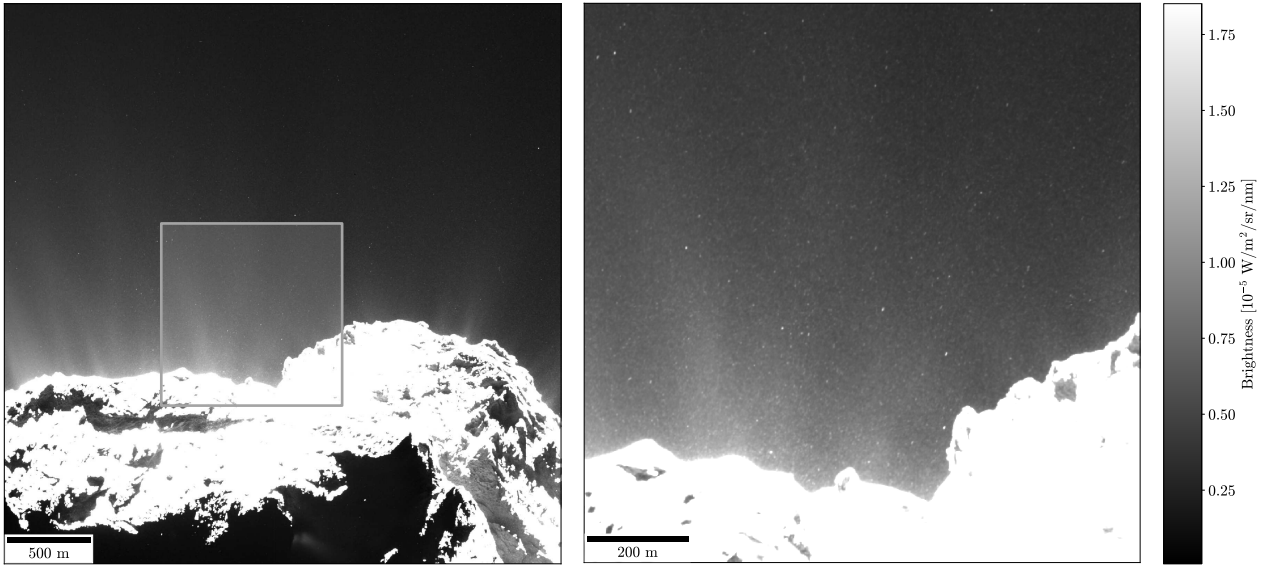


Figure 4.2: Comparison of detection results (red spots) highlighting the potential effect of cosmic ray hits. In both cases, no cosmic ray removal (CRR) was performed. While in the left case, the cosmic ray hit clearly prevented detections in its vicinity, in the right case, its impact is significantly reduced, due to the finer background mesh and the more sensitive detection process.

Table 1. Mission details for sequence STP090.

Date of recording	January 6, 2016
Time of recording	UT 07:01:03–UT 08:51:15
Total duration	1 h 50 min 11 s
Heliocentric distance	~2.06 AU
Nucleocentric distance	~86 km
Camera	OSIRIS NAC
Field of view (FOV)	$2.208^\circ \times 2.208^\circ$
CCD resolution	2048×2048 px $\sim 3.3 \times 3.3$ km
Pixel resolution	18.6×18.6 μ rd $\sim 1.6 \times 1.6$ m
Filter (NAC F22)	center: 649.2 nm, bandwidth: 85 nm


Fig. 1. Timeline of image sequence STP090. The sequence was constructed from the two subsequences “JETS_MOVIE” (20 images, principal sequence) and “DUST_JET” (24 images, extended sequence). The whole sequence spans almost two hours. Due to the alternating time intervals between recordings, the images come in pairs.

Fig. 2. One of the source images of STP090. It showcases the appearance of dust particles as small point sources, as well as the bright surface of the irradiated nucleus and its radiant features. Full image on the left, close-up of central region on the right (contrast enhanced for visibility).

January 6, 2016, starting from UT 07:01:03 when Rosetta was ~86 km away from the nucleus, and 67P was at a heliocentric distance of ~2.06 AU post-perihelion. We constructed STP090 from two sub-sequences, a short and a long one. The short sequence (OSIRIS activity tag “JETS_MOVIE”) consists of 20 images and covers roughly six minutes, while the long sequence (OSIRIS activity tag “DUST_JET”) contains 24 images and spans almost two hours, starting roughly two minutes before the short one (see Fig. 1). While the exposure time for the short sequence is constant at 0.24 s, it alternates between 0.24 and 6 s for the long one. In the following we refer to the short and long one as the principal and extended sequences respectively, a distinction that becomes clearer in Sect. 3.3. The relevant mission details are summarized in Table 1.

We use OSIRIS images of calibration level 3E (Committee on Data Management, Archiving, and Computing, CODMAC, level 4), which includes solar and in-field stray-light correction, radiometric calibration and geometric distortion correction¹ (Tubiana et al. 2015). The pixel values of this level are provided in radiance units ($\text{W m}^{-2} \text{sr}^{-1} \text{nm}^{-1}$).

¹ The data are available at the Planetary Science Archive of the European Space Agency under <https://www.cosmos.esa.int/web/psa/rosetta>

At this “raw” stage, it is already possible to see some of the brighter particles (see Fig. 2). To also detect fainter particles however and track their motion, the images are first cleaned before the point source coordinates are extracted (see Sect. 2.2).

2.1. Image cleaning

To optimize particle detection, we aim to minimize signals not associated with point sources. Of those, we identify three types: (1) ambient background noise that stems from the diffuse coma and bright, roughly cone-shaped dust streams radiating from the nucleus (in the following called radiant features, Fig. 2); (2) prints of cosmic ray hits; and (3) the nucleus itself. While cosmic ray hits may confuse the point source detector occasionally, we found that due to their small number, they do not significantly affect the tracking results. The background noise and the nucleus however need to be removed.

The diffuse coma signal is determined by the background estimator from the library for Source Extraction and Photometry (SEP, Barbary 2016; Bertin & Arnouts 1996; Stetson 1987). It subdivides an image into a grid of rectangular sections, calculates the background locally for each (with the help of iterative κ - σ -clipping and mode estimation), and merges the resulting background patches smoothly back together (via natural bicubic spline interpolation) to form the global background map. This

Because the background subtraction is an essential step of our particle tracking routine, I wanted to understand exactly how it works, especially because we use a third-party tool (a luxurious endeavor that I unfortunately could not afford throughout my whole PhD project). The original paper that introduced the Source Extractor (SExtractor) software (Bertin et al. 1996), as well as its documentation were however not always very clear. And while I failed to reach the original authors, I was luckily able to talk to Kyle Barbary (the author of the SEP Python package, Barbary 2016), Benne Holwerda (the author of the SExtractor guide), and Peter Stetson (the author of the DAOPHOT program which the background estimator is based on, Stetson 1987), who were extremely helpful.

Pearson (1895), who coined the term “mode”, might have chosen it because he may have been familiar with the French expression «à la mode», meaning fashionable, or that which is most popular (George Udny Yule 1911; Codogno 2013). Conversely, when visualizing the frequency-distribution of the dataset, the clipping always reminded me of a bowl-cut.

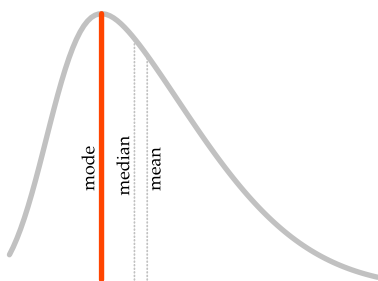


Figure 4.4: Relation between mode, median, and mean in case of a skew-normal distribution.

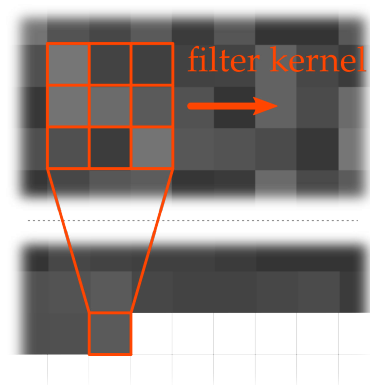


Figure 4.5: Application of a median filter with a 3×3 -kernel. Input image on the top, filtered image below.

In the following comments I refer to it as the master image, which is the term that I also use in the science paper. Because most tracks are easy to spot on this image, it is essential for the tracking assessment, whereas the algorithm works much better with the individual images.

In the hopes that it may be helpful to somebody else, here is a more detailed description of how the background signal is estimated:

Subdivision: The source image is divided into subsections starting from its origin (i. e., the $(0, 0)$ -position of the pixel matrix, typically the top left corner). To better fit the image’s (background) structure, the number and aspect ratio of the sections can be adjusted.

Iteration: Each section is assigned a single background value valid for all the pixels it contains. The value is determined iteratively with the help of κ - σ -clipping and mode estimation, an approach based on Stetson (1987)’s algorithm for crowded-field stellar photometry (see also Da Costa 1992). Kappa-sigma-clipping is a technique where the ends of a sorted dataset—in our case the pixel values of a section—are trimmed to a limit around a central value—in our case the median. The limit is a multiple (κ) of the standard deviation (σ).

The mode marks the most frequently occurring value in a dataset, or the highest peak of a distribution. In a symmetrical distribution, it coincides with both median and mean, but this is rarely the case with the pixel data of an astronomical image. Pearson (1895) observed that for such skewed distributions (see Fig 4.4), the mode can be estimated via

$$\text{mode} = 3 \times \text{median} - 2 \times \text{mean},$$

which Bertin et al. (1996) adapted for their datasets as

$$\text{mode} = 2.5 \times \text{median} - 1.5 \times \text{mean}.$$

The iterative process then works as follows: (1) check if all pixel values of a section lie within $\pm 3\sigma$ around their median. If so, use the mode as the section’s background. If not, (2) remove the excess values outside $\pm 3\sigma$ and repeat step (1) with the clipped dataset, unless the new σ varied by less than 20%. In that case, use the new mean as the background instead.

Choosing the mode as a background estimator has the benefit that “it is itself a maximum-likelihood estimator—it represents the most probable value of the brightness of a randomly chosen pixel in that part of the image” (Stetson 1987). Bertin et al. (1996) opt for the mean only if the field is uncrowded, that is, if the image section contains only few distinct light sources. They argue that in that case, the mean is the more reliable estimator. Bertin et al. (1996) may have chosen the 20%-criterion as the condition for the switch since bright features typically lie far from the median and are thus clipped off during the iteration. But if they are only few, clipping them off will only have a small effect on σ .

Assembly: To form the background of the whole image, the local background tiles are assembled and potentially subjected to a median filter. The median filter is a method to adjust the brightness levels of adjacent background tiles (see Fig. 4.5): Each tile is assigned the median brightness of a tile subset that includes the tile itself and some of its neighbors, which are determined by a distinct pattern that slides across the tile array, the so-called (filter) kernel (e. g., Burger et al. 2009). Finally, a (natural) bicubic-spline interpolation (which I cannot explain here) is applied on the pixel scale to smooth out the tile transitions even further.

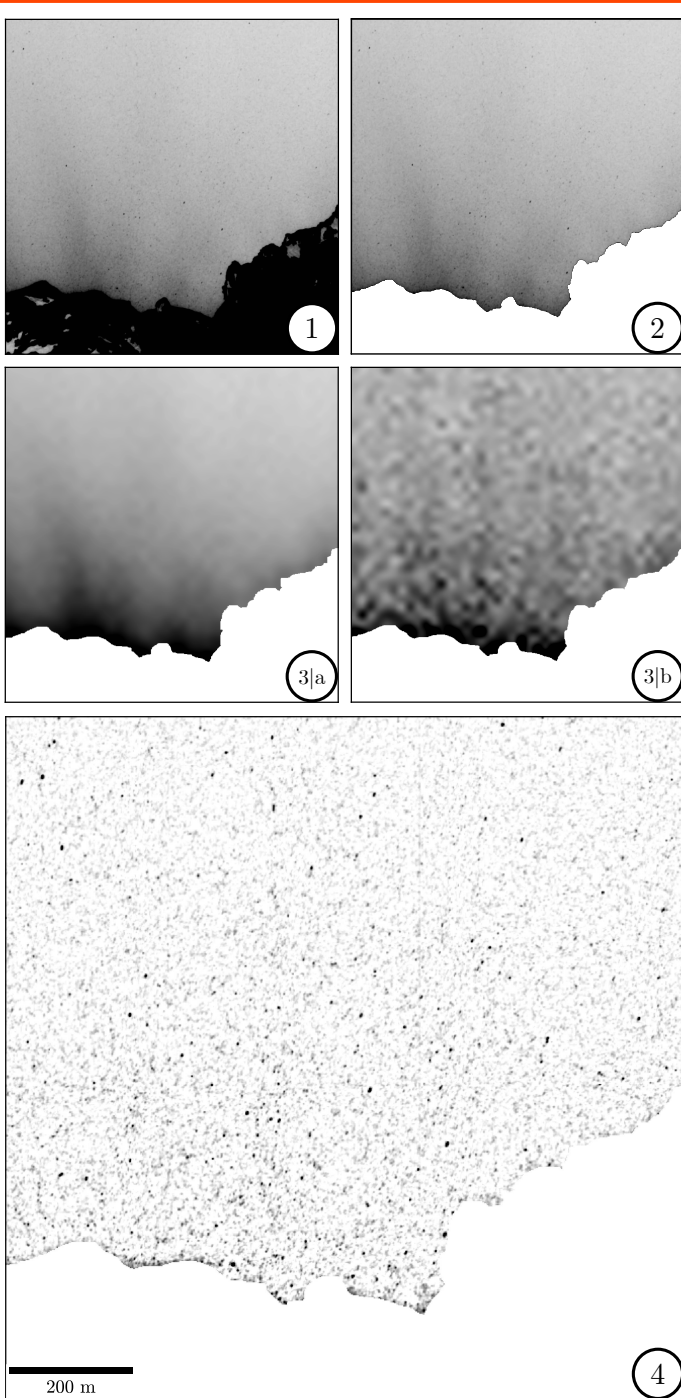


Fig. 3. Illustration of the cleaning pipeline: (1) the unaltered source image (OSIRIS level 3E); (2) the masked-out nucleus; (3) the estimated background level (a) and the corresponding RMS map of the background-subtracted image (b); (4) the background- and nucleus-subtracted image predominated by dust particles. All images show the same central region indicated in Fig. 2 and are brightness-inverted for better reading.

approach has the advantage that it can account for medium-scale changes in the background level—such as radiant features—and is therefore generally well-suited for our datasets (Fig. 3).

The bright nucleus on the other hand poses an issue for the background estimation. For sections at its limb that include both nucleus and coma the background level would be overestimated. To prevent this, we mask out the entire nucleus using its approxi-

mate shape retrieved from the OSIRIS level 4S (CODMAC level 5) georeferencing layers, and subsequently refine the mask with the help of edge-detection algorithms. The shape is then passed on to the background estimator which ignores the masked area during processing. Because particle detection is not possible in front of the illuminated surface, by removing the nucleus we only lose information of particles that appear in front shadowed regions.

The background estimation also renders a root mean square (RMS) map. It is calculated in a similar fashion as the background signal, where the RMS values are first determined locally, before being smoothed out to form the global map. Since the RMS map is calculated from the background-subtracted image, it gives us an idea about the remaining random noise. This information is used during the point source detection.

With the nucleus and background removed, the images are predominated by the signal of dust particles. We call the remaining area that still contains data the dust field.

Lastly, the processed images are stacked by selecting the maximum value that each pixel assumed over the sequence (see Fig. 4). Unlike Agarwal et al. (2016) however, we do not use this stacked image to track the particles, but instead only as a visual aid to check the tracking results and identify sidereal objects.

2.2. Point source detection

The particles are detected with the help of the SEP software (Barbary 2016; Bertin & Arnouts 1996). It employs a thresholding approach based on Lutz (1980)'s one-pass algorithm that can be used to identify point sources. Only pixels whose values are above the local RMS level (see Fig. 3) multiplied by some user-defined detection threshold are considered during the detection process.

The algorithm then extracts sources based on the number of contiguous pixels, which are later-on deblended (using their brightness topology, Beard et al. 1990) to separate neighboring point sources that have been extracted together. The resulting dataset can additionally be “cleaned”, meaning it is checked whether each source would have also been detected without its neighbors being present. In the following we call identified sources detections, and the entirety of all sources detected in a single image a detection set. Figure 5 shows a sample of such a set.

3. Tracking algorithm

In the following we assume an image sequence comprised of N images recorded at times t_n ($n \in \{0, 1, \dots, N-1\}$), thus containing $N/2$ image pairs. We start by briefly defining key concepts:

- Track and candidate track. Track refers to a collection of detections that are all of the same object and thus depict the object's path through the recorded scene. Candidate track refers to any collection of detections, independent of whether or not they belong to the same object. They are only accepted as tracks once they pass a quality check.

- Pursuit and tracking run. Pursuit refers to the tracking of a single object throughout a dataset, while tracking run describes the exhaustive analysis of an entire dataset, encompassing every possible pursuit for a fixed set of tracking parameters.

- Tracking parameters. Tracking parameters are the parameters that govern the execution of a tracking run and each of its pursuits. They influence for example which detections and detection pairs are considered during a pursuit and define how many of them candidate tracks must contain to be accepted.

Notably, Marschall (2017) also came up with a simple but effective way to detect particles in OSIRIS images.

The detection process is arguably an even more important step of our tracking procedure than the background subtraction, but it is also significantly more complex (in particular the deblending), so my descriptions are mostly qualitative.

SEP also offers the option to apply a matched filter instead of the convolution (Barbary 2016). A matched filter accounts for the individual noise in each pixel (e. g., provided by the RMS map) and maximizes the local signal-to-noise ratio specifically for the used filter kernel (e. g., Pratt 2007). Curiously, we found that neither the regular convolution nor the matched filter yielded the best results, so we skipped this step. They might have failed because our simple particle PSF model does not match the actual PSFs well, or more likely, because the local noise around the PSFs is not Gaussian (see the RMS map in Fig. 4.12), which is required for the matched filter to work (e. g., Vio et al. 2021).

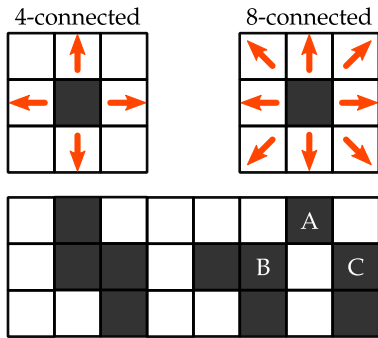


Figure 4.6: Difference between 4- and 8-connectivity. In case of 4-connectivity, only the vertical and horizontal pixel neighbors are considered, while in case of 8-connectivity, the diagonal ones are considered as well. In the example, the left group of pixels would be considered both 4- and 8-connected, while the right group would only be considered 8-connected, made up of the 4-connected groups A, B, and C. Connectivity only dictates how individual pixels must be connected to be considered part of the same group, but not how many pixels a group must at least consist of.

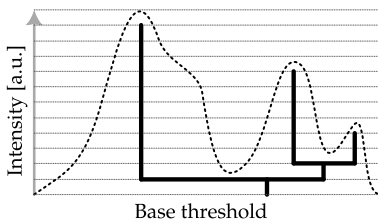


Figure 4.7: Schematic of the deblending tree structure of an extracted pixel group.

Although the SExtractor was designed to identify more conventional sources such as stars and galaxies, it also works well for our particles. Still, Bertin et al. (1996) note that in case of stars, peak finding is more appropriate than their thresholding approach. Potential alternatives to the SExtractor might be astropy's photutils (Bradley et al. 2022), the pspshot program developed for Pan-STARRS data (Magnier et al. 2020), or possibly even DeepSource (Vafaei Sadr et al. 2019), a point source detector based on neural networks. Another interesting option to improve the detection results might have been also the Tractor software (Lang et al. 2016), which uses probability methods to pinpoint light sources in astronomical images. Lastly, the SExtractor now also seems to have received a complete overhaul (Bertin et al. 2020; Kümmel et al. 2020).

Analogous to the previous in-situ discussion of the background subtraction, I briefly expand on some of the detection algorithm's key aspects in the following:

Convolution: Prior to the thresholding, it is possible to enhance the signal of point sources by convolving the background-subtracted image with an appropriate filter kernel. Convolution is a mathematical concept that operates similar to the median filter application in case of image processing (e. g., Burger et al. 2009). But instead of the median, it calculates the weighted sum of the affected pixel values, where the weights are provided by the kernel (in our case, e. g., a discretized PSF or 2D Gaussian, Irwin 1985).

Thresholding: As explained in the methods paper, the threshold is the product of a user-defined factor and an estimate for the noise in each pixel, in our case derived from the root mean square (RMS). Analogous to the background, the RMS is calculated locally for each subsection of the background-subtracted image via

$$\text{RMS} = \sqrt{\frac{1}{n_j} \sum_{i=1}^{n_j} y_i^2},$$

where n_j is the number of pixels in the j th subsection of the image, and y_i is the value of the i th pixel of said section. While the RMS is generally an average similar to the mean or median, in our case it is a good estimate of the remaining noise in the image (if it is not too crowded), since we already removed the background, which should leave only residue noise or signal. So if pixels are significantly brighter than the RMS, chances are that their signal came from a light source.

Detection: The algorithm now scans the image for pixel groups that are above the threshold and are 8-connected (as opposed to, e. g., 4-connected; see Fig 4.6 and e. g., Rosenfeld 1970; Lutz 1980). To count as a detection, a group of 8-connected pixels additionally needs to consist of more than a minimum number of pixels that is specified by the user.

Deblending: Very briefly, for each extracted pixel group, the algorithm calculates a (user-specified) number of intermediate thresholds that are logarithmically spaced between the base threshold of the pixel group and its peak value. Next, it creates a tree-like structure based on the group's brightness profile (see Fig. 4.7), and follows the branches down toward the stump. At each junction it then decides if the traversed branches are bright enough to be extracted as a separate source.

M. Pfeifer et al.: On the trail of a comet's tail: A particle tracking algorithm for comet 67P/Churyumov-Gerasimenko

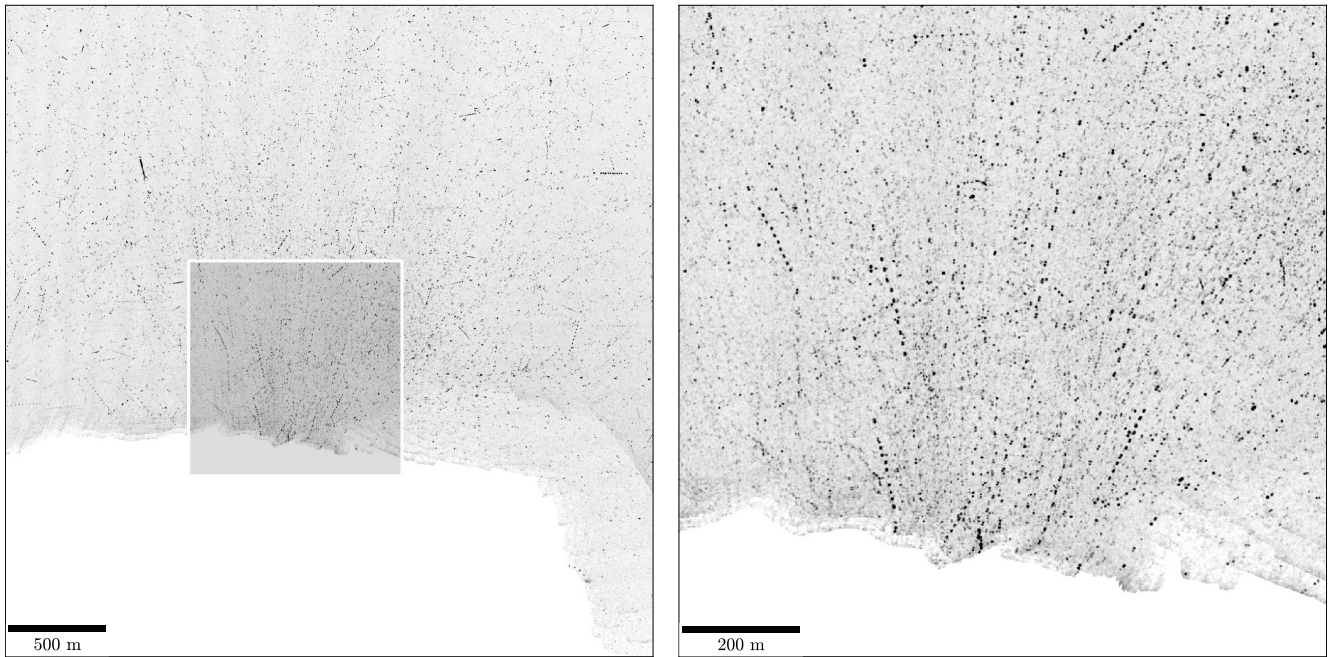


Fig. 4. Stacked image of sequence STP090. It was created by selecting the maximum value for each pixel across the image sequence. Full (brightness-inverted) image on the left, close-up of central region on the right. The stacked image is only used to check the tracking results and identify sidereal objects.

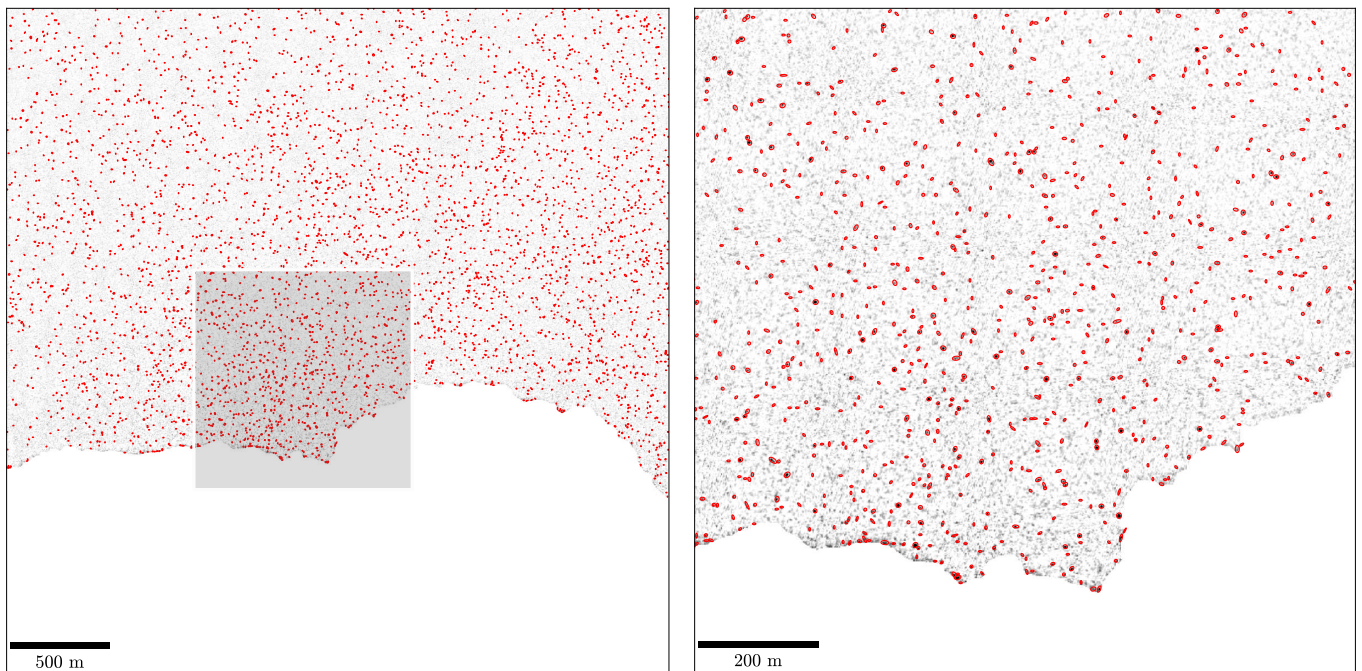


Fig. 5. Sample detection set (red ellipses) from one of the processed images of sequence STP090. Full image on the left, close-up of central region on the right.

3.1. Pair-tracking

A central aspect of our tracking algorithm is the exploit of the image sequences' pair-nature. We assume that during the time interval of an image pair, the particles only travel a short distance (typically no more than a few pixels). This allows us to pair neighboring detections, one from each of the images, and analyze them as a unit: close detections likely belong to the same object. Consequently, our tracking algorithm predominantly operates pairwise, reverting to search for single detections

only when there are no suitable pairs. We call this process pair-tracking.

To create the detection pairs, our algorithm iterates over the detection sets of each image pair. For every detection in the first set, the algorithm looks for detections in the second set within a predefined search radius we call the initial search radius. Each secondary detection found this way then forms a detection pair with the primary detection (see Fig. 9a). Thus, any detection can be part of multiple detection pairs.

Although I didn't directly test this, there is also a technical limit to the initial search radius. Because the detections are roughly homogeneously distributed, the number of possible pairs will grow with R_{init}^2 . But that really means that the number of *spurious* pairs will grow with R_{init}^2 , since a primary detection can only form a single genuine pair at most. Increasing the initial search radius will thus very quickly add a tremendous amount of noise (and along the way also significantly scale up the computation time). Another objective limit to this parameter (and all the others) is of course always how much physical sense they make.

To minimize the bias against very fast particles, this parameter should be maximized. After a certain distance however, it becomes impossible to tell whether two detections belong to the same particle. Hence there is a subjective upper limit to this parameter.

I put this measure into place for several reasons: For one, I believe that accepted tracks should not share any detections, since I assume that at this stage, they are genuine. No shared detections also means not having to decide which of the affected tracks has the best claim to the shared parts, and what to do with the other tracks—two difficult problems to solve. Should the latter be declared spurious and be deleted? Or should they continue to exist, but without the misattributed parts? Of course this introduces a bias by way of “first come first serve”, but it can also be an advantage.

Making these constituents unavailable during subsequent pursuits cleans the parameter space from unrelated detections, which increases the quality of subsequently pursued tracks. I observed this for example when I used very high acceptance thresholds to only allow for the most complete tracks to make it past candidate status. While this resulted in a lower number of recovered tracks, I also expected their overall quality to improve, however the opposite was the case. Because “lower-quality” tracks were not accepted and their constituents therefore not removed, the parameter space was still crowded with unrelated detections, causing the tracking algorithm to go off trail more often. There hence exists a sweet spot for the acceptance threshold that allows for just enough lower-quality tracks and even spurious tracks to make it through so that the parameter space is sufficiently cleaned.

Effectively removing the constituents from their respective pools also has the positive side effect of speeding up the tracking run. Not only are there fewer and fewer candidates available during each subsequent pursuit, but more significantly, the number of potential origins, and thus overall pursuits, is constantly falling.

Lastly, but very importantly, it prevents the algorithm from pursuing and accepting the same track many times, starting only at different origins. Obviously this would be a waste of resources, but more crucially, it would require the removal of duplicate tracks. If any of the duplicates have the slightest variation however (due to missing or incorporating different detections e. g., which can happen depending on the origin and initial tracking direction), this becomes very difficult to solve (see Sect. 2.2).

Accordingly, the tracking process is sequential. I tested the proficiency of parallel tracking in earlier versions, but the results were not convincing. In theory, parallel tracking should be fairer to each individual track, because it is harder for other (spurious) tracks to “steal” their detections. But it also means either (a) that the initial pool of available pairs (and detections) remains untouched throughout the whole tracking procedure (which is not good, see above), or (b) that candidate tracks are already allowed to lock down their constituents during their pursuit. But since there is no distinction between genuine and spurious tracks at that stage, and since there are many more spurious tracks than genuine ones, having spurious tracks locking down detections and potentially stealing them from genuine tracks becomes a serious issue. The sequential method is therefore much better.

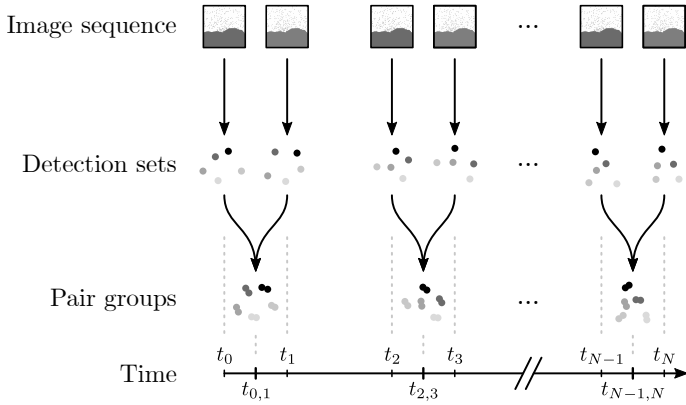


Fig. 6. Illustration of the relation between image sequence, detection sets, and pair groups. Together, the pair groups comprise the pool of available pairs.

During a tracking run, we treat each pair as a singular unit with its own location in time $t_{i,i+1} = (t_i + t_{i+1})/2$ and space $\mathbf{p}_{\text{pair}} = (\mathbf{p}_{\text{det},i} + \mathbf{p}_{\text{det},i+1})/2$, where $\mathbf{p}_{\text{det},i}$ and t_i are the positions and recording times of its two detections, $i \in \{0, 2, 4, \dots, N-2\}$ (for simplicity we refer to any time-step as t_i following Eq. (1)). What discriminates pairs from single detections however, is that we additionally attribute each pair with a velocity vector:

$$\mathbf{v}_{\text{pair}} = \frac{\mathbf{p}_{\text{det},i+1} - \mathbf{p}_{\text{det},i}}{t_{i+1} - t_i}. \quad (1)$$

Once all the pairs are created and their properties computed, they make up the initial pool of available pairs. Because pairs that stem from the same two images all share the same point in time, the pool of available pairs is quantized into $N/2$ pair groups (see Fig. 6).

Each pair from this pool is considered as part of a candidate track at least once: either to establish a new one, or to become part of another. We allow detections and pairs to be associated with only one track however, thus as soon as a candidate track is accepted, its components (and any other unrelated pairs its detections were part of) become unavailable throughout the rest of the tracking run.

Accordingly, a complete tracking run consists of a series of individual pursuits of one candidate track at a time (see Fig. 7). The algorithm walks forward in time through the pool of available pairs, and starts a new candidate track with each (though successful pursuits lower the number of remaining available pairs). We call this initial pair of a candidate track its origin, and track from it forward and backward in time.

Each candidate track is pursued from one pair group to the next, an operation quantized in what we call pair-steps (see Fig. 8). If at any pair-step no suitable pair could be found, the algorithm switches for that instance to single-steps, looking for a single suitable detection instead. Afterwards, the algorithm switches back to pair-tracking, searching the next pair group in line.

In this manner, each candidate track is pursued throughout the whole dataset, independent of how many pairs or detections may have been missed along the way. The pursuit only stops prematurely if, after no suitable pair or detection were found at a given step, it is determined that the center of the search area lies outside the dust field. The pursuit at the other end of the candidate track remains unaffected by this. Any pursuit concludes by checking if the candidate track qualifies as a track (see below). Only then does the algorithm move on to pursue a new candidate track.

3.2. Tracking parameters

Whether a candidate track qualifies as a track and which criteria single detections and pairs need to satisfy to become part of one is governed by a set of tracking parameters. While some of them are static and do not change during the whole tracking run, others are dynamic and adjust as the candidate track in pursuit evolves. The static tracking parameters only play a role at the beginning and end of a pursuit. They are (see Fig. 9):

- The initial search radius R_{init} , which is used to create the detection pairs (Fig. 9a). It limits the maximum velocity any pair can have and sets the stage for individual pursuits of candidate tracks, as the properties of the origin are decisive in what the algorithm is looking for.

- The residual offset R_{off} , which is the final tracking parameter that affects the candidate track itself (Fig. 9b). Once the pursuit of a candidate track is over, a final curve is fitted to its detections, and the distances d_{off} between them ($\mathbf{p}_{\text{det},i}$) and the locations where they should lie according to the fit ($\mathbf{p}_{\text{fit}}(t_i)$) are calculated. Any detection where $d_{\text{off}} > R_{\text{off}}$ is removed from the candidate track.

- The minimum number of detections N_{det} and detection pairs N_{pair} , which define the acceptance thresholds (Fig. 9c). After the residual offsets have been checked, any candidate track must have at least that many detections and detection pairs to be accepted.

Even though exceeding the acceptance thresholds does not guarantee that a group of detections all belong to the same object, it does increase our confidence in the tracking results. The more detections a candidate track contains, the less likely it is that they are unrelated (i.e., stem from different particles or sources). Thus, for the remainder of the tracking run, we treat any candidate track that passes these thresholds as a valid track.

Avoiding to add unrelated detections is also helped by the dynamic tracking parameters: They repeatedly adjust to the properties of the candidate track during its pursuit and therefore narrow the track-specific parameter space that the algorithm searches for suitable detections and detection pairs. With the exception of the first pair-step, where the properties of the origin are used, these parameters depend on the properties of a curve that is fitted to the candidate track at every step. We refer to the detections or detection pairs that satisfy the criteria derived from these parameters as candidate pairs or detections. The dynamic tracking parameters are (see Fig. 10):

- The dynamic search radius R_{dyn} , which defines the area within which the algorithm looks for candidate pairs and detections (Fig. 10a). The size of the area depends on the distance d : the spatial distance between the candidate track's pair \mathbf{p}_{pair} that is closest in time to the investigated step (in case of single-tracking the closest detection), and the predicted position $\mathbf{p}_{\text{fit}}(t_i)$ of where the next pair (or detection) is expected to lie according to the curve fitted to the candidate track. We chose the relation between the search radius and distance to be that of an arctangent, whose free parameters R_{min} , R_{max} , \hat{d} (shift), and \bar{d} (stretch) we can control at the beginning of the tracking run:

$$R_{\text{dyn}}(d) := R_{\text{min}} + \left(\frac{R_{\text{max}} - R_{\text{min}}}{2} \right) \left(1 + \frac{2}{\pi} \arctan \left(\frac{d - \hat{d}}{\bar{d}} \right) \right). \quad (2)$$

Increasing with distance, this function still allows for meaningful search radii at the smallest distances, while being capped at larger distances, as to not include candidate pairs or detections that are too far out.

- The (maximum) offset angle Ω , which defines a circular sector within which the candidate pairs or detections must lie

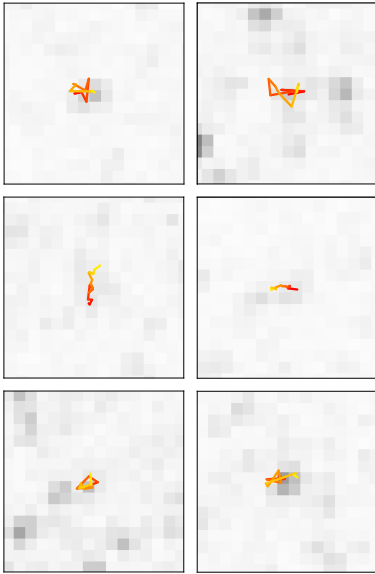


Figure 4.8: Selection of quasi-stationary particles found in sequence STP090. The particles were only tracked throughout the first 20 “principal” images (6 min). The time intervals between “extended” image pairs are too large (~ 10 min) and the particle dynamics too unconstrained for the algorithm to find subsequent detections.

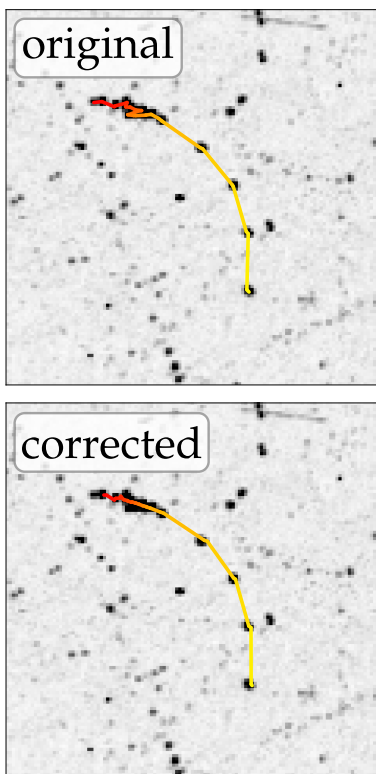


Figure 4.9: Curvy particle track from image sequence STP089 that was particularly hard to recover due to the residual noise induced by the camera pointing fluctuation. Even though the pointing fluctuation was pretty well accounted for, the residual noise made the choice of appropriate tracking parameter values extremely difficult.

This extreme adaptability of the tracking parameters proved to be vital for a successful tracking run, and led to the discovery of particles that appeared to be quasi-stationary relative to the observer (see Fig. 4.8). This was a pretty surprising find, both in terms of the algorithm being able to track them even though I did not consciously account for them, and in terms of such a population of particles existing in our data sets. Since they do not seem to remain in the same positions during the extended sequence, dead pixels or other artifacts are no plausible explanations. Instead, they are likely particles that—at least for the roughly six minutes that we observed them—moved parallel to the camera pointing.

At the other end of the spectrum, the same parameter settings still allow for the tracking of very fast particles as well (see Fig. 4.10). Even though such particles have a fairly constrained parameter range, tracking them is not as trivial as it might seem—precisely *because* of their reasonably straight dynamics. They only allow for candidates pairs and detections to deviate little from the predicted configurations, which in theory should make it easier to choose the correct ones. But due to pointing fluctuations of the camera (see Sect. 4 in the methods paper) and inaccuracies in the measured point source positions, especially the orientation and velocity of detection pairs can vary notably. It is thus quite difficult to make sure that such tracks are as complete as possible, while also not allowing for an entire class of spurious tracks to be extracted as well.

Between those two extremes lie the particles with moderate speed. Their tracks are typically easy to identify by eye and often show substantial curvature (see Fig. 4.9). This makes them very interesting targets, but as with the fast particles, it is difficult to choose just the right amount of leniency in the tracking parameters. Curving tracks require considerable parameter tolerances, but at the same time, this can open the door for similar looking, but entirely spurious tracks.

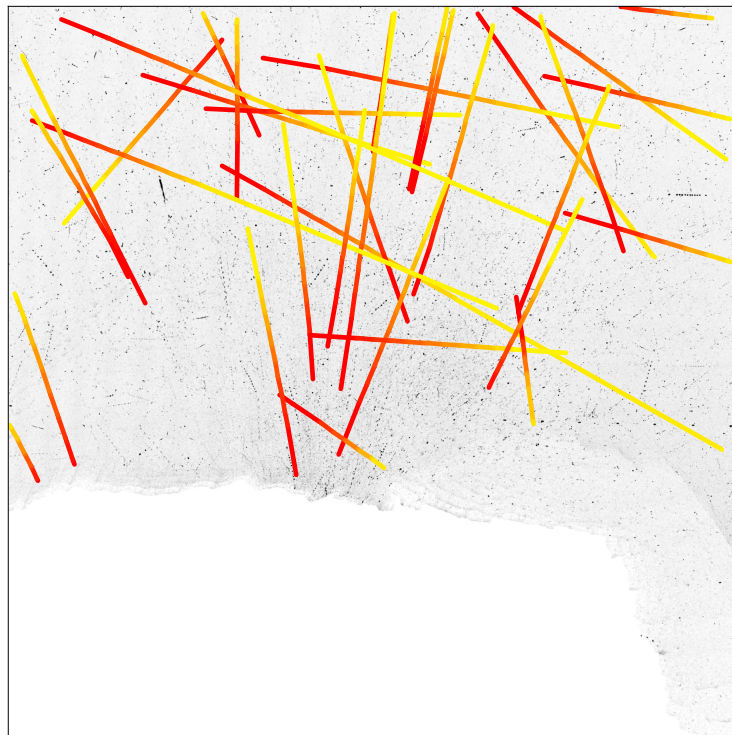


Figure 4.10: A selection of the fastest particles tracked in image sequence STP090.

M. Pfeifer et al.: On the trail of a comet's tail: A particle tracking algorithm for comet 67P/Churyumov-Gerasimenko

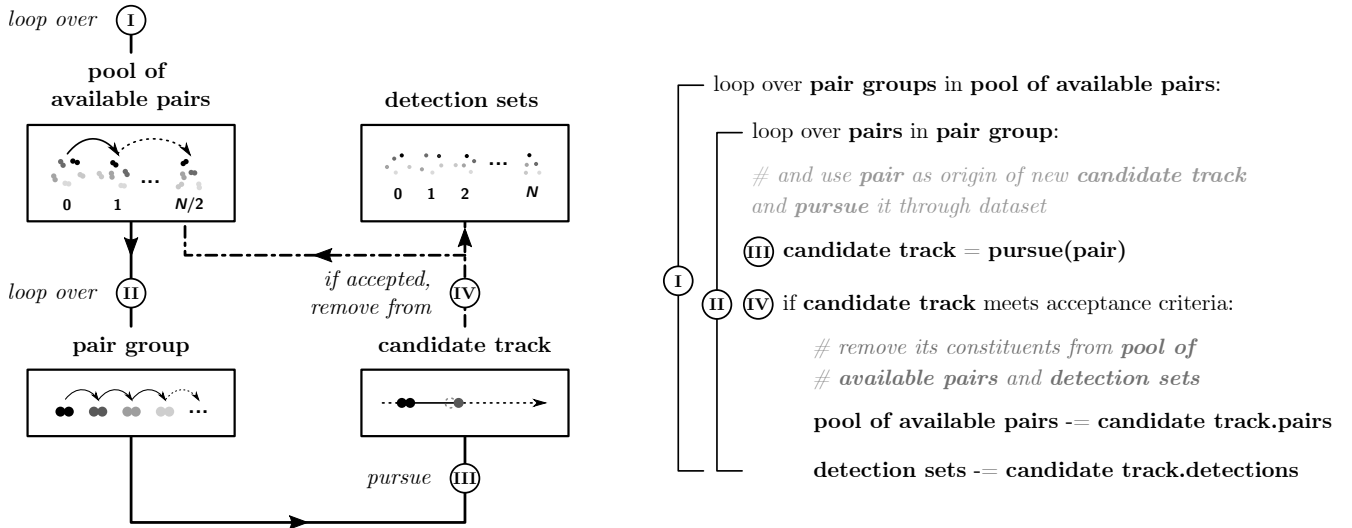


Fig. 7. Flowchart and pseudo-code illustrating the structure of an entire tracking run. The algorithm iterates over the pool of available pairs (I), using each pair as the starting point for a new candidate track (II, III). If a candidate track is accepted (IV), its pairs and detections are removed from the respective sources (as well as any other available pair that shares detections with the track) and cannot be used to create future tracks.

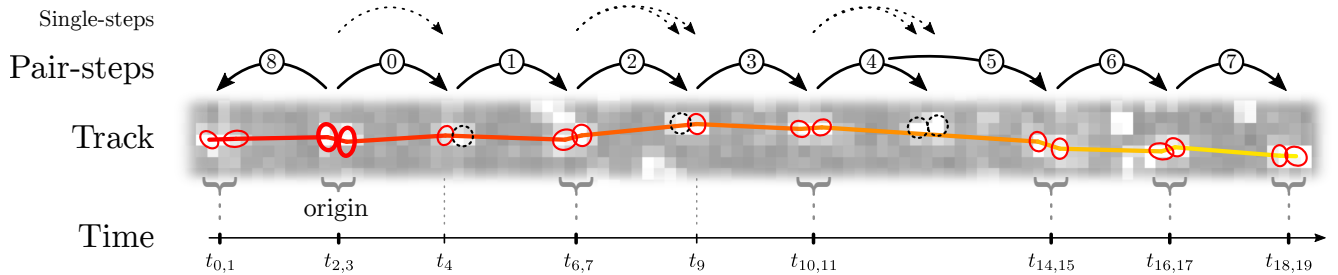


Fig. 8. Typical track demonstrating the pursuit process. The algorithm operates pair-step-wise, going from one pair group to the next. In this case, it starts with a pair from the second group. Because the origin lies in the first half of the image sequence, the candidate track is first tracked forward, then backward in time (indicated by the circled numbers). If no suitable pair is found at a given step, the algorithm switches to searching for suitable single detections (single-step) instead, starting with the detection set that is closer in time to the previous step. The algorithm only searches the second set as well if it finds no suitable detection in the first. Afterwards, the pair-tracking continues. The track's color gradient from red to yellow indicates the direction of time (and therefore the object's motion through space). While the red ellipses mark the detections that make up the track, the black, dashed circles indicate where detections are missing. The background image is part of the stacked image similar to Fig. 4.

(Fig. 10b). It measures from the vector that points in the same direction as the fitted curve at the time of the investigated step ($v_{\text{fit}}(t_i)$), and, like the dynamic search radius, it depends on the distance d . The sector originates from the center of the candidate track's closest pair (or closest detection in case of single-tracking), and opens up in tracking direction. Its arc spans twice the offset angle. The relation between Ω and d is otherwise identical to that of Eq. (2), but with the arctangent flipped:

$$\Omega(d) := \Omega_{\min} + \left(\frac{\Omega_{\max} - \Omega_{\min}}{2} \right) \left(1 - \frac{2}{\pi} \arctan \left(\frac{d - \hat{d}_{\Omega}}{\bar{d}_{\Omega}} \right) \right), \quad (3)$$

where we again have control over the free parameters Ω_{\min} , Ω_{\max} , \hat{d}_{Ω} , and \bar{d}_{Ω} . In this case however, we allow the largest deviations for the smallest distances, since even small positional changes perpendicular to the candidate track can mean large angular ones. The opposite is true for large distances.

– The (maximum) inclination angle I , which is also measured with respect to the candidate track's direction at the investigated time-step ($v_{\text{fit}}(t_i)$, Fig. 10c). It shares the same value as Ω , but instead limits the inclination that pairs can have toward

the reference vector. Because single detections do not have an inclination, this parameter is only relevant during pair-tracking.

– The relative difference in speed ΔV , which restricts how much the speed of candidate pairs can stray from that of the fitted curve at the investigated time-step ($|v_{\text{fit}}(t_i)|$, Fig. 10d). It is calculated as the relative deviation from $|v_{\text{fit}}(t_i)|$ in percent, from a relation that has the same shape as Eq. (3):

$$\Delta V(|v_{\text{fit}}|) := \Delta V_{\min} + \left(\frac{\Delta V_{\max} - \Delta V_{\min}}{2} \right) \left(1 - \frac{2}{\pi} \arctan \left(\frac{|v_{\text{fit}}| - \hat{v}}{\bar{v}} \right) \right), \quad (4)$$

where we also have control over the free parameters ΔV_{\min} , ΔV_{\max} , \hat{v} , and \bar{v} . Analogous to the offset and inclination angle, we allow the largest relative deviation for the smallest speeds, because in this regime, pixelization and uncertainties in the pointing of the camera and source detection can have a significant effect. For high speeds on the other hand, we only expect small deviations, for example due to a curved flight path. Because single detections cannot be assigned a velocity, this parameter is also only relevant during pair-tracking.

For each candidate pair or detection that satisfies all criteria set up by the dynamic tracking parameters, we compute a match-factor M as a proxy for the candidate's validity. The match-factor

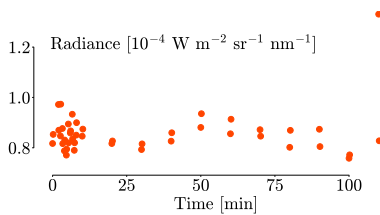


Figure 4.11: Light curve of the (non-variable) star HD 25627, extracted from image sequence STP090 (it is the same star that is also shown in Fig. 13 in the methods paper). Notably, the extreme outlier in the upper right corner is not the result of an unrelated detection. Instead, it is likely caused by a particle that just so happened to cross in front of the star at just the right moment. It would be interesting to see if this difference in radiance also remains when comparing the average radiance of consecutive images. Since during the extended sequence two images of a pair are only taken ~ 12 s apart, nothing much should change content-wise. Any difference in the averages might then be attributed to the different exposure times.

The ellipses semi-major and -minor axes “represent the maximum and minimum spatial dispersion of the object profile along any direction” (Bertin 2023), and are scaled up by a factor of 3, as the resulting ellipse generally describes the isophotal limit (the contour of equal brightness) of the detected object well.

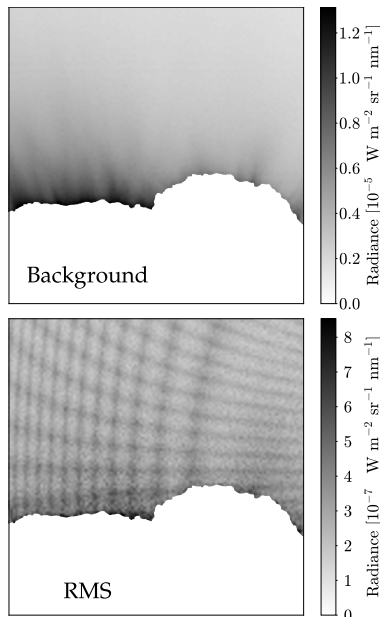


Figure 4.12: Background and RMS map of the first image of sequence STP090 (brightness-inverted and with masked-out nucleus). While the background captures the features of the diffuse coma very well, the RMS map clearly shows some kind of artificial signal, which is likely a moiré pattern introduced by the image calibration. In retrospect, this may have been taken care of by dividing the image by the RMS map.

Another parameter that was frequently suggested to use for tracking is the particle radiance. Unfortunately, this parameter is very unreliable for a number of reasons: For one, as explained in the methods paper, two alternating and vastly different (factor of 25) exposure times are used during the extended part of the sequence. In theory, the images are all normalized to 1 second of exposure (Tubiana et al. 2015; Kovács 2018), however as Figure 4.11 shows (see also Fig. 7.18), there is often a considerable difference in radiance between two consecutive detections, even in case of a star whose radiance should otherwise be constant. This may be because the images that were only exposed for 0.24 seconds have a significantly worse signal-to-noise ratio than the images that were exposed for 6 seconds. So when their signal is scaled up to match that of 1 second exposure, their noise is scaled up, too.

Another reason may be that we deliberately do not subtract any background signal during photometry (e.g., derived from elliptical annuli around the detections), because we already removed the local background in preparation for the detection process, on a scale (16×16 px) very similar to typical annuli radii (~ 11 – 17 px). The radiance values are simply calculated by integrating over the elliptic apertures and the RMS maps show that the remaining background signal is roughly two orders of magnitude weaker than the signal we are usually interested in (see Fig. 4.12). Nevertheless, the noise might still influence the integrated radiance, as the RMS maps are used to determine the detection threshold.

Lastly, but most importantly, many of the particles are evidently oblate rotators (see Fig. 4.13). Their signal therefore naturally changes periodically, which is virtually impossible to account for. Purely from visual inspection of the master images, it seems that many of these particles have rotation frequencies on the order of at least minutes, however due to the other issues mentioned above and the low time resolution, it is likely impossible to reliably fit their periodic signal (although Lomb-Scargle periodograms may be an option; e.g., VanderPlas 2018).

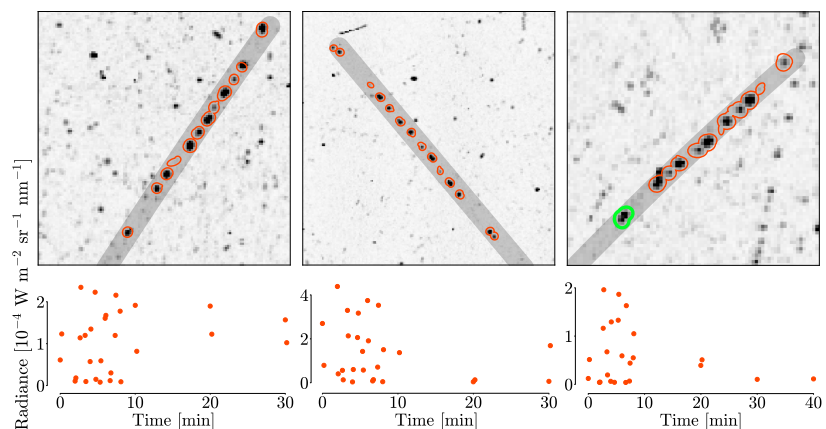


Figure 4.13: Three tracks from sequence STP090 that seem to stem from oblate, rotating particles. The master images on the top row show the first 24 detections of each track, indicated by the orange contours and the gray, semi-transparent curves. The varying shapes of the PSFs can clearly be seen. The track on the right is also an example of a track that had two of its detections (thick green contour) stolen by another track (in this case also a highly spurious one). The plots on the bottom row show the particles’ light curves, which are significantly dispersed.

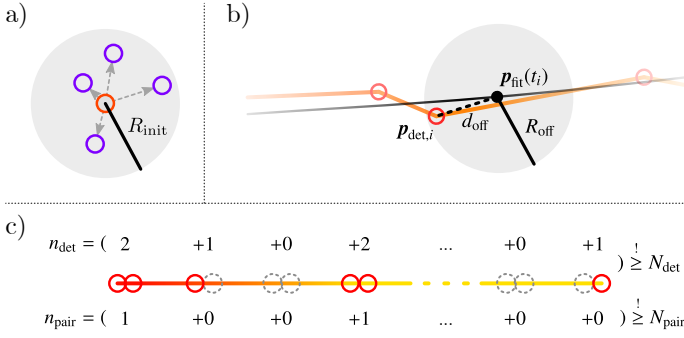


Fig. 9. Diagrams illustrating how the static tracking parameters operate: (a) the initial search radius R_{init} around a primary detection (orange circle), used to create pairs with secondary detections (violet circles); (b) the residual offset R_{off} , which defines the maximum distance d_{off} any detection $p_{\text{det},i}$ (red circle) can have from the corresponding location $p_{\text{fit}}(t_i)$ of the curve (black line) fitted to the candidate track (orange path); and (c) the minimum number of detections N_{det} and detection pairs N_{pair} , which any candidate track (n_{det} , n_{pair}) must have to be accepted as a track. The candidate track is shown as a gradient line from red to yellow, the present and missing detections as red, and gray dashed circles, respectively.

is used in two ways: to decide between different candidate pairs or detections, and to weigh the contribution of the selected one on the curve fitted to the candidate track:

$$M_{\text{cand}} := 1 - \frac{1}{4} \left(\frac{r_{\text{cand}}}{R_{\text{dyn}}} + \frac{\omega_{\text{cand}} + I_{\text{cand}}}{\Omega} + \frac{\Delta v_{\text{cand}}}{\Delta V} \right), \quad (5)$$

for pair-tracking, or

$$M_{\text{cand}} := 1 - \frac{1}{2} \left(\frac{r_{\text{cand}}}{R_{\text{dyn}}} + \frac{\omega_{\text{cand}}}{\Omega} \right), \quad (6)$$

for single-tracking, where r_{cand} , ω_{cand} , I_{cand} and Δv_{cand} are the dynamic parameter values of the candidate pair or detection, which are normalized by the respective maximum values as determined by Eqs. (2)–(4). We then choose the pair or detection with the highest match-factor to become part of the candidate track.

3.3. Principal and extended tracking

To address the different time-steps of the two sub-sequences (see Fig. 1), our tracking algorithm has two operating modes on the pursuit level: principal, and extended tracking. Due to the shorter intervals of the principal sequence, particle tracks are generally easier to identify during principal tracking—both visually and by the tracking algorithm. Thus, candidate tracks are only pursued during extended tracking if they passed the acceptance thresholds after principal tracking. For the same reason, any track becomes part of the final tracking results independent of how many detections were missed during this second stage.

Both modes have their own set of predefined tracking parameters. Extended tracking however has an additional parameter we call life. The lives of a track define how many detection pairs are allowed to be missed during extended tracking. If no pair and no single detection is found at a given step, then the life counter is reduced by 1. Lives also cannot be replenished: should the counter fall to zero, the pursuit is stopped. This prevents adding unrelated detections to a track, something that becomes increasingly more likely the further the search area is away from the established part of the track.

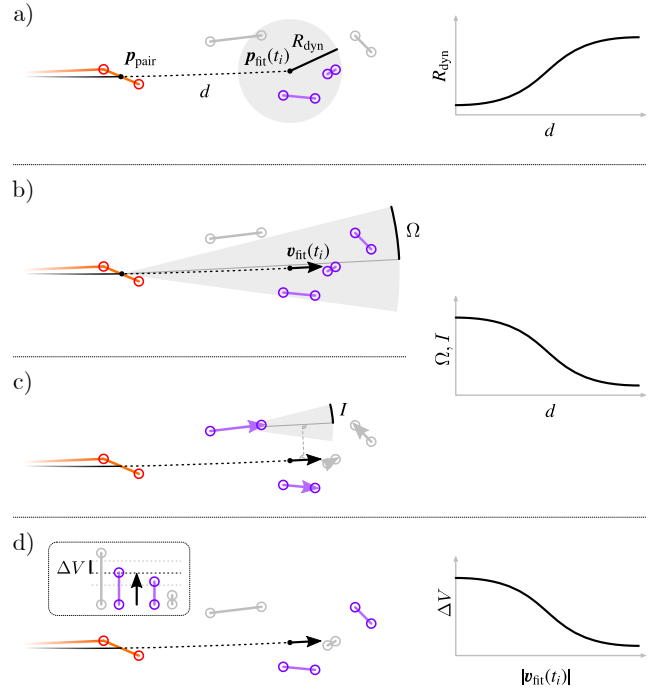


Fig. 10. Diagrams illustrating how the dynamic tracking parameters operate (pairs that satisfy the respective criteria are shown in violet, the ones that do not in gray): (a) the dynamic search radius R_{dyn} , which defines the area the algorithm searches for candidate pairs or detections. It depends on the distance d between the candidate track's pair p_{pair} closest in time to the investigated step, and the predicted position $p_{\text{fit}}(t_i)$ where the next pair is expected to lie according the curve (black, partly dashed line) fitted to the track (orange path). The relation between R_{dyn} and d is that of an arctangent (see Eq. (2)) shown by the graph on the right. (b) the (maximum) offset angle Ω , which defines a circular sector within which candidate pairs or detections must lie. The sector originates from the candidate track's closest pair and opens up in the same direction as the fitted curve at the investigated time-step ($v_{\text{fit}}(t_i)$, black arrow). The offset angle also depends on d in the form of an arctangent, although reversed, as shown by the graph on the right (see Eq. (3)). (c) the (maximum) inclination angle I , whose value is equal to that of Ω . It defines the maximum inclination candidate pairs can have with respect to $v_{\text{fit}}(t_i)$. (d) the relative difference in speed ΔV , which determines how much the speed of a candidate pair can relatively deviate from $|v_{\text{fit}}(t_i)|$. The relation between ΔV and $|v_{\text{fit}}(t_i)|$ is also that of a reversed arctangent as shown by the graph on the right (see Eq. (4)).

Once the algorithm checked the residual offset again after extended tracking, another control mechanism executes. Because detections may have been removed during the residual offset check, the extended part of the track is inspected for larger gaps (i.e., missing pairs). Should any individual gap or the sum of all gaps be larger than the granted extra lives, then all detections that come after the critical gap (i.e., the gap that let the sum of all gaps exceed the number of extra lives) are removed as well.

Finally, principal and extended tracking differ by the kind of curve that is fitted to the candidate track during its pursuit. Because the particles only travel relatively short distances during the principal sequence, we fit their tracks with straight lines. This is more robust than a parabola for example, since we found that the parabola's extra degree of freedom often causes the tracking algorithm to trail off in the wrong direction when the detections of a candidate track are not perfectly aligned. During the extended sequence however, we expect tracks to curve significantly because it covers a much longer time period. Thus at this

Adding the wrong detections to a track can have a number of different effects. In the least severe case, usually when the track already consists of a good amount of related detections, the algorithm is not irritated enough and goes back on track immediately afterwards. These detections are often removed during the residual offset check (which is why we introduced it in the first place). But even if they remain part of a track, they do not drastically change its properties (and hence neither the overall statistics of a tracking run, see also Sect. 5.2).

A more severe case happens when unrelated detections cause the algorithm to literally lose track, leaving it unable to add further detections, and the track shorter than it could be. If this happens during the early stages of a pursuit, the trajectory might even fail to pass the acceptance threshold and end up being rejected. This would not only mean one less recovered particle track, but also more noise during subsequent pursuits, since its constituents remain available.

The most severe case is likely when unrelated detections cause the algorithm to add even more unrelated detections to the track. Even if the first part of the track belongs to a real particle, it ends up spurious.

Also, as already discussed, if the unrelated detections actually belong to another track, that other track might be significantly affected. At the same time, should the detections that actually belong to the original track exist, then they add to the noise during subsequent pursuits.

As far as I know, there is currently no definitive explanation for this phenomenon. Probable causes include:

A defective reaction wheel: Reaction wheels are spinning metal wheels that utilize the conservation of angular momentum to precisely orient a spacecraft. During the Rosetta mission, two of Rosetta's reaction wheels showed abnormal behavior (McMahon et al. 2017). This might be a source for the pointing fluctuation that we see in our image sequences, although during Rosetta's comet phase, there were apparently no real issues with the reaction wheels (Cecilia Tubiana, priv. com.).

A timing offset that translates into a pointing offset: During dust observations like ours, spacecraft maneuvers were often scheduled with not too stringent pointing accuracy (which was instead reserved for limb observations, Cecilia Tubiana, priv. com.). The timing offset between a maneuver and the recording of an image can thus effectively translate into a pointing offset.

Cometary particles hitting the spacecraft: This is by far the most exiting option. Kyriazis (2021) therefore created a 3D computer model of Rosetta to investigate how particle impacts would affect its moment of inertia. He then retrieved the pointing fluctuation data from Rosetta's attitude monitor and correlated it with 67P's phases of increased activity. While he does not rule out particle impacts as a possible cause, he concludes that technical causes are more probable.

Star tracker confusion: Kyriazis (2021) also suggests another potential cause. As explained in Section 40, Rosetta's star trackers were occasionally irritated by the signal of dust particles. Kyriazis (2021) shows that such events can cause pointing fluctuations of the same order as we have observed. It seems unlikely to me however, that the star trackers were irritated virtually every time when one of our sequences was recorded (and also during other surveys).

stage, we fit parabolas to the tracks, which is also less likely to fail now that the tracks already consist of a considerable amount of detections.

The curve fitted to a candidate track to determine the residual offsets on the other hand is always a parabola. And no matter the circumstance under which a curve is fitted, the detections are always weighted by the match-factor (Eqs. (5) and (6)) they were assigned when added to the track.

3.4. Sidereal-motion-based attitude correction

This process precedes any particle tracking, but as it uses the same tracking algorithm, it is described only now. While studying the stacked image of sequence STP090, we noticed a pointing fluctuation with a typical amplitude of a few pixels that occurred during the principal sequence and which can be observed in every track (see Fig. 11). It compromises the tracking results in several ways: (1) A significant spread of detections from their expected positions can quickly lead the algorithm to go off trail. (2) To account for a higher variance in location, velocity, and orientation of candidate pairs and detections, we need to choose more lenient tracking parameters. Inevitably, this further increases the chances of adding **unrelated detections** and going off trail. (3) Drastic changes in velocity also translate into incorrectly computed accelerations. This makes extended tracking based on parabolas virtually impossible, as predictions over the long time intervals between image pairs require accurate accelerations; otherwise, the search areas are too far off, again leading the candidate track to go astray.

Since the deviations are systematic, we attribute them to unexpected changes in **spacecraft attitude**. During STP090 (and other sequences like it), Rosetta's orbit around 67P is noticeable. But to keep the camera's reference frame fixed to the comet's center of mass, the spacecraft's attitude was constantly adjusted. Sidereal objects therefore describe an apparent linear motion across the dust field. By comparing the pointing data of the image headers—which represent the commanded pointing—with the actual motion derived from tracks, we can thus reconstruct the pointing fluctuation.

To identify sidereal objects in a sequence, we query the SIMBAD Astronomical Database (Wenger et al. 2000) via the astroquery library (Ginsburg et al. 2019). Objects such as binaries that are spaced too close to each other to be distinguishable in the images are recorded only once. We then use gnomonic projection to transform the objects' equatorial coordinates back to image coordinates and generate the expected motions (see Fig. 12).

Next, we run the tracking algorithm in a local area around each of the identified objects, visually compare the tracking results to the expected motions, and match them manually. Figure 13 shows an example of such a track we call sidereal track, and its companion, the previously estimated motion. By choosing a reference image, calculating the relative distances of the commanded positions to that reference image, doing the same for the detections of the sidereal tracks, and subtracting the former distances from the latter, we can calculate the relative offsets induced by the pointing fluctuation:

$$\delta_i = (\mathbf{p}_{\text{det},i} - \mathbf{p}_{\text{det,ref}}) - (\mathbf{p}_{\text{com},i} - \mathbf{p}_{\text{com,ref}}), \quad (7)$$

where δ_i is the relative offset of a sidereal track at the i th image, $\mathbf{p}_{\text{det,ref}}$ the position of the track's detection in the reference image, and $\mathbf{p}_{\text{com},i}$ the commanded position of the i th image relative to the position of the reference image $\mathbf{p}_{\text{com,ref}}$.

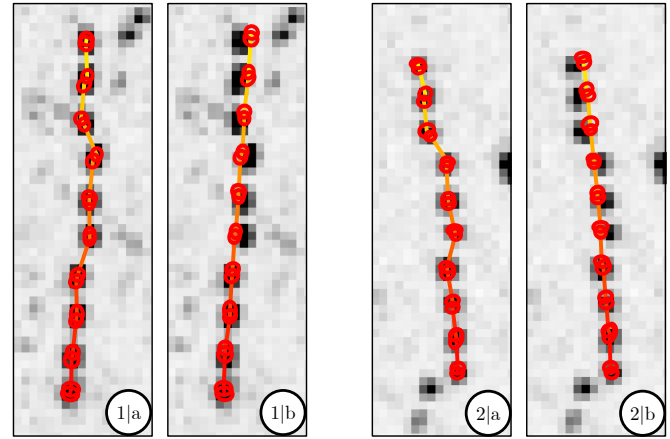


Fig. 11. Two sample tracks (1, 2) from the principal sequence, once without (a) and once with (b) the pointing correction applied (the image shown in the background is left unchanged). Tracks are shown as colored lines from red to yellow, detections indicated by red ellipses.

However, because we need to choose particularly liberal tracking parameters during the pursuit of sidereal tracks to account for the still present pointing fluctuation, there is an increased chance to pick up unrelated detections. Thus before we estimate the pointing fluctuation, we calculate the mean absolute offset values:

$$|\bar{\delta}_i| = \frac{1}{M_i} \sum_{j=0}^{M_i} |\delta_{i,j}|, \quad (8)$$

where M_i is the number of sidereal tracks that have a detection in the i th image, and exclude any data point from the signal estimation whose absolute offset lies outside a certain range around its mean ($\pm 1.7 \sigma_i$ in case of sequence STP090). Only then do we calculate the mean offsets (see Fig. 14) and use them to correct our detection sets:

$$\tilde{\delta}_i = \frac{1}{\tilde{M}_i} \sum_{j=0}^{\tilde{M}_i} \delta_{i,j}, \quad (9)$$

where \tilde{M}_i is M_i minus the excluded data points. Figure 11 shows two sample tracks from the principal sequence with and without the pointing correction.

The choice of the reference point that is used to calculate the relative distances is crucial in this, since a) sidereal tracks that are missing the respective detection cannot be considered for the signature estimation, and b) sidereal tracks that have an unrelated detection as the reference end up with shifted offsets. For sequence STP090, we decided to use the first image of the principal sequence as the reference, as we found that detections from this image are usually not only included in all sidereal tracks but also the most reliable.

Finally, identifying the sidereal tracks also allows us to remove their constituents from the detection sets prior to the actual tracking run, ridding the tracking results of a statistical bias.

4. Parameter optimization

The whole tracking process—including image cleaning, point source detection, attitude correction and the tracking run itself—involves far too many parameters (> 74) for a systematic grid

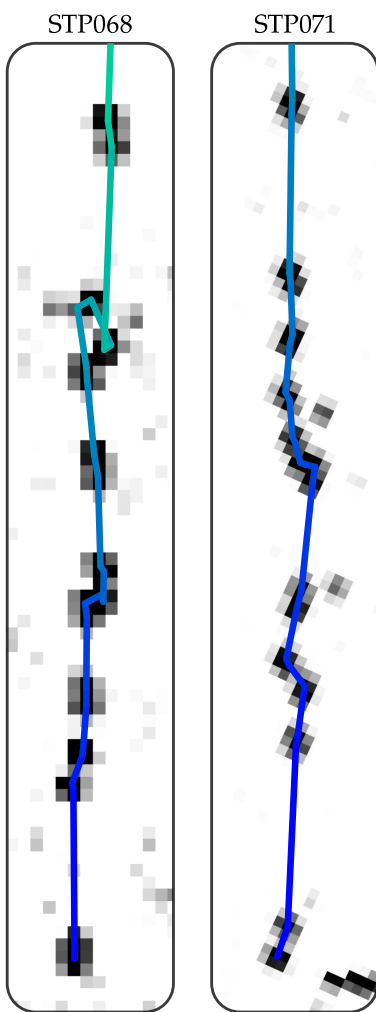


Figure 4.14: The first 24 detections of two sidereal tracks from sequences STP068 and STP071 (images rotated for better presentation).

This is actually a comparatively mild case. In case of sequences STP068 and STP071 for example, the pointing fluctuation is much more severe and accordingly difficult to recover. The maximum offset between two consecutive images of these sequences is about 10 px, which corresponds to an attitude change of almost 0.2 μ rd. As a result, sidereal tracks can even turn in on themselves (see Fig. 4.14). And as Figure 4.15 shows, tracking particles in these sequences would be impossible without correcting for the pointing fluctuation.

In a weird way, we were actually lucky that the pointing fluctuation was so prominent and easy to spot in the principal sequence, since it also affects the extended sequence, but is essentially impossible to spot during that phase due to the large distances between detection pairs. And so without its presence in the principal sequence, we would have likely missed it, which would have given us a very hard time during extended tracking.

Lastly, even if it were possible to track the particles without the attitude correction and all the tracks were complete and did not contain any unrelated detections, the derived dynamics would be drastically off, and we would not be able to extrapolate the tracks at all. The attitude correction is therefore crucial.

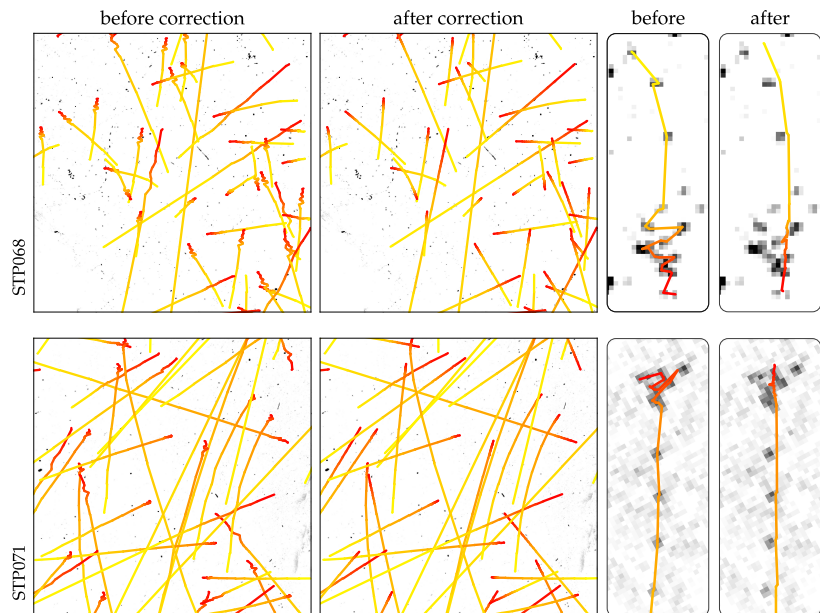


Figure 4.15: Sample particle tracks from sequences STP068 and STP071, demonstrating the extreme pointing fluctuations and the efficacy of our correction method, once on a more general level for small groups of tracks, and once focusing on two individual tracks (bottom right images rotated). Notably, the “before” tracks are merely reconstructions by undoing the correction. They were not originally tracked that way.

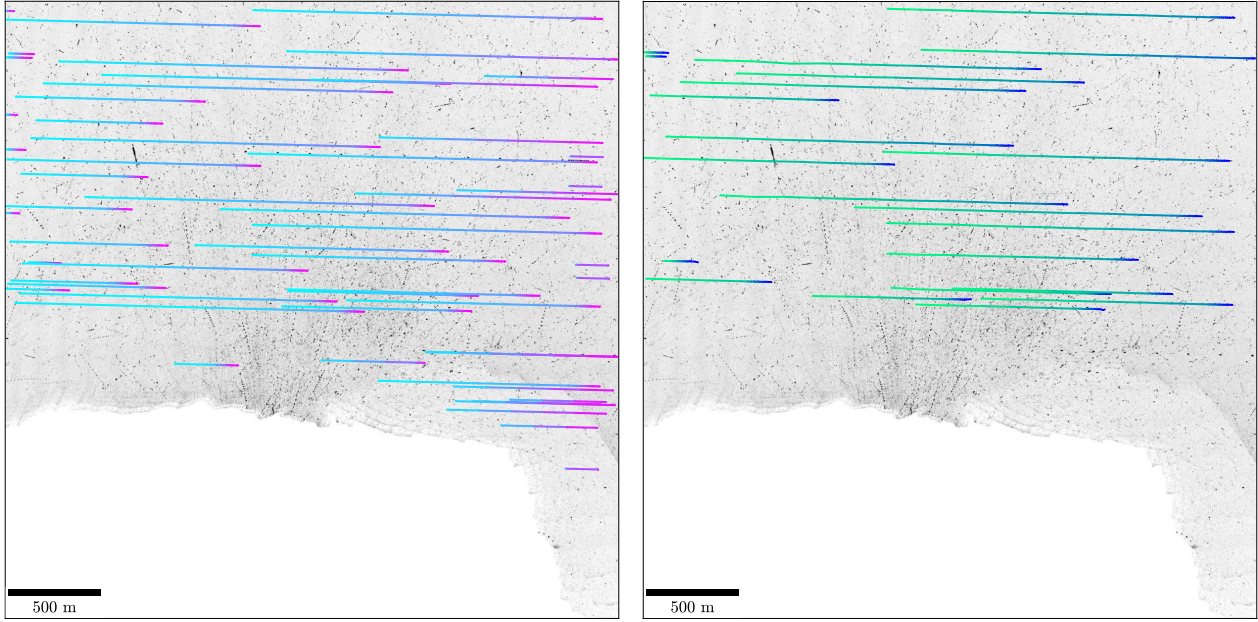


Fig. 12. Sidereal objects identified in the dust field of sequence STP090. *On the left:* results from searching the SIMBAD database (lines colored violet to aquamarine). *On the right:* sidereal tracks obtained from our tracking algorithm that matched some of those results (lines colored dark blue to green). The objects move from right to left.

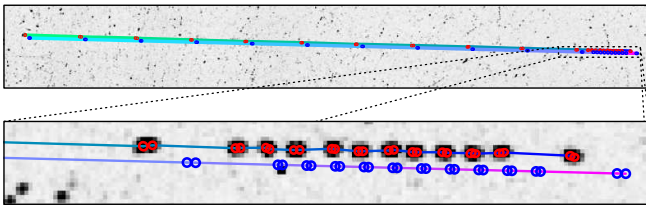


Fig. 13. Sample of a sidereal track (top line from dark blue to green, detections indicated by red ellipses) and the expected motion of a sidereal object it was matched with (bottom line from violet to aquamarine, expected positions indicated by blue circles). The top panel shows the whole track, the bottom one a close-up of the first 24 detections, including the entire principal sequence. The pointing fluctuation is mainly acting along the direction of motion from right to left.

search. However for most parameters, preliminary tests indicate that their exact value is (within some range) secondary to achieving good results. We therefore focused on optimizing only the detection threshold (see Sect. 2.2) and 15 dynamic tracking parameters of the principal and extended tracking (in the following referred to as principal and extended parameters, cf. Table A.1), which we found to be more influential. In the following, we analyze their effect using a single quality index: the miss-rate Γ . It measures the percentage of detections that were missed during the pursuit of a track (i.e., whenever no suitable pair or detection was found, or when detections were later-on removed during offset checks):

$$\Gamma := 100 \cdot \frac{\tilde{N}_{\text{det}} - n_{\text{det}}}{\tilde{N}_{\text{det}}}, \quad (10)$$

where $\tilde{N}_{\text{det}} \leq N$ is the maximum possible number of detections a specific track can have, which depends on whether and when the track supposedly left the dust field (e.g., if it lies close to the edge, the detections expected outside the field do not count toward the total). We then estimated the quality of tracking results by looking not only at the total number of tracks, but

more importantly at the numbers of tracks with $\Gamma = 0\%$ and $\Gamma < 30\%$. By visual inspection we found 30% to be a reasonable threshold where most tracks still belong to real particles and only occasionally incorporate unrelated detections.

Because the principal parameters directly affect the total number of tracks (as the acceptance criteria are applied only once after the principal tracking), we optimized them first. Each of the twelve free parameters from Eqs. (2)–(4) was varied at least ten times around an initial guess. Since testing all value combinations would still take 10^{12} individual tracking runs, we decided on a different strategy: First, we reduced the tracking runs to principal tracking only; and second, we tested each parameter value only once, keeping all other parameters constant. After the full value range for a given parameter was explored, we chose the value that produced the best results and used it as the parameter's new fixed value for the remaining runs. The results of this process are listed in Table A.1.

Next, we optimized the extended parameters. Since we decoupled principal and extended tracking, and on its own the latter runs much faster than the former, we adapted our approach. Instead of testing the whole set, we only varied the three parameters that we deemed the most influential (R_{max} , Ω_{max} , and ΔV_{max}), and used the optimized principal values for the rest. We again chose ten different values for each of the three variable parameters, but this time, we explored all of the 1000 corresponding value combinations. The parameter set that produced the best results according to our miss-rate criteria is also shown in Table A.1.

Lastly, we estimated the optimal detection threshold (in units of signal-to-noise S/N). This dimensionless parameter determines the sensitivity of the detection algorithm toward weaker sources and is therefore directly linked to the number of detections per image. While being able to detect weaker sources can be beneficial in case of fainter particles or oblate rotators (i.e., particles that strongly vary in brightness), it also means to pick up more noise. Hence the detection threshold can neither be too high, as a significant portion of signal would be ignored, nor too low, as the signal would be overwhelmed by noise.

Another short philosophical parenthesis: Despite all the objective parameters, in the end, judging the quality of the tracking results still comes down to subjective interpretation (see also Chap. 5). As I explain in Section 5.1 of the methods paper, I thus rigorously tested the predictive proficiency of the miss-rate criterion, and assessed the quality of every single track. But using the miss-rate and the number of tracks as criteria only works given a reasonable set of tracking parameter values. This is especially true for the detection threshold, as it single-handedly determines the number of available detections. Obviously with a low enough threshold, we would be able to find many times more tracks than with our more conservative setting, and most of them would likely also not miss a single detection. But most—if not all—of them would also be spurious, and so it would of course be highly counter-productive. The question is, where is the sweet spot? At what point does the net quality of the tracks actually decline? This is not so easy to say.

Of course it would be possible to use different tracking parameter sets to track different particle populations in the same image sequence. But then it becomes a question of how to combine these results, which would likely involve cross-correlation. And as I discussed in Section 2.2, figuring out when two tracks are the same is not trivial.

Background and RMS map parameters include, for example: the size and shape of the local areas, the degree to which they are smoothed out, and even parameters that are hard-coded into the methods that we use but have no control over (e.g. parameters that govern the iterative kappa-sigma-clipping), and of course the methods themselves.

Detection parameters include, for example: the minimum number of pixels required to constitute a detection, whether a filter is applied to the image prior to the detection process, the filter kernel and how it is applied (i. e., using simple convolution or a matched filter), and the parameters that determine the deblending and cleaning processes.

Explicitly constant parameters that we are aware of include, for example: the attitude correction, the polynomial degree of the fitted curve, the removal of cosmic ray hits, and how the match-factor is calculated (e. g., how different parameters are weighed; it might also be reasonable to have a lower match-factor threshold that candidates must pass to be incorporated).

Explicitly constant parameters that we are semi-aware of include, for example: bugs in my code or the third-party software that we use, or the quality of the images and the accuracy of their calibration.

Another aspect to consider regarding the overall quality of tracking results is how well they represent what is actually present in the data. While it is important that each individual track is as complete as possible and preferably does not contain any unrelated detections, it is also important that the tracking parameters do not favor certain kinds of tracks over others. It is possible that even though a large number of high-quality particle tracks was recovered, an entire population of tracks was ignored. A large number of high-quality tracks on its own is therefore not sufficient.

In fact, given a good amount of tracks to support reasonable statistics, not much is gained if the statistics do not change with the addition of new tracks (and certainly not if they are spurious). There is hence little reason to optimize the tracking parameters with the goal of retrieving additional tracks if they do not provide new information. Instead, it actually makes more sense to optimize the parameters insofar as to reduce the number of spurious tracks. This may effectively also decrease the total number of retrieved tracks, but improve their overall quality and representation.

There are also quite a few other parameters that influence the tracking results which I disregarded here. They include: how the shape of the nucleus is estimated and thus how much additional area is cut from the dust field; how the background signal and the RMS maps are calculated; how detections are created; and parameters that were implicitly kept constant, ranging from things that we are aware of, over things we are semi-conscious about, to things that we are literally unaware of but that might nevertheless play a role.

All that being said however, there is ample evidence (see next double page) that we found a good set of tracking parameter values. Since the parameter optimization is a so-called multi-dimensional “rugged-landscape” problem (where the landscape is spanned by our tracking parameters and we are looking for the highest peak), there are likely at least several viable parameter value combinations. And while our solution may not be the “Mount Everest”, I am confident it is located in the “Himalayas”. During the many times that I inspected the tracks and the master image of sequence STP090 and others, I did not find any obvious tracks that were missed.

M. Pfeifer et al.: On the trail of a comet's tail: A particle tracking algorithm for comet 67P/Churyumov-Gerasimenko

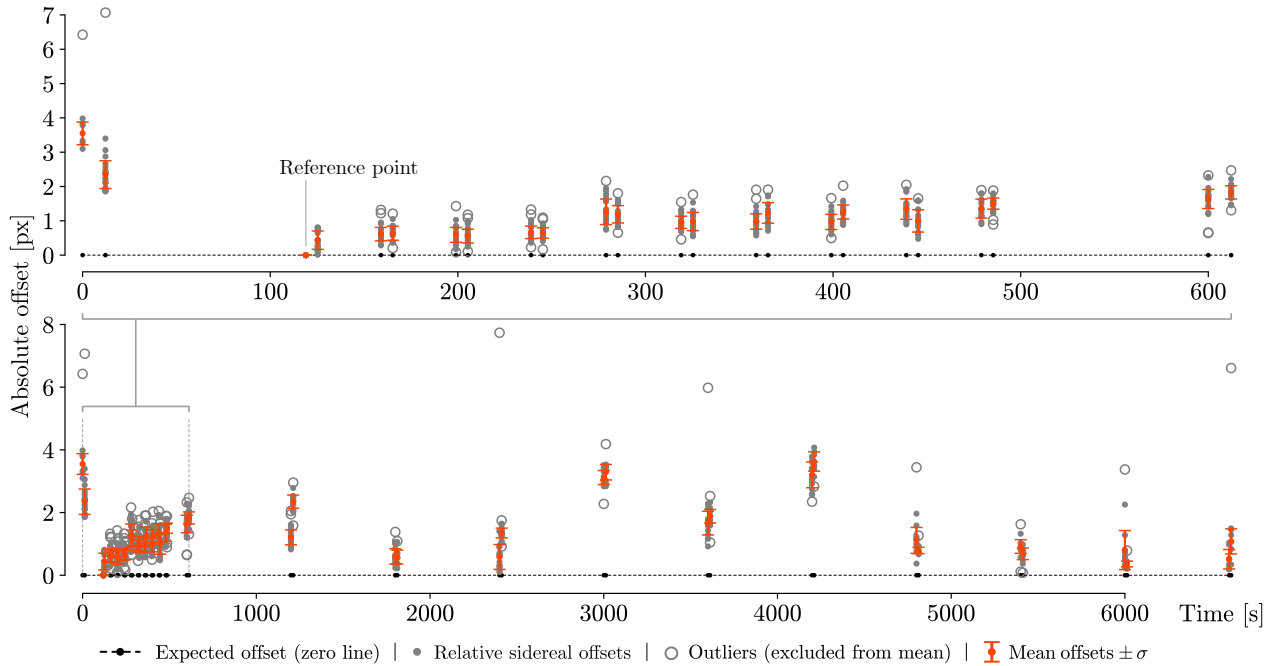


Fig. 14. Pointing fluctuation derived from the apparent motion of 21 sidereal objects in the dust field of sequence STP090 (see Eqs. (7)–(9)). The reference point indicates which image and therefore which detections we used to calculate the relative distances. The black circles and dashed line mark the zero line (no pointing fluctuation). The filled and the open gray circles show the measured offsets from sidereal tracks: while the filled ones were used to calculate the mean values that represent the pointing fluctuation (orange circles with errorbars), the open ones are outliers that were excluded from the calculations, as they are assumed to result from unrelated detections.

So to optimize the detection threshold, we again chose ten values around an initial guess and measured the average detection density (within the dust field). The detection density however also strongly depends on exposure time (T_{exp}). In case of sequence STP090, the average detection density for images with $T_{\text{exp}} = 6$ s was roughly twice of that for images with $T_{\text{exp}} = 0.24$ s. Thus to keep the detection densities roughly constant, we adopted two separate detection thresholds, one for each exposure time. The one for $T_{\text{exp}} = 6$ s was then adjusted so that its corresponding detection densities would approximately match those of the $T_{\text{exp}} = 0.24$ s one. The detection sets produced by each of the ten threshold pairs then underwent their own attitude correction before their tracking runs were started (using the parameters listed in Table A.1). As with the previous optimization processes, we surveyed the total number of tracks, and the numbers of tracks with $\Gamma = 0\%$ and $\Gamma < 30\%$. After inspecting the most promising results more closely, we found that the best were produced by detection thresholds of $S/N = 2.7$ ($T_{\text{exp}} = 6$ s) and $S/N = 3.6$ ($T_{\text{exp}} = 0.24$ s). They roughly correspond to an average detection density of 27.12×10^{-4} detections per pixel, or about 7000 detections per image.

Compared to the results produced by our initial set of tracking parameters (see Fig. 15), the optimization increased the total number of tracks by $\sim 18\%$ (from 1922 to 2268), the number tracks with $\Gamma < 30\%$ by $\sim 21\%$ (from 642 to 775), and the number of tracks without missing detections by $\sim 46\%$ (from 96 to 140)².

² While Fig. 15 and the numbers discussed here are based on data produced by the latest version of the tracking algorithm, the optimization was unfortunately run on a previous version where the pointing fluctuation was slightly miscalculated due to a bug. However, because the error in the pointing fluctuation was small (< 0.5 px), and because the selected parameter values are only estimates of the optimal values that also work well with the correct pointing fluctuation, we decided against rerunning the optimization procedure.

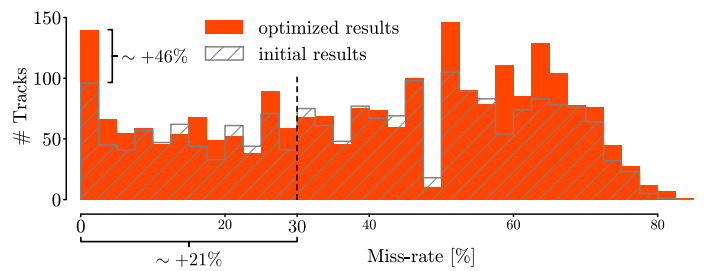


Fig. 15. Effect of parameter optimization on the miss-rate distribution. Gray, hatched bars show the results produced by the initial set of tracking parameters, orange ones the optimized set.

5. Results and discussion

The goal of this study was to develop a robust algorithm to track dust particles of 67P in image sequences recorded by OSIRIS NAC. As proof of concept, we applied the algorithm to sequence STP090 and optimized the tracking parameters. In the following, we first assess the general reliability of the tracking algorithm, and then give examples of how the tracking results can be evaluated to answer scientific questions.

5.1. Algorithm assessment

5.1.1. Simulation

To test our algorithm's tendency to create spurious tracks we simulated datasets which consisted entirely of random noise (i.e., “detections”), with detection densities ranging from 27.59×10^{-4} to 39.42×10^{-4} det. px⁻¹. Although the algorithm identified a few hundred to more than two thousand spurious tracks in the simulations depending on their detection density, it found few to none in the critical miss-rate regime below 30%. In particular, we

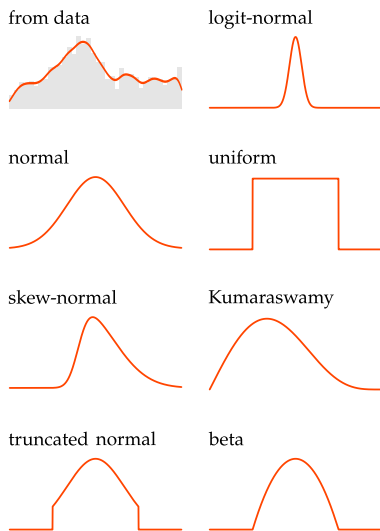


Figure 4.16: Sample distributions that can be used to generate simulation parameters. The data distribution at the top left shows the distribution of the horizontal starting points of tracks in sequence STP090.

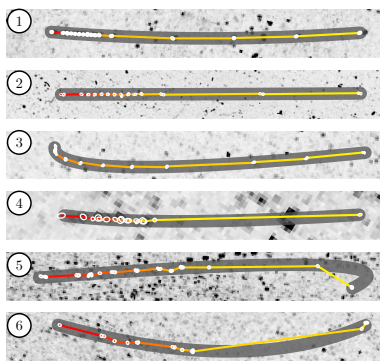


Figure 4.17: Exemplary tracks identified as being ① pure, ② contaminated, ③ aliased (notably, in this case, I believe that all detections are of the same particle), ④ inconclusive, ⑤ compromised, or ⑥ spurious. Tracks are shown as gradient lines from red to yellow, detections as white ellipses. Semi-transparent, thick curves indicate the parabolas fitted to the tracks. Images have been rotated to better fit the page.

Things that can influence the flagging of tracks are, for example: the detection offset from the fit, the detection alignment in the master image with PSFs that are actually from a different image, faint yet real particle PSFs, large gaps between detections, and the shape of the curves. There is likely also a bias against faster particles, because at the same number of detections it might still be possible to verify a short track, but not a long one. Theoretically, the manual evaluation could be tested on simulated data, but that would at least also require a realistic master image.

As already mentioned in Section 2.2, the simulation software can actually do much more than just simulate noise. It can for example extract modeling parameters directly from an image sequence and its detection and tracking results. These parameters include:

- ▶ sequence-specific parameters such as image dimensions, number of images, duration, and time intervals
- ▶ the camera motion and pointing fluctuation
- ▶ the (image-specific) detection density
- ▶ the (image-specific) signal-to-noise ratio
- ▶ the number of sidereal objects and their miss-rates
- ▶ the number of particle tracks, their dynamics, origins, detection offsets, and miss-rates

Many of these parameters of course follow some kind of probability distribution, so I used Gaussian kernel density estimation to model the distributions based on their histograms (not super accurate but good enough), and implemented methods that allow to draw samples from them. But at the same time, I also implemented several other probability distributions that could be used instead. They include normal, skew-normal, truncated normal, logit-normal, uniform, Kumaraswamy, and beta distributions (see Fig. 4.16). All these distributions and parameters can then be further customized. Unfortunately, I never had the chance to really explore these options, but test runs showed that simulated tracks were generally well recovered. The most influential parameters were typically the scatter of detections from their true locations, the miss-rate, and eventually the signal-to-noise ratio.

Originally, I used a more elaborate system, where I additionally flagged genuine tracks if they showed signs of being:

- ▶ *contaminated*, that is, if they seem to contain unrelated detections;
- ▶ *aliased*, that is, if the orientations of their detection pairs are misaligned with their general shape, creating a step-like effect (this can e. g. happen if tracks are crossing and pairs from one track are incorporated in another, but can also be due to inaccurate detection locations);
- ▶ *inconclusive*, that is, if the extended part of a track may be correct (usually the case when it consists of only very few detections), but does not seem to significantly affect the track's properties (like velocity and acceleration);
- ▶ *compromised*, that is, if unrelated detections incorporated into a track seem to significantly affect its properties.

If they did not show any of those signs, I flagged them as *pure*, and if they did not seem to be genuine, I flagged them as *spurious*. Figure 4.17 shows examples for each of the cases. But because this system was rather complex, it was also more susceptible to subjective biases, and so we ultimately decided to simplify it.

Judging the validity of a track is of course still fairly subjective (even flagging the same data twice on separate days will yield slightly different results, see also Sect. 5.2). Yet the general trends are very solid, especially regarding the clear distinction between the two populations based on their miss-rate distributions (as shown in Fig. 17.1 in the methods paper).

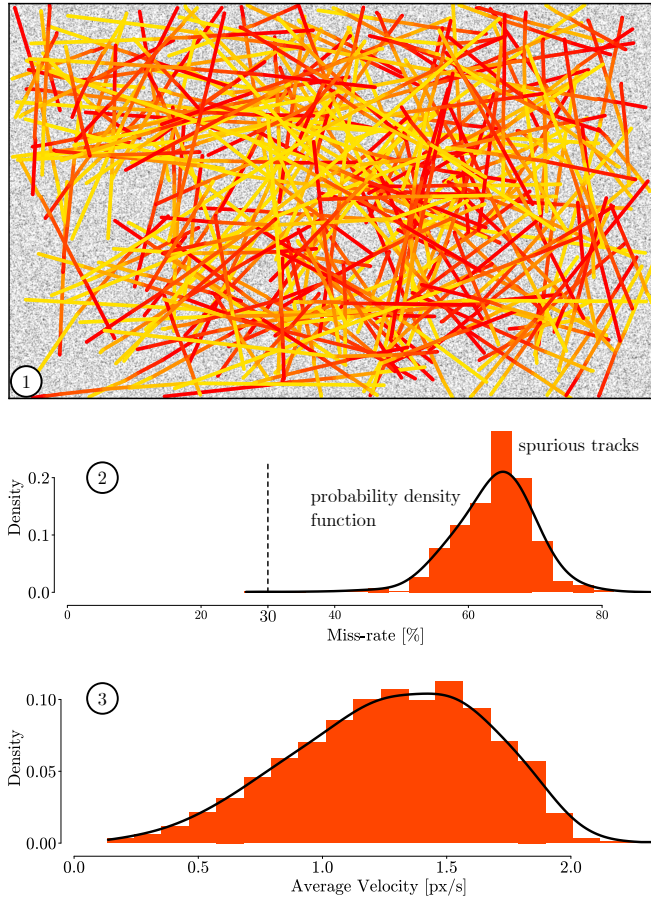


Fig. 16. Results from simulated data: (1) one of the ten simulations with a detection density of 27.59×10^{-4} det. px $^{-1}$. The identified tracks are shown as gradient lines from red to yellow. The background image serves merely as a visual aid, showing the rough locations of detections (it is not a stack of images created to run the detection algorithm on; instead the detections were simulated first and the background image was created retroactively). (2) the combined miss-rate distribution from the ten simulations with a detection density of 27.59×10^{-4} det. px $^{-1}$. (3) the velocity distribution of the same track population, showing a clear tendency of the algorithm to create more fast spurious tracks, especially when compared to velocity distributions from real data (Fig. 17.2). The probability density functions were created with Gaussian kernel density estimation.

simulated ten different datasets for the detection density closest to that of the optimal detection thresholds (27.59×10^{-4} det. px $^{-1}$, Fig. 16). In those cases, only 260 tracks were found on average, and in total only 6 with $\Gamma < 30\%$.

5.1.2. Manual assessment

To further assess the reliability of our algorithm, we inspected and manually flagged each track found in sequence STP090 according to the following system: if they are (a) genuine, that is, whether we believe that they belong to actual particles and contain few to no unrelated detections, or if they are (b) ambiguous, that is, whether we believe that (the majority of) their detections do not belong to the same particle, stem from noise, or when it is impossible to tell.

Of the 2268 tracks, we flagged 1081 (~48%) as ambiguous, leaving 1187 (~52%) as genuine. Figure 17.1 shows that the miss-rate distributions of the ambiguous and genuine tracks have distinct shapes. In particular, only very few (4) of the ambiguous

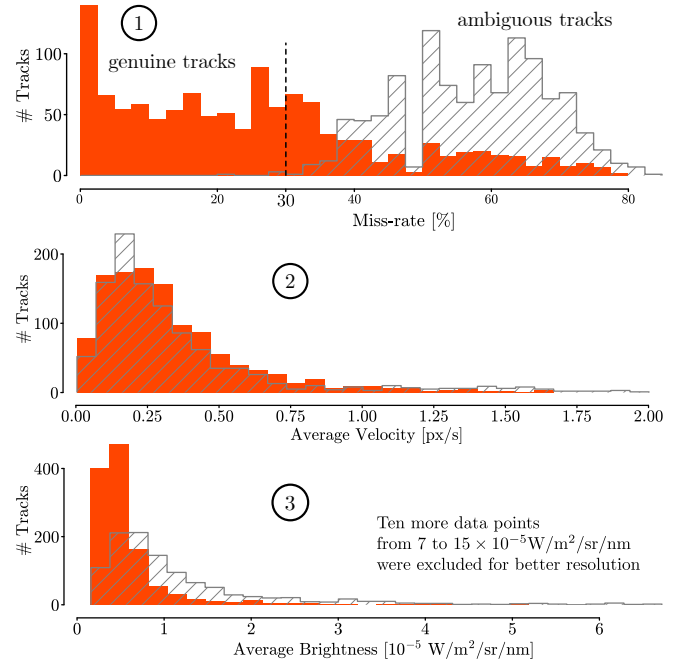


Fig. 17. Miss-rate (1), velocity (2), and brightness (3) distributions of tracks identified as either genuine (orange) or ambiguous (gray hatched).

tracks have miss-rates less than 30%. This is a good sign that our decision to base the parameter optimization on the number of tracks with $\Gamma < 30\%$ was appropriate. This is also further supported by the fact that the miss-rate distribution of the spurious tracks (Fig. 16.2) is very similar in shape to that of the ambiguous ones.

Because manually judging the validity of tracks becomes increasingly difficult with the spread of their detections, we expect a bias against faster particles in the flagged tracks. Figure 17.2 shows that such a trend seems to exist in our data, though only slightly. Figure 16.3 on the other hand shows that our algorithm tends to create more fast than slow spurious tracks. Both effects probably contribute to the excess of fast ambiguous tracks.

We also expect a bias toward flagging faint tracks more often as ambiguous. Figure 17.3 however shows that the opposite was the case. This is likely caused by the overabundance of detections in the bright active area in the center of sequence STP090 (e.g., see Fig. 2): while of the genuine tracks only ~15% originate from here, of the ambiguous ones it is ~22% (the section indicated in Fig. 19.1 was used to calculate those numbers).

5.2. First results

In the following, we present examples of how our tracking results can be used and interpreted. Since they mainly serve as a technical demonstration, we do not perform detailed analyses. Nevertheless, because $\Gamma < 30\%$ proved to be a good criterion to identify genuine tracks, we only consider the 775 tracks that satisfy it—more than three times as many tracks than were identified by Agarwal et al. (2016).

Figure 18 shows the velocity- and acceleration-angle distributions of all 775 tracks. The projected velocity components of most tracks point upward, seemingly away from the nucleus and the central active area. This aligns well with what would be expected and Agarwal et al. (2016)'s findings. The projected

Although Figure 18 in the methods paper clearly shows that there are predominant directions for the particle velocities and accelerations (and even though their distributions are pretty much continuous), it is still interesting to look at other “dynamical groups”. I show some of them on the last two double-pages of this chapter (pp. 80 and 78).

The velocity vector of a track and especially its orientation can of course drastically change during its observation. So the projected velocity that we are referring to here is just the velocity that the particle had when we first detected it according to the fit (same for the projected acceleration).

This criterion actually turned out to be incredibly accurate (at least for sequence STP090). For the science paper, I developed a more sophisticated method to select tracks and associate them with a surface area on the nucleus. In case of sequence STP090, this allowed me to identify 178 tracks (so coincidentally exactly twice as many as here, but also using results from a slightly improved tracking algorithm). The new method is more reliable, but as Figure 4.18 shows, almost all 178 tracks are pointing upward within $\pm 45^\circ$ (only 6 do not). For sequences STP089 and STP087, which we also analyze in the science paper, this old criterion does however not really work.

I also tried to see if there are any other areas where particles are grouped closer together, which might have been an indication of bursts or clusters (e. g., as reported by Shi et al. 2019, 2024). But Figure 4.19 shows that this does not seem to be the case. Instead, it seems that the activity was more or less constant over the hour leading up to the beginning of sequence STP090 (since the particles we observe were likely ejected at least half an hour earlier).

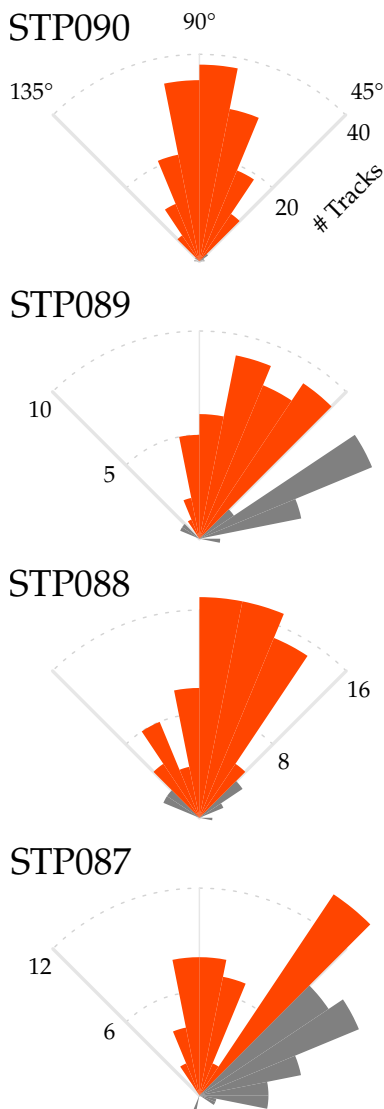


Figure 4.18: Velocity angle distributions of the particle populations that we selected with our more sophisticated method described in the science paper. The upward directions (90°) correspond to the direction that is approximately normal to the surface regions where the particles are assumed to originate from (bars within $\pm 45^\circ$ of upward direction orange, bars outside gray). In case of sequence STP090 that direction just happens to be parallel to the y-axis of the master image.

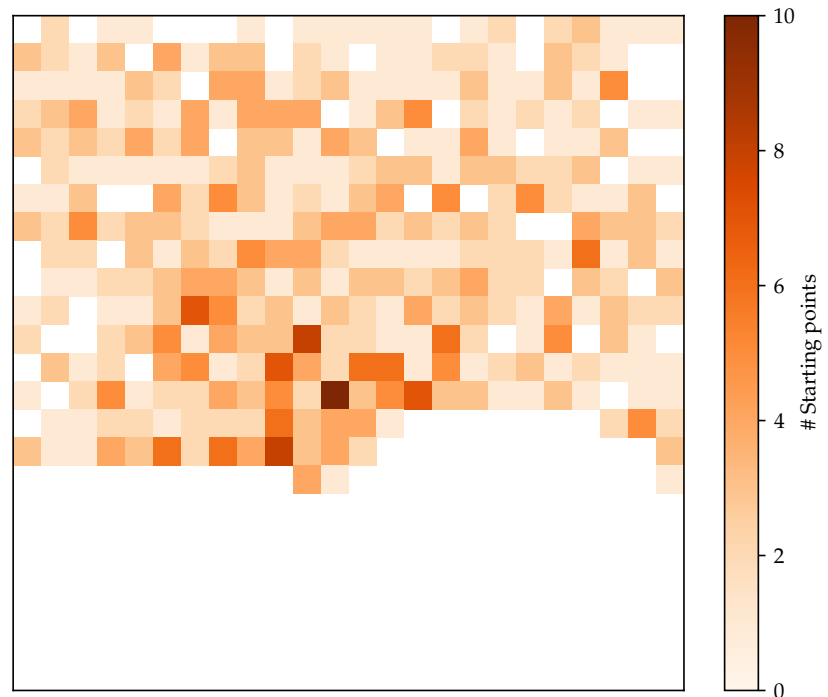


Figure 4.19: Two-dimensional histogram of the track starting point locations.

M. Pfeifer et al.: On the trail of a comet's tail: A particle tracking algorithm for comet 67P/Churyumov-Gerasimenko

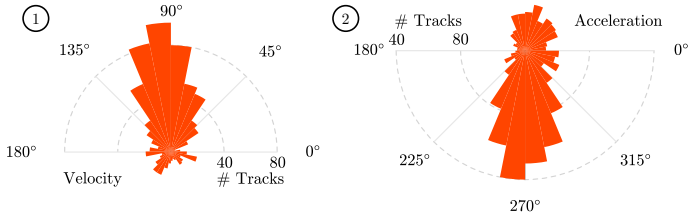


Fig. 18. Angle distributions of the projected velocity (1) and acceleration (2) of all 775 selected tracks. The orientations of the diagrams coincide with how the images of sequence STP090 are displayed (i.e., 0° corresponds to the right direction, 90° to the up direction, etc.). While the projected velocity of most tracks seems to be pointing away from the nucleus, the acceleration of a similar number of tracks seems to be pointing toward it.

acceleration components on the other hand mostly point downward and seem to be dominated by the nucleus' gravity.

To derive particle radii and convert particle velocities and accelerations to physical units (e.g., from px s^{-1} to m s^{-1}), we need to know the particle distances to the spacecraft. Since the only accurate distance measurement we have is of the nucleus (~ 86 km), we focus on particles which were seemingly just ejected from the active area in the center of the images (at that distance $1 \text{ px} \equiv \sim 1.6$ m). In the following example, we isolated this group in two steps. First, we chose a region around the active area and selected the tracks that originate within it (106 tracks, Fig. 19.1); then, we further reduced the group by selecting only tracks whose projected velocities are pointing upward within $\pm 45^\circ$ (89 tracks, Fig. 19.2). Figure 20 shows the selected tracks as they appear in front of the stacked image of sequence STP090.

Figure 19.3 shows that roughly 47% of the selected tracks have a projected acceleration that points away from the nucleus. The velocity distribution (Fig. 19.4) shows that they are on average faster than the particles that are accelerated downward. Most particles show a net acceleration less negative than gravity (Fig. 19.5). Assuming that on a first order the gravitational acceleration is comparable for all particles they must be experiencing an upward directed acceleration of variable strength that partially compensates or even exceeds gravity. A likely candidate for this upward force is gas drag.

Figure 19.6 shows the distribution of the particle radii, which were calculated as:

$$r = \sqrt{J \frac{r_h^2 \Delta^2}{RI_\odot}}, \quad (11)$$

where r is the radius in m, J the average particle flux in $\text{W m}^{-2} \text{ nm}^{-1}$, r_h the dimensionless heliocentric distance measured in units of AU, Δ the observer-particle distance in m, $R = 0.0021$ the particle reflectance (computed for decimeter-sized particles using the model in Markkanen et al. 2018), and $I_\odot = 1.565 \text{ W m}^{-2} \text{ nm}^{-1}$ the solar flux in the NAC F22 filter at 1 AU. The distribution agrees with Agarwal et al. (2016)'s findings when considering that their calculation is affected by a numerical error that leads them to systematically underestimate the radii by a factor of 4.4 (Agarwal et al., in prep.). It furthermore shows no clear trend between the upward- and downward-accelerated particles, which is remarkable because the gas drag we deem responsible for the upward-acceleration should be stronger for smaller particles.

If we assume that the particles have the same bulk density as the nucleus (533 kg m^{-3} , Pätzold et al. 2016), then

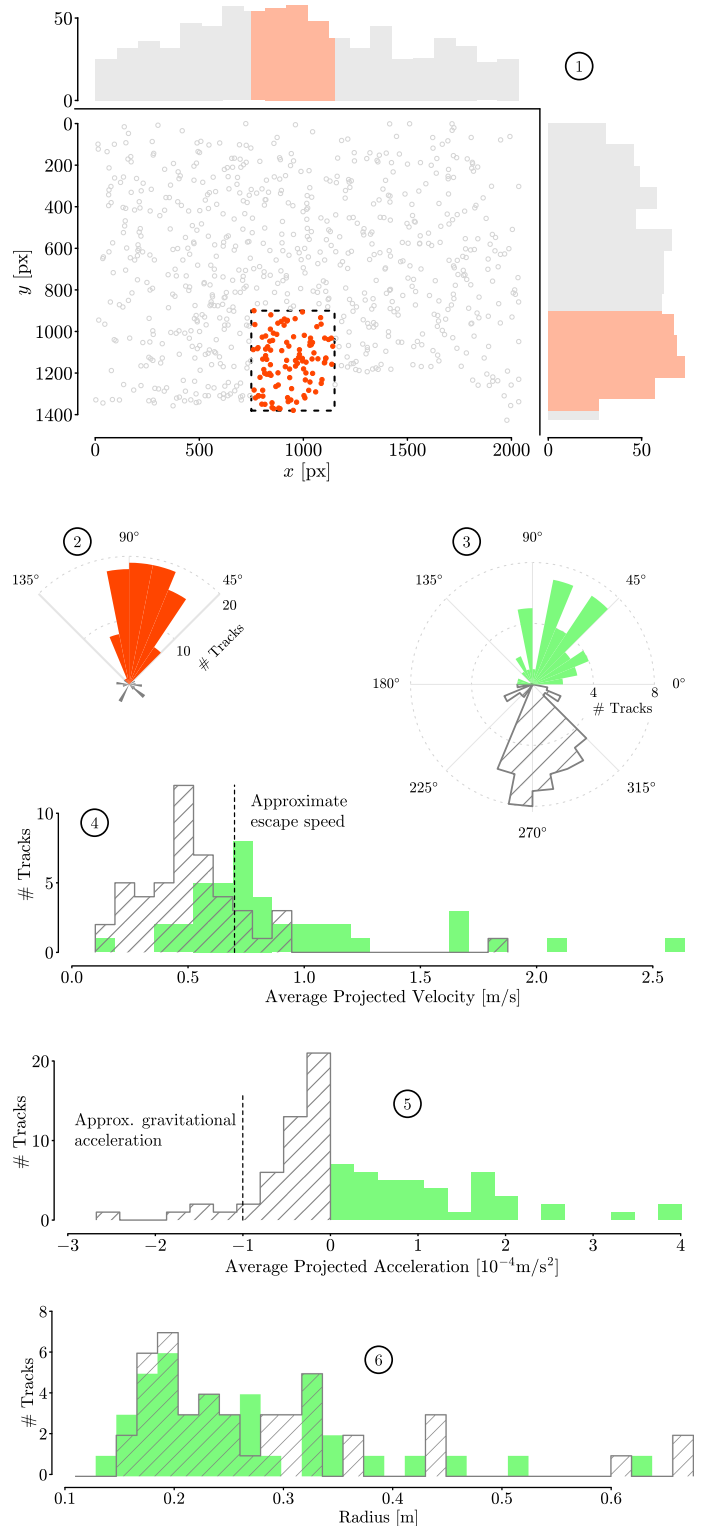


Fig. 19. Selection process and statistics of particles that likely originated from the central active area: (1) the starting points of all 775 tracks (i.e., their earliest confirmed locations) and the tracks we selected (orange circles) that start near the active area. (2) a further reduction of the tracks selected in (1) by choosing only the ones directed upward $\pm 45^\circ$ (orange). (3) the acceleration angle distribution of the tracks selected in (2), which is further divided into tracks that are accelerated upward (green) and downward (gray hashed). (4, 5, 6) the projected velocity, magnitude of acceleration and radius distributions for the two track populations defined in (3). Escape speed and gravitational acceleration based on Pätzold et al. (2016).

Even though the residual offset is checked during a pursuit, its scatter after the fact might have still been an indicator of a track's "cohesiveness". Yet even the best tracks are affected by residual noise from the pointing fluctuation, and in some cases, our simple dynamical model of second-order polynomials is also not good enough to properly describe the trajectory of a particle, as I discuss in the science paper.

Because tracks have a discrete number of detections, the miss-rate favors particles with a long residence time (i.e., a single missing detection e.g. has a stronger effect on particles that were only briefly visible). So the number of missing detections might have allowed to distinguish some of the shorter genuine tracks.

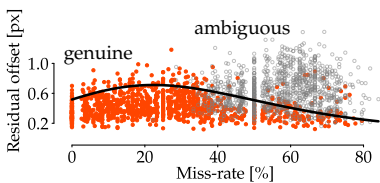


Figure 4.20: Residual offset vs. miss-rate for genuine and ambiguous tracks. Together, these parameters might yield a better criterion than just the miss-rate alone, but discerning their optimal relationship is non-trivial. A skew normal distribution (black curve, fitted by eye) might be an option. Indeed, since populations are usually normally distributed, it was suggested to me to use the expectation-maximization (EM) algorithm for Gaussian mixtures (e.g., Dempster et al. 1977; Bishop 2006; McLachlan et al. 2007). Other options may also be principal component analysis (e.g., Jolliffe et al. 2016) or even a decision tree.

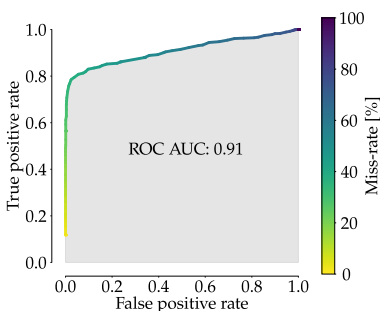


Figure 4.21: ROC curve of the miss-rate illustrating its predictive ability. The true (false) positive rate is the ratio between the number of genuine (ambiguous) tracks that a certain miss-rate correctly (wrongly) marks as genuine, and the total number of tracks that I flagged as genuine (ambiguous). The area under the curve (AUC) indicates how well the predictor is generally performing (random guessing e.g. corresponds to the angle bisector or an AUC of 0.5; see e.g., Fawcett 2006).

There seem to be no other obvious parameters (or combinations thereof) that are as reliable and simple as the miss-rate criterion. I for example tested the mean particle radiance and its standard deviation, the average residual offset, the number of missing detections, and miss-rates specific to the principal and extended part of a track (because principal tracking is much more reliable than extended tracking, so tracks with high "extended" miss-rates may have been more ambiguous). For some the parameters, there are certain trends (see Figs. 4.20 and 4.22), but none of them are as distinct as in case of the miss-rate. The miss-rate criterion remains the strongest predictor by far, which is also shown by the receiver operating characteristic (ROC) curve in Figure 4.21.

Yet even with the miss-rate, it is important where to set the threshold. Relevant factors in this regard are for example the (expected) total number of genuine and ambiguous tracks below the threshold, their ratio, and how these numbers change with varying thresholds. Our 30%-threshold is a very conservative choice, but it guaranties that virtually all the tracks with lower miss-rates are genuine. Figure 4.23 for example shows that even a 40%-threshold would still be a viable choice.

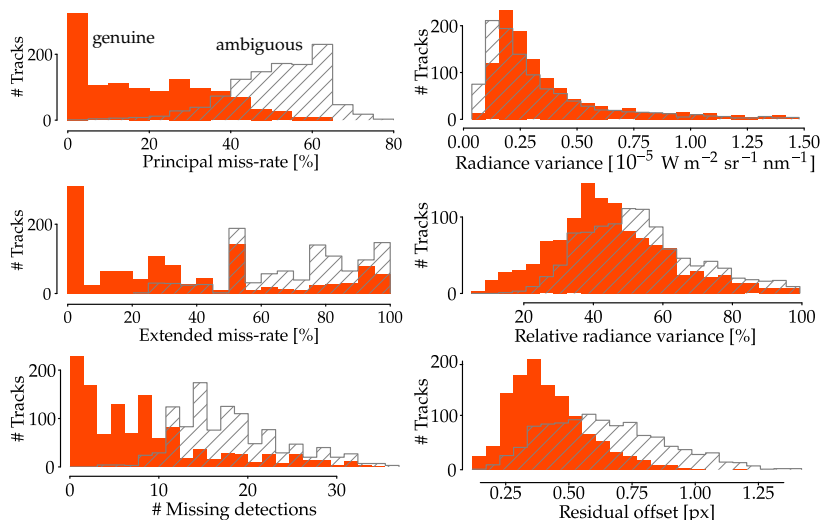


Figure 4.22: Distributions of potential predictor parameters for genuine and ambiguous tracks (as identified in the methods paper). The distributions in the three plots on the right have very long tails that are cut off for a better presentation.

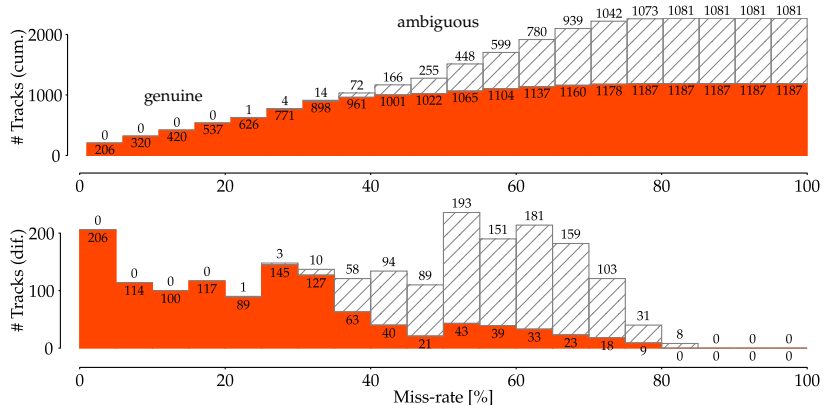


Figure 4.23: Cumulative (top) and differential (bottom) number of genuine and ambiguous tracks as a function of their miss-rate (in steps of 5%). Below $\Lambda = 30\%$, only $\sim 0.5\%$ of tracks are ambiguous, while below a $\Lambda = 40\%$, it's $\sim 7\%$. Going beyond $\Lambda = 40\%$ however, likely only yields diminishing returns (at best).

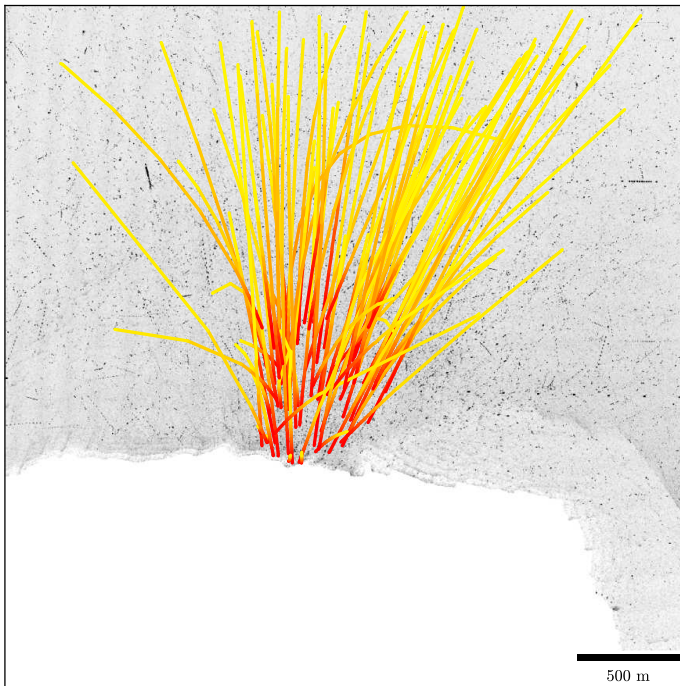


Fig. 20. 89 selected tracks near the central active area.

the upward-accelerated particles contain about 1300 kg, while the downward-accelerated ones contain roughly 3000 kg. The largest boulder alone contains more than half of the mass of the upward-accelerated particles.

A similar extended analysis would be interesting to compare to typical models of cometary dust size distributions (e.g., [Blum et al. 2017](#), and references therein), as they predict that the majority of mass lost due to refractory material is likely contained in the largest specimen. Hence knowing the size limit and emission rate of the largest chunks is crucial to estimate a comet's contribution to the interplanetary dust environment and the zodiacal cloud ([Nesvorný et al. 2011](#)).

Lastly, we can also extrapolate our tracks back in time to find out when and where the particles were likely ejected. As the process behind lifting decimeter-sized debris from the surface is not entirely understood (although it appears now to be more straightforward to explain than the lifting of smaller, micron-sized dust, [Gundlach et al. 2015](#)), this can provide us with possible clues about the lifting mechanism or its conditions.

6. Summary and outlook

In this paper we present our algorithm for tracking the motion of debris near the nucleus of comet 67P. The algorithm operates on image sequences recorded by Rosetta's camera system OSIRIS. The sequences typically show part of 67P's surface that ideally has at least one clearly discernible active area which is ejecting particles that appear as point sources against the dark backdrop of interplanetary space.

As an example and to assess the algorithm's reliability as well as presenting tentative first results, we applied our algorithm to image sequence STP090. The evaluation not only showed that our algorithm can find a large number of tracks, but also revealed a robust criterion—having a miss rate $\Gamma < 30\%$ —to separate genuine from ambiguous tracks. Our first results from a group of particles that satisfied the criterion and likely originated from

the central area in sequence STP090 demonstrate one way of how our tracking results can be used. And finally, knowing the projected particle velocities and accelerations can help us estimate the fall-back fraction and the refractory-to-ice ratio—which are key to understanding more about cometary interiors and the role comets play in planetesimal formation.

Acknowledgements. We thank Eberhard Bodenschatz, Ulrich Christensen, and Pablo Lemos for our fruitful discussions; Carsten Güttler, Michael Mommert, and Jakob Deller for their early support; Kyle Barbary, Benne Holwerda, Peter Stetson, Gábor Kovács, Cecilia Tubiana, Guus Bertens, Jan Molacek, and Maurizio Berti for their technical support; Asmus Freytag for proofreading; and Steve Chesley for reviewing our paper and providing constructive comments. We acknowledge the operation and calibration team at MPS and the Principal Investigator Holger Sierks on behalf of the OSIRIS Team for providing the OSIRIS images and related datasets. OSIRIS was built by a consortium of the Max-Planck-Institut für Sonnensystemforschung, Göttingen, Germany; the CISAS University of Padova, Italy; the Laboratoire d'Astrophysique de Marseille, France; the Instituto de Astrofísica de Andalucía, CSIC, Granada, Spain; the Research and Scientific Support Department of the European Space Agency, Noordwijk, The Netherlands; the Instituto Nacional de Técnica Aeroespacial, Madrid, Spain; the Universidad Politécnica de Madrid, Spain; the Department of Physics and Astronomy of Uppsala University, Sweden; and the Institut für Datentechnik und Kommunikationsnetze der Technischen Universität Braunschweig, Germany. The support of the national funding agencies of Germany (DLR), France (CNES), Italy (ASI), Spain (MEC), Sweden (SNSB), and the ESA Technical Directorate is gratefully acknowledged. We thank the Rosetta Science Ground Segment at ESAC, the Rosetta Missions Operations Centre at ESOC and the Rosetta Project at ESTEC for their outstanding work enabling the science return of the Rosetta Mission. M. P. and J. A. acknowledge funding by the ERC Starting Grant No. 757390 Comet and Asteroid Re-Shaping through Activity (CAstRA). J. A. acknowledges funding by the Volkswagen Foundation.

References

- Agarwal, J., A'Hearn, M. F., Vincent, J.-B., et al. 2016, *MNRAS*, 462, S78
 Bannister, M. T., Kavelaars, J. J., Petit, J.-M., et al. 2016, *AJ*, 152, 70
 Barbary, K. 2016, *J. Open Source Software*, 1, 58
 Beard, S. M., MacGillivray, H. T., & Thanisch, P. F. 1990, *MNRAS*, 247, 311
 Bertin, E., & Arnouts, S. 1996, *A&AS*, 117, 393
 Bertini, I., Gutiérrez, P. J., Lara, L. M., et al. 2015, *A&A*, 583, A19
 Blum, J., Gundlach, B., Krause, M., et al. 2017, *MNRAS*, 469, S755
 Canny, J. 1986, *IEEE Trans. Pattern Anal. Mach. Intell.*, PAMI-8, 679
 Chenouard, N., Smal, I., de Chaumont, F., et al. 2014, *Nat. Methods*, 11, 281
 Chesley, S. R., French, A. S., Davis, A. B., et al. 2020, *J. Geophys. Res.: Planets*, 125, 2019JE006363
 Choukroun, M., Altwegg, K., Kühr, E., et al. 2020, *Space Sci. Rev.*, 216, 44
 Davidsson, B. J. R., Gutiérrez, P. J., Sierks, H., et al. 2015, *A&A*, 583, A16
 Denneau, L., Jedicke, R., Grav, T., et al. 2013, *PASP*, 125, 357
 Drolshagen, E., Ott, T., Koschny, D., et al. 2017, *Planet. Space Sci.*, 143, 256
 Frattin, E., Cremonese, G., Simioni, E., et al. 2017, *MNRAS*, 469, S195
 Frattin, E., Bertini, I., Ivanovski, S. L., et al. 2021, *MNRAS*, 504, 4687
 Fulle, M., Marzari, F., Corte, V. D., et al. 2016, *AJ*, 821, 19
 Ginsburg, A., Sipőcz, B. M., Brasseur, C. E., et al. 2019, *AJ*, 157, 98
 Gladman, B. J., Davis, D. R., Neese, C., et al. 2009, *Icarus*, 202, 104
 Gundlach, B., & Blum, J. 2016, *A&A*, 589, A111
 Gundlach, B., Blum, J., Keller, H. U., & Skorov, Y. V. 2015, *A&A*, 583, A12
 Güttler, C., Hasselmann, P. H., Li, Y., et al. 2017, *MNRAS*, 469, S312
 Hergenrother, C. W., Maleszewski, C. K., Nolan, M. C., et al. 2019, *Nat. Commun.*, 10, 1291
 Hergenrother, C. W., Adam, C. D., Chesley, S. R., & Lauretta, D. S. 2020, *J. Geophys. Res.: Planets*, 125, 2020JE006549
 Holman, M. J., Payne, M. J., Blankley, P., Janssen, R., & Kuindersma, S. 2018, *AJ*, 156, 135
 Hough, P. V. C. 1959, in *Proc. of the International Conference on High Energy Accelerators and Instrumentation*, ed. L. Kowarski, 590914, 554
 Jones, R. L., Slater, C. T., Moeyens, J., et al. 2018, *Icarus*, 303, 181
 Keller, H. U., Barbieri, C., Lamy, P., et al. 2007, *Space Sci. Rev.*, 128, 433
 Keller, H. U., Mottola, S., Davidsson, B., et al. 2015, *A&A*, 583, A34
 Keller, H. U., Mottola, S., Hviid, S. F., et al. 2017, *MNRAS*, 469, S357
 Kelley, M. S., Lindler, D. J., Bodewits, D., et al. 2013, *Icarus*, 222, 634
 Kelley, M. S., Lindler, D. J., Bodewits, D., et al. 2015, *Icarus*, 262, 187
 Kubica, J., Denneau, L., Grav, T., et al. 2007, *Icarus*, 189, 151
 Lai, I.-L., Ip, W.-H., Su, C.-C., et al. 2016, *MNRAS*, 462, S533

Because it is currently not possible to include pdf pages with working hyperlinks in a \LaTeX -document, I manually added all hyperlinks back into the methods paper (except for those found in the bibliography here). Citations within the digital version of this document therefore redirect to the bibliography at the end of this dissertation.

* * *

The following Figures 4.25–4.27 show some dynamic particle populations from sequence STP090. So far, in every plot that showed tracks (featured in the methods paper but for consistency also in the in-situ discussions), the color gradient of the tracks went from red to yellow and was generally used to indicate the direction of flight. The gradient was however always track-specific, that is, while the time was used to parameterize the gradient, it was always fit to the duration of each individual track. The same color could therefore correspond to different times depending on the track. Because this can be misleading and because it can be interesting to compare the timing of different tracks, from now on, the gradients follow a “global” parameterization that is also used in the science paper. This means that the gradients of all the tracks shown in a single image are scaled to the same time interval, which starts with the first detection of the earliest track and ends with the last detection of the latest (i. e., the maximum time interval, which is usually equal to the observational period of the respective sequence). Consequently, the same color now corresponds to the same time. But because red is a much “stronger” color (by which I mean that it is easier to spot), and because most tracks have left the FOV before they would really start turning yellow using the previous gradient, the color gradient is from now on also flipped, going from yellow to red (see Fig. 4.24).

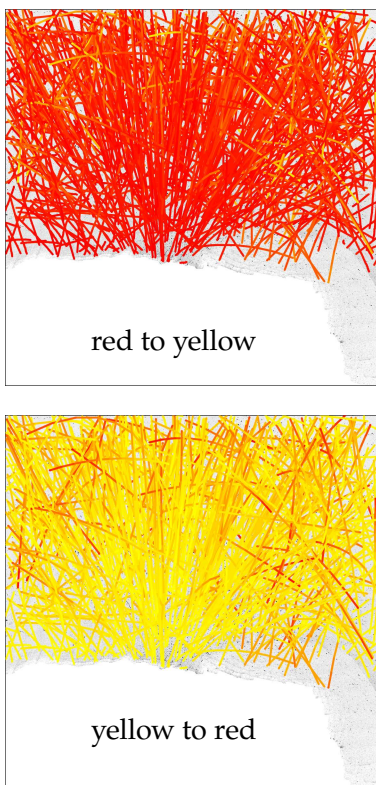


Figure 4.24: The 775 tracks identified in the methods paper with $\Gamma < 30\%$, once with a global gradient from red to yellow (top), and once from yellow to red (bottom). Despite the high density of tracks, some kind of structure can still be made out in the bottom image, while in the top image, that is virtually impossible. Nevertheless, the bottom image is still much too crowded, even though it only shows around one third of all tracks. Because of this, there is no point in ever showing more than a few hundred tracks at once.

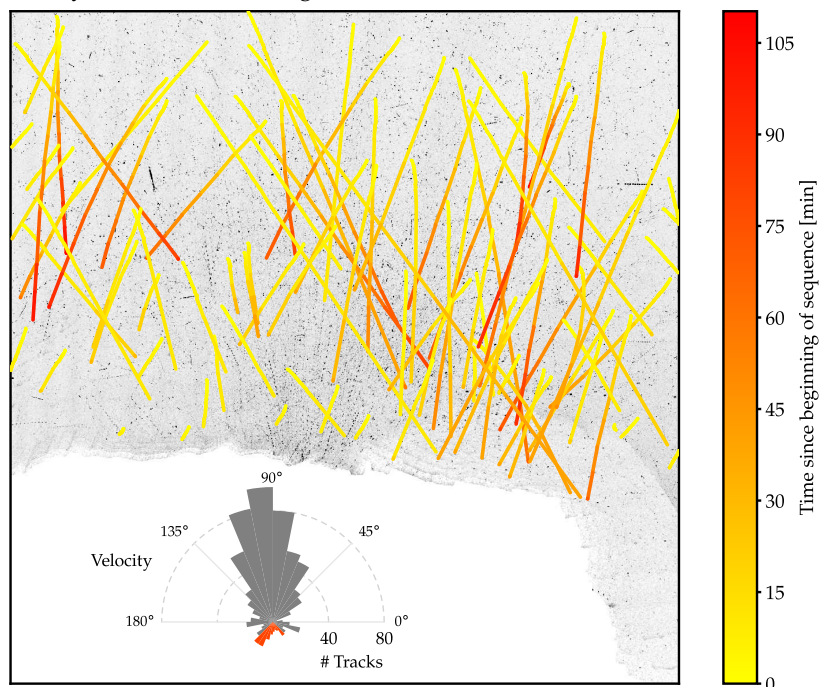


Figure 4.25: The group of tracks (of the 775 tracks with $\Gamma < 30\%$) whose velocity mainly points downward. Some of the corresponding particles seem to fly straight back down toward the nucleus, but unfortunately, it is impossible to tell if they were actually “above” the nucleus or far behind or in front of it.

M. Pfeifer et al.: On the trail of a comet's tail: A particle tracking algorithm for comet 67P/Churyumov-Gerasimenko

- Lauretta, D. S., Hergenrother, C. W., Chesley, S. R., et al. 2019, *Science*, **366**, eaay3544
- Leonard, J. M., Adam, C. D., Pelgrift, J. Y., et al. 2020, *Earth Space Sci.*, **7**, 2019EA000937
- Liounis, A. J., Small, J. L., Swenson, J. C., et al. 2020, *Earth Space Sci.*, **7**, 2019EA000843
- Lutz, R. K. 1980, *Comput. J.*, **23**, 262
- Mainzer, A., Grav, T., Bauer, J., et al. 2011, *AJ*, **743**, 156
- Marín-Yaseli de la Parra, J., Kueppers, M., Roger Pérez, J., & Osiris Team, T. 2020, in *Europlanet Science Congress 2020*
- Markkanen, J., Agarwal, J., Väisänen, T., Penttilä, A., & Muinonen, K. 2018, *ApJS*, **868**
- Masci, F. J., Laher, R. R., Rusholme, B., et al. 2018, *PASP*, **131**, 018003
- Moeyens, J., Jurić, M., Ford, J., et al. 2021, *AJ*, **162**, 143
- Mottola, S., Arnold, G., Grothues, H. G., et al. 2015, *Science*, **349**
- Nesvorný, D., Janches, D., Vokrouhlický, D., et al. 2011, *ApJ*, **743**, 129
- Ohsawa, R. 2021, *J. Space Sci. Inf. Jpn.*, submitted [arXiv:2109.09064]
- Ott, T., Drolshagen, E., Koschny, D., & Poppe, B. 2016, *International Meteor Conference, Egmond, the Netherlands*, 209
- Ott, T., Drolshagen, E., Koschny, D., et al. 2017, *MNRAS*, **469**, S276
- Pajola, M., Mottola, S., Hamm, M., et al. 2016, *MNRAS*, **462**, S242
- Pajola, M., Lucchetti, A., Fulle, M., et al. 2017, *MNRAS*, **469**, S636
- Pätzold, M., Andert, T., Hahn, M., et al. 2016, *Nature*, **530**, 63
- Pelgrift, J. Y., Lessac-Chenen, E. J., Adam, C. D., et al. 2020, *Earth Space Sci.*, **7**, 2019EA000938
- Petit, J.-M., Holman, M., Scholl, H., Kavelaars, J., & Gladman, B. 2004, *MNRAS*, **347**, 471
- Rabinowitz, D. L. 1991, *AJ*, **101**, 1518
- Reach, W. T., Vaubaillon, J., Kelley, M. S., Lisse, C. M., & Sykes, M. V. 2009, *Icarus*, **203**, 571
- Roger, J. 2019, @landru79, Twitter, 1126179023892242435
- Rose, K. A., Molaie, M., Boyle, M. J., et al. 2020, *J. Appl. Phys.*, **127**, 191101
- Rotundi, A., Sierks, H., Della Corte, V., et al. 2015, *Science*, **347**, aaa3905
- Stetson, P. B. 1987, *PASP*, **99**, 191
- Sykes, M. V., & Walker, R. G. 1992, *Icarus*, **95**, 180
- Thomas, N., Davidsson, B., El-Maarry, M. R., et al. 2015, *A&A*, **583**, A17
- Tinevez, J.-Y., Perry, N., Schindelin, J., et al. 2017, *Methods*, **115**, 80
- Tubiana, C., Güttler, C., Kovacs, G., et al. 2015, *A&A*, **583**, A46
- Ulman, V., Maška, M., Magnusson, K. E. G., et al. 2017, *Nat. Methods*, **14**, 1141
- Van Rossum, G., & Drake, Jr., F. L. 1995, *Python Reference Manual* (Centrum voor Wiskunde en Informatica Amsterdam)
- Waszczak, A., Ofek, E. O., Aharonson, O., et al. 2013, *MNRAS*, **433**, 3115
- Wenger, M., Ochsenbein, F., Egret, D., et al. 2000, *A&AS*, **143**, 9
- Westerweel, J., Elsinga, G. E., & Adrian, R. J. 2013, *Ann. Rev. Fluid Mech.*, **45**, 409

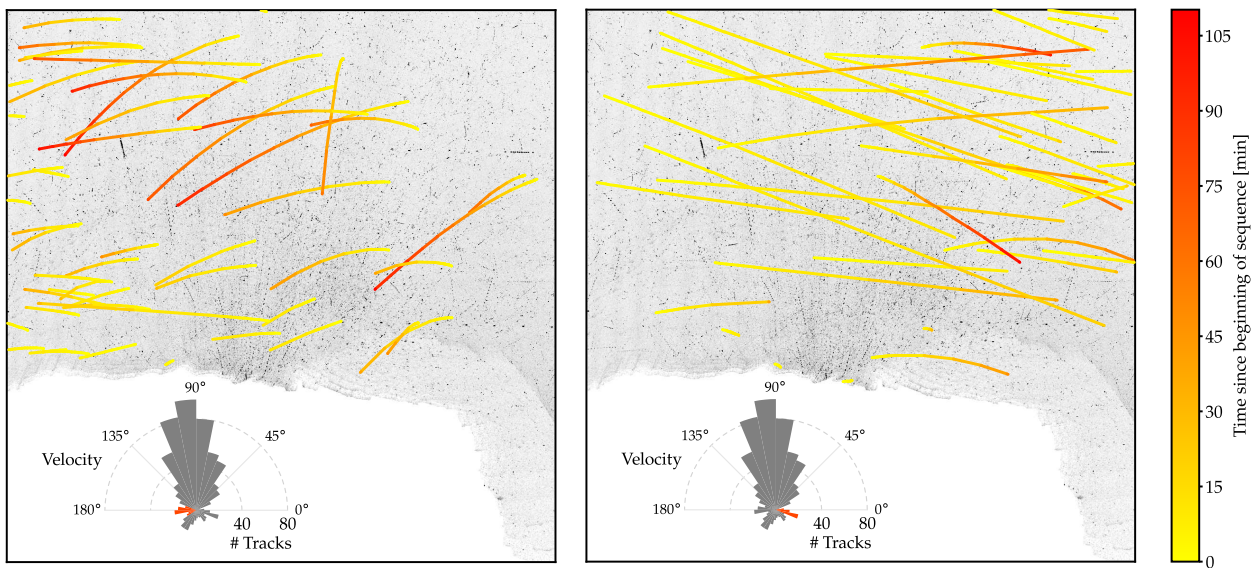
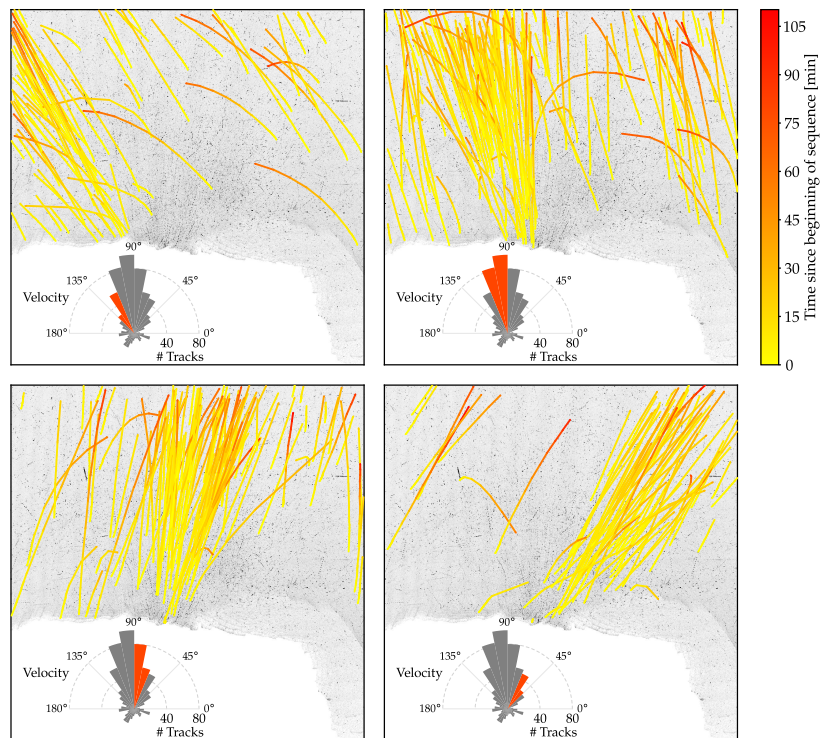


Figure 4.26: The two groups of tracks (of the 775 tracks with $\Gamma < 30\%$) that mostly fly to the left (left) or right (right). Interestingly, the corresponding particles that fly to the right seem to be a bit faster than the ones that fly to the left. Maybe this has to do with the rotation of the nucleus, which is rotating roughly clockwise in this sequence.

Figure 4.27: Four groups of tracks (of the 775 tracks with $\Gamma < 30\%$) that mostly fly upward. Interestingly, the dynamical groups also cluster spatially rather well. This may be because most of them come from a fairly confined area on the nucleus, while their ejection angles are governed by the local topography. Large walls (e. g., from fractures, hills, or valleys) might for example restrict certain ejection angles by blocking the flight path of particles that fly toward them. Likewise, the ejection angle might also be a consequence of particles being ejected from surface areas that face in the respective directions. This is further discussed in the science paper.



Appendix A: Tracking parameter values

Table A.1. Tracking parameter values used for sequence STP090.

Parameter	Principal tracking	Extended tracking
Educated Guesses		
R_{init} [px]	12	–
R_{off} [px]	2	–
N_{det}	8	0
N_{pair}	3	0
Lives	0	2
Systematic Optimization		
R_{max} [px]	6.5	9.5
R_{min} [px]	1.7	–
\hat{d} [px]	1.5	–
\bar{d}	7.8	–
Ω_{max} [°]	290	210
Ω_{min} [°]	40	–
\hat{d}_{Ω} [°]	4.4	–
\bar{d}_{Ω}	2.0	–
ΔV_{max} [%]	700	500
ΔV_{min} [%]	100	–
\hat{v} [px/s]	0.8	–
\bar{v}	0.8	–

Dashes indicate when the parameter values are the same for both principal and extended tracking, 0 when the parameter is not used in the given mode.

ADDITIONAL THOUGHTS

Since all models are wrong, the scientist must be alert to what is importantly wrong. It is inappropriate to be concerned about mice when there are tigers abroad.

— Box (1976). “Science and Statistics”.

BECAUSE the tracking parameters are such an elemental part of my tracking algorithm, in the following, I share some more (elaborate) thoughts and findings regarding their potential effects and the evaluation of tracking results.

5.1 THE DETECTION THRESHOLD

As previously explained on page 70, lowering the detection threshold is favorable to a certain point: being more sensitive to picking up fainter sources not only allows us to potentially track fainter particles, but it also lowers the miss-rate of tracks that for example vary strongly in brightness (such as oblate rotators), and consequently pushes borderline cases above the acceptance thresholds. Yet there exists a natural (subjective) lower bound for the threshold: the point at which detections cannot be identified as point sources by eye anymore. Even if these detections stem from real particles and not from noise artifacts, as soon as it becomes impossible to tell whether tracks are based on real signal, the results lose their meaning.

But there are also (at least) two technical criteria. For one, if the threshold is lowered to a level where noise can compete with the signal, a lot of noise will be picked up as well. This would for example lower the quality of genuine tracks and increase the number of spurious tracks (see also the discussion on p. 60). But even if all detections belong to real particles, at a certain detection density, the algorithm will end up creating tracks from unrelated detections (e. g., by an effect similar to aliasing, see Fig. 5.1). Improving the tracking results by lowering the detection threshold therefore only works to a certain limit, below which the quality of tracking results starts to decline again.

When optimizing the detection threshold, it turned out that the number of detections increased roughly exponentially with decreasing detection threshold (see Fig. 5.2). Interestingly, at higher thresholds, the first images generally have an overall lower number of detections than later images (plot ① in Fig. 5.2), but then the image order inverts with decreasing detection threshold. This may be because at higher thresholds, the algorithm mostly detects signal, while at lower thresholds, it falsely detects a lot more noise. And since half the extended images have significantly longer exposure times (6 vs 0.24 s, see p. 55) and thus much

CHAPTER CONTENTS

The Detection Threshold	83
More on Quality Control	85
Last Words on Simulations	87

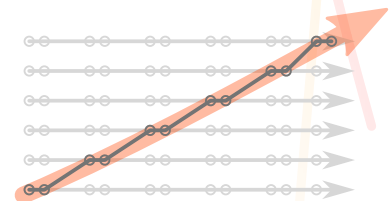


Figure 5.1: Simple illustration of the aliasing effect of a spurious track (semi-transparent orange arrow) created from unrelated detections (dark gray line and circles) that belong to genuine tracks (light gray arrows and circles). A similar effect can also be seen in genuine tracks (see Fig. 4.17), which is likely caused by residual pointing fluctuation noise.

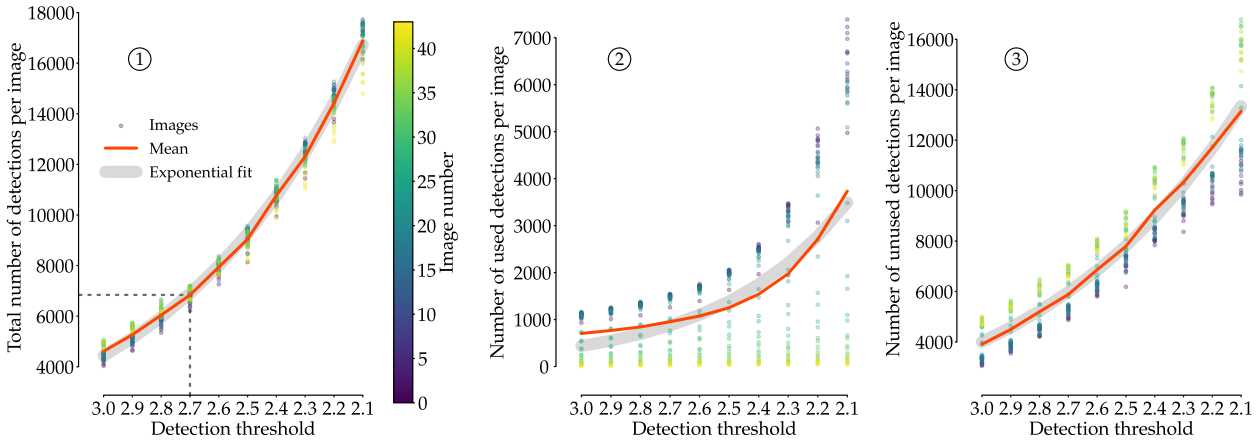


Figure 5.2: Total number ① and number of used ② and unused ③ detections (i. e., detections that did or did not become part of tracks) per image if sequence STP090, as a function of the detection threshold. For simplicity, the x -axis only shows the threshold values for the images with $T_{\text{exp}} = 0.24$ s (see p. 71). The dashed lines indicate the threshold value that we chose in the methods paper (2.7) and the corresponding mean number of detections per image. The latter is averaged over the whole image sequence and its trend can be roughly described by an exponential function. Also shown are the individual numbers of detections per image, color-coded by their image number.

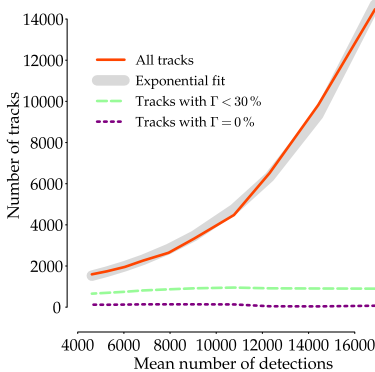


Figure 5.3: Total number of tracks and number of tracks with $\Gamma < 30\%$ and $\Gamma = 0\%$ as a function of mean number of detections per image. The total number of tracks can be roughly described by an exponential function, while the numbers of tracks with $\Gamma < 30\%$ and $\Gamma = 0\%$ are virtually constant.

better signal-to-noise ratios, they have more point sources that can cross the higher thresholds. At lower thresholds however, the noise from the noisier principal images with their short exposure times (0.24 s) is picked up faster. Another interesting feature is the large spread in the image data when it comes to the number of used detection (plot ② in Fig. 5.2). This is a direct result of principal and extended tracking, the acceptance thresholds, but also the residence time of the tracks. While the acceptance thresholds dictate that each track has to be detected at least a certain number of times in the principal sequence, in the extended sequence, many of them will not be found again, often because they already left the FOV.

Likewise, the total number of tracks also increased roughly exponentially with an increasing number of detections (see Fig. 5.3). This makes intuitive sense, as more detections not only beget more tracks, but they also close gaps within tracks that would have otherwise not made it past the acceptance thresholds. The trend in the total number of tracks shown in Figure 5.3 is therefore not unexpected, but it is still somewhat surprising, since after a certain point, the relation should become linear (if a track e. g. has to have at least ten detections and there are 100 detections in total, then in the perfect case, 10 tracks are recovered, but it cannot go beyond that). But it seems that this point was not yet reached.

Additionally, the number of tracks with $\Gamma < 30\%$ and $\Gamma = 0\%$ remained virtually constant with increasing number of detections. This may be a testament to the robustness of our tracking algorithm, but there could also be other mechanisms at play. At the highest detection densities, I would expect there to be suitable detections at every step, which would result in dropping miss-rates. But maybe the velocities and accelerations of most spurious tracks quickly become outlandish so that their pursuits fail during extended tracking.

The statistics of the other parameters that we optimized are however not worth showing. The number of tracks was almost unaffected by the tested parameter ranges, showing only small peaks. Accordingly, our initial guesses were already pretty good.

5.2 MORE ON QUALITY CONTROL

As already mentioned on page 70, the quality of the tracking results can ultimately only be assessed by a human. One of the criteria that I used to determine the validity of a track was the number of unrelated detections that it included (although I did so only qualitatively; I never literally counted all the unrelated detections). While I generally believe that this is a good criterion because it not only reflects the “purity” of a track but also indicates how reliable its derived dynamics likely are, in reality, it is often hard to discern (and if the algorithm were able to do it, tracks would not have unrelated detections in the first place).

To better or worse, humans are particularly susceptible to a bias called *apophenia*—the tendency to see patterns everywhere even if there are none (e. g., Hubscher 2007). Thus, I always tried to be conservative with my judgment and rather dismiss than accept tracks whose validity was not immediately clear. As an example, Figure 5.4 shows three tracks that I flagged as ambiguous, but unfortunately, it is impossible to convey the “actual” appearance of the tracks on paper. In my program, I can for example pan or zoom around, blend in and out different elements, or adjust the contrast of the background image. This interactivity gives a much better “feeling” for the tracks. Nevertheless, Figure 5.4 hopefully shows that things like the shape of the fitted curve or the arrangement of the detections can be deceiving (in one way or the other). The dense, linear arrangement of detections at the beginning of track #118 is for example a generally good indicator that this part of the track is genuine, which cannot be said with certainty about the rest of the detections. The overall shapes of the tracks however look convincing (they usually do), so there is a chance that they are genuine. Sometimes, it also helps to look at the orientation of the velocity and acceleration vectors of a track to see if they make sense, but this is rarely the case (especially without knowing where those tracks are supposed to be in relation to the observer). But ultimately, the signal of their detections was just too weak to really stand out from the noise, so I flagged them as ambiguous.

A different case is shown in Figure 5.5. Here, the track is actually genuine, although its shape is very unusual. From the looks of the detection arrangement and the straight, gradient lines that connect them, the track seems odd, especially because of the sharp kink after the first 24 detections (there are many tracks that start out the same way, but they usually continue to be fairly straight). The fitted curve and the velocity and acceleration vectors on the other hand seem reasonable, and the master image shows that the associated detections clearly stand out from the background noise. But in this case, that was not sufficient. The distance between the later detection pairs is simply too large for an observer to be certain that they belong to the same particle. So I switched back and forth between the individual images of the sequence to study the actual particle motion, which ultimately allowed me to confirm that the track was genuine.

Generally however, missing and unrelated detections in an otherwise genuine track are often not the (direct) result of shortcomings of the tracking algorithm or its setup, but of the detection algorithm not identifying the point sources in the first place—where there is no detection, none can be added to the track. This happens for example when the particle

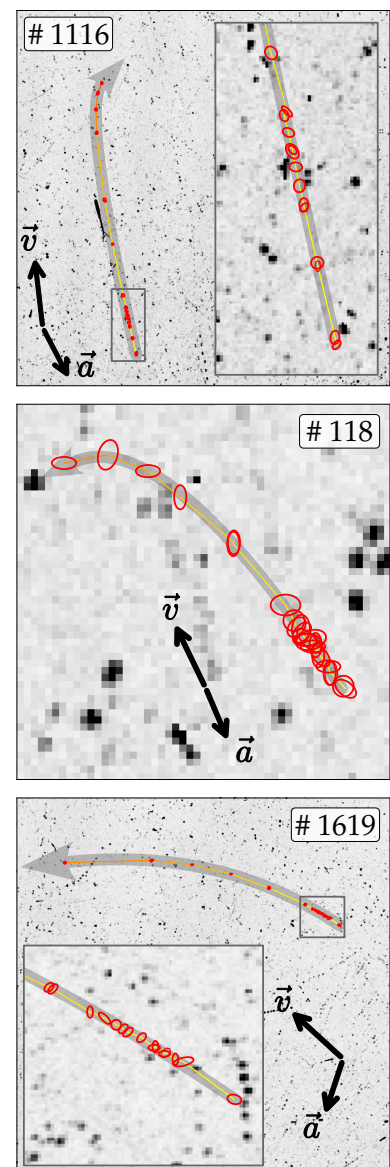


Figure 5.4: Three tracks from sequence STP090 that I flagged as ambiguous. The red ellipses mark their detections, which are connected by the gradient line from yellow to red. Also shown are the fitted curve in gray, and the orientations of their velocity, \vec{v} , and acceleration vectors, \vec{a} .

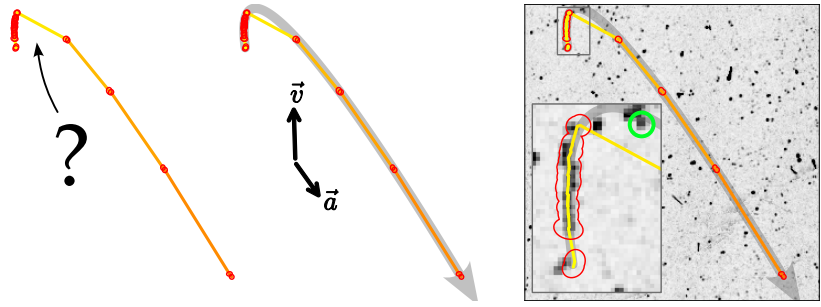


Figure 5.5: Example of a genuine particle track with a unique shape, demonstrating my assessment process and the difficulty of distinguishing between genuine and ambiguous tracks. The uncharacteristic kink (marked by the arrow), is also the result of a missing detection pair (thick green circle).

Testing the effects of missing or unrelated detections incorporated into a track is also a reason why my simulation software can generate tracks with inherent miss-rates.

When looking at the overall statistics of a tracking result, the deviations induced by such residual offsets should also average out given a large enough data set. A similar argument might even be made regarding the dynamics of spurious tracks. The velocity and acceleration distributions of genuine and ambiguous tracks look quite similar (see, e. g., Fig. 17 in the methods paper; otherwise, they might have been used to distinguish between the two groups). But importantly, to estimate their physical dynamics and particle sizes (i. e., in meters instead of pixels), the particle-observer distance has to be known (e. g., by associating them with the nucleus), which is impossible if their fits are unreliable on an individual level.

is rotating and osculates in brightness, which then leads the tracking algorithm to choose the next best (but wrong) candidate. But luckily, the “presence” of missing or unrelated detections in an otherwise genuine track is only a minor issue as long as its properties are not significantly affected, which is what we ultimately care most about. In that regard, they have an effect similar to the residual pointing fluctuation.

I tentatively investigated the effects of such spatial offsets by adding random noise to the fit of a sample particle track, and then refitting the new data points to see how drastically the derived velocity and acceleration vectors change. The random noise was created in two ways: (a) via bootstrapping of the measured offset values, and (b) by sampling the offset values from a Gaussian distribution, which they generally follow in reality (see Fig. 5.6). Nevertheless, Figure 5.7 shows that there is essentially no difference between the two methods, and more importantly, that the noise only seems to have minor effects on the derived velocity and acceleration vectors (at least on the offset scales that we generally allow). So at least from a quality-of-fit point of view, the particle dynamics that we obtain from the fitted particle tracks should be fairly reliable.

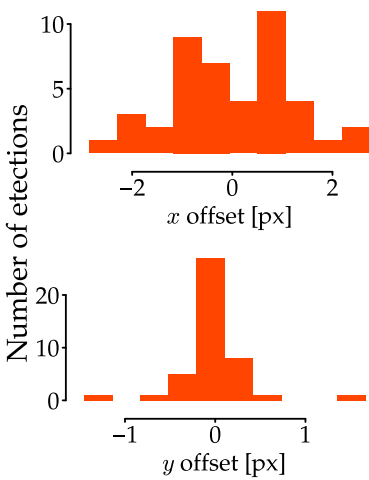


Figure 5.6: Residual offset distribution of a sample track (the same one shown in Figure 3 in the science paper). These distributions were used to investigate how the spatial offset might affect the track properties.

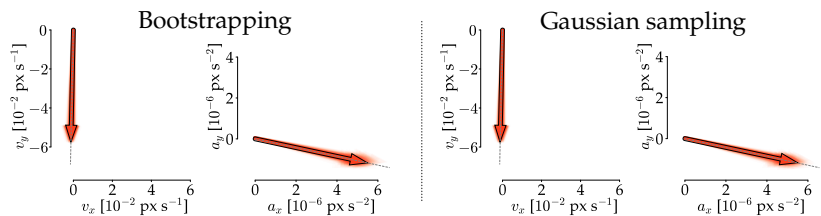


Figure 5.7: Derived velocity and acceleration vectors obtained from adding random noise to the fit of a sample track (see Fig. 5.6), once via bootstrapping, and once by Gaussian sampling. In both cases, 300 different data sets were created and subsequently fitted. The resulting vectors (orange) were plotted with a transparency of 1/300 to create a kind of “probability cloud”. The dashed gray lines point in their average directions, while the black-contour arrows correspond the vectors derived from the real data.

5.3 LAST WORDS ON SIMULATIONS

As already described on page 72, my simulation software is able to simulate data based either on concrete tracking results, or on user-specified parameters and synthetic distributions. It can thus simulate data in three different flavors:

Simulating data solely based on assumptions: This entails coming up with reasonable estimates for velocity, acceleration, orientation, positioning (e. g. clustering), miss-rate, residual offset, detection signal-to-noise ratio (i. e., the ratio between detections from tracks vs. those from noise), and other minor distributions, as well as the general number of tracks. The strength of this approach is that the parameter space to choose from is essentially limitless. It allows to make up any kind of (unphysical) track populations and detection sets, which can help to identify limitations and biases of the tracking algorithm. Such data sets can for example be used to determine the parameter-dependent tendency of the tracking algorithm to retrieve spurious tracks. This was shown in Section 5.1.1 of the methods paper, where data sets that only consisted of random noise were used to test how many spurious tracks the algorithm retrieved as a function of detection density, which is directly related to the detection threshold. But in theory, this approach could also be used to study the effect of other tracking parameters. Another application would be to test the sensitivity of parabola fitting by creating a data set that only consists of random noise and straight tracks with detections that are slightly offset. It could then be tested how resistant the algorithm is against noise and offset before it goes off trail and creates curved tracks. Opposed to simulating data solely based on tracking results, this approach also has the advantage that it is free from any biases that may be inherent to the tracking results (although it may of course be prone to others).

Simulating data solely based on tracking results: In this case, distributions for velocity, acceleration, orientation, positioning, miss-rate, offset, signal-to-noise, etc., are all directly inferred from the tracking results of real data. As long as the underlying tracking results are good, this approach has the obvious advantage that the parameter distributions will generally be close to reality. But because it relies on Gaussian kernel density estimation to create the distributions, they are sensitive to the binning of the histogram data, which therefore must be chosen with care. Additionally, this approach can only ever simulate data within a limited parameter space, since it not only excludes tracks that are not part of the underlying tracking results (but that might very well exist), but it may also be based on parameter distributions that are inherently wrong due to the inclusion of spurious tracks. On the other hand however, it might allow to make the following statement: if a) the simulation shows that for a given set of tracking parameters, the true positive and false positive rates of the algorithm are relatively stable and independent of the number of simulated tracks, and b) the shape of the parameter distributions of the underlying tracking results is “preserved” (i. e., reproduced by the tracking results of the simulated data), then the true positive rate is likely also valid for the underlying data.

Notably, in the current implementation of the simulation software, the parameters are drawn independently from one another, while in reality, many of them are correlated (such as velocity and acceleration). As a consequence, the simulated parameter space actually allows for a larger variety of parameter combinations, which may also be an advantage.

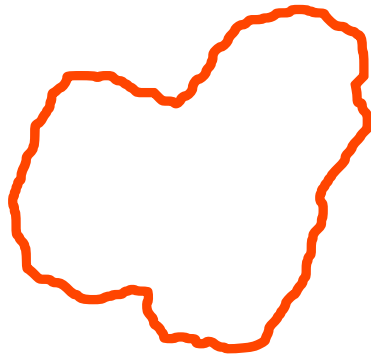
It might also be useful to test the stability of this preservation of parameter distributions by continuously feeding the tracking results back into the simulation to use as the new basis for the next simulated data set. The evolution of the parameter distributions (or the lack thereof) might then make certain biases more visible.

The idea of this statement is that if true, the real data set should be statistically no different from any other data set drawn from the underlying distributions. Thus any conclusions that can be made about the simulated data should also apply to the real data.

A hybrid simulation based on assumptions and tracking results: This middle ground might prove the most useful, since it allows to keep the simulation close to real data, while also being flexible. There are obviously all kinds of ways of how assumption- and tracking-result-based parameters could be combined. Here are a four suggestions:

- ▶ Using tracking-result-based parameters, but varying the detection density (while keeping the detection signal-to-noise ratio constant). This could be useful to find a more sensible lower bound for the detection threshold than by simulating noise only.
- ▶ Using tracking-result-based parameters, but varying the detection signal-to-noise ratio, for example by changing the number of simulated tracks while keeping the noise constant or vice versa. At the one extreme, this might give an idea about when the algorithm would start generating spurious tracks even if most of the detections are genuine. At the other extreme, it might give an idea about when the algorithm stops being able to pursue a genuine track and gets lost in the noise (“needle in the haystack”). Another way would be by changing the miss-rate of the simulated tracks, which might give an idea about when low-quality tracks become inseparable from noise.
- ▶ Using tracking-result-based parameters, but adding specific track populations on top that were not found in the real data. If these artificial tracks are found with the same set of tracking parameters that was used for the real data, then this should be a good indication that those tracks do not exist in the real data. Something similar was for example also done by Denneau et al. (2013), who added synthetic measurements of asteroid populations to their real data sets to test the efficiency of their tracking engine for SSSBs, or Kelley et al. (2013, 2015), who added artificial point sources to their observations to test their tracking algorithm of dust particles at comet 103P/Hartley 2.
- ▶ Using tracking-result-based parameters, but simulating the noise by creating tracks that consist of too few detections to make it past the acceptance threshold. This way, the simulated noise might be closer to reality, since most of the noise in real data likely comes from very faint particles on the verge of merging with the diffuse coma.

THE SCIENCE PAPER



PREAMBLE

IN my second paper, “Dynamics and potential origins of decimeter-sized particles around comet 67P/Churyumov-Gerasimenko” (which in this dissertation is called the “science paper” for convenience), I focused on the application of my tracking algorithm and the implications of my findings to cometary science. As with the methods paper, the science paper is now presented unaltered and in full following the layout described in the Preface. Each page of the original paper is reprinted on the right side of a double-page and regularly augmented by in-situ discussions on the left side to provide additional information (although this time, not every double-page contains in-situ discussions because many of them have by now found their way into the science paper during its review process). Because it is currently not possible to include pdf pages with working hyperlinks in a \LaTeX -document, I manually added all hyperlinks back into the science paper (except for those found in its bibliography). Citations within the digital version of this document therefore redirect to the bibliography at the end of the dissertation.

* * *

Contribution disclosure

I wrote the entire science paper and created all its figures. The analysis I performed under the advice of my co-authors. Raphael Marschall additionally provided his gas and dust coma modeling software and helped with its usage and the implementation of code changes. Björn Grieger additionally transformed data into the QuACK coordinate system.

PART CONTENTS

Preamble	91
The Science Paper	92
Introduction	93
Data selection	95
Particle tracking	95
Results and discussion	103
Summary and conclusions	123
Appendix	129



7

Dynamics and potential origins of decimeter-sized particles around comet 67P/Churyumov-Gerasimenko

Marius Pfeifer¹ , Jessica Agarwal^{1,2}, Raphael Marschall³, Björn Grieger⁴, and Pablo Lemos^{1,2} 

¹ Max Planck Institute for Solar System Research, Justus-von-Liebig-Weg 3, 37077 Göttingen, Germany
 e-mail: pfeifer@mps.mpg.de

² Institute for Geophysics and Extraterrestrial Physics, TU Braunschweig, Mendelssohnstraße 3, 38106 Braunschweig, Germany

³ CNRS, Laboratoire J.-L. Lagrange, Observatoire de la Côte d'Azur, 06304 Nice, France

⁴ Aurora Technology B.V. for ESA, ESAC, Madrid, Spain

Received 10 March 2023 / Accepted 16 February 2024

ABSTRACT

Context. One of the primary goals of the European Space Agency's Rosetta mission to comet 67P/Churyumov-Gerasimenko was to investigate the mechanisms responsible for cometary activity.

Aims. Our aim is to learn more about the ejection process of large refractory material by studying the dynamics of decimeter-sized dust particles in the coma of 67P and estimating their potential source regions.

Methods. We algorithmically tracked thousands of individual particles through four OSIRIS/NAC image sequences of 67P's near-nucleus coma. We then traced concentrated particle groups back to the nucleus surface, and estimated their potential source regions, size distributions, and projected dynamical parameters. Finally, we compared the observed activity to dust coma simulations.

Results. We traced back 409 decimeter-sized particles to four suspected source regions. The regions strongly overlap and are mostly confined to the Khonsu-Atum-Anubis area. The activity may be linked to rugged terrain, and the erosion of fine dust and the ejection of large boulders may be mutually exclusive. Power-law indices fitted to the particle size–frequency distributions range from 3.4 ± 0.3 to 3.8 ± 0.4 . Gas drag fits to the radial particle accelerations provide an estimate for the local gas production rates ($Q_g = 3.6 \times 10^{-5} \text{ kg s}^{-1} \text{ m}^{-2}$), which is several times higher than our model predictions based on purely insolation-driven water ice sublimation. Our observational results and our modeling results both reveal that our particles were likely ejected with substantial nonzero initial velocities of around $0.5\text{--}0.6 \text{ m s}^{-1}$.

Conclusions. Our findings strongly suggest that the observed ejection of decimeter-sized particles cannot be explained by water ice sublimation and favorable illumination conditions alone. Instead, the local structures and compositions of the source regions likely play a major role. In line with current ejection models of decimeter-sized particles, we deem an overabundance of CO_2 ice and its sublimation to be the most probable driver. In addition, because of the significant initial velocities, we suspect the ejection events to be considerably more energetic than gradual liftoffs.

Key words. comets: general – zodiacal dust – comets: individual: 67P/Churyumov-Gerasimenko

1. Introduction

Comets are small Solar System objects that formed in the outer regions of our protoplanetary disk beyond the snowline (e.g., Weissman et al. 2020). At these heliocentric distances, water and other (super-)volatiles like CO_2 can remain solid over astronomical timescales. These ices make up a significant part of cometary material, which otherwise consists mainly of refractory aggregates. Because of this ice content, comets become active once they enter the inner Solar System: their ices start to sublimate. If this happens beneath the cometary surface, the expanding gas can get trapped and build up pressure. Eventually, this pressure may overcome the gravity and tensile strength of the overlying material, expel the gas, and eject some of the refractory material along with it. The released gas and dust then form the characteristic cometary coma, tail, and trail (e.g., Agarwal et al. 2023).

Decimeter-sized particles¹ are likely ejected by CO_2 ice sublimation in deeper surface layers (e.g., Gundlach et al. 2020; Fulle et al. 2020; Wesolowski et al. 2020; Ciarniello et al. 2022; Davidsson et al. 2022), but the responsible mechanisms are not

¹ Following the classification of cometary dust by Güttler et al. (2019), we use the term “particle” as a generic term for any unspecified dust particle, independently of its size.

yet fully understood (e.g., Zakharov et al. 2022; Bischoff et al. 2023; Agarwal et al. 2023, and even less so for small particles where cohesion forces dominate, e.g., Gundlach et al. 2015; Skorov et al. 2017; Markkanen & Agarwal 2020).

Learning more about these processes was, and still is, one of the primary science goals of the European Space Agency's Rosetta mission to comet 67P/Churyumov-Gerasimenko (e.g., Taylor et al. 2017). The spacecraft rendezvoused with 67P in August 2014 and accompanied the comet through its perihelion passage in August 2015, until Rosetta was set on an intercept course with 67P on September 30, 2016, and landed on its surface. Among the suite of Rosetta's science instruments was the Optical, Spectroscopic, and Infrared Remote Imaging System (OSIRIS), which consisted of a wide-angle and a narrow-angle camera (WAC and NAC, Keller et al. 2007). During the rendezvous phase, these cameras recorded many image sequences of the near-nucleus coma, which also captured the motion of individual dust particles shortly after their ejection. Because the study of their dynamics can help to understand their ejection process, we developed a particle tracking algorithm for OSIRIS images in Pfeifer et al. (2022).

For the current paper we have now applied an enhanced version of this algorithm to four OSIRIS/NAC image sequences. In

Some of those sequences are shown on this and the next two double-pages to highlight some of the issues (all images are brightness-inverted and their contrasts improved for better readability).

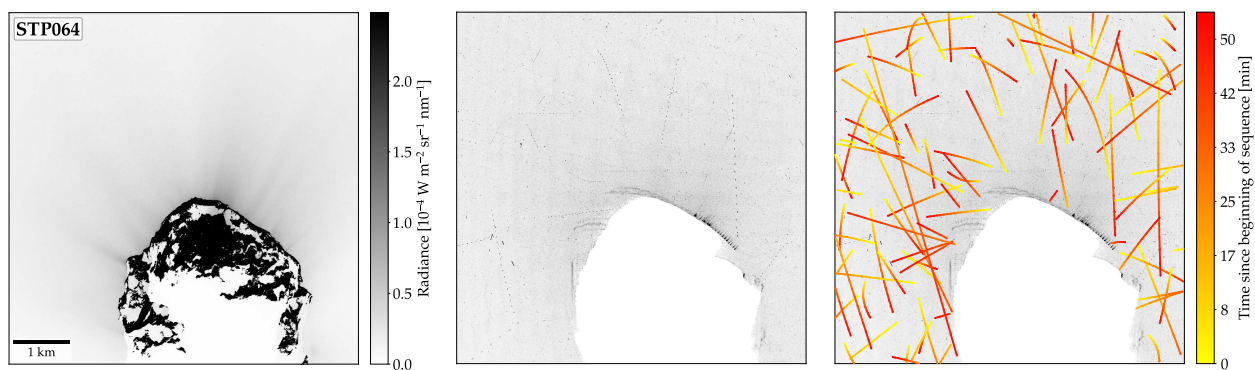


Figure 7.1: Sample images of sequence STP064. First image of the sequence on the left, master image in the middle and again with a sample of identified tracks ($\Gamma < 30\%$) on the right. The sequence consists of 57 images and was recorded on July 14, 2015, at roughly 1.3 AU from the Sun and 162 km from the nucleus. It has two main “issues”. For one, it was recorded in image triplets instead of pairs, which our tracking algorithm cannot handle by default (I still got it running with some small tweaks to the source code, but it is certainly not optimized for such sequences; the results are surprisingly good, however). Second, there are only a handful of tracks, and nothing that would allow to associate them with the nucleus or otherwise determine their particle-observer distance.

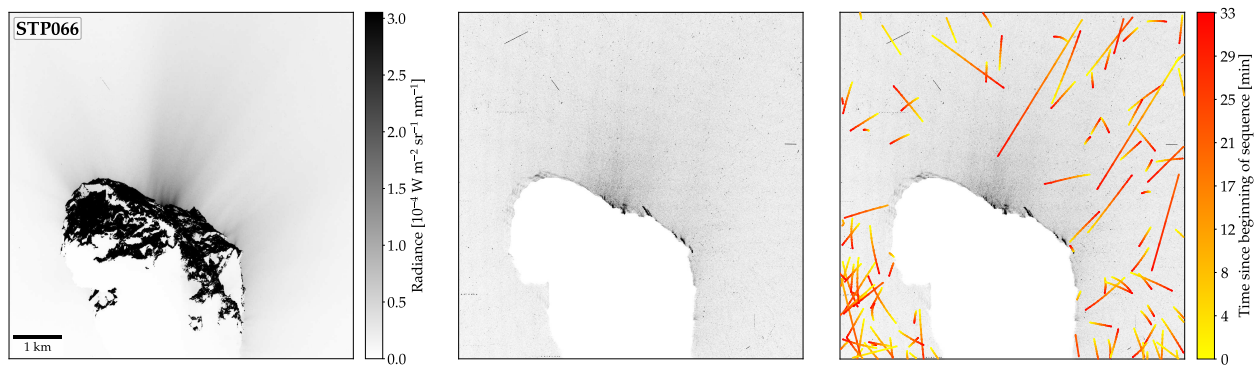


Figure 7.2: Sample images of sequence STP066 (figure layout analogous to Fig. 7.1). It consists of 36 images and was recorded on July 24, 2015, at roughly 1.3 AU from the Sun and 185 km from the nucleus. It has the same issues as sequence STP064.

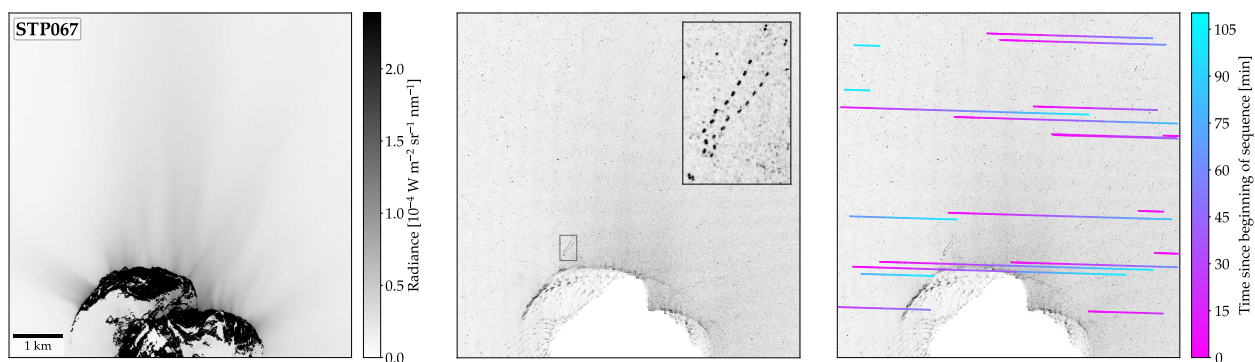


Figure 7.3: Sample images of sequence STP067 (figure layout analogous to Fig. 7.1). It consists of 44 images and was recorded on July 29, 2015, at roughly 1.3 AU from the Sun and 181 km from the nucleus. This sequence has different issues than the previous two. Unlike STP064 and STP066, which also only consist of a single sub-sequence, this one has the same format as the other sequences that I analyze in the science paper (i. e., consisting of a short and a long sub-sequence recorded in image pairs). Unfortunately however, as the inlet in the central image shows, it is strongly affected by pointing fluctuation. Generally, this is manageable, but there are no sidereal objects visible in the background that could be used to correct for it. The right figure shows where such objects should theoretically be visible in the master image, but they are simply not bright enough. Additionally, even if they were visible, there are only two that stay within the FOV throughout the entire sequence, but one is partly covered by the nucleus, and the other is very close to it. But for the sidereal-motion-based correction to work, at least one object should be tracked throughout the entire sequence. Thus, while it is important for a sequence to be long enough to allow for a reliable determination of the particle dynamics, it is also important that it is not too long either, because then there will be no sidereal object that is visible throughout the entire sequence. As it turns out, the roughly two hours of the sequences that we analyze in the science paper are pretty optimal.

Sect. 2 we give an overview of the image sequences. In Sect. 3, we briefly discuss how we improved the tracking algorithm, and explain why we only focus on certain particle groups for our analysis, and how we selected them and identified their suspected source regions. In Sect. 4, we investigate these regions, determine the particle size–frequency distributions, reconstruct the local illumination conditions and surface accelerations, analyze the particle dynamics, and compare the results to dust coma simulations. Finally, in Sect. 5 we summarize our findings and conclusions.

2. Data selection

We chose the four most suitable image sequences for our analysis from a group of about 100 similar sequences. The others were rejected for various reasons (listed in Appendix B), but to summarize, we looked for (preferably complete) image sequences that were recorded in image pairs over a roughly 2-h time span and no farther than ≈ 150 km from the nucleus, and that consist of two subsequences (one short, one long), contain (trackable) sidereal objects, and show at least one concentrated group of high-quality particle tracks.

The four selected sequences were recorded by OSIRIS/NAC between December 16, 2015, and January 6, 2016 (see Table 1 and Keller et al. 2007). They each consist of 44 images and are the result of merging two subsequences (OSIRIS activity tags “JETS_MOVIE” and “DUST_JET”). Figure 1 shows the typical timeline of such a sequence, and Table 2 lists relevant meta-data (see also Pfeifer et al. 2022). In the following, we call these sequences according to their designated (Rosetta mission) short-time-planning (STP) numbers: STP087, STP088, STP089, and STP090.

As did Pfeifer et al. (2022), we used images of OSIRIS calibration level 3E (Tubiana et al. 2015, see sample images in Figs. 2 and A.1)². Images of this level are radiometrically calibrated, corrected for in-field and solar stay-light, geometric distortion, and boresight offset (resampled), and are expressed in radiance units ($\text{W m}^{-2} \text{sr}^{-1} \text{nm}^{-1}$). In preparation for the particle tracking, the images additionally underwent a number of pre-processing steps, where the diffuse coma background was removed, the bright nucleus masked out, and the point-source-like particles were detected (Pfeifer et al. 2022). For visual confirmation, we then also stacked the cleaned images using only the maximum value that each pixel assumed over the course of the sequence to create a “master image” (see, e.g., Fig. 2). The identified point source coordinates, on the other hand, are passed on to the tracking algorithm, where they are used to reconstruct the particle trajectories.

3. Particle tracking

3.1. Tracking algorithm

To track the detected particles, we used the algorithm described in Pfeifer et al. (2022, see this reference for definitions of technical terms used in the following), which we improved in three significant ways:

1) Because we found that for some tracks, fitting a second-order polynomial is inadequate, we now also allow fitting of third-order polynomials during the extended tracking phase, but

² The data are available at the Planetary Science Archive of the European Space Agency under <https://www.cosmos.esa.int/web/psa/rosetta>

Table 1. OSIRIS/NAC specifications.

Field of view (FOV)	$2.208^\circ \times 2.208^\circ$
Pixel resolution	$18.6 \mu\text{rad} \times 18.6 \mu\text{rad}$
CCD resolution	$2048 \text{ px} \times 2048 \text{ px}$
Filter (NAC F22)	Center: 649.2 nm, bandwidth: 85 nm

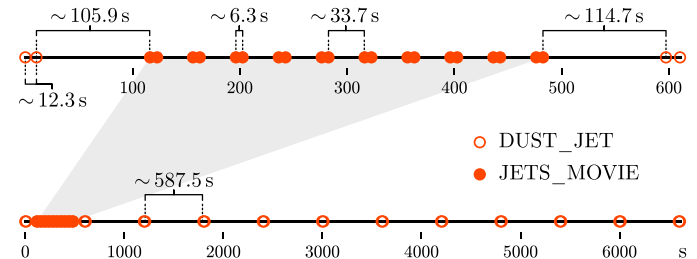


Fig. 1. Typical timeline of the four image sequences analyzed, in this case STP089. The other sequences deviate from this structure only by a few seconds at most.

only under the condition that the absolute jerk (i.e., change in acceleration) is lower than a certain user-defined threshold. This condition is necessary because the jerk is very sensitive to inaccurate data points. Thus, high jerk values more likely result from pointing fluctuation that we could not completely correct for or from unrelated detections that were erroneously incorporated into a track, rather than from actual physical forces that acted on the particles. Because the tracks generally have a lot more data points than the polynomials have degrees of freedom, and because their fits yield median adjusted R^2 values (a measure for the goodness of fit; e.g., Ezekiel 1930; Fahrmeir et al. 2021) that are extremely close to unity ($\gtrsim 0.9999$), we are confident that we are not overfitting our data. Nevertheless, there are other caveats that come with the choice of polynomial degree, specifically concerning the extrapolation of such fits (see Appendix C). We therefore limit extrapolations to a maximum of 30 minutes.

2) Originally, some detections were rejected during the tracking process, even though they were located close to their track and could be visually confirmed to be part of it. We found that they were rejected because their residual offset was too large with respect to their expected location at the corresponding time, according to the fit. We now calculate the residual offset as the shortest distance to the fit, effectively dropping the timing criterion.

3) The radiance values of particle detections are now more accurate. Instead of integrating only over the member-pixels of a point source that are above a certain radiance threshold, we now integrate over all the (sub)pixels that lie within an ellipse containing most of the source’s signal (see also Bertin & Arnouts 1996; Barbary 2016). During the photometry however, we are deliberately not removing any background signal (e.g., derived from elliptical annuli around the detections), because we already removed the local background in preparation for the detection process, on a scale ($16 \times 16 \text{ px}$) very similar to typical annuli radii (≈ 11 – 17 px ; see also Pfeifer et al. 2022).

Figure 3 shows how fitting third-order polynomials in certain cases, and generally calculating the residual offset as the shortest distance to the fit, improves the particle tracking. In the demonstrated case, fitting a third-order polynomial is even necessary to track the particle at all. If a second-order polynomial were

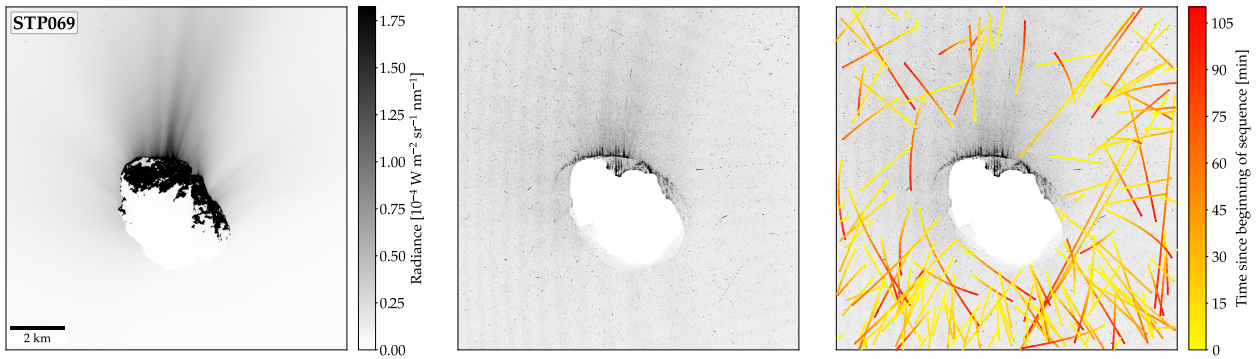


Figure 7.4: Sample images of sequence STP069 (figure layout analogous to Fig. 7.1). It consists of 44 images and was recorded on August 16, 2015, at roughly 1.2 AU from the Sun and 328 km from the nucleus. This sequence has no technical issues, but it was unfortunately recorded very far away from the nucleus (Rosetta was put on a safe distance because this was just after 67P passed through its perihelion on August 13, 2015, so during its most active phase). Hence despite the intense activity, not many individual particles can be observed (which, to be fair, is also an issue with the previous three sequences). Judging from the image on the right, if the tracks were at the same distance as the nucleus (which they are likely not), they must be at least about 50 cm in radius to be detectable, but there are likely only relatively few particles that large (especially during this most active phase, see discussion on p. 103).

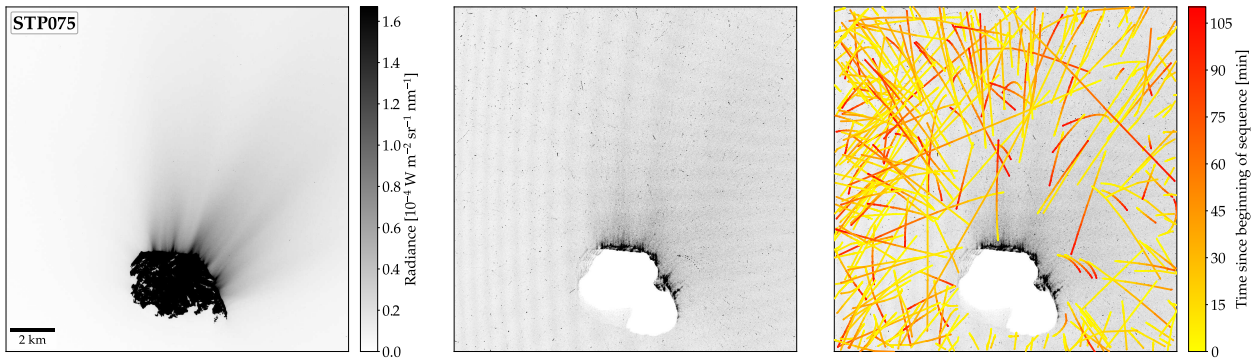


Figure 7.5: Sample images of sequence STP075 (figure layout and issues analogous to Fig. 7.4). It consists of 44 images and was recorded on September 23, 2015, at roughly 1.3 AU from the Sun and 401 km from the nucleus. Even though this sequence was recorded even further away from the nucleus than sequence STP069, there are significantly more particles that can be tracked. Nevertheless, most of the tracks start too far away from the nucleus to reasonably associate them with its surface. In fact, most of the particles that seem to fly straight away from the nucleus in radial direction are likely far away from the nucleus and much closer to the camera, which is why they can be seen and why their tracks start at a significant distance from the nucleus. Curiously, there are three particles to the north-west of the nucleus that almost seem to orbit the nucleus in unison—even following its rotation. If they were truly at roughly nucleocentric distance from the camera, the two brighter ones may have been around 2 and 3.5 m (in equivalent) radius. Maybe they even share the same origin.

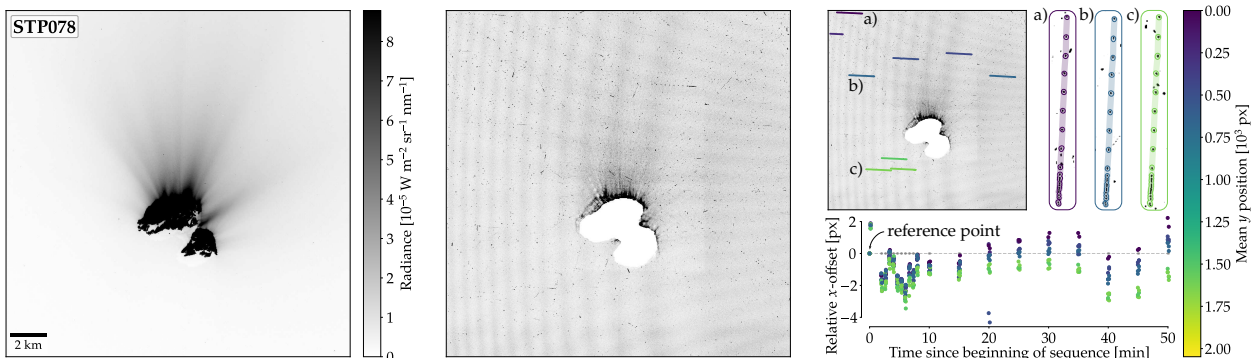


Figure 7.6: Sample images of sequence STP078 (figure layout similar to Fig. 7.1, except for the image on the right). It consists of 40 images and was recorded on October 14, 2015, at roughly 1.5 AU from the Sun and 497 km from the nucleus. This sequence is one of a few with a very peculiar issue: its inherent pointing fluctuation is strongly location-dependent. The smaller image on the right shows the identified sidereal tracks, color-coded by their mean vertical position. Next to it are three (rotated) close-ups of the sidereal tracks a), b), and c), to show that the objects are clearly visible and have been perfectly tracked. Nevertheless, as the plot below shows, there is a significant difference in relative (horizontal) offset, depending on the image location. This is likely due to insufficient distortion correction, making it impossible to accurately correct for the pointing fluctuation. (Theoretically, the sequence actually consists of 72 images, spanning roughly 2 h 20 min, but after the first 40 images, there is a significant jump in pointing, so the remaining 32 images have to be disregarded.)

Table 2. Metadata of the four sequences analyzed.

Name	Date	$t_0^{(a)}$ (UT)	$\Delta t^{(b)}$	$\bar{r}_h^{(c)}$ (AU)	$\bar{\Delta}^{(d)}$ (km)	$\bar{\delta}_{\text{px}}^{(e)}$ (m ²)	$\bar{\delta}_{\text{FOV}}^{(f)}$ (km ²)	$\bar{\phi}_s^{(g)}$ (°)	$\lambda_s^{(h)}$ (°)	$\bar{\alpha}^{(i)}$ (°)
STP087	2015-12-16	7:01:06	1:50:10	1.90	113	2.1×2.1	4.35×4.35	-21.1	122–177	90.9
STP088	2015-12-26	6:30:06	1:50:11	1.98	79	1.5×1.5	3.06×3.06	-18.2	185–240	91.2
STP089	2015-12-30	7:01:06	1:50:10	2.01	88	1.7×1.7	3.39×3.39	-17.1	188–243	91.3
STP090	2016-01-06	7:01:04	1:50:11	2.06	86	1.6×1.6	3.33×3.33	-15.3	219–274	91.2

Notes. ^(a)Starting time. ^(b)Total duration. ^(c)Mean heliocentric distance. ^(d)Mean nucleocentric distance. ^(e)Mean pixel resolution at nucleocentric distance. ^(f)Mean CCD FOV at nucleocentric distance. ^(g)Mean sub-solar latitude. ^(h)Sub-solar longitude range. ⁽ⁱ⁾Mean phase angle.

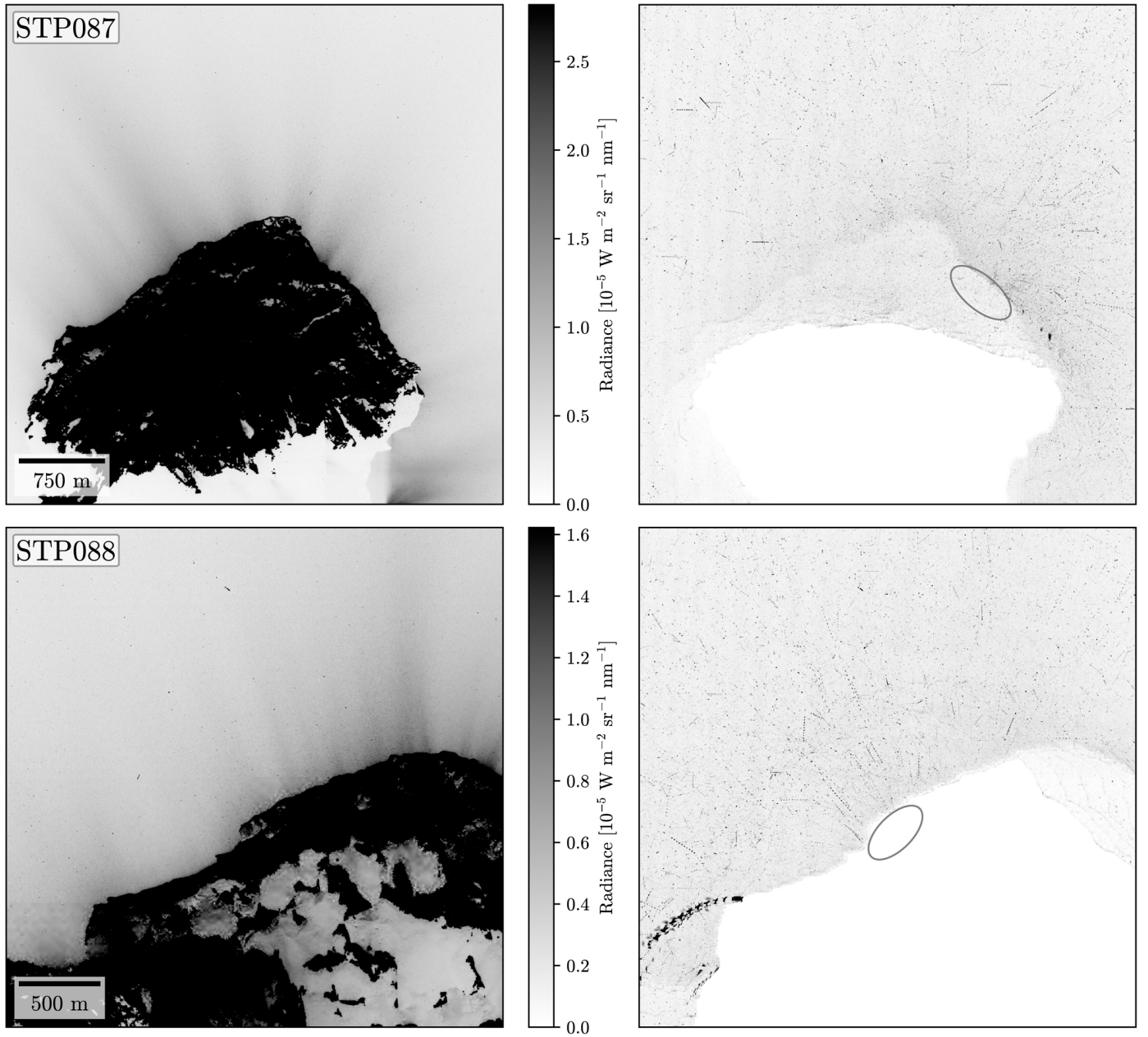


Fig. 2. Sample images from sequences STP087 and STP088. First images of the respective sequences on the left, master images on the right. The ellipses in the master images mark the suspected source regions of the concentrated particle groups. All images are brightness-inverted and had their contrasts improved for better readability (for sequences STP089 and STP090 see Fig. A.1).

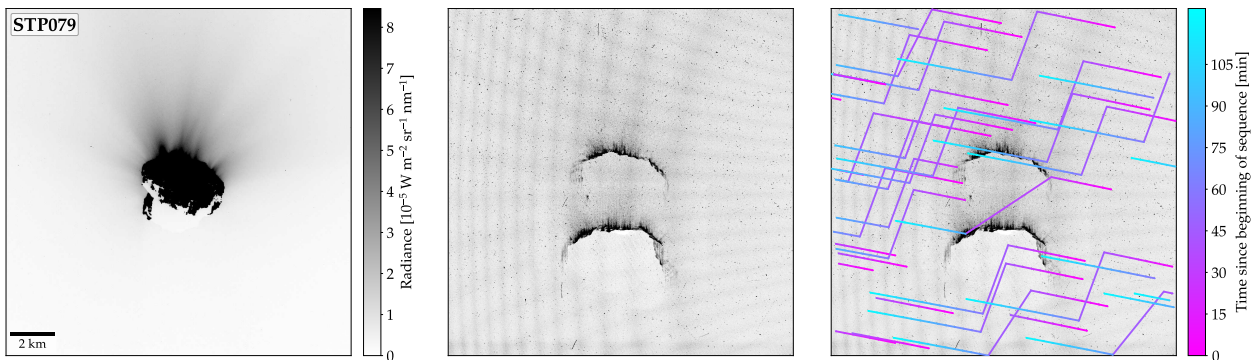


Figure 7.7: Sample images of sequence STP079 (figure layout analogous to Fig. 7.3). It consists of 48 images and was recorded on October 21, 2015, at roughly 1.5 AU from the Sun and 406 km from the nucleus. While this sequence was also recorded very far away from the nucleus, its main issue is that there is a big jump in the camera pointing after the first 20 images, as demonstrated by the two “nuclei ghosts” in the master image and the sudden jumps in the sidereal tracks (the different angles are because some objects briefly left the FOV or were covered by the nucleus). To make the tracking work in this case, the jump would need to be corrected for, which is non-trivial. But even with the correction, it would be difficult to say if a track was correctly continued after the jump (although this may be solvable by creating a new master image that accounts for the jump, but that is also not straightforward as the pixels won’t align anymore). In theory, this sequence even has a third part of another 20 images, but they were recorded roughly five days after the first two.

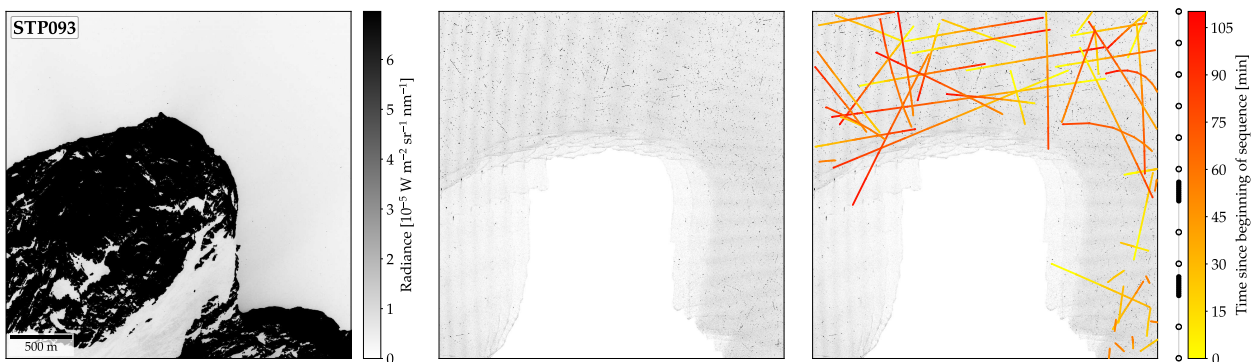


Figure 7.8: Sample images of sequence STP093 (figure layout analogous to Fig. 7.1). It consists of 44 images and was recorded on January 27, 2016, at roughly 2.2 AU from the Sun and 73 km from the nucleus. This sequence also has several issues. Generally, it was recorded at a nucleocentric distance that should work well for particle tracking, but unfortunately, the nucleus takes up way too much space in the images. And since we cannot track particles in front of it because most of its surface is usually oversaturated and point sources cannot easily be distinguished from other surface features, there is only a small area in the sequence where particles can be tracked. Additionally, its recording pattern is more complicated than usual (indicated by the line with circles next to the color bar). While it consists of a shorter (filled circles) and a longer (open circles) sub-sequence, the shorter one does not consist of image pairs, but is instead split into two sets of ten equally-spaced images. This makes the default principal and extended tracking impossible.

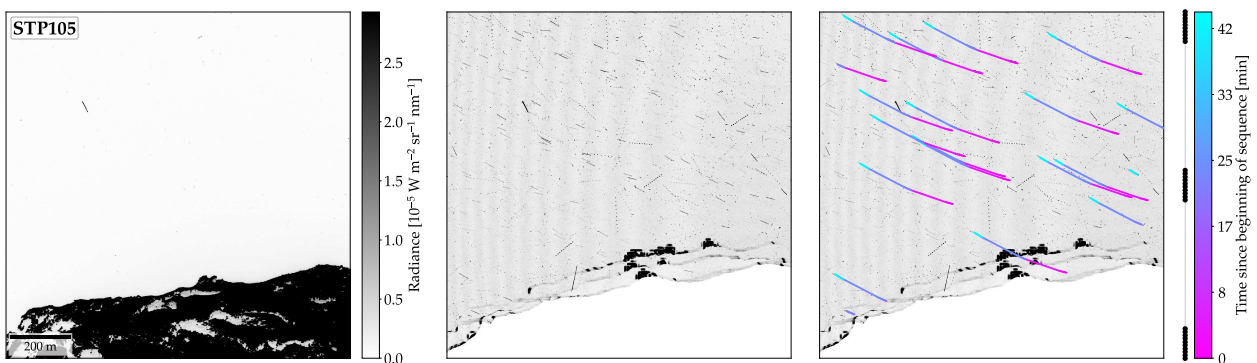


Figure 7.9: Sample images of sequence STP105 (figure layout analogous to Fig. 7.3). It consists of 30 images and was recorded on April 20, 2016, at roughly 2.8 AU from the Sun and 30 km from the nucleus. This is one of the last sequences of this kind that was recorded. Unfortunately, its recording pattern is different yet again, with three groups of ten equally-spaced images. This issue alone would likely be solvable, but in between these image groups, the spacecraft was seemingly rotating along the camera line of sight. This makes the default tracking of sidereal objects impossible.

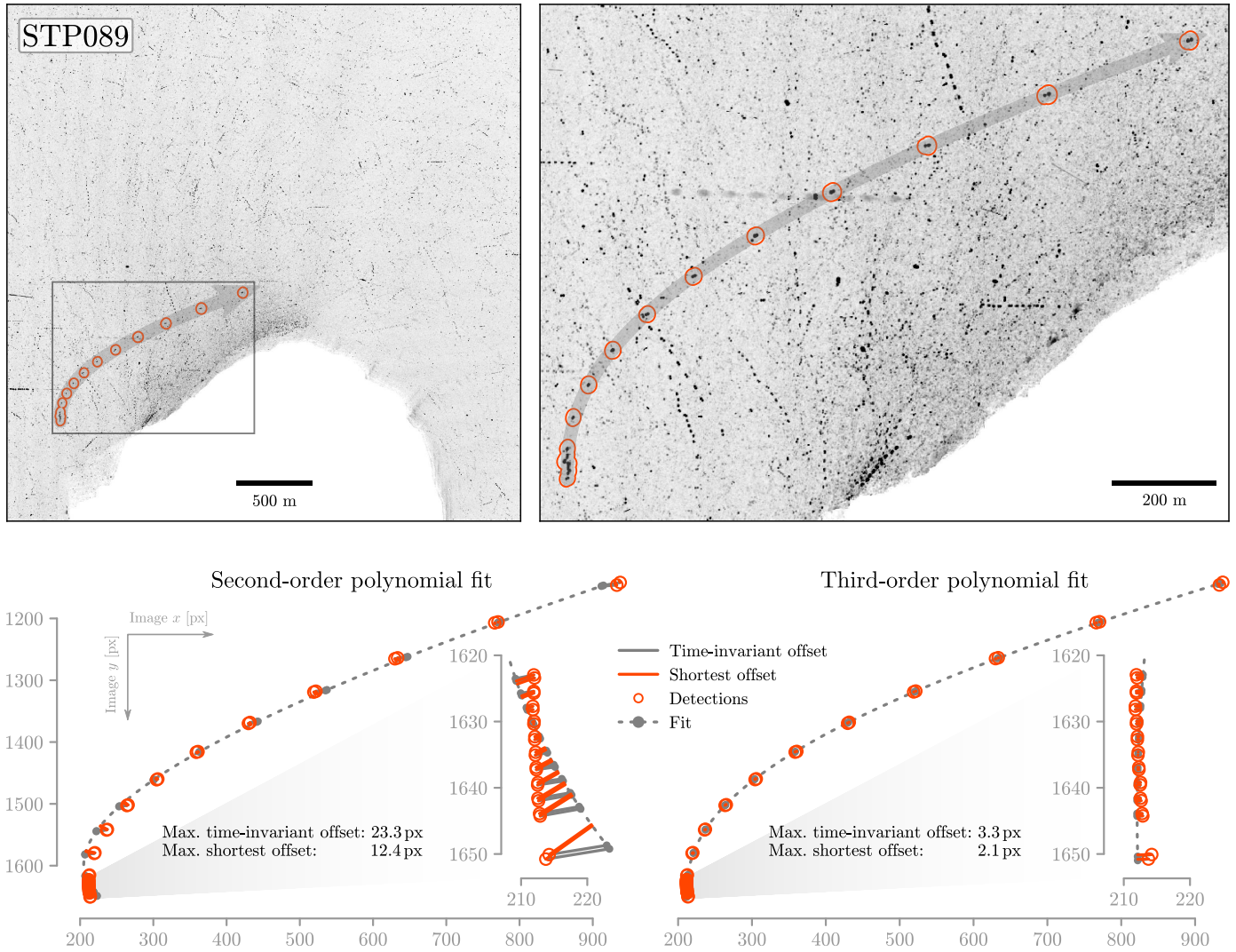


Fig. 3. Sample track from sequence STP089 demonstrating how fitting third-order polynomials and calculating the residual as the shortest offset instead of the time-invariant offset can significantly improve the tracking results. Full (brightness-inverted) master image on the top left, close-up on the top right. The sample track is highlighted by the gray arrow, while the orange contours indicate the corresponding point sources.

used, the tracking parameters would have to be too lenient, which would result in highly inaccurate velocity and acceleration vectors and thus predictions during tracking, causing the algorithm to go astray.

3.2. Track selection

In Pfeifer et al. (2022), we introduced a simple but effective criterion—a miss-rate $\Gamma < 30\%$ —to separate genuine from ambiguous tracks, and demonstrated potential applications for our tracking algorithm with tentative first results. While we continue to use the miss-rate criterion as a means of pre-selection, we have now substantially refined the analysis that follows it.

To derive physical properties of ejected particles, such as their sizes and dynamics, it is essential to know the particle-observer distances. Chesley et al. (2020, and references therein), for example, were able to retrieve particle-observer distances and reconstruct the full 3D trajectories of particles around asteroid 101955 Benu; but doing the same for particles near an active cometary nucleus is extremely difficult. For one, in addition to a complex gravity field, active comets have unknown

gaseous environments, whose influence on the particles is complex (Skorov et al. 2016, 2018; Reshetnyk et al. 2018; Ivanovski et al. 2017a,b; Moreno et al. 2022). Secondly, if the (decimeter-sized) particles retain large amounts of water ice after ejection (Gundlach et al. 2020; Davidsson et al. 2021), they may even be outgassing themselves and produce a measurable rocket force (Kelley et al. 2013, 2015; Agarwal et al. 2016; Güttler et al. 2017). Finally, due to the aforementioned residual pointing fluctuation, our positional data is generally not precise enough to account for such effects and reconstruct 3D trajectories. We hence have to work in the 2D image plane and use a different way to approximate the particle-observer distance.

In Pfeifer et al. (2022), we made the basic assumption that particles, whose tracks started close to a central active area on the surface of 67P, and whose velocity vector pointed in the same direction as the estimated surface normal $\pm 45^\circ$, likely originated from that area. This allowed us to use the nucleocentric distance as a proxy for the particle-observer distance.

While we still use the nucleocentric distance as an estimate for the particle-observer distance, we now change how the particles for which we make this assumption are selected. First, we

There are also a few more image sequences that didn't suffer from any serious technical issues, but which simply lacked enough (concentrated) tracks to do reasonable statistics (see Fig. 7.10).

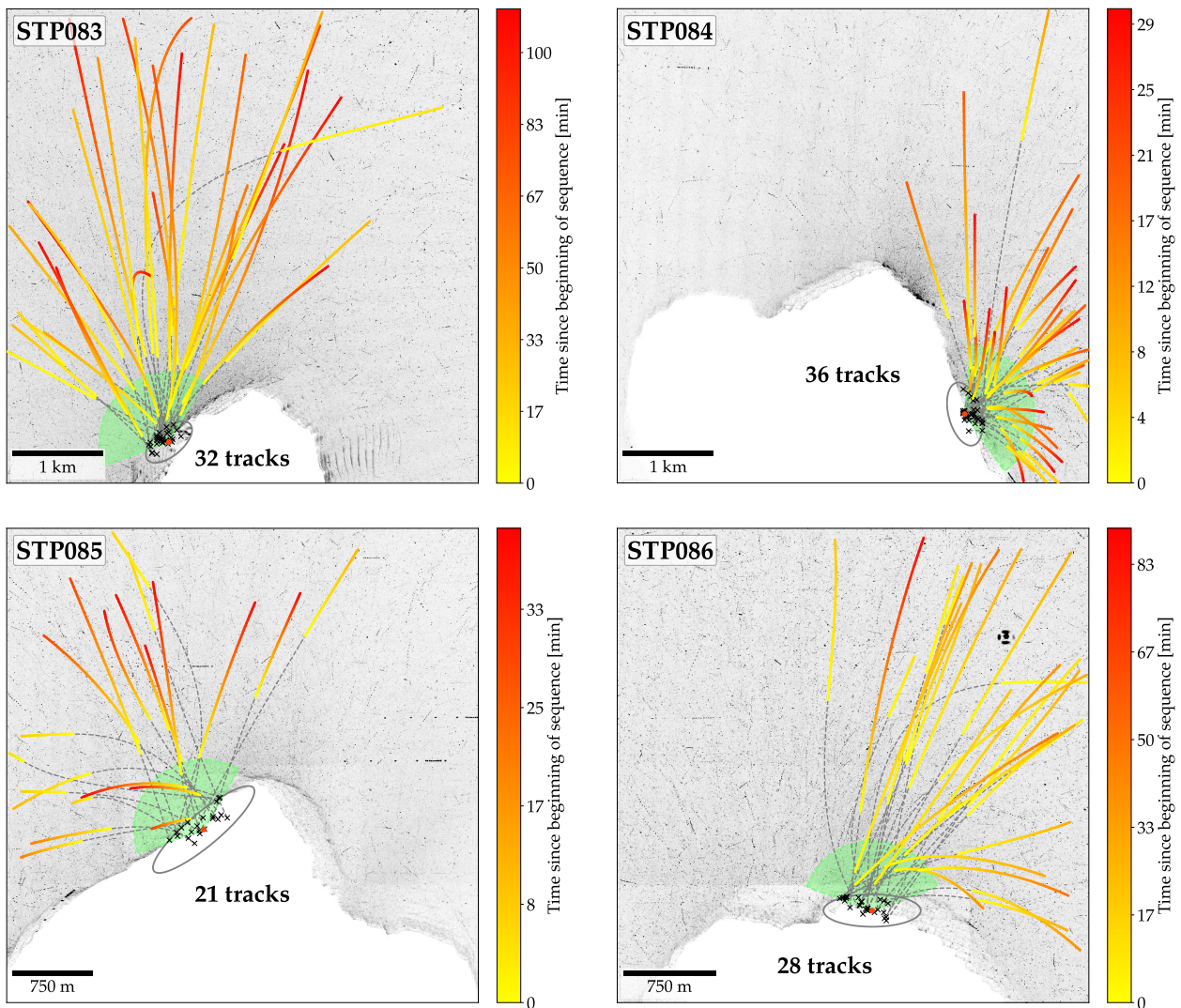


Figure 7.10: Four more image sequences with selected groups of tracks. The legend is analogous to that of Figure 4 in the science paper. Generally, all these sequences contain a lot of tracks—especially sequence STP086, where we identified 1067 tracks with $\Gamma < 30\%$, the most out of all the sequences (and that despite heavy artifacts around the nucleus which are present in all the images with short exposure time and can be seen as the squareish “ghost feature” in the lower part of the master image). The sequences however do not show surface areas that seem to be significantly more active in ejecting large particles than others (or at least not in the same intensity as the sequences discussed in the science paper). The most promising may have been sequence STP084, but the suspected source region is unfortunately located very close to the edge of the FOV, which likely prevents the detection of many additional particles that might have been ejected from it.

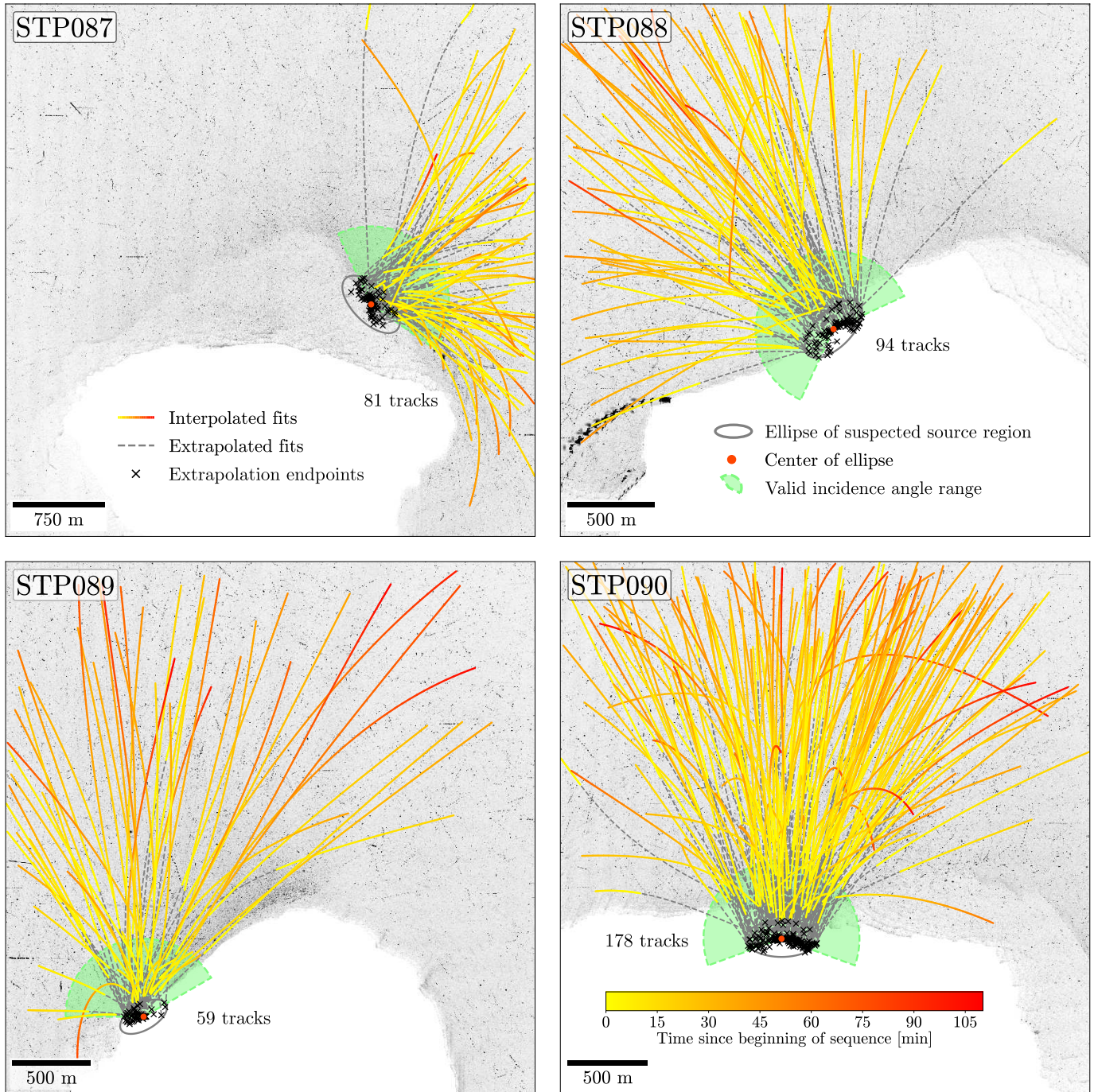


Fig. 4. Selected tracks from the four sequences. The fits were extrapolated back in time for a maximum of 30 min. The extrapolated curves end where they are closest to the ellipse centers. The endpoints are hence not intended to mark the exact ejection times or places.

find a concentrated group of particles in the master image. Such groups are key, because their tracks intersect the nucleus within a relatively well-defined area. This allows us to assume that the particles (a) were ejected only recently, and (b) share a common origin (two assumptions that are unreasonable to make about the more randomly or homogeneously distributed tracks). Then, we define an ellipse that roughly outlines their suspected source region in the first image of a sequence, placed on the nucleus close to its limb and slightly following its contour (see Fig. 2). Next, we extrapolate the 2D fits of the particle tracks back in time for a maximum of 30 minutes. Within this period, the nucleus

rotates at most 14.5° , which results in a displacement of the suspected source region that we still deem acceptable. Lastly, we check whether the tracks intersect with the ellipse within a certain incidence angle range. For those that do, we assume that they likely originated from this area (see Fig. 4). Even though this approach is still relatively simple and some of the selected particles likely originated from somewhere else, in Sect. 4, we show that the general areas are nevertheless plausible.

In the past, it was also suggested that the crossing of particle “streams” can lead to apparent (artificial) features in the particle number/coma density and the average particle motion

Some of those sequences are shown in Figures 7.1, 7.2, 7.4, and 7.5. In these cases, there is a distinct lack of large particles in the radiant gas and dust features above the active areas. At first, I thought that no particles could be seen in those areas because they were simply too densely yet diffusely populated, and that the signal of the particles was removed together with the background. But then I discovered sidereal background objects that “moved” through these areas and were perfectly visible and detectable.

The corresponding results have by now been published in Attree et al. (2024a).

(and specifically so in the case of coma simulations using fluid dynamics, e.g., Crifo et al. 1995, 2005; Rodionov et al. 2002; Zakharov et al. 2009). More recently, Shi et al. (2018) indeed confirmed that collimated gas and dust flows can result from topographic focusing, but additionally note that apparent jet-like features can also be optical illusions that emerge from projections along the viewing direction. Since we are tracking individual particles however, and thus are not concerned with average coma densities or particle motions within certain volumes along the line of sight, the crossing of particle trajectories is irrelevant in this regard.

During the tracking procedure itself, crossing trajectories are also generally unproblematic. For the tracking algorithm to get confused and jump from one trajectory to the other, they also need to cross at the same time, and have relatively similar speeds, accelerations, and directions. While this can still happen occasionally, such cases are effectively filtered out by our acceptance thresholds and the miss-rate criterion (see Pfeifer et al. 2022). In total, we recovered 11 858 potential particle tracks from the four image sequences, of which 3626 have miss-rates less than 30%. Of those, we traced back 409 to the suspected source regions and visually inspected them several times. We are hence confident that none of the 409 particle tracks that we analyze in the following consist, or were affected by, crossing trajectories. During the entire process, we also did not see any particles colliding or breaking apart.

4. Results and discussion

4.1. Suspected source regions

To get a better idea about where the suspected source regions are located on the nucleus, we used the SPICE toolkit (spacecraft–planet–instrument–c–matrix–events, Acton 1996; ESA SPICE Service 2020) to project the ellipses onto the nucleus surface as it was oriented in the first image of each sequence. For every pixel inside the ellipses, we calculated the points of intersection between the corresponding line of sight and the nucleus shape model SHAP5 (Jorda et al. 2016, in the “cheops” reference frame). Due to 67P’s concave shape however, not every point on its highly irregular nucleus is uniquely identified by the typically-used equidistant cylindrical map projection. Hence, we instead use the recently developed quincuncial adaptive closed Kohonen (QuACK) projection (Grieger 2019; Leon-Dasi et al. 2021) to present our data. Figure 5, for example, shows how the four suspected source regions project onto the south-centered QuACK map.

As already indicated in Sect. 2, we chose the suspected source regions according to which parts in the master images looked to be most active. Because the diffuse coma and jet-like features have mostly been removed in these images, the choices were based on where the largest, concentrated groups of point-source-like particles appeared to originate from. Interestingly, the suspected source regions do not necessarily coincide with the locations of the strongest diffuse features. In other words, it seems that the ejection of large particles (likely of at least a few centimeters) does not always correlate in location, strength, or orientation with that of small (probably subcentimeter) particles (cf. images in Figs. 2 and A.1).

We also observed this seeming anti-correlation in several other sequences not discussed in detail here. In some of those cases, the spacecraft may have been too far away from the nucleus to distinguish even boulders from the diffuse dust features above its surface, and in others, the phenomenon may

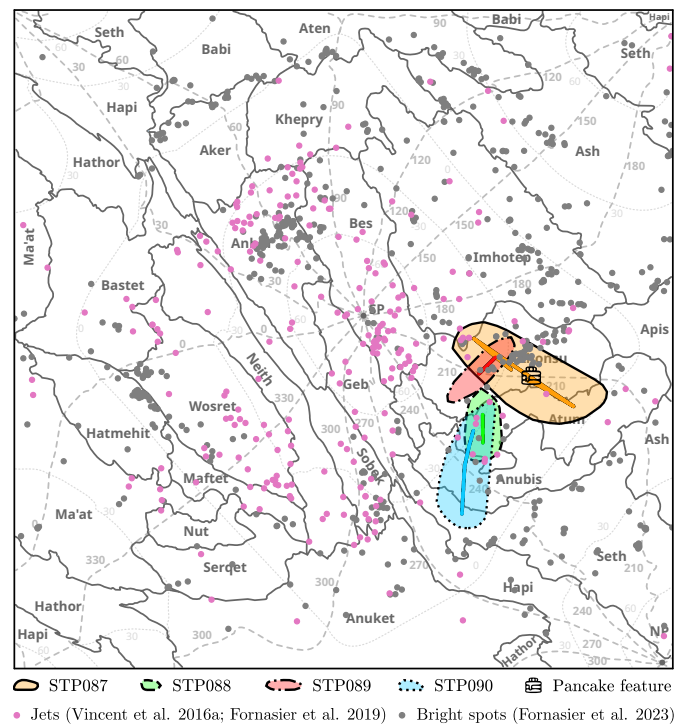


Fig. 5. QuACK-map of 67P’s nucleus, centered on its south pole (SP). The colored shapes show how the ellipses that mark the suspected source regions project onto the surface. The lines in the respective colors indicate the projected ellipse centers. For the geographic data such as surface regions (black lines), latitudes (dotted, light gray lines), and longitudes (dashed, gray lines), the publicly available maps provided by Leon-Dasi et al. (2021)³ were used (slightly modified). For the data of the bright spots, see also Oklay et al. (2017); Deshapriya et al. (2018); Hasselmann et al. (2019); Fornasier et al. (2016, 2017).

be explained by the fact that the sequences were recorded during 67P’s perihelion phase, when the comet was most active and dominated by water ice sublimation (e.g., Combi et al. 2020; Läuter et al. 2020), which, according to current activity models, can only eject fine dust particles (≤ 1 cm) due to its shallow sublimation front, while CO₂ ice sublimation is responsible for the ejection of larger chunks (e.g., Gundlach et al. 2020; Fulle et al. 2020; Wesofowski et al. 2020; Ciarniello et al. 2022; Davidsson et al. 2022). Yet according to recent thermal modeling by Nicholas Attree (priv. comm.)⁴, the fine-dust erosion driven by water ice sublimation and the ejection of large particles driven by CO₂ ice sublimation cannot happen simultaneously at the same location. The observed lack of large particles within the strong, diffuse dust features may therefore be evidence of this activity-based separation. Notably, Kelley et al. (2013, 2015) already observed the same phenomenon for comet 103P/Hartley 2, but they suspected dynamical processes like the rotation of the nucleus, solar radiation pressure, or rocket forces from asymmetric outgassing to be responsible.

It may also seem as if the nucleus is not homogeneously, but only locally active in this particle size regime. This observation could be biased however due to our selection criteria of the image sequences (cf. Sect. 2), as we were specifically looking for sequences with strong, local activity to fulfill our basic assumptions. Nevertheless, our data clearly show that there are times when inhomogeneous activity occurs.

³ Maps available here: <https://doi.org/10.5270/esa-kokoti7>

⁴ Presented at the Rosetta Dust Workshop 2023.

Here is some more information about the related phenomena, which I did not mention in the science paper for brevity: meteorite impacts in similar size regimes typically involve much higher energies and are the result of completely different mechanics (see, e. g., also Öpik 1958b; Kadono et al. 2020); volcanic eruptions are likely much closer related to the phenomena we observed, since the underlying mechanisms (i. e., the sub-surface buildup and subsequent release of pressure) should be similar, although they still occur on very different (energy) regimes; cryovolcanism as observed on some ice moons may be a little bit closer related (see, e. g., also Porco et al. 2006; Tian et al. 2007; Schmidt et al. 2008; Postberg et al. 2011; Berne et al. 2024); and finally the physics of (terrestrial) geysers (which I didn't mention in science paper at all) may also be related (see, e. g., White 1967; Hurwitz et al. 2017; but also Mao et al. 2020).

More importantly however, currently conducted laboratory experiments with illuminated water-ice pebbles ($r = 2.4 \mu\text{m}$) also show similar ejection cones and indicate that their shapes strongly depend on the surface structure (see Fig. 7.11).

Figure 7.11: Cumulative particle trajectories from micrometer-sized water-ice particles (data kindly provided by Calvin Knoop). The images are similar to our master images and were created by reducing 21-minute-long videos. The top image shows the particle trajectories generated by a flat (but somewhat rough) surface, while the bottom image shows the particle trajectories generated by a crater of ~ 1 cm depth and ~ 2 cm radius.

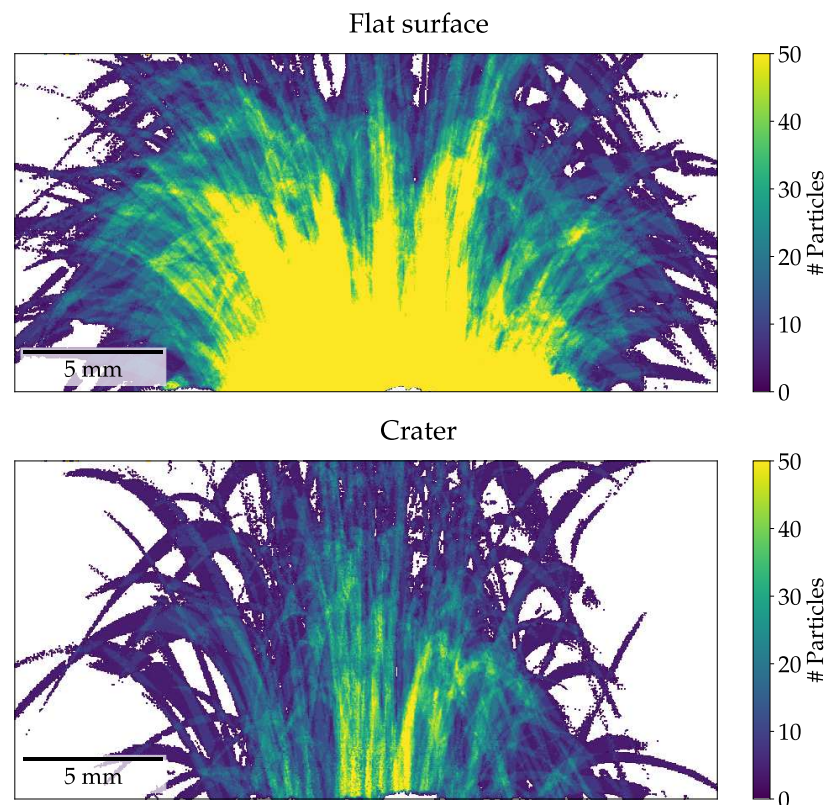


Table 3. Summarized findings regarding the four suspected source regions.

Sequence	$N_t^{(a)}$	$\lambda_c^{(b)}$ (°)	$\tau^{(c)}$ (LT)	Covered surface regions ^(d)	Source characteristics ^(e)	$b^{(f)}$
STP087	81	206	13:57–17:35 ± 2:14	Im[b], Kn[a, b, c, d], Am[a]	Rough, boulders, bright spots, jets	3.8 ± 0.4
STP088	94	226	11:06–14:45 ± 1:24	Kn[d], Am[a]	Rough, terrace, scarp, jets	3.6 ± 0.4
STP089	59	211	9:54–13:33 ± 2:00	Kn[a, d]	Rough, boulders, bright spots, jets	3.7 ± 0.6
STP090	178	238	9:36–13:15 ± 2:18	Am[a], Ab, Se	Smooth, scarp, fractures	3.4 ± 0.3

Notes. ^(a)Number of associated tracks. ^(b)Longitude center. ^(c)Observational period in local time at source region center. Time shift provides local times at source region edges. Universal duration: 03:39. ^(d)Covered surface regions and subregions as defined by [Thomas et al. \(2018\)](#). ^(e)Terrain features. ^(f)Differential power-law index of associated particle SFD.

As illustrated in Fig. 5, all four suspected source regions overlap substantially. While the recorded local time periods of the four sequences are very similar (with the exception of sequence STP087, see Table 3), these areas are not the only ones that were illuminated and visible during the observations (see Figs. 8–10, especially because of the different viewing geometries). We could thus have picked areas that lie much farther apart, had there been stronger activity elsewhere. This indicates that the observed activity was likely locally confined and reoccurring.

It also shows that despite our relatively simple selection process, we likely located the general areas of the source regions correctly. This is further supported by the distinct ejection cones formed by the trajectories that taper toward the ellipse centers (see Fig. 4). To some extent, these ejection cones are likely a consequence of our selection criteria (such as the incidence angle range) and the viewing geometries. Yet their shapes, orientations, and opening angles also suggest that they were likely notably affected by the local surface morphology. Since, to our knowledge, this is the first time such ejection cones have been observed or described, there are currently no theories that explain their occurrence. Their appearance is nevertheless reminiscent of meteorite impacts (e.g., [Opik 1936](#); [Arakawa et al. 2017, 2020](#); [Wada et al. 2021](#)), volcanic eruptions (e.g., [Tsunematsu et al. 2016](#); [Cigala et al. 2017, 2021](#); [Schmid et al. 2020](#)), cryovolcanism (e.g., [Quick et al. 2013](#); [Liu et al. 2016](#); [Fagents et al. 2022](#)), and, of course, cometary jets/geysers/outbursts (e.g., [Keller et al. 1987](#); [Wallis & Chandra Wickramasinghe 1992](#); [Yelle et al. 2004](#); [A’Hearn et al. 2011](#); [Lin et al. 2017](#); [Shi et al. 2019](#); [Wesołowski et al. 2020](#)). The relatively slow and decentralized release of dust particles however (i.e., resulting not from a singular responsible event, but rather many small, independent ones), from a rough, cometary terrain into the vacuum of space, seems to be unique.

According to Fig. 5, the selected particles should have been predominantly ejected from the Khonsu, Atum, and Anubis regions, and potentially also from Imhotep and Seth (following the regional definitions of [El-Maarry et al. 2015, 2016, 2017b](#); [Thomas et al. 2018](#)). The terrains of these regions are very diverse. Generally, the relatively compact area that is covered by the suspected source regions contains almost every kind of (geomorphological) feature that was observed on the nucleus, be it smooth, or consolidated and outcropped. This includes ridges, terraces, scarps, niches, (coarse or fine grained) dust-blankets, boulders ([El-Maarry et al. 2015, 2016](#); [Ferrari et al. 2018](#); [Thomas et al. 2015b, 2018](#); [Leon-Dasi et al. 2021](#)), (steep) cliffs ([Attree et al. 2018a](#)), fractures and other linear features ([Giacomini et al. 2016](#); [Lee et al. 2016](#)), bright spots (associated with freshly exposed volatiles, [Deshapriya et al. 2016, 2018](#); [Fornasier et al. 2023](#)), jet sources ([Vincent et al. 2016a](#);

[Fornasier et al. 2019](#); [Lai et al. 2019](#)), and potentially even clods or “goosebumps” ([Sierks et al. 2015](#); [Davidsson et al. 2016](#)). Khonsu in particular also contains the striking landmark dubbed “pancake feature” ([El-Maarry et al. 2016](#)), and has been found to be one of 67P’s most active regions ([Deshapriya et al. 2016](#); [Hasselmann et al. 2019](#)).

Due to this variety in morphology, there are several locations within the suspected source regions that could be the origin of the observed activity. In the area near the pancake feature, for example, [Vincent et al. \(2016a\)](#) and [Fornasier et al. \(2019\)](#) located several jet sources, [Fornasier et al. \(2023\)](#) identified many bright spots (see Fig. 5), and [Hasselmann et al. \(2019\)](#) discovered surface changes such as boulder movements and cavity formations. All these occurrences however essentially happened throughout Rosetta’s entire rendezvous phase with 67P, and not specifically during our observational period. Nevertheless, the area near the pancake feature substantially overlaps with the suspected source regions (and even the ellipse centers) of sequences STP087 and STP089, which identifies it as a probable source of the particles associated with these regions.

The suspected source regions of sequences STP088 and STP090, on the other hand, predominantly coincide with Atum and Anubis, which are two vastly different areas. While Atum is an elevated region that mainly consists of consolidated structures like terraces, ridges, and scarps, Anubis is a flat area, which is mostly covered in smooth material, but that also displays some fractures ([El-Maarry et al. 2015, 2016](#); [Thomas et al. 2018](#); [Leon-Dasi et al. 2021](#)). Even though these areas have not yet been studied as closely as Khonsu, Fig. 5 shows that especially around the suspected source region of sequence STP088, [Vincent et al. \(2016a\)](#) and [Fornasier et al. \(2019\)](#) have located several jet sources, which might be related to the activity we observed. Additionally, there is a long terrace with a scarp in this area ([Lee et al. 2016](#); [Leon-Dasi et al. 2021](#)), so the activity might have also come from an event similar to the cliff collapse discovered at the Aswan site ([Pajola et al. 2016c](#)).

In the case of sequence STP090, it is also possible that the activity was caused by retreating scarps of fine material that were reported in this area ([El-Maarry et al. 2017a](#)), or by the formation and deepening of fractures ([Leon-Dasi et al. 2021](#)), which can facilitate activity ([Höfner et al. 2017](#)). STP090’s suspected source region also includes steep cliffs located in Seth ([Attree et al. 2018a](#)), but it seems less likely that the observed particles originated from there since the cliffs were not as strongly illuminated during the observational period as the other areas (see Sect. 4.3).

Finally, the suspected source regions not only lie close to where [Combi et al. \(2020\)](#) estimates the four major volatiles (H₂O, CO₂, CO, and O₂) have caused the most erosion between 67P’s inbound equinox and August 2016, but they also notably

Although this figure indicates that the suspected source regions have generally low average emission rates, these regions are also relatively large. The observed activity however more likely stems from much more confined areas within these larger regions, which are neither resolved by the emission data, nor the QuACK-map. The figure nevertheless clearly shows water emission rate peaks close to or within the suspected source regions, supporting their approximate locations.

There is also the citizen science project called Rosetta Zoo (Vincent et al. 2021, 2022). The project aims to document every surface change that could be observed in OSIRIS images over the course of the entire Rosetta mission. To achieve this, the project relies on the power of crowdsourcing: volunteers are presented with pairs of images that show roughly the same surface region under roughly the same conditions, but once recorded at an early phase of the mission and once at late phase. The volunteers are then asked to mark all the differences they can spot. Unfortunately however, the results have yet to be published.

Originally, I intended to compare the particle SFDs and fitted power-law indices from all the different studies to provide a good context for my results. But this quickly turned out to be too time-intensive for a small “side-project”: Some of the studies use different techniques to fit the power-laws, and their derived indices also need to be converted into the same system to be comparable. Admittedly, converting the index values is easy enough, since most of the indices are for example derived from cumulative distributions instead of differential ones, which means that the differential power-law indices are just the cumulative indices minus one. But with so many data points that need to be checked manually, it is easy to make a mistake.

The most appropriate approach however would be to refit all the different data sets with the same coherent method—which I attempted. But it turned out that such comprehensive work actually deserves its own paper and thus may be a project for the future. The particle SFDs of ejected material may for example also be reminiscent of the SFD of the primordial particles that formed the nucleus (Kretke et al. 2015; Davidsson et al. 2016; Blum et al. 2017; Fulle et al. 2017a, 2020a; Blum et al. 2022; Ciarniello et al. 2022). Meanwhile, the use of a power-law to describe cometary particles might have been a natural development from its use to describe meteors and the zodiacal dust (Watson et al. 1937; Whipple 1955; Öpik 1956, 1958a; Finson et al. 1968b), but that is as far as I managed to trace back the source.

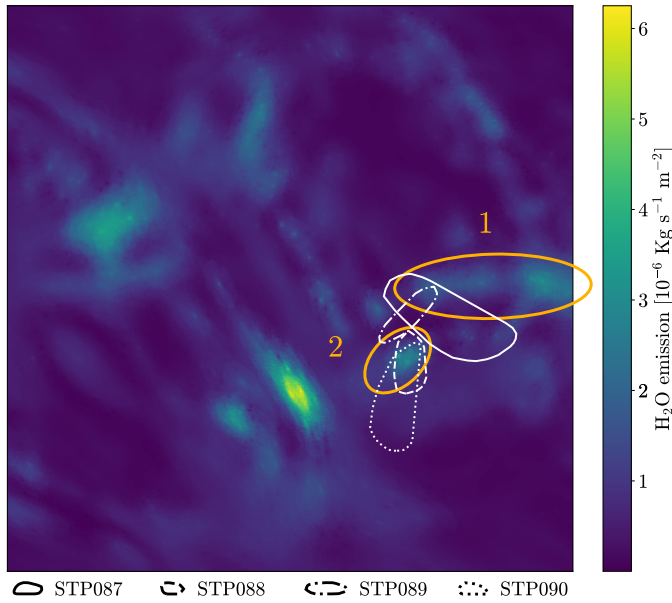


Fig. 6. South-centered QuACK-map of the water emission rates predicted by Lauter et al. (2022), averaged over the period between December 13, 2015, and January 14, 2016 (data kindly provided by Matthias Lauter and Tobias Kramer). Also shown are the four suspected source regions and the approximate locations of areas 1 and 2 (orange ellipses, drawn in by hand) from Lauter et al. (2022).

overlap with two areas that Lauter et al. (2019, 2020, 2022) estimate to be among the most active in water and CO₂ production (and possibly many other species) during the perihelion phase, but also long afterward. Figure 6 shows the QuACK-map of the water emission rates predicted by Lauter et al. (2022). The data was averaged over the period between December 13, 2015, and January 14, 2016, which aligns closely with the overarching time frame of our observations. While the suspected source regions of STP087 and STP089 partly overlap with their area 1, the regions of STP088 and STP090 do so with their area 2.

Overall, we can generally associate the ejected particles with areas that contain rugged terrain or steep slopes, be it scarps, cliffs, or fractures. Such geological features are also considered to favor activity, because they (a) should make it easier for particles to overcome the local gravity and tensile strength that keep them in place (Groussin et al. 2015; Attree et al. 2018a,b), (b) can absorb and store energy more efficiently than flat or smooth areas (Hofner et al. 2017), and (c) do not get covered by loose material that could quench their activity (Vincent et al. 2016b). Additionally, we can likely link some of the observed activity to surface areas with a high concentration of jet sources and bright spots, which fits well with our assumptions: Both features indicate (recent) activity, as bright spots may be the remnants of meter-sized, water-ice-enriched blocks (WEBs, Ciarniello et al. 2022) that were exposed due to erosion driven by CO₂ ice sublimation.

4.2. Particle size-frequency distribution

Because we associated the particle groups with regions on the nucleus surface, we can use the average nucleocentric distances of the spacecraft (see Table 2) as rough estimates for the particle-observer distances. By further assuming that the particles are

spherical, we can approximate their equivalent radii via

$$r = \sqrt{J \frac{r_h^2 \Delta^2}{R I_\odot}}, \quad (1)$$

where r is the particle radius in m, J the particle flux averaged over all its detections in $\text{W m}^{-2} \text{nm}^{-1}$, r_h the dimensionless heliocentric distance measured in units of AU, Δ the particle-observer distance in m, $R = 0.0021$ the particle reflectance (computed for decimeter-sized particles at a 90° phase angle using the model from Markkanen et al. 2018), and $I_\odot = 1.565 \text{ W m}^{-2} \text{ nm}^{-1}$ the solar flux in the NAC F22 filter at 1 AU.

For distinct size ranges, it is generally assumed that the size-frequency distribution (SFD) of cometary particles follows a power law. When it comes to particles that are found on the nucleus surface (other than fall-back material), there is good reason to believe that they mostly formed under fractal fragmentation processes like thermal fatigue or gravitational collapse (Pajola et al. 2015, 2017a; Attree et al. 2018b; Cambianica et al. 2019), which have been studied extensively for terrestrial material (e.g., Mandelbrot 1982; Turcotte 1986; Sanchidrian et al. 2014; Fowler & Scheu 2016). Impact and collisional fragmentation, as seen in asteroids for example, also produce fractal SFDs (Dohnanyi 1969; Hartmann 1969; Brown 1989), but likely only play a minor role in the case of 67P (so far, evidence for just a single impact crater has been found, Thomas et al. 2015b).

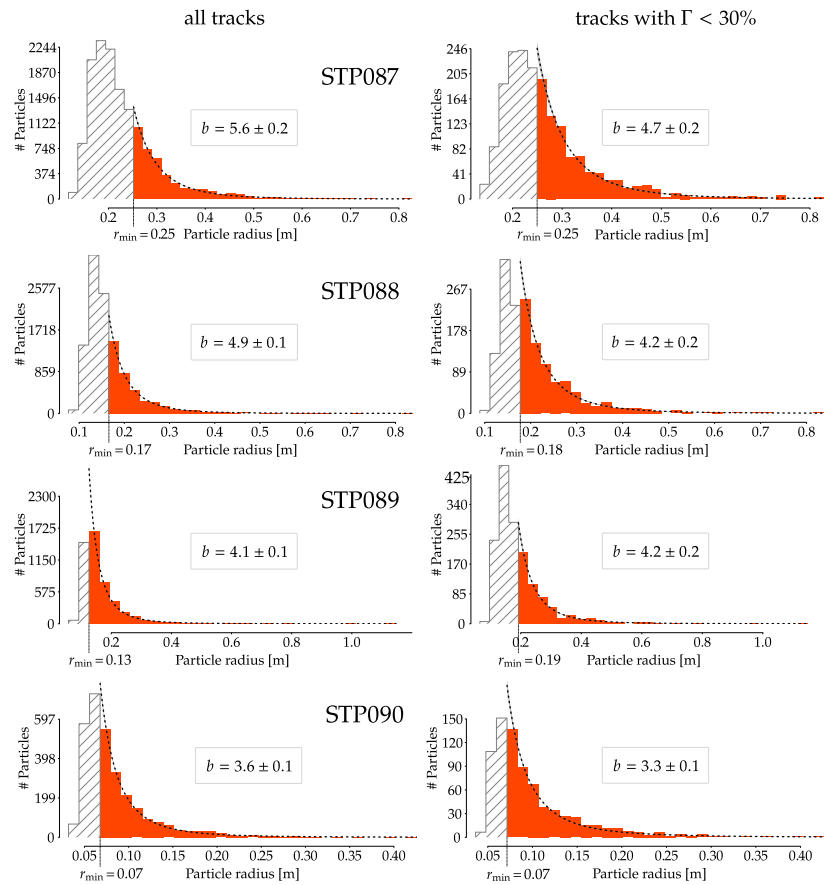
Numerous studies have determined SFDs of 67P’s surface material and fitted them with power laws (e.g., Auger et al. 2015; Mottola et al. 2015; La Forgia et al. 2015; Pommerol et al. 2015; Vincent et al. 2015, 2016b; Pajola et al. 2015, 2016a,b,c, 2017a,b, 2019; Deshapriya et al. 2016; Poulet et al. 2016; Oklay et al. 2016, 2017; Lucchetti et al. 2016, 2017; Tang et al. 2017; Hasselmann et al. 2019; Cambianica et al. 2019). Likewise, power laws have been used for a long time to fit or model the cometary dust environment (e.g., Finson & Probst 1968a,b; Fulle 1989; Clark et al. 2004; Ishiguro 2008; Kelley et al. 2008, 2009; Agarwal et al. 2010, 2017; Fulle et al. 2010; Soja et al. 2015; Lai et al. 2016; Marschall et al. 2016, 2017, 2019, 2020b; Markkanen et al. 2018), and more recently to describe the SFDs of particles observed by Deep Impact/EPOXI’s camera system around comet 103P/Hartley 2 (Kelley et al. 2013, 2015), and Rosetta’s dust detectors and camera system around comet 67P (e.g., Rotundi et al. 2015; Merouane et al. 2016, 2017; Hilchenbach et al. 2016; Agarwal et al. 2016, 2017; Fulle et al. 2016; Rinaldi et al. 2017). There is however no proven link between the assumption of a power law and the physical origin of the particle SFD (Marco Fulle, priv. comm.). Instead, the power law is mainly of practical use when fitted to a limited size range, because it allows to easily compare different size regimes, and immediately indicates which size range dominates the cross section and volume (mass) distribution (e.g., Fulle et al. 2010, 2016; Rotundi et al. 2015; Blum et al. 2017). We therefore also use power laws to describe the SFDs of our particles.

Generally, if an SFD follows a power law, it means that the radii were drawn from a probability distribution in the form of

$$p(r) \propto r^{-b}, \quad (2)$$

where in our context, the exponent b is often called the (differential) power-law index. A common method to fit a power law to data is to construct a histogram from the data and plot it on a log-log scale with logarithmic bins and counts. In this representation, the data form a straight line with slope $-b$ if the

Figure 7.12: “Particle” SFDs and fitted power-laws derived for all tracks and those with miss-rates $\Gamma < 30\%$ for the four sequences. The elements in the plots are analogous to Fig. 7 in the science paper.



As I mention at the end of Section 5.2, the velocity and acceleration distributions look very similar for genuine and ambiguous tracks. So while these parameters cannot be used to separate between the two populations, it also means that the overall distributions (including all the tracks) already give a pretty good idea about what the distributions for the genuine tracks should look like. But for the derived particle SFDs, this is not the case (at least when they are quantified by a power-law; visually they may be very similar). Figure 7.12 shows that except for sequence STP090, the particle SFDs that include all tracks or just the ones with miss-rates $< 30\%$ are generally not good predictors for the SFDs of particles that we associated with the nucleus (at least in terms of the fitted power-law index).

This may be due to the following reasons: For one, spurious tracks will likely produce different “particle” SFDs than genuine ones (although spurious tracks of course don’t have corresponding particles), because they typically contain a lot of background noise instead of genuine particle detections. Second, even though most of the tracks with miss-rates $< 30\%$ are likely genuine, a large number of them likely belong to particles at very different particle-observer distances, which means their radii cannot be reliably estimated. And third, specific surface areas may produce particle SFDs that are notably different from the global particle SFD, which is also something that our dust coma simulations indicate (see final paragraph on p. 121).

In theory, spurious tracks can also consist entirely of genuine detections that are unrelated (e. g., in case of aliasing, see Fig. 5.1). In that regard, it would be interesting to know if the brightness distribution of genuine and spurious detections are similar, which might be a way of separating them. These populations are however not easy to separate, but the distributions of used versus unused detections might give an idea (see also Fig. 5.2).

histogram follows a power law, which makes it easy to determine the power-law index via least-squares linear regression, but due to systematic errors (like the arbitrary binning intervals), this approach should generally not be trusted (Clauset et al. 2009).

So instead, we rely on maximum-likelihood estimators (MLEs) and Kolmogorov–Smirnov (KS) tests (see, e.g., Feller 1948 for KS tests, but also Snodgrass et al. 2011, who nevertheless favor least-square regression). To fit our data, we use the Python-package powerlaw (Alstott et al. 2014), which is based on the statistical methods of Klaus et al. (2011) and Clauset et al. (2009, see also Virkar & Clauset 2014). Since our data are drawn from a continuous distribution, Eq. (2) can be written as

$$p(r) = Cr^{-b}, \quad (3)$$

with normalization constant

$$C = (b - 1)r_{\min}^{b-1}, \quad (4)$$

where r_{\min} is the lower fitting bound, which is required because $p(r)$ diverges for $r \rightarrow 0$. The MLE of b can then be computed as (Muniruzzaman 1957)

$$\hat{b} = 1 + n \left[\sum_{i=1}^n \ln \frac{r_i}{r_{\min}} \right]^{-1}, \quad (5)$$

where $r_i \geq r_{\min}$ ($i = 1, \dots, n$) are the measured radii. We additionally used KS tests to find the r_{\min} and \hat{b} values that produce the best fits (although in the case of sequence STP089, we slightly restricted the allowed range for r_{\min} due to the small number of data points)⁵.

Figure 7 shows the resulting particle SFDs and fitted power laws. The size ranges of the four SFDs largely overlap, covering mostly the decimeter-scale. Only sequence STP090 differs notably from the other three, with its SFD shifted toward smaller radii, peaking below 10 cm, and containing the smallest detected particles at roughly 5 cm. In sequence STP089 on the other hand, we detected the largest particle with an equivalent radius of about 1.15 m. Many particles strongly fluctuate in brightness over the course of their tracks however (in large part likely because they are nonspherical rotators), so their mean-flux-based radii only represent the most likely average values. In contrast, the errors from residual background signals and inaccurate particle-observer distances, as well as the uncertainty in the albedo, are typically much smaller than these fluctuations. Our results therefore remain sufficiently precise, and following the terminology of Pajola et al. (2016b), the particles classify as either pebbles (<25 cm) or boulders (>25 cm).

The values of the fitted power-law indices range from 3.4 ± 0.3 to 3.8 ± 0.4 and are all within each others' error bars, suggesting that most of the mass is contained in the larger particles. Yet most of the large particles were likely not fast enough to leave the gravitational field of the nucleus (see Figs. 12 and 13 in Sect. 4.4), and should have later fallen back onto its surface. Farther out in the coma, the SFDs in this size range might hence be a little steeper. So far however, there are no other studies that report power-law indices for coma particle SFDs in a similar size range (or time period) to corroborate our findings.

⁵ Strictly speaking, a good fit alone is also not sufficient to conclude that the underlying distribution is truly a power law. In addition to a good theoretical model that explains the data, Clauset et al. (2009) recommend elaborate hypothesis testing (see, e.g., Kelley et al. 2013, 2015), but that is outside of the scope of this work.

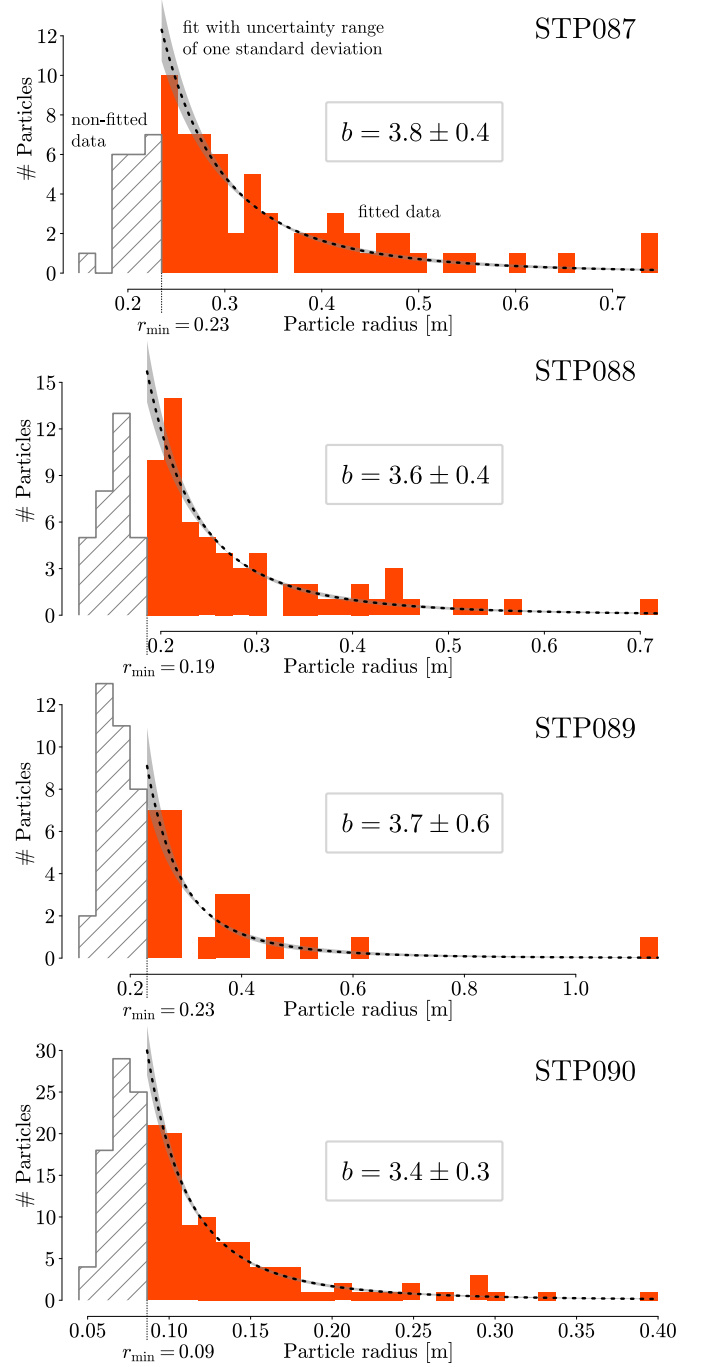


Fig. 7. Particle SFDs and fitted power laws of the four particle groups (Fig. 4).

Nevertheless, our index values agree notably well with those obtained for submillimeter-sized particles, despite the likely fundamentally different ejection mechanisms: Fulle et al. (2016) report $b \approx 3.7$ for dust particles captured during the perihelion phase, and Merouane et al. (2016) report $b = 3.1 \pm 0.5$ for those captured between perihelion and April 2016 (these are currently the two observational periods that most closely match ours and for which b -values exist).

Regarding surface material, the most relevant b -values were obtained by Deshapriya et al. (2016) and Hasselmann et al. (2019), who counted boulders in the Khonsu region (no studies exist yet for Atum or Anubis). Deshapriya et al. (2016) surveyed

the entire region using images recorded pre-perihelion on May 2, 2015, and report $b = 4.1 + 0.2 / - 0.3$ for boulders ranging from 7 to 40 m, whereas [Hasselmann et al. \(2019\)](#) studied a small patch near the pancake feature in images recorded post-perihelion on June 25, 2016, and report $b = 2.6 \pm 0.01$ for boulders ranging from 1.2 to 10 m. This significant flattening of the particle SFD over the course of the perihelion phase might indicate that most of the smaller boulders were removed from the surveyed area, while most of the larger ones remained or fell back onto it. Since our observations were recorded post-perihelion but well before June 25, 2016, the fact that our power-law indices lie in between those reported by [Deshapriya et al. \(2016\)](#) and [Hasselmann et al. \(2019\)](#) might be a reflection of this particle SFD transition.

Overall, our particles may therefore be a link between the debris studied on 67P's surface and the particles observed and collected in its coma. Not only do they cover a size range that on the upper end overlaps with that of the typically much larger boulders counted on the nucleus surface, and on the lower end with that of the typically much smaller particles detected farther out in the coma (see also [Güttler et al. 2017](#); [Ott et al. 2017](#); [Frattin et al. 2021](#); [Lemos et al. 2023, 2024](#)); but from an evolutionary standpoint, they also sit between the relatively pristine surface material which has not yet been ejected (excluding fall-back material), and the more processed material found in the coma and beyond which has escaped the nucleus gravity.

4.3. Illumination and surface acceleration

Because solar irradiation fundamentally drives the activity of comets, we created QuACK-maps that show 67P's average surface illumination during the time periods when our sequences were recorded, to estimate the insolation that our suspected source regions received. The maps were generated using the same approach as described by [Grieger \(2019\)](#), which accounts for the relative orientation between the solar irradiation vector and the surface normals of the QuACK shape model tiles, as well as self-shadowing effects. Because the QuACK shape model is relatively rough however (160 000 tiles), the resulting illumination maps are somewhat blurred. In reality, small-scale surface parts, such as cliff faces, may receive insolation that is much stronger than the average ([Pajola et al. 2017a](#)). Activity from such sites may be significantly enhanced, which our employed model would not reflect, but since we are mainly interested in general areas, the illumination maps are adequate.

Because the four sequences were recorded within less than a month (which corresponds to a change in sub-solar latitude of less than six degrees), the illumination conditions averaged over a whole comet day are almost identical on the respective dates and differ mostly in overall intensity. Figure 8 shows the average daily illumination for sequence STP088, which is a good representation for the entire period as its sub-solar latitude is at the center of the covered value range (see Table 2). Additionally, we created two more illumination maps for each of our sequences. The first set shows the average illumination received solely during the observational periods of the respective sequences (see Fig. 9); but because our particles were likely ejected up to half an hour before the sequences were recorded, and because the activity does not immediately follow the exposure to sunlight as temperature and gas pressure first need to build up, the other set shows the average illumination received over the 2 h (roughly 3 h and 51 min in local time) leading up to the observational periods (see Fig. 10).

According to Fig. 8, the suspected source regions clearly received some of the most sunlight over the course of a full

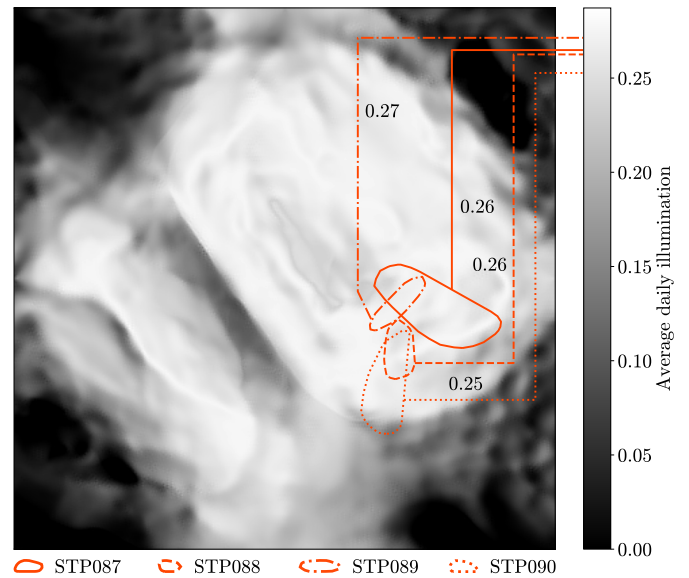


Fig. 8. South-centered QuACK-map of the average nucleus illumination received over a whole comet day at the time of sequence STP088 (December 26, 2015). The intensity is measured in units of the average illumination at 1 AU from the Sun at the equator of the Earth over one Earth-day during equinox. The orange shapes and lines indicate the mean values within the suspected source regions.

comet day at that time. Conversely, Fig. 9 shows that this was not always the case during the observational periods. Surface areas other than the suspected source regions were illuminated just as, or even more strongly during these periods, but did not show nearly the same levels of activity in our image sequences. Yet if the back-extrapolations of our tracks are approximately correct, most of our particles should have been ejected up to half an hour before the observations started (or possibly even earlier). Figure 10 shows that during the 2 h prior to the observations, the illumination conditions for other areas (such as the neck, the small lobe, or Hapi) were a lot different, while the suspected source regions were already well illuminated. This further supports our choice of their general locations. Yet since we did not observe similar activity from areas that received comparable insolation (during either period), it also suggests that strong illumination is necessary, but not sufficient to explain the observed activity.

We thus also investigated the intensity of the local surface acceleration, a_S (i.e., the sum of gravity and centrifugal acceleration). Figure 11 shows two QuACK-maps of a_S , once normal to the shape model facets and once in radial direction. In both cases, the average downward accelerations within the suspected source regions are relatively high, which means that they cannot explain the localized release of decimeter-sized particles either. The local surface composition and structure therefore seem to be the most probable causes. For one, activity-enhancing topographies as discussed in Sect. 4.1 may play a role (see also [Reshetnyk et al. 2021, 2022](#); [Skorov et al. 2021, 2022a,b, 2023](#), who use models to explore how structural parameters such as porosity and dust layer thickness can affect the gas production rate), but more importantly, we regard a local overabundance of CO₂ ice as the most likely driver of decimeter-sized particle ejection (in line with current ejection models, e.g., [Gundlach et al. 2020](#); [Fulle et al. 2020](#); [Wesołowski et al. 2020](#); [Ciarniello et al. 2022](#); [Davidsson et al. 2022](#)).

Figure 7.13: Selected particle tracks of sequence STP090, color-coded according to their particle size.

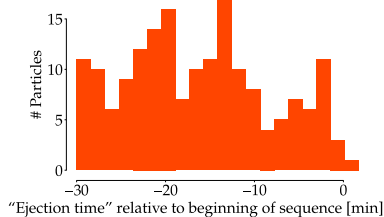
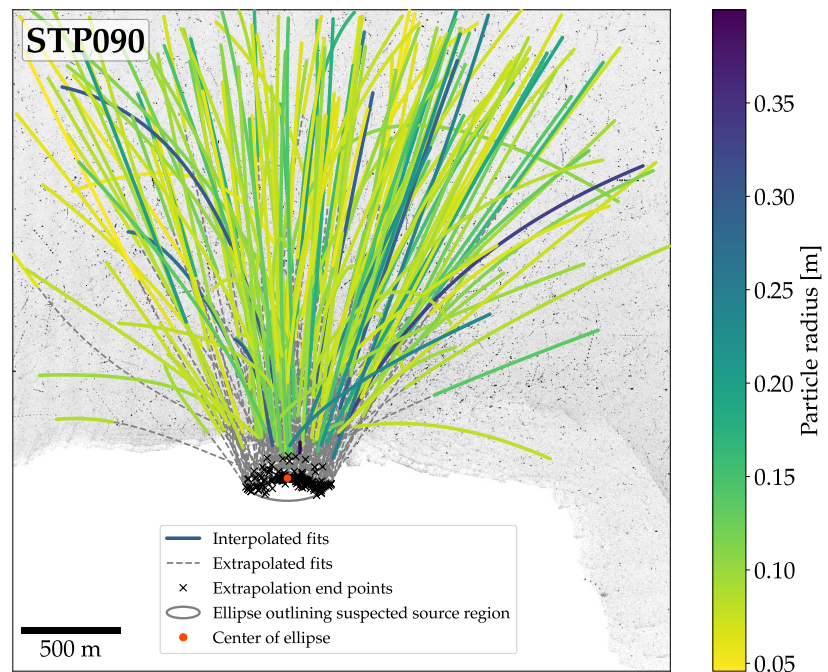


Figure 7.14: Histogram of the particle “ejection times” for the selected particles of sequence STP090. The ejection times are calculated as the times when the back-extrapolated fits are closest to the ellipse center (i. e., the extrapolation end points as e. g. shown in Fig. 7.13).

Other than what is mentioned in this section, we also looked at many other parameter distributions and their correlations, such as “ejection times”, different velocity and acceleration components (e. g., in the solar direction), or the particle–source-region distance over time, but none of them really allowed for reliable conclusions. Figure 7.14 for example shows the “ejection time” histogram for the selected particles of sequence STP090. The histogram has clearly several peaks, which may hint at some burst-like ejection pattern. The pattern even seems roughly periodic, which could indicate the time it takes for enough gas pressure to build up beneath the surface to overcome the forces that keep the surface material in place and eject it. But because it is difficult to say how accurate the ejection times really are, the histogram data may also be misleading. So for now, this is certainly an interesting result, but it requires further investigation.

Another example is presented in Figure 7.13, which shows the same particle tracks of sequence STP090 shown in Figure 4 in the science paper, but color-coded as a function of the particle radius. This figure might have for example indicated a relation between the curvature of a track and the particle size, or between the size and origin of a particle, but unfortunately, no obvious pattern can be observed.

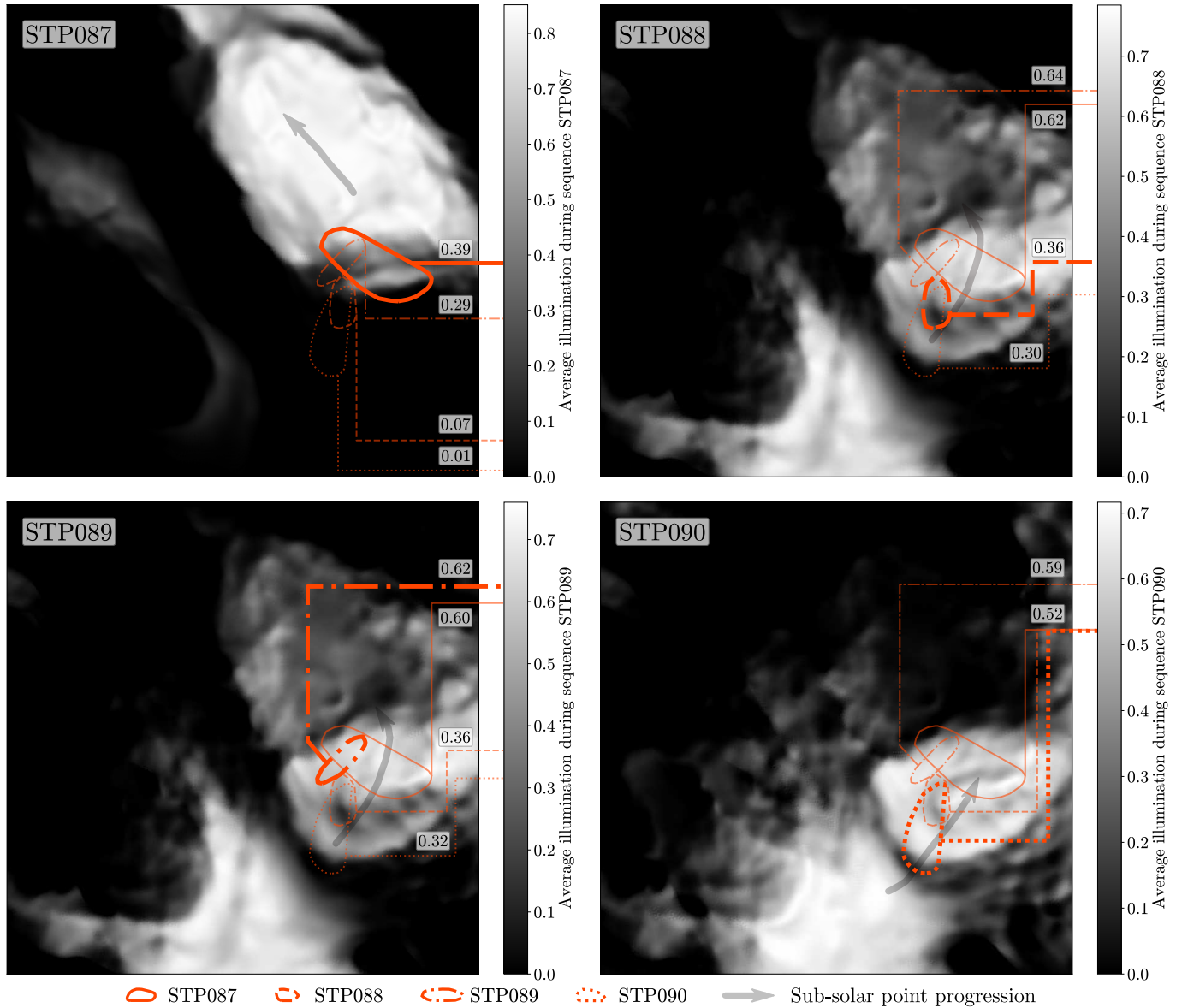


Fig. 9. South-centered QuACK-maps of the average surface illumination received during the respective observational periods of the four sequences. The intensity units are the same as in Fig. 8. The mean values within the suspected source regions are indicated by the orange shapes and lines, with the areas that were selected during the respective sequences highlighted in bold. The values here are generally higher than in Fig. 8 because here the illumination was averaged over time periods when the areas were mostly in sunlight, while in Fig. 8 the illumination was averaged over a whole day-and-night cycle.

4.4. Particle dynamics

From the polynomial fits to the particle tracks we immediately obtain the projected particle velocities and accelerations. Initially, they are measured in terms of the image coordinate system (e.g., in px s^{-1}), so to translate them into physical units, we again need to know the particle-observer distance and thus again use the nucleocentric distance as a proxy (see also Table 2).

Figure 12 shows how the radial components (relative to the nucleus' center of mass) of the resulting projected particle velocities, v_{rad} , distribute as a function of particle radius, and how they compare to the local escape speed, v_{esc} . Assuming a local surface acceleration at the suspected source regions of approximately $-1.8 \times 10^{-4} \text{ m s}^{-2}$ (based on the data shown in Fig. 11), we find that $v_{\text{esc}} \approx 0.85 \text{ m s}^{-1}$. Overall, roughly 75 to 91% of the selected

particles are slower than this escape speed. Some particles even have negative radial velocities, reflecting the fact that some of the tracks in Fig. 4 already curve back toward the nucleus. Although these velocities are merely projected, the percentages of particles slower than the escape speed directly provide upper-limit estimates of the fall-back fractions, ϕ_{fb} . In particular, almost all particles with $r \geq 40 \text{ cm}$ seem to be too slow to leave the gravitational field of the nucleus (although some of them may still reach escape speed later on due to gas drag acceleration). These particles may for example contribute to the dust blankets found on the northern hemisphere of the nucleus such as the Hapi region (e.g., Thomas et al. 2015a; Keller et al. 2015, 2017; Lai et al. 2016; Cambianica et al. 2020; Davidsson et al. 2021).

The sizes and radial velocities of the particles that are faster than the escape speed, on the other hand, generally fit well

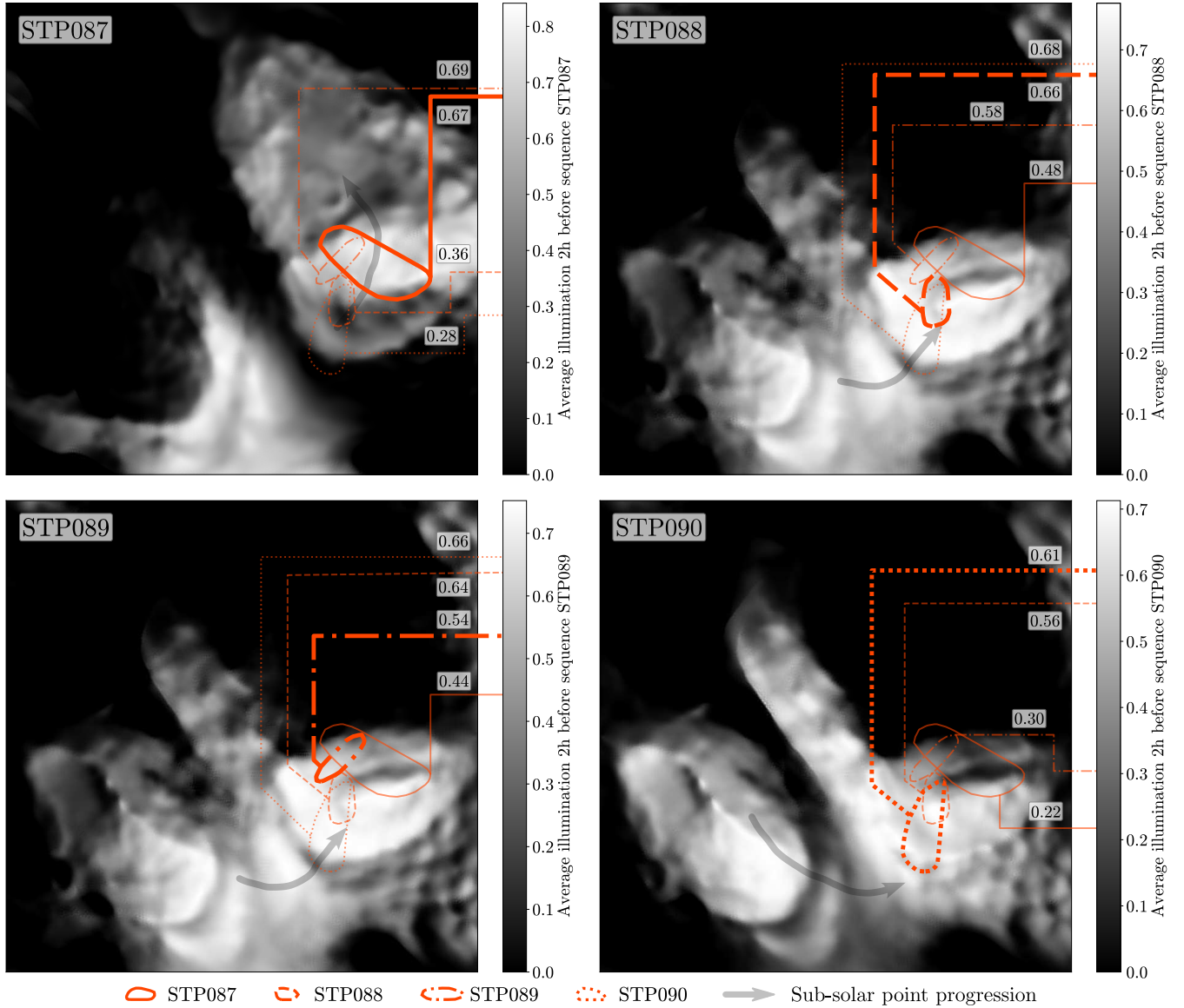


Fig. 10. South-centered QuACK-maps of the average surface illumination received during the 2 h prior to the respective observational periods. The figure elements and intensity scale are analogous to those in Fig. 9.

with those of particles detected farther out in the coma by Ott et al. (2017). Their particles are mostly centimeter-sized and on average about twice as fast as ours, which seems reasonable given that our particles are mostly decimeter-sized and still accelerating away from the nucleus.

This is illustrated by Fig. 13, which shows the projected radial particle accelerations as a function of particle radius. In this context of decimeter-sized particles, we assume that there are mainly three forces acting along the radial direction: gravity, centrifugal force, and gas drag. Solar radiation pressure and solar tides are generally several orders of magnitude weaker than these three, and therefore negligible. Rocket forces exerted by the particles themselves due to asymmetric outgassing, on the other hand, are difficult to estimate (see, e.g., Kelley et al. 2013, 2015; Agarwal et al. 2016; Güttler et al. 2017). The particles' sublimation rate and in particular their ice fraction are still topics of debate, and may be high or insignificant, depending on the model (e.g., Davidsson et al. 2016, 2021; Blum et al. 2017, 2022; Gundlach et al. 2020; Fulle et al. 2020; Cambianica et al. 2020;

Choukroun et al. 2020; Ciarniello et al. 2022). We thus also ignore rocket forces (for discussions of other minor forces that act in such scenarios, see, e.g., Chesley et al. 2020; Jiang & Schmidt 2020), and model the radial component of the particle acceleration, a_{rad} , via

$$a_{\text{rad}} = \frac{1}{m} (F_G + F_C + F_D), \quad (6)$$

where m is the particle mass, F_G and F_C are the (radial components of) gravitational and centrifugal force, respectively, and

$$F_D = \frac{1}{2} C_D m_g n_g \sigma_p |v_g - v_p| (v_g - v_p) \quad (7)$$

is the (radial component of) gas drag, where C_D is the (dimensionless) drag coefficient, m_g the mass of a gas molecule, n_g the gas number density, σ_p the particle cross section, and v_g and v_p are the radial velocities of the gas and the particles, respectively.

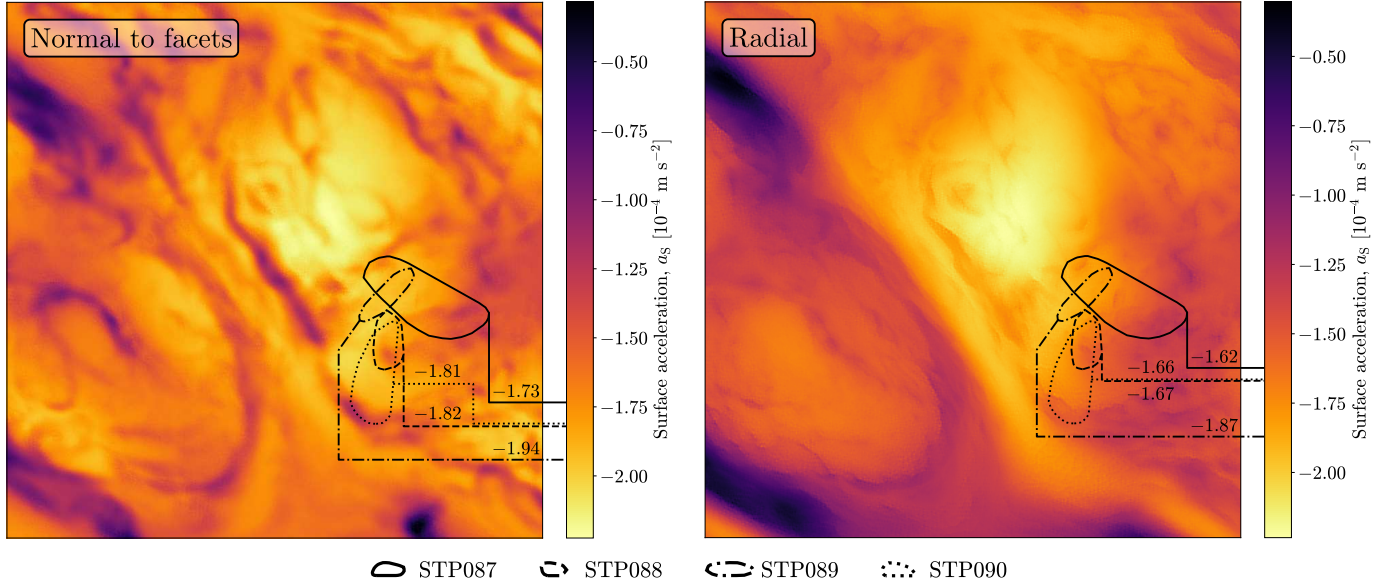


Fig. 11. South-centered QuACK-maps of the approximate surface acceleration, a_s , on 67P's nucleus. Component parallel to the facet normal on the left, radial component on the right. The mean values within the suspected source regions are also indicated.

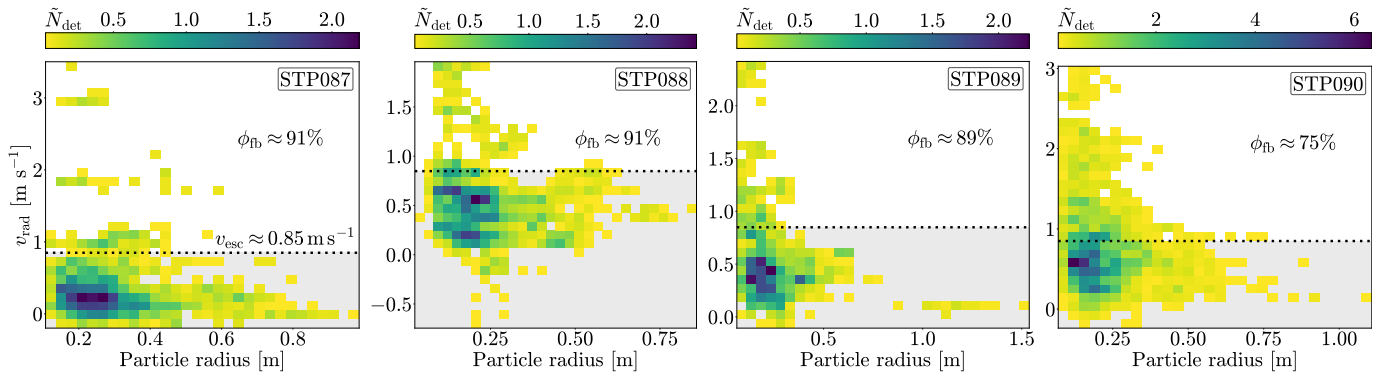


Fig. 12. 2D histograms of the projected radial particle velocities, v_{rad} , as a function of particle radius (for the selected particles, see Fig. 4). Because the polynomial fits to the particle tracks also approximate the particle accelerations, instead of using values averaged over a track, the particle velocities and radii were determined for each detection of a track individually and the results were weighted by the number of detections of the respective track (residence time weighting). The histogram data thus represent the weighted number of detections, \tilde{N}_{det} . Also shown are the approximate escape speeds at the suspected source regions, v_{esc} (dotted line), and the corresponding maximum fall-back fractions, ϕ_{fb} (gray area).

Plugging Eq. (7) into Eq. (6) and assuming $v_g \gg v_p$, as well as spherical particles with bulk density ρ_p and radius r , we get

$$a_{\text{rad}} = a_s + \xi r^{-1}, \quad (8)$$

where $a_s = (F_G + F_C)m^{-1}$ is the surface acceleration, and roughly equal to $-1.8 \times 10^{-4} \text{ m s}^{-2}$ at our suspected source regions according to the data shown in Fig. 11, and

$$\xi = \frac{3}{2} C_D Q_g v_g \rho_p^{-1}, \quad (9)$$

where $Q_g = \frac{1}{4} m_g n_g v_g$ (Bird 1994) is the local gas production rate at the suspected source regions.

The parameters that constitute ξ , however, are difficult to constrain. The particle density, for instance, might be significantly lower than the bulk density of the nucleus, if the particles lost most of their volatiles but kept their structure and thus volume intact. Likewise, the drag coefficient also depends on particle shape, macro porosity, and other parameters, and could

consequently vary a lot (e.g., Skorov et al. 2016, 2018; Ivanovski et al. 2017a,b; Reshetnyk et al. 2018), and in correlation with the gas velocity and number density, the local gas production rate could even differ by one or two orders of magnitude (see also Marschall et al. 2020a,c, 2023).

Nevertheless, from fitting Eq. (8) visually to our data, we find that $\xi \approx 2 \times 10^{-4} \text{ m}^2 \text{ s}^{-2}$ describes the upper limit of the measured a_{rad} rather well for all four sequences (see solid curves in Fig. 13). To achieve such a value, we for example propose the following parameter combination: $C_D = 4$, $Q_g = 3.6 \times 10^{-5} \text{ kg s}^{-1} \text{ m}^{-2}$, $v_g = 500 \text{ m s}^{-1}$, and $\rho_p = 533 \text{ kg m}^{-3}$. While the particle density value is a conservative estimate based on the nucleus bulk density (Pätzold et al. 2016) and may be notably lower, the other parameter values are based on our water activity model ($m_g = m_{\text{H}_2\text{O}} = 3 \times 10^{-26} \text{ kg}$, $n_g = 1.9 \times 10^{18} \text{ m}^{-3}$; see Fig. D.1, Sect. 4.5, and Marschall et al. 2020b), assuming that the local gas production is about five times higher than our model prediction ($Q_g = 7.1 \times 10^{-6} \text{ kg s}^{-1} \text{ m}^{-2}$, which is also very similar to the peak average production rates estimated by Läuter et al. (2022), see Fig. 6 and dashed curves in Fig. 13). This fits well

Figure 7.15 shows the corresponding particle populations.

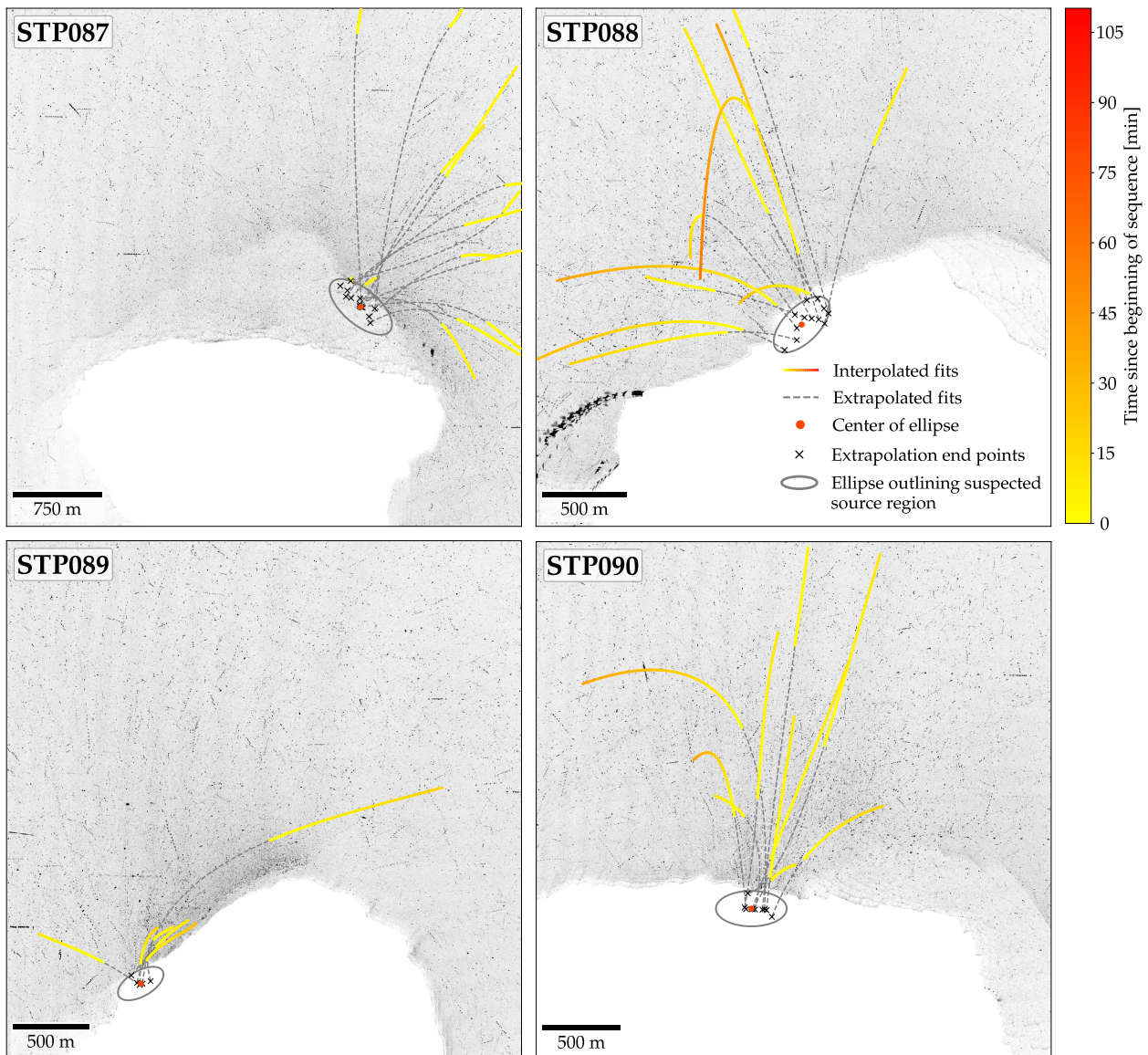


Figure 7.15: Particle tracks that exhibit downward accelerations smaller than the local gravitational acceleration at least once during the observational period.

The full simulation pipeline is divided into several self-contained steps (Marschall 2017; Marschall et al. 2016, 2017, 2019, 2020a,b). At the base sits a shape model of 67P's nucleus, in our case the stereo-photogrammetric SHAP7 model of Preusker et al. (2017), decimated to roughly 440 000 facets. Next, the insolation is calculated for each facet, depending on the heliocentric distance and the incidence angle, and accounting for self-shadowing (but neglecting re-radiation). This is followed by a simple thermal model that balances the incoming solar energy with thermal radiation and water-ice sublimation, but ignores thermal conductivity because comets (Huebner et al. 2006; Fernández et al. 2013) and 67P specifically (Choukroun et al. 2015; Gulikis et al. 2015; Schloerb et al. 2015; Spohn et al. 2015; Marshall et al. 2018) were observed to have very low thermal inertia. The gas production rate is then directly computed from this equilibrium, assuming pure ice sublimation (discussion continues on the next double-page).

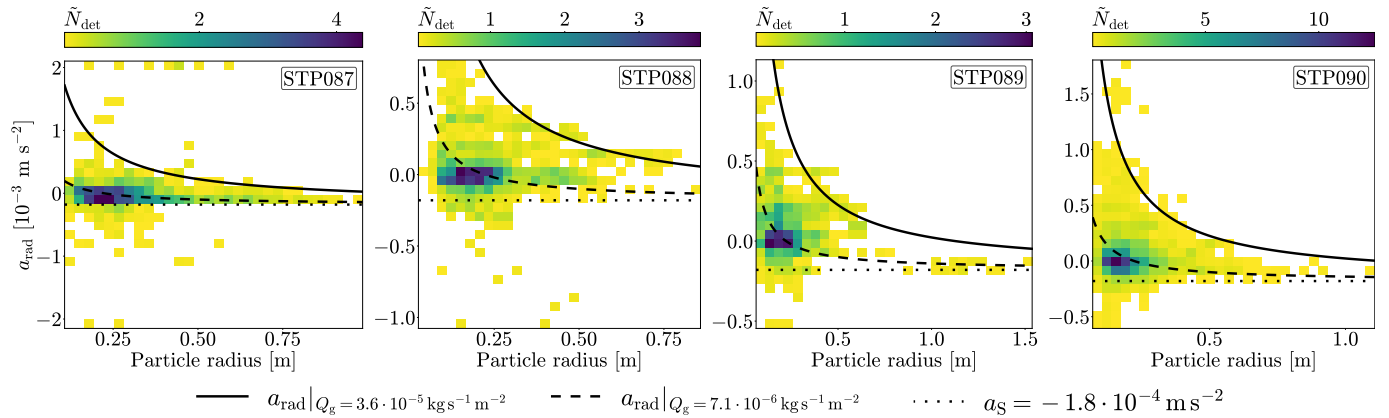


Fig. 13. 2D histograms of the projected radial particle accelerations, a_{rad} , as a function of particle radius (for the selected particles, see Fig. 4). The histogram values were determined analogously to the description in Fig. 12. Also shown are the predicted surface acceleration, a_s (dotted line, see also Fig. 11), and two models (dashed and solid curves) of the particle acceleration, as described by Eqs. (8) and (9). The parameters for both curves are based on our gas models (see Sect. 4.5), but for the solid curve, a local gas production rate was assumed that is about five times higher.

with our observations of strong, localized activity, likely driven by CO_2 ice sublimation. Additionally, the lower bound of the measured radial accelerations also agrees particularly well with the estimated surface acceleration.

There are some measurements in Fig. 13 however, that clearly lie outside these theoretical bounds. More curiously, there is an apparent trend for outliers with radii $\lesssim 40$ cm to have radial accelerations that are much lower than the predicted surface acceleration. To investigate this trend, we looked at all the particles that exhibited downward accelerations smaller than a_S at least once while they were observed. The corresponding tracks indicate that some of the outliers likely belong to particles that do not actually originate from the suspected source regions, but were instead flying in the fore- or background and just passed through the ellipses by chance. Others may have inaccurate back-extrapolated fits, and a third group of particles seem to “orbit” around the nucleus at a distance and orientation where the “downward” direction as defined by the ellipses is inadequate, and so they only seem to have such strong downward accelerations due to the 2D projection. These causes should also apply to the other outliers, but the described trend is likely at least in part a statistical effect, since most of our particles lie in this size regime (see also Fig. 7), and so we expect most outliers to lie in this size regime, too. Yet, even though under standard assumptions, solar radiation pressure and rocket forces are not strong enough to produce the measured downward accelerations, small particles may have a much higher water ice content than larger ones, which they would also lose more quickly to sublimation (Markkanen & Agarwal 2020). The observed trend might thus also be a sign of asymmetric outgassing in the anti-solar direction.

Finally, we used the extrapolation endpoints shown in Fig. 4 to roughly estimate the particle ejection velocities. As stated in the caption, these endpoints do not mark the exact ejection times or places, but simply the points where the extrapolated tracks are closest to the ellipse centers. This choice is fairly arbitrary, but since the individual particle origins are impossible to locate precisely, the endpoints nevertheless serve as useful references to roughly estimate when the particles were ejected and at what speed. Accordingly, we find that the initial particle velocities were likely distinctly nonzero. The median initial velocities obtained for the four sequences are also notably similar, centering around ≈ 0.59 m s $^{-1}$ (STP087: 0.68 m s $^{-1}$, STP088:

0.56 m s $^{-1}$, STP089: 0.45 m s $^{-1}$, STP090: 0.65 m s $^{-1}$; averaged over the respective particle groups). This supports the notion that particles of such sizes are only weakly affected by gas drag, and indicates that they instead gained most of their speed from the initial ejection event. It further agrees well with a growing number of studies that postulate or measured initial particle velocities: Bischoff et al. (2019) observed the activity of dust-covered water ice in the lab and find that millimeter-sized particles were ejected with a nonzero initial velocity; Lemos et al. (2023, 2024) modeled particle tracks to recreate OSIRIS images of (mostly centimeter-sized) particles recorded farther out in the coma of 67P, and find that the simulated particles required an initial velocity of about 1 m s $^{-1}$ to match the observations; Shi et al. (2024) analyzed the diurnal ejection of boulder clusters from a common source region on 67P’s nucleus, and find that their median initial velocity is likely around 0.5 m s $^{-1}$; and Kwon et al. (2023) investigated the dust coma of comet C/2017 K2 and find that their models necessitate nonzero initial particle velocities to reproduce part of the observed coma structure. It therefore seems that the ejection mechanism must be considerably more energetic than a slow or gradual liftoff (see also, e.g., Yelle et al. 2004; Huebner et al. 2006; Belton 2010; Kramer & Noack 2015, 2016; Knollenberg et al. 2016; Vincent et al. 2016b; Wesolowski et al. 2020).

4.5. Dust coma simulations

To put our observations into perspective, we used an enhanced version of the water and dust coma modeling software by Marschall et al. (2020b) to simulate the particle dynamics around 67P and its diffuse coma during the time of our observations. The enhanced version of this software now also takes solar radiation pressure, centrifugal force, Coriolis force, and solar tides into account, and allows us to give particles an initial velocity normal to the shape model’s surface facet from which they are released. The initial velocities are drawn from a Maxwell-Boltzmann distribution defined via its peak value, v_{init} (which is the value we refer to as initial velocity in the following), and are assigned to all particles indiscriminately, even if the modeled gas pressure is theoretically not strong enough to lift them.

For each of the four sequences, we chose the static gas solution that best matched their respective observational conditions (see Fig. D.1). The solutions were all computed for epoch 16 of

(Continued discussion from previous double-page.) The production rate in turn dictates the initial velocity distribution (described by a “half-Maxwellian”, see Fig. 1.17) and the number density of the gas molecules. But because the comet does not consist of pure water-ice, the production rate is scaled down to match observations. The scaling factor (called effective active fraction, *eah*) is determined globally for all facets by comparing the modeled number densities to measurements made by the Rosetta Orbiter Spectrometer for Ion and Neutral Analysis (ROSINA, Balsiger et al. 2007).

The expanding gas field is then calculated with the direct simulation Monte Carlo method (DSMC, Bird 1994). This probabilistic method was developed to model rarefied gas flows, which cannot be described analytically (see Sect. 1.3.4). The DSMC implementation that is used in our model is called Ultra-fast Statistical Particle Simulation Package (ultraSPARTS), which is a commercial derivative of the PDSC++ code (Su 2013) that can simulate 3D flow fields (Marschall 2017). In our case, the simulation domain is a 10 km sphere expanding from the nucleus shape, filled with an unstructured grid of tetrahedron cells, within which the local gas and particle properties are calculated (see Fig. 7.20).

DSMC is however a very computationally expensive method, so only static gas solutions and a low temporal resolution are feasible. Marschall et al. (2020b) therefore divided Rosetta’s rendezvous phase into 20 epochs and calculated 12 different static gas solutions for each (with sub-solar longitudes ranging from 0° to 330° in steps of 30°). We use the solutions from epoch 16, which covers the time period from the 7th of December, 2015 to the 12th of January, 2016, with an *eah* of 6.84%. The dust particles are then injected into the gas flow field and their trajectories calculated according to the acting forces, under the assumption that the gas flow is not affected by the particles and that there is no particle-particle interaction.

Finally, to recreate OSIRIS images of the coma, the dust particle densities are first integrated within the pixel columns along the camera line of sight for a specific viewing geometry, and then convolved with the optical properties of the relevant particle sizes: while for particles smaller than $1\ \mu\text{m}$ we use classic Mie scattering (e. g., Hahn 2009), for larger particles, we assume that they are irregular aggregates made from sub-micrometer-sized organic grains and micrometer-sized silicate grains (Marschall et al. 2020b), and model their scattering properties via the radiative transfer with reciprocal transactions method (R^2T^2 , Markkanen et al. 2018a; Markkanen et al. 2018b; Muinonen et al. 2018).

Notably, using another derivative of Marschall’s modeling software, Pinzón-Rodríguez et al. (2021) simulated the coupled sublimation of water- and CO_2 -ice of a spherical comet, and showed that even low thermal inertia values and the presence of CO_2 -ice sublimation can substantially affect the gas flow field of comets (although regarding mostly the night-side activity in case of CO_2 -ice sublimation). Still, such a model is much more computationally expensive, and while our modeling results already match the observations rather well, the need for CO_2 -ice sublimation as a means to explain the observed activity fits well with our main (data-driven) conclusions (see also Bischoff et al. 2023).

Marschall et al. (2020b), which covers the time period from Dec. 7, 2015 to Jan. 12, 2016, when 67P was roughly 1.98 AU from the Sun at a sub-solar latitude of -18.2° (which is right at the center of the sequences' latitude value range, see Table 2). The solution setups only differ in sub-solar longitude, where we used 150° for sequence STP087, 210° for sequences STP088 and STP089, and 240° for sequence STP090. All three values almost exactly coincide with the centers of the covered sub-solar latitude value ranges of the respective sequences (see Table 2).

Based on these three gas solutions, we then simulated nine different scenarios for each of our sequences. The scenarios are defined by every combination of three different initial velocities (0, 0.25, and 0.5 m s^{-1}) and three different activity distributions: only local (i.e., Khonsu, Atum, and Anubis), global, and nonlocal (i.e., global without local activity). For each of these runs, we simulated spherical particles in 17 different size bins distributed logarithmically over a radius range from 10^{-8} to 1 m, where each particle has the same bulk density as the nucleus (533 kg m^{-3} , Pätzold et al. 2016). To reduce computation time however, we only allowed for one particle to be emitted per model facet and size regime⁶.

Figures D.2–D.5 show the results from the particle trajectory simulations for particle sizes similar to those we obtained from the OSIRIS data. For each sequence, initial velocity, and size bin, we randomly selected (up to) 150 simulated particles that were ejected from within the suspected source regions, and projected their trajectories onto the 2D planes of the corresponding OSIRIS/NAC FOVs (via SpiceyPy, a Python wrapper for SPICE, Annex et al. 2020). The trajectories start with the beginning of each sequence (the nucleus shapes in their initial configurations are shown for reference), and unless they leave the FOV, they represent the particle motions over a time period of up to 2 h. The simulated particles however do not (and are not intended to) retrace our observations. We merely use these simulated particle ensembles to compare them to our observations regarding their general appearance and statistical properties.

According to Figs. D.2–D.5, the initial velocities are essential for reproducing our observed particle tracks (cf. Fig. 4). Of the tested values, $v_{\text{init}} = 0.5 \text{ m s}^{-1}$ provides the best results for all sequences, which is remarkably similar to the average value we derived from the OSIRIS data (0.59 m s^{-1}). In the case of our model, the initial velocities are also not only necessary for ejecting decimeter-sized particles at all, but also for recreating the observed ejection cones. This indicates that besides the particle speed, the shape of the ejection cones may most notably be affected by the local topography. Without the initial velocity, the simulated trajectories of the larger particles appear to “bend” predominantly in either the clockwise or counterclockwise direction, an effect caused by the viewing geometry and the rotation of the nucleus. Yet when particles are ejected with enough speed from surface areas that face in the opposite direction, their trajectories also appear to bend the other way. In the case of sequence STP090 however, even an initial velocity of 0.5 m s^{-1} is not enough to reproduce the almost symmetric shape of the observed ejection cone (cf. Figs. 4 and D.5).

Despite the initial velocities however, the overall projected (radial) accelerations and velocities of the simulated particles

⁶ Because of this, especially for flat particle SFDs, the simulations of the diffuse coma appear a bit patchy (Figs. D.7–D.14), since the software has to interpolate the column densities from sparse data. With large amounts of simulated particles, the patchiness disappears. For the same reason, the coma maps of the drag coefficients in Fig. D.1 show some artifacts where not enough particles passed through the affected cells.

are still lower than what we measured for the real particles (cf. Figs. 12, 13, and D.6). This indicates that even higher initial velocities, locally higher gas production rates (especially of CO_2 , which was not included in the simulations), or lower particle bulk densities (as discussed in Sect. 4.4), may be necessary to reproduce our observations. We also did not model rocket forces, which might have a noticeable effect.

We additionally used the same simulated data from which we recovered the individual trajectories to generate images of the diffuse dust coma as it appeared in the first image of each sequence (cf. Figs. 2 and A.1). In this case, particles from every simulated size bin in the range from 10^{-8} to 1 m contributed. Generally, we find that the simulated images fit our observations well (but because we ran 36 different simulations, we do not present all the results here). As an example, Figs. D.7–D.10 show the dust coma simulations of sequence STP090 for all three activity distributions (local, nonlocal, and global), given $v_{\text{init}} = 0.5 \text{ m s}^{-1}$. The first three of these figures primarily illustrate how the coma simulations are affected by different particle SFDs, which are modeled according to a power law (see, e.g., Eq. (3) and the discussion in Sect. 4.2). By visually comparing the diffuse coma structures in these images to those recorded in the OSIRIS images, we find that power-law indices between 3 and 3.5 best reproduce our observations, across all sequences. This agrees well with the value range that we derived for our real, decimeter-sized particles (3.4 ± 0.3 – 3.8 ± 0.4 , see Sect. 4.2), suggesting that a single power-law exponent can describe the SFD of both small and large particles.

By comparing the results from the three different activity distributions across all sequences, we also find further evidence that the locations of our suspected source regions are likely correct. For one, images with only local activity show strong dust features above the suspected source regions similar to our observations. Secondly, images with nonlocal activity show that the space above the suspected source regions is only significantly “contaminated” by dust features from other areas in the cases where the particle SFDs are steep. Because the corresponding particles are much smaller and faster than the particles that we observed however, their contamination is irrelevant. In the relevant particle size range, only relatively weak dust features from other areas appear above the suspected source regions (see Fig. D.10). Still, in the case of sequence STP090, such contamination might at least in part explain the missing left side of the simulated ejection cone (cf. Figs. 4 and D.5), by creating an optical illusion akin to the jet-like features described by Shi et al. (2018). Another reason might be that our gas solutions are static and do not follow the rotation of the nucleus. Depending on the viewing geometry and on how strongly the particles couple with the gas, this could also noticeably affect the projected trajectories.

Like the trajectory simulations, the coma simulations also match our observations best when the initial velocity is highest, as demonstrated by Figs. D.11–D.14 (for the case of sequence STP087). Clearly, the initial velocity strongly affects the features generated by the largest particles, which seem to make up an essential part of the simulated diffuse coma. The figures also show that different surface regions require different particle SFDs to best reproduce the observed dust features. In the case of sequence STP087 for example, the features near the suspected source region that radiate toward the top right corner are well described by a power-law index $b \approx 3$, while the features on the opposite side that radiate toward the top left corner are better described by a power-law index of at least 3.5.

Finally, Fig. D.14 shows that our model failed to reproduce the strong diffuse coma features seen in the lower right corner

of the first image of sequence STP087 (cf. Fig. 2). These features may have resulted from night-time activity driven by water ice sublimation and sustained by thermal lag, akin to the sunset jets discussed by Shi et al. (2016), or possibly even from CO₂ ice sublimation (Gerig et al. 2018, 2020; Pinzón-Rodríguez et al. 2021).

5. Summary and conclusions

We analyzed the dynamics and potential origins of 409 decimeter-sized dust particles that were recorded in four OSIRIS/NAC image sequences of 67P's near-nucleus dust coma between December 16, 2015, and January 6, 2016 (post-perihelion). After tracking thousands of individual dust particles through these sequences, we identified four concentrated groups of recently ejected particles and traced them back to four suspected source regions on the nucleus surface. This allowed us not only to examine their potential origins, but also to derive their approximate sizes, speeds, and accelerations. Finally, we compared our observations and results to simulations of 67P's dust coma for further evaluation.

Although we were limited to tracking particles only in the 2D image plane and not in the full 3D environment, our data analysis provides much evidence that the general locations of the suspected source regions are likely correct:

- (i) The particle trajectories form distinct ejection cones that taper toward the centers of the suspected source regions.
- (ii) Even though the suspected source regions were chosen independently from one another, they turned out to be rather well confined and to strongly overlap.
- (iii) The suspected source regions contain (or are near) areas where global activity models estimate high surface erosion and gas emission rates (Combi et al. 2020; Läuter et al. 2022).
- (iv) In particular, the suspected source regions derived from image sequences STP087 and STP089 largely coincide with an area in the Khonsu region for which a lot of activity and surface changes have been documented (e.g., Deshapriya et al. 2016; Hasselmann et al. 2019).
- (v) Unlike other areas, the suspected source regions were continuously well illuminated during the observational periods and the roughly 4 h in local time leading up to them.
- (vi) Trajectory simulations of particles released from the suspected source regions generally reproduce the observed particle tracks well.
- (vii) Comparisons between different simulations of the diffuse dust coma (local vs. nonlocal) show that most of the simulated dust features above the suspected source regions come from local activity.

Throughout this paper, we drew several conclusions regarding the nature of the observed activity:

- (i) Instead of homogeneous activity, the ejection of large particles ($\gtrsim 1$ cm) can occur distinctly localized.
- (ii) The concentrated ejection of large particles does not necessarily correlate (in strength, location, or orientation) with that of small particles ($\lesssim 1$ cm) that make up the diffuse coma. This may be evidence that water-driven erosion and CO₂-driven ejection of large chunks cannot happen simultaneously at the same location.
- (iii) The suspected source regions of the particles that we traced back to the nucleus surface predominantly lie in the Khonsu-Atum-Anubis area, and the observed activity may be linked to rugged terrain or steep slopes like scarps, cliffs, or fractures.

- (iv) The studied particles range in size from about 5 cm to 1.15 m in (equivalent) radius. Power-law fits to their SFDs best describe the data with power-law indices between 3.4 ± 0.3 and 3.8 ± 0.4 . This indicates that shortly after ejection, most of the mass is still contained in the larger particles, although ultimately most of them likely did not escape the nucleus gravity. The index values also agree notably well with those obtained for submillimeter-sized particles (3.7 and 3.1 ± 0.5 , Fulle et al. 2016; Merouane et al. 2016), and might reflect an SFD transition of the surface material located in the suspected source regions (Deshapriya et al. 2016; Hasselmann et al. 2019).
- (v) Solar irradiation alone cannot explain the locality of the observed activity. Additionally, surface accelerations in the suspected source regions are relatively high, ruling out gravity and centrifugal forces as decisive factors as well.
- (vi) The projected radial particle velocities directly provide upper limit estimates for the particle fall-back fractions, which lie between 75 and 91%. The data indicate that essentially all particles larger than 40 cm likely fell back onto the nucleus surface.
- (vii) The distributions of the projected radial particle accelerations as functions of the particle radii are well described by the local surface acceleration (lower bound) and gas drag (upper bound). The gas drag parameters, however, are degenerate and cannot be precisely constrained. Values from our water and dust coma simulations nevertheless indicate that the local gas production rate was likely several times higher ($Q_g = 3.6 \times 10^{-5} \text{ kg s}^{-1} \text{ m}^{-2}$) than the prediction by our purely insolation-driven model and the peak average production rates estimated by Läuter et al. (2022).
- (viii) Some particles exhibit downward accelerations that are much stronger than the local surface accelerations. Most of these outliers are likely caused by inaccurate measurements and statistical effects, but their general trend might also be a sign of asymmetric outgassing.
- (ix) Rough estimates of the initial particle velocities are distinctly nonzero and average around 0.59 m s^{-1} , which indicates that the particles likely gained most of their speed from the initial ejection event.
- (x) Our dynamics simulations of decimeter-sized particles in the coma of 67P support the need for higher local activity to reproduce the observed trajectories. Simulated particles larger than ≈ 32 cm could not be lifted from the suspected source regions without introducing initial velocities in addition to gas drag. Even with an initial velocity of $\approx 0.5 \text{ m s}^{-1}$ the simulated particles were generally still slower than those we observed.
- (xi) The inclusion of initial velocities also shows that they are necessary for reproducing the observed ejection cones, which indicates that the local topography plays an important role in shaping these cones.
- (xii) Both, the simulated dynamics of individual particles, and the simulated images of the diffuse dust coma, match the observations best when the initial velocity is the highest ($\approx 0.5 \text{ m s}^{-1}$). This is further evidence that initial velocities are an essential aspect of the ejection process.
- (xiii) The simulated images additionally reproduce our observations best given particle SFDs described by power laws with indices equal to 3 or 3.5. This agrees well with the value range that we obtained from our real particle populations, but we also found that some dust features require different size distributions to be well reproduced.

Because it is currently not possible to include pdf pages with working hyperlinks in a \LaTeX -document, as with the methods paper, I manually added all hyperlinks back into the science paper (except for those found in the bibliography here). Citations within the digital version of this paper therefore redirect to the bibliography at the end of the dissertation.

Pfeifer, M., et al.: A&A, 685, A136 (2024)

Overall, our observational and modeling results strongly suggest that the concentrated local ejection of decimeter-sized particles cannot be explained with water-driven activity and favorable illumination conditions alone. Instead, the composition and structure of the suspected source regions seem to be the deciding factors; of these, we deem an overabundance of volatiles, in particular of CO₂ ice, to be the most probable cause. This is in line with current particle ejection models (e.g., Gundlach et al. 2020; Fulle et al. 2020; Wesolowski et al. 2020; Ciarniello et al. 2022; Davidsson et al. 2022), which necessitate the sublimation of CO₂ ice in deeper surface layers to eject decimeter-sized particles. Additionally, our results show that decimeter-sized particles are very likely ejected with substantial nonzero initial velocities, which agrees well with other recent studies (e.g., Bischoff et al. 2019; Lemos et al. 2023, 2024; Kwon et al. 2023; Shi et al. 2024), and implies that the ejection mechanism must be considerably more energetic than a slow or gradual liftoff.

Acknowledgements. We thank the anonymous referee for their valuable feedback; Xian Shi, Nicholas Attree, Yuri Skorov, Marco Fulle, and Asmus Freitag for (proof)reading our manuscript and providing helpful comments; Miryam Merk, for statistical consulting; Sonia Fornasier, Matthias L auter, and Tobias Kramer for providing their data; Aaron Clauset for discussing the intricacies of power-law fitting with us; and Pedro Hasselmann, Maurizio Pajola, Mohamed Ramy El-Maarry, Nicolas Thomas, Frank Preusker, Michael Combi, Koji Wada, Jean-Baptiste Vincent, Johannes Markkanen, and Giovanna Rinaldi for providing tools and discussing certain aspects of our paper. We acknowledge the operation and calibration team at MPS and the Principal Investigator Holger Sierks on behalf of the OSIRIS Team for providing the OSIRIS images and related data sets. OSIRIS was built by a consortium of the Max-Planck-Institut f ur Sonnensystemforschung, G ttingen, Germany; the CISAS University of Padova, Italy; the Laboratoire d'Astrophysique de Marseille, France; the Instituto de Astrof sica de Andaluc a, CSIC, Granada, Spain; the Research and Scientific Support Department of the European Space Agency, Noordwijk, The Netherlands; the Instituto Nacional de T cnica Aeroespacial, Madrid, Spain; the Universidad Polit cnica de Madrid, Spain; the Department of Physics and Astronomy of Uppsala University, Sweden; and the Institut f ur Datentechnik und Kommunikationsnetze der Technischen Universit t Braunschweig, Germany. The support of the national funding agencies of Germany (DLR), France (CNES), Italy (ASI), Spain (MEC), Sweden (SNSB), and the ESA Technical Directorate is gratefully acknowledged. We thank the Rosetta Science Ground Segment at ESAC, the Rosetta Missions Operations Centre at ESOC and the Rosetta Project at ESTEC for their outstanding work enabling the science return of the Rosetta Mission. M.P., J.A., and P.L. acknowledge funding by the ERC Starting Grant No. 757390 Comet and Asteroid Re-Shaping through Activity (CAstRA). J.A. acknowledges funding by the Volkswagen Foundation. M.P. and P.L. conducted the work in this paper in the framework of the International Max-Planck Research School (IMPRS) for Solar System Science at the University of G ttingen.

References

Acton, C. H. 1996, *Planet. Space Sci.*, **44**, 65
 Agarwal, J., M uller, M., Reach, W. T., et al. 2010, *Icarus*, **207**, 992
 Agarwal, J., A'Hearn, M. F., Vincent, J.-B., et al. 2016, *MNRAS*, **462**, S78
 Agarwal, J., Della Corte, V., Feldman, P. D., et al. 2017, *MNRAS*, **469**, s606
 Agarwal, J., Kim, Y., Kelley, M. S. P., & Marschall, R. 2023, arXiv e-prints [arXiv:2309.12759]
 Alstott, J., Bullmore, E., & Plenz, D. 2014, *PLOS ONE*, **9**, e85777
 Annex, A. M., Pearson, B., Seignovert, B., et al. 2020, *J. Open Source Softw.*, **5**, 2050
 Arakawa, M., Wada, K., Saiki, T., et al. 2017, *Space Sci. Rev.*, **208**, 187
 Arakawa, M., Saiki, T., Wada, K., et al. 2020, *Science*, **368**, 67
 Attree, N., Groussin, O., Jorda, L., et al. 2018a, *A&A*, **611**, A33
 Attree, N., Groussin, O., Jorda, L., et al. 2018b, *A&A*, **610**, A76
 Auger, A.-T., Groussin, O., Jorda, L., et al. 2015, *A&A*, **583**, A35
 A'Hearn, M. F., Belton, M. J. S., Delamere, W. A., et al. 2011, *Science*, **332**, 1396
 Barbary, K. 2016, *J. Open Source Softw.*, **1**, 58
 Belton, M. J. S. 2010, *Icarus*, **210**, 881
 Bertin, E., & Arnouts, S. 1996, *A&ASS*, **117**, 393
 Bird, G. A. 1994, *Molecular Gas Dynamics And The Direct Simulation Of Gas Flows* (Oxford: Clarendon Press)

Bischoff, D., Gundlach, B., Neuhaus, M., & Blum, J. 2019, *MNRAS*, **483**, 1202
 Bischoff, D., Schuckart, C., Attree, N., Gundlach, B., & Blum, J. 2023, *MNRAS*, **523**, 5171
 Blum, J., Gundlach, B., Krause, M., et al. 2017, *MNRAS*, **469**, S755
 Blum, J., Bischoff, D., & Gundlach, B. 2022, *Universe*, **8**, 381
 Brown, W. K. 1989, *J. Astrophys. Astron.*, **10**, 89
 Cambianica, P., Cremonese, G., Naletto, G., et al. 2019, *A&A*, **630**, A15
 Cambianica, P., Fulle, M., Cremonese, G., et al. 2020, *A&A*, **636**, A91
 Chesley, S. R., French, A. S., Davis, A. B., et al. 2020, *J. Geophys. Res.: Planets*, **125**
 Choukroun, M., Altwegg, K., K uhr, E., et al. 2020, *Space Sci. Rev.*, **216**, 44
 Ciarniello, M., Fulle, M., Raponi, A., et al. 2022, *Nat. Astron.*, **6**, 546
 Cigala, V., Kueppers, U., Pe a Fern andez, J. J., et al. 2017, *J. Geophys. Res.: Solid Earth*, **122**, 6031
 Cigala, V., Kueppers, U., Fern andez, J. J. P., & Dingwell, D. B. 2021, *Bull. Volcanol.*, **83**, 53
 Clark, B. C., Green, S. F., Economou, T. E., et al. 2004, *J. Geophys. Res.: Planets*, **109**, E12S03
 Clauset, A., Shalizi, C. R., & Newman, M. E. J. 2009, *SIAM Rev.*, **51**, 661
 Combi, M., Shou, Y., Fougere, N., et al. 2020, *Icarus*, **335**, 113421
 Crifo, J. F., Itkin, A. L., & Rodionov, A. V. 1995, *Icarus*, **116**, 77
 Crifo, J. F., Loukianov, G. A., Rodionov, A. V., & Zakharov, V. V. 2005, *Icarus*, **176**, 192
 Davidsson, B. J. R., Sierks, H., G ttler, C., et al. 2016, *A&A*, **592**, A63
 Davidsson, B. J. R., Birch, S., Blake, G. A., et al. 2021, *Icarus*, **354**, 114004
 Davidsson, B. J. R., Schloerb, F. P., Fornasier, S., et al. 2022, *MNRAS*, **516**, 6009
 Deshapriya, J. D. P., Barucci, M. A., Fornasier, S., et al. 2016, *MNRAS*, **462**, S274
 Deshapriya, J. D. P., Barucci, M. A., Fornasier, S., et al. 2018, *A&A*, **613**, A36
 Dohnanyi, J. S. 1969, *J. Geophys. Res.*, **74**, 2531
 El-Maarry, M. R., Thomas, N., Giacomini, L., et al. 2015, *A&A*, **583**, A26
 El-Maarry, M. R., Thomas, N., Gracia-Bern a, A., et al. 2016, *A&A*, **593**, A110
 El-Maarry, M. R., Groussin, O., Thomas, N., et al. 2017a, *Science*, **355**, 1392
 El-Maarry, M. R., Thomas, N., Gracia-Bern a, A., et al. 2017b, *A&A*, **598**, C2
 ESA SPICE Service 2020, Rosetta Operational SPICE Kernel Dataset, <https://doi.org/10.5270/esa-tyidsbu>
 Ezekiel, M. 1930, *Methods Of Correlation Analysis* (John Wiley & Sons Inc)
 Fagents, S. A., Lopes, R. M. C., Quick, L. C., & Gregg, T. K. P. 2022, in *Comparative Planetology*, 1, Planetary Volcanism across the Solar System, eds. T. K. P. Gregg, R. M. C. Lopes, & S. A. Fagents (Elsevier), 161
 Fahrmeir, L., Kneib, T., Lang, S., & Marx, B. D. 2021, *Regression: Models, Methods and Applications* (Springer)
 Feller, W. 1948, *Ann. Math. Stat.*, **19**, 177
 Ferrari, S., Penasa, L., La Forgia, F., et al. 2018, *MNRAS*, **479**, 1555
 Finson, M. L., & Probst, R. F. 1968a, *ApJ*, **154**, 327
 Finson, M. L., & Probst, R. F. 1968b, *ApJ*, **154**, 353
 Fornasier, S., Mottola, S., Keller, H. U., et al. 2016, *Science*, **354**, 1566
 Fornasier, S., Feller, C., Lee, J.-C., et al. 2017, *MNRAS*, **469**, S93
 Fornasier, S., Hoang, V. H., Hasselmann, P. H., et al. 2019, *A&A*, **630**, A7
 Fornasier, S., Hoang, H. V., Fulle, M., Quirico, E., & Ciarniello, M. 2023, *A&A*, **672**, A136
 Fowler, A. C., & Scheu, B. 2016, *Proc. Roy. Soc. A: Math. Phys. Eng. Sci.*, **472**, 20150843
 Frattin, E., Bertini, I., Ivanovski, S. L., et al. 2021, *MNRAS*, **504**, 4687
 Fulle, M. 1989, *A&A*, **217**, 283
 Fulle, M., Colangeli, L., Agarwal, J., et al. 2010, *A&A*, **522**, A63
 Fulle, M., Marzari, F., Corte, V. D., et al. 2016, *ApJ*, **821**, 19
 Fulle, M., Blum, J., Rotundi, A., et al. 2020, *MNRAS*, **493**, 4039
 Gerig, S.-B., Marschall, R., Thomas, N., et al. 2018, *Icarus*, **311**, 1
 Gerig, S.-B., Pinz n-Rodr guez, O., Marschall, R., Wu, J.-S., & Thomas, N. 2020, *Icarus*, **351**, 113968
 Giacomini, L., Massironi, M., El-Maarry, M. R., et al. 2016, *MNRAS*, **462**, S352
 Grieger, B. 2019, *A&A*, **630**, A1
 Groussin, O., Jorda, L., Auger, A.-T., et al. 2015, *A&A*, **583**, A32
 Gundlach, B., Blum, J., Keller, H. U., & Skorov, Y. V. 2015, *A&A*, **583**, A12
 Gundlach, B., Fulle, M., & Blum, J. 2020, *MNRAS*, **493**, 3690
 G ttler, C., Hasselmann, P. H., Li, Y., et al. 2017, *MNRAS*, **469**, S312
 G ttler, C., Mannel, T., Rotundi, A., et al. 2019, *A&A*, **630**, A24
 Hartmann, W. K. 1969, *Icarus*, **10**, 201
 Hasselmann, P. H., Barucci, M. A., Fornasier, S., et al. 2019, *A&A*, **630**, A8
 Hilchenbach, M., Kissel, J., Langevin, Y., et al. 2016, *ApJ*, **816**, L32
 H fner, S., Vincent, J.-B., Blum, J., et al. 2017, *A&A*, **608**, A121
 Huebner, W. F., Benkhoff, J., Capria, M.-T., et al. 2006, *Heat And Gas Diffusion in Comet Nuclei* (International Space Science Institute)
 Ishiguro, M. 2008, *Icarus*, **193**, 96
 Ivanovski, S., Zakharov, V., Della Corte, V., et al. 2017a, *Icarus*, **282**, 333
 Ivanovski, S. L., Della Corte, V., Rotundi, A., et al. 2017b, *MNRAS*, **469**, S774
 Jiang, Y., & Schmidt, J. 2020, *Heliyon*, **6**, e05275

Pfeifer, M., et al.: A&A, 685, A136 (2024)

- Jorda, L., Gaskell, R., Capanna, C., et al. 2016, *Icarus*, 277, 257
- Keller, H. U., Delamere, W. A., Reitsema, H. J., Huebner, W. F., & Schmidt, H. U. 1987, *A&A*, 187, 807
- Keller, H. U., Barbieri, C., Lamy, P., et al. 2007, *Space Sci. Rev.*, 128, 433
- Keller, H. U., Mottola, S., Davidsson, B., et al. 2015, *A&A*, 583, A34
- Keller, H. U., Mottola, S., Hviid, S. F., et al. 2017, *MNRAS*, 469, S357
- Kelley, M. S., Reach, W. T., & Lien, D. J. 2008, *Icarus*, 193, 572
- Kelley, M. S., Wooden, D. H., Tubiana, C., et al. 2009, *AJ*, 137, 4633
- Kelley, M. S., Lindler, D. J., Bodewits, D., et al. 2013, *Icarus*, 222, 634
- Kelley, M. S. P., Lindler, D. J., Bodewits, D., et al. 2015, *Icarus*, 262, 187
- Klaus, A., Yu, S., & Plenz, D. 2011, *PLOS ONE*, 6, e19779
- Knollenberg, J., Lin, Z. Y., Hviid, S. F., et al. 2016, *A&A*, 596, A89
- Kramer, T., & Noack, M. 2015, *ApJ*, 813, L33
- Kramer, T., & Noack, M. 2016, *ApJ*, 823, L11
- Kwon, Y. G., Opitom, C., & Lippi, M. 2023, *A&A*, 674, A206
- La Forgia, F., Giacomini, L., Lazzarin, M., et al. 2015, *A&A*, 583, A41
- Lai, I.-L., Ip, W.-H., Su, C.-C., et al. 2016, *MNRAS*, 462, S533
- Lai, I.-L., Ip, W.-H., Lee, J.-C., et al. 2019, *A&A*, 630, A17
- Läuter, M., Kramer, T., Rubin, M., & Altwegg, K. 2019, *MNRAS*, 483, 852
- Läuter, M., Kramer, T., Rubin, M., & Altwegg, K. 2020, *MNRAS*, 498, 3995
- Läuter, M., Kramer, T., Rubin, M., & Altwegg, K. 2022, *ACS Earth Space Chem.*, 6, 1189
- Lee, J.-C., Massironi, M., Ip, W.-H., et al. 2016, *MNRAS*, 462, S573
- Lemos, P., Agarwal, J., & Schröter, M. 2023, *MNRAS*, 519, 5775
- Lemos, P., Agarwal, J., Marschall, R., & Pfeifer, M. 2024, *A&A*, submitted
- Leon-Dasi, M., Besse, S., Grieger, B., & Küppers, M. 2021, *A&A*, 652, A52
- Lin, Z.-Y., Knollenberg, J., Vincent, J.-B., et al. 2017, *MNRAS*, 469, S731
- Liu, X., Sachse, M., Spahn, F., & Schmidt, J. 2016, *J. Geophys. Res.: Planets*, 121, 1141
- Lucchetti, A., Cremonese, G., Jorda, L., et al. 2016, *A&A*, 585, L1
- Lucchetti, A., Pajola, M., Fornasier, S., et al. 2017, *MNRAS*, 469, S238
- Mandelbrot, B. B. 1982, *The Fractal Geometry of Nature* (San Francisco : W.H. Freeman)
- Markkanen, J., & Agarwal, J. 2020, *A&A*, 643, A16
- Markkanen, J., Agarwal, J., Väisänen, T., Penttilä, A., & Muinonen, K. 2018, *ApJ*, 868, L16
- Marschall, R., Su, C. C., Liao, Y., et al. 2016, *A&A*, 589, A90
- Marschall, R., Mottola, S., Su, C. C., et al. 2017, *A&A*, 605, A112
- Marschall, R., Rezac, L., Kappel, D., et al. 2019, *Icarus*, 328, 104
- Marschall, R., Liao, Y., Thomas, N., & Wu, J.-S. 2020a, *Icarus*, 346, 113742
- Marschall, R., Markkanen, J., Gerig, S.-B., et al. 2020b, *Front. Phys.*, 8, 227
- Marschall, R., Skorov, Y., Zakharov, V., et al. 2020c, *Space Sci. Rev.*, 216, 130
- Marschall, R., Davidsson, B. J. R., Rubin, M., & Tennishev, V. 2023, arXiv e-prints [arXiv:2308.05797]
- Merouane, S., Zaprudin, B., Stenzel, O., et al. 2016, *A&A*, 596, A87
- Merouane, S., Stenzel, O., Hilchenbach, M., et al. 2017, *MNRAS*, 469, S459
- Moreno, F., Guirado, D., Muñoz, O., et al. 2022, *MNRAS*, 510, 5142
- Mottola, S., Arnold, G., Grothues, H.-G., et al. 2015, *Science*, 349, aab0232
- Muniruzzaman, A. N. M. 1957, *Calcutta Stat. Assoc. Bull.*, 7, 115
- Oklay, N., Sunshine, J. M., Pajola, M., et al. 2016, *MNRAS*, 462, S394
- Oklay, N., Mottola, S., Vincent, J.-B., et al. 2017, *MNRAS*, 469, S582
- Opik, E. J. 1936, *Publications of the Tartu Astrofizika Observatory*, 28, 1
- Ott, T., Drolshagen, E., Koschny, D., et al. 2017, *MNRAS*, 469, S276
- Pajola, M., Vincent, J.-B., Güttler, C., et al. 2015, *A&A*, 583, A37
- Pajola, M., Lucchetti, A., Vincent, J.-B., et al. 2016a, *A&A*, 592, A2
- Pajola, M., Mottola, S., Hamm, M., et al. 2016b, *MNRAS*, 462, S242
- Pajola, M., Oklay, N., Forgia, F. L., et al. 2016c, *A&A*, 592, A69
- Pajola, M., Höfner, S., Vincent, J. B., et al. 2017a, *Nat. Astron.*, 1, 0092
- Pajola, M., Lucchetti, A., Fulle, M., et al. 2017b, *MNRAS*, 469, S636
- Pajola, M., Lee, J.-C., Oklay, N., et al. 2019, *MNRAS*, 485, 2139
- Pätzold, M., Andert, T., Hahn, M., et al. 2016, *Nature*, 530, 63
- Pfeifer, M., Agarwal, J., & Schröter, M. 2022, *A&A*, 659, A171
- Pinzón-Rodríguez, O., Marschall, R., Gerig, S.-B., et al. 2021, *A&A*, 655, A20
- Pommerol, A., Thomas, N., El-Maarry, M. R., et al. 2015, *A&A*, 583, A25
- Poulet, F., Lucchetti, A., Bibring, J.-P., et al. 2016, *MNRAS*, 462, S23
- Quick, L. C., Barnouin, O. S., Prockter, L. M., & Patterson, G. W. 2013, *Planet. Space Sci.*, 86, 1
- Reshetnyk, V. M., Skorov, Y. V., Lacerda, P., Hartogh, P., & Rezac, L. 2018, *Solar Syst. Res.*, 52, 266
- Reshetnyk, V., Skorov, Y., Vasyuta, M., et al. 2021, *Solar Syst. Res.*, 55, 106
- Reshetnyk, V., Skorov, Y., Bentley, M., et al. 2022, *Solar Syst. Res.*, 56, 100
- Rinaldi, G., Della Corte, V., Fulle, M., et al. 2017, *MNRAS*, 469, S598
- Rodionov, A. V., Crifo, J. F., Szegő, K., Lagerros, J., & Fulle, M. 2002, *Planet. Space Sci.*, 50, 983
- Rotundi, A., Sierks, H., Della Corte, V., et al. 2015, *Science*, 347, aaa3905
- Sanchidrián, J. A., Ouchterlony, F., Segarra, P., & Moser, P. 2014, *Int. J. Rock Mech. Mining Sci.*, 71, 381
- Schmid, M., Kueppers, U., Cigala, V., Sesterhenn, J., & Dingwell, D. B. 2020, *Bull. Volcanol.*, 82, 68
- Shi, X., Hu, X., Sierks, H., et al. 2016, *A&A*, 586, A7
- Shi, X., Hu, X., Mottola, S., et al. 2018, *Nat. Astron.*, 2, 562
- Shi, X., Hu, X., Rose, M., et al. 2019, in *EPSC Abstracts*, 13, 2
- Shi, X., Hu, X., Agarwal, J., et al. 2024, *ApJ*, 961, L16
- Sierks, H., Barbieri, C., Lamy, P. L., et al. 2015, *Science*, 347, aaa1044
- Skorov, Y., Reshetnyk, V., Lacerda, P., Hartogh, P., & Blum, J. 2016, *MNRAS*, 461, 3410
- Skorov, Y. V., Rezac, L., Hartogh, P., & Keller, H. U. 2017, *A&A*, 600, A142
- Skorov, Y., Reshetnyk, V., Rezac, L., et al. 2018, *MNRAS*, 477, 4896
- Skorov, Y., Reshetnyk, V., Bentley, M., et al. 2021, *MNRAS*, 501, 2635
- Skorov, Y., Reshetnyk, V., Bentley, M. S., et al. 2022a, *MNRAS*, 510, 5520
- Skorov, Y., Reshetnyk, V., Küppers, M., et al. 2022b, *MNRAS*, 519, 59
- Skorov, Y., Markkanen, J., Reshetnyk, V., et al. 2023, *MNRAS*, 522, 4781
- Snodgrass, C., Fitzsimmons, A., Lowry, S. C., & Weissman, P. 2011, *MNRAS*, 414, 458
- Soja, R. H., Sommer, M., Herzog, J., et al. 2015, *A&A*, 583, A18
- Tang, Y., Birch, S. P. D., Hayes, A. G., de Freitas Bart, R., & Squyres, S. W. 2017, in *48th Annual Lunar and Planetary Science Conference*, 2796
- Taylor, M. G. G. T., Altobelli, N., Buratti, B. J., & Choukroun, M. 2017, *Philos. Trans. Roy. Soc. A: Math. Phys. Eng. Sci.*, 375, 20160262
- Thomas, N., Davidsson, B., El-Maarry, M. R., et al. 2015a, *A&A*, 583, A17
- Thomas, N., Sierks, H., Barbieri, C., et al. 2015b, *Science*, 347, aaa0440
- Thomas, N., El Maarry, M. R., Theologou, P., et al. 2018, *Planet. Space Sci.*, 164, 19
- Tsunematsu, K., Ishimine, Y., Kaneko, T., et al. 2016, *Earth Planets Space*, 68, 88
- Tubiana, C., Güttler, C., Kovacs, G., et al. 2015, *A&A*, 583, A46
- Turcotte, D. L. 1986, *J. Geophys. Res.: Solid Earth*, 91, 1921
- Vincent, J.-B., Bodewits, D., Besse, S., et al. 2015, *Nature*, 523, 63
- Vincent, J.-B., A'Hearn, M. F., Lin, Z.-Y., et al. 2016a, *MNRAS*, 462, S184
- Vincent, J.-B., Oklay, N., Pajola, M., et al. 2016b, *A&A*, 587, A14
- Virkar, Y., & Clauset, A. 2014, *Ann. Appl. Stat.*, 8, 89
- Wada, K., Ishibashi, K., Kimura, H., et al. 2021, *A&A*, 647, A43
- Wallis, M. K., & Chandra Wickramasinghe, N. 1992, *Adv. Space Res.*, 12, 133
- Weissman, P., Morbidelli, A., Davidsson, B., & Blum, J. 2020, *Space Sci. Rev.*, 216, 6
- Wesołowski, M., Gronkowski, P., & Tralle, I. 2020, *Icarus*, 338, 113546
- Yelle, R. V., Soderblom, L. A., & Jokipii, J. R. 2004, *Icarus*, 167, 30
- Zakharov, V. V., Rodionov, A. V., Lukianov, G. A., & Crifo, J. F. 2009, *Icarus*, 201, 358
- Zakharov, A. V., Popel, S. I., Kuznetsov, I. A., et al. 2022, *Phys. Plasmas*, 29, 110501

Appendix A: Sample images from sequences STP089 and STP090

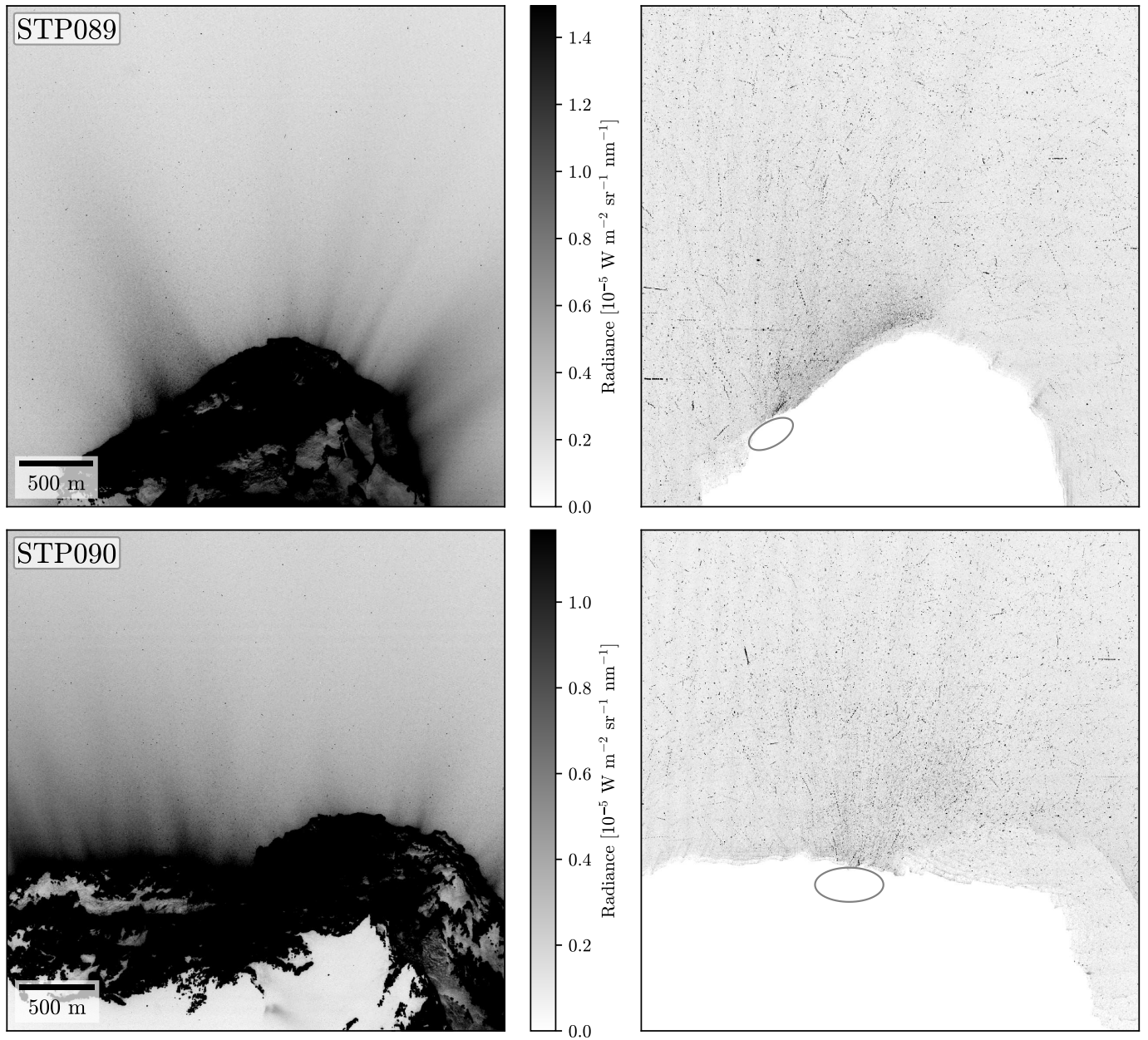


Fig. A.1. Sample images from sequences STP089 and STP090. The first images of the respective sequences are on the left, the master images on the right. The ellipses in the master images mark the suspected source regions of the concentrated particle groups. All images are brightness-inverted and had their contrasts improved for better readability (continuation of Fig. 2).

Appendix B: Reasons for rejection of image sequences

In the following, we list the reasons why we excluded other OSIRIS image sequences from our analysis (roughly from most to least critical):

- An incomplete pair of subsequences (i.e., only one exists) or an insufficient number of images (many subsequences consist of less than twenty images). If the covered time period is long, subsequent particle detections can lie far apart, which makes particle tracking very difficult, especially if there is no “stem” of detections linked over a short interval (cf. Fig. 1), that provides accurate predictions. Conversely, if the covered time period is short, the derived particle dynamics can be unreliable because the tracks do not evolve enough for fits to be resistant against smaller deviations like pointing fluctuations or the inclusion of unrelated detections.
- Binning, which severely hampers particle detection.
- A lack of sidereal objects, which are needed to correct for pointing fluctuations.
- An abrupt and substantial change in (commanded) camera pointing, which is nontrivial to correct for, and makes visual confirmation of particle tracks mostly impossible.
- Long time gaps/periods, which make the continuous tracking of the same particles difficult and result in many particles to have left the FOV.
- No concentrated group(s) of particles that seemingly originate from the same surface area (see Sect. 3.2 as to why this is important).

Although there is no consensus, the fourth, fifth, and sixth derivatives of position are apparently somewhat facetiously called snap, crackle, and pop, after the three mascots of Kellogg’s Rice Krispies cereal (Thompson 2011; Eager et al. 2016).

While polynomial orders beyond four are likely no longer physically justifiable, Figure 7.16 nevertheless illustrates how extreme these effects become for higher orders. Meanwhile, Figure 7.17 shows that the median adjusted R^2 values remain extremely good up until polynomial orders around 12, when the fits have long become unreasonable. This qualifier alone should therefore not be trusted.

Higher-order polynomials are also more sensitive to inaccurate detection locations during the pursuit of a track, so when the track only consists of a few detections, the algorithm can quickly go astray (see also discussion on p. 66). Yet as I show in Section 5.2, the fitting results are relatively stable against scatter in the data points when the track is well established.

Figure 7.16: Effect of polynomial order on fitting quality. The core figure layout is identical to that of Figure C.1 in the science paper, but the top plots additionally include fits with polynomial orders from 5 to 9 (light-green), and the bottom plots polynomial orders from 5 to 43 (the highest possible value).

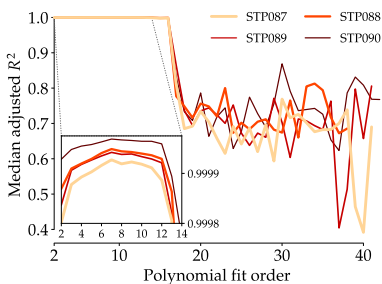
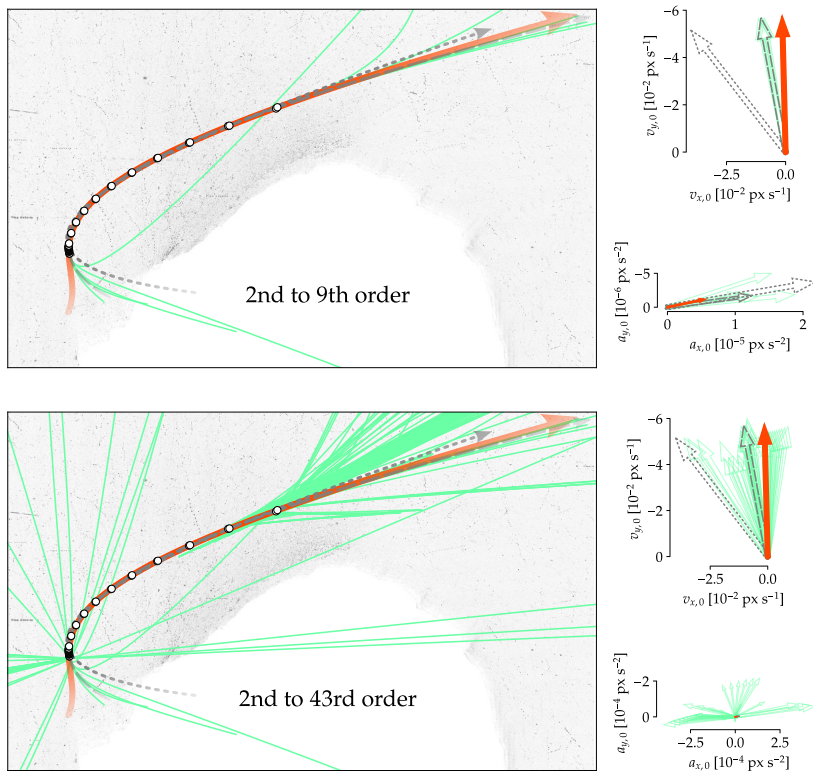


Figure 7.17: Mean adjusted R^2 values as a function of polynomial fit order for tracks with miss-rates < 30% from the four image sequences. The sudden drop at a polynomial order of around 14 might have to do with the acceptance criteria.



A third reason against long extrapolation times (the second one being the nucleus rotation, see p. 59) is of course that it also becomes unreasonable to assume that particles that require such long extrapolation times were still close to the nucleus during the observational period.

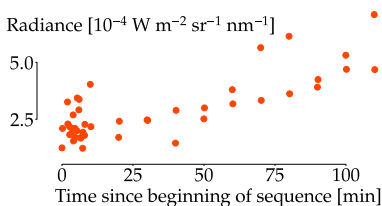


Figure 7.18: The light curve of the sample track shown in Figs. 3 & C.1 in the science paper.

Of the particles for which we checked their light curve, this is also one of the few with a light curve that actually shows a clear trend (see Fig. 7.18 and discussion on p. 64). Since the average intensity is steadily increasing over the course of the track, it is likely that this particle was flying toward the observer, potentially coming from the backside of the nucleus. It is also one of the larger particles with an equivalent radius around one meter.

Pfeifer, M., et al.: A&A, 685, A136 (2024)

- A low number of (reliable) tracks (e.g., due to a low number of particles).
- Nucleus outside the FOV, which makes associating particles with potential source regions on its surface much more speculative.
- Too large nucleocentric distances of the spacecraft, which do not allow for particles near the nucleus to be distinguishable from the diffuse coma or associated with potential source regions.
- Different time signatures (i.e., images come in singles or triplets instead of pairs, which require at minimum an adaptation of the tracking algorithm).
- Missing or an uneven number of images (e.g., in the used calibration levels).
- Defect/artifact-riddled/incomplete images (see, e.g., the artifacts around the nucleus in the first image of sequence STP088, shown in Fig. 2).

Appendix C: Caveats of polynomial fitting

As Figure 3 shows, fitting third-order polynomials is sometimes not only required for tracking particles successfully, but often simply the more appropriate choice. From a physical standpoint,

third-order polynomials are justified, since the particle acceleration changes over time due to the complex gas and micro-gravity environment and the possibility for asymmetric outgassing. Even fourth-order polynomials may be fair. Yet because of residual pointing fluctuation and other effects, the positional data of our particles are not precise enough to allow for the detection of such delicate signals. In some cases, the order of the fitted polynomial can also substantially affect the derived velocity and acceleration vectors and change the extrapolated course of the track (see Fig. C.1 for an extreme example). Our ability to extrapolate particle tracks is thus limited, which is one reason why we only trace back particles for at most half an hour.

To ensure that our statistical results are nonetheless reliable, we tested how much they are affected by the order of the fitted polynomials (second or third). The most notable difference was in the track populations that intersect with the suspected source regions. Some tracks only do so when using a second- but not a third-order polynomial, and others vice versa. The corresponding radius, velocity, and acceleration distributions, however, are very similar, and do not significantly change the derived qualities. The fitted SFD power-law indices, for example, differ by no more than 0.1. Based on this analysis, we consider our statistical results reliable, and our conclusions remain unaffected.

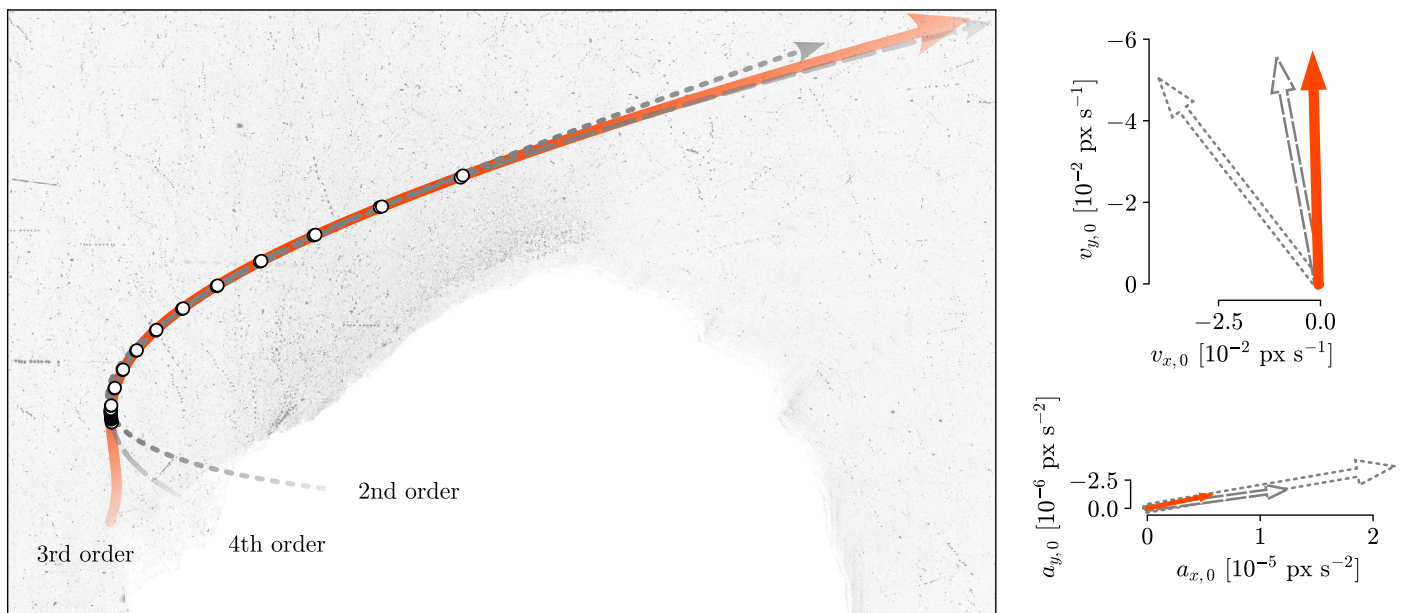


Fig. C.1. Same particle track shown in Fig. 3 (white circles), but this time fitted with a second-, third-, and fourth-order polynomial, each extrapolated an hour back and over two and a half hours forward in time. The plots on the right show the respective derived vertical and horizontal particle velocities and accelerations at $t = 0$ s.

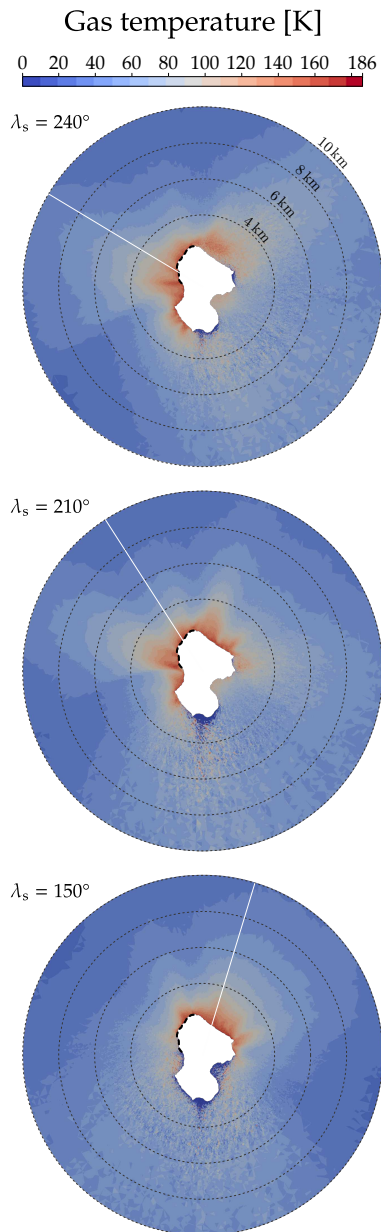


Figure 7.19: Slice through the simulation domain showing the gas temperature gradients of the three gas solutions. Figure elements analogous to those in Figure D.1 in the science paper.

Another interesting parameter is the gas temperature, shown in Figure 7.19. It falls off quickly with increasing nucleocentric distance because the thermal energy is converted essentially adiabatically into kinetic energy as the gas expands into the vacuum of space.

This transition region can clearly be seen in Figure 7.20, which shows the wireframe representation of a slice through the simulation domain. The transition region was created to make sure that the tetrahedron cells would not become too large too fast with increasing nucleocentric distance, which is important for the gas simulation (Raphael Marschall, priv. com.). But as a consequence, dust particles may not traverse through the many of the tiny cells, which creates the artifacts seen in the drag coefficient diagrams.

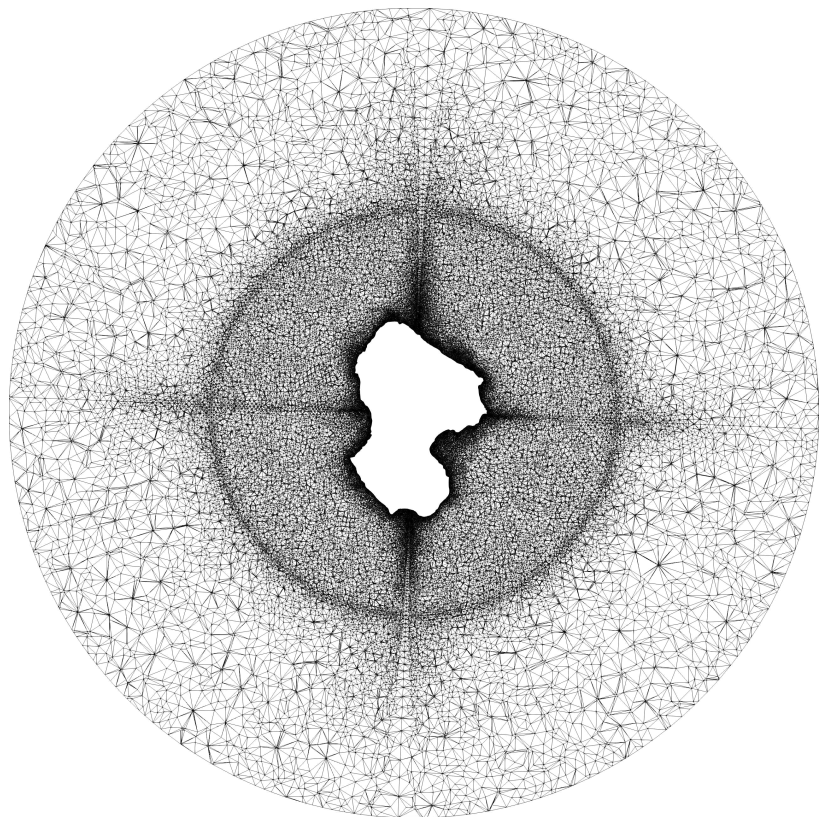


Figure 7.20: Wireframe representation of a slice through the simulation domain highlighting the cell arrangement of the unstructured tetrahedron grid.

* * *

Because the rest of the science paper appendix only contains figures, some of the following paper pages are reorganized or appear on both sides of a double-page to allow for better and more coherent reading.

Appendix D: Dust coma simulation results

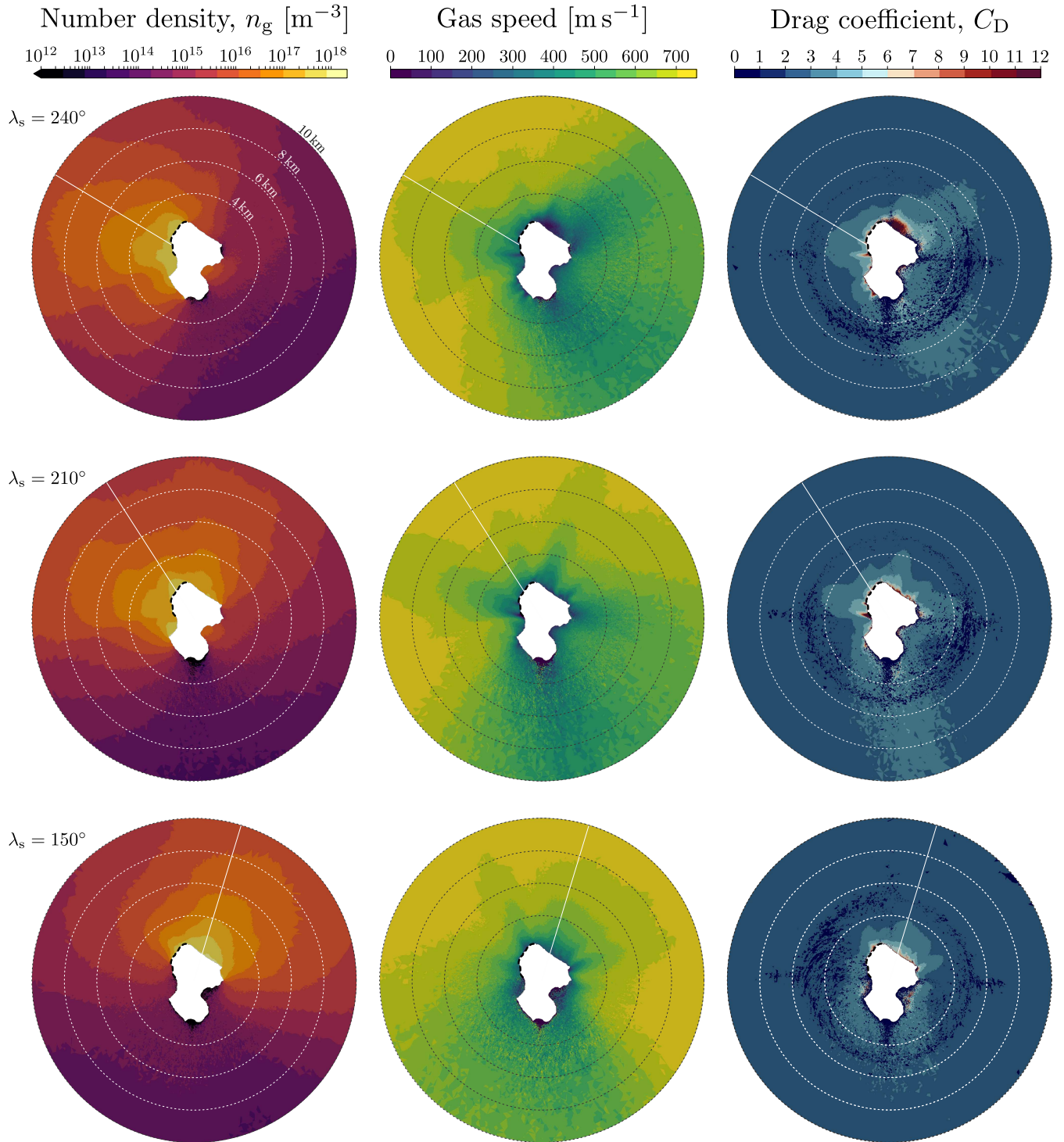


Fig. D.1. Properties of the three static gas solutions that we used for our dust coma models. The plots show model cross sections that slice through the suspected source regions, which are indicated by the bold dashed curves on the top left side of the nucleus. The solar directions are highlighted by the white lines. The drag coefficient plots show the results computed for global activity of 32 cm particles, which are representative for the whole relevant size range from 1 cm to 1 m. The circular artifacts in these plots, around 3 km from the nucleus, are a consequence of how the simulation domain was built (with a transition region between an inner sphere with very small cells and an outer region with much larger cells) and the low number of simulated particles.

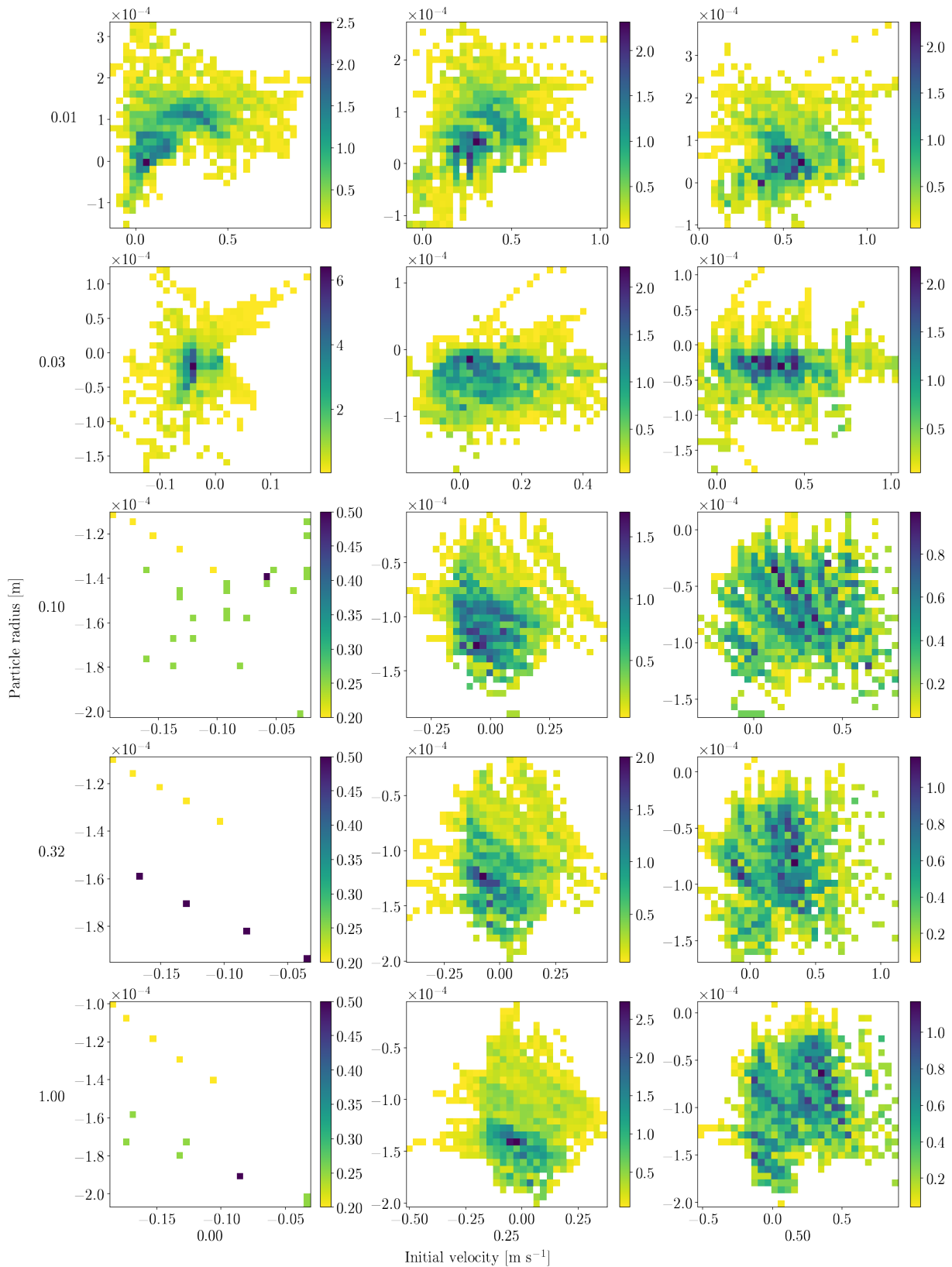


Figure 7.21: Projected radial particle accelerations and velocities of the particles shown in Fig. D.2 in the science paper (sequence STP087). As with the OSIRIS data, the values were determined by fitting third-order polynomials to the projected tracks. In each subplot, the x -axis shows the projected radial velocity in m s^{-1} , the y -axis the projected radial acceleration in m s^{-2} , and the color bar the number of measurements, which are again weighted by the number of measurements per respective track (residence time weighting).

Pfeifer, M., et al.: A&A, 685, A136 (2024)

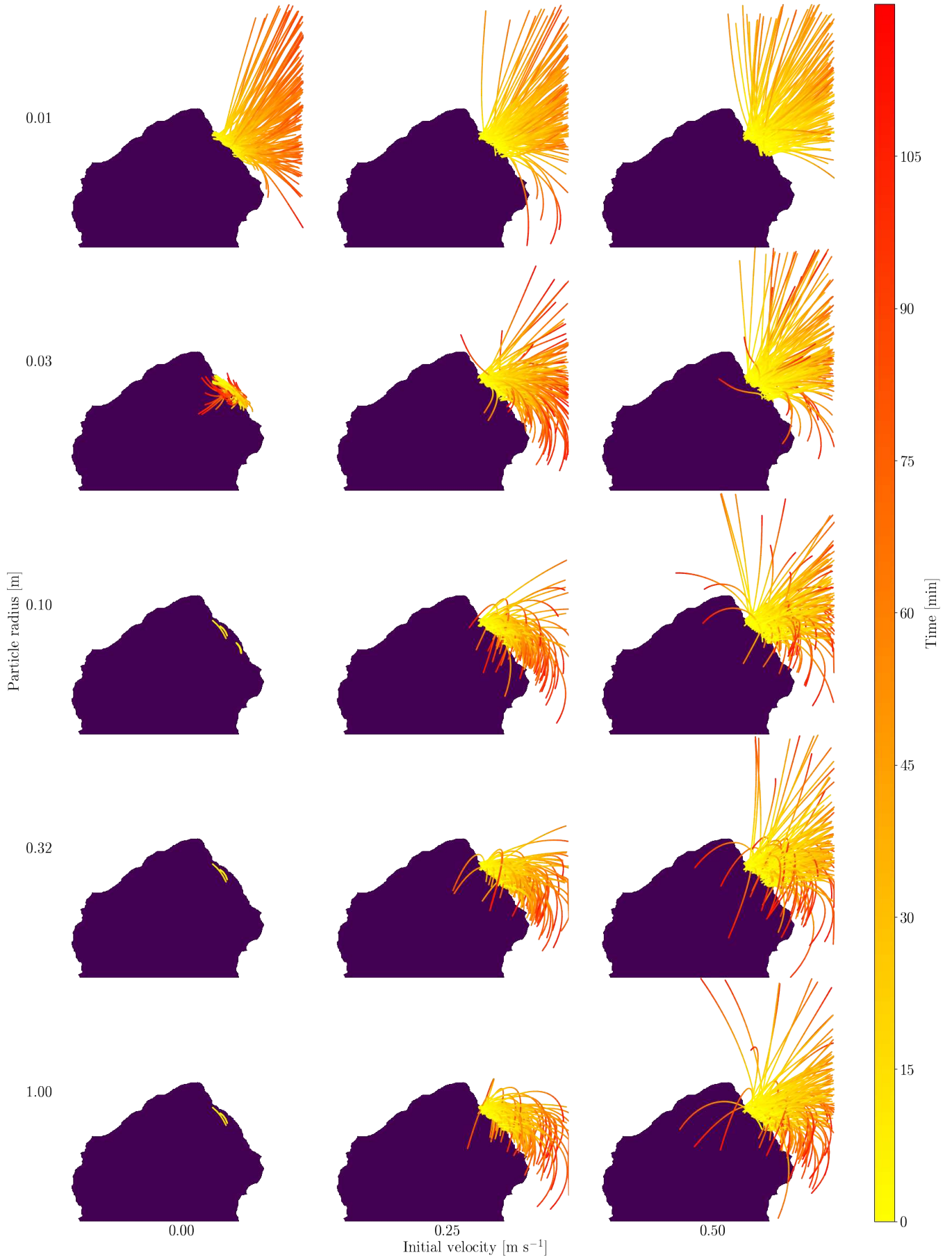


Fig. D.2. Trajectory simulations of up to 150 randomly selected particles ejected from within the suspected source region of sequence STP087. A136, page 22 of 30

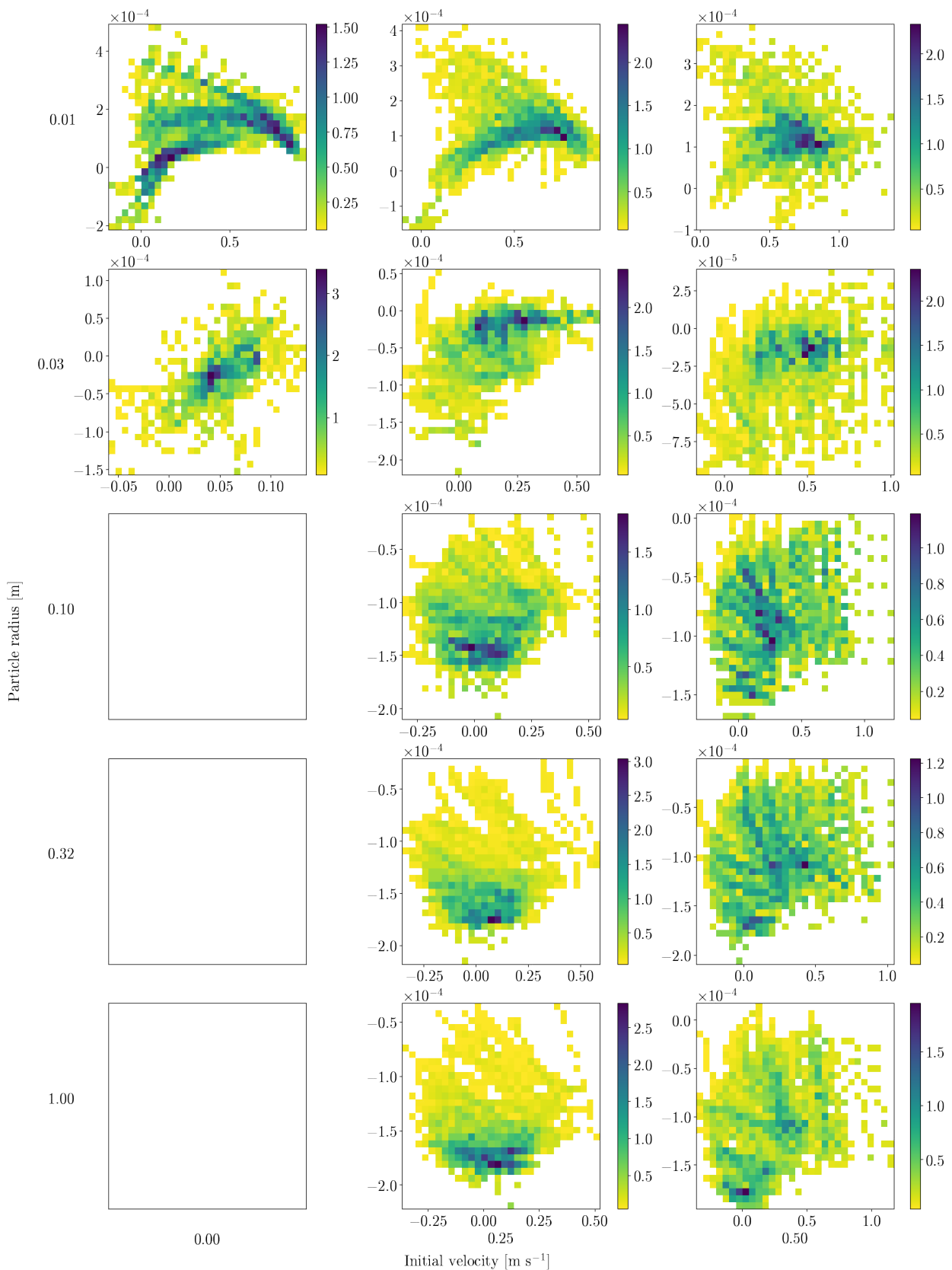


Figure 7.22: Projected radial particle accelerations and velocities of the particles shown in Fig. D.3 in the science paper (sequence STP088). Description analogous to Fig. 7.21. The three bottom left panels are blank because no particles were ejected in these instances.

Pfeifer, M., et al.: A&A, 685, A136 (2024)

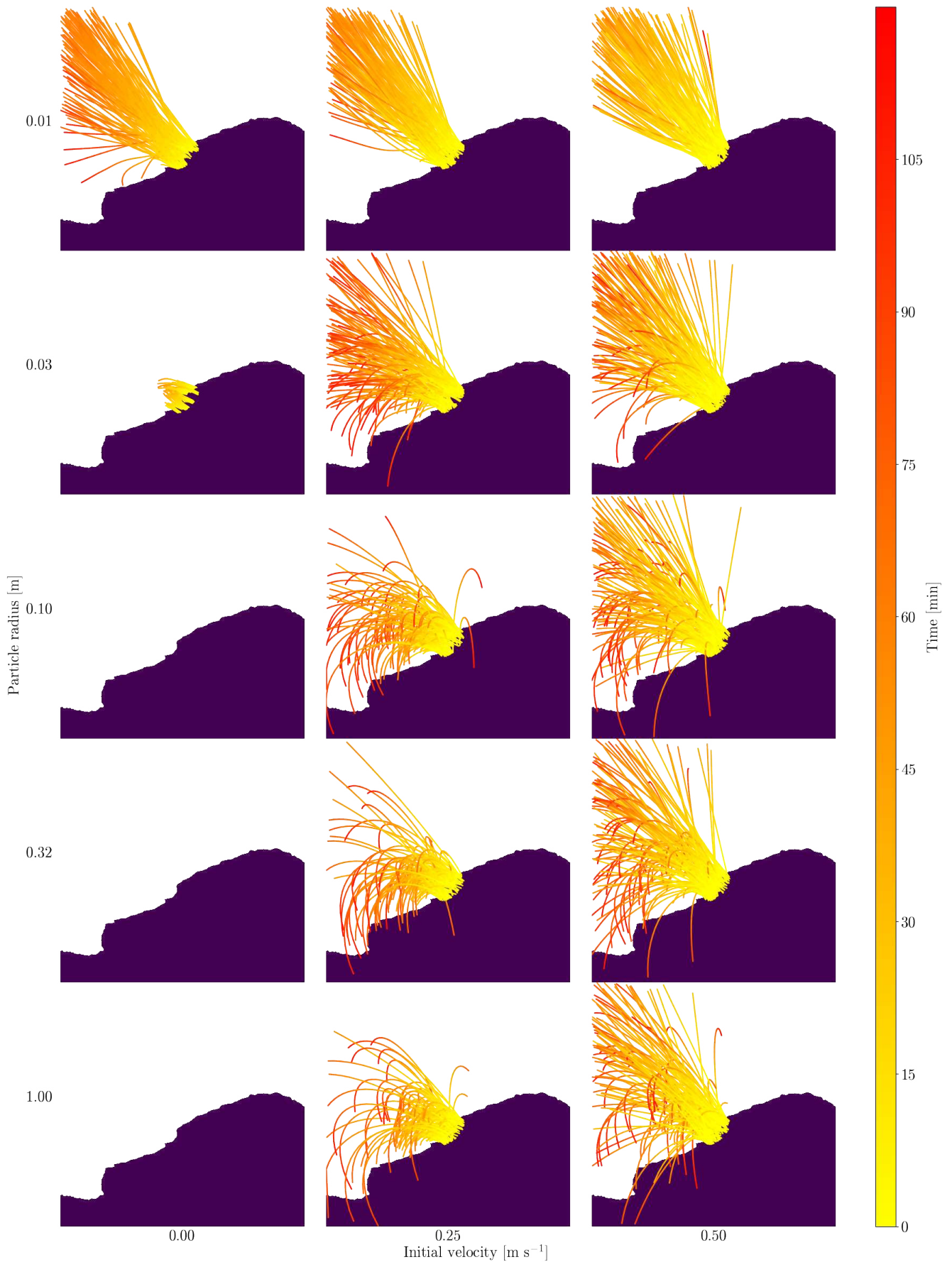


Fig. D.3. Trajectory simulations of up to 150 randomly selected particles ejected from within the suspected source region of sequence STP088.

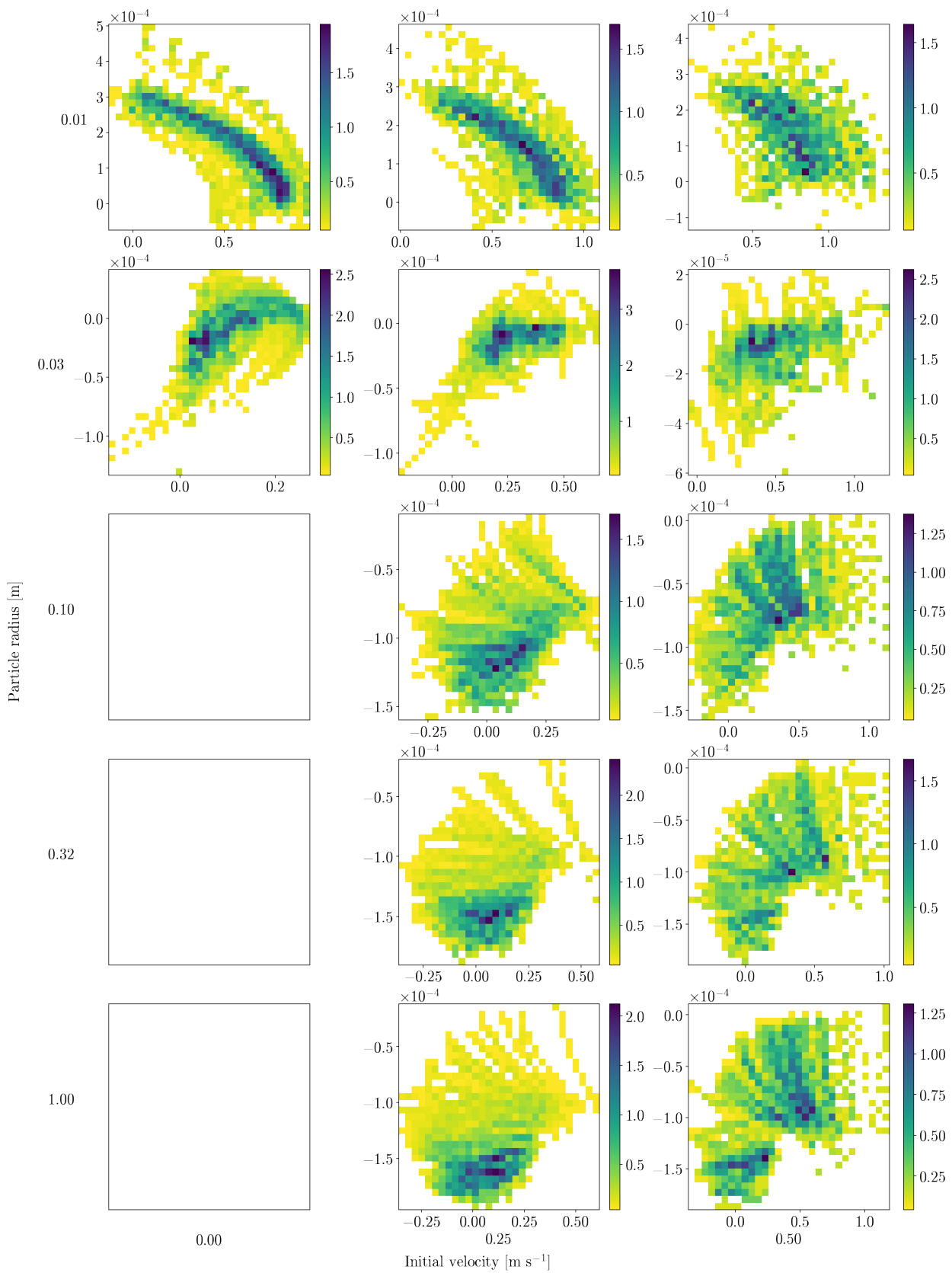


Figure 7.23: Projected radial particle accelerations and velocities of the particles shown in Fig. D.4 in the science paper (sequence STP089). Description analogous to Fig. 7.21. The three bottom left panels are blank because no particles were ejected in these instances.

Pfeifer, M., et al.: A&A, 685, A136 (2024)

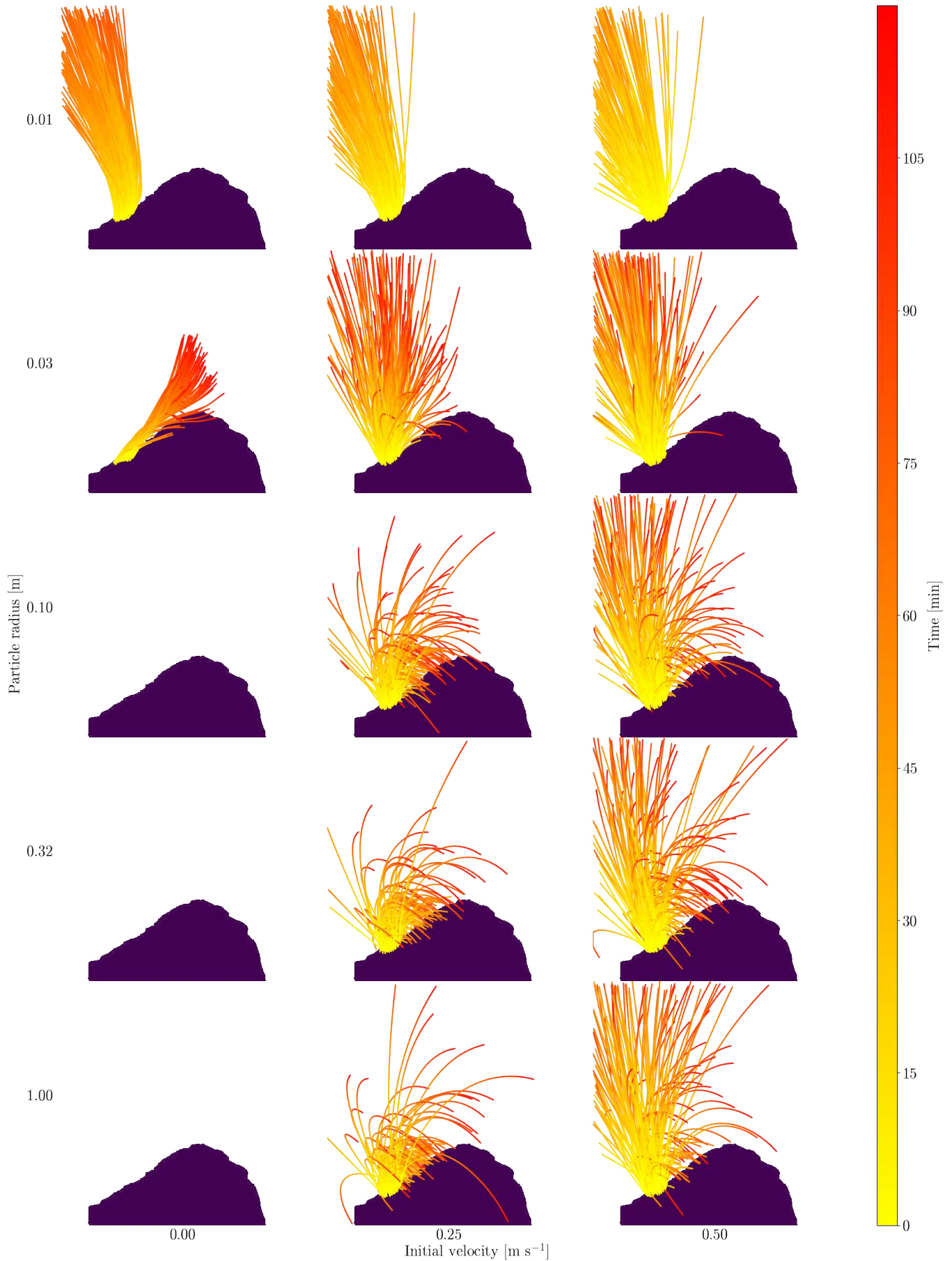


Fig. D.4. Trajectory simulations of up to 150 randomly selected particles ejected from within the suspected source region of sequence STP089. A136, page 24 of 30

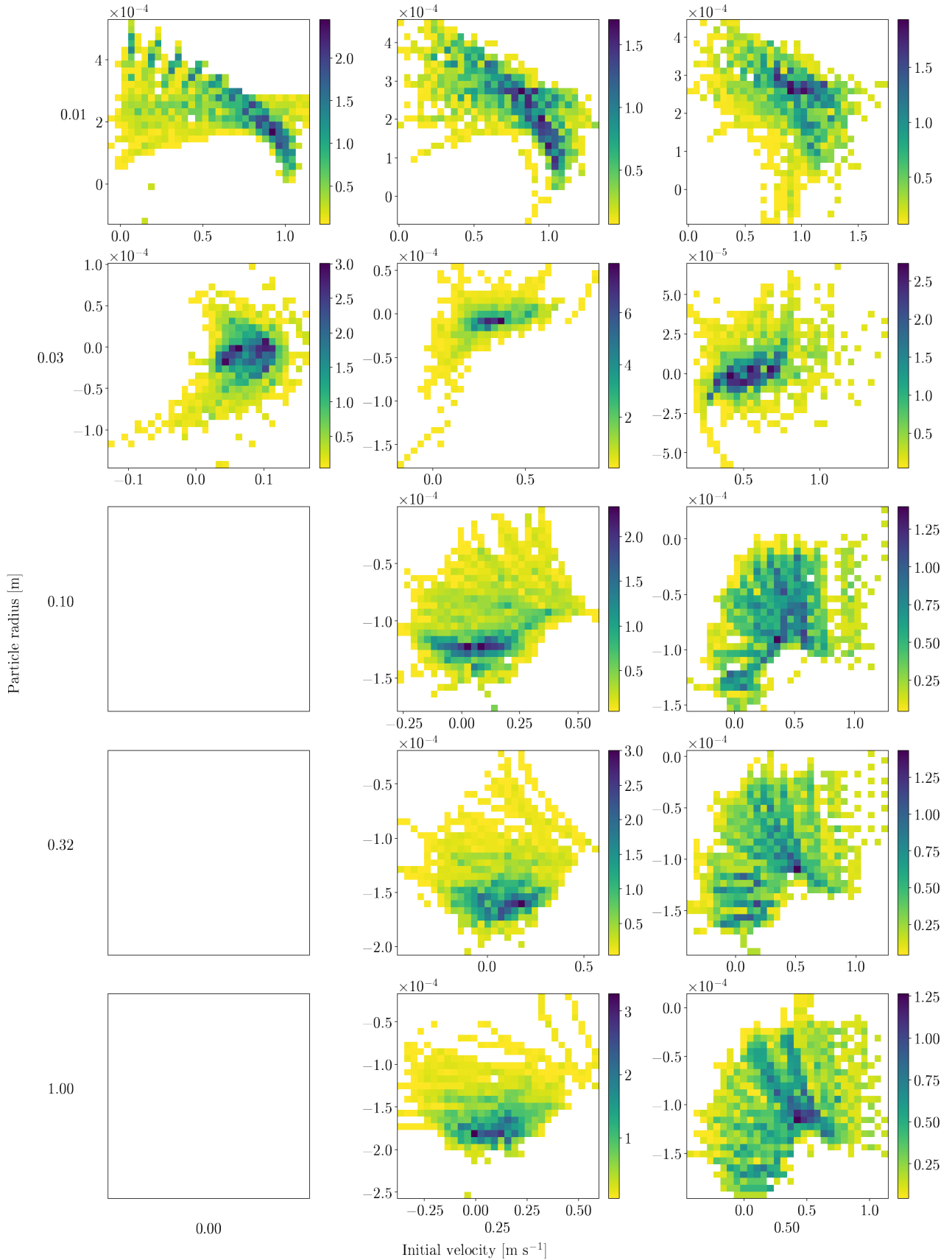


Fig. D.6. Projected radial accelerations and velocities of the particles shown in Fig. D.5 (sequence STP090). As with the OSIRIS data, the values were determined by fitting third-order polynomials to the projected tracks. In each subplot, the x-axis shows the projected radial velocity in m s^{-1} , the y-axis the projected radial acceleration in m s^{-2} , and the color bar the number of measurements, which are again weighted by the number of measurements per respective track (residence time weighting). The three bottom left panels are blank because no particles were ejected in these instances.

Pfeifer, M., et al.: A&A, 685, A136 (2024)

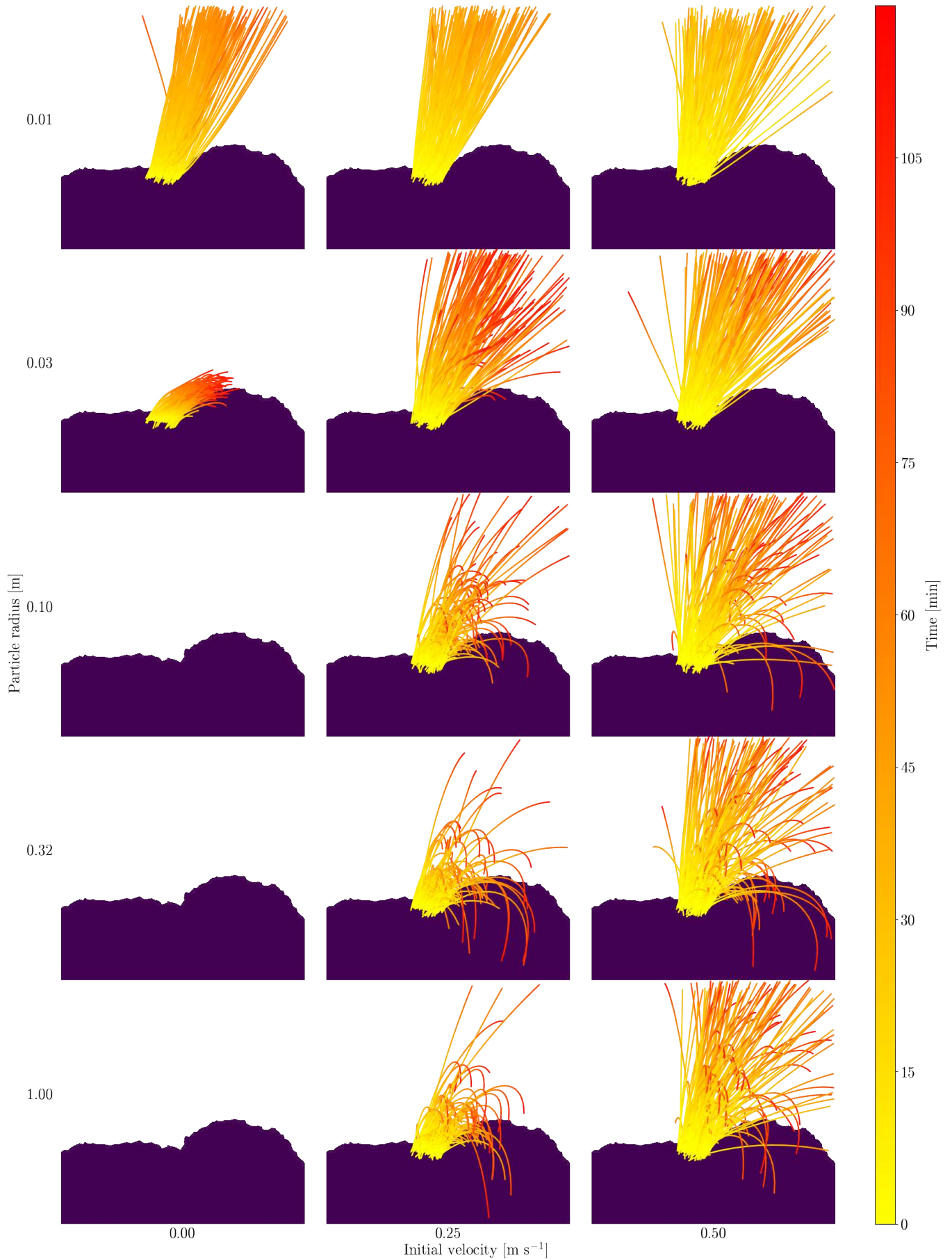


Fig. D.5. Trajectory simulations of up to 150 randomly selected particles ejected from within the suspected source region of sequence STP090.

Pfeifer, M., et al.: A&A, 685, A136 (2024)

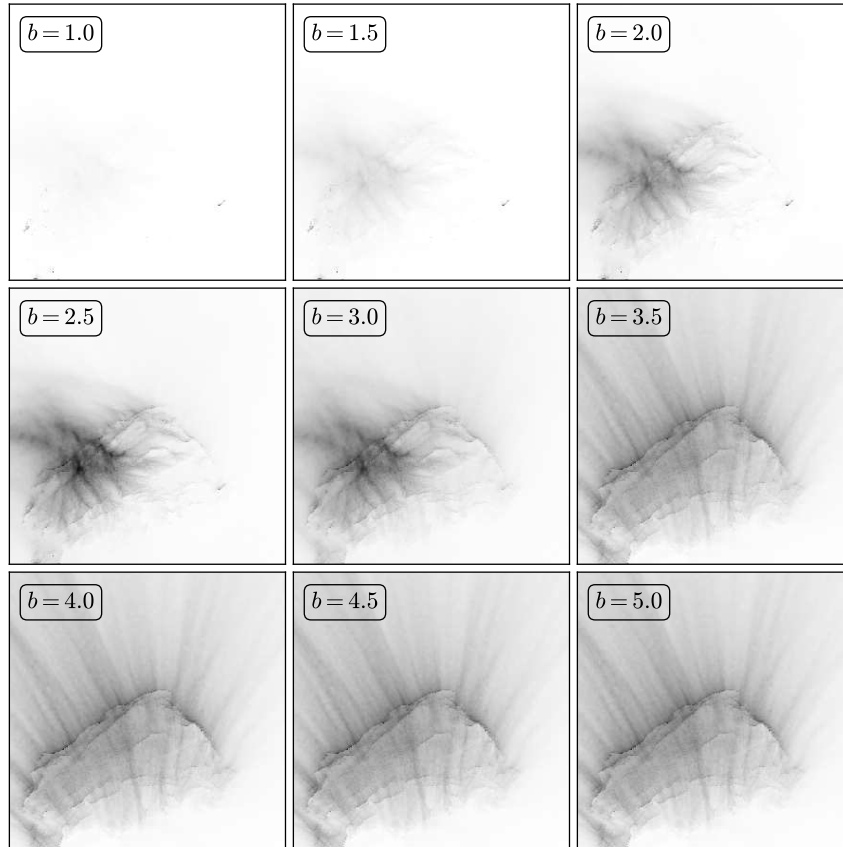


Fig. D.11. Global coma simulations for sequence STP087 as a function of the particle SFD power-law index, b , given $v_{\text{init}} = 0.0 \text{ m s}^{-1}$.

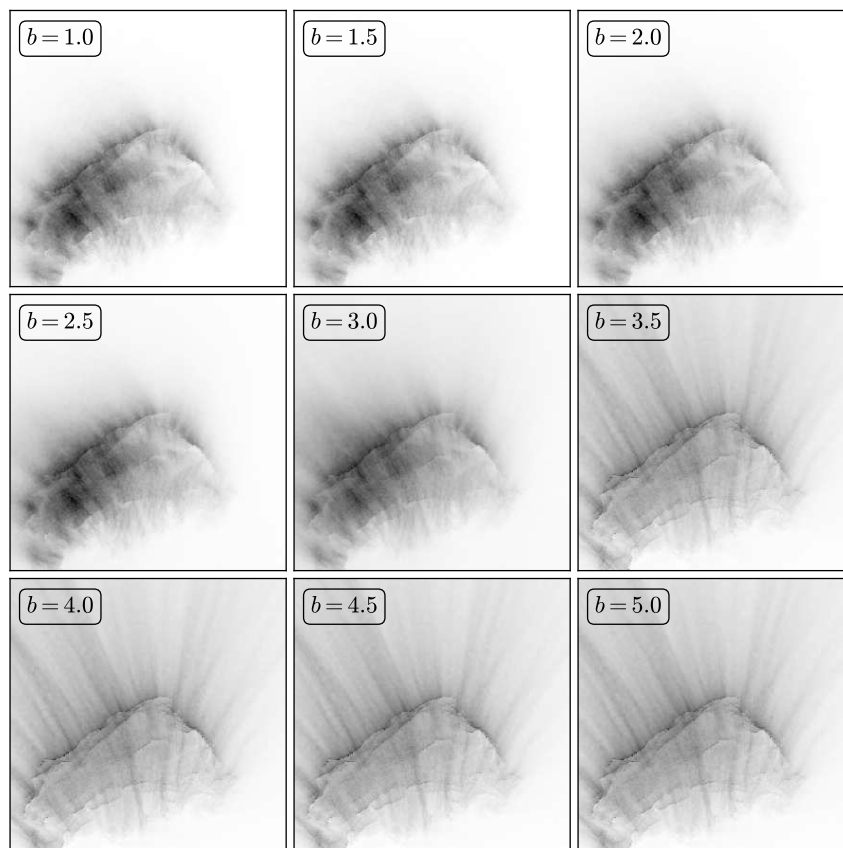


Fig. D.12. Global coma simulations for sequence STP087 as a function of the particle SFD power-law index, b , given $v_{\text{init}} = 0.25 \text{ m s}^{-1}$.

Pfeifer, M., et al.: A&A, 685, A136 (2024)

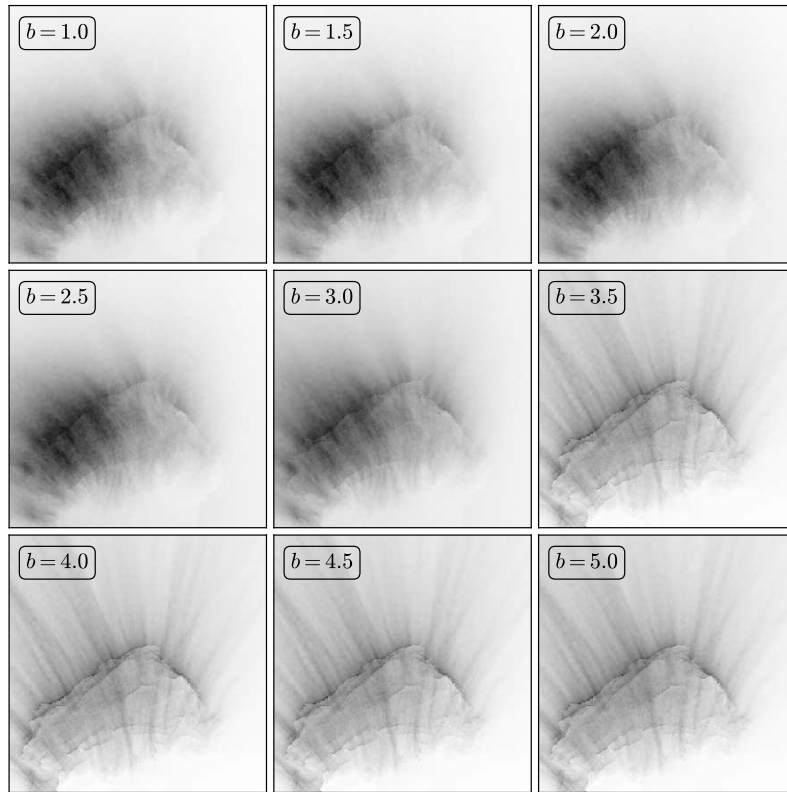


Fig. D.13. Global coma simulations for sequence STP087 as a function of the particle SFD power-law index, b , given $v_{\text{init}} = 0.5 \text{ m s}^{-1}$.

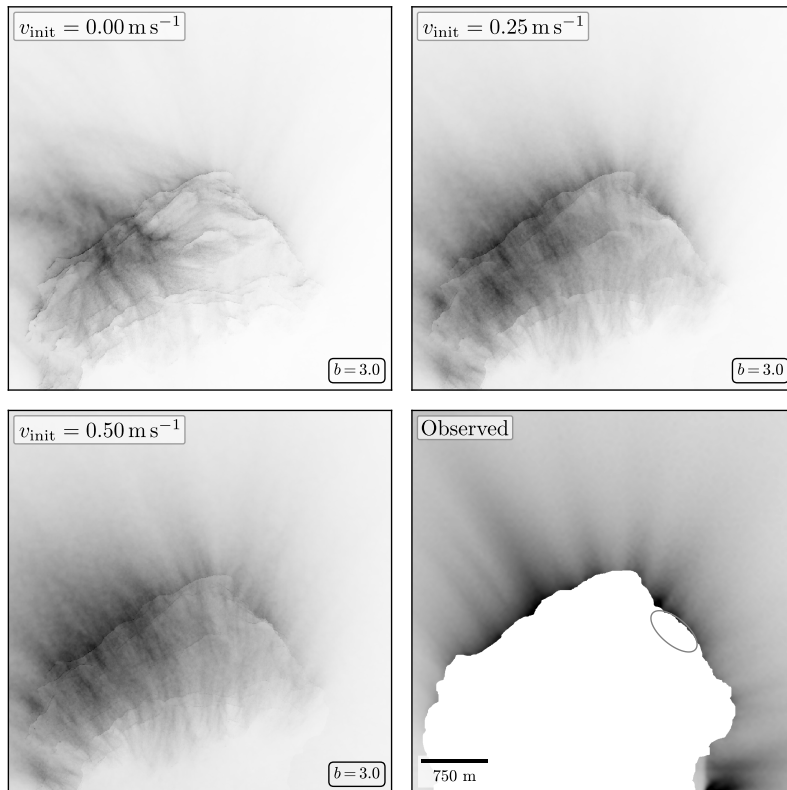


Fig. D.14. Comparison between global coma simulations given different initial velocities, v_{init} , and the observed coma in the first image of sequence STP087. The image of the observed coma is the background signal subtracted during the preparation for the tracking procedure (see Sect. 2 and Pfeifer et al. 2022). The ellipse indicates the suspected source region. All images are brightness-inverted and had their contrasts improved individually for better readability. Because of this, the absolute intensity levels should not be compared across images, but only relative to other areas of the same image.

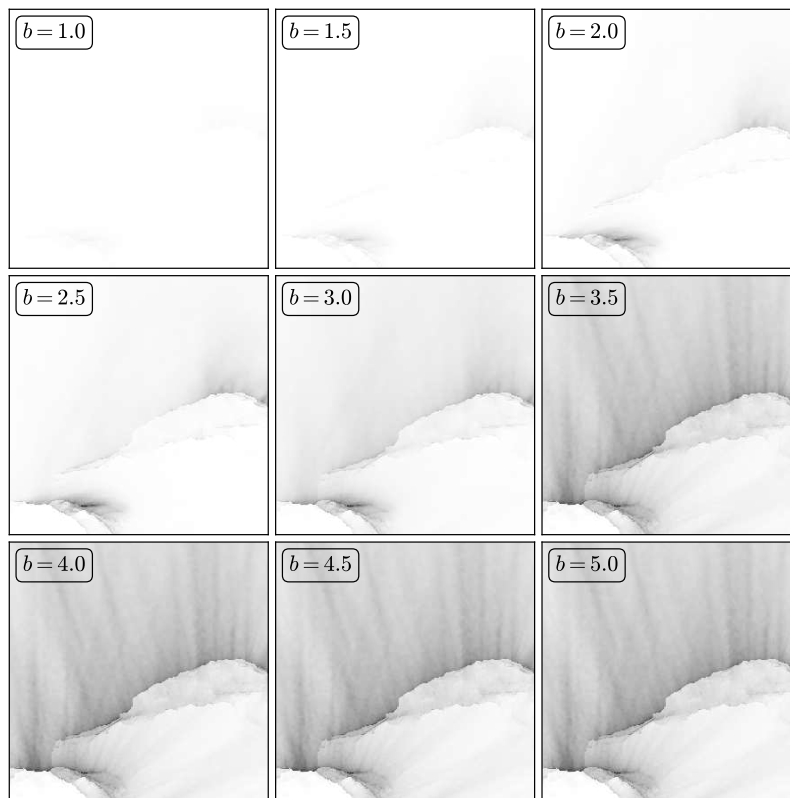


Figure 7.24: Global coma simulations for sequence STP088 as a function of the particle SFD power-law index, b , given $v_{\text{init}} = 0.0 \text{ m s}^{-1}$.

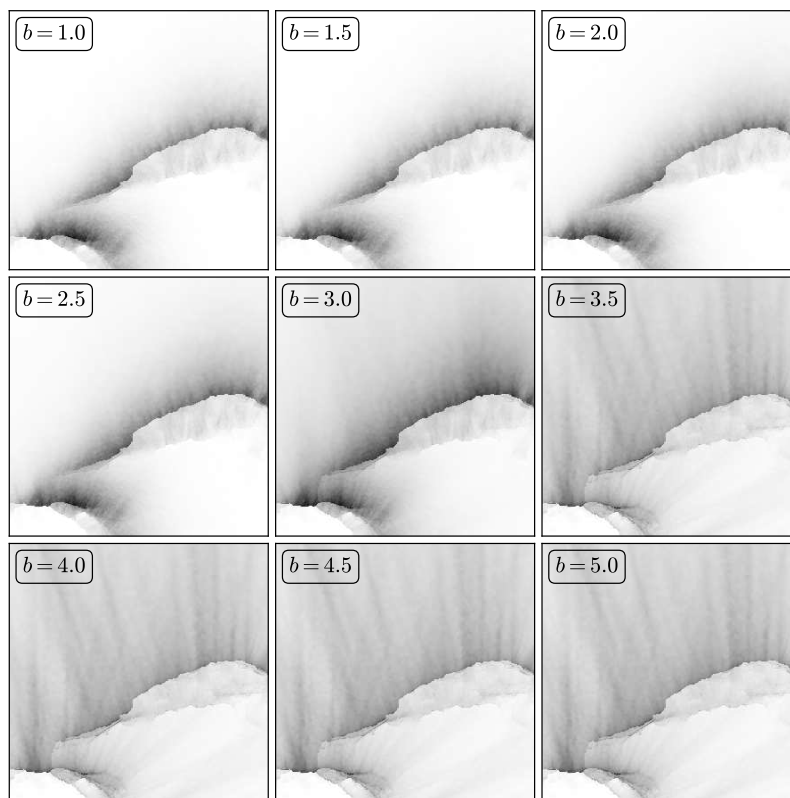


Figure 7.25: Global coma simulations for sequence STP088 as a function of the particle SFD power-law index, b , given $v_{\text{init}} = 0.25 \text{ m s}^{-1}$.

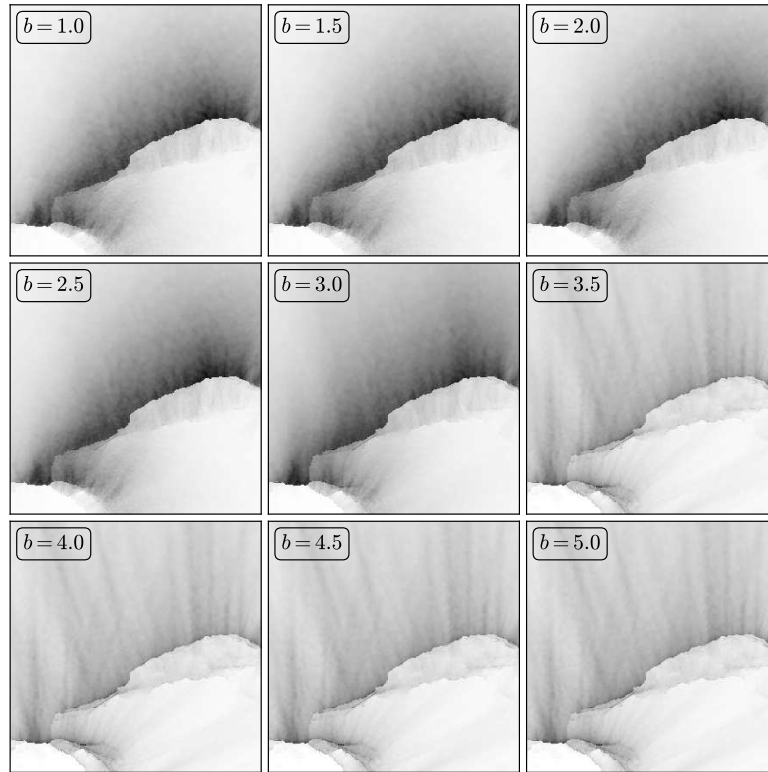


Figure 7.26: Global coma simulations for sequence STP088 as a function of the particle SFD power-law index, b , given $v_{\text{init}} = 0.5 \text{ m s}^{-1}$.

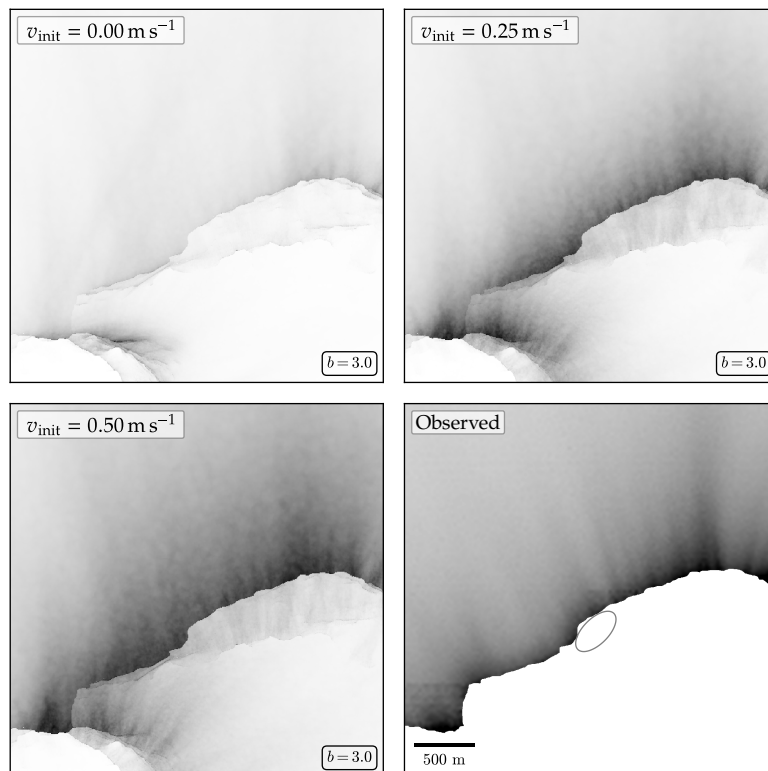


Figure 7.27: Comparison between global coma simulations given different initial velocities, v_{init} , and the observed coma in the first image of sequence STP088. The image of the observed coma is the background signal that we subtracted from the first image of the sequence during the preparation for the tracking procedure (see p. 56 & 57). The ellipse again indicates the suspected source region. All images are brightness-inverted and their contrasts have been adapted for each image individually for better reading. Because of this, the absolute intensity levels should not be compared across images, but only relative to other areas of the same image.

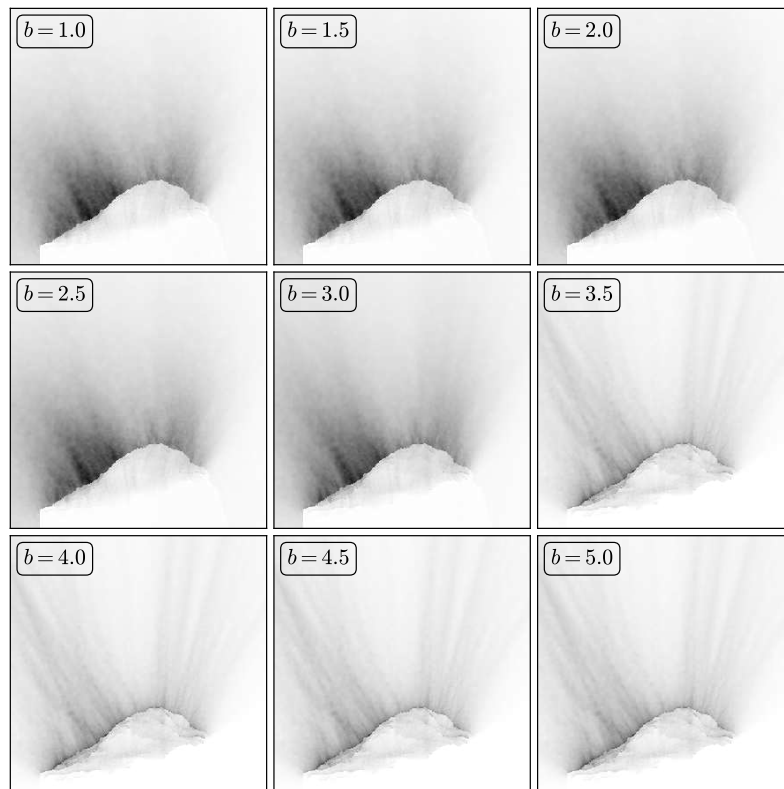


Figure 7.28: Coma simulations for sequence STP089 as a function of the particle SFD power-law index, b , given local activity and $v_{\text{init}} = 0.5 \text{ m s}^{-1}$.

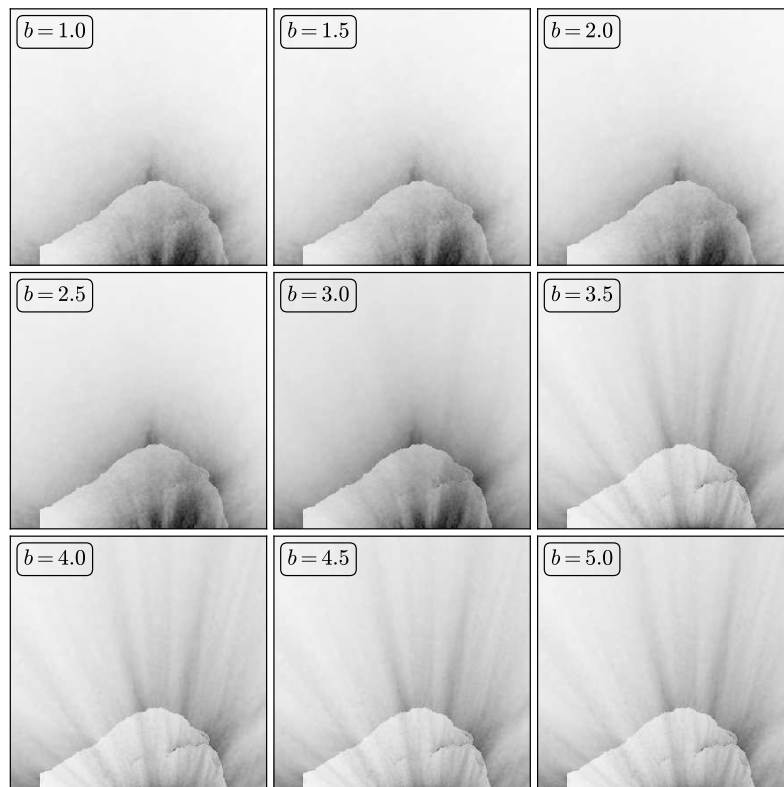


Figure 7.29: Coma simulations for sequence STP089 as a function of the particle SFD power-law index, b , given global except local activity and $v_{\text{init}} = 0.5 \text{ m s}^{-1}$.

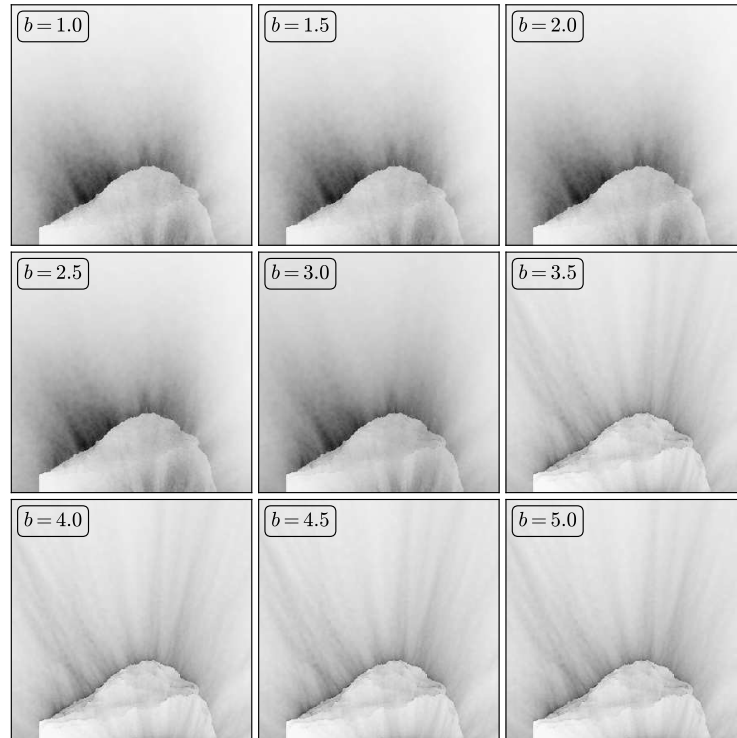


Figure 7.30: Coma simulations for sequence STP089 as a function of the particle SFD power-law index, b , given global activity and $v_{\text{init}} = 0.5 \text{ m s}^{-1}$.

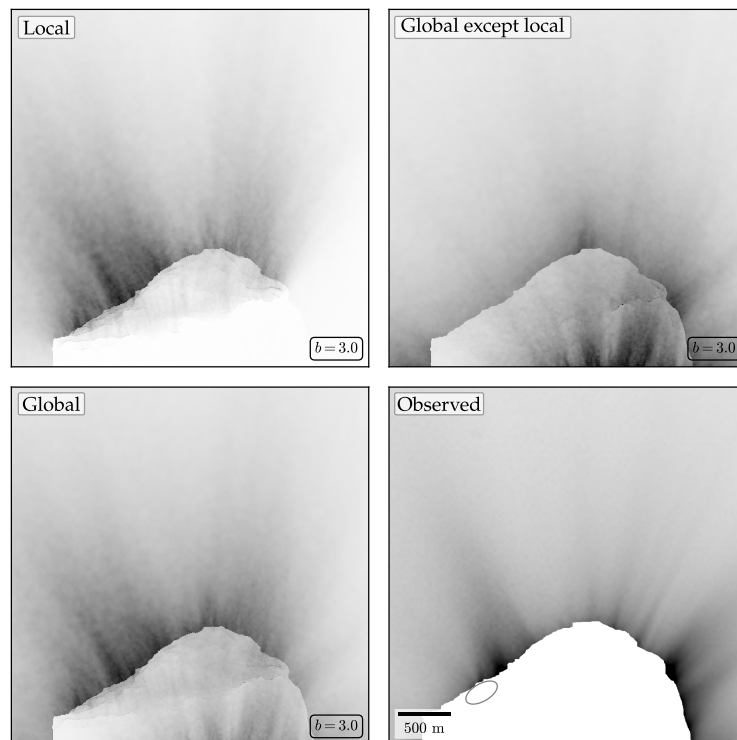


Figure 7.31: Comparison between coma simulations of local, global except local, and global activity distributions given $v_{\text{init}} = 0.5 \text{ m s}^{-1}$, and the observed coma in the first image of sequence STP089. The image of the observed coma is the background signal that we subtracted from the first image of the sequence during the preparation for the tracking procedure (see p. 56 & 57). The ellipse again indicates the suspected source region. All images are brightness-inverted and their contrasts have been adapted for each image individually for better reading. Because of this, the absolute intensity levels should not be compared across images, but only relative to other areas of the same image.

Pfeifer, M., et al.: A&A, 685, A136 (2024)

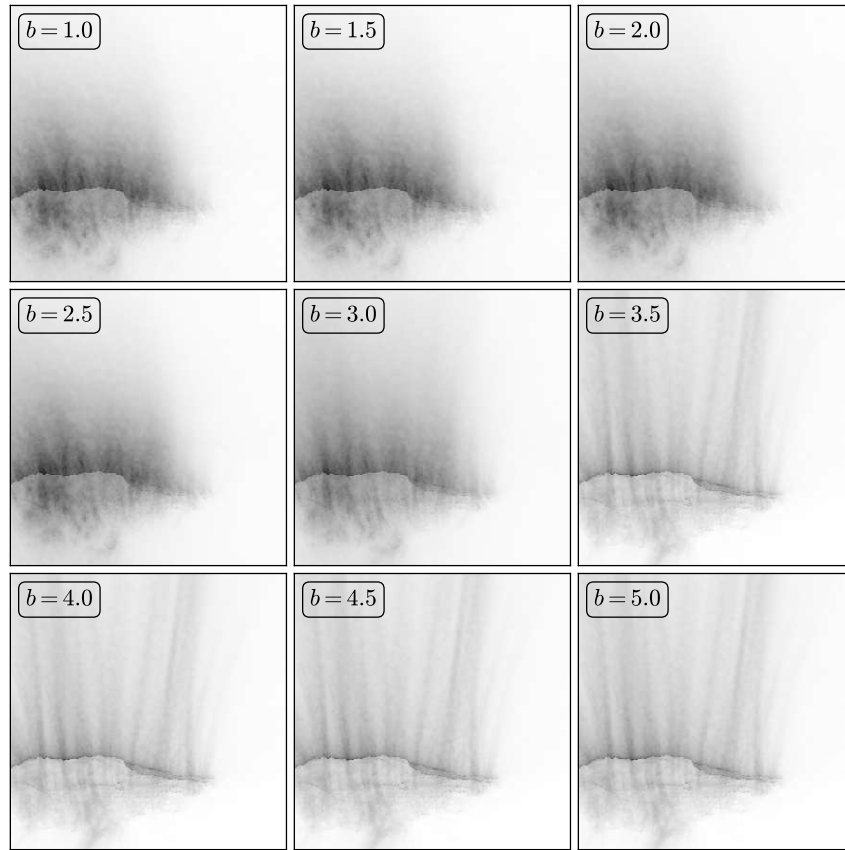


Fig. D.7. Coma simulations for sequence STP090 as a function of the particle SFD power-law index, b , given local activity and $v_{\text{init}} = 0.5 \text{ m s}^{-1}$.

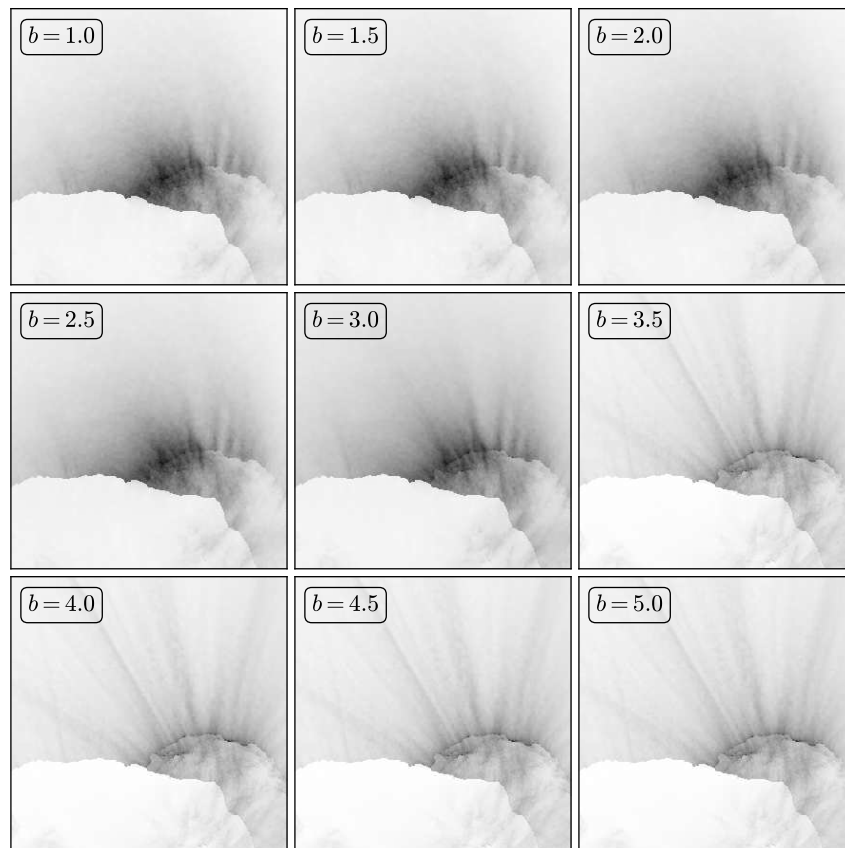


Fig. D.8. Coma simulations for sequence STP090 as a function of the particle SFD power-law index, b , given nonlocal activity and $v_{\text{init}} = 0.5 \text{ m s}^{-1}$.

Pfeifer, M., et al.: A&A, 685, A136 (2024)

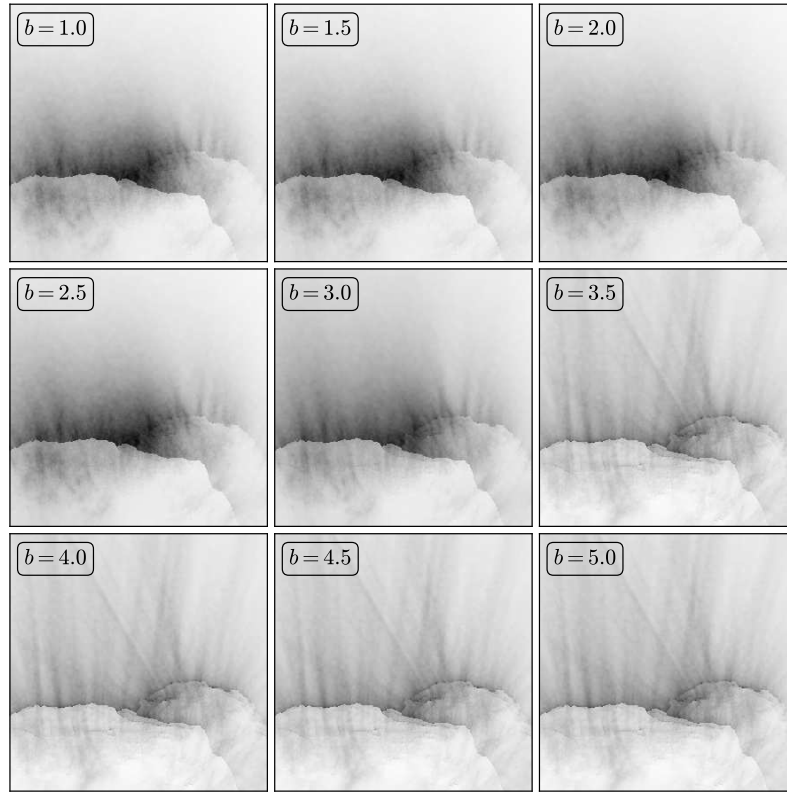


Fig. D.9. Coma simulations for sequence STP090 as a function of the particle SFD power-law index, b , given global activity and $v_{\text{init}} = 0.5 \text{ m s}^{-1}$.

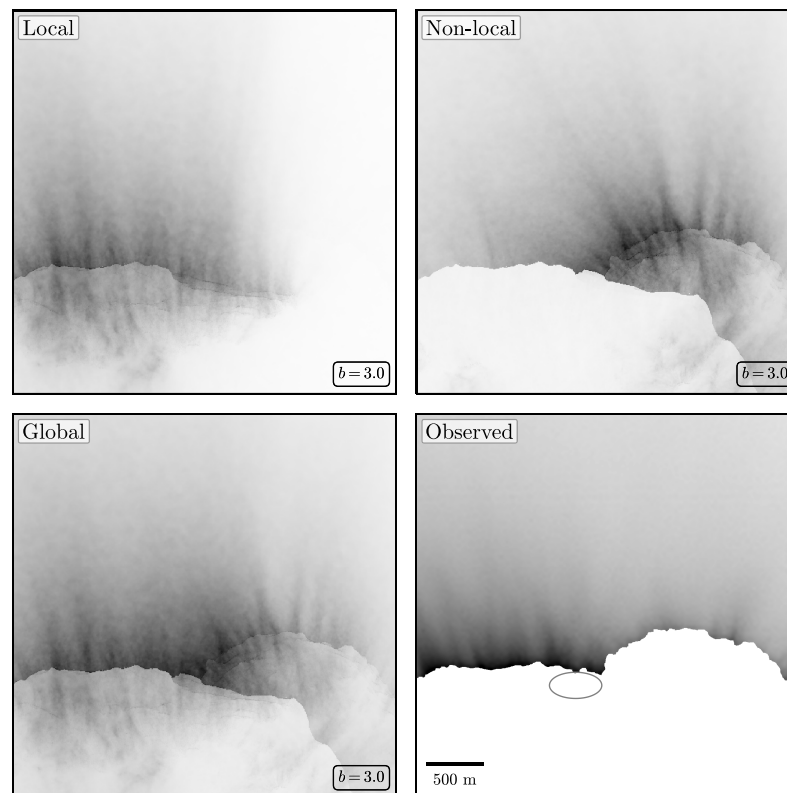
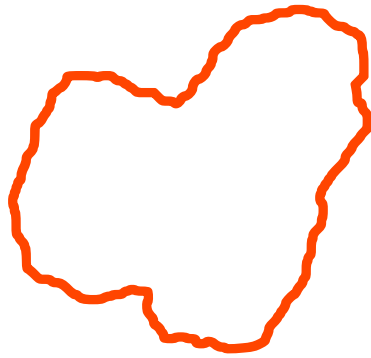


Fig. D.10. Comparison between coma simulations with different activity distributions given $v_{\text{init}} = 0.5 \text{ m s}^{-1}$, and the observed coma in the first image of sequence STP090. The image of the observed coma is the background signal that we subtracted during the preparation for the tracking procedure (see Sect. 2 and Pfeifer et al. 2022). The ellipse indicates the suspected source region. All images are brightness-inverted and had their contrasts improved individually for better reading. Because of this, the absolute intensity levels should not be compared across images, but only relative to other areas of the same image.

FINAL REFLECTIONS



FINAL REFLECTIONS

*“Oh, dear me!” [Moomintroll] lamented. “The raft has floated off and I suppose it’s gone down that awful hole by now.”
 “Well, never mind. We’re not on it,” said Snufkin gaily.
 “What’s a kettle here or there when you’re out looking for a comet!”*

— Jansson (2003). *Comet in Moominland*.

PART CONTENTS

Final Reflections	153
Methodology	153
Comet Physics	154

To conclude this thesis, I briefly summarize and reflect on the content of the previous chapters, starting with the methodology followed by the scientific results and their implications.

8.1 METHODOLOGY

In Chapter 2, I showed that our particle tracking method belongs to a large family of applications and techniques, with some closer, but many more distant relatives. Due to the unique challenges posed by our data however, relying on these other techniques was not feasible, and so we developed our own tracking engine from scratch.

The main challenge during its development was the combination of sparse data with crowded fields, complex particle dynamics, and random fluctuations in the camera pointing. To solve these issues and reliably track potentially thousands of particles per image sequence, we introduced pair tracking as a core concept of our tracking algorithm, used sidereal objects to correct for the pointing fluctuations, and defined several tracking parameters, of which many dynamically adapt to the properties of a track during its pursuit. To scrutinize our tracking results, I additionally built an extensive simulation software, systematically optimized the most relevant tracking parameters, manually inspected and flagged thousands of tracks, and ultimately came up with a robust parameter that can accurately predict the authenticity of a track: the miss-rate criterion.

While our approach yielded very satisfying results, there are still plenty of open questions and tasks that may be addressed in the future, such as:

- If there is a way to correct for the pointing fluctuation in sequences that do not contain trackable sidereal objects. As I for example discuss on page 94, the absence of such objects was one of the reasons we had to dismiss certain image sequences that otherwise would have been interesting to analyze. Similarly, it would be useful to implement a correction method that is sensitive to the CCD location, because as Figure 7.6 shows, some image sequences may still be significantly distorted. To a lesser degree this is likely also the case for the other sequences. Being able to account for this would likely yield much more precise particle tracks, which would

allow to detect weaker effects like the rocket force more reliably, and make back-extrapolations more precise. If the pointing fluctuation can be corrected to well below sub-pixel level, this might even make it possible to reconstruct 3D particle trajectories.

- ▶ How to correlate two sets of tracking results. This would for example allow to see what kind of tracks are better recovered with what kind of tracking parameters and might help to significantly improve tracking results.
- ▶ If the automatic separation between genuine and ambiguous tracks can still be significantly improved. Although the miss-rate is already an extremely good predictor, as discussed on page 76, there may still be ways to reliably identify even more genuine tracks. Different parameters like the miss-rate and residual offset may for example be combined to yield an even better predictor, while the expectation-maximization algorithm for Gaussian mixtures or principal component analysis may also be viable approaches.
- ▶ Make the algorithm more versatile that it can also be applied to other data sets, especially from other space missions (see below). In light of the many different particle tracking tools, it would also be interesting to test all these techniques on the same data set to see which methods performs best.

Finally, it is important to stress that there currently exists no community in the field of dust particle tracking around SSSBs. There are simply too few relevant space missions separated by too much time, while each is also unique in its design, challenges, and data. So far, there have only been three space missions where particle tracking was possible, and until now, there was not even a (comprehensive) overview of all the employed and relevant methods and applications. Yet even though due to the rapid advancement in technology, the old techniques may already be outdated by the time the next mission arrives at a SSSB, there are new and exciting space missions to SSSBs on the horizon (such as Comet Interceptor, DESTINY+, Hera, Lucy, and possibly RAMSES, e. g., Snodgrass et al. 2019; Levison et al. 2021; Michel et al. 2022; Ozaki et al. 2022; Kueppers et al. 2023; see also Snodgrass et al. 2022), and so I believe it is nevertheless important to establish standards in this emerging field and to start build a community. I hope that this dissertation may be a first step in this direction.

8.2 COMET PHYSICS

Before I continue to discuss our particle tracking results and their implications for cometary science, there are two other ideas that I would briefly like to mention. For one, as I already noted on page 50, I find the difference between the smooth and consolidated terrain curious. If comets truly formed by the gentle gravitational collapse of a pebble cloud, as the currently more popular theory predicts (e. g., Blum et al. 2017, 2022), and 67P subsequently experienced no significant compression (although it is likely the result of two merging cometesimals, e. g., Jutzi et al. 2015; Massironi et al. 2015; de Niem et al. 2018; Nesvorný et al. 2018), then why is there such a structural difference between the deposits of fall-back material and the pristine consolidated material? To me, the most

likely explanation seems to be that this difference is because for one, the fall-back material consists not just of pebbles but also of larger boulders that may also be notably dryer than the consolidated material, but more importantly, the fall-back material is likely missing the fluffy particle “glue” that fill the gaps of the consolidated material, as suggested by Blum et al. (2017) and Longobardo et al. (2020). The structural difference between these two terrain types might therefore be further evidence in support of the gravitational collapse scenario.

Second, to understand how the nucleus layering formed (see, e. g., Sect. 1.5.1), I wonder if it may be helpful to ask why these layers are observed in comets, but not in (primitive) asteroids, which might have at least initially formed via similar processes (e. g., Simon et al. 2022). While it is highly plausible that any initial layering in asteroids was eventually destroyed due to (catastrophic) collisions, the constant meteorite impacts, and other space weathering effects that they experienced (e. g., Beitz et al. 2016; Jourdan et al. 2023), or that in case of rubble-pile asteroids, such layering never existed because they consist of fragments from larger parent bodies (e. g., Okada et al. 2020), an important factor for forming such layers may also be the relative abundance and distribution of volatiles. Also, because the layers always remind me of the layers that build up when creating a large snow ball by rolling it through the snow, maybe an equivalent process of one-sided accretion might also be conceivable. But whatever the reason, finding the cause for the layering of cometary nuclei may be helpful in finding consensus about their formation process. That being said, I now continue to discuss our scientific results.

Once the development of our tracking algorithm was concluded, we focused on its application to the OSIRIS image sequences. It became quickly apparent however that the image sequences recorded by OSIRIS/NAC were far better suited for our purposes, since OSIRIS/NAC resolved the nucleus and its immediate surroundings in much more detail than OSIRIS/WAC (see Fig. 1.21). While OSIRIS/NAC images generally showed thousands of individual point-source-like dust particles, OSIRIS/WAC images were generally zoomed too far out to distinguish any particles close to the nucleus. Even boulders blended in with the diffuse coma. Consequently, there are several image sequences that we had to disregard, which is also particularly unfortunate because OSIRIS/NAC and OSIRIS/VAC were occasionally recording image sequences simultaneously. This should have made it possible to continue tracking particles in OSIRIS/WAC images that were initially observed by OSIRIS/NAC and thus learn more about how they behave further out in the coma.

Yet as I showed and discussed on pages 94, 96, 98, and 100, we also realized that even with the OSIRIS/NAC image sequences, there are several serious issues that prevented us from using them for our purposes. Ultimately, we decided to focus on four image sequences that showed the most promising results, but that does not mean that the other sequences may not also be analyzed in a similar way. Just like there may be a way to correct for the pointing fluctuation without trackable sidereal objects, there for example also be another way of determining particle-observer distances. Especially the cases where particle tracking was in principle possible, but that did not contain concentrated groups of particle tracks and thus did not allow for associating the particles with the nucleus or for reliable statistics, likely already provide evidence for the emerging

theory that water-driven erosion and CO₂-driven boulder ejection cannot happen simultaneously at the same location. This anti-correlation is not only a consequence of the recently developed WEB-based model, which states that the water-driven erosion is concentrated on the WEBs, which themselves only contain marginal amounts of CO₂-ice (Fulle 2021; Ciarniello et al. 2022), but it was also independently predicted by subsequent thermophysical modeling (Attree et al. 2024a). Finding more evidence for this anti-correlation in the future may therefore be an important contribution.

For our analysis, we concentrated on four image sequences, all recorded within a period of less than a month between December 2015 and early January 2016. These sequences proved to be suitable for our application because they showed high local activity that allowed us to trace concentrated groups of particles back to four suspected source regions on the nucleus surface. These four regions turned out to all lie in vicinity of one another and to even partly overlap. They additionally correlate with other signs of activity and surface changes that were documented within this region, such as dust jets (e. g., Vincent et al. 2016a; Fornasier et al. 2019), bright spots (e. g., Deshapriya et al. 2018; Hasselmann et al. 2019; Fornasier et al. 2023), or retreating scarps (El-Maarry et al. 2017b), and likely lie in an area that exhibited some of the highest gas production rates during the Rosetta mission (Combi et al. 2020; Lauter et al. 2022). And generally, they may be linked to rough terrain or steep slopes, such as scarps, cliffs, or fractures (e. g., Lee et al. 2016; Leon-Dasi et al. 2021) that likely enhance activity (Hofner et al. 2017). This correlation therefore seems highly plausible and for example also agrees with the recent WEB model that predicts that large particles should generally originate from the more consolidated pristine surface areas (e. g., Fulle 2021; Ciarniello et al. 2022).

Associating these particle groups with the nucleus then also allowed us to estimate their particle-observer distance, and in turn derive their (projected) dynamics and (equivalent) sizes. According to the decimeter size range of the particles and the fitted power-law indices ($3.4 \pm 0.3 \leq b \leq 3.8 \pm 0.4$), the particles fit well between the population of particles that were observed further out in the coma ($r \lesssim 1$ cm; $3.1 \pm 0.5 \leq b \leq 3.7$ for submillimeter-sized particles, Fulle et al. 2016b; Merouane et al. 2016) and boulders studied on the surface ($\gtrsim 1$ dm). In particular, they might even reflect an SFD transition of the surface material in the corresponding source regions, as our measured power-law index value lies in between those measured pre-perihelion ($b = 4.1 + 0.2/-0.3$, Deshapriya et al. 2016) and those measured over five months after our observations ($b = 2.6 \pm 0.01$, Hasselmann et al. 2019). This transition might indicate that most of the smaller material was removed from the area, while the larger boulders remained on the surface or fell back onto it, which might be another seasonal effect.

We additionally analyzed the illumination conditions during, and roughly four hours (in local time) before the respective observational periods, as well as the local gravity and centrifugal force. It turned out that the suspected source regions were neither favorable in terms of the local surface acceleration, nor were their local illumination conditions sufficient to explain the observed localized ejection of decimeter-sized particles. It therefore seems likely that the local surface composition and structure

is important for ejecting (large amounts of) decimeter-sized particles, possibly due to an interplay between activity-enhancing topographies and an overabundance of CO₂-ice, which is universally seen as the driver of decimeter-sized particle ejection (e. g., Fulle et al. 2020a; Gundlach et al. 2020; Wesolowski et al. 2020; Ciarniello et al. 2022).

Another phenomenon that may also be linked to the local surface morphology are the observed ejection cones. As discussed on page 104, they are reminiscent of several other phenomena, such as volcanism, cryovolcanism, or geysers. But most notably, similar ejection cones have also been observed in laboratory experiments with illuminated micrometer-sized water-ice particles. These experiments are currently conducted to investigate how the local surface structure affects the activity, and initial results already show a strong correlation. This is in line with our own suspicion that the shape of the ejection cones is significantly influenced by the local surface morphology. Once this dependency is better understood, it may be possible to learn something about the surface morphology of the source regions by studying the respective ejection cones. But already now it seems that narrower ejection cones correspond to surface regions that in one way or another lie “deeper”, than their surroundings, while wider ejection cones indicate flatter source regions.

Regarding the derived particle dynamics, we found that the particle accelerations can generally be well described by the local surface acceleration as a lower bound and the gas drag as an upper bound. But since we cannot precisely constrain most of the parameters that determine the gas drag (such as particle density, drag coefficient, and gas production rate), the upper gas drag limit may result from several factors. Based on conservative estimates however, we find that the local gas production rate may be significantly stronger than more global averages during the observational periods, which again agrees with the idea of locally different surface structures and an overabundance in CO₂-ice.

Additionally, although most of the measured particle accelerations are well-defined by the above-mentioned limits, their distribution also showed that there is a significant number of particles that experience unusually high downward accelerations. While this is in part likely due to statistics and other effects, this downward acceleration may also be evidence of asymmetric outgassing. Yet if true, it sparks the question why only so few particles are affected by it and so strongly at that. It is thus difficult to regard this as clear evidence for asymmetric outgassing. But there is another aspect to consider: in the science paper, the lower bound of the particle accelerations is defined by the *surface* acceleration, but assuming the particles travel with radial velocities of around 0.5 m/s (which is a conservative estimate based on the 2D projection), within an hour, they are already almost two kilometers above the surface (which is a reasonable travel time considering that the observational periods are almost two hours long and that most particles were likely ejected up to half an hour earlier). At that distance, the gravitational acceleration of the nucleus is only around a quarter of what it was at the surface. Accordingly, the more appropriate “lower bound” for the particle accelerations may actually lie up to four times closer to zero, which would put a large amount of measured particle accelerations below this value. In that case, the discrepancy cannot be explained by outliers alone anymore, but is instead systematic. And since the rocket force from asymmetric

outgassing can reasonably be of the same order of magnitude as the nucleus gravity, it may be the most probable explanation.

Although this is only tentative evidence, it may be worth to investigate further, as clear evidence for asymmetric outgassing would immediately tell us something about the particles' ice content and thermal properties, which is also why such research was originally one of the main scientific motivations for this work. For one, if a significant rocket force exists, this means that the heat conduction of the particles is not efficient enough to redistribute the incoming solar energy homogeneously, as that would lead to isotropic outgassing and a net rocket force of zero. Likewise, since the rocket force should act in the anti-solar direction given negligible thermal inertia, the angle between the anti-solar direction and the direction of the rocket force can be used to determine the thermal inertia of a particle if its rotational period and orientation is well-known. Or conversely, if it can be assumed that the thermal inertia of the particle is similar to that of the nucleus, the just mentioned angle can be used to determine the particle's rotational frequency. The magnitude of the rocket force on the other hand would allow us to constrain the ice content of the particle and thus its refractory-to-ice ratio. Yet if no significant rocket forces can be detected, this could either mean that the particles have negligible thermal inertia and are thus outgassing homogeneously, or support the hypothesis that (the outer layers of) coma particles are effectively dehydrated.

But the particle dynamics also revealed something that we did not initially predict: the back-extrapolations of the particle tracks showed that the particles were likely ejected with significant initial velocities on the order of 0.5 m/s. The particles therefore likely gained most of their momentum during their ejection events and afterwards only weakly couple with the gas. Although the latter part is unsurprising, the existence of these initial velocities is an important discovery as it should help to constrain the responsible ejection mechanisms. Notably, several other recent independent studies also postulated or observed similar initial velocities for cometary particles (e. g., Protopapa et al. 2014; Bischoff et al. 2019; Kwon et al. 2023; Lemos et al. 2023; Lemos et al. 2024; Shi et al. 2024), which strongly indicates that initial velocities are essential to the ejection process.

In this regard, I can think of two potential mechanisms: for one, we know that there are diurnal water-cycles where water vapor re-deposits on the night-side of the nucleus or other shadowed areas (e. g., De Sanctis et al. 2015; Ciarniello et al. 2016; Fornasier et al. 2016; Tosi et al. 2019; Hu et al. 2021). Maybe this happens not just on the surface, but also below, where the water-ice fills cracks and holes, and thus seals in the CO₂-ice in deeper surface layers (at least to a certain degree). This might create the necessary environment for the sublimating CO₂-ice to build up enough gas pressure and eject decimeter-sized particles in small "explosions". Such "frost-sealing" may lead to a situation similar to the model of Fulle et al. (2019b) (2019b, 2020a), who argue that the water diffusion inside pebbles turns them into "pressure cookers", allowing them to eject small dust particles; but it may also be corroborated by the recent thermal modeling of Bischoff et al. (2023), which required reduced diffusivity for the gas pressure to overcome the nucleus gravity and tensile strength.

Another option might be that just as with the WEBs, there are also CO₂-ice-enriched blocks (CEBs). While it is currently unclear how the WEBs

formed, their existence cannot be denied. WEBS are therefore formed somehow, so a similar process might also be feasible for CO₂, although CEBs would likely have to be less abundant or smaller. It would also be difficult to confirm their existence, since they would have evaporated long before erosion would expose them to the surface. But if they exist (maybe the “goosebumps” observed by Sierks et al. (2015) and Davidsson et al. (2016) are CEB remnants?), the local overabundance of CO₂-ice may be enough to eject decimeter-sized particles with significant initial velocities.

Finally, we also simulated the observed particle dynamics using an enhanced version of the gas and dust coma model of Marschall et al. (2020b). The simulation results turned out to corroborate all our findings: they reproduced the observed ejection cones and the diffuse dust coma, and in doing so predict particle SFDs and dynamics very similar to our measurements. In particular, they also require an initial velocity on the order of 0.5 m/s to not only reproduce our observations, but also to lift decimeter-sized particles in the first place.

In conclusion, this work allowed us to gain new insights regarding several aspects of comet physics. The obtained particle dynamics showed that the local surface structure and (volatile) composition likely plays a significant role in driving the corresponding activity, and although our results did not provide unequivocal evidence of asymmetric outgassing, they did allow us to discover other unexpected but important phenomena like the ejection cones and especially the initial velocities. We may therefore be a step closer to solving the activity paradox. But to get there, we likely still need to answer many other open questions first. In the context of this work, I suggest to address the following tasks in the future:

- ▶ First and foremost, investigating the cause for the initial velocities should lead to a better understanding of the involved ejection processes. Their existence is therefore likely the most promising lead in solving the activity paradox.
- ▶ Next, asymmetric outgassing remains an interesting phenomenon that can provide valuable insights. Scrutinizing our results further may thus prove fruitful. Another way of detecting it may also be via the rotational frequency of particles, as it may cause them to spin up or down. If it does, it might also be interesting to know if it is capable of disintegrating the particles via rotational fracturing (see also Fulle et al. 2015b). And if the outgassing is isotropic, it might also be possible to detect it via the particles brightness profile, as it should be broader than the PSF. In this case, I also wonder if the generated force could be strong enough to compact the particle interior (which might also happen with surface material, Davidsson et al. 2022b).
- ▶ Regarding rotating particles, it would also be useful to improve the accuracy of the detected particle radiance. This might allow us to fit the rotation periods of oblate rotators, which is currently not possible due to the strong radiance variations (cf. Fig. 4.11). More accurate particle radiance measurements might then even be used as an additional tracking parameter.
- ▶ Since laboratory experiments that investigate how surface properties may influence cometary activity are already underway, a closer

collaboration would be helpful to find out under what conditions the observed ejection cones are recreated.

- ▶ As mentioned on page 106, I already started to review all the studies that determined particle sizes and suggested to re-analyze their data with a single coherent method. I believe this may be useful to the community since it allows for unbiased comparisons. Ideally, this should be coupled with elaborate hypothesis testing to see if power-laws are actually the best model to describe our data.
- ▶ Finally, a more sophisticated thermophysical model that can simulate the simultaneous sublimation of both water- and CO₂-ice (such as those of Pinzón-Rodríguez et al. 2021; Bischoff et al. 2023) would be useful as the basis for our gas and dust coma simulations in the future, as it could help to corroborate the role of CO₂-ice in the activity events that we observed and thus may lead to a better understanding of the initial velocities and the responsible ejection mechanism.

BIBLIOGRAPHY

- A'Hearn, M. F., Belton, M. J. S., Delamere, A., et al. (2005). "Deep Impact: A Large-Scale Active Experiment on a Cometary Nucleus". In: *Space Science Reviews* 117.1, pp. 1–21. doi: 10.1007/s11214-005-3387-3 (cited on page 23).
- A'Hearn, M. F., Belton, M. J. S., Delamere, W. A., et al. (2011). "EPOXI at Comet Hartley 2". In: *Science* 332.6036, pp. 1396–1400. doi: 10.1126/science.1204054 (cited on pages 18, 23, 33, 105).
- El-Abbadi, M. (2023). "Library of Alexandria". In: *Encyclopedia Britannica*. (Visited on 03/04/2024) (cited on page xvi).
- Accomazzo, A., Ferri, P., Lodioli, S., et al. (2016). "Rosetta Following a Living Comet". In: *Acta Astronautica. Space Flight Safety* 126, pp. 190–198. doi: 10.1016/j.actastro.2016.04.023 (cited on page 40).
- Accomazzo, A., Ferri, P., Lodioli, S., et al. (2017). "The Final Year of the Rosetta Mission". In: *Acta Astronautica* 136, pp. 354–359. doi: 10/gnkm7t (cited on page 40).
- Ackroyd, P. (2006). *Newton*. New York : Nan A. Talese/Doubleday (cited on page 6).
- Acton, C. H. (1996). "Ancillary Data Services of NASA's Navigation and Ancillary Information Facility". In: *Planetary and Space Science. Planetary Data System* 44.1, pp. 65–70. doi: 10.1016/0032-0633(95)00107-7 (cited on page 103).
- Adachi, I., Hayashi, C., and Nakazawa, K. (1976). "The Gas Drag Effect on the Elliptic Motion of a Solid Body in the Primordial Solar Nebula". In: *Progress of Theoretical Physics* 56.6, pp. 1756–1771. doi: 10.1143/PTP.56.1756 (cited on page 19).
- Adema, J. (2015). *The Monograph Crisis Revisited*. URL: <https://openreflections.wordpress.com/2015/01/29/the-monograph-crisis-revisited/> (visited on 02/20/2024) (cited on page xiii).
- Adler, M. J. and Doren, C. V. (2014). *How to Read a Book: The Classic Guide to Intelligent Reading*. Simon and Schuster (cited on pages xiii, xiv).
- Afghan, Q., Jones, G. H., Battams, K., et al. (2024). "Characterization of the Dust and Sodium Tails of Comet C/2020 F3 (NEOWISE) from Parker Solar Probe and Amateur Observations". In: *The Planetary Science Journal* 5.12, p. 264. doi: 10.3847/PSJ/ad856b (cited on page 16).
- Agarwal, J., A'Hearn, M. F., Vincent, J.-B., et al. (2016). "Acceleration of Individual, Decimetre-Sized Aggregates in the Lower Coma of Comet 67P/Churyumov-Gerasimenko". In: *Monthly Notices of the Royal Astronomical Society* 462.Suppl 1, S78–S88. doi: 10/gbjgn5. (Visited on 11/19/2021) (cited on pages 34, 53, 57, 73, 75, 99, 107, 115).
- Agarwal, J., Della Corte, V., Feldman, P. D., et al. (2017). "Evidence of Sub-Surface Energy Storage in Comet 67P from the Outburst of 2016 July 03". In: *Monthly Notices of the Royal Astronomical Society* 469.Suppl_2, s606–s625. doi: 10/gfbs3k (cited on page 107).
- Agarwal, J., Kim, Y., Kelley, M. S. P., et al. (2023). *Dust Emission and Dynamics*. doi: 10.48550/arXiv.2309.12759. preprint (cited on pages 3, 15, 16, 21, 22, 34, 93).
- Agarwal, J., Müller, M., Reach, W. T., et al. (2010). "The Dust Trail of Comet 67P/Churyumov-Gerasimenko between 2004 and 2006". In: *Icarus* 207.2, pp. 992–1012. doi: 10.1016/j.icarus.2010.01.003 (cited on page 107).
- Aguilar, C., Ortner, M., and Zerubia, J. (2022). "Small Object Detection and Tracking in Satellite Videos With Motion Informed-CNN and GM-PHD Filter". In: *Frontiers in Signal Processing* 2. doi: 10.3389/frsip.2022.827160 (cited on page 42).
- Airey, S. P., Berrighi, G., and Procopio, D. (2003). "Seeing Through Dust – Tracking Stars from within a Cometary Dust Cloud". In: *Proceedings of the Annual AAS Rocky Mountain Guidance and Control Conference*. Ed. by I. J. Gravseth and R. D. Culp. Vol. 113. Advances in Astronautical Sciences. Breckenridge, Colorado, U.S.A.: American Astronautical Society, p. 19 (cited on page 40).
- Airy, G. B. (1835). "On the Diffraction of an Object-glass with Circular Aperture". In: *Transactions of the Cambridge Philosophical Society* 5, p. 283 (cited on page 50).
- Akiba, K., Beuzekom, M. van, Beveren, V. van, et al. (2023). "Reconstruction of Charged Tracks with Timepix4 ASICs". In: *Journal of Instrumentation* 18.02, P02011. doi: 10.1088/1748-0221/18/02/P02011 (cited on page 43).

- Allan, D. B., Caswell, T., Keim, N. C., et al. (2021). *Soft-Matter/Trackpy: Trackpy v0.5.0*. Zenodo. doi: 10.5281/zenodo.4682814 (cited on page 42).
- Allweiss, W. (1979). "Von der Disputation zur Dissertation. Das Promotionswesen in Deutschland vom Mittelalter bis zum 19. Jahrhundert". In: *Dissertationen in Wissenschaft und Bibliotheken*. Ed. by R. Jung and P. Kaegbein. K. G. Saur, pp. 13–28. doi: 10.1515/9783111325941.13 (cited on page xiv).
- Alstott, J., Bullmore, E., and Plenz, D. (2014). "Powerlaw: A Python Package for Analysis of Heavy-Tailed Distributions". In: *PLOS ONE* 9.1, e85777. doi: 10/gc4n4j (cited on page 109).
- Altwegg, K., Balsiger, H., Bar-Nun, A., et al. (2016). "Prebiotic Chemicals—Amino Acid and Phosphorus—in the Coma of Comet 67P/Churyumov-Gerasimenko". In: *Science Advances* 2.5, e1600285. doi: 10.1126/sciadv.1600285 (cited on page 33).
- Altwegg, K., Balsiger, H., and Fuselier, S. A. (2019). "Cometary Chemistry and the Origin of Icy Solar System Bodies: The View After Rosetta". In: *Annual Review of Astronomy and Astrophysics* 57. Volume 57, 2019, pp. 113–155. doi: 10.1146/annurev-astro-091918-104409 (cited on page 3).
- Anderson, T., Alexander, I., and Saunders, G. (2020). "An Examination of Education-Based Dissertation Macrostructures". In: *Journal of English for Academic Purposes* 45, p. 100845. doi: 10.1016/j.jeap.2020.100845. (Visited on 02/23/2024) (cited on page xv).
- Anderson, T. and Okuda, T. (2021). "Temporal Change in Dissertation Macrostructures". In: *English for Specific Purposes* 64, pp. 1–12. doi: 10.1016/j.esp.2021.06.001. (Visited on 02/23/2024) (cited on page xv).
- Annex, A. M., Pearson, B., Seignovert, B., et al. (2020). "SpicyPy: A Pythonic Wrapper for the SPICE Toolkit". In: *Journal of Open Source Software* 5.46, p. 2050. doi: 10.21105/joss.02050 (cited on page 121).
- Arakawa, M., Saiki, T., Wada, K., et al. (2020). "An Artificial Impact on the Asteroid (162173) Ryugu Formed a Crater in the Gravity-Dominated Regime". In: *Science* 368.6486, pp. 67–71. doi: 10/dp6q (cited on page 105).
- Arakawa, M., Wada, K., Saiki, T., et al. (2017). "Scientific Objectives of Small Carry-on Impactor (SCI) and Deployable Camera 3 Digital (DCAM3-D): Observation of an Ejecta Curtain and a Crater Formed on the Surface of Ryugu by an Artificial High-Velocity Impact". In: *Space Science Reviews* 208.1-4, pp. 187–212. doi: 10/gbmzwx (cited on page 105).
- Aristotle (1952). *Meteorologica*. Trans. by H. D. P. Lee. Cambridge, MA: Harvard University Press (cited on page 4).
- Armato, D. (2012). *What Was a University Press?: The Monograph*. Page. URL: <https://www.upress.umn.edu/about-us/history-and-fact-sheet-folder/what-was-a-university-press-1/iii.-the-monograph> (visited on 02/20/2024) (cited on page xiii).
- Asher, D. J., Bailey, M. E., Hahn, G., et al. (1994). "Asteroid 5335 Damocles and Its Implications for Cometary Dynamics". In: *Monthly Notices of the Royal Astronomical Society* 267.1, pp. 26–42. doi: 10.1093/mnras/267.1.26. (Visited on 04/29/2024) (cited on page 14).
- Asphaug, E. (2009). "Growth and Evolution of Asteroids". In: *Annual Review of Earth and Planetary Sciences* 37.1, pp. 413–448. doi: 10.1146/annurev.earth.36.031207.124214. (Visited on 03/11/2024) (cited on page 3).
- Asphaug, E., Collins, G., and Jutzi, M. (2015). "Global-Scale Impacts". In: *Asteroids IV*. Ed. by W. F. Bottke, F. E. DeMeo, and P. Michel. University of Arizona Press. doi: 10.2458/azu_uapress_9780816532131-ch034 (cited on page 3).
- Atkinson, D. (1998). *Scientific Discourse in Sociohistorical Context: The Philosophical Transactions of the Royal Society of London, 1675-1975*. Routledge (cited on page xiv).
- Attree, N., Schuckart, C., Bischoff, D., et al. (2024a). "Localized Ejection of Dust and Chunks on Comet 67P/Churyumov-Gerasimenko: Testing How Comets Work". In: *Monthly Notices of the Royal Astronomical Society* 535.1, pp. 65–77. doi: 10.1093/mnras/stae2315 (cited on pages 17, 102, 156).
- Attree, N., Groussin, O., Jorda, L., et al. (2018a). "Tensile Strength of 67P/Churyumov-Gerasimenko Nucleus Material from Overhangs". In: *Astronomy & Astrophysics* 611, A33. doi: 10/gdmz2r (cited on pages 17, 31, 105, 107).
- Attree, N., Groussin, O., Jorda, L., et al. (2018b). "Thermal Fracturing on Comets - Applications to 67P/Churyumov-Gerasimenko". In: *Astronomy & Astrophysics* 610, A76. doi: 10.1051/0004-6361/201731937 (cited on page 107).

- Attree, N., Gutiérrez, P., Groussin, O., et al. (2024b). "Varying Water Activity and Momentum Transfer on Comet 67P/Churyumov-Gerasimenko from Its Non-Gravitational Forces and Torques". In: *Astronomy & Astrophysics* 690, A82. doi: 10.1051/0004-6361/202450728 (cited on pages 12, 16, 29).
- Attree, N., Jorda, L., Groussin, O., et al. (2019). "Constraining Models of Activity on Comet 67P/Churyumov-Gerasimenko with Rosetta Trajectory, Rotation, and Water Production Measurements". In: *Astronomy & Astrophysics* 630, A18. doi: 10.1051/0004-6361/201834415 (cited on pages 12, 16, 29).
- Attree, N., Jorda, L., Groussin, O., et al. (2023). "Activity Distribution of Comet 67P/Churyumov-Gerasimenko from Combined Measurements of Non-Gravitational Forces and Torques". In: *Astronomy & Astrophysics* 670, A170. doi: 10.1051/0004-6361/202245243 (cited on pages 12, 16, 29).
- Auger, A.-T., Groussin, O., Jorda, L., et al. (2015). "Geomorphology of the Imhotep Region on Comet 67P/Churyumov-Gerasimenko from OSIRIS Observations". In: *Astronomy & Astrophysics* 583, A35. doi: 10.1051/0004-6361/201525947 (cited on page 107).
- Autry, M. K. and Wojcik, K. (2016). *Dissertations at NC State University: A Guide to Understanding What Dissertations Look Like*. Tech. rep. NC State University (cited on page xv).
- Azzalini, L. J. and Izzo, D. (2023). "Tracking Particles Ejected from Active Asteroid Bennu with Event-Based Vision". In: *Materials Research Proceedings*. Millersville PA, USA: Materials Research Forum LLC. doi: 10.21741/9781644902813-124 (cited on page 39).
- Bailey, M. E., Chambers, J. E., and Hahn, G. (1992). "Origin of Sungrazers: A Frequent Cometary End-State". In: *Astronomy and Astrophysics* 257, pp. 315–322 (cited on page 10).
- Bailey, M. E., Clube, S. V. M., Napier, W. M., et al. (1990). *The Origin of Comets*. Elsevier Science & Technology Books (cited on page 11).
- Baines, M. J., Williams, I. P., Asebiomo, A. S., et al. (1965). "Resistance to the Motion of a Small Sphere Moving Through a Gas". In: *Monthly Notices of the Royal Astronomical Society* 130.1, pp. 63–74. doi: 10.1093/mnras/130.1.63 (cited on page 22).
- Ball, P. (2017). "It's Not Just You: Science Papers Are Getting Harder to Read". In: *Nature*. doi: 10.1038/nature.2017.21751 (cited on page xiv).
- Balsiger, H., Altwegg, K., Bochsler, P., et al. (2007). "Rosina – Rosetta Orbiter Spectrometer for Ion and Neutral Analysis". In: *Space Science Reviews* 128.1, pp. 745–801. doi: 10.1007/s11214-006-8335-3 (cited on pages 24, 120).
- Bannister, M. T., Kavelaars, J. J., Petit, J.-M., et al. (2016). "The Outer Solar System Origins Survey. I. Design And First-Quarter Discoveries". In: *The Astronomical Journal* 152.3, p. 70. doi: 10.3847/0004-6256/152/3/70. (Visited on 11/19/2021) (cited on pages 41, 53).
- Barbary, K. (2016). "SEP: Source Extractor as a Library". In: *The Journal of Open Source Software* 1.6, p. 58. doi: 10.21105/joss.00058. (Visited on 11/19/2021) (cited on pages 55–58, 95).
- Barboianu, C. (2022). *Galileo and the Birth of Modern Science*. <https://www.thecollector.com/galileo-modern-science/> (cited on page 4).
- Bardyn, A., Baklouti, D., Cottin, H., et al. (2017). "Carbon-Rich Dust in Comet 67P/Churyumov-Gerasimenko Measured by COSIMA/Rosetta". In: *Monthly Notices of the Royal Astronomical Society* 469.Suppl_2, S712–S722. doi: 10.1093/mnras/stx2640 (cited on page 31).
- Baron, N. S. (2015). *Words Onscreen: The Fate of Reading in a Digital World*. Oxford University Press (cited on page xvi).
- Baron, N. S., Calixte, R. M., and Havewala, M. (2017). "The Persistence of Print among University Students: An Exploratory Study". In: *Telematics and Informatics* 34.5, pp. 590–604. doi: 10.1016/j.tele.2016.11.008 (cited on page xvii).
- Baron, N. S. and Mangan, A. (2021). "Doing the Reading: The Decline of Long Long-Form Reading in Higher Education". In: *Poetics Today* 42.2, pp. 253–279. doi: 10.1215/03335372-8883248 (cited on page xvi).
- Batygin, K., Brown, M. E., and Fraser, W. C. (2011). "Retention Of A Primordial Cold Classical Kuiper Belt In An Instability-Driven Model Of Solar System Formation". In: *The Astrophysical Journal* 738.1, p. 13. doi: 10.1088/0004-637X/738/1/13. (Visited on 04/08/2024) (cited on page 8).
- Bazerman, C. (1988). *Shaping Written Knowledge: The Genre and Activity of the Experimental Article in Science*. University of Wisconsin Press. 376 pp. (cited on page xiv).

- Beard, S. M., MacGillivray, H. T., and Thanisch, P. F. (1990). "The COSMOS System for Crowded-Field Analysis of Digitized Photographie Plate Scans". In: *Monthly Notices of the Royal Astronomical Society* 247, pp. 311–321 (cited on page 57).
- Beitz, E., Blum, J., Parisi, M. G., et al. (2016). "The Collisional Evolution Of Undifferentiated Asteroids And The Formation Of Chondritic Meteoroids". In: *The Astrophysical Journal* 824.1, p. 12. doi: 10.3847/0004-637X/824/1/12 (cited on page 155).
- Belton, M. J. S. (2010). "Cometary Activity, Active Areas, and a Mechanism for Collimated Outflows on 1P, 9P, 19P, and 81P". In: *Icarus* 210.2, pp. 881–897. doi: 10.1016/j.icarus.2010.07.007 (cited on page 119).
- Belton, M. J. S., Thomas, P., Veverka, J., et al. (2007). "The Internal Structure of Jupiter Family Cometary Nuclei from Deep Impact Observations: The "Talps" or "Layered Pile" Model". In: *Icarus*. Deep Impact Mission to Comet 9P/Tempel 1, Part 1 187.1, pp. 332–344. doi: 10.1016/j.icarus.2006.09.005 (cited on page 20).
- Belton, M. J. S., Zou, X.-D., Li, J.-Y., et al. (2018). "On the Origin of Internal Layers in Comet Nuclei". In: *Icarus* 314, pp. 364–375. doi: 10.1016/j.icarus.2018.05.031 (cited on page 20).
- Belyaev, N. A., Kresák, L., Pittich, E. M., et al. (1986). *Catalogue of Short-Period Comets*. Veda, Bratislava: Astronomical Institute, Slovak Academy of Sciences (cited on page 26).
- Bentley, M. S., Schmied, R., Mannel, T., et al. (2016). "Aggregate Dust Particles at Comet 67P/Churyumov–Gerasimenko". In: *Nature* 537.7618, pp. 73–75. doi: 10.1038/nature19091 (cited on page 32).
- Berne, A., Simons, M., Keane, J. T., et al. (2024). "Jet Activity on Enceladus Linked to Tidally Driven Strike-Slip Motion along Tiger Stripes". In: *Nature Geoscience*, pp. 1–7. doi: 10.1038/s41561-024-01418-0 (cited on page 104).
- Bertin, E. (2023). *Isophotal Measurements*. URL: <https://web.archive.org/web/20240219035013/https://astromatic.github.io/sexttractor/Position.html> (cited on page 64).
- Bertin, E. and Arnouts, S. (1996). "SExttractor: Software for Source Extraction". In: *Astronomy and Astrophysics Supplement Series* 117.2, pp. 393–404. doi: 10.1051/aas:1996164. (Visited on 11/19/2021) (cited on pages 53, 55–58, 95).
- Bertin, E., Schefer, M., Apostolakos, N., et al. (2020). "The SourceXtractor++ Software". In: *Astronomical Data Analysis Software and Systems XXIX* 527, p. 461 (cited on page 58).
- Bertini, I., Gutiérrez, P. J., Lara, L. M., et al. (2015). "Search for Satellites near Comet 67P/Churyumov–Gerasimenko Using Rosetta/OSIRIS Images". In: *Astronomy & Astrophysics* 583, A19. doi: 10.1051/0004-6361/201525979 (cited on page 53).
- Bessel, F. W. (1836a). "Bemerkungen Über Mögliche Unzulänglichkeit Der Die Anziehungen Allein Berücksichtigenden Theorie Der Kometen. Von Herrn Geheimen-Rath u Ritter Bessel". In: *Astronomische Nachrichten* 13, p. 345. doi: 10.1002/asna.18360132302 (cited on page 7).
- Bessel, F. W. (1836b). "Beobachtungen Über Die Physische Beschaffenheit Des Halley'schen Kometen Und Dadurch Veranlasste Bemerkungen". In: *Astronomische Nachrichten* 13.13-15, pp. 185–232. doi: 10.1002/asna.18360131302 (cited on page 16).
- Beth, A., Galand, M., Wedlund, C. S., et al. (2022). *Cometary Ionospheres: An Updated Tutorial*. doi: 10.48550/arXiv.2211.03868. URL: <http://arxiv.org/abs/2211.03868> (cited on pages 15, 16).
- Biele, J., Vincent, J.-B., and Knollenberg, J. (2022). "Mechanical Properties of Cometary Surfaces". In: *Universe* 8.9, p. 487. doi: 10.3390/universe8090487 (cited on page 17).
- Biermann, L. (1951). "Kometenschweife Und Solare Korpuskularstrahlung". In: *Zeitschrift fur Astrophysik* 29, p. 274 (cited on page 16).
- Biermann, L. (1952). "Physical Processes in Comet Tails and Their Relation to Solar Activity". In: *La Physique Des Comètes: Communications Présentées Au Quatrième Colloque International d'astrophysique*. Vol. 4. Liège: Société Royale des Sciences de Liège, pp. 251–262 (cited on page 16).
- Bird, G. A. (1994). *Molecular Gas Dynamics And The Direct Simulation Of Gas Flows*. Oxford: Clarendon Press (cited on pages 22, 117, 120).
- Birkett, K. S. (2017). "Investigating the Neutral Sodium Emissions Observed at Comets". Doctoral. UCL (University College London) (cited on page 16).
- Bischoff, D., Gundlach, B., Neuhaus, M., et al. (2019). "Experiments on Cometary Activity: Ejection of Dust Aggregates from a Sublimating Water-Ice Surface". In: *Monthly Notices of the Royal Astronomical Society* 483.1, pp. 1202–1210. doi: 10/gnh7hq (cited on pages 119, 125, 158).

- Bischoff, D., Kreuzig, C., Haack, D., et al. (2020). "Sticky or Not Sticky? Measurements of the Tensile Strength of Microgranular Organic Materials". In: *Monthly Notices of the Royal Astronomical Society* 497.3, pp. 2517–2528. doi: 10.1093/mnras/staa2126 (cited on page 17).
- Bischoff, D., Schuckart, C., Attree, N., et al. (2023). "A Quantitative Description of Comet 67P's Dust and Gas Production Remains Enigmatic". In: *Monthly Notices of the Royal Astronomical Society* 523.4, pp. 5171–5186. doi: 10.1093/mnras/stad1766 (cited on pages 3, 16–18, 93, 120, 158, 160).
- Bishop, C. (2006). *Pattern Recognition and Machine Learning*. Springer Science+Business Media (cited on page 76).
- Bistafa, S. R. (2017). "On the Development of the Navier-Stokes Equation by Navier". In: *Revista Brasileira de Ensino de Física* 40. doi: 10.1590/1806-9126-RBEF-2017-0239 (cited on page 21).
- Biver, N., Bockelée-Morvan, D., Hofstadter, M., et al. (2019). "Long-Term Monitoring of the Outgassing and Composition of Comet 67P/Churyumov-Gerasimenko with the Rosetta/MIRO Instrument". In: *Astronomy & Astrophysics* 630, A19. doi: 10.1051/0004-6361/201834960 (cited on page 33).
- Blackford, J. R. (2007). "Sintering and Microstructure of Ice: A Review". In: *Journal of Physics D: Applied Physics* 40.21, R355. doi: 10.1088/0022-3727/40/21/R02 (cited on page 18).
- Blackman, S. (2004). "Multiple Hypothesis Tracking for Multiple Target Tracking". In: *IEEE Aerospace and Electronic Systems Magazine* 19.1, pp. 5–18. doi: 10.1109/MAES.2004.1263228. (Visited on 05/03/2024) (cited on page 38).
- Blum, J., Bischoff, D., and Gundlach, B. (2022). "Formation of Comets". In: *Universe* 8.7, p. 381. doi: 10.3390/universe8070381 (cited on pages 3, 17, 19, 20, 32, 106, 115, 154).
- Blum, J., Gundlach, B., Mühle, S., et al. (2014). "Comets Formed in Solar-Nebula Instabilities! – An Experimental and Modeling Attempt to Relate the Activity of Comets to Their Formation Process". In: *Icarus* 235, pp. 156–169. doi: 10.1016/j.icarus.2014.03.016 (cited on pages 16, 17).
- Blum, J., Gundlach, B., Mühle, S., et al. (2015). "Corrigendum to "Comets Formed in Solar-Nebula Instabilities! – An Experimental and Modeling Attempt to Relate the Activity of Comets to Their Formation Process" [Icarus 235 (2014) 156–169]". In: *Icarus* 248, pp. 135–136. doi: 10.1016/j.icarus.2014.10.025 (cited on page 17).
- Blum, J., Gundlach, B., Krause, M., et al. (2017). "Evidence for the Formation of Comet 67P/Churyumov-Gerasimenko through Gravitational Collapse of a Bound Clump of Pebbles". In: *Monthly Notices of the Royal Astronomical Society* 469.Suppl_2, S755–S773. doi: 10.1093/mnras/stx2741. (Visited on 11/19/2021) (cited on pages 19, 20, 32, 77, 106, 107, 115, 154, 155).
- Blum, J. and Münch, M. (1993). "Experimental Investigations on Aggregate-Aggregate Collisions in the Early Solar Nebula". In: *Icarus* 106.1, pp. 151–167. doi: 10.1006/icar.1993.1163 (cited on page 19).
- Blum, J., Schräpler, R., Davidsson, B. J. R., et al. (2006). "The Physics of Protoplanetary Dust Agglomerates. I. Mechanical Properties and Relations to Primitive Bodies in the Solar System". In: *The Astrophysical Journal* 652.2, p. 1768. doi: 10.1086/508017 (cited on page 17).
- Blum, J. and Wurm, G. (2008). "The Growth Mechanisms of Macroscopic Bodies in Protoplanetary Disks". In: *Annual Review of Astronomy and Astrophysics* 46. Volume 46, 2008, pp. 21–56. doi: 10.1146/annurev.astro.46.060407.145152 (cited on page 19).
- Bochkovskiy, A., Wang, C.-Y., and Liao, H.-Y. M. (2020). *YOLOv4: Optimal Speed and Accuracy of Object Detection*. doi: 10.48550/arXiv.2004.10934. URL: <http://arxiv.org/abs/2004.10934> (cited on page 42).
- Bockelée-Morvan, D. and Biver, N. (2017). "The Composition of Cometary Ices". In: *Philosophical Transactions of the Royal Society A: Mathematical, Physical and Engineering Sciences* 375.2097, p. 20160252. doi: 10.1098/rsta.2016.0252 (cited on page 3).
- Bockelée-Morvan, D., Debout, V., Erard, S., et al. (2015). "First Observations of H₂O and CO₂ Vapor in Comet 67P/Churyumov-Gerasimenko Made by VIRTIS Onboard Rosetta". In: *Astronomy & Astrophysics* 583, A6. doi: 10.1051/0004-6361/201526303 (cited on page 30).
- Boehnhardt, H. (2003). "The Anti-Tail of Comet C/1995 O1 (Hale-Bopp) in 1997/1998". In: *Earth, Moon, and Planets* 93.1, pp. 19–35. doi: 10.1023/B:M00N.0000034496.28985.ef (cited on page 15).
- Boice, D. C., Soderblom, L. A., Britt, D. T., et al. (2002). "The Deep Space 1 Encounter with Comet 19p/Borrelly". In: *Earth, Moon, and Planets* 89.1, pp. 301–324. doi: 10.1023/A:1021519124588 (cited on page 23).
- Boltzmann, L. (1872). *Weitere Studien über das Wärmegleichgewicht unter Gasmolekülen: vorgelegt in der Sitzung am 10. October 1872*. k. und k. Hof- und Staatsdr. (cited on page 21).

- Bond, P. (2020). *Rosetta: The Remarkable Story of Europe's Comet Explorer*. Cham: Springer International Publishing (cited on page 23).
- Bonnet, R. M. (1985). "The New Mandatory Scientific Programme for ESA". In: *ESA Bulletin-European Space Agency* 43, pp. 8–13 (cited on pages 3, 22).
- Borisov, G. V. and Shustov, B. M. (2021). "Discovery of the First Interstellar Comet and the Spatial Density of Interstellar Objects in the Solar Neighborhood". In: *Solar System Research* 55.2, pp. 124–131. doi: 10.1134/S0038094621020027. (Visited on 04/29/2024) (cited on page 14).
- Bosch, S., Albee, B., and Romaine, S. (2022). *Are We There Yet? | Periodicals Price Survey 2022*. URL: <https://www.libraryjournal.com/story/Are-We-There-Yet-Periodicals-Price-Survey-2022> (visited on 02/21/2024) (cited on page xiii).
- Bottke, W. F., Moorhead, A. V., Connolly, H. C., et al. (2020). "Meteoroid Impacts as a Source of Bennu's Particle Ejection Events". In: *Journal of Geophysical Research: Planets* 125.8. doi: 10/gnh596 (cited on page 14).
- Bottke Jr., W. F., Vokrouhlický, D., Rubincam, D. P., et al. (2006). "The Yarkovsky and Yorp Effects: Implications for Asteroid Dynamics". In: *Annual Review of Earth and Planetary Sciences* 34, pp. 157–191. doi: 10.1146/annurev.earth.34.031405.125154 (cited on page 16).
- Box, G. E. P. (1976). "Science and Statistics". In: *Journal of the American Statistical Association* 71.356, pp. 791–799. doi: 10.2307/2286841 (cited on page 83).
- Boyer, C. B. (B. (1959). *The Rainbow from Myth to Mathematics*. New York, T. Yoseloff (cited on page 4).
- Bradley, L., Sipőcz, B., Robitaille, T., et al. (2022). *Astropy/Photutils: 1.6.0*. Zenodo. doi: 10.5281/zenodo.7419741 (cited on page 58).
- Brahe, T. (1588). *De Mundi Aetherei Recentioribus Phaenomenis Liber Secundus*. Uraniborg (cited on page 4).
- Brandt, J. C. (2014). "Physics and Chemistry of Comets". In: *Encyclopedia of the Solar System (Third Edition)*. Ed. by T. Spohn, D. Breuer, and T. V. Johnson. Boston: Elsevier, pp. 683–703. doi: 10.1016/B978-0-12-415845-0.00030-X; <https://web.archive.org/web/20240517112902/https://www.sciencedirect.com/science/article/abs/pii/B978012415845000030X> (cited on pages 15, 16).
- Bringinghurst, R. (2004). *The Elements of Typographic Style*. Hartley & Marks, Publishers (cited on page xviii).
- Brisset, J., Heißelmann, D., Kothe, S., et al. (2016). "Submillimetre-Sized Dust Aggregate Collision and Growth Properties - Experimental Study of a Multi-Particle System on a Suborbital Rocket". In: *Astronomy & Astrophysics* 593, A3. doi: 10.1051/0004-6361/201527288 (cited on page 19).
- Brown, M. E. (2001). "The Inclination Distribution of the Kuiper Belt". In: *The Astronomical Journal* 121.5, p. 2804. doi: 10.1086/320391. (Visited on 04/06/2024) (cited on page 8).
- Brown, W. K. (1989). "A Theory of Sequential Fragmentation and Its Astronomical Applications". In: *Journal of Astrophysics and Astronomy* 10.1, pp. 89–112. doi: 10.1007/BF02714980 (cited on page 107).
- Brownlee, D. E. (2014). "The Stardust Mission: Analyzing Samples from the Edge of the Solar System". In: *Annual Review of Earth and Planetary Sciences* 42. Volume 42, 2014, pp. 179–205. doi: 10.1146/annurev-earth-050212-124203 (cited on page 23).
- Brownlee, D. E., Horz, F., Newburn, R. L., et al. (2004). "Surface of Young Jupiter Family Comet 81P/Wild 2: View from the Stardust Spacecraft". In: *Science* 304.5678, pp. 1764–1769. doi: 10.1126/science.1097899 (cited on page 23).
- Brownlee, D. E., Tsou, P., Anderson, J. D., et al. (2003). "Stardust: Comet and Interstellar Dust Sample Return Mission". In: *Journal of Geophysical Research: Planets* 108.E10. doi: 10.1029/2003JE002087 (cited on page 23).
- Brownlee, D. E., Tsou, P., Aléon, J., et al. (2006). "Comet 81P/Wild 2 Under a Microscope". In: *Science* 314.5806, pp. 1711–1716. doi: 10.1126/science.1135840 (cited on page 23).
- Budge, E. A. W. (1913). *The Rosetta Stone*. London: British Museum (cited on page 23).
- Buemi, M., Landi, A., and Procopio, D. (2000). "Autonomous Star Tracker for Rosetta". In: *4th ESA International Conference. Spacecraft Guidance, Navigation and Control Systems*, p. 9 (cited on page 40).
- Buranyi, S. (2017). "Is the Staggeringly Profitable Business of Scientific Publishing Bad for Science?" In: *The Guardian*. (Visited on 02/20/2024) (cited on page xiii).
- Burger, W. and Burge, M. J. (2009). *Principles of Digital Image Processing: Fundamental Techniques*. Undergraduate Topics in Computer Science. London: Springer (cited on pages 52, 56, 58).
- Burns, J. A., Lamy, P. L., and Soter, S. (1979). "Radiation Forces on Small Particles in the Solar System". In: *Icarus* 40.1, pp. 1–48. doi: 10.1016/0019-1035(79)90050-2 (cited on page 15).

- Cairo, A. (2012). *The Functional Art: An Introduction to Information Graphics and Visualization*. New Riders. 546 pp. (cited on page xviii).
- Cambianica, P., Cremonese, G., Fulle, M., et al. (2021). "Long-Term Measurements of the Erosion and Accretion of Dust Deposits on Comet 67P/Churyumov–Gerasimenko with the OSIRIS Instrument". In: *Monthly Notices of the Royal Astronomical Society* 504.2, pp. 2895–2910. doi: 10.1093/mnras/stab950 (cited on page 30).
- Cambianica, P., Cremonese, G., Naletto, G., et al. (2019). "Quantitative Analysis of Isolated Boulder Fields on Comet 67P/Churyumov-Gerasimenko". In: *Astronomy & Astrophysics* 630, A15. doi: 10.1051/0004-6361/201834775 (cited on page 107).
- Cambianica, P., Fulle, M., Cremonese, G., et al. (2020). "Time Evolution of Dust Deposits in the Hapi Region of Comet 67P/Churyumov-Gerasimenko". In: *Astronomy & Astrophysics* 636, A91. doi: 10.1051/0004-6361/202037485 (cited on pages 30, 32, 113, 115).
- Cameron, A. G. W. (1962). "The Formation of the Sun and Planets". In: *Icarus* 1.1, pp. 13–69. doi: 10.1016/0019-1035(62)90005-2 (cited on page 7).
- Canny, J. (1986). "A Computational Approach to Edge Detection". In: *IEEE Transactions on Pattern Analysis and Machine Intelligence* 6, pp. 679–698. doi: 10.1109/tpami.1986.4767851 (cited on page 53).
- Carr, C., Cupido, E., Lee, C. G. Y., et al. (2007). "RPC: The Rosetta Plasma Consortium". In: *Space Science Reviews* 128.1, pp. 629–647. doi: 10.1007/s11214-006-9136-4 (cited on page 25).
- Carson, A. (2017). "Owning My Masters: The Rhetorics of Rhymes & Revolutions". PhD thesis. Clemson University (cited on page xiv).
- Carusi, A., Kresak, L., Perozzi, E., et al. (1985). *Long-Term Evolution of Short-Period Comets* (cited on page 26).
- Carusi, A., Kresak, L., Perozzi, E., et al. (1987a). "High-Order Librations of Halley-Type Comets". In: *Astronomy and Astrophysics* 187, p. 899 (cited on page 12).
- Carusi, A., Kresák, L., Perozzi, E., et al. (1987b). "Long-Term Resonances and Orbital Evolutions of Halley-type Comets." In: *Publications of the Astronomical Institute of the Czechoslovak Academy of Sciences* 2, pp. 29–32 (cited on page 12).
- Caspar, M. and Hellman, C. D. (1993). *Kepler*. Courier Corporation (cited on page 4).
- Cassini, G. D. (1681). *Observations sur la Comete qui a paru au mois de Decembre 1680 et en Janvier 1681*. Paris: Michallet (cited on page 5).
- Cauchy, A.-L. (1846). "Méthodes nouvelles pour la détermination des orbites des corps célestes, et, en particulier, des comètes". In: *Oeuvres complètes d'Augustin Cauchy*. Vol. 10. 1. Paris: Gauthier-Villars et fils, pp. 196–202 (cited on page 7).
- Chenouard, N., Smal, I., de Chaumont, F., et al. (2014). "Objective Comparison of Particle Tracking Methods". In: *Nature Methods* 11.3, pp. 281–289. doi: 10.1038/nmeth.2808. (Visited on 11/19/2021) (cited on pages 42, 53).
- Chesley, S. R., French, A. S., Davis, A. B., et al. (2020). "Trajectory Estimation for Particles Observed in the Vicinity of (101955) Bennu". In: *Journal of Geophysical Research: Planets* 125.9. doi: 10.1029/2019je006363. (Visited on 11/19/2021) (cited on pages 22, 53, 99, 115).
- Chiang, E. I. and Brown, M. E. (1999). "Keck Pencil-Beam Survey for Faint Kuiper Belt Objects". In: *The Astronomical Journal* 118.3, p. 1411. doi: 10.1086/301005. (Visited on 04/08/2024) (cited on page 10).
- Chong, S. W. and Johnson, N., eds. (2022). *Landscapes and Narratives of PhD by Publication: Demystifying Students' and Supervisors' Perspectives*. Cham: Springer International Publishing (cited on page xiii).
- Choukroun, M., Keilm, S., Schloerb, F. P., et al. (2015). "Dark Side of Comet 67P/Churyumov-Gerasimenko in Aug.–Oct. 2014 - MIRO/Rosetta Continuum Observations of Polar Night in the Southern Regions". In: *Astronomy & Astrophysics* 583, A28. doi: 10.1051/0004-6361/201526181 (cited on page 118).
- Choukroun, M., Altwegg, K., Kührt, E., et al. (2020). "Dust-to-Gas and Refractory-to-Ice Mass Ratios of Comet 67P/Churyumov-Gerasimenko from Rosetta Observations". In: *Space Science Reviews* 216.3, p. 44. doi: 10.1007/s11214-020-00662-1. (Visited on 11/19/2021) (cited on pages 27, 51, 115).
- Christian, J. A. and Crassidis, J. L. (2021). "Star Identification and Attitude Determination With Projective Cameras". In: *IEEE Access* 9, pp. 25768–25794. doi: 10/gn38fq (cited on page 40).
- Ciarletti, V., Herique, A., Lasue, J., et al. (2017). "CONSERT Constrains the Internal Structure of 67P at a Few Metres Size Scale". In: *Monthly Notices of the Royal Astronomical Society* 469.Suppl_2, S805–S817. doi: 10.1093/mnras/stx3132 (cited on page 27).

- Ciarniello, M., Fulle, M., Tosi, F., et al. (2023). "Comparison of a Pebbles-Based Model with the Observed Evolution of the Water and Carbon Dioxide Outgassing of Comet 67P/Churyumov-Gerasimenko". In: *Monthly Notices of the Royal Astronomical Society* 523.4, pp. 5841–5852. doi: 10.1093/mnras/stad1663 (cited on pages 18, 30, 32, 33).
- Ciarniello, M., Fulle, M., Raponi, A., et al. (2022). "Macro and Micro Structures of Pebble-Made Cometary Nuclei Reconciled by Seasonal Evolution". In: *Nature Astronomy*, pp. 1–8. doi: 10.1038/s41550-022-01625-y (cited on pages 17, 18, 30, 32, 93, 103, 106, 107, 111, 115, 125, 156, 157).
- Ciarniello, M., Raponi, A., Capaccioni, F., et al. (2016). "The Global Surface Composition of 67P/Churyumov-Gerasimenko Nucleus by Rosetta/VIRTIS. II) Diurnal and Seasonal Variability". In: *Monthly Notices of the Royal Astronomical Society* 462.Suppl_1, S443–S458. doi: 10.1093/mnras/stw3177 (cited on pages 30, 158).
- Cigala, V., Kueppers, U., Fernández, J. J. P., et al. (2021). "Linking Gas and Particle Ejection Dynamics to Boundary Conditions in Scaled Shock-Tube Experiments". In: *Bulletin of Volcanology* 83.8, p. 53. doi: 10.1007/s00445-021-01473-0 (cited on page 105).
- Cigala, V., Kueppers, U., Peña Fernández, J. J., et al. (2017). "The Dynamics of Volcanic Jets: Temporal Evolution of Particles Exit Velocity from Shock-Tube Experiments". In: *Journal of Geophysical Research: Solid Earth* 122.8, pp. 6031–6045. doi: 10.1002/2017JB014149 (cited on page 105).
- Clairaut, A.-C. (1760). *Théorie du mouvement des comètes* (cited on page 6).
- Clark, B. C., Green, S. F., Economou, T. E., et al. (2004). "Release and Fragmentation of Aggregates to Produce Heterogeneous, Lumpy Coma Streams". In: *Journal of Geophysical Research: Planets* 109.E12. doi: 10.1029/2004JE002319 (cited on page 107).
- Clark, D. and Hill, M. (2020). "Researchers' Perspectives on the Purpose and Value of the Monograph". In: *Commonplace*. doi: 10.21428/6ffd8432.6489b1ba. (Visited on 02/16/2024) (cited on pages xiii–xv).
- Clauset, A., Shalizi, C. R., and Newman, M. E. J. (2009). "Power-Law Distributions in Empirical Data". In: *SIAM Review* 51.4, pp. 661–703. doi: 10/dd7xhj (cited on page 109).
- Clinton, V. (2019). "Reading from Paper Compared to Screens: A Systematic Review and Meta-Analysis". In: *Journal of Research in Reading* 42.2, pp. 288–325. doi: 10.1111/1467-9817.12269. (Visited on 03/08/2024) (cited on page xvii).
- Cochran, A., Veverka, J., Bell, J., et al. (2003). "The Comet Nucleus Tour (Contour)". In: *Cometary Science after Hale-Bopp*. Ed. by H. Boehnhardt, M. Combi, M. R. Kidger, et al. Dordrecht: Springer Netherlands, pp. 289–300. doi: 10.1007/978-94-017-1086-2_13 (cited on page 23).
- Cochran, A. L., Levasseur-Regourd, A.-C., Cordiner, M., et al. (2015). "The Composition of Comets". In: *Space Science Reviews* 197.1, pp. 9–46. doi: 10.1007/s11214-015-0183-6 (cited on page 3).
- Codogno, M. (2013). *Parole matematiche: moda*. URL: <https://web.archive.org/web/20230320144023/https://www.ilpost.it/mauriziocodogno/2013/03/12/parole-matematiche-moda/#more-441061> (cited on page 56).
- Colangeli, L., Lopez Moreno, J. J., Palumbo, P., et al. (2007). "GIADA: The Grain Impact Analyser and Dust Accumulator for the Rosetta Space Mission". In: *Advances in Space Research* 39.3, pp. 446–450. doi: 10.1016/j.asr.2006.12.048 (cited on pages 24, 43).
- Cole, C. L. and Crassidis, J. (2004). "Fast Star Pattern Recognition Using Spherical Triangles". In: *AIAA/AAS Astrodynamics Specialist Conference and Exhibit*. Providence, Rhode Island: American Institute of Aeronautics and Astronautics. doi: 10/gnh59x (cited on page 40).
- Cole, C. L. and Crassidis, J. L. (2006). "Fast Star-Pattern Recognition Using Planar Triangles". In: *Journal of Guidance, Control, and Dynamics* 29.1, pp. 64–71. doi: 10/cpxdcp (cited on page 40).
- Combi, M., Shou, Y., Fougere, N., et al. (2020). "The Surface Distributions of the Production of the Major Volatile Species, H₂O, CO₂, CO and O₂, from the Nucleus of Comet 67P/Churyumov-Gerasimenko throughout the Rosetta Mission as Measured by the ROSINA Double Focusing Mass Spectrometer". In: *Icarus* 335, p. 113421. doi: 10/gpb34h (cited on pages 103, 105, 123, 156).
- Copernicus, N., Petrejus, J., Poccianti, M., et al. (1543). *De revolutionibus orbium coelestium*. Nürnberg: Apud Ioh. Petreium (cited on page 4).
- Coradini, A., Capaccioni, F., Drossart, P., et al. (2007). "Virtis: An Imaging Spectrometer for the Rosetta Mission". In: *Space Science Reviews* 128.1, pp. 529–559. doi: 10.1007/s11214-006-9127-5 (cited on page 25).
- Cottin, H. and Fray, N. (2008). "Distributed Sources in Comets". In: *Space Science Reviews* 138.1, pp. 179–197. doi: 10.1007/s11214-008-9399-z (cited on page 33).

- Cremonese, G., Boehnhardt, H., Crovisier, J., et al. (1997). "Neutral Sodium from Comet Hale-Bopp: A Third Type of Tail". In: *The Astrophysical Journal* 490.2, p. L199. doi: 10.1086/311040 (cited on page 16).
- Cremonese, G., Huebner, W. F., Rauer, H., et al. (2002). "Neutral Sodium Tails in Comets". In: *Advances in Space Research* 29.8, pp. 1187–1197. doi: 10.1016/S0273-1177(02)00136-9 (cited on page 16).
- Cremonese, G., Simioni, E., Ragazzoni, R., et al. (2016). "Photometry of Dust Grains of Comet 67P and Connection with Nucleus Regions". In: *Astronomy & Astrophysics* 588, A59. doi: 10.1051/0004-6361/201527307 (cited on page 52).
- Crifo, J. F., Itkin, A. L., and Rodionov, A. V. (1995). "The Near-Nucleus Coma Formed by Interacting Dusty Gas Jets Effusing from a Cometary Nucleus: I". In: *Icarus* 116.1, pp. 77–112. doi: 10.1006/icar.1995.1114 (cited on page 103).
- Crifo, J. F., Loukianov, G. A., Rodionov, A. V., et al. (2005). "Direct Monte Carlo and Multifluid Modeling of the Circumnuclear Dust Coma: Spherical Grain Dynamics Revisited". In: *Icarus* 176.1, pp. 192–219. doi: 10.1016/j.icarus.2005.01.003 (cited on page 103).
- Crocker, J. C. and Grier, D. G. (1996). "Methods of Digital Video Microscopy for Colloidal Studies". In: *Journal of Colloid and Interface Science* 179.1, pp. 298–310. doi: 10/bw4g88 (cited on page 42).
- Crossick, G. (2016). "Why Monographs Matter". In: *Against the Grain* 28.3. doi: 10.7771/2380-176X.7358. (Visited on 02/19/2024) (cited on page xiii).
- Curti, F., Spiller, D., Ansalone, L., et al. (2015). "High Angular Rate Determination Algorithm Based on Star Sensing". In: *Proceedings of the AAS* (cited on page 40).
- Da Costa, G. S. (1992). "Basic Photometry Techniques". In: *Astronomical CCD Observing and Reduction Techniques*. Vol. 23. San Francisco: Astronomical Society of the Pacific, p. 90 (cited on page 56).
- Davidsson, B. J. R. (2008). "Comet Knudsen Layers". In: *Space Science Reviews* 138.1, pp. 207–223. doi: 10.1007/s11214-008-9305-8 (cited on page 21).
- Davidsson, B. J. R., Birch, S., Blake, G. A., et al. (2021). "Airfall on Comet 67P/Churyumov–Gerasimenko". In: *Icarus* 354, p. 114004. doi: 10.1016/j.icarus.2020.114004 (cited on pages 30, 33, 99, 113, 115).
- Davidsson, B. J. R., Gutiérrez, P. J., Sierks, H., et al. (2015). "Orbital Elements of the Material Surrounding Comet 67P/Churyumov–Gerasimenko". In: *Astronomy & Astrophysics* 583, A16. doi: 10.1051/0004-6361/201525841 (cited on page 53).
- Davidsson, B. J. R., Samarasinha, N. H., Farnocchia, D., et al. (2022a). "Modelling the Water and Carbon Dioxide Production Rates of Comet 67P/Churyumov–Gerasimenko". In: *Monthly Notices of the Royal Astronomical Society* 509.2, pp. 3065–3085. doi: 10.1093/mnras/stab3191 (cited on pages 17, 18, 33).
- Davidsson, B. J. R., Schloerb, F. P., Fornasier, S., et al. (2022b). "CO₂-driven Surface Changes in the Hapi Region on Comet 67P/Churyumov–Gerasimenko". In: *Monthly Notices of the Royal Astronomical Society* 516.4, pp. 6009–6040. doi: 10.1093/mnras/stac2560 (cited on pages 93, 103, 111, 125, 159).
- Davidsson, B. J. R., Sierks, H., Güttler, C., et al. (2016). "The Primordial Nucleus of Comet 67P/Churyumov–Gerasimenko". In: *Astronomy & Astrophysics* 592, A63. doi: 10/f3tpzv (cited on pages 19, 20, 31, 105, 106, 115, 159).
- Dawson, R. I. and Murray-Clay, R. (2012). "Neptune's Wild Days: Constraints From The Eccentricity Distribution Of The Classical Kuiper Belt". In: *The Astrophysical Journal* 750.1, p. 43. doi: 10.1088/0004-637X/750/1/43. (Visited on 04/08/2024) (cited on page 8).
- Day, R. A. (1989). "The Origins of the Scientific Paper: The IMRAD Format". In: *American Medical Writers Association Journal* 4.2 (cited on page xiv).
- De Keyser, J., Dhooghe, F., Altwegg, K., et al. (2017). "Evidence for Distributed Gas Sources of Hydrogen Halides in the Coma of Comet 67P/Churyumov–Gerasimenko". In: *Monthly Notices of the Royal Astronomical Society* 469.Suppl_2, S695–S711. doi: 10.1093/mnras/stx2725 (cited on page 33).
- de la Fuente Marcos, C. and de la Fuente Marcos, R. (2024). "Past the Outer Rim, into the Unknown: Structures beyond the Kuiper Cliff". In: *Monthly Notices of the Royal Astronomical Society: Letters* 527.1, pp. L110–L114. doi: 10.1093/mnrasl/slad132 (cited on page 10).
- de Niem, D., Kührt, E., Hviid, S., et al. (2018). "Low Velocity Collisions of Porous Planetesimals in the Early Solar System". In: *Icarus* 301, pp. 196–218. doi: 10.1016/j.icarus.2017.09.024 (cited on pages 26, 154).
- De Sanctis, M. C., Capaccioni, F., Ciarniello, M., et al. (2015). "The Diurnal Cycle of Water Ice on Comet 67P/Churyumov–Gerasimenko". In: *Nature* 525.7570, pp. 500–503. doi: 10.1038/nature14869 (cited on pages 30, 158).

- Delgado, P., Vargas, C., Ackerman, R., et al. (2018). "Don't Throw Away Your Printed Books: A Meta-Analysis on the Effects of Reading Media on Reading Comprehension". In: *Educational Research Review* 25, pp. 23–38. doi: 10.1016/j.edurev.2018.09.003 (cited on page xvii).
- Della Corte, V., Rotundi, A., Accolla, M., et al. (2014). "Giada: Its Status after the Rosetta Cruise Phase and on-Ground Activity in Support of the Encounter with Comet 67p/Churyumov-Gerasimenko". In: *Journal of Astronomical Instrumentation* 03.01, p. 1350011. doi: 10.1142/S2251171713500116 (cited on page 43).
- Delsanti, A. and Jewitt, D. (2006). "The Solar System Beyond The Planets". In: *Solar System Update*. Ed. by P. Blondel and J. W. Mason. Berlin, Heidelberg: Springer-Verlag, pp. 267–293. doi: 10.1007/3-540-37683-6_11 (cited on pages 8, 10).
- Dempster, A. P., Laird, N. M., and Rubin, D. B. (1977). "Maximum Likelihood from Incomplete Data Via the EM Algorithm". In: *Journal of the Royal Statistical Society: Series B (Methodological)* 39.1, pp. 1–22. doi: 10.1111/j.2517-6161.1977.tb01600.x (cited on page 76).
- Denneau, L., Jedicke, R., Grav, T., et al. (2013). "The Pan-STARRS Moving Object Processing System". In: *Publications of the Astronomical Society of the Pacific* 125.926, pp. 357–395. doi: 10.1086/670337. (Visited on 11/19/2021) (cited on pages 41, 53, 88).
- Deshapriya, J. D. P., Barucci, M. A., Fornasier, S., et al. (2016). "Spectrophotometry of the Khonsu Region on the Comet 67P/Churyumov-Gerasimenko Using OSIRIS Instrument Images". In: *Monthly Notices of the Royal Astronomical Society* 462.Supp_1, S274–S286. doi: 10.1093/mnras/stw2530 (cited on pages 105, 107, 109, 111, 123, 156).
- Deshapriya, J. D. P., Barucci, M. A., Fornasier, S., et al. (2018). "Exposed Bright Features on the Comet 67P/Churyumov-Gerasimenko: Distribution and Evolution". In: *Astronomy & Astrophysics* 613, A36. doi: 10.1051/0004-6361/201732112 (cited on pages 30, 103, 105, 156).
- Deshapriya, J. D. P., Hasselmann, P. H., Gai, I., et al. (2023). "Characterization of the DART Impact Ejecta Plume on Dimorphos from LICIAcube Observations". In: *The Planetary Science Journal* 4.12, p. 231. doi: 10.3847/PSJ/ad09ba (cited on page 39).
- Deslandres, H. and Bernard, A. (1907). "Étude Spectrale de La Comète Danuel (1907 d): Particularités de La Queue". In: *Comptes rendus hebdomadaires des séances de l'Académie des sciences*, pp. 445–448 (cited on page 16).
- Deutsch, H. and Garbacz, P. (2022). "Relative Identity". In: *The Stanford Encyclopedia of Philosophy*. Ed. by E. N. Zalta and U. Nodelman. Winter 2022. Metaphysics Research Lab, Stanford University (cited on page 43).
- DeZoort, G., Thais, S., Duarte, J., et al. (2021). "Charged Particle Tracking via Edge-Classifying Interaction Networks". In: *Computing and Software for Big Science* 5.1, p. 26. doi: 10.1007/s41781-021-00073-z (cited on page 43).
- Dietz, B. (2022). "Towards a History of Scientific Publishing". In: *History of Science* 60.2, pp. 155–165. doi: 10.1177/00732753221074609. (Visited on 03/06/2024) (cited on page xv).
- Dohnanyi, J. S. (1969). "Collisional Model of Asteroids and Their Debris". In: *Journal of Geophysical Research* (1896-1977) 74.10, pp. 2531–2554. doi: 10.1029/JB074i010p02531 (cited on page 107).
- Dominik, C. and Tielens, A. G. G. M. (1997). "The Physics of Dust Coagulation and the Structure of Dust Aggregates in Space". In: *The Astrophysical Journal* 480.2, p. 647. doi: 10.1086/303996 (cited on page 19).
- Dong, Y. R. (1998). "Non-Native Graduate Students' Thesis/Dissertation Writing in Science: Self-reports by Students and Their Advisors from Two U.S. Institutions". In: *English for Specific Purposes* 17.4, pp. 369–390. doi: 10.1016/S0889-4906(97)00054-9. (Visited on 02/26/2024) (cited on page xv).
- Donner, P. (2021). "Identifying Constitutive Articles of Cumulative Dissertation Theses by Bilingual Text Similarity. Evaluation of Similarity Methods on a New Short Text Task". In: *Quantitative Science Studies* 2.3, pp. 1071–1091. doi: 10.1162/qss_a_00152. (Visited on 03/06/2024) (cited on page xv).
- Dotto, E., Deshapriya, J. D. P., Gai, I., et al. (2024). "The Dimorphos Ejecta Plume Properties Revealed by LICIAcube". In: *Nature* 627.8004, pp. 505–509. doi: 10.1038/s41586-023-06998-2 (cited on page 39).
- Doumont, J.-I. (2009). *Trees, Maps, and Theorems: Effective Communication for Rational Minds*. Principiæ (cited on pages xvii, xviii).
- Drahus, M., Guzik, P., Waniak, W., et al. (2018). "Tumbling Motion of 1I/'Oumuamua and Its Implications for the Body's Distant Past". In: *Nature Astronomy* 2.5, pp. 407–412. doi: 10.1038/s41550-018-0440-1 (cited on page 14).

- Drażkowska, J., Bitsch, B., Lambrechts, M., et al. (2023). "Planet Formation Theory in the Era of ALMA and Kepler: From Pebbles to Exoplanets". In: *Protostars and Planets VII*. Vol. 534. eprint: arXiv:2203.09759: Astronomical Society of the Pacific, p. 717. doi: 10.48550/arXiv.2203.09759 (cited on page 19).
- Drażkowska, J., Windmark, F., and Dullemond, C. P. (2013). "Planetesimal Formation via Sweep-up Growth at the Inner Edge of Dead Zones". In: *Astronomy & Astrophysics* 556, A37. doi: 10.1051/0004-6361/201321566 (cited on page 20).
- Drolshagen, E., Ott, T., Koschny, D., et al. (2017). "Distance Determination Method of Dust Particles Using Rosetta OSIRIS NAC and WAC Data". In: *Planetary and Space Science*. SI:Meteoroids 2016 143, pp. 256–264. doi: 10.1016/j.pss.2017.04.018 (cited on page 53).
- Ducharme, J. (2023). *Why No One Feels Like They Can Focus Anymore*. URL: <https://time.com/6302294/why-you-cant-focus-anymore-and-what-to-do-about-it/> (visited on 02/14/2024) (cited on page xv).
- Duffy, B. and Thain, M. (2022). *Do We Have Your Attention? How People Focus and Live in the Modern Information Environment*. Tech. rep. King's College London: Policy Institute and Centre for Attention Studies (cited on page xv).
- Duke, N. K. and Beck, S. W. (1999). "Research News And Comment: Education Should Consider Alternative Formats for the Dissertation". In: *Educational Researcher* 28.3, pp. 31–36. doi: 10.3102/0013189X028003031. (Visited on 02/23/2024) (cited on page xiii).
- Duncan, M. J., Levison, H., and Dones, L. (2004). "Dynamical Evolution of Ecliptic Comets". In: *Comets II*. Ed. by M. C. Festou, H. U. Keller, and H. A. Weaver. University of Arizona Press. doi: 10.2307/j.ctv1v7zdq5 (cited on pages 11, 13).
- Duncan, M. J. and Levison, H. F. (1997). "A Disk of Scattered Icy Objects and the Origin of Jupiter-Family Comets". In: *Science* 276.5319, pp. 1670–1672. doi: 10.1126/science.276.5319.1670 (cited on pages 7, 9).
- Duncan, M. J., Quinn, T., and Tremaine, S. (1987). "The Formation and Extent of the Solar System Comet Cloud". In: *The Astronomical Journal* 94, p. 1330. doi: 10.1086/114571 (cited on pages 7, 9).
- Duncan, M. J., Quinn, T., and Tremaine, S. (1988). "The Origin of Short-Period Comets". In: *The Astrophysical Journal* 328, p. L69. doi: 10.1086/185162 (cited on page 7).
- Eager, D., Pendrill, A.-M., and Reistad, N. (2016). "Beyond Velocity and Acceleration: Jerk, Snap and Higher Derivatives". In: *European Journal of Physics* 37.6, p. 065008. doi: 10.1088/0143-0807/37/6/065008 (cited on page 130).
- Edgeworth, K. E. (1943). "The Evolution of Our Planetary System". In: *Journal of the British Astronomical Association* 53, pp. 181–188 (cited on page 7).
- Edgeworth, K. E. (1949). "The Origin and Evolution of the Solar System". In: *Monthly Notices of the Royal Astronomical Society* 109, pp. 600–609. doi: 10.1093/mnras/109.5.600 (cited on page 7).
- Elbroch, M. (2003). *Mammal Tracks & Sign: A Guide to North American Species*. Stackpole Books (cited on page 37).
- Elliot, J. L., Kern, S. D., Clancy, K. B., et al. (2005). "The Deep Ecliptic Survey: A Search for Kuiper Belt Objects and Centaurs. II. Dynamical Classification, the Kuiper Belt Plane, and the Core Population". In: *The Astronomical Journal* 129.2, p. 1117. doi: 10.1086/427395. (Visited on 04/06/2024) (cited on page 7).
- Elst, E. W., Pizarro, O., Pollas, C., et al. (1996). "Comet P/1996 N2 (Elst-Pizarro)". In: *International Astronomical Union Circular* 6456, p. 1 (cited on page 13).
- Emel'yanenko, V. V., Asher, D. J., and Bailey, M. E. (2003). "A New Class of Trans-Neptunian Objects in High-Eccentricity Orbits". In: *Monthly Notices of the Royal Astronomical Society* 338.2, pp. 443–451. doi: 10.1046/j.1365-8711.2003.06066.x (cited on page 10).
- Encke, J. F. (1819). "Nouvelles et Annonces II: Comètes". In: *Correspondance astronomique, géographique, hydrographique et statistique* 2, p. 305. (Visited on 04/28/2024) (cited on page 12).
- Englander, K. (2014). *Writing and Publishing Science Research Papers in English: A Global Perspective*. SpringerBriefs in Education. Dordrecht: Springer Netherlands (cited on page xiii).
- Ermilov, A. A., Fleit, G., Conevski, S., et al. (2022). "Bedload Transport Analysis Using Image Processing Techniques". In: *Acta Geophysica* 70.5, pp. 2341–2360. doi: 10.1007/s11600-022-00791-x (cited on page 42).
- Ershov, D., Phan, M.-S., Pylvänäinen, J. W., et al. (2022). "TrackMate 7: Integrating State-of-the-Art Segmentation Algorithms into Tracking Pipelines". In: *Nature Methods* 19.7, pp. 829–832. doi: 10.1038/s41592-022-01507-1 (cited on page 38).

- ESA SPICE Service (2020). *Rosetta Operational SPICE Kernel Dataset*. doi: 10.5270/esa-tyidsbu (cited on page 103).
- Euler, L. (1743). *Determinatio orbitae cometae qui mense Martio huius anni 1742 potissimum fuit observatus*. Vol. 7. *Miscellanea Berolinensia* (cited on page 7).
- Euler, L. (1757). "Principes Généraux Du Mouvement Des Fluides". In: *Mémoires de l'académie des sciences de Berlin*, pp. 274–315 (cited on page 21).
- Evershed, J. (1907). "The Spectrum of Comet 1907 d (Daniel)". In: *Monthly Notices of the Royal Astronomical Society* 68.1, pp. 16–18. doi: 10.1093/mnras/68.1.16 (cited on page 16).
- Ezekiel, M. (1930). *Methods Of Correlation Analysis*. New York: John Wiley & Sons Inc (cited on page 95).
- Fabry, L. (1893). "Étude Sur La Probabilité Des Comètes Hyperboliques et l'origine Des Comètes". PhD thesis. Marseille: L'Observatoire de Marseille (cited on page 11).
- Fagents, S. A., Lopes, R. M. C., Quick, L. C., et al. (2022). "Cryovolcanism". In: *Planetary Volcanism across the Solar System*. Ed. by T. K. P. Gregg, R. M. C. Lopes, and S. A. Fagents. Vol. 1. Comparative Planetology. Elsevier, pp. 161–234. doi: 10.1016/B978-0-12-813987-5.00005-5 (cited on page 105).
- Fahrmeir, L., Kneib, T., Lang, S., et al. (2021). *Regression: Models, Methods and Applications*. Berlin, Heidelberg: Springer (cited on page 95).
- Fanale, F. P. and Salvail, J. R. (1989). "The Water Regime of Asteroid (1) Ceres". In: *Icarus* 82.1, pp. 97–110. doi: 10.1016/0019-1035(89)90026-2 (cited on page 13).
- Farinella, P. and Davis, D. R. (1996). "Short-Period Comets: Primordial Bodies or Collisional Fragments?" In: *Science* 273.5277, pp. 938–941. doi: 10.1126/science.273.5277.938 (cited on page 19).
- Farnham, T. L., Kelley, M. S. P., and Bauer, J. M. (2021). "Early Activity in Comet C/2014 UN271 Bernardinelli-Bernstein as Observed by TESS". In: *The Planetary Science Journal* 2.6, p. 236. doi: 10.3847/PSJ/ac323d (cited on page 14).
- Faure, G. and Mensing, T. M. (2007). "Comets: Coming Inside from the Cold". In: *Introduction to Planetary Science: The Geological Perspective*. Ed. by G. Faure and T. M. Mensing. Dordrecht: Springer Netherlands, pp. 421–440. doi: 10.1007/978-1-4020-5544-7_22 (cited on page 14).
- Fawcett, T. (2006). "An Introduction to ROC Analysis". In: *Pattern Recognition Letters*. ROC Analysis in Pattern Recognition 27.8, pp. 861–874. doi: 10.1016/j.patrec.2005.10.010 (cited on page 76).
- Fayet, G. (1906). "Recherches Concernant Les Excentricités Des Comètes". PhD thesis. Paris: Université de Paris (cited on page 11).
- Feiteirinha, J. L. F., Kairiss, V., Reggestad, V., et al. (2019). "STR4SD - Exploring the concept of opportunistically using star-trackers for space debris observations". In: *1st NEO and Debris Detection Conference* (cited on page 40).
- Feller, W. (1948). "On the Kolmogorov-Smirnov Limit Theorems for Empirical Distributions". In: *The Annals of Mathematical Statistics* 19.2, pp. 177–189. doi: 10.1214/aoms/1177730243 (cited on page 109).
- Fernández, J. A. (1980). "On the Existence of a Comet Belt beyond Neptune". In: *Monthly Notices of the Royal Astronomical Society* 192.3, pp. 481–491. doi: 10.1093/mnras/192.3.481 (cited on page 7).
- Fernández, Y. R., Kelley, M. S., Lamy, P. L., et al. (2013). "Thermal Properties, Sizes, and Size Distribution of Jupiter-family Cometary Nuclei". In: *Icarus* 226.1, pp. 1138–1170. doi: 10.1016/j.icarus.2013.07.021. (Visited on 04/17/2023) (cited on page 118).
- Ferrari, S., Penasa, L., La Forgia, F., et al. (2018). "The Big Lobe of 67P/Churyumov-Gerasimenko Comet: Morphological and Spectrophotometric Evidences of Layering as from OSIRIS Data". In: *Monthly Notices of the Royal Astronomical Society* 479.2, pp. 1555–1568. doi: 10.1093/mnras/sty1656 (cited on pages 31, 105).
- Fiaz, M., Mahmood, A., Javed, S., et al. (2019). "Handcrafted and Deep Trackers: Recent Visual Object Tracking Approaches and Trends". In: *ACM Computing Surveys* 52.2, 43:1–43:44. doi: 10.1145/3309665 (cited on page 42).
- Filacchione, G., Raponi, A., Capaccioni, F., et al. (2016). "Seasonal Exposure of Carbon Dioxide Ice on the Nucleus of Comet 67P/Churyumov-Gerasimenko". In: *Science* 354.6319, pp. 1563–1566. doi: 10.1126/science.aag3161 (cited on page 30).
- Filacchione, G., Capaccioni, F., Ciarniello, M., et al. (2020). "An Orbital Water-Ice Cycle on Comet 67P from Colour Changes". In: *Nature* 578.7793, pp. 49–52. doi: 10.1038/s41586-020-1960-2 (cited on page 30).
- Filacchione, G., Ciarniello, M., Fornasier, S., et al. (2022). *Comet Nuclei Composition and Evolution*. doi: 10.48550/arXiv.2210.02741 (cited on page 3).

- Finson, M. L. and Probst, R. F. (1968a). "A Theory of Dust Comets. I. Model and Equations". In: *The Astrophysical Journal* 154, pp. 327–352. doi: 10.1086/149761 (cited on pages 21, 107).
- Finson, M. L. and Probst, R. F. (1968b). "A Theory of Dust Comets. II. Results for Comet Arend-Roland". In: *The Astrophysical Journal* 154, pp. 353–380. doi: 10.1086/149762 (cited on pages 106, 107).
- Fire, M. and Guestrin, C. (2019). "Over-Optimization of Academic Publishing Metrics: Observing Goodhart's Law in Action". In: *GigaScience* 8.6, giz053. doi: 10.1093/gigascience/giz053 (cited on page xv).
- Fornasier, S., Feller, C., Lee, J.-C., et al. (2017). "The Highly Active Anhur–Bes Regions in the 67P/Churyumov–Gerasimenko Comet: Results from OSIRIS/ROSETTA Observations". In: *Monthly Notices of the Royal Astronomical Society* 469.Suppl_2, S93–S107. doi: 10.1093/mnras/stx1275 (cited on pages 30, 103).
- Fornasier, S., Hasselmann, P. H., Barucci, M. A., et al. (2015). "Spectrophotometric Properties of the Nucleus of Comet 67P/Churyumov-Gerasimenko from the OSIRIS Instrument Onboard the ROSETTA Spacecraft". In: *Astronomy & Astrophysics* 583, A30. doi: 10.1051/0004-6361/201525901 (cited on page 34).
- Fornasier, S., Hoang, H. V., Fulle, M., et al. (2023). "Volatile Exposures on the 67P/Churyumov-Gerasimenko Nucleus". In: *Astronomy & Astrophysics* 672, A136. doi: 10.1051/0004-6361/202245614 (cited on pages 18, 30, 105, 156).
- Fornasier, S., Hoang, V. H., Hasselmann, P. H., et al. (2019). "Linking Surface Morphology, Composition, and Activity on the Nucleus of 67P/Churyumov-Gerasimenko". In: *Astronomy & Astrophysics* 630, A7. doi: 10.1051/0004-6361/201833803 (cited on pages 105, 156).
- Fornasier, S., Mottola, S., Keller, H. U., et al. (2016). "Rosetta's Comet 67P/Churyumov-Gerasimenko Sheds Its Dusty Mantle to Reveal Its Icy Nature". In: *Science* 354.6319, pp. 1566–1570. doi: 10.1126/science.aag2671 (cited on pages 30, 103, 158).
- Fouchard, M., Rickman, H., Froeschlé, C., et al. (2017a). "Distribution of Long-Period Comets: Comparison between Simulations and Observations". In: *Astronomy & Astrophysics* 604, A24. doi: 10.1051/0004-6361/201630343 (cited on pages 3, 11).
- Fouchard, M., Rickman, H., Froeschlé, C., et al. (2017b). "On the Present Shape of the Oort Cloud and the Flux of "New" Comets". In: *Icarus* 292, pp. 218–233. doi: 10.1016/j.icarus.2017.01.013 (cited on pages 3, 11).
- Fougere, N., Altwegg, K., Berthelier, J.-J., et al. (2016). "Three-Dimensional Direct Simulation Monte-Carlo Modeling of the Coma of Comet 67P/Churyumov-Gerasimenko Observed by the VIRTIS and ROSINA Instruments on Board Rosetta". In: *Astronomy & Astrophysics* 588, A134. doi: 10.1051/0004-6361/201527889 (cited on page 30).
- Fowler, A. C. and Scheu, B. (2016). "A Theoretical Explanation of Grain Size Distributions in Explosive Rock Fragmentation". In: *Proceedings of the Royal Society A: Mathematical, Physical and Engineering Sciences* 472.2190, p. 20150843. doi: 10.1098/rspa.2015.0843 (cited on page 107).
- Frasca-Spada, M. and Jardine, N., eds. (2000). *Books and the Sciences in History*. New York: Cambridge University Press (cited on page xvi).
- Frattin, E., Bertini, I., Ivanovski, S. L., et al. (2021). "Observational Constraints to the Dynamics of Dust Particles in the Coma of Comet 67P/Churyumov–Gerasimenko". In: *Monthly Notices of the Royal Astronomical Society* 504.4, pp. 4687–4705. doi: 10.1093/mnras/stab1152 (cited on pages 52, 53, 111).
- Frattin, E., Cremonese, G., Simioni, E., et al. (2017). "Post-Perihelion Photometry of Dust Grains in the Coma of 67P Churyumov–Gerasimenko". In: *Monthly Notices of the Royal Astronomical Society* 469.Suppl_2, S195–S203. doi: 10.1093/mnras/stx1395 (cited on page 53).
- Fray, N., Bardyn, A., Cottin, H., et al. (2016). "High-Molecular-Weight Organic Matter in the Particles of Comet 67P/Churyumov–Gerasimenko". In: *Nature* 538.7623, pp. 72–74. doi: 10.1038/nature19320 (cited on page 31).
- Freedman, R. and Kaufmann, W. J. (2007). *Universe*. W. H. Freeman (cited on page 14).
- Freeman, S. (2018). "The Manuscript Dissertation: A Means of Increasing Competitive Edge for Tenure-track Faculty Positions". In: *International Journal of Doctoral Studies* 13, pp. 273–292. (Visited on 02/23/2024) (cited on page xiii).
- Frick, L. (2016). "PHD by publication: an institutional analysis". In: *PHD by publication : an institutional analysis*. AFRICAN SUN MeDIA (cited on page xv).

- Fritscher, M. and Teiser, J. (2022). "Tensile Strength and Surface Energy of CO₂ Ice in the Context of Planet Formation". In: *Monthly Notices of the Royal Astronomical Society* 512.3, pp. 3754–3758. doi: 10.1093/mnras/stac676 (cited on page 17).
- Fukai, Y. T. and Kawaguchi, K. (2023). "LapTrack: Linear Assignment Particle Tracking with Tunable Metrics". In: *Bioinformatics* 39.1. doi: 10.1093/bioinformatics/btac799 (cited on page 42).
- Fulle, M., Leblanc, F., Harrison, R. A., et al. (2007). "Discovery of the Atomic Iron Tail of Comet MCNaught Using the Heliospheric Imager on STEREO". In: *The Astrophysical Journal* 661.1, p. L93. doi: 10.1086/518719 (cited on page 16).
- Fulle, M. (1989). "Evaluation of Cometary Dust Parameters from Numerical Simulations: Comparison with an Analytical Approach and the Role of Anisotropic Emissions." In: *Astronomy and Astrophysics, Vol. 217, p. 283–297* (1989) 217, p. 283 (cited on page 107).
- Fulle, M. (2021). "Water and Deuterium-to-Hydrogen Ratio in Comets". In: *Monthly Notices of the Royal Astronomical Society* 505.2, pp. 3107–3112. doi: 10.1093/mnras/stab1507 (cited on pages 18, 32, 33, 156).
- Fulle, M., Altabelli, N., Buratti, B., et al. (2016a). "Unexpected and Significant Findings in Comet 67P/Churyumov–Gerasimenko: An Interdisciplinary View". In: *Monthly Notices of the Royal Astronomical Society* 462.Suppl_1, S2–S8. doi: 10.1093/mnras/stw1663 (cited on page 33).
- Fulle, M., Blum, J., Green, S. F., et al. (2019a). "The Refractory-to-Ice Mass Ratio in Comets". In: *Monthly Notices of the Royal Astronomical Society* 482.3, pp. 3326–3340. doi: 10.1093/mnras/sty2926 (cited on page 27).
- Fulle, M., Blum, J., Rotundi, A., et al. (2020a). "How Comets Work: Nucleus Erosion versus Dehydration". In: *Monthly Notices of the Royal Astronomical Society* 493.3, pp. 4039–4044. doi: 10/gnh7hs (cited on pages 17, 18, 32, 106, 111, 115, 157, 158).
- Fulle, M. and Blum, J. (2017a). "Fractal Dust Constrains the Collisional History of Comets". In: *Monthly Notices of the Royal Astronomical Society* 469.Suppl_2, S39–S44. doi: 10.1093/mnras/stx971 (cited on pages 19, 32, 106).
- Fulle, M., Blum, J., and Rotundi, A. (2019b). "How Comets Work". In: *The Astrophysical Journal Letters* 879.1, p. L8. doi: 10.3847/2041-8213/ab2898 (cited on pages 16–18, 158).
- Fulle, M., Blum, J., and Rotundi, A. (2020b). "CO-driven Activity Constrains the Origin of Comets". In: *Astronomy & Astrophysics* 636, p. L3. doi: 10.1051/0004-6361/202037805 (cited on pages 18, 93, 103, 125).
- Fulle, M., Colangeli, L., Agarwal, J., et al. (2010). "Comet 67P/Churyumov-Gerasimenko: The GIADA Dust Environment Model of the Rosetta Mission Target". In: *Astronomy & Astrophysics* 522, A63. doi: 10.1051/0004-6361/201014928 (cited on page 107).
- Fulle, M., Corte, V. D., Rotundi, A., et al. (2015a). "Density And Charge Of Pristine Fluffy Particles From Comet 67P/Churyumov–Gerasimenko". In: *The Astrophysical Journal Letters* 802.1, p. L12. doi: 10.1088/2041-8205/802/1/L12 (cited on page 32).
- Fulle, M., Della Corte, V., Rotundi, A., et al. (2017b). "The Dust-to-Ices Ratio in Comets and Kuiper Belt Objects". In: *Monthly Notices of the Royal Astronomical Society* 469.Suppl_2, S45–S49. doi: 10.1093/mnras/stx983 (cited on page 27).
- Fulle, M., Ivanovski, S. L., Bertini, I., et al. (2015b). "Rotating Dust Particles in the Coma of Comet 67P/Churyumov-Gerasimenko". In: *Astronomy & Astrophysics* 583, A14. doi: 10.1051/0004-6361/201526158 (cited on page 159).
- Fulle, M., Levasseur-Regourd, A. C., McBride, N., et al. (2000). "In Situ Dust Measurements From within the Coma of 1P/Halley: First-Order Approximation with a Dust Dynamical Model". In: *The Astronomical Journal* 119.4, p. 1968. doi: 10.1086/301285 (cited on page 17).
- Fulle, M., Marzari, F., Corte, V. D., et al. (2016b). "Evolution Of The Dust Size Distribution Of Comet 67P/Churyumov–Gerasimenko From 2.2 Au To Perihelion". In: *The Astrophysical Journal* 821.1, p. 19. doi: 10.3847/0004-637x/821/1/19. (Visited on 11/24/2021) (cited on pages 53, 107, 109, 123, 156).
- Fyfe, A., Moxham, N., McDougall-Waters, J., et al. (2022). *A History of Scientific Journals: Publishing at the Royal Society 1665-2015*. London, UK: UCL Press (cited on page xiv).
- Galilei, G. (1623). *Il saggliatore*. appresso Giacomo Mascardi (cited on page 4).
- Galilei, G., Grassi, H., Guiducci, M., et al. (1960). "The Assayer". In: *The Controversy on the Comets of 1618*. Trans. by S. Drake and C. D. O'Malley. University of Pennsylvania Press. doi: 10.9783/9781512801453 (cited on page 4).

- Gauss, C. F. (1809). *Theoria Motus Corporum Coelestium in Sectionibus Conicis Solem Ambientium*. Hamburg (cited on page 7).
- Gehrels, T. (1981). "Faint Comet Searching". In: *Icarus* 47.3, pp. 518–522. doi: 10.1016/0019-1035(81)90200-1. (Visited on 05/05/2024) (cited on page 41).
- Gehrels, T. (1991). "Scanning with Charge-Coupled Devices". In: *Space Science Reviews* 58.1, pp. 347–375. doi: 10.1007/bf01206004 (cited on page 41).
- George Udny Yule (1911). *An Introduction to the Theory of Statistics*. C. Griffin and Company, limited (cited on page 56).
- Gerig, S.-B., Marschall, R., Thomas, N., et al. (2018). "On Deviations from Free-Radial Outflow in the Inner Coma of Comet 67P/Churyumov–Gerasimenko". In: *Icarus* 311, pp. 1–22. doi: 10.1016/j.icarus.2018.03.012 (cited on page 123).
- Gerig, S.-B., Pinzón-Rodríguez, O., Marschall, R., et al. (2020). "Dayside-to-Nightside Dust Coma Brightness Asymmetry and Its Implications for Nightside Activity at Comet 67P/Churyumov–Gerasimenko". In: *Icarus* 351, p. 113968. doi: 10.1016/j.icarus.2020.113968 (cited on page 123).
- Giacomini, L., Massironi, M., El-Maarry, M. R., et al. (2016). "Geologic Mapping of the Comet 67P/Churyumov–Gerasimenko's Northern Hemisphere". In: *Monthly Notices of the Royal Astronomical Society* 462.Suppl_1, S352–S367. doi: 10.1093/mnras/stw2848 (cited on pages 31, 105).
- Ginsburg, A., Sipőcz, B. M., Brasseur, C. E., et al. (2019). "Astroquery: An Astronomical Web-querying Package in Python". In: *The Astronomical Journal* 157.3, p. 98. doi: 10.3847/1538-3881/aaf333. (Visited on 03/17/2023) (cited on page 67).
- Gkotsinas, A., Guilbert-Lepoutre, A., Raymond, S. N., et al. (2022). "Thermal Processing of Jupiter-family Comets during Their Chaotic Orbital Evolution". In: *The Astrophysical Journal* 928.1, p. 43. doi: 10.3847/1538-4357/ac54ac (cited on page 14).
- Gladman, B. J. (2005). "The Kuiper Belt and the Solar System's Comet Disk". In: *Science* 307.5706, pp. 71–75. doi: 10.1126/science.1100553. (Visited on 04/09/2024) (cited on page 9).
- Gladman, B. J., Davis, D. R., Neese, C., et al. (2009). "On the Asteroid Belt's Orbital and Size Distribution". In: *Icarus* 202.1, pp. 104–118. doi: 10.1016/j.icarus.2009.02.012. (Visited on 11/22/2021) (cited on pages 41, 53).
- Gladman, B. J., Marsden, B. G., and Vanlaerhoven, C. (2008). "Nomenclature in the Outer Solar System". In: *The Solar System Beyond Neptune*. Ed. by M. A. Barucci, H. Boehnhardt, D. P. Cruikshank, et al. University of Arizona Press, pp. 43–57 (cited on pages 7–10, 13).
- Gladman, B. J. and Volk, K. (2021). "Transneptunian Space". In: *Annual Review of Astronomy and Astrophysics* 59. Volume 59, 2021, pp. 203–246. doi: 10.1146/annurev-astro-120920-010005. (Visited on 04/08/2024) (cited on pages 7, 9, 10).
- Glassmeier, K.-H., Boehnhardt, H., Koschny, D., et al. (2007). "The Rosetta Mission: Flying Towards the Origin of the Solar System". In: *Space Science Reviews* 128.1-4, pp. 1–21. doi: 10.1007/s11214-007-9021-0 (cited on pages 3, 22, 23).
- Godard, B., Budnik, F., Bellei, G., et al. (2017). "Multi-Arc Orbit Determination to Determine Rosetta Trajectory and 67P Physical Parameters". In: *Proceedings of the 26th International Symposium on Space Flight Dynamics*. Matsuyama, Japan (cited on page 29).
- Gombosi, T. I., Cravens, T. E., and Nagy, A. F. (1985). "Time-Dependent Dusty Gasdynamical Flow near Cometary Nuclei". In: *The Astrophysical Journal* 293, pp. 328–341. doi: 10.1086/163240 (cited on page 21).
- Gombosi, T. I., Nagy, A. F., and Cravens, T. E. (1986). "Dust and Neutral Gas Modeling of the Inner Atmospheres of Comets". In: *Reviews of Geophysics* 24.3, pp. 667–700. doi: 10.1029/RG024i003p0667 (cited on page 21).
- Gombosi, T. I. (1987). "Dusty Cometary Atmospheres". In: *Advances in Space Research*. Proceedings of the Topical Meeting of the COSPAR Interdisciplinary Scientific Commission C (Meeting C3), Workshop III and Symposium 8 of the COSPAR Twenty-sixth Plenary Meeting 7.12, pp. 137–145. doi: 10.1016/0273-1177(87)90211-0 (cited on page 21).
- Gomes, R. (2021). "The Formation of the Cold Classical Kuiper Belt by a Short Range Transport Mechanism". In: *Icarus* 357, p. 114121. doi: 10.1016/j.icarus.2020.114121 (cited on page 8).
- Götz, C., Behar, E., Beth, A., et al. (2022a). "The Plasma Environment of Comet 67P/Churyumov-Gerasimenko". In: *Space Science Reviews* 218.8, p. 65. doi: 10.1007/s11214-022-00931-1 (cited on page 16).

- Götz, C., Deca, J., Mandt, K., et al. (2022b). *Solar Wind Interaction with a Comet: Evolution, Variability, and Implication*. DOI: 10.48550/arXiv.2211.04887. URL: <http://arxiv.org/abs/2211.04887> (cited on page 16).
- Gould, J. (2016). "What's the Point of the PhD Thesis?" In: *Nature* 535.7610, pp. 26–28. DOI: 10.1038/535026a (cited on page xiii).
- Green, D. W. E. (1999). *What Is Improper about the Term "Kuiper Belt"?* <http://www.icq.eps.harvard.edu/kb.html> (cited on page 7).
- Green, D. W. E. (2004). "Assessment of Early-Modern Observations of Comets and Supernovae: Focus on Pre-Telescopic European Astrometric and Physical Data". Doctoral. Durham University (cited on pages 4, 6).
- Greene, A. E. (2013). *Writing Science in Plain English*. University of Chicago Press (cited on page xiv).
- Grewal, M. S. and Andrews, A. P. (2010). "Applications of Kalman Filtering in Aerospace 1960 to the Present [Historical Perspectives]". In: *IEEE Control Systems Magazine* 30.3, pp. 69–78. DOI: 10.1109/MCS.2010.936465 (cited on page 38).
- Grieger, B. (2019). "Quincuncial Adaptive Closed Kohonen (QuACK) Map for the Irregularly Shaped Comet 67P/Churyumov-Gerasimenko". In: *Astronomy & Astrophysics* 630, A1. DOI: 10.1051/0004-6361/201834841 (cited on pages 103, 111).
- Grimme, S., Taylor, M., Elliott, M. A., et al. (2019). *The State of Open Monographs*. Report. Digital Science. DOI: 10.6084/m9.figshare.8197625.v4. (Visited on 02/25/2024) (cited on page xiv).
- Groeneveld, I. and Kuiper, G. P. (1954). "Photometric Studies of Asteroids. I". In: *The Astrophysical Journal* 120, p. 200. DOI: 10.1086/145904 (cited on page 41).
- Groussin, O., Hahn, G., Lamy, P. L., et al. (2007). "The Long-Term Evolution and Initial Size of Comets 46P/Wirtanen and 67P/Churyumov-Gerasimenko". In: *Monthly Notices of the Royal Astronomical Society* 376.3, pp. 1399–1406. DOI: 10.1111/j.1365-2966.2007.11553.x (cited on page 26).
- Groussin, O., Jorda, L., Auger, A.-T., et al. (2015). "Gravitational Slopes, Geomorphology, and Material Strengths of the Nucleus of Comet 67P/Churyumov-Gerasimenko from OSIRIS Observations". In: *Astronomy & Astrophysics* 583, A32. DOI: 10/f3pcj9 (cited on pages 31, 107).
- Grün, E., Agarwal, J., Altabelli, N., et al. (2016). "The 2016 Feb 19 Outburst of Comet 67P/CG: An ESA Rosetta Multi-Instrument Study". In: *Monthly Notices of the Royal Astronomical Society* 462.Suppl_1, S220–S234. DOI: 10.1093/mnras/stw2088 (cited on page 40).
- Gu, T. F. (1978). "The Cometary Atlas in the Silk Book of the Han Tomb at Mawangdui". In: *Wen Wu (Cultural Relics)*. DOI: 10.13619/j.cnki.cn11-1532/k.1978.02.001 (cited on page 4).
- Gulkis, S., Frerking, M., Crovisier, J., et al. (2007). "MIRO: Microwave Instrument for Rosetta Orbiter". In: *Space Science Reviews* 128.1, pp. 561–597. DOI: 10.1007/s11214-006-9032-y (cited on page 24).
- Gulkis, S., Allen, M., von Allmen, P., et al. (2015). "Subsurface Properties and Early Activity of Comet 67P/Churyumov-Gerasimenko". In: *Science* 347.6220, aaa0709. DOI: 10.1126/science.aaa0709 (cited on page 118).
- Gundlach, B., Fulle, M., and Blum, J. (2020). "On the Activity of Comets: Understanding the Gas and Dust Emission from Comet 67/Churyumov-Gerasimenko's South-Pole Region during Perihelion". In: *Monthly Notices of the Royal Astronomical Society* 493.3, pp. 3690–3715. DOI: 10/gnh7h4 (cited on pages 16–18, 33, 93, 99, 103, 111, 115, 125, 157).
- Gundlach, B., Ratte, J., Blum, J., et al. (2018a). "Sintering and Sublimation of Micrometre-Sized Water-Ice Particles: The Formation of Surface Crusts on Icy Solar System Bodies". In: *Monthly Notices of the Royal Astronomical Society* 479.4, pp. 5272–5287. DOI: 10.1093/mnras/sty1839 (cited on page 18).
- Gundlach, B., Schmidt, K. P., Kreuzig, C., et al. (2018b). "The Tensile Strength of Ice and Dust Aggregates and Its Dependence on Particle Properties". In: *Monthly Notices of the Royal Astronomical Society* 479.1, pp. 1273–1277. DOI: 10.1093/mnras/sty1550 (cited on page 17).
- Gundlach, B. and Blum, J. (2015a). "The Stickiness Of Micrometer-Sized Water-Ice Particles". In: *The Astrophysical Journal* 798.1, p. 34. DOI: 10.1088/0004-637X/798/1/34 (cited on page 19).
- Gundlach, B. and Blum, J. (2016). "Why Are Jupiter-family Comets Active and Asteroids in Cometary-like Orbits Inactive? - How Hydrostatic Compression Leads to Inactivity". In: *Astronomy & Astrophysics* 589, A111. DOI: 10.1051/0004-6361/201527260 (cited on pages 14, 51).

- Gundlach, B., Blum, J., Keller, H. U., et al. (2015b). "What Drives the Dust Activity of Comet 67P/Churyumov-Gerasimenko?" In: *Astronomy & Astrophysics* 583, A12. doi: 10.1051/0004-6361/201525828 (cited on pages 3, 17, 77, 93).
- Güttler, C., Blum, J., Zsom, A., et al. (2010). "The Outcome of Protoplanetary Dust Growth: Pebbles, Boulders, or Planetesimals? - I. Mapping the Zoo of Laboratory Collision Experiments". In: *Astronomy & Astrophysics* 513, A56. doi: 10.1051/0004-6361/200912852 (cited on page 19).
- Güttler, C., Hasselmann, P. H., Li, Y., et al. (2017). "Characterization of Dust Aggregates in the Vicinity of the Rosetta Spacecraft". In: *Monthly Notices of the Royal Astronomical Society* 469.Suppl_2, S312–S320. doi: 10.1093/mnras/stx1692 (cited on pages 34, 53, 99, 111, 115).
- Güttler, C., Mannel, T., Rotundi, A., et al. (2019). "Synthesis of the Morphological Description of Cometary Dust at Comet 67P/Churyumov-Gerasimenko". In: *Astronomy & Astrophysics* 630, A24. doi: 10/gnh7jm (cited on pages 17, 32, 93).
- Guzzo, M. and Lega, E. (2015). "A Study of the Past Dynamics of Comet 67P/Churyumov-Gerasimenko with Fast Lyapunov Indicators". In: *Astronomy & Astrophysics* 579, A79. doi: 10.1051/0004-6361/201525878 (cited on page 26).
- Guzzo, M. and Lega, E. (2017). "Scenarios for the Dynamics of Comet 67P/Churyumov-Gerasimenko over the Past 500 Kyr". In: *Monthly Notices of the Royal Astronomical Society* 469.Suppl_2, S321–S328. doi: 10.1093/mnras/stx1669 (cited on page 26).
- Hadraoui, K., Cottin, H., Ivanovski, S. L., et al. (2019). "Distributed Glycine in Comet 67P/Churyumov-Gerasimenko". In: *Astronomy & Astrophysics* 630, A32. doi: 10.1051/0004-6361/201935018 (cited on page 33).
- Hadraoui, K., Cottin, H., Ivanovski, S. L., et al. (2021). "Distributed Glycine in Comet 67P/Churyumov-Gerasimenko (Corrigendum)". In: *Astronomy & Astrophysics* 651, p. C2. doi: 10.1051/0004-6361/201935018e (cited on page 33).
- Haghighipour, N., Maindl, T. I., Schäfer, C., et al. (2016). "Triggering Sublimation-Driven Activity of Main Belt Comets". In: *The Astrophysical Journal* 830.1, p. 22. doi: 10.3847/0004-637X/830/1/22 (cited on page 14).
- Hahn, D. W. (2009). *Light Scattering Theory* (cited on page 120).
- Halley, E. (1705). *A Synopsis of the Astronomy of Comets*. Printed for John Senex, next to the Fleece Tavern, in Cornhill (cited on page 6).
- Hamel, R. E. (2007). "The Dominance of English in the International Scientific Periodical Literature and the Future of Language Use in Science". In: *AILA Review* 20.1, pp. 53–71. doi: 10.1075/aila.20.06ham. (Visited on 03/01/2024) (cited on page xiii).
- Hänni, N., Altwegg, K., Pestoni, B., et al. (2020). "First in Situ Detection of the CN Radical in Comets and Evidence for a Distributed Source". In: *Monthly Notices of the Royal Astronomical Society* 498.2, pp. 2239–2248. doi: 10.1093/mnras/staa2387 (cited on page 33).
- Hartley, R. and Zisserman, A. (2003). *Multiple View Geometry in Computer Vision*. Cambridge University Press (cited on page 38).
- Hartmann, W. K. (1969). "Terrestrial, Lunar, and Interplanetary Rock Fragmentation". In: *Icarus* 10.2, pp. 201–213. doi: 10.1016/0019-1035(69)90022-0 (cited on page 107).
- Hartmann, W. K., Tholen, D. J., and Cruikshank, D. P. (1987). "The Relationship of Active Comets, "Extinct" Comets, and Dark Asteroids". In: *Icarus* 69.1, pp. 33–50. doi: 10.1016/0019-1035(87)90005-4 (cited on page 14).
- Hasselmann, P. H., Barucci, M. A., Fornasier, S., et al. (2019). "Pronounced Morphological Changes in a Southern Active Zone on Comet 67P/Churyumov-Gerasimenko". In: *Astronomy & Astrophysics* 630, A8. doi: 10.1051/0004-6361/201833940 (cited on pages 103, 105, 107, 109, 111, 123, 156).
- Heard, S. B. (2016). *The Scientist's Guide to Writing: How to Write More Easily and Effectively throughout Your Scientific Career*. Princeton University Press (cited on page xiv).
- Heck, A. (2003). "Astronomy Professional Communication". In: *Astronomy Communication*. Ed. by A. Heck and C. Madsen. Dordrecht: Springer Netherlands, pp. 203–220. doi: 10.1007/978-94-017-0801-2_12 (cited on page xvi).
- Hein, A. M., Eubanks, T. M., Lingam, M., et al. (2022). "Interstellar Now! Missions to Explore Nearby Interstellar Objects". In: *Advances in Space Research* 69.1, pp. 402–414. doi: 10.1016/j.asr.2021.06.052 (cited on page 14).

- Heinisch, P., Auster, H.-U., Gundlach, B., et al. (2019). "Compressive Strength of Comet 67P/Churyumov-Gerasimenko Derived from Philae Surface Contacts". In: *Astronomy & Astrophysics* 630, A2. doi: 10.1051/0004-6361/201833889 (cited on page 31).
- Helin, E. F., Pravdo, S. H., Rabinowitz, D. L., et al. (1997). "Near-Earth Asteroid Tracking (NEAT) Program". In: *Proceedings of the International Conference Held*. Vol. 822. New York, USA: Annals of the New York Academy of Sciences, pp. 6–24 (cited on page 41).
- Hellman, C. D. (1975). "Kepler and Comets". In: *Vistas in Astronomy* 18, pp. 789–796. doi: 10.1016/0083-6656(75)90169-5 (cited on page 5).
- Hergenrother, C. W., Adam, C. D., Chesley, S. R., et al. (2020). "Introduction to the Special Issue: Exploration of the Activity of Asteroid (101955) Bennu". In: *Journal of Geophysical Research: Planets* 125.9. doi: 10.1029/2020je006549. (Visited on 11/19/2021) (cited on pages 14, 53).
- Hergenrother, C. W., Maleszewski, C. K., Nolan, M. C., et al. (2019). "The Operational Environment and Rotational Acceleration of Asteroid (101955) Bennu from OSIRIS-REx Observations". In: *Nature Communications* 10.1, p. 1291. doi: 10.1038/s41467-019-09213-x. (Visited on 11/19/2021) (cited on page 53).
- Herique, A., Kofman, W., Beck, P., et al. (2016). "Cosmochemical Implications of CONSERT Permittivity Characterization of 67P/CG". In: *Monthly Notices of the Royal Astronomical Society* 462.Suppl_1, S516–S532. doi: 10.1093/mnras/stx040 (cited on page 27).
- Heritier, K. L., Galand, M., Henri, P., et al. (2018). "Plasma Source and Loss at Comet 67P during the Rosetta Mission". In: *Astronomy & Astrophysics* 618, A77. doi: 10.1051/0004-6361/201832881 (cited on page 16).
- Hermalyn, B., Farnham, T. L., Collins, S. M., et al. (2013). "The Detection, Localization, and Dynamics of Large Icy Particles Surrounding Comet 103P/Hartley 2". In: *Icarus*. Stardust/EPOXI 222.2, pp. 625–633. doi: 10/f4qq8h (cited on page 38).
- Herman, A. (2013). *The Cave and the Light: Plato Versus Aristotle, and the Struggle for the Soul of Western Civilization*. Random House Publishing Group (cited on page xvi).
- Herny, C., Mousis, O., Marschall, R., et al. (2021). "New Constraints on the Chemical Composition and Outgassing of 67P/Churyumov-Gerasimenko". In: *Planetary and Space Science* 200, p. 105194. doi: 10.1016/j.pss.2021.105194 (cited on page 18).
- Hibberd, A., Perakis, N., and Hein, A. M. (2021). "Sending a Spacecraft to Interstellar Comet 2I/Borisov". In: *Acta Astronautica* 189, pp. 584–592. doi: 10.1016/j.actaastro.2021.09.006 (cited on page 14).
- Hilchenbach, M., Kissel, J., Langevin, Y., et al. (2016). "Comet 67P/Churyumov-Gerasimenko: Close-Up On Dust Particle Fragments". In: *The Astrophysical Journal* 816.2, p. L32. doi: 10.3847/2041-8205/816/2/L32 (cited on pages 32, 107).
- Hirao, K. and Itoh, T. (1988). "The Sakigake/Suisei Encounter with Comet P/Halley". In: *Exploration of Halley's Comet*. Ed. by M. Grewing, F. Praderie, and R. Reinhard. Berlin, Heidelberg: Springer, pp. 39–46. doi: 10.1007/978-3-642-82971-0_6 (cited on page 23).
- Hirshfeld, A. W. (2013). *Parallax: The Race to Measure the Cosmos*. Courier Corporation (cited on page 4).
- Hoag, D. G. (1983). "The History of Apollo Onboard Guidance, Navigation, and Control". In: *Journal of Guidance, Control, and Dynamics* 6.1, pp. 4–13. doi: 10/b8x8fq (cited on page 40).
- Hoffmeister, C. (1943). "Physikalische Untersuchungen an Kometen. I. Die Beziehungen Des Primären Schweifstrahls Zum Radiusvektor. Mit 2 Abbildungen." In: *Zeitschrift für Astrophysik* 22, p. 265 (cited on page 16).
- Höfner, S., Vincent, J.-B., Blum, J., et al. (2017). "Thermophysics of Fractures on Comet 67P/Churyumov-Gerasimenko". In: *Astronomy & Astrophysics* 608, A121. doi: 10.1051/0004-6361/201628726 (cited on pages 105, 107, 156).
- Holman, M. J., Payne, M. J., Blankley, P., et al. (2018). "HelioLinC: A Novel Approach to the Minor Planet Linking Problem". In: *The Astronomical Journal* 156.3, p. 135. doi: 10.3847/1538-3881/aad69a. (Visited on 11/19/2021) (cited on pages 41, 53).
- Hough, P. V. C. (1959). "Machine Analysis of Bubble Chamber Pictures". In: *Proc. of the International Conference on High Energy Accelerators and Instrumentation*. Ed. by L. Kowarski. Vol. 590914, pp. 554–558 (cited on page 53).

- Hsieh, C.-H., Laughlin, G., and Arce, H. G. (2021). "Evidence Suggesting That 'Oumuamua Is the ~30 Myr Old Product of a Molecular Cloud". In: *The Astrophysical Journal* 917.1, p. 20. doi: 10.3847/1538-4357/ac0729. (Visited on 04/29/2024) (cited on page 14).
- Hsieh, H. H. (2015). "Main-Belt Comets: Sublimation-Driven Activity in the Asteroid Belt". In: *Proceedings of the International Astronomical Union* 10.S318, pp. 99–110. doi: 10.1017/S1743921315008546 (cited on page 13).
- Hsieh, H. H. (2017). "Asteroid–Comet Continuum Objects in the Solar System". In: *Philosophical Transactions of the Royal Society A: Mathematical, Physical and Engineering Sciences* 375.2097, p. 20160259. doi: 10.1098/rsta.2016.0259 (cited on page 13).
- Hsieh, H. H. and Jewitt, D. (2006). "A Population of Comets in the Main Asteroid Belt". In: *Science* 312.5773, pp. 561–563. doi: 10.1126/science.1125150 (cited on page 13).
- Hsieh, H. H., Jewitt, D. C., and Fernández, Y. R. (2004). "The Strange Case of 133P/Elst-Pizarro: A Comet among the Asteroids". In: *The Astronomical Journal* 127.5, p. 2997. doi: 10.1086/383208 (cited on pages 13, 14).
- Hsieh, H. H., Jewitt, D. C., Lacerda, P., et al. (2010). "The Return of Activity in Main-Belt Comet 133P/Elst-Pizarro". In: *Monthly Notices of the Royal Astronomical Society* 403.1, pp. 363–377. doi: 10.1111/j.1365-2966.2009.16120.x (cited on page 13).
- Hu, X., Shi, X., Sierks, H., et al. (2017a). "Seasonal Erosion and Restoration of the Dust Cover on Comet 67P/Churyumov-Gerasimenko as Observed by OSIRIS Onboard Rosetta". In: *Astronomy & Astrophysics* 604, A114. doi: 10.1051/0004-6361/201629910 (cited on page 30).
- Hu, X., Shi, X., Sierks, H., et al. (2017b). "Thermal Modelling of Water Activity on Comet 67P/Churyumov-Gerasimenko with Global Dust Mantle and Plural Dust-to-Ice Ratio". In: *Monthly Notices of the Royal Astronomical Society* 469.Suppl_2, S295–S311. doi: 10.1093/mnras/stx1607 (cited on page 18).
- Hu, X. and Shi, X. (2021). "Thermophysical Characterization of Cyclic Frost Formation in the Subsurface and Nominal Water Activity on Comets: Case Study of 67P/Churyumov-Gerasimenko". In: *The Astrophysical Journal* 910.1, p. 10. doi: 10.3847/1538-4357/abdbbf (cited on pages 30, 158).
- Hubscher, S. L. (2007). *Apophenia: Definition and Analysis*. <https://archive.ph/5B2UI> (cited on page 85).
- Huebner, W. F., Benkhoff, J., Capria, M.-T., et al. (2006). *Heat And Gas Diffusion In Comet Nuclei* (cited on pages 118, 119).
- Hughes, D. W. (1988). "The 'Principia' and Comets". In: *Notes and Records of the Royal Society of London* 42.1, pp. 53–74. doi: 10.1098/rsnr.1988.0007 (cited on page 5).
- Hui, M.-T., Farnocchia, D., and Micheli, M. (2019). "C/2010 U3 (Boattini): A Bizarre Comet Active at Record Heliocentric Distance". In: *The Astronomical Journal* 157.4, p. 162. doi: 10.3847/1538-3881/ab0e09 (cited on page 14).
- Humpherys, J., Redd, P., and West, J. (2012). "A Fresh Look at the Kalman Filter". In: *SIAM Review* 54.4, pp. 801–823. doi: 10.1137/100799666. (Visited on 05/04/2024) (cited on pages 38, 39).
- Hunter, A., ed. (2016). *Thornton and Tully's Scientific Books, Libraries and Collectors: A Study of Bibliography and the Book Trade in Relation to the History of Science*. Routledge (cited on pages xiv, xvi).
- Hurwitz, S. and Manga, M. (2017). "The Fascinating and Complex Dynamics of Geyser Eruptions". In: *Annual Review of Earth and Planetary Sciences* 45. Volume 45, 2017, pp. 31–59. doi: 10.1146/annurev-earth-063016-015605. (Visited on 05/01/2024) (cited on page 104).
- Huxley, T. H. (1885). "Anniversary Meeting". In: *Proceedings of the Royal Society of London*. Vol. 39. The Royal Society; <https://web.archive.org/web/20240306093904/https://www.jstor.org/stable/114186>, pp. 277–313. (Visited on 03/06/2024) (cited on page xvi).
- Ip, W. -. and Mendis, D. A. (1974). "Neutral Atmospheres of Comets: A Distributed Source Model". In: *Astrophysics and Space Science* 26, pp. 153–166. doi: 10.1007/BF00642630 (cited on page 33).
- Ip, W.-H. and Jorda, L. (1998). "Can the Sodium Tail of Comet Hale-Bopp Have a Dust-Impact Origin?" In: *The Astrophysical Journal* 496.1, p. L47. doi: 10.1086/311241 (cited on page 16).
- Irwin, M. J. (1985). "Automatic Analysis of Crowded Fields". In: *Monthly Notices of the Royal Astronomical Society* 214.4, pp. 575–604. doi: 10.1093/mnras/214.4.575 (cited on page 58).
- Ishiguro, M. (2008). "Cometary Dust Trail Associated with Rosetta Mission Target: 67P/Churyumov-Gerasimenko". In: *Icarus* 193.1, pp. 96–104. doi: 10.1016/j.icarus.2007.08.027 (cited on page 107).

- Ivanovski, S. L., Della Corte, V., Rotundi, A., et al. (2017a). “Dynamics of Non-Spherical Dust in the Coma of 67P/Churyumov–Gerasimenko Constrained by GIADA and ROSINA Data”. In: *Monthly Notices of the Royal Astronomical Society* 469.Suppl_2, S774–S786. doi: 10.1093/mnras/stx3008 (cited on pages 22, 99, 117).
- Ivanovski, S. L., Zakharov, V. V., Moreno, F., et al. (2024). “On the Similarity of Rotational Motion of Dust Particles in the Inner Atmosphere of Comets”. In: *Monthly Notices of the Royal Astronomical Society* 528.4, pp. 5723–5729. doi: 10.1093/mnras/stad2665 (cited on page 22).
- Ivanovski, S. L., Zakharov, V., Della Corte, V., et al. (2017b). “Dynamics of Aspherical Dust Grains in a Cometary Atmosphere: I. Axially Symmetric Grains in a Spherically Symmetric Atmosphere”. In: *Icarus* 282, pp. 333–350. doi: 10/gnh7hp (cited on pages 22, 99, 117).
- Jackman, C. D. and Dumont, P. J. (2013). “Optical Navigation Capabilities for Deep Space Missions”. In: *Proceedings of the 23rd AAS/AIAA Space Flight Mechanics Conference* (cited on page 40).
- Jackman, C. D., Nelson, D. S., Mccarthy, L. K., et al. (2017). “Optical Navigation Concept of Operations for the OSIRIS-REX Mission”. In: *27th AAS/AIAA Space Flight Mechanics Meeting, Washington, DC* (cited on page 40).
- Jacobi, C. G. J. (1836). “Sur Le Mouvement d’un Point et Sur Un Cas Particulier Du Problème Des Trois Corps”. In: *Comptes Rendus de l’Académie des Sciences de Paris* 3, pp. 59–61 (cited on pages 7, 12).
- Jansson, T. (2003). *Comet in Moominland*. Penguin UK (cited on page 153).
- Jardine, N. (1988). *The Birth of History and Philosophy of Science: Kepler’s ‘A Defence of Tycho against Ursus’ with Essays on Its Provenance and Significance*. Cambridge University Press (cited on page xvi).
- Jewitt, D. C. (2002). “From Kuiper Belt Object to Cometary Nucleus: The Missing Ultrared Matter”. In: *The Astronomical Journal* 123.2, p. 1039. doi: 10.1086/338692 (cited on page 10).
- Jewitt, D. C. (2005). “A First Look at the Damocloids”. In: *The Astronomical Journal* 129.1, p. 530. doi: 10.1086/426328. (Visited on 04/29/2024) (cited on page 14).
- Jewitt, D. C. (2012). “The Active Asteroids”. In: *The Astronomical Journal* 143.3, p. 66. doi: 10.1088/0004-6256/143/3/66 (cited on page 13).
- Jewitt, D. C., Agarwal, J., Hui, M.-T., et al. (2019a). “Distant Comet C/2017 K2 and the Cohesion Bottleneck”. In: *The Astronomical Journal* 157.2, p. 65. doi: 10.3847/1538-3881/aaef38c (cited on page 17).
- Jewitt, D. C., Hsieh, H., and Agarwal, J. (2015). “The Active Asteroids”. In: *Asteroids IV*. Ed. by P. Michel, F. E. DeMeo, and W. F. Bottke. University of Arizona Press, pp. 221–241. doi: 10.2458/azu_uapress_9780816532131-ch012 (cited on pages 13, 14).
- Jewitt, D. C. and Hsieh, H. H. (2022). *The Asteroid-Comet Continuum*. doi: 10.48550/arXiv.2203.01397. URL: <http://arxiv.org/abs/2203.01397> (cited on page 13).
- Jewitt, D. C., Hui, M.-T., Mutchler, M., et al. (2017). “A Comet Active Beyond the Crystallization Zone”. In: *The Astrophysical Journal Letters* 847.2, p. L19. doi: 10.3847/2041-8213/aa88b4 (cited on page 14).
- Jewitt, D. C., Ishiguro, M., Weaver, H., et al. (2014). “Hubble Space Telescope Investigation of Main-Belt Comet 133P/Elst-Pizarro”. In: *The Astronomical Journal* 147.5, p. 117. doi: 10.1088/0004-6256/147/5/117 (cited on page 13).
- Jewitt, D. C., Kim, Y., Mutchler, M., et al. (2021). “Cometary Activity Begins at Kuiper Belt Distances: Evidence from C/2017 K2”. In: *The Astronomical Journal* 161.4, p. 188. doi: 10/gnh7hb (cited on page 14).
- Jewitt, D. C. and Luu, J. (2019b). “Initial Characterization of Interstellar Comet 2I/2019 Q4 (Borisov)”. In: *The Astrophysical Journal Letters* 886.2, p. L29. doi: 10.3847/2041-8213/ab530b. (Visited on 04/29/2024) (cited on page 14).
- Jiang, Y. and Schmidt, J. (2020). “Motion of Dust Ejected from the Surface of Asteroid (101955) Bennu”. In: *Heliyon* 6.10, e05275. doi: 10/gnkwmf (cited on pages 22, 115).
- Johansen, A., Blum, J., Tanaka, H., et al. (2014). “The Multifaceted Planetesimal Formation Process”. In: *Protostars and Planets VI*. Ed. by H. Beuther, R. S. Klessen, C. P. Dullemond, et al. eprint: arXiv:1402.1344: University of Arizona Press (cited on page 19).
- Johansen, A., Oishi, J. S., Low, M.-M. M., et al. (2007). “Rapid Planetesimal Formation in Turbulent Circumstellar Disks”. In: *Nature* 448.7157, pp. 1022–1025. doi: 10.1038/nature06086 (cited on pages 19, 20).
- Johnson, R., Watkinson, A., and Mabe, M. A. (2018). *The STM Report: An Overview of Scientific and Scholarly Publishing*. Tech. rep. International Association of Scientific, Technical and Medical Publishers (cited on page xv).

- Jolliffe, I. T. and Cadima, J. (2016). "Principal Component Analysis: A Review and Recent Developments". In: *Philosophical Transactions of the Royal Society A: Mathematical, Physical and Engineering Sciences* 374.2065, p. 20150202. doi: 10.1098/rsta.2015.0202 (cited on page 76).
- Jones, G. H., Knight, M. M., Battams, K., et al. (2017). "The Science of Sungrazers, Sunskirters, and Other Near-Sun Comets". In: *Space Science Reviews* 214.1, p. 20. doi: 10.1007/s11214-017-0446-5 (cited on page 15).
- Jones, G. H., Snodgrass, C., Tubiana, C., et al. (2024). "The Comet Interceptor Mission". In: *Space Science Reviews* 220.1, p. 9. doi: 10.1007/s11214-023-01035-0 (cited on page 23).
- Jones, R. L., Slater, C. T., Moeyens, J., et al. (2018). "The Large Synoptic Survey Telescope as a Near-Earth Object Discovery Machine". In: *Icarus* 303, pp. 181–202. doi: 10.1016/j.icarus.2017.11.033. (Visited on 11/19/2021) (cited on pages 41, 53).
- Jorda, L., Gaskell, R., Capanna, C., et al. (2016). "The Global Shape, Density and Rotation of Comet 67P/Churyumov-Gerasimenko from Preperihelion Rosetta/OSIRIS Observations". In: *Icarus* 277, pp. 257–278. doi: 10.1016/j.icarus.2016.05.002 (cited on pages 29, 103).
- Jourdan, F., Timms, N. E., Nakamura, T., et al. (2023). "Rubble Pile Asteroids Are Forever". In: *Proceedings of the National Academy of Sciences* 120.5, e2214353120. doi: 10.1073/pnas.2214353120 (cited on page 155).
- Junkins, J. L., White, C. C., and Turner, J. D. (1977). "Star Pattern Recognition for Real Time Attitude Determination". In: *Journal of the Astronautical Sciences* 25.3, pp. 251–270 (cited on page 40).
- Jutzi, M. and Asphaug, E. (2015). "The Shape and Structure of Cometary Nuclei as a Result of Low-Velocity Accretion". In: *Science* 348.6241, pp. 1355–1358. doi: 10.1126/science.aaa4747 (cited on pages 26, 154).
- Jutzi, M. and Benz, W. (2017a). "Formation of Bi-Lobed Shapes by Sub-Catastrophic Collisions - A Late Origin of Comet 67P's Structure". In: *Astronomy & Astrophysics* 597, A62. doi: 10.1051/0004-6361/201628964 (cited on page 27).
- Jutzi, M., Benz, W., Toliou, A., et al. (2017b). "How Primordial Is the Structure of Comet 67P? - Combined Collisional and Dynamical Models Suggest a Late Formation". In: *Astronomy & Astrophysics* 597, A61. doi: 10.1051/0004-6361/201628963 (cited on page 27).
- Kadono, T., Arakawa, M., Honda, R., et al. (2020). "Impact Experiment on Asteroid (162173) Ryugu: Structure beneath the Impact Point Revealed by In Situ Observations of the Ejecta Curtain". In: *The Astrophysical Journal* 899.1, p. L22. doi: 10/gnh592 (cited on page 104).
- Kaib, N. A., Parsells, A., Grimm, S., et al. (2024). "More Realistic Planetesimal Masses Alter Kuiper Belt Formation Models and Add Stochasticity". In: *Icarus* 415, p. 116057. doi: 10.1016/j.icarus.2024.116057. (Visited on 04/08/2024) (cited on page 10).
- Kalman, R. E. (1960). "A New Approach to Linear Filtering and Prediction Problems". In: *Journal of Basic Engineering* 82.1, pp. 35–45. doi: 10.1115/1.3662552 (cited on page 38).
- Kant, I. (1755). *Allgemeine Naturgeschichte Und Theorie Des Himmels*. 1. Auflage. Königsberg; Leipzig: Petersen (cited on page 19).
- Kavelaars, J. J., Petit, J.-M., Gladman, B., et al. (2021). "OSSOS Finds an Exponential Cutoff in the Size Distribution of the Cold Classical Kuiper Belt". In: *The Astrophysical Journal Letters* 920.2, p. L28. doi: 10.3847/2041-8213/ac2c72. (Visited on 04/08/2024) (cited on page 8).
- Keller, H. U. (1989). "Comets - Dirty Snowballs or Icy Dirtballs?" In: *Proceedings of an International Workshop on Physics and Mechanics of Cometary Materials*. Vol. 302. ESA, pp. 39–45 (cited on page 17).
- Keller, H. U., Arpigny, C., Barbieri, C., et al. (1986). "First Halley Multicolour Camera Imaging Results from Giotto". In: *Nature* 321.6067, pp. 320–326. doi: 10.1038/321320a0 (cited on page 16).
- Keller, H. U., Barbieri, C., Lamy, P., et al. (2007). "OSIRIS – The Scientific Camera System Onboard Rosetta". In: *Space Science Reviews* 128.1-4, pp. 433–506. doi: 10.1007/s11214-006-9128-4 (cited on pages 3, 24, 25, 53, 93, 95).
- Keller, H. U., Delamere, W. A., Reitsema, H. J., et al. (1987). "Comet P/Halley's Nucleus and Its Activity". In: *Astronomy and Astrophysics* 187, pp. 807–823 (cited on page 105).
- Keller, H. U., Mottola, S., Davidsson, B., et al. (2015a). "Insolation, Erosion, and Morphology of Comet 67P/Churyumov-Gerasimenko". In: *Astronomy & Astrophysics* 583, A34. doi: 10.1051/0004-6361/201525964 (cited on pages 30, 113).

- Keller, H. U., Mottola, S., Hviid, S. F., et al. (2017). “Seasonal Mass Transfer on the Nucleus of Comet 67P/Churyumov–Gerasimenko”. In: *Monthly Notices of the Royal Astronomical Society* 469.Suppl_2, S357–S371. doi: 10.1093/mnras/stx1726 (cited on pages 30, 33, 53, 113).
- Keller, H. U., Mottola, S., Skorov, Y., et al. (2015b). “The Changing Rotation Period of Comet 67P/Churyumov–Gerasimenko Controlled by Its Activity”. In: *Astronomy & Astrophysics* 579, p. L5. doi: 10.1051/0004-6361/201526421 (cited on pages 29, 51).
- Kelley, M. S., Lindler, D. J., Bodewits, D., et al. (2013). “A Distribution of Large Particles in the Coma of Comet 103P/Hartley 2”. In: *Icarus. Stardust/EPOXI* 222.2, pp. 634–652. doi: 10.1016/j.icarus.2012.09.037. (Visited on 02/08/2022) (cited on pages 34, 38, 53, 88, 99, 103, 107, 109, 115).
- Kelley, M. S., Lindler, D. J., Bodewits, D., et al. (2015). “Erratum to “A Distribution of Large Particles in the Coma of Comet 103P/Hartley 2””. In: *Icarus* 262, pp. 187–189. doi: 10.1016/j.icarus.2015.09.004 (cited on pages 38, 53, 88, 99, 103, 107, 109, 115).
- Kelley, M. S., Reach, W. T., and Lien, D. J. (2008). “The Dust Trail of Comet 67P/Churyumov–Gerasimenko”. In: *Icarus. Saturn’s Icy Satellites from Cassini* 193.2, pp. 572–587. doi: 10.1016/j.icarus.2007.08.018 (cited on page 107).
- Kelley, M. S., Wooden, D. H., Tubiana, C., et al. (2009). “Spitzer Observations Of Comet 67P/Churyumov–Gerasimenko At 5.5–4.3 Au From The Sun”. In: *The Astronomical Journal* 137.6, pp. 4633–4642. doi: 10.1088/0004-6256/137/6/4633 (cited on page 107).
- Kepler, J. (1606). *De Stella nova in pede serpentarii*. Ex officina Pauli Sessii (cited on page xvi).
- Kepler, J. (1619a). *De cometis libelli tres*. Augsburg: Apergeri, Andreae (cited on pages 5, 15).
- Kepler, J. (1619b). *Harmonices mundi*. Linz, Austria: Johann Planck (cited on page 11).
- Kepler, J., Brahe, T., Rudolph II, e. o. G., et al. (1609). *Astronomia nova*. Heidelberg: G. Voegelinus (cited on page 4).
- Kerr, R. A. (2003). “Failed CONTOUR Comet Mission Melted Itself Down”. In: *Science* 302.5645, pp. 546–546. doi: 10.1126/science.302.5645.546a (cited on page 23).
- Kim, M., Mannel, T., Boakes, P. D., et al. (2023). “Cometary Dust Collected by MIDAS on Board Rosetta - I. Dust Particle Catalog and Statistics”. In: *Astronomy & Astrophysics* 673, A129. doi: 10.1051/0004-6361/202245262 (cited on page 32).
- Kim, Y., Agarwal, J., Jewitt, D., et al. (2022). “Sublimation Origin of Active Asteroid P/2018 P3”. In: *Astronomy & Astrophysics* 666, A163. doi: 10.1051/0004-6361/202244356 (cited on page 13).
- Kimura, H. and Liu, C.-p. (1977). “On the Structure of Cometary Dust Tails”. In: *Chinese Astronomy* 1.2, pp. 235–264. doi: 10.1016/0146-6364(77)90004-4 (cited on page 16).
- Kissel, J., Altwegg, K., Clark, B. C., et al. (2007). “Cosima – High Resolution Time-of-Flight Secondary Ion Mass Spectrometer for the Analysis of Cometary Dust Particles Onboard Rosetta”. In: *Space Science Reviews* 128.1, pp. 823–867. doi: 10.1007/s11214-006-9083-0 (cited on page 24).
- Klaus, A., Yu, S., and Plenz, D. (2011). “Statistical Analyses Support Power Law Distributions Found in Neuronal Avalanches”. In: *PLOS ONE* 6.5, e19779. doi: 10.1371/journal.pone.0019779 (cited on page 109).
- Knollenberg, J., Lin, Z. Y., Hviid, S. F., et al. (2016). “A Mini Outburst from the Nightside of Comet 67P/Churyumov–Gerasimenko Observed by the OSIRIS Camera on Rosetta”. In: *Astronomy & Astrophysics* 596, A89. doi: 10.1051/0004-6361/201527744 (cited on page 119).
- Knox-Shaw, H. (1934). “Apology to a Blink-Microscope”. In: *The Observatory* 57, pp. 382–382 (cited on page 41).
- Knudsen, M. (1909). “Die Gesetze Der Molekularströmung Und Der Inneren Reibungsströmung Der Gase Durch Röhren”. In: *Annalen der Physik* 333, pp. 75–130. doi: 10.1002/andp.19093330106 (cited on page 21).
- Kofman, W., Herique, A., Goutail, J.-P., et al. (2007). “The Comet Nucleus Sounding Experiment by Radiowave Transmission (CONSERT): A Short Description of the Instrument and of the Commissioning Stages”. In: *Space Science Reviews* 128.1, pp. 413–432. doi: 10.1007/s11214-006-9034-9 (cited on page 24).
- Kofman, W., Herique, A., Barbin, Y., et al. (2015). “Properties of the 67P/Churyumov–Gerasimenko Interior Revealed by CONSERT Radar”. In: *Science* 349.6247, aab0639. doi: 10.1126/science.aab0639 (cited on page 27).
- Kofman, W., Zine, S., Herique, A., et al. (2020). “The Interior of Comet 67P/C–G; Revisiting CONSERT Results with the Exact Position of the Philae Lander”. In: *Monthly Notices of the Royal Astronomical Society* 497.3, pp. 2616–2622. doi: 10.1093/mnras/staa2001 (cited on page 27).

- Kolbe, D. and Best, R. (1997). "The ROSETTA Mission". In: *Acta Astronautica*. Developing Business 41.4, pp. 569–577. doi: 10.1016/S0094-5765(98)00072-1 (cited on page 22).
- Kong, Y., Seo, Y. S., and Zhai, L. (2018). "Comparison of Reading Performance on Screen and on Paper: A Meta-Analysis". In: *Computers & Education* 123, pp. 138–149. doi: 10.1016/j.compedu.2018.05.005 (cited on page xvii).
- Kothe, S. (2017). "Mikrogravitationsexperimente zur Entwicklung eines empirischen Stoßmodells für proto-planetare Staubagglomerate". PhD thesis. Technische Universität Braunschweig. doi: 10.24355/dbbs.084-201701031210-0 (cited on page 19).
- Kovács, G. (2018). *OSIRIS Calibration Pipeline OsiCalliope* (cited on page 64).
- Kowal, C. T., Liller, W., and Marsden, B. G. (1979). "The Discovery and Orbit of (2060) Chiron". In: *Proceedings of the Symposium*. Vol. 81. Tokyo, Japan: D. Reidel Publishing Co., p. 245 (cited on page 12).
- Kramer, T. and Läuter, M. (2019a). "Outgassing-Induced Acceleration of Comet 67P/Churyumov-Gerasimenko". In: *Astronomy & Astrophysics* 630, A4. doi: 10.1051/0004-6361/201935229 (cited on pages 12, 16, 29).
- Kramer, T., Läuter, M., Hviid, S., et al. (2019b). "Comet 67P/Churyumov-Gerasimenko Rotation Changes Derived from Sublimation-Induced Torques". In: *Astronomy & Astrophysics* 630, A3. doi: 10.1051/0004-6361/201834349 (cited on page 29).
- Kramer, T. and Noack, M. (2015). "Prevailing Dust-Transport Directions On Comet 67P/Churyumov-Gerasimenko". In: *The Astrophysical Journal* 813.2, p. L33. doi: 10.1088/2041-8205/813/2/L33 (cited on page 119).
- Kramer, T. and Noack, M. (2016). "On The Origin Of Inner Coma Structures Observed By Rosetta During A Diurnal Rotation Of Comet 67P/Churyumov-Gerasimenko". In: *The Astrophysical Journal Letters* 823.1, p. L11. doi: 10.3847/2041-8205/823/1/L11 (cited on page 119).
- Kresák, L. (1954). "On a Criterion Concerning the Perturbing Action of the Earth on Meteor Streams". In: *Bulletin of the Astronomical Institutes of Czechoslovakia* 5, p. 45 (cited on page 12).
- Kresák, L. (1972). "Jacobian Integral as a Classificational and Evolutionary Parameter of Interplanetary Bodies". In: *Bulletin of the Astronomical Institutes of Czechoslovakia* 23, p. 1 (cited on page 12).
- Kretke, K. A. and Levison, H. F. (2015). "Evidence for Pebbles in Comets". In: *Icarus* 262, pp. 9–13. doi: 10.1016/j.icarus.2015.08.017 (cited on page 106).
- Krolikowska, M. (2003). "67P/Churyumov-Gerasimenko – Potential Target for the Rosetta Mission". In: *Acta Astronomica* 53, pp. 195–209. doi: 10.48550/arXiv.astro-ph/0309130 (cited on page 26).
- Królikowska, M. and Dybczyński, P. A. (2020). "The Catalogue of Cometary Orbits and Their Dynamical Evolution". In: *Astronomy & Astrophysics* 640, A97. doi: 10.1051/0004-6361/202038451 (cited on pages 10, 11).
- Kronk, G. W. (1999). *Cometography: Volume 2, 1800-1899: A Catalog of Comets*. Cambridge University Press (cited on page 7).
- Kruse, O. (2006). "The Origins of Writing in the Disciplines: Traditions of Seminar Writing and the Humboldtian Ideal of the Research University". In: *Written Communication* 23.3, pp. 331–352. doi: 10.1177/0741088306289259. (Visited on 02/26/2024) (cited on page xiv).
- Kubica, J., Denneau, L., Grav, T., et al. (2007). "Efficient Intra- and Inter-Night Linking of Asteroid Detections Using Kd-Trees". In: *Icarus* 189.1, pp. 151–168. doi: 10.1016/j.icarus.2007.01.008. (Visited on 11/19/2021) (cited on pages 41, 53).
- Kubota, F. I., Cauchick-Miguel, P. A., Tortorella, G., et al. (2021). "Paper-Based Thesis and Dissertations: Analysis of Fundamental Characteristics for Achieving a Robust Structure". In: *Production* 31, e20200100. doi: 10.1590/0103-6513.20200100. (Visited on 02/28/2024) (cited on page xv).
- Kueppers, M., Martino, P., Carnelli, I., et al. (2023). "Ramses – ESA's Study for a Small Mission to Apophis". In: *Bulletin of the AAS* 55.8 (cited on page 154).
- Kührt, E. and Keller, H. U. (1994). "The Formation of Cometary Surface Crusts". In: *Icarus* 109.1, pp. 121–132. doi: 10.1006/icar.1994.1080 (cited on pages 16, 17).
- Kuiper, G. P. (1951). "On the Origin of the Solar System". In: *Proceedings of the National Academy of Sciences* 37.1, pp. 1–14. doi: 10.1073/pnas.37.1.1 (cited on page 7).
- Kümmel, M., Bertin, E., Schefer, M., et al. (2020). "Working With the SourceXtractor++ Software". In: *Astronomical Data Analysis Software and Systems XXIX*. Vol. 527. Groningen, the Netherlands: Astronomical Society of the Pacific, p. 29 (cited on page 58).

- Kwon, Y. G., Opitom, C., and Lippi, M. (2023). “Coma Environment of Comet C/2017 K2 around the Water Ice Sublimation Boundary Observed with VLT/MUSE”. In: *Astronomy & Astrophysics* 674, A206. doi: 10.1051/0004-6361/202345989 (cited on pages 119, 125, 158).
- Kyriazis, N. (2021). “Attitude-Schwankungen und -korrekturen der Rosetta-Sonde am Kometen 67P”. PhD thesis. Braunschweig: Technische Universität Braunschweig (cited on page 66).
- La Forgia, F., Giacomini, L., Lazzarin, M., et al. (2015). “Geomorphology and Spectrophotometry of Philae’s Landing Site on Comet 67P/Churyumov-Gerasimenko”. In: *Astronomy & Astrophysics* 583, A41. doi: 10.1051/0004-6361/201525983 (cited on page 107).
- Lagrange, J.-L. (1785). “Recherches Sur La Theorie Des Perturbations Que Les Comètes Peuvent Eprouver Par L’Action Des Planètes”. In: *Mémoires de Mathématique et de Physique, Présentés à l’Académie Royale Des Sciences, Par Divers Sçavans & Lûs Dans Ses Assemblées*. Vol. 10. Paris, pp. 65–160 (cited on page 7).
- Lai, I.-L., Ip, W.-H., Lee, J.-C., et al. (2019). “Seasonal Variations in Source Regions of the Dust Jets on Comet 67P/Churyumov-Gerasimenko”. In: *Astronomy & Astrophysics* 630, A17. doi: 10/gjfd42 (cited on page 105).
- Lai, I.-L., Ip, W.-H., Su, C.-C., et al. (2016). “Gas Outflow and Dust Transport of Comet 67P/Churyumov-Gerasimenko”. In: *Monthly Notices of the Royal Astronomical Society* 462.Suppl_1, S533–S546. doi: 10.1093/mnras/stx332 (cited on pages 30, 53, 107, 113).
- Lamy, P. L., Toth, I., Weaver, H. A., et al. (2006). “Hubble Space Telescope Observations of the Nucleus and Inner Coma of Comet 67P/Churyumov-Gerasimenko”. In: *Astronomy & Astrophysics* 458.2, pp. 669–678. doi: 10.1051/0004-6361:20065253 (cited on page 26).
- Lamy, P. L., Toth, I., Davidsson, B. J. R., et al. (2007). “A Portrait of the Nucleus of Comet 67P/Churyumov-Gerasimenko”. In: *Space Science Reviews* 128.1, pp. 23–66. doi: 10.1007/s11214-007-9146-x (cited on pages 23, 26).
- Lang, D., Hogg, D. W., and Mykytyn, D. (2016). “The Tractor: Probabilistic Astronomical Source Detection and Measurement”. In: *Astrophysics Source Code Library*, ascl:1604.008 (cited on page 58).
- Langevin, Y., Hilchenbach, M., Ligier, N., et al. (2016). “Typology of Dust Particles Collected by the COSIMA Mass Spectrometer in the Inner Coma of 67P/Churyumov Gerasimenko”. In: *Icarus* 271, pp. 76–97. doi: 10.1016/j.icarus.2016.01.027 (cited on page 32).
- Langevin, Y., Hilchenbach, M., Vincendon, M., et al. (2017). “Optical Properties of Cometary Particles Collected by the COSIMA Mass Spectrometer On-Board Rosetta during the Rendezvous Phase around Comet 67P/Churyumov-Gerasimenko”. In: *Monthly Notices of the Royal Astronomical Society* 469.Suppl_2, S535–S549. doi: 10.1093/mnras/stx2070 (cited on page 32).
- Laplace, P. S. de (1805). *Traité de mécanique céleste*. Vol. 4. Paris: chez Courcier (cited on page 7).
- Laplace, P. S. de (1813). *Exposition du Système du Monde*. 4th ed. Paris: Courcier (cited on page 16).
- Lara, L. M., Lowry, S., Vincent, J.-B., et al. (2015). “Large-Scale Dust Jets in the Coma of 67P/Churyumov-Gerasimenko as Seen by the OSIRIS Instrument Onboard Rosetta”. In: *Astronomy & Astrophysics* 583, A9. doi: 10.1051/0004-6361/201526103 (cited on page 30).
- Larsen, J. A., Roe, E. S., Albert, C. E., et al. (2007). “The Search for Distant Objects in the Solar System Using Spacewatch”. In: *The Astronomical Journal* 133.4, pp. 1247–1270. doi: 10.1086/511155. (Visited on 11/19/2021) (cited on page 41).
- Larsson, M., Geppert, W. D., and Nyman, G. (2012). “Ion Chemistry in Space”. In: *Reports on Progress in Physics* 75.6, p. 066901. doi: 10.1088/0034-4885/75/6/066901 (cited on page 16).
- Laurent-Varin, J., James, T., Marty, J.-C., et al. (2024). *New Gravity Field of Comet 67P/C-G Based on Rosetta’s Doppler and Optical Data*. doi: 10.48550/arXiv.2409.02692 (cited on page 29).
- Lauretta, D. S., Hergenrother, C. W., Chesley, S. R., et al. (2019). “Episodes of Particle Ejection from the Surface of the Active Asteroid (101955) Bennu”. In: *Science* 366.6470, eaay3544. doi: 10.1126/science.aay3544. (Visited on 11/19/2021) (cited on page 53).
- Läuter, M., Kramer, T., Rubin, M., et al. (2019). “Surface Localization of Gas Sources on Comet 67P/Churyumov-Gerasimenko Based on DFMS/COPS Data”. In: *Monthly Notices of the Royal Astronomical Society* 483.1, pp. 852–861. doi: 10.1093/mnras/sty3103 (cited on page 107).
- Läuter, M., Kramer, T., Rubin, M., et al. (2020). “The Gas Production of 14 Species from Comet 67P/Churyumov-Gerasimenko Based on DFMS/COPS Data from 2014 to 2016”. In: *Monthly Notices of the Royal Astronomical Society* 498.3, pp. 3995–4004. doi: 10.1093/mnras/staa2643 (cited on pages 103, 107).

- Läuter, M., Kramer, T., Rubin, M., et al. (2022). “The Ice Composition Close to the Surface of Comet 67P/Churyumov-Gerasimenko”. In: *ACS Earth and Space Chemistry* 6.5, pp. 1189–1203. doi: 10.1021/acsearthspacechem.1c00378 (cited on pages 107, 117, 123, 156).
- Lebofsky, L. A., Feierberg, M. A., Tokunaga, A. T., et al. (1981). “The 1.7- to 4.2-Mm Spectrum of Asteroid 1 Ceres: Evidence for Structural Water in Clay Minerals”. In: *Icarus* 48.3, pp. 453–459. doi: 10.1016/0019-1035(81)90055-5 (cited on page 13).
- Lee, J.-C., Massironi, M., Ip, W.-H., et al. (2016). “Geomorphological Mapping of Comet 67P/Churyumov-Gerasimenko’s Southern Hemisphere”. In: *Monthly Notices of the Royal Astronomical Society* 462.Supp_1, S573–S592. doi: 10.1093/mnras/stx450 (cited on pages 31, 105, 156).
- Leeuwen, J. van (2016). “Manuscripts”. In: *A Companion to the History of Science*. Ed. by B. Lightman. John Wiley & Sons, Ltd. Chap. 23, pp. 329–343. doi: 10.1002/9781118620762.ch23 (cited on page xiii).
- Legendre, A. M. (1805). *Nouvelles méthodes pour la détermination des orbites des comètes*. F. Didot (cited on page 7).
- Lemos, P., Agarwal, J., Marschall, R., and Pfeifer, M. (2024). “Ejection and Dynamics of Aggregates in the Coma of Comet 67P/Churyumov-Gerasimenko”. In: *A&A* 687, A289. doi: 10.1051/0004-6361/202348692 (cited on pages 52, 111, 119, 125, 158).
- Lemos, P., Agarwal, J., and Schröter, M. (2023). “Distribution and Dynamics of Decimetre-Sized Dust Agglomerates in the Coma of 67P/Churyumov-Gerasimenko”. In: *Monthly Notices of the Royal Astronomical Society* 519.4, pp. 5775–5786. doi: 10.1093/mnras/stad032 (cited on pages 52, 111, 119, 125, 158).
- Leon-Dasi, M., Besse, S., Grieger, B., et al. (2021). “Mapping a Duck: Geological Features and Region Definitions on Comet 67P/Churyumov-Gerasimenko”. In: *Astronomy & Astrophysics* 652, A52. doi: 10.1051/0004-6361/202140497 (cited on pages 31, 103, 105, 156).
- Leonard, F. C. (1930). “The New Planet Pluto”. In: *Leaflet of the Astronomical Society of the Pacific* 1, p. 121 (cited on page 7).
- Leonard, J. M., Adam, C. D., Pelgrift, J. Y., et al. (2020). “Initial Orbit Determination and Event Reconstruction From Estimation of Particle Trajectories About (101955) Bennu”. In: *Earth and Space Science* 7.9. doi: 10.1029/2019ea000937. (Visited on 11/19/2021) (cited on page 53).
- Leuschner, A. O. (1907). “Preliminary Statistics on the Eccentricities of Comet Orbits”. In: *Publications of the Astronomical Society of the Pacific* 19, p. 67. doi: 10.1086/121723 (cited on page 7).
- Levesque, M. and Lelievre, M. (2008). *Evaluation of the Iterative Method for Image Background Removal in Astronomical Images*. Tech. rep. TN 2007-344. Canada – Valcartier: Defence Research and Development, p. 30 (cited on page 39).
- Levison, H. F. (1996). “Comet Taxonomy”. In: *Astronomical Society of the Pacific Conference Proceedings*. Vol. 107, pp. 173–191 (cited on pages 11–13).
- Levison, H. F. and Dones, L. (2007). “Comet Populations and Cometary Dynamics”. In: *Encyclopedia of the Solar System*. Ed. by L.-A. McFadden, P. R. Weissman, and T. V. Johnson. San Diego: Academic Press, pp. 575–588. doi: 10.1016/B978-012088589-3/50035-9 (cited on pages 10, 11).
- Levison, H. F. and Dones, L. (2014). “Comet Populations and Cometary Dynamics”. In: *Encyclopedia of the Solar System (Third Edition)*. Ed. by T. Spohn, D. Breuer, and T. V. Johnson. Boston: Elsevier, pp. 705–719. doi: 10.1016/B978-0-12-415845-0.00031-1 (cited on page 12).
- Levison, H. F., Dones, L., and Duncan, M. J. (2001a). “The Origin of Halley-Type Comets: Probing the Inner Oort Cloud”. In: *The Astronomical Journal* 121.4, p. 2253. doi: 10.1086/319943. (Visited on 04/14/2024) (cited on page 10).
- Levison, H. F. and Duncan, M. J. (1994). “The Long-Term Dynamical Behavior of Short-Period Comets”. In: *Icarus* 108.1, pp. 18–36. doi: 10.1006/icar.1994.1039 (cited on page 10).
- Levison, H. F. and Duncan, M. J. (1997). “From the Kuiper Belt to Jupiter-Family Comets: The Spatial Distribution of Ecliptic Comets”. In: *Icarus* 127.1, pp. 13–32. doi: 10.1006/icar.1996.5637 (cited on pages 3, 7, 9, 10).
- Levison, H. F. and Morbidelli, A. (2003). “The Formation of the Kuiper Belt by the Outward Transport of Bodies during Neptune’s Migration”. In: *Nature* 426.6965, pp. 419–421. doi: 10.1038/nature02120 (cited on page 8).
- Levison, H. F., Olkin, C. B., Noll, K. S., et al. (2021). “Lucy Mission to the Trojan Asteroids: Science Goals”. In: *The Planetary Science Journal* 2.5, p. 171. doi: 10.3847/PSJ/abf840 (cited on page 154).

- Levison, H. F. and Stern, S. A. (2001b). "On the Size Dependence of the Inclination Distribution of the Main Kuiper Belt". In: *The Astronomical Journal* 121.3, p. 1730. doi: 10.1086/319420. (Visited on 04/07/2024) (cited on page 8).
- Levy, D. H. (1998). *Comets: Creators and Destroyers*. Touchstone (cited on page 3).
- Li, X., Li, Q., Yin, C., et al. (2022). "Autonomous Navigation Technology for Low-Speed Small Unmanned Vehicle: An Overview". In: *World Electric Vehicle Journal* 13.9, p. 165. doi: 10.3390/wevj13090165 (cited on page 42).
- Lin, T.-P., Matzarakis, A., Hwang, R., et al. (2010). "Effect of Pavements Albedo on Long-Term Outdoor Thermal Comfort". In: *7th Conference on Biometeorology*. Freiburg (cited on page 30).
- Lin, Z.-Y., Ip, W.-H., Lai, I.-L., et al. (2015). "Morphology and Dynamics of the Jets of Comet 67P/Churyumov-Gerasimenko: Early-phase Development". In: *Astronomy & Astrophysics* 583, A11. doi: 10.1051/0004-6361/201525961 (cited on page 30).
- Lin, Z.-Y., Knollenberg, J., Vincent, J.-B., et al. (2017). "Investigating the Physical Properties of Outbursts on Comet 67P/Churyumov-Gerasimenko". In: *Monthly Notices of the Royal Astronomical Society* 469 (Suppl_2), S731-S740. doi: 10.1093/mnras/stx2768 (cited on page 105).
- Liounis, A. J., Small, J. L., Swenson, J. C., et al. (2020). "Autonomous Detection of Particles and Tracks in Optical Images". In: *Earth and Space Science* 7.8. doi: 10.1029/2019ea000843. (Visited on 11/19/2021) (cited on pages 39-41, 53).
- Liounis, A. J., Swenson, J., Small, J., et al. (2019). "Independent Optical Navigation Processing for the OSIRIS-REx Mission Using the Goddard Image Analysis and Navigation Tool". In: *2nd RPI Space Imaging Workshop*. GSFC-E-DAA-TN74562. Saratoga Springs, NY. (cited on page 40).
- Lis, D. C., Bockelée-Morvan, D., Güsten, R., et al. (2019). "Terrestrial Deuterium-to-Hydrogen Ratio in Water in Hyperactive Comets". In: *Astronomy & Astrophysics* 625, p. L5. doi: 10.1051/0004-6361/201935554 (cited on page 33).
- Liu, Q., Li, Z., Yuan, S., et al. (2021). "Review on Vehicle Detection Technology for Unmanned Ground Vehicles". In: *Sensors* 21.4, p. 1354. doi: 10.3390/s21041354 (cited on page 42).
- Liu, X., Sachse, M., Spahn, F., et al. (2016). "Dynamics and Distribution of Jovian Dust Ejected from the Galilean Satellites". In: *Journal of Geophysical Research: Planets* 121.7, pp. 1141-1173. doi: 10.1002/2016JE004999 (cited on page 105).
- Long, P. O. (2003). *Openness, Secrecy, Authorship: Technical Arts and the Culture of Knowledge from Antiquity to the Renaissance*. JHU Press (cited on page xiv).
- Longobardo, A., Della Corte, V., Rotundi, A., et al. (2020). "67P/Churyumov-Gerasimenko's Dust Activity from Pre- to Post-Perihelion as Detected by Rosetta/GIADA". In: *Monthly Notices of the Royal Astronomical Society* 496.1, pp. 125-137. doi: 10/gnh7g5 (cited on pages 32, 43, 155).
- Longobardo, A., Mannel, T., Kim, M., et al. (2022). "Combining Rosetta's GIADA and MIDAS Data: Morphological versus Dynamical Properties of Dust at 67P/Churyumov-Gerasimenko". In: *Monthly Notices of the Royal Astronomical Society* 516.4, pp. 5611-5617. doi: 10.1093/mnras/stac2544 (cited on pages 32, 43).
- Longobardo, A., Della Corte, V., Ivanovski, S., et al. (2019). "67P/Churyumov-Gerasimenko Active Areas before Perihelion Identified by GIADA and VIRTIS Data Fusion". In: *Monthly Notices of the Royal Astronomical Society* 483.2, pp. 2165-2176. doi: 10.1093/mnras/sty3244 (cited on pages 17, 32, 43).
- Lorek, S., Lacerda, P., and Blum, J. (2018). "Local Growth of Dust- and Ice-Mixed Aggregates as Cometary Building Blocks in the Solar Nebula". In: *Astronomy & Astrophysics* 611, A18. doi: 10.1051/0004-6361/201630175 (cited on page 19).
- Lowry, S., Duddy, S. R., Rozitis, B., et al. (2012). "The Nucleus of Comet 67P/Churyumov-Gerasimenko - A New Shape Model and Thermophysical Analysis". In: *Astronomy & Astrophysics* 548, A12. doi: 10.1051/0004-6361/201220116 (cited on page 26).
- Lucchetti, A., Pajola, M., Fornasier, S., et al. (2017). "Geomorphological and Spectrophotometric Analysis of Seth's Circular Niches on Comet 67P/Churyumov-Gerasimenko Using OSIRIS Images". In: *Monthly Notices of the Royal Astronomical Society* 469.Suppl_2, S238-S251. doi: 10.1093/mnras/stx1590 (cited on page 107).

- Lucchetti, A., Cremonese, G., Jorda, L., et al. (2016). "Characterization of the Abydos Region through OSIRIS High-Resolution Images in Support of CIVA Measurements". In: *Astronomy & Astrophysics* 585, p. L1. doi: 10.1051/0004-6361/201527330 (cited on page 107).
- Lucien Price (1954). *Dialogues Of Alfred North Whitehead*. (Visited on 02/29/2024) (cited on page xiii).
- Luhn, H. P. (1958). "The Automatic Creation of Literature Abstracts". In: *IBM Journal of Research and Development* 2.2, pp. 159–165. doi: 10.1147/rd.22.0159. (Visited on 03/06/2024) (cited on page xvi).
- Lutz, R. K. (1980). "An Algorithm for the Real Time Analysis of Digitised Images". In: *The Computer Journal* 23.3, pp. 262–269. doi: 10.1093/comjnl/23.3.262. (Visited on 11/19/2021) (cited on pages 57, 58).
- Luu, J. X. and Jewitt, D. C. (2002). "Kuiper Belt Objects: Relics from the Accretion Disk of the Sun". In: *Annual Review of Astronomy and Astrophysics* 40. Volume 40, 2002, pp. 63–101. doi: 10.1146/annurev.astro.40.060401.093818. (Visited on 04/14/2024) (cited on page 10).
- El-Maarry, M. R., Groussin, O., Keller, H. U., et al. (2019). "Surface Morphology of Comets and Associated Evolutionary Processes: A Review of Rosetta's Observations of 67P/Churyumov-Gerasimenko". In: *Space Science Reviews* 215.4, p. 36. doi: 10.1007/s11214-019-0602-1 (cited on page 30).
- El-Maarry, M. R., Thomas, N., Giacomini, L., et al. (2015). "Regional Surface Morphology of Comet 67P/Churyumov-Gerasimenko from Rosetta/OSIRIS Images". In: *Astronomy & Astrophysics* 583, A26. doi: 10.1051/0004-6361/201525723 (cited on pages 30, 31, 105).
- El-Maarry, M. R., Thomas, N., Gracia-Berná, A., et al. (2016). "Regional Surface Morphology of Comet 67P/Churyumov-Gerasimenko from Rosetta/OSIRIS Images: The Southern Hemisphere". In: *Astronomy & Astrophysics* 593, A110. doi: 10.1051/0004-6361/201628634 (cited on pages 30, 31, 105).
- El-Maarry, M. R., Thomas, N., Gracia-Berná, A., et al. (2017a). "Regional Surface Morphology of Comet 67P/Churyumov-Gerasimenko from Rosetta/OSIRIS Images: The Southern Hemisphere (Corrigendum)". In: *Astronomy & Astrophysics* 598, p. C2. doi: 10.1051/0004-6361/201628634e (cited on pages 30, 31, 105).
- El-Maarry, M. R., Groussin, O., Thomas, N., et al. (2017b). "Surface Changes on Comet 67P/Churyumov-Gerasimenko Suggest a More Active Past". In: *Science* 355.6332, pp. 1392–1395. doi: 10/b4r6 (cited on pages 105, 156).
- Mabe, M. A. (2009). "Scholarly Publishing". In: *European Review* 17.1, pp. 3–22. doi: 10.1017/S1062798709000532 (cited on page xv).
- Mabe, M. A. (2010). "Scholarly Communication: A Long View". In: *New Review of Academic Librarianship* 16.sup1, pp. 132–144. doi: 10.1080/13614533.2010.512242. (Visited on 02/21/2024) (cited on page xv).
- Mabe, M. A. and Mulligan, A. (2011). "What Journal Authors Want: Ten Years of Results from Elsevier's Author Feedback Programme". In: *New Review of Information Networking* 16.1, pp. 71–89. doi: 10.1080/13614576.2011.574495. (Visited on 02/21/2024) (cited on page xv).
- Macher, W., Kömle, N., Skorov, Y., et al. (2019). "3D Thermal Modeling of Two Selected Regions on Comet 67P and Comparison with Rosetta/MIRO Measurements". In: *Astronomy & Astrophysics* 630, A12. doi: 10.1051/0004-6361/201834798 (cited on page 18).
- Magnier, E. A., Sweeney, W. E., Chambers, K. C., et al. (2020). "Pan-STARRS Pixel Analysis: Source Detection and Characterization". In: *The Astrophysical Journal Supplement Series* 251.1, p. 5. doi: 10.3847/1538-4365/abb82c (cited on page 58).
- Mainzer, A., Grav, T., Bauer, J., et al. (2011). "Neowise Observations Of Near-Earth Objects: Preliminary Results". In: *The Astrophysical Journal* 743.2, p. 156. doi: 10.1088/0004-637x/743/2/156. (Visited on 11/19/2021) (cited on pages 41, 53).
- Malhotra, R. (2019). "Resonant Kuiper Belt Objects: A Review". In: *Geoscience Letters* 6.1, p. 12. doi: 10.1186/s40562-019-0142-2. (Visited on 04/14/2024) (cited on page 10).
- Mandelbrot, B. B. (1982). *The Fractal Geometry of Nature*. San Francisco : W.H. Freeman (cited on page 107).
- Mannel, T., Bentley, M. S., Boakes, P. D., et al. (2019). "Dust of Comet 67P/Churyumov-Gerasimenko Collected by Rosetta/MIDAS: Classification and Extension to the Nanometer Scale". In: *Astronomy & Astrophysics* 630, A26. doi: 10.1051/0004-6361/201834851 (cited on page 32).
- Mannel, T., Bentley, M. S., Schmied, R., et al. (2016). "Fractal Cometary Dust – a Window into the Early Solar System". In: *Monthly Notices of the Royal Astronomical Society* 462.Suppl_1, S304–S311. doi: 10.1093/mnras/stw2898 (cited on pages 17, 32).

- Mao, H., Li, Y., Wang, L., et al. (2020). "Numerical Investigation on the Mechanism of Geyser in Cryogenic Fluid Pipes". In: *International Journal of Heat and Mass Transfer* 154, p. 119670. doi: 10.1016/j.ijheatmasstransfer.2020.119670. (Visited on 05/01/2024) (cited on page 104).
- Maquet, L. (2015). "The Recent Dynamical History of Comet 67P/Churyumov-Gerasimenko". In: *Astronomy & Astrophysics* 579, A78. doi: 10.1051/0004-6361/201425461 (cited on page 26).
- Marín-Yaseli de la Parra, J., Kueppers, M., Roger Pérez, J., et al. (2020). "Analysis of a Particle in the Surroundings of 67P". In: *Europlanet Science Congress 2020*. doi: 10.5194/epsc2020-801. (Visited on 11/19/2021) (cited on pages 38, 53).
- Mark, G. (2023). *Attention Span: A Groundbreaking Way to Restore Balance, Happiness and Productivity*. Harlequin (cited on page xv).
- Markkanen, J. and Agarwal, J. (2020). "Thermophysical Model for Icy Cometary Dust Particles". In: *Astronomy & Astrophysics* 643, A16. doi: 10.1051/0004-6361/202039092 (cited on pages 3, 33, 93, 119).
- Markkanen, J., Väisänen, T., Penttilä, A., et al. (2018a). "Scattering and Absorption in Dense Discrete Random Media of Irregular Particles". In: *Optics Letters* 43.12, pp. 2925–2928. doi: 10.1364/OL.43.002925 (cited on page 120).
- Markkanen, J., Agarwal, J., Väisänen, T., et al. (2018b). "Interpretation of the Phase Functions Measured by the OSIRIS Instrument for Comet 67P/Churyumov-Gerasimenko". In: *The Astrophysical Journal* 868.1, p. L16. doi: 10.3847/2041-8213/aabee10. (Visited on 02/10/2022) (cited on pages 75, 107, 120).
- Marschall, R. (2017). "Inner Gas and Dust Comae of Comets". PhD thesis. Bern: University of Bern (cited on pages 29, 58, 118, 120).
- Marschall, R., Davidsson, B. J. R., Rubin, M., et al. (2023). *Neutral Gas Coma Dynamics: Modeling of Flows and Attempts to Link Inner Coma Structures to Properties of the Nucleus*. doi: 10.48550/arXiv.2308.05797. preprint (cited on page 117).
- Marschall, R., Liao, Y., Thomas, N., et al. (2020a). "Limitations in the Determination of Surface Emission Distributions on Comets through Modelling of Observational Data - A Case Study Based on Rosetta Observations". In: *Icarus* 346, p. 113742. doi: 10/gnh7hw (cited on pages 117, 118).
- Marschall, R., Markkanen, J., Gerig, S.-B., et al. (2020b). "The Dust-to-Gas Ratio, Size Distribution, and Dust Fall-Back Fraction of Comet 67P/Churyumov-Gerasimenko: Inferences From Linking the Optical and Dynamical Properties of the Inner Comae". In: *Frontiers in Physics* 8, p. 227. doi: 10/gnh7jq (cited on pages 107, 117–121, 159).
- Marschall, R., Mottola, S., Su, C. C., et al. (2017). "Cliffs versus Plains: Can ROSINA/COPS and OSIRIS Data of Comet 67P/Churyumov-Gerasimenko in Autumn 2014 Constrain Inhomogeneous Outgassing?" In: *Astronomy & Astrophysics* 605, A112. doi: 10.1051/0004-6361/201730849 (cited on pages 107, 118).
- Marschall, R., Rezac, L., Kappel, D., et al. (2019). "A Comparison of Multiple Rosetta Data Sets and 3D Model Calculations of 67P/Churyumov-Gerasimenko Coma around Equinox (May 2015)". In: *Icarus* 328, pp. 104–126. doi: 10.1016/j.icarus.2019.02.008 (cited on pages 107, 118).
- Marschall, R., Skorov, Y., Zakharov, V., et al. (2020c). "Cometary Comae-Surface Links: The Physics of Gas and Dust from the Surface to a Spacecraft". In: *Space Science Reviews* 216.8, p. 130. doi: 10/gnh7hc (cited on pages 21, 117).
- Marschall, R., Su, C. C., Liao, Y., et al. (2016). "Modelling Observations of the Inner Gas and Dust Coma of Comet 67P/Churyumov-Gerasimenko Using ROSINA/COPS and OSIRIS Data: First Results". In: *Astronomy & Astrophysics* 589, A90. doi: 10.1051/0004-6361/201628085 (cited on pages 21, 30, 107, 118).
- Marsden, B. G. (1974). "Cometary Motions". In: *Celestial mechanics* 9.3, pp. 303–314. doi: 10.1007/BF01228573 (cited on page 7).
- Marsden, B. G. and Williams, G. V. (1994). *Cometary Designation System*. Tech. rep. 23803-4. ambridge, MA: Minor Planet Center, Smithsonian Astrophysical Observatory, (cited on page 11).
- Marsden, B. G., Sekanina, Z., and Yeomans, D. K. (1973). "Comets and Nongravitational Forces. V". In: *The Astronomical Journal* 78, p. 211. doi: 10.1086/111402 (cited on pages 12, 16).
- Marshall, D., Groussin, O., Vincent, J.-B., et al. (2018). "Thermal Inertia and Roughness of the Nucleus of Comet 67P/Churyumov-Gerasimenko from MIRO and VIRTIS Observations". In: *Astronomy & Astrophysics* 616, A122. doi: 10.1051/0004-6361/201833104 (cited on page 118).

- Masci, F. J., Laher, R. R., Rusholme, B., et al. (2019). "The Zwicky Transient Facility: Data Processing, Products, and Archive". In: *Publications of the Astronomical Society of the Pacific* 131.995, p. 018003. doi: 10.1088/1538-3873/aae8ac. (Visited on 11/19/2021) (cited on pages 41, 53).
- Mason, S. (2018). "Publications in the Doctoral Thesis: Challenges for Doctoral Candidates, Supervisors, Examiners and Administrators". In: *Higher Education Research & Development* 37.6, pp. 1231–1244. doi: 10.1080/07294360.2018.1462307. (Visited on 02/23/2024) (cited on page xiii).
- Massironi, M., Simioni, E., Marzari, F., et al. (2015). "Two Independent and Primitive Envelopes of the Bilobate Nucleus of Comet 67P". In: *Nature* 526.7573, pp. 402–405. doi: 10.1038/nature15511 (cited on pages 20, 26, 154).
- Mastrofini, M., Goracci, G., Agostinelli, I., et al. (2023). "YOLO v4 Based Algorithm for Resident Space Object Detection and Tracking". In: *The Use of Artificial Intelligence for Space Applications*. Ed. by C. Ieracitano, N. Mammone, M. Di Clemente, et al. Cham: Springer Nature Switzerland, pp. 19–33. doi: 10.1007/978-3-031-25755-1_2 (cited on page 40).
- Mastropietro, M., Kim, Y., Hsieh, H. H., et al. (2024). "Activity of Main-Belt Comet 324P/La Sagra". In: *Astronomy & Astrophysics* 690, A298. doi: 10.1051/0004-6361/202451090 (cited on page 13).
- Mathis, A., Schneider, S., Lauer, J., et al. (2020). "A Primer on Motion Capture with Deep Learning: Principles, Pitfalls, and Perspectives". In: *Neuron* 108.1, pp. 44–65. doi: 10.1016/j.neuron.2020.09.017 (cited on page 42).
- Mathis, B. A., Rush, J. E., and Young, C. E. (1973). "Improvement of Automatic Abstracts by the Use of Structural Analysis". In: *Journal of the American Society for Information Science* 24.2, pp. 101–109. doi: 10.1002/asi.4630240205 (cited on page xvi).
- Maxwell, J. C. (1860a). "Illustrations of the Dynamical Theory of Gases. Part I. On the Motions and Collisions of Perfectly Elastic Spheres". In: *The London, Edinburgh, and Dublin Philosophical Magazine and Journal of Science* 19.124, pp. 19–32. doi: 10.1080/147864460008642818. (Visited on 05/02/2024) (cited on page 21).
- Maxwell, J. C. (1860b). "Illustrations of the Dynamical Theory of Gases. Part II. On the Process of Diffusion of Two or More Kinds of Moving Particles among One Another." In: *The London, Edinburgh, and Dublin Philosophical Magazine and Journal of Science* 20.130, pp. 21–37. doi: 10.1080/147864460008642902. (Visited on 05/02/2024) (cited on page 21).
- McBride, N., Green, S. F., Chantal Levasseur-Regourd, A., et al. (1997). "The Inner Dust Coma of Comet 26P/Grigg-Skjellerup: Multiple Jets and Nucleus Fragments?" In: *Monthly Notices of the Royal Astronomical Society* 289, pp. 535–553. doi: 10.1093/mnras/289.3.535 (cited on page 23).
- McCully, C., Crawford, S., Kovacs, G., et al. (2018). *Astropy/Astrocrappy: V1.0.5 Zenodo Release*. Zenodo. doi: 10.5281/zenodo.1482019 (cited on page 54).
- McLachlan, G. J. and Krishnan, T. (2007). *The EM Algorithm and Extensions*. John Wiley & Sons (cited on page 76).
- McMahon, P., Seiler, R., Accomazzo, A., et al. (2017). "Inorbit Maintenance Of The Rosetta Reaction Wheels (RWAs)". In: *Conference: European Space Mechanisms and Tribology Symposium*. Hatfield, UK (cited on page 66).
- McMillan, R. S., Scotti, J. V., Frecker, J. E., et al. (1986). "Use Of A Scanning Ccd To Discriminate Asteroid Images Moving In A Field Of Stars". In: *Proc.SPIE*. Vol. 0627. doi: 10.1117/12.968084 (cited on page 41).
- Meadows, A. J. (1980). *Development of Science Publishing in Europe*. Elsevier Science Publishers (cited on pages xiii, xiv).
- Meech, K. J., Kleyna, J. T., Hainaut, O., et al. (2017a). "CO-driven Activity in Comet C/2017 K2 (PANSTARRS)". In: *The Astrophysical Journal Letters* 849.1, p. L8. doi: 10.3847/2041-8213/aa921f (cited on page 14).
- Meech, K. J., Weryk, R., Micheli, M., et al. (2017b). "A Brief Visit from a Red and Extremely Elongated Interstellar Asteroid". In: *Nature* 552.7685, pp. 378–381. doi: 10.1038/nature25020 (cited on page 14).
- Melosh, H. J. and Schenk, P. (1993). "Split Comets and the Origin of Crater Chains on Ganymede and Callisto". In: *Nature* 365.6448, pp. 731–733. doi: 10.1038/365731a0 (cited on page 13).
- Mendis, D. A. (1988). "A Postencounter View of Comets". In: *Annual Review of Astronomy and Astrophysics* 26, pp. 11–49. doi: 10.1146/annurev.aa.26.090188.000303 (cited on page 16).
- Merk, R. and Prialnik, D. (2006). "Combined Modeling of Thermal Evolution and Accretion of Trans-Neptunian Objects—Occurrence of High Temperatures and Liquid Water". In: *Icarus* 183.2, pp. 283–295. doi: 10.1016/j.icarus.2006.02.011 (cited on page 20).

- Merouane, S., Stenzel, O., Hilchenbach, M., et al. (2017). "Evolution of the Physical Properties of Dust and Cometary Dust Activity from 67P/Churyumov–Gerasimenko Measured in Situ by Rosetta/COSIMA". In: *Monthly Notices of the Royal Astronomical Society* 469.Suppl_2, S459–S474. doi: 10.1093/mnras/stx2018 (cited on pages 32, 107).
- Merouane, S., Zaprudin, B., Stenzel, O., et al. (2016). "Dust Particle Flux and Size Distribution in the Coma of 67P/Churyumov-Gerasimenko Measured in Situ by the COSIMA Instrument on Board Rosetta". In: *Astronomy & Astrophysics* 596, A87. doi: 10.1051/0004-6361/201527958 (cited on pages 17, 32, 107, 109, 123, 156).
- Michel, P., Küppers, M., Bagatin, A. C., et al. (2022). "The ESA Hera Mission: Detailed Characterization of the DART Impact Outcome and of the Binary Asteroid (65803) Didymos". In: *The Planetary Science Journal* 3.7, p. 160. doi: 10.3847/PSJ/ac6f52 (cited on page 154).
- Micheli, M., Farnocchia, D., Meech, K. J., et al. (2018). "Non-Gravitational Acceleration in the Trajectory of 1I/2017 U1 ('Oumuamua)". In: *Nature* 559.7713, pp. 223–226. doi: 10.1038/s41586-018-0254-4 (cited on pages 12, 16).
- Mizrachi, D., Salaz, A. M., Kurbanoglu, S., et al. (2018). "Academic Reading Format Preferences and Behaviors among University Students Worldwide: A Comparative Survey Analysis". In: *PLOS ONE* 13.5, e0197444. doi: 10.1371/journal.pone.0197444. (Visited on 03/08/2024) (cited on page xvii).
- Moeyens, J., Jurić, M., Ford, J., et al. (2021). "THOR: An Algorithm for Cadence-independent Asteroid Discovery". In: *The Astronomical Journal* 162.4, p. 143. doi: 10.3847/1538-3881/ac042b. (Visited on 11/19/2021) (cited on pages 41, 53).
- Molaro, J. L., Hergenrother, C. W., Chesley, S. R., et al. (2020). "Thermal Fatigue as a Driving Mechanism for Activity on Asteroid Bennu". In: *Journal of Geophysical Research: Planets* 125.8, e2019JE006325. doi: 10.1029/2019JE006325 (cited on page 14).
- Monaghan, P. (1989). "Some Fields Are Reassessing the Value of the Traditional Doctoral Dissertation". In: *Chronicle of Higher Education* 35.29 (cited on page xiii).
- Morbidelli, A., Gaspar, H. S., and Nesvorný, D. (2014). "Origin of the Peculiar Eccentricity Distribution of the Inner Cold Kuiper Belt". In: *Icarus* 232, pp. 81–87. doi: 10.1016/j.icarus.2013.12.023 (cited on page 8).
- Morbidelli, A. and Rickman, H. (2015). "Comets as Collisional Fragments of a Primordial Planetesimal Disk". In: *Astronomy & Astrophysics* 583, A43. doi: 10.1051/0004-6361/201526116 (cited on pages 26, 27).
- Morbidelli, A., Thomas, F., and Moons, M. (1995). "The Resonant Structure of the Kuiper Belt and the Dynamics of the First Five Trans-Neptunian Objects". In: *Icarus* 118.2, pp. 322–340. doi: 10.1006/icar.1995.1194. (Visited on 04/10/2024) (cited on pages 8, 9).
- Morbidelli, A. (1997). "Chaotic Diffusion and the Origin of Comets from the 2/3 Resonance in the Kuiper Belt". In: *Icarus* 127.1, pp. 1–12. doi: 10.1006/icar.1997.5681. (Visited on 04/14/2024) (cited on page 9).
- Morbidelli, A. (2008). "Comets and Their Reservoirs: Current Dynamics and Primordial Evolution". In: *Trans-Neptunian Objects and Comets*. Ed. by D. Jewitt, A. Morbidelli, and H. Rauer. Heidelberg: Springer Berlin (cited on page 9).
- Morbidelli, A. and Levison, H. F. (2007). "Kuiper Belt: Dynamics". In: *Encyclopedia of the Solar System*. Ed. by L.-A. McFadden, P. R. Weissman, and T. V. Johnson. San Diego: Academic Press, pp. 589–604. doi: 10.1016/B978-012088589-3/50036-0 (cited on pages 7–10).
- Moreno, F., Bagatin, A. C., Tancredi, G., et al. (2023). "Characterization of the Ejecta from the NASA/DART Impact on Dimorphos: Observations and Monte Carlo Models". In: *The Planetary Science Journal* 4.8, p. 138. doi: 10.3847/PSJ/ace827 (cited on page 39).
- Moreno, F., Guirado, D., Muñoz, O., et al. (2022). "Dynamics of Irregularly Shaped Cometary Particles Subjected to Outflowing Gas and Solar Radiative Forces and Torques". In: *Monthly Notices of the Royal Astronomical Society* 510.4, pp. 5142–5153. doi: 10.1093/mnras/stab3769 (cited on pages 22, 99).
- Moretto, M. J. and Holzinger, M. J. (2023). "Automatic Detection, Tracking, and Characterization of Grains about Active Comets Using Multiple Hypothesis Tracking". In: *Asteroids, Comets, Meteors Conference*. Flagstaff, AZ (cited on pages 38, 39, 52).
- Moro-Martín, A. and Norman, C. (2022). "Interstellar Planetesimals: Potential Seeds for Planet Formation?". In: *The Astrophysical Journal* 924.2, p. 96. doi: 10.3847/1538-4357/ac32cc. (Visited on 04/29/2024) (cited on page 14).

- Mortari, D., Samaan, M. A., Bruccoleri, C., et al. (2004). "The Pyramid Star Identification Technique". In: *Navigation* 51.3, pp. 171–183. doi: 10/gh678h (cited on page 40).
- Mottola, S., Arnold, G., Grothues, H.-G., et al. (2015). "The Structure of the Regolith on 67P/Churyumov-Gerasimenko from ROLIS Descent Imaging". In: *Science* 349.6247, aab0232. doi: 10.1126/science.aab0232. (Visited on 02/14/2022) (cited on pages 51, 107).
- Mottola, S., Lowry, S., Snodgrass, C., et al. (2014). "The Rotation State of 67P/Churyumov-Gerasimenko from Approach Observations with the OSIRIS Cameras on Rosetta". In: *Astronomy & Astrophysics* 569, p. L2. doi: 10.1051/0004-6361/201424590 (cited on page 29).
- Mrva-Montoya, A. (2016). "The Ecology, Evolution and Future of the Monograph". In: *Against the Grain* 28.3. doi: 10.7771/2380-176X.7354. (Visited on 02/19/2024) (cited on page xiii).
- Muinonen, K., Markkanen, J., Väisänen, T., et al. (2018). "Multiple Scattering of Light in Discrete Random Media Using Incoherent Interactions". In: *Optics Letters* 43.4, pp. 683–686. doi: 10.1364/OL.43.000683 (cited on page 120).
- Muniruzzaman, A. N. M. (1957). "On Measures of Location and Dispersion and Tests of Hypotheses in a Pare to Population". In: *Calcutta Statistical Association Bulletin* 7.3, pp. 115–123. doi: 10.1177/0008068319570303 (cited on page 109).
- Murdoch, N., Sanchez, P., Schwartz, S. R., et al. (2015). "Asteroid Surface Geophysics". In: *Asteroids IV*. Ed. by W. F. Bottke, F. E. DeMeo, and P. Michel. University of Arizona Press. doi: 10.2458/azu_uapress_9780816532131-ch039 (cited on page 3).
- Murphy, D. M. and Koop, T. (2005). "Review of the Vapour Pressures of Ice and Supercooled Water for Atmospheric Applications". In: *Quarterly Journal of the Royal Meteorological Society* 131.608, pp. 1539–1565. doi: 10.1256/qj.04.94 (cited on page 34).
- Murray, C. D. and Dermott, S. F. (1999). *Solar System Dynamics*. Cambridge University Press (cited on pages 9, 12).
- Musiela, Z. E. and Quarles, B. (2014). "The Three-Body Problem". In: *Reports on Progress in Physics* 77.6, p. 065901. doi: 10.1088/0034-4885/77/6/065901 (cited on pages 7, 12).
- Nesvorný, D. (2018). "Dynamical Evolution of the Early Solar System". In: *Annual Review of Astronomy and Astrophysics* 56. Volume 56, 2018, pp. 137–174. doi: 10.1146/annurev-astro-081817-052028. (Visited on 04/08/2024) (cited on page 9).
- Nesvorný, D., Janches, D., Vokrouhlický, D., et al. (2011). "Dynamical Model for the Zodiacal Cloud and Sporadic Meteors". In: *The Astrophysical Journal* 743.2, p. 129. doi: 10.1088/0004-637X/743/2/129. (Visited on 04/08/2022) (cited on page 77).
- Nesvorný, D., Parker, J., and Vokrouhlický, D. (2018). "Bi-Lobed Shape of Comet 67P from a Collapsed Binary". In: *The Astronomical Journal* 155.6, p. 246. doi: 10.3847/1538-3881/aac01f (cited on pages 26, 154).
- Newton, I. (1687). *Philosophiæ Naturalis Principia Mathematica* (cited on page 5).
- Nicholas, D., Huntington, P., Jamali, H. R., et al. (2007). "Characterising and Evaluating Information Seeking Behaviour in a Digital Environment: Spotlight on the 'Bouncer'". In: *Information Processing & Management* 43.4, pp. 1085–1102. doi: 10.1016/j.ipm.2006.08.007 (cited on page xvi).
- Nicholas, D., Huntington, P., Williams, P., et al. (2004). "Re-appraising Information Seeking Behaviour in a Digital Environment: Bouncers, Checkers, Returnees and the Like". In: *Journal of Documentation* 60.1, pp. 24–43. doi: 10.1108/00220410410516635. (Visited on 03/06/2024) (cited on page xvi).
- niplav (2023). *Have Attention Spans Been Declining?* URL: <https://shorturl.at/Ge0Ye> (visited on 02/21/2024) (cited on page xv).
- Noll, K. S., Grundy, W. M., Chiang, E. I., et al. (2008). "Binaries in the Kuiper Belt". In: *The Solar System Beyond Neptune*. Ed. by M. A. Barucci, H. Boehnhardt, D. P. Cruikshank, et al. University of Arizona Press, pp. 345–363 (cited on pages 9, 26).
- Nummedal, T. (2016). "The Alchemist". In: *A Companion to the History of Science*. Ed. by B. Lightman. John Wiley & Sons, Ltd. Chap. 4, pp. 58–70. doi: 10.1002/9781118620762.ch4 (cited on page xiv).
- O'Rourke, L., Heinisch, P., Blum, J., et al. (2020). "The Philae Lander Reveals Low-Strength Primitive Ice inside Cometary Boulders". In: *Nature* 586.7831, pp. 697–701. doi: 10.1038/s41586-020-2834-3 (cited on page 31).

- Ohsawa, R. (2021). "Development of a Tracklet Extraction Engine". In: *Journal of Space Science Informatics Japan* 11.in press (cited on pages 41, 53).
- Okada, T., Fukuhara, T., Tanaka, S., et al. (2020). "Highly Porous Nature of a Primitive Asteroid Revealed by Thermal Imaging". In: *Nature* 579.7800, pp. 518–522. doi: 10.1038/s41586-020-2102-6 (cited on page 155).
- Oklay, N., Mottola, S., Vincent, J.-B., et al. (2017). "Long-Term Survival of Surface Water Ice on Comet 67P". In: *Monthly Notices of the Royal Astronomical Society* 469.Suppl_2, S582–S597. doi: 10.1093/mnras/stx2298 (cited on pages 30, 103, 107).
- Oklay, N., Sunshine, J. M., Pajola, M., et al. (2016). "Comparative Study of Water Ice Exposures on Cometary Nuclei Using Multispectral Imaging Data". In: *Monthly Notices of the Royal Astronomical Society* 462.Suppl_1, S394–S414. doi: 10.1093/mnras/stw2918 (cited on pages 30, 107).
- Oort, J. H. (1950). "The Structure of the Cloud of Comets Surrounding the Solar System and a Hypothesis Concerning Its Origin". In: *Bulletin of the Astronomical Institutes of the Netherlands* 11, pp. 91–110 (cited on pages 7, 10, 11).
- Oort, J. H. and Schmidt, M. (1951). "Differences between New and Old Comets". In: *Bulletin of the Astronomical Institutes of the Netherlands* 11, p. 259 (cited on page 12).
- Opik, E. J. (1936). "Researches on the Physical Theory of Meteor Phenomena. I. Theory of the Formation of Meteor Craters." In: *Publications of the Tartu Astrofizica Observatory* 28, pp. 1–12 (cited on page 105).
- Öpik, E. J. (1932). "Note on Stellar Perturbations of Nearly Parabolic Orbits". In: *Proceedings of the American Academy of Arts and Sciences* 67.6, pp. 169–183. doi: 10.2307/20022899 (cited on page 7).
- Öpik, E. J. (1951). "Collision Probabilities with the Planets and the Distribution of Interplanetary Matter". In: *Proceedings of the Royal Irish Academy. Section A: Mathematical and Physical Sciences* 54, pp. 165–199 (cited on page 16).
- Öpik, E. J. (1956). "Interplanetary Dust and Terrestrial Accretion of Meteoric Matter". In: *Irish Astronomical Journal* 4, p. 84 (cited on page 106).
- Öpik, E. J. (1958a). "Spike of Comet Arend-Roland 1956h". In: *Irish Astronomical Journal* 5, p. 37 (cited on page 106).
- Öpik, E. J. (1958b). "Meteor Impact on Solid Surface". In: *Irish Astronomical Journal* 5, p. 14 (cited on page 104).
- Opitom, C., Jehin, E., Hutsemékers, D., et al. (2021). "The Similarity of the Interstellar Comet 2I/Borisov to Solar System Comets from High-Resolution Optical Spectroscopy". In: *Astronomy & Astrophysics* 650, p. L19. doi: 10.1051/0004-6361/202141245 (cited on page 14).
- Ott, T., Drolshagen, E., Koschny, D., et al. (2017). "Dust Mass Distribution around Comet 67P/Churyumov–Gerasimenko Determined via Parallax Measurements Using Rosetta's OSIRIS Cameras". In: *Monthly Notices of the Royal Astronomical Society* 469.Suppl_2, S276–S284. doi: 10.1093/mnras/stx1419 (cited on pages 53, 111, 115).
- Ott, T., Drolshagen, E., Koschny, D., et al. (2016). "PaDe - The Particle Detection Program". In: *International Meteor Conference*. Egmond, the Netherlands, pp. 209–213 (cited on page 53).
- Ouellette, N. T., Xu, H., and Bodenschatz, E. (2006). "A Quantitative Study of Three-Dimensional Lagrangian Particle Tracking Algorithms". In: *Experiments in Fluids* 40.2, pp. 301–313. doi: 10/dkrzv6 (cited on page 41).
- Ozaki, N., Yamamoto, T., Gonzalez-Franquesa, F., et al. (2022). "Mission Design of DESTINY+: Toward Active Asteroid (3200) Phaethon and Multiple Small Bodies". In: *Acta Astronautica* 196, pp. 42–56. doi: 10.1016/j.actaastro.2022.03.029 (cited on page 154).
- Pajola, M., Höfner, S., Vincent, J. B., et al. (2017a). "The Pristine Interior of Comet 67P Revealed by the Combined Aswan Outburst and Cliff Collapse". In: *Nature Astronomy* 1.5, pp. 1–8. doi: 10.1038/s41550-017-0092 (cited on pages 107, 111).
- Pajola, M., Lee, J.-C., Oklay, N., et al. (2019). "Multidisciplinary Analysis of the Hapi Region Located on Comet 67P/Churyumov–Gerasimenko". In: *Monthly Notices of the Royal Astronomical Society* 485.2, pp. 2139–2154. doi: 10.1093/mnras/stz446 (cited on page 107).
- Pajola, M., Lucchetti, A., Fulle, M., et al. (2017b). "The Pebbles/Boulders Size Distributions on Sais: Rosetta's Final Landing Site on Comet 67P/Churyumov–Gerasimenko". In: *Monthly Notices of the Royal Astronomical Society* 469.Suppl_2, S636–S645. doi: 10.1093/mnras/stx1620 (cited on pages 17, 51, 107).

- Pajola, M., Lucchetti, A., Vincent, J.-B., et al. (2016a). "The Southern Hemisphere of 67P/Churyumov-Gerasimenko: Analysis of the Preperihelion Size-Frequency Distribution of Boulders ≥ 7 m". In: *Astronomy & Astrophysics* 592, p. L2. doi: 10.1051/0004-6361/201628887 (cited on page 107).
- Pajola, M., Mottola, S., Hamm, M., et al. (2016b). "The Agilkia Boulders/Pebbles Size-Frequency Distributions: OSIRIS and ROLIS Joint Observations of 67P Surface". In: *Monthly Notices of the Royal Astronomical Society* 462.Suppl_1, S242–S252. doi: 10.1093/mnras/stw2720 (cited on pages 51, 107, 109).
- Pajola, M., Oklay, N., Forgia, F. L., et al. (2016c). "Aswan Site on Comet 67P/Churyumov-Gerasimenko: Morphology, Boulder Evolution, and Spectrophotometry". In: *Astronomy & Astrophysics* 592, A69. doi: 10.1051/0004-6361/201527865 (cited on pages 105, 107).
- Pajola, M., Vincent, J.-B., Güttler, C., et al. (2015). "Size-Frequency Distribution of Boulders ≥ 7 m on Comet 67P/Churyumov-Gerasimenko". In: *Astronomy & Astrophysics* 583, A37. doi: 10.1051/0004-6361/201525975 (cited on page 107).
- Paltridge, B. (2002). "Thesis and Dissertation Writing: An Examination of Published Advice and Actual Practice". In: *English for Specific Purposes* 21.2, pp. 125–143. doi: 10.1016/S0889-4906(00)00025-9. (Visited on 02/22/2024) (cited on pages xiii, xiv).
- Paltridge, B. and Starfield, S. (2020). "Change and Continuity in Thesis and Dissertation Writing: The Evolution of an Academic Genre". In: *Journal of English for Academic Purposes* 48, p. 100910. doi: 10.1016/j.jeap.2020.100910. (Visited on 02/20/2024) (cited on page xiii).
- Paltridge, B. and Starfield, S. (2023). "The PhD by Publication in the Humanities and Social Sciences: A Cross Country Analysis". In: *Journal of Further and Higher Education* 47.7, pp. 863–874. doi: 10.1080/0309877X.2023.2190450. (Visited on 02/23/2024) (cited on pages xiii, xv).
- Paré, A. (2019). "Re-Writing the Doctorate: New Contexts, Identities, and Genres". In: *Journal of Second Language Writing*. Special Issue: Thesis and Dissertation Writing in a Second Language: Context, Identity, Genre 43, pp. 80–84. doi: 10.1016/j.jslw.2018.08.004. (Visited on 02/23/2024) (cited on page xiii).
- Parker, E. N. (1958). "Dynamics of the Interplanetary Gas and Magnetic Fields." In: *The Astrophysical Journal* 128, p. 664. doi: 10.1086/146579 (cited on page 16).
- Pätzold, M., Andert, T., Hahn, M., et al. (2016). "A Homogeneous Nucleus for Comet 67P/Churyumov-Gerasimenko from Its Gravity Field". In: *Nature* 530.7588, pp. 63–65. doi: 10.1038/nature16535 (cited on pages 27, 75, 117, 121).
- Pätzold, M., Andert, T. P., Hahn, M., et al. (2019). "The Nucleus of Comet 67P/Churyumov-Gerasimenko – Part I: The Global View – Nucleus Mass, Mass-Loss, Porosity, and Implications". In: *Monthly Notices of the Royal Astronomical Society* 483.2, pp. 2337–2346. doi: 10.1093/mnras/sty3171 (cited on pages 27, 34).
- Pätzold, M., Häusler, B., Aksnes, K., et al. (2007). "Rosetta Radio Science Investigations (RSI)". In: *Space Science Reviews* 128.1, pp. 599–627. doi: 10.1007/s11214-006-9117-7 (cited on page 25).
- Pearson, K. (1895). *Contributions to the Mathematical Theory of Evolution. II. Skew Variation in Homogeneous Material*. Royal Society of London (cited on page 56).
- Peixinho, N., Lacerda, P., and Jewitt, D. (2008). "Color-Inclination Relation Of The Classical Kuiper Belt Objects". In: *The Astronomical Journal* 136.5, p. 1837. doi: 10.1088/0004-6256/136/5/1837. (Visited on 04/07/2024) (cited on page 8).
- Pelgrift, J. Y., Lessac-Chenen, E. J., Adam, C. D., et al. (2020). "Reconstruction of Bennu Particle Events From Sparse Data". In: *Earth and Space Science* 7.8. doi: 10.1029/2019ea000938. (Visited on 11/19/2021) (cited on page 53).
- Peltonen, M., ed. (1996). *The Cambridge Companion to Bacon*. Cambridge Companions to Philosophy. Cambridge: Cambridge University Press (cited on page xiv).
- Penasa, L., Massironi, M., Naletto, G., et al. (2017). "A Three-Dimensional Modelling of the Layered Structure of Comet 67P/Churyumov-Gerasimenko". In: *Monthly Notices of the Royal Astronomical Society* 469.Suppl_2, S741–S754. doi: 10.1093/mnras/stx2899 (cited on pages 26, 29).
- Pestoni, B., Altwegg, K., Corte, V. D., et al. (2023). "Multi-Instrument Analysis of 67P/Churyumov-Gerasimenko Coma Particles: COPS-GIADA Data Fusion". In: *Astronomy & Astrophysics* 671, A168. doi: 10.1051/0004-6361/202245279 (cited on page 32).
- Petit, J.-M., Holman, M., Scholl, H., et al. (2004a). "A Highly Automated Moving Object Detection Package". In: *Monthly Notices of the Royal Astronomical Society* 347.2, pp. 471–480. doi: 10.1111/j.1365-2966.2004.07217.x (cited on pages 41, 53).

- Petit, J.-M., Kavelaars, J. J., Gladman, B. J., et al. (2011). "The Canada–France Ecliptic Plane Survey—Full Data Release: The Orbital Structure Of The Kuiper Belt*". In: *The Astronomical Journal* 142.4, p. 131. doi: 10.1088/0004-6256/142/4/131. (Visited on 04/06/2024) (cited on page 7).
- Petit, J.-M. and Mousis, O. (2004b). "KBO Binaries: How Numerous Were They?" In: *Icarus* 168.2, pp. 409–419. doi: 10.1016/j.icarus.2003.12.013. (Visited on 04/08/2024) (cited on page 9).
- Petit, J.-M., Gladman, B., Kavelaars, J. J., et al. (2023). "The Hot Main Kuiper Belt Size Distribution from OSSOS". In: *The Astrophysical Journal Letters* 947.1, p. L4. doi: 10.3847/2041-8213/acc525. (Visited on 04/08/2024) (cited on page 8).
- Pfeifer, M., Agarwal, J., Marschall, R., Grieger, B., and Lemos, P. (2024). "Dynamics and Potential Origins of Decimeter-Sized Particles around Comet 67P/Churyumov-Gerasimenko". In: *A&A* 685, A136. doi: 10.1051/0004-6361/202346380 (cited on page xiii).
- Pfeifer, M., Agarwal, J., and Schröter, M. (2022). "On the Trail of a Comet's Tail: A Particle Tracking Algorithm for Comet 67P/Churyumov-Gerasimenko". In: *A&A* 659, A171. doi: 10.1051/0004-6361/202141953 (cited on pages xiii, 93, 95, 99, 103, 143, 149).
- Phillips, A. and Kovač, M. (2022). *Is This a Book?* Cambridge University Press (cited on page xvi).
- Pieters, C. M. and Noble, S. K. (2016). "Space Weathering on Airless Bodies". In: *Journal of Geophysical Research: Planets* 121.10, pp. 1865–1884. doi: 10.1002/2016JE005128 (cited on page 3).
- Pinker, S. (2014). *The Sense of Style: The Thinking Person's Guide to Writing in the 21st Century*. Penguin (cited on page xiv).
- Pinzón-Rodríguez, O., Marschall, R., Gerig, S.-B., et al. (2021). "The Effect of Thermal Conductivity on the Outgassing and Local Gas Dynamics from Cometary Nuclei". In: *Astronomy & Astrophysics* 655, A20. doi: 10.1051/0004-6361/202039824 (cited on pages 120, 123, 160).
- Pires, R., Dorotovic, I., Ribeiro, R., et al. (2019). "CBPTracker - a Web Tool to Detect and Track Solar Features from SDO/ AIA Images". In: *2019 International Young Engineers Forum (YEF-ECE)*, pp. 72–76. doi: 10.1109/YEF-ECE.2019.8740819 (cited on page 42).
- Plato (2006). *The Dialogues of Plato*. Random House Publishing Group (cited on page xiii).
- Poincaré, H. (1890). *Sur le problème des trois corps et les équations de la dynamique*. Acta mathematica (cited on page 7).
- Pommerol, A., Thomas, N., El-Maarry, M. R., et al. (2015). "OSIRIS Observations of Meter-Sized Exposures of H₂O Ice at the Surface of 67P/Churyumov-Gerasimenko and Interpretation Using Laboratory Experiments". In: *Astronomy & Astrophysics* 583, A25. doi: 10.1051/0004-6361/201525977 (cited on page 107).
- Porco, C. C., Helfenstein, P., Thomas, P. C., et al. (2006). "Cassini Observes the Active South Pole of Enceladus". In: *Science* 311.5766, pp. 1393–1401. doi: 10.1126/science.1123013 (cited on page 104).
- Postberg, F., Schmidt, J., Hillier, J., et al. (2011). "A Salt-Water Reservoir as the Source of a Compositionally Stratified Plume on Enceladus". In: *Nature* 474.7353, pp. 620–622. doi: 10.1038/nature10175 (cited on page 104).
- Poulet, F., Lucchetti, A., Bibring, J.-P., et al. (2016). "Origin of the Local Structures at the Philae Landing Site and Possible Implications on the Formation and Evolution of 67P/Churyumov-Gerasimenko". In: *Monthly Notices of the Royal Astronomical Society* 462.Suppl_1, S23–S32. doi: 10.1093/mnras/stw1959 (cited on page 107).
- Pratt, W. K. (2007). *Digital Image Processing*. Fourth Edition. 605 Third Avenue New York, NY United States: John Wiley & Sons, Ltd (cited on page 58).
- Preusker, F., Scholten, F., Matz, K.-D., et al. (2017). "The Global Meter-Level Shape Model of Comet 67P/Churyumov-Gerasimenko". In: *Astronomy & Astrophysics* 607, p. L1. doi: 10.1051/0004-6361/201731798 (cited on pages 27, 29, 118).
- Prialnik, D. and Rosenberg, E. D. (2009). "Can Ice Survive in Main-Belt Comets? Long-term Evolution Models of Comet 133P/Elst-Pizarro". In: *Monthly Notices of the Royal Astronomical Society: Letters* 399.1, pp. L79–L83. doi: 10.1111/j.1745-3933.2009.00727.x (cited on page 13).
- Price, O., Jones, G. H., Morrill, J., et al. (2019). "Fine-Scale Structure in Cometary Dust Tails I: Analysis of Striae in Comet C/2006 P1 (McNaught) through Temporal Mapping". In: *Icarus* 319, pp. 540–557. doi: 10.1016/j.icarus.2018.09.013 (cited on page 15).
- Protopapa, S., Sunshine, J. M., Feaga, L. M., et al. (2014). "Water Ice and Dust in the Innermost Coma of Comet 103P/Hartley 2". In: *Icarus* 238, pp. 191–204. doi: 10.1016/j.icarus.2014.04.008 (cited on page 158).

- Quick, L. C., Barnouin, O. S., Prockter, L. M., et al. (2013). "Constraints on the Detection of Cryovolcanic Plumes on Europa". In: *Planetary and Space Science* 86, pp. 1–9. doi: 10.1016/j.pss.2013.06.028 (cited on page 105).
- Rabinowitz, D. L. (1991). "Detection of Earth-Approaching Asteroids in near Real Time". In: *The Astronomical Journal* 101, p. 1518. doi: 10.1086/115785. (Visited on 11/19/2021) (cited on pages 41, 53).
- Reach, W. T., Vaubaillon, J., Kelley, M. S., et al. (2009). "Distribution and Properties of Fragments and Debris from the Split Comet 73P/Schwassmann-Wachmann 3 as Revealed by Spitzer Space Telescope". In: *Icarus* 203.2, pp. 571–588. doi: 10.1016/j.icarus.2009.05.027 (cited on pages 34, 51).
- Redmon, J. and Farhadi, A. (2018). *YOLOv3: An Incremental Improvement*. doi: 10.48550/arXiv.1804.02767. URL: <http://arxiv.org/abs/1804.02767> (cited on page 42).
- Regnier, P., Vidal, P., Lodirot, S., et al. (2016). "ROSETTA Star Trackers in the Comet Dust: Understanding and Improving the in-Flight Behaviour through on-Ground Testing of the STR EQM with the microSTO". In: *Proceedings of the 13th International Planetary Probe Workshop*. Laurel (USA) (cited on page 40).
- Reid, W. M. (1978). "Commentary: Will the Future Generations of Biologists Write a Dissertation?" In: *BioScience* 28.10, pp. 651–654. doi: 10.2307/1307396 (cited on page xiii).
- Reinhard, R. (1986). "The Giotto Encounter with Comet Halley". In: *Nature* 321.6067, pp. 313–318. doi: 10.1038/321313a0 (cited on page 23).
- Reshetnyk, V., Skorov, Y., Bentley, M., et al. (2022). "Transport Characteristics of a Hierarchical Near-Surface Layer of the Nucleus of Comet 67P/Churyumov–Gerasimenko". In: *Solar System Research* 56.2, pp. 100–121. doi: 10.1134/S0038094622020071 (cited on page 111).
- Reshetnyk, V., Skorov, Y., Vasyuta, M., et al. (2021). "Transport Characteristics of the Near-Surface Layer of the Nucleus of Comet 67P/Churyumov–Gerasimenko". In: *Solar System Research* 55.2, pp. 106–123. doi: 10.1134/S0038094621020040 (cited on page 111).
- Reshetnyk, V. M., Skorov, Y. V., Lacerda, P., et al. (2018). "Dynamics of Dust Particles of Different Structure: Application to the Modeling of Dust Motion in the Vicinity of the Nucleus of Comet 67P/Churyumov–Gerasimenko". In: *Solar System Research* 52.3, pp. 266–281. doi: 10.1134/S0038094618030085 (cited on pages 22, 99, 117).
- Richardson, J., Melosh, H., Lisse, C., et al. (2007). "A Ballistics Analysis of the Deep Impact Ejecta Plume: Determining Comet Tempel 1's Gravity, Mass, and Density". In: *Icarus* 190.2, pp. 357–390. doi: 10/d6zq68 (cited on page 39).
- Rickman, H. and Jorda, L. (1998). "Comet 46P/Wirtanen, the Target of the Rosetta Mission". In: *Advances in Space Research* 21.11, pp. 1491–1504. doi: 10.1016/S0273-1177(97)00942-3 (cited on page 33).
- Rickman, H., Marchi, S., A'Hearn, M. F., et al. (2015). "Comet 67P/Churyumov–Gerasimenko: Constraints on Its Origin from OSIRIS Observations". In: *Astronomy & Astrophysics* 583, A44. doi: 10.1051/0004-6361/201526093 (cited on page 27).
- Rickman, H. (2017). *Origin and Evolution of Comets*. Vol. 2. Advances in Planetary Science. WORLD SCIENTIFIC (cited on page 11).
- Riedler, W., Torkar, K., Jeszenszky, H., et al. (2007). "MIDAS – The Micro-Imaging Dust Analysis System for the Rosetta Mission". In: *Space Science Reviews* 128.1, pp. 869–904. doi: 10.1007/s11214-006-9040-y (cited on page 24).
- Rigby, J. and Jones, B. (2020). "Bringing the Doctoral Thesis by Published Papers to the Social Sciences and the Humanities: A Quantitative Easing? A Small Study of Doctoral Thesis Submission Rules and Practice in Two Disciplines in the UK". In: *Scientometrics* 124.2, pp. 1387–1409. doi: 10.1007/s11192-020-03483-9 (cited on page xiii).
- Rimrott, F. P. J. (1989). *Introductory Orbit Dynamics*. Friedr. Vieweg & Sohn (cited on page 11).
- Rinaldi, G., Della Corte, V., Fulle, M., et al. (2017). "Cometary Coma Dust Size Distribution from in Situ IR Spectra". In: *Monthly Notices of the Royal Astronomical Society* 469.Suppl_2, S598–S605. doi: 10.1093/mnras/stx1873 (cited on page 107).
- Robutel, P. and Laskar, J. (2001). "Frequency Map and Global Dynamics in the Solar System I: Short Period Dynamics of Massless Particles". In: *Icarus* 152.1, pp. 4–28. doi: 10.1006/icar.2000.6576. (Visited on 04/10/2024) (cited on pages 8, 9).
- Rodionov, A. V., Crifo, J. -, Szegő, K., et al. (2002). "An Advanced Physical Model of Cometary Activity". In: *Planetary and Space Science* 50.10, pp. 983–1024. doi: 10.1016/S0032-0633(02)00047-8 (cited on page 103).

- Roger, J. (2019). *¿Maybe Little Coorbital Chunk?* Tweet. URL: <https://twitter.com/landru79/status/1126179023892242435> (visited on 11/24/2021) (cited on page 53).
- Rose, K. A., Molaei, M., Boyle, M. J., et al. (2020). "Particle Tracking of Nanoparticles in Soft Matter". In: *Journal of Applied Physics* 127.19, p. 191101. doi: 10.1063/5.0003322. (Visited on 11/24/2021) (cited on pages 42, 53).
- Rosenfeld, A. (1970). "Connectivity in Digital Pictures". In: *Journal of the ACM* 17.1, pp. 146–160. doi: 10.1145/321556.321570 (cited on page 58).
- Rotundi, A., Sierks, H., Della Corte, V., et al. (2015). "Dust Measurements in the Coma of Comet 67P/Churyumov-Gerasimenko Inbound to the Sun". In: *Science* 347.6220, aaa3905. doi: 10.1126/science.aaa3905. (Visited on 03/01/2024) (cited on pages 32, 53, 107).
- Rubin, M., Engrand, C., Snodgrass, C., et al. (2020). "On the Origin and Evolution of the Material in 67P/Churyumov-Gerasimenko". In: *Space Science Reviews* 216.5, p. 102. doi: 10.1007/s11214-020-00718-2 (cited on pages 3, 31).
- Rubincam, D. P. (2000). "Radiative Spin-up and Spin-down of Small Asteroids". In: *Icarus* 148.1, pp. 2–11. doi: 10.1006/icar.2000.6485 (cited on page 16).
- Rud, M. (1992). *The Bayeux Tapestry and the Battle of Hastings, 1066*. Copenhagen : C. Eilers (cited on page 6).
- Ruzicka, B.-K., Penasa, L., Boehnhardt, H., et al. (2019). "Analysis of Layering-Related Linear Features on Comet 67P/Churyumov-Gerasimenko". In: *Monthly Notices of the Royal Astronomical Society* 482.4, pp. 5007–5011. doi: 10.1093/mnras/sty3079 (cited on page 26).
- Sagan, C. and Druyan, A. (2011). *Comet*. Random House Publishing Group (cited on pages 4, 5).
- Sagdeev, R. Z., Blamont, J., Galeev, A. A., et al. (1986a). "Vega Spacecraft Encounters with Comet Halley". In: *Nature* 321.6067, pp. 259–262. doi: 10.1038/321259a0 (cited on page 23).
- Sagdeev, R. Z., Szabó, F., Avanesov, G. A., et al. (1986b). "Television Observations of Comet Halley from Vega Spacecraft". In: *Nature* 321.6067, pp. 262–266. doi: 10.1038/321262a0 (cited on page 16).
- Sanchidrián, J. A., Ouchterlony, F., Segarra, P., et al. (2014). "Size Distribution Functions for Rock Fragments". In: *International Journal of Rock Mechanics and Mining Sciences* 71, pp. 381–394. doi: 10.1016/j.ijrmms.2014.08.007 (cited on page 107).
- Savage, W. W. (2010). "Monographs: The Sounds of Silence: The Transom". In: *Journal of Scholarly Publishing* 41.4, pp. 483–488. doi: 10.1353/scp.0.0094. (Visited on 02/19/2024) (cited on page xiii).
- Schimel, J. (2012). *Writing Science: How to Write Papers That Get Cited and Proposals That Get Funded*. Oxford University Press, USA (cited on page xiv).
- Schloerb, F. P., Keihm, S., Allmen, P. von, et al. (2015). "MIRO Observations of Subsurface Temperatures of the Nucleus of 67P/Churyumov-Gerasimenko". In: *Astronomy & Astrophysics* 583, A29. doi: 10.1051/0004-6361/201526152 (cited on page 118).
- Schmid, M., Kueppers, U., Cigala, V., et al. (2020). "Release Characteristics of Overpressurised Gas from Complex Vents: Implications for Volcanic Hazards". In: *Bulletin of Volcanology* 82.11, p. 68. doi: 10.1007/s00445-020-01407-2 (cited on page 105).
- Schmidt, J., Brilliantov, N., Spahn, F., et al. (2008). "Slow Dust in Enceladus' Plume from Condensation and Wall Collisions in Tiger Stripe Fractures". In: *Nature* 451.7179, pp. 685–688. doi: 10.1038/nature06491 (cited on page 104).
- Schorghofer, N. (2008). "The Lifetime of Ice on Main Belt Asteroids". In: *The Astrophysical Journal* 682.1, p. 697. doi: 10.1086/588633 (cited on page 13).
- Schorghofer, N. (2016). "Predictions of Depth-to-Ice on Asteroids Based on an Asynchronous Model of Temperature, Impact Stirring, and Ice Loss". In: *Icarus* 276, pp. 88–95. doi: 10.1016/j.icarus.2016.04.037 (cited on page 13).
- Schräpler, R., Blum, J., Krijt, S., et al. (2018). "The Physics of Protoplanetary Dust Agglomerates. X. High-velocity Collisions between Small and Large Dust Agglomerates as a Growth Barrier". In: *The Astrophysical Journal* 853.1, p. 74. doi: 10.3847/1538-4357/aaa0d2 (cited on page 19).
- Schröder, A. and Schanz, D. (2023). "3D Lagrangian Particle Tracking in Fluid Mechanics". In: *Annual Review of Fluid Mechanics* 55.1, pp. 511–540. doi: 10.1146/annurev-fluid-031822-041721 (cited on pages 41, 52).
- Schroeder I, I. R. H. G., Altwegg, K., Balsiger, H., et al. (2019). "A Comparison between the Two Lobes of Comet 67P/Churyumov-Gerasimenko Based on D/H Ratios in H₂O Measured with the Rosetta/ROSINA DFMS".

- In: *Monthly Notices of the Royal Astronomical Society* 489.4, pp. 4734–4740. doi: 10.1093/mnras/stz2482 (cited on page 27).
- Schroeter, M., Lyv, C., Huang, J., et al. (2022). “Challenges of ‘imaging’ Particulate Materials in Three Dimensions”. In: *Papers in Physics* 14, pp. 140015–140015. doi: 10.4279/pip.140015 (cited on page 42).
- Schuhmann, M., Altwegg, K., Balsiger, H., et al. (2019). “Aliphatic and Aromatic Hydrocarbons in Comet 67P/Churyumov-Gerasimenko Seen by ROSINA”. In: *Astronomy & Astrophysics* 630, A31. doi: 10.1051/0004-6361/201834666 (cited on page 33).
- Schultz, P. H., Eberhardy, C. A., Ernst, C. M., et al. (2007). “The Deep Impact Oblique Impact Cratering Experiment”. In: *Icarus. Deep Impact Mission to Comet 9P/Tempel 1, Part 2* 190.2, pp. 295–333. doi: 10.1016/j.icarus.2007.06.006 (cited on page 23).
- Schulz, R. (2010). “The Rosetta Mission and Its Fly-by at Asteroid 2867 Steins”. In: *Planetary and Space Science. Special Issue: Rosetta Fly-by at Asteroid (2867) Steins* 58.9, p. 1057. doi: 10.1016/j.pss.2010.04.026 (cited on page 23).
- Schulz, R., Sierks, H., Küppers, M., et al. (2012). “Rosetta Fly-by at Asteroid (21) Lutetia: An Overview”. In: *Planetary and Space Science. Rosetta Fly-by at Asteroid (21) Lutetia* 66.1, pp. 2–8. doi: 10.1016/j.pss.2011.11.013 (cited on page 23).
- Schwamb, M. E., Fraser, W. C., Bannister, M. T., et al. (2019). “Col-OSSOS: The Colors of the Outer Solar System Origins Survey”. In: *The Astrophysical Journal Supplement Series* 243.1, p. 12. doi: 10.3847/1538-4365/ab2194. (Visited on 04/08/2024) (cited on pages 8, 9).
- Schwehm, G. and Schulz, R. (1999). “Rosetta Goes to Comet Wirtanen”. In: *Space Science Reviews* 90.1, pp. 313–319. doi: 10.1023/A:1005231006010 (cited on page 23).
- Schwehm, G. (1989). “Rosetta/CNSR, ESA’s Planetary Cornerstone Mission”. In: *Proceedings of an International Workshop on Physics and Mechanics of Cometary Materials*. Vol. 302. ESA, pp. 11–15 (cited on page 22).
- Schwehm, G. and Hechler, M. (1994). “Rosetta - ESA’s Planetary Cornerstone Mission”. In: *ESA Bulletin* 77, pp. 7–18 (cited on page 22).
- Seargent, D. A. J. (2008). *The Greatest Comets in History: Broom Stars and Celestial Scimitars*. Springer Science & Business Media (cited on page 5).
- Seneca (1972). *Natural Questions, Volume II*. Trans. by T. H. Corcoran. Cambridge, MA: Harvard University Press (cited on page 5).
- Sengers, J. V., Lin Wang, Y. .-, Kamgar-Parsi, B., et al. (2014). “Kinetic Theory of Drag on Objects in Nearly Free Molecular Flow”. In: *Physica A: Statistical Mechanics and its Applications* 413, pp. 409–425. doi: 10.1016/j.physa.2014.06.026 (cited on page 21).
- Shahamatnia, E., Dorotovič, I., Fonseca, J. M., et al. (2016). “An Evolutionary Computation Based Algorithm for Calculating Solar Differential Rotation by Automatic Tracking of Coronal Bright Points”. In: *Journal of Space Weather and Space Climate* 6, A16. doi: 10.1051/swsc/2016010 (cited on page 42).
- Al-Shakarji, N. M., Seetharaman, G., Bunyak, F., et al. (2017). “Robust Multi-Object Tracking with Semantic Color Correlation”. In: *2017 14th IEEE International Conference on Advanced Video and Signal Based Surveillance (AVSS)*, pp. 1–7. doi: 10.1109/AVSS.2017.8078507. (Visited on 05/03/2024) (cited on page 39).
- Sharmini, S., Spronken-Smith, R., Golding, C., et al. (2015). “Assessing the Doctoral Thesis When It Includes Published Work”. In: *Assessment & Evaluation in Higher Education* 40.1, pp. 89–102. doi: 10.1080/02602938.2014.888535. (Visited on 02/23/2024) (cited on pages xiii, xv).
- Shaw, P., Phillips, A., and Gutiérrez, M. B. (2022). “The Death of the Monograph?” In: *Publishing Research Quarterly* 38.2, pp. 382–395. doi: 10.1007/s12109-022-09885-2 (cited on pages xiii, xiv).
- Sheppard, S. S., Trujillo, C. A., Tholen, D. J., et al. (2019). “A New High Perihelion Trans-Plutonian Inner Oort Cloud Object: 2015 TG387”. In: *The Astronomical Journal* 157.4, p. 139. doi: 10.3847/1538-3881/ab0895. (Visited on 04/08/2024) (cited on page 10).
- Shi, X., Hu, X., Mottola, S., et al. (2018). “Coma Morphology of Comet 67P Controlled by Insolation over Irregular Nucleus”. In: *Nature Astronomy* 2.7, pp. 562–567. doi: 10.1038/s41550-018-0481-5 (cited on pages 103, 121).
- Shi, X., Hu, X., Sierks, H., et al. (2016). “Sunset Jets Observed on Comet 67P/Churyumov-Gerasimenko Sustained by Subsurface Thermal Lag”. In: *Astronomy & Astrophysics* 586, A7. doi: 10.1051/0004-6361/201628113 (cited on page 123).

- Shi, X., Hu, X., Agarwal, J., et al. (2024). “Diurnal Ejection of Boulder Clusters on Comet 67P Lasting beyond 3 Au”. In: *The Astrophysical Journal Letters* 961.1, p. L16. doi: 10.3847/2041-8213/ad18d9. (Visited on 03/01/2024) (cited on pages 52, 74, 119, 125, 158).
- Shi, X., Hu, X., Rose, M., et al. (2019). “Clustered Ejection of Metre-Sized Boulders on Comet 67P”. In: *EPSC Abstracts*. Vol. 13. EPSC-DPS2019-1410-1. EPSC-DPS2019-1410, p. 2 (cited on pages 74, 105).
- Shou, Y., Combi, M., Toth, G., et al. (2017). “A New 3D Multi-fluid Dust Model: A Study of the Effects of Activity and Nucleus Rotation on Dust Grain Behavior at Comet 67P/Churyumov–Gerasimenko”. In: *The Astrophysical Journal* 850.1, p. 72. doi: 10.3847/1538-4357/aa91ca (cited on page 21).
- Sierks, H., Barbieri, C., Lamy, P. L., et al. (2015). “On the Nucleus Structure and Activity of Comet 67P/Churyumov-Gerasimenko”. In: *Science* 347.6220, aaa1044. doi: 10 / zp2 (cited on pages 26, 29–31, 105, 159).
- Sighencea, B. I., Stanciu, R. I., and Căleanu, C. D. (2021). “A Review of Deep Learning-Based Methods for Pedestrian Trajectory Prediction”. In: *Sensors* 21.22, p. 7543. doi: 10.3390/s21227543 (cited on page 42).
- Simon, J. B., Blum, J., Birnstiel, T., et al. (2022). *Comets and Planetesimal Formation*. doi: 10.48550/arXiv.2212.04509. URL: <http://arxiv.org/abs/2212.04509> (cited on pages 19, 155).
- Singer, K. N., McKinnon, W. B., Gladman, B., et al. (2019). “Impact Craters on Pluto and Charon Indicate a Deficit of Small Kuiper Belt Objects”. In: *Science* 363.6430, pp. 955–959. doi: 10.1126/science.aap8628. (Visited on 04/08/2024) (cited on page 9).
- Siraj, A. and Loeb, A. (2020). “Observable Signatures of the Ejection Speed of Interstellar Objects from Their Birth Systems”. In: *The Astrophysical Journal Letters* 903.1, p. L20. doi: 10.3847/2041-8213/abc170. (Visited on 04/29/2024) (cited on page 14).
- Skorov, Y., Keller, H. U., Mottola, S., et al. (2020). “Near-Perihelion Activity of Comet 67P/Churyumov–Gerasimenko. A First Attempt of Non-Static Analysis”. In: *Monthly Notices of the Royal Astronomical Society* 494.3, pp. 3310–3316. doi: 10.1093/mnras/staa865 (cited on page 18).
- Skorov, Y. and Blum, J. (2012). “Dust Release and Tensile Strength of the Non-Volatile Layer of Cometary Nuclei”. In: *Icarus* 221.1, pp. 1–11. doi: 10.1016/j.icarus.2012.01.012 (cited on pages 16–18).
- Skorov, Y., Markkanen, J., Reshetnyk, V., et al. (2023). “Cometary Surface Dust Layers Built out of Millimetre-Scale Aggregates: Dependence of Modelled Cometary Gas Production on the Layer Transport Properties”. In: *Monthly Notices of the Royal Astronomical Society* 522.3, pp. 4781–4800. doi: 10.1093/mnras/stad1330 (cited on page 111).
- Skorov, Y., Reshetnyk, V., Bentley, M. S., et al. (2022a). “The Effect of Hierarchical Structure of the Surface Dust Layer on the Modelling of Comet Gas Production”. In: *Monthly Notices of the Royal Astronomical Society* 510.4, pp. 5520–5534. doi: 10.1093/mnras/stab3760 (cited on page 111).
- Skorov, Y., Reshetnyk, V., Küppers, M., et al. (2022b). “Sensitivity of Modelled Cometary Gas Production on the Properties of the Surface Layer of the Nucleus”. In: *Monthly Notices of the Royal Astronomical Society* 519.1, pp. 59–73. doi: 10.1093/mnras/stac3242 (cited on page 111).
- Skorov, Y., Reshetnyk, V., Bentley, M., et al. (2021). “The Effect of Varying Porosity and Inhomogeneities of the Surface Dust Layer on the Modelling of Comet Gas Production”. In: *Monthly Notices of the Royal Astronomical Society* 501.2, pp. 2635–2646. doi: 10.1093/mnras/staa3735 (cited on page 111).
- Skorov, Y., Reshetnyk, V., Lacerda, P., et al. (2016). “Acceleration of Cometary Dust near the Nucleus: Application to 67P/Churyumov–Gerasimenko”. In: *Monthly Notices of the Royal Astronomical Society* 461.4, pp. 3410–3420. doi: 10.1093/mnras/stw1470 (cited on pages 22, 99, 117).
- Skorov, Y., Reshetnyk, V., Rezac, L., et al. (2018). “Dynamical Properties and Acceleration of Hierarchical Dust in the Vicinity of Comet 67P/Churyumov–Gerasimenko”. In: *Monthly Notices of the Royal Astronomical Society* 477.4, pp. 4896–4907. doi: 10.1093/mnras/sty1014 (cited on pages 22, 99, 117).
- Skorov, Y., Rezac, L., Hartogh, P., et al. (2017). “Is Near-Surface Ice the Driver of Dust Activity on 67P/Churyumov-Gerasimenko”. In: *Astronomy & Astrophysics* 600, A142. doi: 10.1051/0004-6361/201630000 (cited on pages 3, 17, 93).
- Smith, P. (1990). *Killing the Spirit: Higher Education in America*. Viking (cited on pages xiii, xiv).
- Smith, P. H. (2004). *The Body of the Artisan: Art and Experience in the Scientific Revolution*. University of Chicago Press (cited on page xiv).
- Smith, S. (2015). *PhD by Published Work: A Practical Guide for Success*. Red Globe Press (cited on page xiii).

- Snodgrass, C., Feaga, L., Jones, G. H., et al. (2022). *Past and Future Comet Missions*. doi: 10.48550/arXiv.2208.08476. URL: <http://arxiv.org/abs/2208.08476> (cited on pages 23, 154).
- Snodgrass, C., Fitzsimmons, A., Lowry, S. C., et al. (2011). "The Size Distribution of Jupiter Family Comet Nuclei". In: *Monthly Notices of the Royal Astronomical Society* 414.1, pp. 458–469. doi: 10.1111/j.1365-2966.2011.18406.x (cited on page 109).
- Snodgrass, C., Agarwal, J., Combi, M., et al. (2017). "The Main Belt Comets and Ice in the Solar System". In: *The Astronomy and Astrophysics Review* 25.1, p. 5. doi: 10.1007/s00159-017-0104-7 (cited on page 13).
- Snodgrass, C. and Jones, G. H. (2019). "The European Space Agency's Comet Interceptor Lies in Wait". In: *Nature Communications* 10.1, p. 5418. doi: 10.1038/s41467-019-13470-1 (cited on page 154).
- Soja, R. H., Sommer, M., Herzog, J., et al. (2015). "Characteristics of the Dust Trail of 67P/Churyumov-Gerasimenko: An Application of the IMEX Model". In: *Astronomy & Astrophysics* 583, A18. doi: 10.1051/0004-6361/201526184 (cited on page 107).
- Sollaci, L. B. and Pereira, M. G. (2004). "The Introduction, Methods, Results, and Discussion (IMRAD) Structure: A Fifty-Year Survey". In: *Journal of the Medical Library Association* 92.3, pp. 364–371 (cited on page xiv).
- Solli, K. and Nygaard, L. P. (2023). "The Doctorate in Pieces: A Scoping Review of Research on the PhD Thesis by Publication". In: *Higher Education Research & Development* 42.4, pp. 984–999. doi: 10.1080/07294360.2022.2110575 (cited on page xv).
- Sousanis, N. (2015). *Unflattering*. Harvard University Press (cited on page xiv).
- Spencer, J. R., Stern, S. A., Moore, J. M., et al. (2020). "The Geology and Geophysics of Kuiper Belt Object (486958) Arrokoth". In: *Science* 367.6481, eaay3999. doi: 10.1126/science.aay3999. (Visited on 04/08/2024) (cited on page 9).
- Spiller, D., Magionami, E., Schiattarella, V., et al. (2020). "On-Orbit Recognition of Resident Space Objects by Using Star Trackers". In: *Acta Astronautica* 177, pp. 478–496. doi: 10/gn33mj (cited on pages 40, 41).
- Spohn, T., Knollenberg, J., Ball, A. J., et al. (2015). "Thermal and Mechanical Properties of the Near-Surface Layers of Comet 67P/Churyumov-Gerasimenko". In: *Science* 349.6247, aab0464. doi: 10.1126/science.aab0464 (cited on page 118).
- Sprat, T. (1667). *The History of the Royal Society of London, for the Improving of Natural Knowledge*. London: T. R. and J. Allestry (cited on page xiv).
- Steele, C. (2008). "Scholarly Monograph Publishing in the 21st Century: The Future More Than Ever Should Be an Open Book". In: *Journal of Electronic Publishing* 11.2. doi: 10.3998/3336451.0011.201. (Visited on 02/20/2024) (cited on page xiii).
- Stern, A. (1988a). "Collisions in the Oort Cloud". In: *Icarus* 73.3, pp. 499–507. doi: 10.1016/0019-1035(88)90059-0 (cited on page 19).
- Stern, A. (1988b). "Collisions in the Oort Cloud: Erratum". In: *Icarus* 76.2, p. 385. doi: 10.1016/0019-1035(88)90080-2 (cited on page 19).
- Stern, A. and Weissman, P. R. (2001). "Rapid Collisional Evolution of Comets during the Formation of the Oort Cloud". In: *Nature* 409.6820, pp. 589–591. doi: 10.1038/35054508 (cited on page 19).
- Stern, S. A., Slater, D. C., Scherrer, J., et al. (2007). "Alice: The Rosetta Ultraviolet Imaging Spectrograph". In: *Space Science Reviews* 128.1, pp. 507–527. doi: 10.1007/s11214-006-9035-8 (cited on page 24).
- Stetson, P. B. (1987). "DAOPHOT - A Computer Program for Crowded-Field Stellar Photometry". In: *Publications of the Astronomical Society of the Pacific* 99, p. 191. doi: 10.1086/131977. (Visited on 11/19/2021) (cited on pages 55, 56).
- Stiegler-Balfour, J. J., Roberts, Z. S., LaChance, A. S., et al. (2023). "Is Reading under Print and Digital Conditions Really Equivalent? Differences in Reading and Recall of Expository Text for Higher and Lower Ability Comprehenders". In: *International Journal of Human-Computer Studies* 176, p. 103036. doi: 10.1016/j.ijhcs.2023.103036 (cited on page xvii).
- Strikwerda, T. E. and Junkins, J. L. (1981). *Star Pattern Recognition and Spacecraft Attitude Determination*. Tech. rep. Virginia Polytechnic Inst And State Univ Blacksburg Dept Of Engineering (cited on page 40).
- Strömgren, E. (1914). "Über Den Ursprung Der Kometen Mit Wesentlicher Unterstützung Des Mag. Johannes Braae". In: *Publikationer og mindre Meddelelser fra Kobenhavns Observatorium* 19, pp. 1–62 (cited on page 11).
- Strunk, W. and White, E. B. (1959). *The Elements of Style*. Macmillan (cited on page xiv).

- Su, C.-C. (2013). "Parallel Direct Simulation Monte Carlo (DSMC) methods for modeling rarefied gas dynamics". In: *Taiwan: National Chiao Tung University* (cited on page 120).
- Sunshine, J. M. and Feaga, L. M. (2021). "All Comets Are Somewhat Hyperactive and the Implications Thereof". In: *The Planetary Science Journal* 2.3, p. 92. doi: 10.3847/PSJ/abf11f (cited on page 33).
- Sword, H. (2012). *Stylish Academic Writing*: Cambridge, MA: Harvard University Press (cited on pages xi, xiv).
- Sykes, M. V. and Walker, R. G. (1992a). "Cometary Dust Trails: I. Survey". In: *Icarus* 95.2, pp. 180–210. doi: 10.1016/0019-1035(92)90037-8. (Visited on 04/08/2022) (cited on pages 16, 53).
- Sykes, M. V. and Walker, R. G. (1992b). "The Nature of Comet Nuclei". In: *Asteroids, Comets, Meteors*. Lunar and Planetary Society, p. 587 (cited on page 17).
- Szebehely, V. (1967). *Theory of Orbit: The Restricted Problem of Three Bodies*. Academic Press (cited on page 7).
- Szenher, M., Delacroix, A., Keto, E., et al. (2022). "A Hardware and Software Platform for Aerial Object Localization". In: *Journal of Astronomical Instrumentation*, p. 2340002. doi: 10.1142/S2251171723400020 (cited on page 42).
- Tang, Y., Birch, S. P. D., Hayes, A. G., et al. (2017). "Boulder Size Frequency Distribution on Comet 67P/Churyumov-Gerasimenko". In: *48th Annual Lunar and Planetary Science Conference*, p. 2796 (cited on page 107).
- Taylor, M. G. G. T., Altobelli, N., Buratti, B. J., et al. (2017). "The Rosetta Mission Orbiter Science Overview: The Comet Phase". In: *Philosophical Transactions of the Royal Society A: Mathematical, Physical and Engineering Sciences* 375.2097, p. 20160262. doi: 10/gkn5v9 (cited on pages 3, 22, 23, 93).
- Tegler, S. C., Romanishin, W., and G. J. Consolmagno, S. J. (2003). "Color Patterns in the Kuiper Belt: A Possible Primordial Origin". In: *The Astrophysical Journal* 599.1, p. L49. doi: 10.1086/381076. (Visited on 04/08/2024) (cited on page 8).
- Tenishev, V., Combi, M. R., and Rubin, M. (2011). "Numerical Simulation Of Dust In A Cometary Coma: Application To Comet 67P/Churyumov-Gerasimenko". In: *The Astrophysical Journal* 732.2, p. 104. doi: 10.1088/0004-637X/732/2/104 (cited on page 22).
- Tenopir, C., Christian, L., and Kaufman, J. (2019). "Seeking, Reading, and Use of Scholarly Articles: An International Study of Perceptions and Behavior of Researchers". In: *Publications* 7.1, p. 18. doi: 10.3390/publications7010018 (cited on pages xv, xvii).
- Tenopir, C., King, D. W., Christian, L., et al. (2015). "Scholarly Article Seeking, Reading, and Use: A Continuing Evolution from Print to Electronic in the Sciences and Social Sciences". In: *Learned Publishing* 28.2, pp. 93–105. doi: 10.1087/20150203. (Visited on 02/22/2024) (cited on pages xvi, xvii).
- Thomas, N. (2020). *An Introduction to Comets: Post-Rosetta Perspectives*. Astronomy and Astrophysics Library. Cham: Springer International Publishing (cited on pages 7, 9, 11, 13).
- Thomas, N., Davidsson, B., El-Maarry, M. R., et al. (2015a). "Redistribution of Particles across the Nucleus of Comet 67P/Churyumov-Gerasimenko". In: *Astronomy & Astrophysics* 583, A17. doi: 10.1051/0004-6361/201526049 (cited on pages 30, 51, 113).
- Thomas, N., El Maarry, M. R., Theologou, P., et al. (2018). "Regional Unit Definition for the Nucleus of Comet 67P/Churyumov-Gerasimenko on the SHAP7 Model". In: *Planetary and Space Science* 164, pp. 19–36. doi: 10.1016/j.pss.2018.05.019 (cited on pages 31, 105).
- Thomas, N., Sierks, H., Barbieri, C., et al. (2015b). "The Morphological Diversity of Comet 67P/Churyumov-Gerasimenko". In: *Science* 347.6220, aaa0440. doi: 10.1126/science.aaa0440 (cited on pages 30, 31, 105, 107).
- Thomas, P. C., Veverka, J., Belton, M. J. S., et al. (2007). "The Shape, Topography, and Geology of Tempel 1 from Deep Impact Observations". In: *Icarus*. Deep Impact Mission to Comet 9P/Tempel 1, Part 1 187.1, pp. 4–15. doi: 10.1016/j.icarus.2006.12.013 (cited on page 20).
- Thomas, R. A., West, R. E., and Rich, P. (2016). "Benefits, Challenges, and Perceptions of the Multiple Article Dissertation Format in Instructional Technology". In: *Australasian Journal of Educational Technology* 32.2. doi: 10.14742/ajet.2573 (cited on page xiii).
- Thompson, J. B. (2005). *Books in the Digital Age: The Transformation of Academic and Higher Education Publishing in Britain and the United States*. Cambridge: Polity Press Ltd. (cited on page xiii).
- Thompson, P. M. (2011). *Snap, Crackle, and Pop* (cited on page 130).
- Thraen, P. A. (1894). "Untersuchung Über Die Vormalige Bahn Des Cometen 1886 II". In: *Astronomische Nachrichten* 136.9, pp. 133–138. doi: 10.1002/asna.18941360903 (cited on page 11).

- Tian, F., Stewart, A. I. F., Toon, O. B., et al. (2007). "Monte Carlo Simulations of the Water Vapor Plumes on Enceladus". In: *Icarus* 188.1, pp. 154–161. doi: 10.1016/j.icarus.2006.11.010 (cited on page 104).
- Tinevez, J.-Y., Perry, N., Schindelin, J., et al. (2017). "TrackMate: An Open and Extensible Platform for Single-Particle Tracking". In: *Methods* 115, pp. 80–90. doi: 10.1016/j.ymeth.2016.09.016. (Visited on 11/19/2021) (cited on pages 38, 53).
- Tiscareno, M. S. and Malhotra, R. (2009). "Chaotic Diffusion Of Resonant Kuiper Belt Object". In: *The Astronomical Journal* 138.3, p. 827. doi: 10.1088/0004-6256/138/3/827. (Visited on 04/14/2024) (cited on page 9).
- Tisserand, F. (1896). *Traité de mécanique céleste*. Vol. 4. Gauthier-Villars et fils (cited on page 12).
- Tosi, F., Capaccioni, F., Capria, M. T., et al. (2019). "The Changing Temperature of the Nucleus of Comet 67P Induced by Morphological and Seasonal Effects". In: *Nature Astronomy* 3.7, pp. 649–658. doi: 10.1038/s41550-019-0740-0 (cited on pages 30, 158).
- Trujillo, C. A. and Brown, M. E. (2002). "A Correlation between Inclination and Color in the Classical Kuiper Belt". In: *The Astrophysical Journal* 566.2, p. L125. doi: 10.1086/339437. (Visited on 04/07/2024) (cited on page 8).
- Trujillo, C. A. and Sheppard, S. S. (2014). "A Sedna-like Body with a Perihelion of 80 Astronomical Units". In: *Nature* 507.7493, pp. 471–474. doi: 10.1038/nature13156 (cited on page 10).
- Tsunematsu, K., Ishimine, Y., Kaneko, T., et al. (2016). "Estimation of Ballistic Block Landing Energy during 2014 Mount Ontake Eruption". In: *Earth, Planets and Space* 68.1, p. 88. doi: 10.1186/s40623-016-0463-8 (cited on page 105).
- Tubiana, C., Güttler, C., Kovacs, G., et al. (2015). "Scientific Assessment of the Quality of OSIRIS Images". In: *Astronomy & Astrophysics* 583, A46. doi: 10.1051/0004-6361/201525985 (cited on pages 55, 64, 95).
- Turcotte, D. L. (1986). "Fractals and Fragmentation". In: *Journal of Geophysical Research: Solid Earth* 91.B2, pp. 1921–1926. doi: 10.1029/JB091iB02p01921 (cited on page 107).
- Ulman, V., Maška, M., Magnusson, K. E. G., et al. (2017). "An Objective Comparison of Cell-Tracking Algorithms". In: *Nature Methods* 14.12, pp. 1141–1152. doi: 10.1038/nmeth.4473 (cited on pages 42, 53).
- Unknown (1757). *An Account of the Remarkable Comet*. The second edition. Proceedings of the National Academy of Sciences. London (cited on page ix).
- ur Rahman, A., Sajid, M., Gillani, S. O., et al. (2019). "Detection and Tracking of Bubbles in Two-Phase Air Water Flow for Non-Convergent Sinusoidal Channel". In: *IET Image Processing* 13.4, pp. 692–697. doi: 10/gnkn5v (cited on page 42).
- Vafaei Sadr, A., Vos, E. E., Bassett, B. A., et al. (2019). "DeepSource: Point Source Detection Using Deep Learning". In: *Monthly Notices of the Royal Astronomical Society* 484.2, pp. 2793–2806. doi: 10.1093/mnras/stz131 (cited on page 58).
- Valtonen, M., Anosova, J., Kholshevnikov, K., et al. (2016). *The Three-body Problem from Pythagoras to Hawking*. Springer Cham (cited on page 7).
- van der Weel, A. (2015). "Reading the Scholarly Monograph". In: *TXT Magazine* 2015 (cited on page xiii).
- van der Weel, A. (2016). "Monographs in a Changing Reading Culture". In: *Against the Grain* 28.3. doi: 10.7717/2380-176X.7359. (Visited on 02/19/2024) (cited on page xiii).
- Van Dokkum, P. G. (2001). "Cosmic-Ray Rejection by Laplacian Edge Detection". In: *Publications of the Astronomical Society of the Pacific* 113.789, p. 1420. doi: 10.1086/323894 (cited on page 54).
- Van Noorden, R. (2014). "Scientists May Be Reaching a Peak in Reading Habits". In: *Nature*. doi: 10.1038/nature.2014.14658 (cited on page xvi).
- van Rossum, G. (1995). *Python Reference Manual*. Technical Report. NLD: CWI (Centre for Mathematics and Computer Science) (cited on page 53).
- van Woerkom, A. J. J. (1948). "On the Origin of Comets". In: *Bulletin of the Astronomical Institutes of the Netherlands* 10, pp. 445–472 (cited on page 11).
- VanderPlas, J. T. (2018). "Understanding the Lomb–Scargle Periodogram". In: *The Astrophysical Journal Supplement Series* 236.1, p. 16. doi: 10.3847/1538-4365/aab766 (cited on page 64).
- Veverka, J., Klaasen, K., A'Hearn, M., et al. (2013). "Return to Comet Tempel 1: Overview of Stardust-NExT Results". In: *Icarus*. Stardust/EPOXI 222.2, pp. 424–435. doi: 10.1016/j.icarus.2012.03.034 (cited on page 23).

- Vincent, J.-B., A'Hearn, M. F., Lin, Z.-Y., et al. (2016a). "Summer Fireworks on Comet 67P". In: *Monthly Notices of the Royal Astronomical Society* 462.Suppl_1, S184–S194. doi: 10.1093/mnras/stw2409 (cited on pages 105, 156).
- Vincent, J.-B., Bodewits, D., Besse, S., et al. (2015). "Large Heterogeneities in Comet 67P as Revealed by Active Pits from Sinkhole Collapse". In: *Nature* 523.7558, pp. 63–66. doi: 10.1038/nature14564 (cited on page 107).
- Vincent, J.-B., Farnham, T., Kührt, E., et al. (2019). "Local Manifestations of Cometary Activity". In: *Space Science Reviews* 215.4, p. 30. doi: 10.1007/s11214-019-0596-8 (cited on page 17).
- Vincent, J.-B., Kruk, S., Fanara, L., et al. (2021). *Automated Detection of Surface Changes on Comet 67P*. Tech. rep. EPSC2021-525. Copernicus Meetings. doi: 10.5194/epsc2021-525 (cited on page 106).
- Vincent, J.-B., Kruk, S., Schallig, E., et al. (2022). *Rosetta Zoo: Finding Changes on Comet 67P*. Tech. rep. EPSC2022-494. Copernicus Meetings. doi: 10.5194/epsc2022-494 (cited on page 106).
- Vincent, J.-B., Oklay, N., Pajola, M., et al. (2016b). "Are Fractured Cliffs the Source of Cometary Dust Jets? Insights from OSIRIS/Rosetta at 67P/Churyumov-Gerasimenko". In: *Astronomy & Astrophysics* 587, A14. doi: 10.1051/0004-6361/201527159 (cited on pages 107, 119).
- Vio, R. and Andreani, P. (2021). *Everything You Always Wanted to Know about Matched Filters (but Were Afraid to Ask)*. doi: 10.48550/arXiv.2107.09378 (cited on page 58).
- Virkar, Y. and Clauset, A. (2014). "Power-Law Distributions in Binned Empirical Data". In: *The Annals of Applied Statistics* 8.1, pp. 89–119. doi: 10/ghqvgw (cited on page 109).
- von Rosening, T. T., Brandt, J. C., and Farquhar, R. W. (1986). "The International Cometary Explorer Mission to Comet Giacobini-Zinner". In: *Science* 232.4748, pp. 353–356. doi: 10.1126/science.232.4748.353 (cited on page 23).
- Wada, K., Ishibashi, K., Kimura, H., et al. (2021). "Size of Particles Ejected from an Artificial Impact Crater on Asteroid 162173 Ryugu". In: *Astronomy & Astrophysics* 647, A43. doi: 10.1051/0004-6361/202039777 (cited on page 105).
- Wada, K., Tanaka, H., Suyama, T., et al. (2009). "Collisional Growth Conditions For Dust Aggregates". In: *The Astrophysical Journal* 702.2, p. 1490. doi: 10.1088/0004-637X/702/2/1490 (cited on page 20).
- Wallis, M. K. and Chandra Wickramasinghe, N. (1992). "Triton's Eruptions Analogous to Comet Halley's?". In: *Advances in Space Research* 12.11, pp. 133–138. doi: 10.1016/0273-1177(92)90429-2 (cited on page 105).
- Wang, C.-Y., Bochkovskiy, A., and Liao, H.-Y. M. (2022). *YOLOv7: Trainable Bag-of-Freebies Sets New State-of-the-Art for Real-Time Object Detectors*. doi: 10.48550/arXiv.2207.02696. URL: <http://arxiv.org/abs/2207.02696> (cited on page 42).
- Ware, M. and Mabe, M. A. (2015). *The STM Report: An Overview of Scientific and Scholarly Journal Publishing*. Tech. rep. : International Association of Scientific, Technical and Medical Publishers (cited on page xv).
- Waszczak, A., Ofek, E. O., Aharonson, O., et al. (2013). "Main-Belt Comets in the Palomar Transient Factory Survey – I. The Search for Extendedness". In: *Monthly Notices of the Royal Astronomical Society* 433.4, pp. 3115–3132. doi: 10.1093/mnras/stt951 (cited on pages 41, 53).
- Watanabe, S., Hirabayashi, M., Hirata, N., et al. (2019). "Hayabusa2 Arrives at the Carbonaceous Asteroid 162173 Ryugu—A Spinning Top-Shaped Rubble Pile". In: *Science* 364.6437, pp. 268–272. doi: 10.1126/science.aav8032. (Visited on 04/29/2024) (cited on page 14).
- Watson, F. G. and Shapley, H. (1937). "Distribution of Meteoric Masses in Interstellar Space". In: *Annals of Harvard College Observatory* 105, pp. 623–632 (cited on page 106).
- Wedlund, C. S., Behar, E., Nilsson, H., et al. (2019). "Solar Wind Charge Exchange in Cometary Atmospheres - III. Results from the Rosetta Mission to Comet 67P/Churyumov-Gerasimenko". In: *Astronomy & Astrophysics* 630, A37. doi: 10.1051/0004-6361/201834881 (cited on page 16).
- Wedlund, C. S., Behar, E., Nilsson, H., et al. (2020). "Solar Wind Charge Exchange in Cometary Atmospheres - III. Results from the Rosetta Mission to Comet 67P/Churyumov-Gerasimenko (Corrigendum)". In: *Astronomy & Astrophysics* 640, p. C3. doi: 10.1051/0004-6361/201834881e (cited on page 16).
- Weidenschilling, S. J. (1977). "Aerodynamics of Solid Bodies in the Solar Nebula". In: *Monthly Notices of the Royal Astronomical Society* 180.2, pp. 57–70. doi: 10.1093/mnras/180.2.57 (cited on page 19).
- Weidenschilling, S. J. (1997). "The Origin of Comets in the Solar Nebula: A Unified Model". In: *Icarus* 127.2, pp. 290–306. doi: 10.1006/icar.1997.5712 (cited on page 19).

- Weidling, R., Güttler, C., and Blum, J. (2012). "Free Collisions in a Microgravity Many-Particle Experiment. I. Dust Aggregate Sticking at Low Velocities". In: *Icarus* 218.1, pp. 688–700. doi: 10.1016/j.icarus.2011.10.002 (cited on page 19).
- Weidling, R., Güttler, C., Blum, J., et al. (2009). "The Physics Of Protoplanetary Dust Agglomerates. III. Compaction In Multiple Collisions". In: *The Astrophysical Journal* 696.2, p. 2036. doi: 10.1088/0004-637X/696/2/2036 (cited on page 19).
- Weissman, P., Morbidelli, A., Davidsson, B., et al. (2020). "Origin and Evolution of Cometary Nuclei". In: *Space Science Reviews* 216.1, p. 6. doi: 10.1007/s11214-019-0625-7 (cited on pages 7, 10, 11, 19, 20, 93).
- Wenger, M., Ochsenbein, F., Egret, D., et al. (2000). "The SIMBAD Astronomical Database - The CDS Reference Database for Astronomical Objects". In: *Astronomy and Astrophysics Supplement Series* 143.1, pp. 9–22. doi: 10.1051/aas:2000332 (cited on page 67).
- Wesołowski, M., Gronkowski, P., and Tralle, I. (2020). "Selected Mechanisms of Matter Ejection out of the Cometary Nuclei". In: *Icarus* 338, p. 113546. doi: 10.1016/j.icarus.2019.113546 (cited on pages 93, 103, 105, 111, 119, 125, 157).
- Westerweel, J., Elsinga, G. E., and Adrian, R. J. (2013). "Particle Image Velocimetry for Complex and Turbulent Flows". In: *Annual Review of Fluid Mechanics* 45.1, pp. 409–436. doi: 10.1146/annurev-fluid-120710-101204 (cited on pages 41, 52, 53).
- Whipple, F. L. (1950). "A Comet Model. I. The Acceleration of Comet Encke". In: *The Astrophysical Journal* 111, pp. 375–394. doi: 10.1086/145272 (cited on pages 12, 16).
- Whipple, F. L. (1972a). "On Certain Aerodynamic Processes for Asteroids and Comets". In: *Proceedings of the Twenty-First Nobel Symposium*. Saltsjöbaden, near Stockholm, Sweden: Wiley Interscience Division (cited on page 19).
- Whipple, F. L. (1972b). "The Origin of Comets". In: *Proceedings from IAU Symposium No. 45*. Vol. 45. Leningrad, U.S.S.R.: International Astronomical Union, p. 401 (cited on page 7).
- Whipple, F. L. (1951). "A Comet Model. II. Physical Relations for Comets and Meteors." In: *The Astrophysical Journal* 113, p. 464. doi: 10.1086/145416 (cited on page 16).
- Whipple, F. L. (1955). "A Comet Model. III. The Zodiacal Light." In: *The Astrophysical Journal* 121, p. 750. doi: 10.1086/146040 (cited on page 106).
- Whipple, F. L. (1964a). "Brightness Changes in Periodic Comets." In: *The Astronomical Journal* 69, p. 152. doi: 10.1086/109434 (cited on page 7).
- Whipple, F. L. (1964b). "Evidence for a Comet Belt beyond Neptune". In: *Proceedings of the National Academy of Sciences* 51.5, pp. 711–718. doi: 10.1073/pnas.51.5.711 (cited on page 7).
- Whipple, F. L. (1974). "The Nature of Comets". In: *Scientific American* 230.2, pp. 48–57 (cited on pages 14, 16).
- White, D. E. (1967). "Some Principles of Geyser Activity, Mainly from Steamboat Springs, Nevada". In: *American Journal of Science* 265, pp. 641–684. doi: 10.2475/ajs.265.8.641 (cited on page 104).
- Wiegert, P. and Tremaine, S. (1999). "The Evolution of Long-Period Comets". In: *Icarus* 137.1, pp. 84–121. doi: 10.1006/icar.1998.6040. (Visited on 04/28/2024) (cited on page 11).
- Wilding, N. (2016). "The Printing Press". In: *A Companion to the History of Science*. Ed. by B. Lightman. John Wiley & Sons, Ltd. Chap. 24, pp. 344–357. doi: 10.1002/9781118620762.ch24 (cited on page xiv).
- Williams, G. V. (2017). *New Designation Scheme For Interstellar Objects*. Tech. rep. 2017-V17. Cambridge, MA: Minor Planet Center (cited on page 11).
- Williams, J. M. and Colomb, G. G. (1995). *Style: Toward Clarity and Grace*. University of Chicago Press (cited on page xiv).
- Wilson, C. (1993). "Clairut's Calculation of the Eighteenth-century Return of Halley's Comet". In: *Journal for the History of Astronomy* 24, p. 1. doi: 10.1177/002182869302400101 (cited on pages 6, 7).
- Wilson, K. (1998). *The Status of Published Work in Submissions for Doctoral Degrees in European Universities*. UK Council for Graduate Education (cited on page xv).
- Wilson, K. (2002). "Quality Assurance Issues for a PhD by Published Work: A Case Study". In: *Quality Assurance in Education* 10.2. Ed. by D. Howard and M. Shaw, pp. 71–78. doi: 10.1108/09684880210423555 (cited on page xiii).
- Windmark, F., Birnstiel, T., Güttler, C., et al. (2012a). "Planetesimal Formation by Sweep-up: How the Bouncing Barrier Can Be Beneficial to Growth". In: *Astronomy & Astrophysics* 540, A73. doi: 10.1051/0004-6361/201118475 (cited on pages 19, 20).

- Windmark, F., Birnstiel, T., Ormel, C. W., et al. (2012b). "Breaking through: The Effects of a Velocity Distribution on Barriers to Dust Growth". In: *Astronomy & Astrophysics* 544, p. L16. doi: 10.1051/0004-6361/201220004 (cited on pages 19, 20).
- Wolff, S., Dawson, R. I., and Murray-Clay, R. A. (2012). "Neptune On Tiptoes: Dynamical Histories That Preserve The Cold Classical Kuiper Belt". In: *The Astrophysical Journal* 746.2, p. 171. doi: 10.1088/0004-637X/746/2/171. (Visited on 04/08/2024) (cited on page 8).
- Wood, J. and Hinse, T. C. (2022). "The Transformation of Centaurs into Jupiter-family Comets". In: *The Astrophysical Journal* 929.2, p. 157. doi: 10.3847/1538-4357/ac5964. (Visited on 04/14/2024) (cited on page 9).
- Wright, C. A., Liounis, A. J., and Ashman, B. W. (2018). "Optical Navigation Algorithm Performance". In: *1st Annual RPI Workshop on Image-Based Modeling and Navigation for Space Applications* (cited on page 40).
- Xi, Z.-z. (1984). "The Cometary Atlas in the Silk Book of the Han Tomb at Mawangdui". In: *Chinese Astronomy and Astrophysics* 8.1, pp. 1–7. doi: 10.1016/0275-1062(84)90002-X (cited on page 4).
- Ye, Q. and Jenniskens, P. (2022). *Comets and Meteor Showers*. doi: 10.48550/arXiv.2209.10654. URL: <http://arxiv.org/abs/2209.10654> (cited on page 16).
- Yelle, R. V., Soderblom, L. A., and Jokipii, J. R. (2004). "Formation of Jets in Comet 19P/Borrelly by Subsurface Geysers". In: *Icarus*. Special Issue on DS1/Comet Borrelly 167.1, pp. 30–36. doi: 10.1016/j.icarus.2003.08.020 (cited on pages 105, 119).
- Yeomans, D. K. (1985). "The Selection of Comets for Future Space Missions". In: *Dynamics of Comets: Their Origin and Evolution*. Ed. by A. Carusi and G. B. Valsecchi. Dordrecht: Springer Netherlands, pp. 415–421. doi: 10.1007/978-94-009-5400-7_36 (cited on page 26).
- Yeomans, D. K., Rahe, J., and Freitag, R. S. (1986). "The History of Comet Halley". In: *Journal of the Royal Astronomical Society of Canada* 80, pp. 62–86 (cited on page 6).
- Youdin, A. N. and Goodman, J. (2005). "Streaming Instabilities in Protoplanetary Disks". In: *The Astrophysical Journal* 620.1, p. 459. doi: 10.1086/426895 (cited on page 19).
- Ytrehus, T. (1975). "Kinetic Theory Description and Experimental Results for Vapor Motion in Arbitrary Strong Evaporation". In: *VKI Training Center for Experimental Aerodynamics Technical Note 112* (cited on page 21).
- Zahnle, K. and Low, M.-M. M. (1994). "The Collision of Jupiter and Comet Shoemaker-Levy 9". In: *Icarus* 108.1, pp. 1–17. doi: 10.1006/icar.1994.1038 (cited on page 13).
- Zakharov, A. V., Popel, S. I., Kuznetsov, I. A., et al. (2022). "Physical Processes Leading to Surface Erosion and Dust Particles Dynamics of Airless Bodies". In: *Physics of Plasmas* 29.11, p. 110501. doi: 10.1063/5.0117833 (cited on page 93).
- Zakharov, V. V., Rodionov, A. V., Lukianov, G. A., et al. (2009). "Monte-Carlo and Multifluid Modelling of the Circumnuclear Dust Coma II. Aspherical-homogeneous, and Spherical-Inhomogeneous Nuclei". In: *Icarus* 201.1, pp. 358–380. doi: 10.1016/j.icarus.2008.12.022 (cited on page 103).
- Zapevalin, P. R., Novoselov, A., and Zharov, V. E. (2023). "Artificial Neural Network for Star Tracker Centroid Computation". In: *Advances in Space Research*. Application of Artificial Intelligence in Tracking Control and Synchronization of Spacecraft 71.9, pp. 3917–3925. doi: 10.1016/j.asr.2022.11.023. (Visited on 05/05/2024) (cited on page 40).
- Zhang, G. (2017). *Star Identification*. Berlin, Heidelberg: Springer Berlin Heidelberg (cited on page 40).
- Zhang, Z., Wang, C., Song, J., et al. (2022). "Object Tracking Based on Satellite Videos: A Literature Review". In: *Remote Sensing* 14.15, p. 3674. doi: 10.3390/rs14153674 (cited on page 42).
- Zhen-Tao, X., Stephenson, F. R., and Yao-Tiao, J. (1995). "Astronomy on Oracle Bone Inscriptions". In: *Quarterly Journal of the Royal Astronomical Society* 36, p. 397 (cited on page 4).
- Zsom, A. and Dullemond, C. P. (2008). "A Representative Particle Approach to Coagulation and Fragmentation of Dust Aggregates and Fluid Droplets". In: *Astronomy & Astrophysics* 489.2, pp. 931–941. doi: 10.1051/0004-6361:200809921 (cited on page 19).
- Zudin, Y. B. (2021). *Non-Equilibrium Evaporation and Condensation Processes: Analytical Solutions*. Springer Nature (cited on page 21).